"ULTRASONIC DETERMINATION OF THE INTERNAL STRUCTURE OF SOLIDS"

A thesis presented for the
degree of Doctor of Philosophy in Electrical Engineering
in the University of Canterbury,
Christchurch, New Zealand.

by

M.G. Maginness, B.E. (Hons.).

1970.

"ULTRASONIC DETERMINATION OF THE INTERNAL STRUCTURE OF SOLIDS"

M.G. Maginness

Errata:

3.22 line above eq. 3.21 .. "then $k_{1,}$ must..." should be; $k_{1,1}$

5.15 Eqn. 5.33(b) - exponential argument should read $e^{-j(\xi x + \eta y + \zeta z - kct)}$ as in 5.33(a).

5.17 Eqn. 5.42 - at the end of the integral reads ".dx_Z.dy_A." should be; .dx_A.dy_A.

5.22 Eqn. 5.48 left hand side reads " $\frac{\partial}{\partial t}$ $U_n(c,y,ct)$" this should be; $\frac{\partial}{\partial t}$ $U_n(x,y,ct)$.

6.3 ninth line reads - "every $\frac{\omega_h}{\pi}$ seconds." this should be; every π/ω_h seconds.

6.15 line five reads "of = $\frac{2\pi}{Qd}$ in from...." should be; of $\xi = \frac{2\pi}{Qd}$ in from...

6.16 First line of Eqn. 6.19, v term arguments. Third argument reads "$\frac{h2\pi}{Sc}$" This should be; $\frac{h2\pi}{Sc\tau}$

6.19 Eqn. 6.25 (i) left hand side, second argument of v reads "$\frac{2KM}{Q}g$" Should be $\frac{2KM}{R}$ g

(ii) right hand side. Second factor in exponential argument reads "$\frac{+qr}{R}$" should be; $\frac{+gr}{R}$ (c.f. eqn. 6.26)

6.20 Eqn. 6.28 right hand side. Argument of first exponential term lacks a 'z'. Presently reads: "$e^{-j2K\sqrt{\quad}}$" should be: $e^{-j2Kz\sqrt{\quad}}$.

Thesis Errata (cont'd)

A similar omission occurs in Eqn. 6.29 (page 6.21). Also because the summation limits run from zero up and not symmetrically about the origin the terms in the z dependant exponential must be altered to give:

$$e^{-j2Kz\sqrt{\left(\frac{h^*}{S}\right)^2-\left(\frac{Lf^*}{Q}\right)^2-\left(\frac{Mg^*}{R}\right)^2}}$$

with $f^* = f \;,\; 0 \leq f \leq Q/2 - 1$

$= Q-f, \; Q/2 \leq f \leq Q-1.$

and similarly for g^* and h^*.

This modification applies to both Eqn. 6.28 and 6.29.

6.37 Eqn. 6.44 "S(s,y)" term should be S(x,y).

6.46 Line above Eqn. 6.62 "then as $F_o(-z) = -F(z)$, the..." should be $F_o(-z) = -F_o(z)$.

6.49 Line three, first word should be "spectra" not spectrum. - eqn. 6.64 second term on right hand side reads "f(f-τ)" this should be f(t-τ).

Figure 6.15. The solid line is the modulus plot and the dotted one shows the phase.

7.25 End of first paragraph "and will cause any significant.." should be: and will not cause any significant....

7.30 Second paragraph Section 7.6, third line, delete "of the plane" at the end of this line.

7.31 Second paragraph, second to last line, change "ingenuous" to ingenious.

8.26 Eqn. 8.16 - there should be an "equals" sign (=) after $A^*(\omega)$.

10.2 Beginning of last paragraph on page "All the programs on this disk were written.." should read: All the programs for this project were written....

11.7 Footnote: last word should be "cone" not "core"

Thesis Errata (cont'd)

13.8 First line "balck box" should read: black box.

A3.1/2 Eqn. A3.1/2(a) Denominator of bracketed term in top line reads "$ZC_o(1+Z_{TX}(\omega).j\omega C_o)$" should be: $Z\omega\ C_o(1+\ ...)$.

A3.1/8 Sentence above section 2 "The measured value (e) was 11mA." should read: The measured value (f) was 11mA.

A3.2/14 Eqn. A3.2/36 Term in square brackets should read:

$$[e^{\eta u}(1+\eta u) + e^{\xi u}(1+\xi u) - \frac{2}{\mu-\xi}(\mu e^{\eta u} - \xi e^{\xi u})]$$

This change does not affect the conclusions drawn below.

A3.3/1 Eqn. A3.3/1 Factor outside integral ("S/SK) should be: S/2K.

A3.4/1 Eqn A3.4/2 First bracketed term in denominator reads "(2R+d)" should be: (2R+d').

PREFACE

This project commenced from the concept that some of the wide variety of signal processing techniques developed in radar and sonar systems should be capable of useful application in the field of materials inspection. The particular aim was to assess the possibilities of an imaging arrangement and with this objective the author's main topic was defined as the signal processing section of an overall system. Inevitably perhaps, a multiplicity of practical difficulties associated largely with transducers and the actual handling of the signals before the imaging operations, diverted the main part of the effort away from the original topic into these other problems.

The thesis itself is organised into four main sections. Section I, containing Chapters 1 and 2, is by way of an introduction to the topic, discussing in particular the pattern of development followed and surveying the work reported in acoustic holography.

Section II, consisting of Chapters 3 through to 7, contains a theoretical analysis of the general problem of reconstruction of fields from measurements taken at some surface (Chapter 5) and of many details relating to specific portions of the complete imaging arrangement.

Section III, (Chapters 8, 9 and 10) is a brief description of the particular solution synthesised in the present work to meet the practical requirements of an imaging system.

The final section, Section IV, presents the experimental results obtained (Chapters 11 and 12) and a general summary of the whole project with suggestions for further development (Chapter 13).

A number of appendices contain details of some pieces of apparatus, discuss a computer simulation of transducer behaviour and hold some lengthy mathematical expositions.

Chapters 5 and 12 are the most important in the whole thesis. The theoretical development of field reconstruction from recordings of wideband, elastic wave signals as presented in Chapter 5 is based on well known mathematical techniques but as far as the author is aware these have not previously been fully applied to the situation treated here.* Chapter 12 contains a record of many of the actual images obtained and discusses the correlation with theoretical predictions.

Chapters 6 and 7 are important to the determination of potential performance of the scheme devised here and similarly Chapter 2 is significant as a record of previous work with which to compare the present results.

During the period of this project the whole topic of ultrasonic imaging has gathered a rapidly increasing number of workers in many laboratories and a large number of results displaying images of

---

* Since the preparation of this Chapter, a paper by Sondhi (J.Acoust. Soc.Am., 46, Pt.2, pp.1158-1164, Nov. 1969) has been published. This contains a similar development but one restricted to monochromatic, acoustic (i.e., scalar) waves.

considerably greater fidelity than any results obtained here, have been published. However, it is considered that the local effort offers much greater potential of a very high level of ultimate performance since the other methods so far reported are near the limits of their capabilities whereas the developments described in this thesis are capable of improvement in nearly every significant aspect by direct extension of the techniques already established by the work to date. The most significant of these is considered to be the extension into wideband imaging, a capability already incorporated in the special apparatus constructed but one which could not be fully exploited because of present computer limitations. As far as is known, no other work in progress offers this possibility.

Maginness M.G. "Comment on Non-Optical Holography"
Proc. IEEE (Letters) 55 pp 2050-1,
Nov. 1967.

Maginness M.G. and Kay L. "Signal processing for acoustic imagining systems"
Paper K-5-3, 6th International Congress on Acoustics, Tokyo, August 1968.

Maginness M.G. and Kay L. "Ultrasonic Imagining in Solids"
Paper presented at 'Conference on Industrial Ultrasonics', Loughborough U.K., 23-25 Sept. 1969.

Cook G.B. and Johnson D.A.H. "Pseudorandom selection of elements in a multielement array".
Radio. Electron. Eng. 38 pp 82-88,
August 1969.

Kay L, Maginness M.G. and Cook G.B. "A method for the production of images of the interior structure of solid objects"
N.Z. Patent Application 154800, Dec. 1968.

A C K N O W L E D G E M E N T S

This project has been conducted as a team effort and consequently I am heavily indebted to many people for their substantial assistance. In particular, however, I must acknowledge the efforts of my supervisor, Professor L. Kay, who provided the initial impetus and continuing guidance and Mr G.B. Cook who was responsible for much of the actual detail design and construction work.

The technicians of the Electrical Engineering and several other departments, the staff of the Engineering Library and of the University Computer Centre, have all provided much appreciated help.

Personal financial assistance was provided by the National Electrical and Engineering Company's Scholarship, the New Zealand University Grants Committee and the National Research Development Corporation of the U.K. The latter two organizations have also generously supported the research and without this finance very little could have been achieved.

Finally, I am deeply indebted to my wife, Helen, for her encouragement and patience and for willingly tackling the major task of typing this thesis.

C O N T E N T S

SECTION III: SYNTHESIS OF METHODS AND TECHNIQUES.

CHAPTER 8. INTERROGATION OF THE RECEIVING TRANSDUCER ARRAY.

CHAPTER 9. SIGNAL CAPTURE AND RECORDING.

CHAPTER 10. COMPUTER ORGANIZATION.

SECTION IV: EXPERIMENTAL WORK. FURTHER DEVELOPMENTS.

CHAPTER 11. PRACTICAL APPLICATION OF TRANSMITTING TRANSDUCERS.

CHAPTER 12. EXPERIMENTAL ARRANGEMENTS AND RESULTS.

CHAPTER 13. GENERAL COMMENTS AND SUGGESTIONS FOR FURTHER DEVELOPMENT.

A P P E N D I C E S

CHAPTER 1.

PROJECT BACKGROUND.

1.1. INTRODUCTION. A STATEMENT OF THE PROBLEM AND GENERAL BACKGROUND.

This project was conceived as an exploration of theory and techniques with the aim of developing (or showing that some fundamental obstacle prevented developing) a system which would be capable of producing pictures of the internal structure of solid objects. Essential requirements were defined as:

Applicability of the method to a range of typical technical materials and possibly biological tissue;

Development in a form that at least encompassed the prototype of a practicable testing apparatus for industrial use.

No form of energy other than ultrasonic waves was considered for the sensing radiation. The only other form offering significant penetration of metals is high energy electromagnetic radiation. This does not permit 'focussing' of attention on specific regions within the volume being examined or one-sided access to a specimen and will not show up many practically significant flaws (e.g., thin laminations) which are readily detectable by ultrasonics.

The general field into which the present effort fits covers a wide range of technologies - radar, sonar, X and gamma ray inspection, ultrasonic flaw detection, infra-red[1] and microwave[2]

devices all with the common purpose of revealing details of optically inaccessible regions. A common tendency in the evolution of these systems is the development of output displays presenting the information through our most developed channel for perceiving spatial relationships, vision, in a form corresponding directly with the actual geometry of the situation. (Examples are plan position indicating (PPI) radar and 'B' scan sonar). Thus it seemed most desirable that this project should aim at providing a similar final display.

It would be safe to say that currently operational ultrasonic pulse-echo flaw detection systems represent a level of sophistication approximately equivalent to that of radar thirty years ago. Even a very cursory examination of the patent literature will show[3,4] that a large amount of ingenuity has been applied to adapting the basic method to a wide variety of physical situations but only very recently have even the most basic tools of signal processing and control been applied.[5,35]. The major difficulty lies in interpretation of the data acquired rather than in lack of information gathering capability.[6] Thus systems offering a display in the form of an image have considerable attraction.

At the time (1966) this project commenced attempts at obtaining images had not significantly advanced from the method proposed by Sokoloff[7] in 1937, nearly all the rather limited effort having been expended in producing a variety of acoustic-electrical conversion devices. All this work was confined to fluid media,

much of it in attempts to provide imaging systems for inspection work in murky water.[8]

Only recently has much attention been paid to the stress fields existing in solid materials under conditions of direct significance to materials testing.[9] A related problem is the behaviour of transducers when used to sample these stress fields. Particularly under conditions where it is desired to employ wideband signals (see below) the exact solution of transducer behaviour is rather complex.

The first reported application of the holographic technique in other than an optical context appears to have been the microwave experiments of Dooley[10] in 1965. Since then much work has been done on the extension of this powerful concept to acoustic systems. So far as is known at the time of writing, nothing has yet been reported on the use of this method when the original medium containing the objects is solid. Acoustic holography and its precise relation to the present system is described in Chapter 2.

1.2. IMAGING SYSTEMS.

1.2.1. Definition of an imaging system.

It is appropriate at this point to define precisely what is meant by the term 'imaging system' in the present context. Referring to Figure 1.1 an imaging system is a collection of devices and procedures which, by measurements of the field existing over an aperture 'A', determine the internal configuration of the

volume 'V', and display this configuration in visible form. The volume 'V', is defined by a bounding surface 'R' of which A forms a part. The effect is that of 'looking' through a 'window' (A) to observe internal details such as O_1,O_2, etc. Implicit in this definition is the presence of some propagating field within V, either produced by self-radiating objects (e.g., as in passive sonar) or by an externally powered source positioned on R, (e.g., radar and active sonar), which is perturbed by the presence of objects. A basic limitation to the performance of any practical system arises from the restriction of A to a (usually small) portion of R. Significant information about O_1,O_2, etc., must generally be assumed to exist in radiations or reflections in all directions. Restriction of view to a limited arc sets a limit on the fineness of detail resolvable, hence the trend towards larger telescopes, radar antennas etc.

The information gathered by an imaging system may be divided into two main categories;

a) positional information about the objects of interest,

b) parameters such as size, shape, velocity.

The distinction is frequently blurred in actual systems but is convenient in classifying methods.

1.2.2. Some imaging systems.

Consider the most familiar form of imaging system - the simple optical lens. Figure 1.2 shows a section through such an arrangement. The wavefront W_1 defines the locus of energy

emanating from an object O_1 at some instant. The lens L of aperture A operates on the available portion of W_1 so as to (ideally) recombine (i.e., focus) all the intercepted energy from O_1 at a single point I_1 at some later instant. Similarly energy from O_2 is made to pass through a point I_2 and so on. The basic operation performed is the insertion of appropriate time delays in the signal paths through the system. This action is the essential feature of all imaging arrangements.

In a simple radar system we may recognise the time delay operation in the shape of the antenna dish. Positional information is determined by the mechanical pointing of the antenna for azimuth and elevation and the third position coordinate by the propagation delay of the echo signal. Other target parameters (often merely presence or absence of an object) are obtained by a distinct decision device (often a human operator).

Mechanical difficulties in the physical movement of large antennas required for high spatial resolution and the desire for more detailed information on the target have led to the development of the 'phased array' method permitting rapid electrical scanning and the use of various systems based on statistical decision theory to estimate target parameters. A further technique, 'synthetic aperture'[11] radar used for high resolution mapping provides an interesting example very closely parallel to the system developed in the present work.

Some background to these developments in radar systems may be found in Skolnik[12] and some further examples of phased array radars

in references 13, 14, 15, 16 and 17. Some sonar phased array systems are described in 19, 20 and 21. One may note the enormous quantity of hardware involved in the more advanced of these systems.[18] This complication arises largely because 'real time' operation is essential. In a system intended for the observation of objects in rigid materials (or where fine target movement is insignificant at the resolution required as in synthetic aperture radar) collection of data can be spread over a larger time interval making repeated use of a single signal processing channel rather than parallel use of many.

1.2.3. Ultrasonic imaging systems.

Figure 1.3 shows a block diagram of the system that will be referred to as the 'conventional' ultrasonic imaging system.[22,23,24] The arrangement stems directly from Sokoloff's original patent and is very similar to a closed circuit television display. The optically sensitive camera surface is replaced by an acoustically sensitive plate and 'illumination' provided from an acoustic transmitter. At the time this project commenced characteristic features of these systems were:

a) Simple shadow casting techniques were most common, the performance of available acoustic lenses being very limited. More recent work offers improvements in this direction.[25] The shadow casting technique necessitates access to two opposite faces of the specimen, a limitation it was considered desirable to avoid.

b) Continuous wave transmission of a steady frequency. Reported values ranged from 1 to 15 MHz, giving in water, wavelengths in the range 1.5mm to 0.10mm.

c) The sensitive faceplate of the tube formed part of the vacuum envelope. This placed a severe restriction on permissible aperture (or if an acoustic lens were used, on field of view).

d) The relatively long wavelengths, combined with small apertures and coherent illumination resulted in poor resolution capabilities and severe interference effects with anything other than thin objects. Judicious orientation of the specimens helped in some cases.[26]

e) Establishment of a suitable field from the transmitter proved very difficult. Images were frequently obscured in the interference pattern of the transmitter field. Attempts to use very small transmitters and thus obtain a 'smoother' field fail in fluid media because the large change in acoustic properties between the solid transducer and the fluid prevents radiation at large angles from the normal to the transmitter surface.

A 'state of the art' survey up to 1965 is in reference 27 and some trends are discussed in 28. The question of transducer tube performance is treated in Chapter 8. Developments in the overall system since 1965 have included the use of the phase information obtained from the tube in the display as colour information via the NTSC colour television system[29] and the use of bursts of

insonification.[30] This later development in particular should enhance the usefulness of such systems by permitting time gating of multiple reflections and other forms of interference out of the display. Use of phase information enhances the sensitivity to small changes in the object being viewed but does not necessarily help in depicting it with greater fidelity.

Although only piezoelectric acoustic-electrical conversion and electron beam scanning have been mentioned above, several other phenomena offer possibilities in the visualization of acoustic fields.[22,24] Few of these methods approach the sensitivity of the piezoelectric effect and many are energy sensitive only, destroying phase information. A number of successful systems have been constructed using mechanical aperture scanning with relatively large probes.[31,32,33] These commonly employ pulse-echo techniques and have proved useful in biological applications, but the ultimate resolution is limited by the coarseness of the samples taken over the inspection surface. Some preliminary applications of electronic beam steering techniques have appeared recently in this field.[34]

1.3. PROJECT HISTORY.

Consideration of a form for the present system commenced from a number of previous developments, the most important of which were:

1. Work on high resolution sonars with electronic scanning and some preliminary experiments on the practicability

of controlling ultrasonic field patterns in solid materials using similar scanning apparatus.[36,37] Control of a transmitted field immediately implies the possibility of being able to achieve the reverse effect - scanning of a receiving array pattern through the space under investigation.

2) The concept of recording a field over an aperture from a number of sample points so spaced as to permit unambiguous reconstruction (at a resolution level determined by aperture size) of the field existing over the whole of the volume 'viewed' by the aperture.[38] The possibility of extending the resolution beyond that normally expected for a given size of aperture[39] was noted but any possibility of achieving this with a practical device is considered remote.

3) The ultrasonic image tube was regarded as means by which an aperture could be sampled and the acoustic signals recorded not just in intensity but in fine time structure. At the time none of the previous applications of this device had required preservation of temporal detail and some types deliberately lost this information either for convenience of scanning method[22] or to permit integration of signal energy over the frame scanning period and thus enhance sensitivity.[40]

Although Sokoloff's original patent apparently indicates direct coupling of the image tube to a solid object all reported work was on systems where the tube face, object, and transmitter were immersed in a liquid bath. Thus some doubt existed as to whether the tube would operate satisfactorily with the faceplate

directly attached to a solid material.

4) The observation by Gericke[41] that information obtainable from a conventional ultrasonic testing apparatus was considerably more consistent and reliable when two frequencies were employed simultaneously. This correlated with the known difficulty of accurate object perception in monochromatic illumination and together with the necessity of a wideband signal if good depth resolution was to be obtained in the proposed system led to the idea of developing a wideband imaging apparatus.

The preliminary concept of the device contained the notion of using the image tube as a very fast space-time sampling device scanning the entire transducer area within one temporal sampling period and feeding the signal to a spatial scanning system developed after the style of the 'within pulse' sonar.[21] This was immediately demonstrated as unfeasible by considering the scanning rate required over the tube face. A 50mm diameter plate scanned in 100 lines requires each line scanned in 1nS for a highest frequency of 5 MHz and correct spatial resolution in a typical metal (5 MHz wavelength approximately 1.1mm.). Attention then turned to the possibilities of performing the imaging operation more slowly but still in a completely self-contained apparatus. This idea seems attractive until one appreciates that in typical materials inspection applications the spacing of the receiving transducer and objects will frequently be such that 'near field' conditions prevail. Under these circumstances the

processing time delays (1.2.2.)* are no longer linear+ functions of position on the aperture. The hardware developed in sonar and radar applications can then perform only one part of the total transformation required to reconstruct the field and hence the object distribution in the viewed region.

It will be noted that once the ideas of fast scanning and self-containment are abandoned then the possibility of real time or at least relatively fast image formation is lost as well. However consideration of the extra complexity needed to produce a complete near-field spatial scanner together with the very large storage requirement if all data were processed on the spot led to the modification of the original concept to one of recording the aperture data through special apparatus onto a media suitable for computer input and performing the main processing to an image there.

A rough calculation will serve to illustrate the magnitude of the data handling problem. Consider an aperture of 50mm. diameter, sampled at 0.5mm intervals for a total of approximately 7860 elements. Let the system bandwidth be 10 MHz (e.g., transmission of a damped pulse of 1-2 cycles of a 5 MHz wave)

---

* Insertions such as (1.2.2.) etc. are cross-references to sections in this thesis.

\+ That is, wavefronts incident on the aperture from nearby scatterers are curved and do not have uniform rate of change of phase along the aperture as do plane waves from distant objects.

then if 10μS* of returning echo is recorded from each aperture element one has a total of 200 time samples for each point or 1.572×10^6 samples. If each of these samples occupied one punching on standard paper tape a total of 13100 feet of tape would be required. No other media was available for the project so it was obvious that some means of reducing this figure by a factor of about 20 was essential.

Firstly, examination of work done in radar systems made it obvious that the large aperture required for good spatial resolution did not need to be completely interrogated but rather that random omission of many elements would have comparatively minor effects on the final performance.[42,43] Secondly, at that time use of the image tube as the aperture sampling means was taken as most probable and some calculations showed that the obtainable signal to noise ratio would be low. Hence coarse amplitude quantization of the time samples would be adequate and several could be accommodated in each punching of the tape.

These considerations, a study of propagation conditions in solid media and of transducer behaviour, together with planning of the required apparatus, occupied most of the first year on this project. The studies are contained in reference 44.

At this point a commercially available image tube was acquired

---

* This value represents a compromise between gathering information from as large a volume as possible on one recording and data storage economy. (See 6.4.2.)

for evaluation and detail work on the data acquisition hardware commenced as a separate project. Lack of experience with vacuum equipment led to rather unsatisfactory performance from the image tube and the consumption of what must be regarded in retrospect as an exorbitant amount of time. Additionally, such tests on tube performance as were conducted indicated that the operating conditions set by the manufacturer were far from optimum and were severely restricting the potential signal gain of the electron multiplier part of the device.

Some considerable attention was given at this time to the development of acoustic holography and to the general question of data processing by optical means.[45] Optical methods appear to offer many advantages in the processing of large amounts of data because of the inherent multiple channel capacity but suffer from the restriction to two dimensional information and the lack of phase preserving sensors.

After prolonged failure to achieve consistent operation of the image tube a simple mechanically scanned transducer was set up on a block of aluminium and readings obtained from this demonstrated that imaging to the limit permitted by the very small aperture was possible. Until the automatic recording apparatus became functional the operation was confined to using bursts of a single frequency making only two readings (amplitude and phase) from each aperture point necessary. These results confirmed a concept which appears to not have received mention, namely, that not only would a thin piezoelectric plate respond

point by point to the local acoustic field when very lightly damped as in a water tank imaging system but that this behaviour continues under conditions of very tight coupling to a bulk solid material.

The data acquisition apparatus, containing random scanning control for apertures up to 128 by 128 elements, high speed analogue to digital converter with a bandwidth of 12 MHz and paper tape punch control was completed in April 1969 and results obtained through this have proved sufficiently promising to warrant further development of the system.

Some preliminary work in metals other than aluminium has been done as a further separate project. Difficulties arise through the grain structure of technical metals once acoustic wavelengths approaching the grain size[46] are reached. Considerable scattering occurs resulting in high attenuation of the desired signal returns and a high level of background return (the 'grass' of pulse-echo testing).

Overall then, at the present stage many of the original ideas have proved unsuitable. The receiving transducer still remains the major bottleneck but developments in the production of integrated semiconductor arrays offer the possibility of a transducer of greatly superior overall characteristics to the image tube. Some feasibility studies for such a device are in Chapter 8. The large quantity of data involved in image formation has resulted in, with the program currently operational, an excessively long

computer processing time and full use cannot yet be made of the wide bandwidth of the signals to improve the images. However development of 'fast' algorithms for computer calculation of multidimensional Fourier transforms[47] offers a means of replacing the present convolution method of image calculation by a more rapid technique. Implementation of this must await the installation of a larger core store in the University computer.

1.4. A SUMMARY OF DEVELOPMENTS.

The advantages of the system developed in this project are seen as:

1. A single set of automatically recorded signals serves to produce a geometrically correct image of the space viewed without any further manual action.

2. Focussing of the received data is achieved thereby obtaining the maximum possible information about the objects examined.

3. The wide bandwidth illuminating signal permits sharp resolution in depth as well as angle. Additionally the particular form chosen - a sharp pulse - minimises direct electromagnetic leakage from the transmitter to receiving transducer. This is a major artefact in conventional imaging systems. The use of pulse transmission also overcomes much of the effect of shear wave propagation in solids. As typically the shear wave velocity is one half that of the longitudinal wave recording of data from a particular region can be complete before shear wave

returns appear. Any shear wave pickup in the recording period must be from a different region and unless the incident waves are the result of shear wave propagation throughout this shear wave image will not focus at the true image depth but at some other depth.

4. The system retains the big advantage of ultrasonic inspection methods of requiring access to only one side of the specimen.

Of course there are also some major drawbacks:

1. The time lag before results are obtained.

2. The necessity that the transducers and the object space remain completely stationary over the recording time. It may be noted here that the imaging computations do not require any information as to the actual position of the transmitting transducer, the only assumption is that it remains fixed.

3. A specially prepared area is required on the specimen for transducer attachment.

4. Restrictions in the recording and processing apparatus confine recordings at any one time to a slice from the entire specimen. This slice will be approximately one half the thickness of material traversed in the length of record from any receiver element. (The 10μS referred to above).

5. A restriction in the ultimate resolution imposed by the transmission properties of the material itself.

However defects of the same size as the grain structure are at the limit of practical significance in any case.

Of these objections, 4., is more a function of resources than inherent in the method and the use of say magnetic tape as the recording material would permit very much faster interrogation of the receiver.

REFERENCES FOR CHAPTER 1.

1. Horan, J.J. 'Spacecraft infrared imaging'.
IEEE Spectrum 5, pp.71-75, June 1968.

2. Jacobs, H. et.al. 'Proposal for a fog penetrating imaging device'.
Proc. IEEE 54, p.907, June 1966.

3. Kortenhoven, P. 'Transducer for ultrasonic testing of pipe'.
U.S. Patent 3 413 843, Dec. 1968.

4. Cowan, J.V. 'Ultrasonic inspection apparatus'.
U.S. Patent 3 130 577, April 1964.

5. Wood, F.M. and Proctor, N.B. 'Method of and apparatus for ultrasonic inspection utilizing correlation techniques'.
U.S. Patent 3 295 362, Jan. 1967.

6. Worlton, D.C. 'Recent non-destructive testing advances at Batelle Memorial Institute, Pacific Northwest Laboratory, Report BNWL-SA-1772.

7. Sokoloff, S. British Patent 477 139, Dec. 1937.

8. Green, P.S., Bellin, J.L.S. and Knollman, G.C. 'Acoustic imaging in a turbid underwater environment'.
Journ. Acoust. Soc. Am. 44, pp.1719-1730, 1968.

9. Christie, D.G. 'Stress wave propagation as applied to the detection of flaws by ultrasonic inspection'.
pp.35-56 of 'Progress in non-destructive testing', (Ed. Stanford, E.G. and Ferron, J.H.), Vol.1, Heywood, London, 1958.

10. Dooley, R.P. 'X-band holography'.
Proc. IEEE (Letters) 53, pp.1733-5, Nov. 1965.

11. I.R.E. Transactions on Military Electronics.
Special issue on synthetic aperture arrays.
MIL-6, No.2, April 1962.

12. Skolnik, M. 'Introduction to radar systems'.
McGraw-Hill, New York, 1962.

13. Allen, J.L. et.al. 'Phased array radar studies'.
M.I.T. Lincoln Laboratory Tech. Reports 228 (August 1960) and 236 (November 1961).

14. Davies, D.E.N. 'Continuous scan beam positioning radars'. Proc. IEE 112, p.439, March 1965.

15. Slattery, B.R. 'Use of Mills Cross receiving arrays in radar systems'. Proc. IEE 113, p.1712, November 1966.

16. Molz, K.F. 'Phased array radar systems'. Radio and Electronic Eng. 28, pp.331-340, Dec. 1964.

17. Burtnyk, N. et.al. 'A wide aperture sampling linear array for direction finding'. I.R.E. Trans. AP-12, p.248, May 1964.

18. Proc. IEEE 56, Special issue on electronic scanning. Nov. 1968, contains many descriptions of specific items and a full system is outlined by -
Lowenschuss, O. 'Digital radar systems', and Thompson, B.J. and Goldstone, B.J. 'Digital signal processing'. Electronic Progress 12, 1, 1968.

19. Welsby, V.G. and Dunn, J.R. 'High resolution sector scanning sonar'. Journ. Brit. I.R.E. 26, p.205, Sept. 1963.

20. McCartney, B.S. 'An improved electronic sector scanning sonar receiver'. Journ. Brit. I.R.E. 22, Dec. 1961, pp.481-488.

21. Tucker, D.G., Welsby, V.G. and Kendal, R. 'Electronic sector scanning'. Journ. Brit. I.R.E. 18, p.465, Aug. 1958.

22. Smyth, C.N. et.al. 'The ultrasound image camera'. Proc. IEE 110, pp.16-28, Jan. 1963.

23. Semmenikov, Iu. B. 'A study of acoustic image converters', Soviet Physics-Acoustics 4, p.72, 1958.

24. Turner, W.R. 'Ultrasonic imaging'. Ultrasonics 3, p.182, Oct.-Dec. 1965.

25. Golis, M.J. 'An analysis of the ultrasonic zone lens'. IEEE Trans. SU-15, pp.105-110, April 1968.

26. Berger, H. and di Novi, R.A. 'Angular positioning of thin metallic samples for optimum continuous wave ultrasonic imaging'. Journ. Acoust. Soc. Am. 36, pp.2053-8, Nov. 1964.

27. McKay, R.S. (Ed.) 'Ultrasonic imaging'.
Mine Advisory Committee, Natl. Acd. Sci., Natl. Res. Council. NRC:MAC:2016, April 1965.

28. Sayers, J.F. 'The future of ultrasonic cameras in industrial inspection'.
Ultrasonics 4, p.22, April 1966.

29. Jacobs, J.E. 'Ultrasound image converter systems utilizing electron-scanning techniques'.
IEEE Trans. SU-15, pp.146-152, July 1968.

30. Dubois, J.L. 'An electron beam acoustic image converter operating in a pulsed transmission mode'.
Paper H-5, 1968 IEEE Ultrasonics Symposium, Sept. 25-27, New York.

31. Greatorex, C.A. and Ireland, H.J.D. 'An experimental scanner for use with ultrasound'.
Brit. J. Radiology 37(453), p.174, March 1964.

32. Klinker, L.G. et.al. 'Inspecting metals by ultrasonic visualization'.
Metal Progress 88, p.82, July 1965.

33. Thurston, F.L. et.al. 'Ultrasonic scanning of biological tissue by a new technique'.
Science 149(3681), p.302, 1965.

34. Somer, J.C. 'Electronic sector scanning for ultrasonic diagnosis'.
Ultrasonics 6, pp.153-159, July 1968.

35. Whittington, K.R. and Cox, B.D. 'Electronic steering and focussing of ultrasonic beams in tube inspection'.
Ultrasonics 7, pp.20-25, Jan. 1969.

36. Kay, L., Whipp, E. and Bishop, M.J. 'The physical factors affecting non-destructive testing'.
Journ. Brit. I.R.E. 23, pp.373-380, May 1962.

37. Kay, L. and Bishop, M.J. 'The effect of a linear phase taper on the near field of an ultrasonic multi-element array'.
Radio and Electronic Eng. 29, pp.207-212, April 1965.

38. Ksienski, A. 'Spatial frequency characteristics of finite aperture antennas'.
Paper at Symposium on 'Electromagnetic Theory and Antennae', Copenhagen, June 1962. (Publ. as 'Electromagnetic waves and antennas'. Ed. E.C. Jordan, Pergammon, 1963).

39. Welsby, V.G. 'The angular resolution of a receiving aperture in the absence of noise'.
Journ. Brit. I.R.E. 26, pp.115-124, Aug. 1963.
- also Departmental Memo 114, Elect. Eng. Dept. Univ. Birmingham, (U.K.)

40. Rocha, H.A.F. 'Ultrasonic image detector'.
U.S. Patent 2 957 340, Oct. 25, 1960.

41. Gericke, O.R. 'Dual frequency pulse echo testing'.
Journ. Acoust. Soc. Am. 36, pp.313-322, Feb. 1964.

42. Ogg, F.C. 'Steerable array radars'.
I.R.E. Trans. MIL-6, pp.80-94, April 1961.

43. Willey, R.F. 'Space tapering of linear and planar arrays'.
I.R.E. Trans. AP-10, pp.369-376, July 1962.

44. Maginness, M.G. 'Studies for an acoustic imaging system'.
Dept. Memo. 3, Elect. Eng. Dept., Univ. Canterbury (N.Z.), April 1967.

45. Cutrona, L.J. et.al. 'On the application of coherent optical processing techniques to synthetic aperture radar'.
Proc. IEEE 58, p.1026, Aug. 1966.

46. Bhatia, A.B. 'Scattering of high frequency sound waves in polycrystalline materials'.
Journ. Acoust. Soc. Am. 31, p.16-23, Jan. 1959.

47. Cooley, J.W. and Tukey, J.W. 'An algorithm for the machine computation of complex Fourier series'.
Mathematics of Computation 19, pp.297-301, April 1965.

48. Marom, E. et.al. 'Ultrasonic holography by electronic scanning of a piezoelectric crystal'.
App. Phys. Lett. 12, pp.26-28, 15 Jan. 1968.

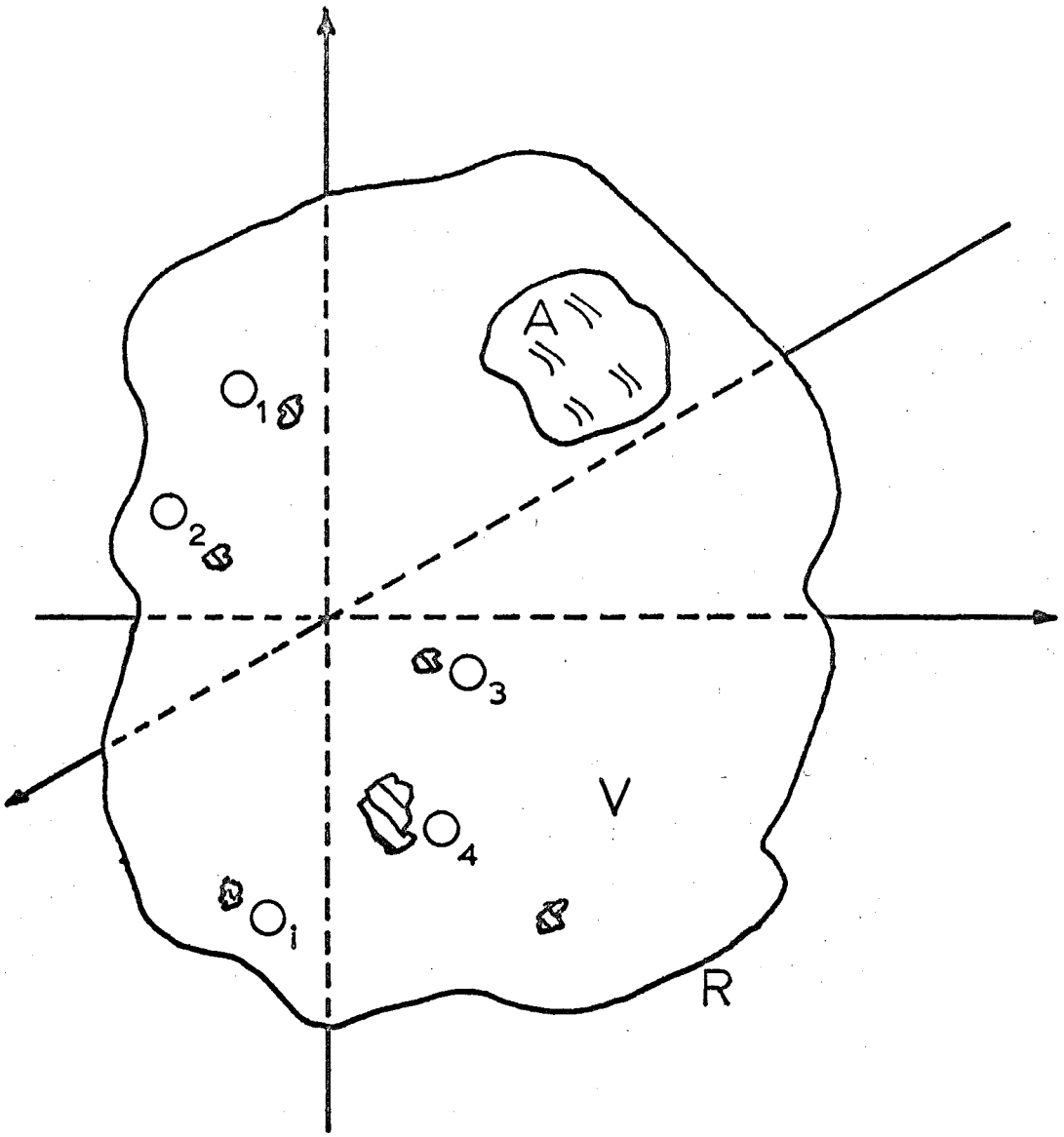

FIG. 1.1: Pertaining to definition of an imaging system

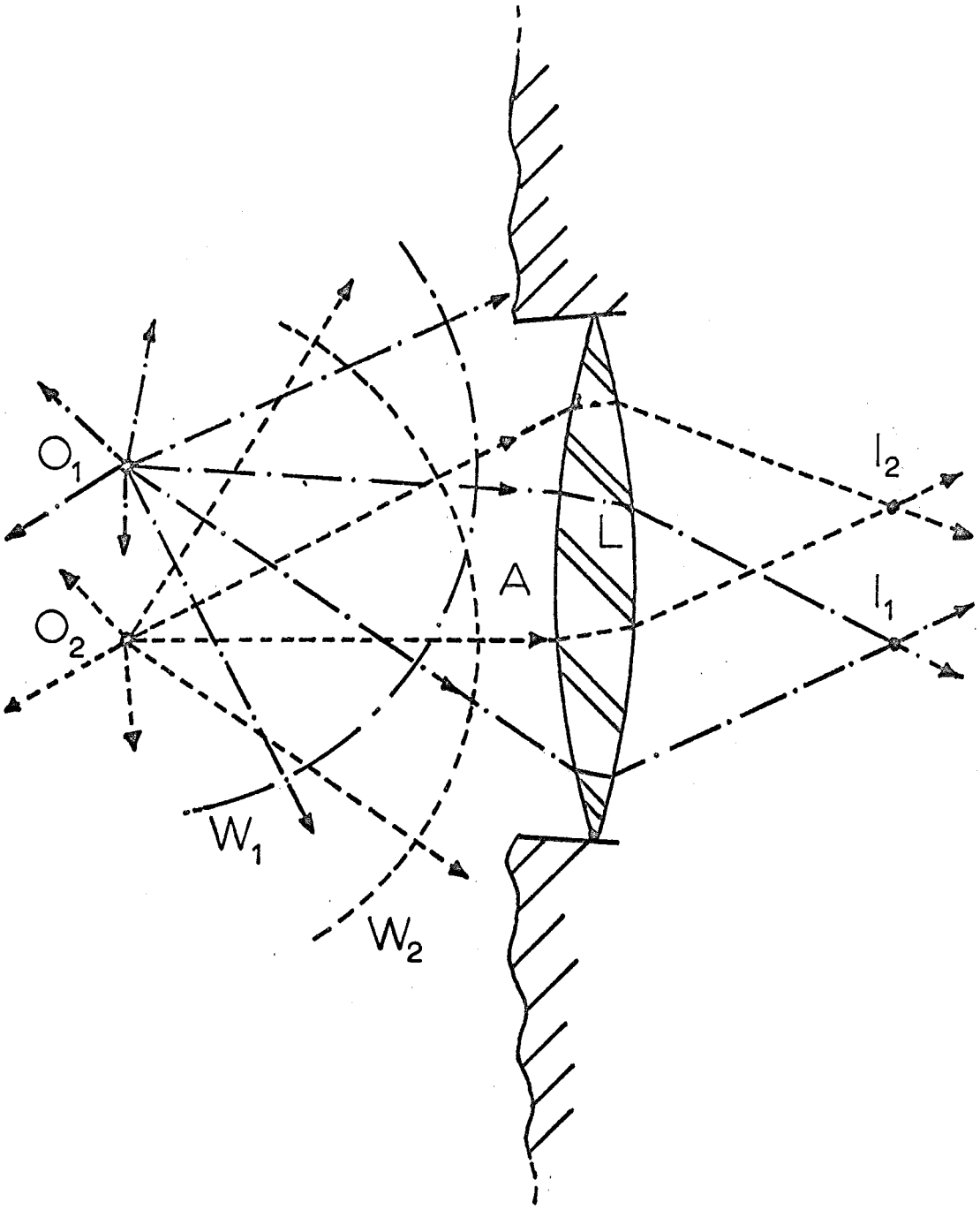

FIG.1.2: Simple optical imaging system

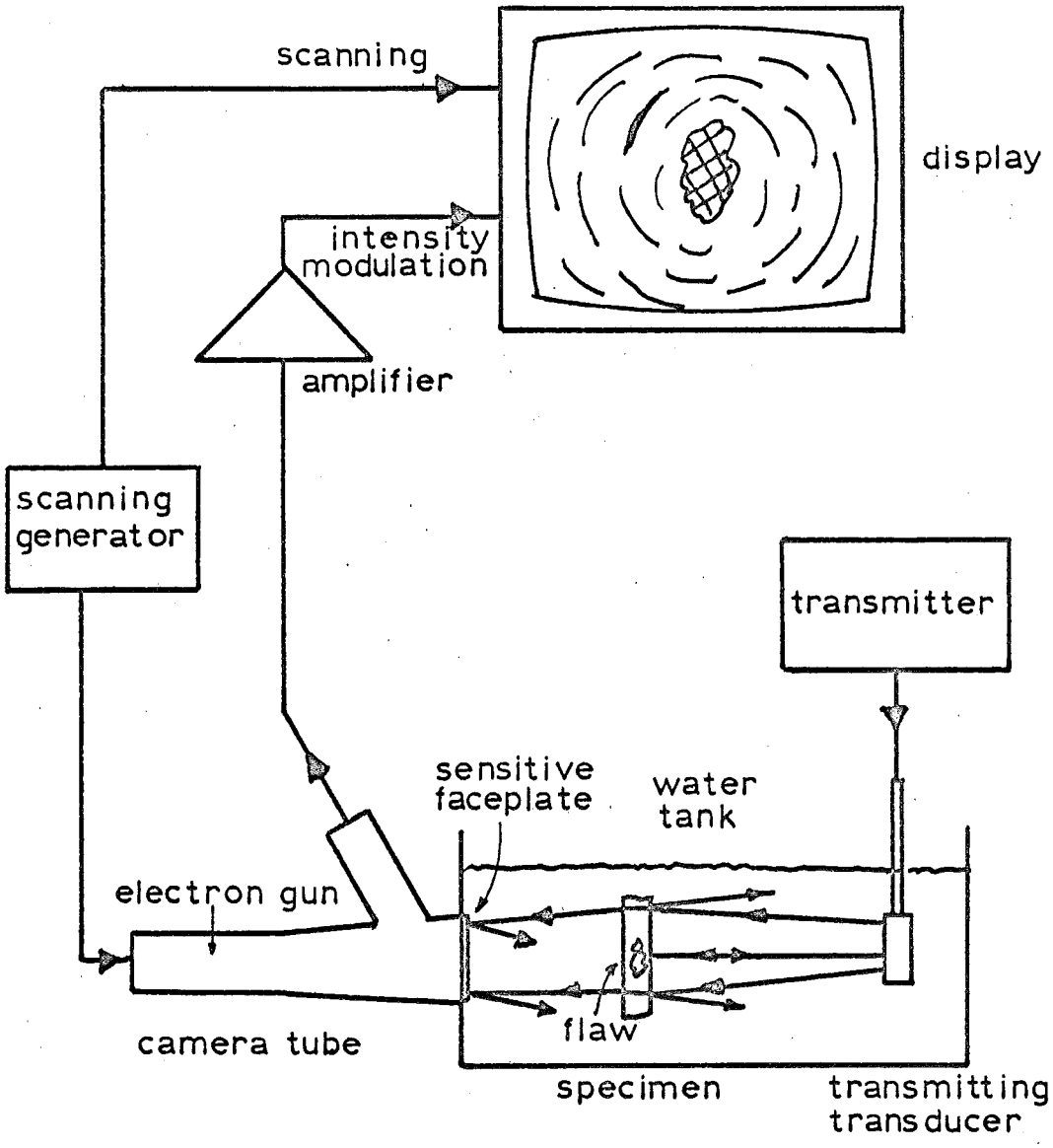

FIG. 1.3: Conventional ultrasonic imaging system

CHAPTER 2.

SOME OTHER VISUALIZATION SYSTEMS AND THEIR RELATION TO THE PRESENT PROJECT.

2.1. INTRODUCTION.

This chapter is a review of the principles and development of some sensing systems using both acoustic and electromagnetic radiation that have proved particularly helpful in considering the present system. The arrangement that has been referred to as the 'conventional' ultrasonic imaging system (1.2.3.) will not be further dealt with here. In Chapter 8 some aspects of the transducer behaviour are considered. The main concern in this chapter will be with synthetic aperture radar and particularly with acoustic holography.

Some discussion of the concepts of phased array radar (and sonar) appears in Chapter 7.

2.2. SYNTHETIC ARRAY RADAR.

In basic terms this is a system for forming high resolution images by correlation of the radar returns obtained through a small antenna carried by an aircraft[50] along a definite path. The geometry is illustrated in Figure 2.1. Pulses are transmitted at regular intervals along the aircraft track and the corresponding

echoes stored (as a video signal*). Commonly this appears on film as successive pictures of a modified 'A' scope display, as shown in the diagram. (The obvious military advantages of this surveillance technique restricts the open literature to rather general material but the precise details of recording etc., are not of great significance in the present discussion). An aircraft moving at (say) 1500km/hr and receiving from a maximum range of 20km will advance only 5.5cm during the signal travel and may be regarded as stationary. Carrier wavelengths of the order of 3cm are suggested in the literature with antenna sizes of 1-2m (i.e., >> aircraft advance) and total path lengths of the order of 1km.

With the sizes suggested the 'far field' zone of the physical antenna commences at less than 200 metres and the null to null beamwidth is about 5^0. (1m circular dish). The details are discussed more fully in succeeding chapters but here we note that a linear array which is to unambiguously image a far, or focussed near field target distribution spread over an angle of $\pm \sin^{-1}U$ to the array normal should be sampled at intervals not exceeding $\lambda/2U$. If $U=\frac{1}{2}$ this would imply sampling at every wavelength (i.e., every 3cm) if the physical antenna were isotropic. With directional array elements however the nulls of the element

---

* Note that the carrier as such does not convey any useful information about the targets. The data collected is contained in the coherently demodulated 'video' signal. (c.f., the method adopted by McCartney.[1]) A bipolar signal may be recorded as intensity variations photographically by the application of a suitable bias to the film.[2] In the ultrasonic system the actual radiated signal is 'lowpass' in nature and no carrier is used.

patterns may be used to suppress the multiple main lobes of the array pattern and if we allow the first of these 'grating lobes' to fall into the first null of the element pattern the successive samples may be taken at 0.5m intervals. Thus about 2000 samples each consisting of a record of say 50μS of the return can give a map of an area extending approximately 7500m normal to the aircraft track and if this region is at the 20km range taken above the $\pm$ 2.5° pattern of the physical antenna will permit imaging of distance about equal to 1.5 times the aircraft path.

The near field of a 1km aperture at 3cm would extend to 1700km and hence focussing is essential to make full use of the information available. If this is performed then the achievable resolution[3] is $\approx \frac{1}{2}$ (physical antenna size). This applies to the azimuth coordinate only. In elevation the resolution is that of the physical antenna only. Normally this is of no concern as the vertical dimensions of the targets are negligible compared with range but for a non-destructive testing system we require three dimensional images. Thus the very elegant optical processing techniques[4] applied to the formation of radar images are unfortunately inapplicable. While the processing operation involved in synthetic aperture radar may be viewed in a number of ways[5] the cross-correlation (or with some symbol manipulation, convolution) formulation is most relevant to the present case (Chapter 5). In McCord's[5] formulation the array output is viewed as the cross-correlation of the signal return with the antenna spatial weighting function. In Chapter 5 the formulation is

reversed but the concept is identical.

Recently, Kock[6,7] has observed that the set of recorded traces on film closely resembles a one dimensional zone plate and that regarded in this light one may consider the stored information as a hologram[8] of the viewed scene.

It is seen that the relevance of the synthetic aperture technique arises from:

1. A very large aperture is covered by interrogating the total backscattered field with a relatively non-directional transducer at a limited number of spatial positions only.

2. The received signal from each spatial sampling point is recorded for a period commencing after some delay defining the region to be imaged.

3. The size of the synthesised aperture is such that the samples of return from a given target cannot be considered as having come from a plane wavefront and the curvature must be allowed for in reconstructing the target field.

All of these features appear in the ultrasonic system. The differences appear in the extra spatial dimension required and the effective doubling of aperture size in the radar arrangement resulting from movement of the transmitter with the receiver. This latter effect has been exploited in some holographic experiments[9] but is not practical in any of the schemes considered for transducers in the present project.

2.3. ACOUSTIC HOLOGRAPHY.

2.3.1. Introductory.

As was mentioned in the previous chapter the first published account of non-optical holography seems to have appeared in 1965. In November 1966 Mueller and Sheridon[10] described an experiment closely following the inclined reference method of Leith and Upatnieks.[11] A photograph of the stationary ripple pattern formed on the surface of the liquid media containing the sound sources and object formed the holographic record. Reconstruction followed by illumination of this with a laser. The actual formation of a hologram (but without reconstruction) appears to have been achieved slightly earlier by Greguss.[32,52]. Other early work was initiated by Thurston.[38,39].

As is not uncommon with such 'discoveries' once made they cause older work to be examined from a new angle. This process frequently reveals that to some extent the wheel has been reinvented once more. Without seeking an extensive documentation of prior work it is sufficient to note the experiments of Kock and Harvey[12] performed concurrently with Gabor's original work.[13] Not only did Kock and Harvey succeed in visualizing microwave and acoustic fields but their method of so doing used the inclined reference concept not applied to the optical field until 1962.[11]

The general principles of holography will be presumed known as at least two books are available.[14,15]. Holography will be defined here as any process by which a field appearing at some region in space may be 'frozen' in a fashion allowing later

reproduction of the field not only in intensity as an ordinary photograph but also in relative phasing (or in the extended sense used here, timing) as well. The record or 'hologram' need not be the photographic plate of optical holography but may extend to other permanent recording media (e.g., the paper tape of the author's present apparatus) or exist in dynamic form, for example in a computer store.[16]

Preoccupation with reproducing existing optical results appeared to inhibit the initial exploitation of a feature of acoustic technology which is lacking in optical systems. This is the availability or rather perhaps the ubiquitousness of phase preserving sensors. While electrical provision of the reference waveform[17] soon followed the initial work it did not appear to be realized that separate preservation of the phase and amplitude (or quadrature components) of the field would permit complete elimination[18] of the multiple images characteristic of optical holography.

For the remainder of this chapter we will follow the development of acoustic holography up to the present, consider the trends which have emerged and discuss their relation to the present project.

2.3.2. Chronological development.

The system of Mueller and Sheridon operated in water with MHz waves (7 MHz). This feature reappeared in work by Preston and Kreuzer[17,19] where electrical simulation of a plane reference

wavefront impinging normally on the receiving aperture was applied. Recording was now achieved via a small piezoelectric transducer scanned over the water surface and carrying with it a small lamp excited in proportion to the acoustic signal. Optical reconstruction from a photograph of the lamp patterns suffered from the collinearity of images characteristic of noninclined reference waves but the paper shows a definite reconstruction of a hole within a metal block. Quality was good enough to exhibit the 'speckly' character of coherent imaging.[20]

During 1967 a number of papers appeared describing work at low frequencies[21,22,23,24] using conventional microphones. Reference 22 contains the first attempt at a definitive treatment of the subject but the actual apparatus was very crude even by the existing standards of the high frequency experiments. (Massey[51] discusses some of the practical problems in forming these holograms).

Some further work on radio wave holography was reported[25] and provoked a discussion of image distortion inherent in all attempts at reconstructing a field with radiation of a wavelength differing greatly from that of the original illumination.[26]

Some developments in recording technique were reported[27] but suffered from rather low sensitivity compared with the other methods. Near the end of 1967 a Symposium* was held devoted to

---

* The proceedings[28] of which have suffered a very long publishing delay and became available only this year (1969).

this topic.

By early 1968 the desire for faster hologram formation resulted in the application of the Sokoloff tube to sampling the acoustic field first with an acoustically supplied reference wave[29] and later an electronically simulated one.[30] This latter development represented some exploitation of the ease of manipulating electrical signals at the frequencies (in the case reported 7 MHz.) used. The effect of an inclined reference corresponds to a continuous phase progression along the aperture at a rate determined by the angle of incidence of the reference. Now in an ultrasonic camera tube the electron beam is scanning vertically over the aperture at a rate say v_s. Thus if the received signal is added to one offset in frequency by an amount $\Delta\omega$ the progressive 'slipping' in phase over the frame scan time simulates a physical reference at an angle to the aperture normal given by;

$$\theta_R = \sin^{-1} \frac{\Delta\omega}{k\, v_s} \qquad (2.1)$$

k being the wave number $= 2\pi/\lambda$, (λ = wavelength) in the medium. Thus for example if $\theta_R = 45^\circ$ and $v_s = 2.5$m/S (50mm aperture in 20mS) then with $k = 3 \times 10^4 m^{-1}$ (7 MHz in water), $\Delta\omega$ must be 53 kHz.

A paper by Halstead[31] covered in detail the holographic process considering,

(a) general theory,

(b) geometrical relations between object and image,

(c) intrinsic aberrations,

(d) limits of resolution, and

(e) performance of a wide variety of potential transducers.

Continuing their work on low frequency apparatus, Metherell et.al. reported on a method whereby the sound source rather than the receiver is scanned.[33] This represents an application of the reciprocity theorem to holography. A further paper[34] by the same authors discusses a rather ingenious modification of the method of reference 30. Instead of mixing an offset signal with the received wave the (in this case horizontal) scanning speed was adjusted to some suitable multiple of the incoming wave velocity. Taking an individual plane wave of incident radiation normally incident, the scan takes successively delayed samples of the wavefront, that is phase shifted values with the phase shift increasing linearly along the scan. The effect is exactly that of adding a physical inclined reference wave.

Near the end of 1968 a number of papers[35,36,37] appeared indicating the beginning of adaption of the method to practical inspection situations, and describing efforts towards the development of industrially practicable devices.

The present year (1969) has so far witnessed a consolidation and refinement in established techniques[40] and the publication of details of a method using a scanned laser beam[41] to detect the minute (3.4.3.) deflections of the surface of a solid material in which ultrasonic waves are propagating. This latter technique appears to be a by-product of a laser television display system.[42]

Two other systems using mechanical scanning of a laser beam have been described.[43,44] In the form presently published the system of Massey[44] does not give a full two-dimensional recording but the extension of his method is obvious.

Some interest has been displayed in the performance achievable when the information gathered from the recording aperture is deliberately restricted. The paper of Metherell et.al.[22] indicates the necessary constraints on the scanning transducer (or area on a large plate interrogated as a 'point') size. Failure to fulfil this condition results in constructions contaminated by ambiguous images. An example provided by Carter[45] illustrates the condition. Although it does not appear to have been reported elsewhere in the acoustic imaging context, consolidation of the spatial information is possible and the achievement of this has been essential to the present project (1.3.).

Compression of the 'temporal' data is easily achieved and techniques using binary amplitude quantization (i.e., 'black and white' only in the hologram)[46] and phase only[47] recording have been discussed. Coldrick and Holt[48] have recently presented details of a complete apparatus for the phase only method.

2.3.3. Discussion.

Taking the number of papers on acoustic holography presented at the annual I.E.E.E. Sonics and Ultrasonics Symposium as a rough measure of innovation we may note that from zero in 1966 the number of papers grew to five in both 1967 and 1968 with special sessions

devoted to the topic. However the 1969 programme contains only two papers specifically on acoustic holography. Of some significance is the fact that these have been classified under 'Industrial Testing and Processing'. It would in fact seem that the initial novelty has diminished considerably. It is this author's belief that this is due to the present systems (at least those operating at high frequencies) having reached a limit in their performance which cannot be exceeded without progression to very much higher frequencies to improve resolution, or, where losses in practical materials make this impossible, maximum exploitation of the frequency band that is available. Full use of wideband information seems to demand the use of computer image construction.[46,47]. This conclusion immediately involves data collection and reduction facilities of much greater complexity than those currently reported. Although the initial studies and design of the system described here did not make specific reference to holographic concepts, nevertheless the arrangement in its current form does represent some start towards a wideband imaging device.

REFERENCES FOR CHAPTER 2.

1. McCartney, B.S. 'Theoretical and experimental properties of two element multiplicative, multifrequency receiving arrays including superdirectivity'. Radio Electron. Eng. 28, pp.129-143, Aug. 1964.

2. Leith, E.N. et.al. 'Coherent optical systems for data processing, spatial filtering, and wavefront reconstruction'. Chapter 8, pp.143-158 in 'Optical and electro optical information processing', (Ed. Tippett, J.T. et.al.) M.I.T. Press, Cambridge, Mass. 1965.

3. Cutrona, L.J. and Hall, G.O. 'A comparison of techniques for achieving fine azimuth resolution'. I.R.E. Trans. MIL-6, pp.119-121, April 1962.

4. Cutrona, L.J. et.al. 'On the application of coherent optical processing techniques to synthetic aperture radar'. Proc. IEEE 54, pp.1026-1032, Aug. 1966.

5. McCord, H.L. 'The equivalence among three approaches to deriving synthetic array patterns and analysing processing techniques'. I.R.E. Trans. MIL-6, pp.116-118, April 1962.

6. Kock, W.E. 'Side looking radar, holography and doppler free coherent radar'. Proc. IEEE (Letters) 56, pp.238-239, Feb. 1968.

7. Kock, W.E. 'Stationary coherent (Hologram) radar and sonar'. Proc. IEEE (Letters) 56, pp.2180-2181, Dec. 1968.

8. Rodgers, G. 'Gabor Diffraction microscopy: The hologram as a generalized zone plate'. Nature 166, p.237, 1950.

9. Hildebrand, B.P. and Haines, K.A. 'Simultaneous object illumination scanning and detector scanning in holography'. Phy. Lett. 27A, p.376, 12 Aug. 1968.

10. Mueller, R.K. and Sheridon, N.K. 'Sound holograms and optical reconstruction'. App. Phys. Lett. 9, pp.319-320, 1 Nov. 1966.

11. Leith, E.N. and Upatnieks, J. 'Wavefront reconstruction with continuous-tone objects'. J.Opt.Soc.Am. 53, p.1377, 1963.

12. Kock, W.E. and Harvey, F.J. 'A photographic method for displaying sound waves and microwave space patterns'. Bell Sys. Tech. J. 30, pp.564-587, July 1951.

13. Gabor, D. 'Microscopy by reconstructed wavefronts'. Proc. Roy. Soc. 197A, pp.454-487, 1949.

14. Stroke, F.W. 'An introduction to coherent optics and holography'. Academic Press, New York and London, 1966.

15. DeVelis, J.B. and Reynolds, G.O. 'Theory and applications of holography'. Addison-Wesley, Reading, Mass. 1967.

16. Lesem, L.B. et.al. 'Computer synthesis of holograms for 3-D display'. Comm. A.C.M. 11, pp.661-674, Oct. 1968.

17. Preston, K. and Kreuzer, J.L. 'Ultrasonic imaging using a synthetic holographic technique'. App. Phys. Lett. 10, pp.150-152, 1 Mar. 1967.

18. Skattebol, L.V. 'Acoustic holograms'. Elect. Lett. 4, pp.583-584, Dec. 1968.

19. Kruezer, J.L. 'Ultrasonic three-dimensional imaging using holographic techniques'. Paper presented at the Symposium on Modern Optics, Polytechnic Institute of Brooklyn, Mar. 22-24, 1967.

20. Oliver, B.M. 'Sparkling spots in random diffraction'. Proc. IEEE (Letters) 51, p.220, 1963.

21. Metherell, A.F. and El-Sum, H.M.A. 'Simulated reference in a coarsely sampled acoustic hologram'. App. Phys. Lett. 11, pp.20-22, 1 July 1967.

22. Metherell, A.F. et.al. 'Introduction to acoustic holography'. J. Acoust. Soc. Am. 42, pp.733-742, Oct. 1967.

23. Aoki, Y. et.al. 'Sound wave holograms and optical reconstruction'. Proc. IEEE (Letters) 55, pp.1622-3, Sept. 1967.

24. Massey, G.A. 'Acoustic holography in air with an electronic reference'. Proc. IEEE (Letters) 55, pp.1115-1117, June 1967.

25. Deschamps, G.A. 'Some remarks on radio frequency holography'. Proc. IEEE (Letters) 55, pp.570-571, April 1967.

26. Maginness, M.G. 'Comment on non-optical holography'. Proc. IEEE (Letters) 55, pp.2050-2051, Nov. 1967.

27. Young, J. and Wolfe, J.E. 'A new recording technique for acoustic holography'. App. Phys. Lett. 11, pp.294-296, 1 Nov. 1967.

28. Metherell, A.F. et.al. (Eds). 'Acoustic Holography'. (Proceedings of the first international symposium). Plenum Press, New York, 1969.

29. Marom, E. et.al. 'Ultrasonic holography by electronic scanning of a piezoelectric crystal'. App. Phys. Lett. 12, pp.26-28, 15 Jan. 1968.

30. Mueller, R.K. et.al. 'Electronic simulation of a variable inclination reference for acoustic holography via the ultrasonic camera'. App. Phys. Lett. 12, pp.394-395, June 1968.

31. Halstead, J. 'Ultrasonic holography'. Ultrasonics, 6, pp.79-87, April 1968.

32. Greguss, P.J. 'Pictures by sound'. Perspective 14, pp.287-302, 1966.

33. Metherell, A.F. and Spinak, S. 'Acoustical holography of non-existent wavefronts detected at a single point in space'. App. Phys. Lett. 13, pp.22-24, 1 July 1968.

34. Metherell, A.F. 'Temporal reference holography'. App. Phys. Lett. 13, pp.340-343, 15 Nov. 1968.

35. Kreuzer, J.L. 'Ultrasonic holography for nondestructive testing'. Materials Evaluation 26, pp.197-202, Oct. 1968.

36. Holt, D. and Watrasiewicz, B.M. 'Optimum receiver arrays for acoustic holography'. British Aircraft Corp. Bristol, U.K., Ref. K03/30/ELO/413, 28 Oct. 1968.

37. Worlton, D.C. 'Recent nondestructive testing advances at Battelle Northwest Laboratory'. Batelle Memorial Inst., Pacific Northwest Lab., Report BNWL-SA-1772, 1968.

38. Thurston, F.L. 'Ultrasound holography and visual reconstruction'. Proc. Symp. Biomed. Eng., Milwaukee, Wis. 1, pp.12-15, 1966.

39. Thurston, F.L. 'Ultrasound holograms for the visualization of sonic fields'.
Proc. Ann. Conf. Eng. Med. Biol. 8, p.222, 1966.

40. Smith, R.B. and Brenden, B.B. 'Refinements and variations in liquid surface and scanned ultrasound holography'.
Ultrasonics 7, pp.125-126, April 1969.

41. Korpel, A. and Desmares, P. 'Rapid sampling of acoustic holograms by laser scanning techniques'.
J. Acoust. Soc. Am. 45, pp.881-884, April 1969.

42. Korpel, A. et.al. 'A television display using acoustic deflection and modulation of coherent light'.
Proc. IEEE 54, pp.1429-1437, Oct. 1966.

43. Gabor, D. French Patent, 1 479 712, 28 March 1967.

44. Massey, G. 'An optical heterodyne ultrasonic image converter'.
Proc. IEEE 56, pp.2157-2161, Dec. 1968.

45. Carter, W.H. 'Aliasing in sampled holograms'.
Proc. IEEE (Letters) 56, pp.96-98, Jan. 1968.

46. Schroeder, M.R. 'Computers in Acoustics'.
Paper GP-6-1, 6th I.C.A. Tokyo, Aug. 21-28, 1968.

47. Metherell, A.F. 'The relative importance of phase and amplitude in acoustic holography'. See Ref. 28.

48. Coldrick, J.R. and Holt, D. 'Phase-only acoustic holography'.
Elect. Lett. 5, pp.169-170, April 1969.

49. Maginness, M.G. and Kay, L. 'Signal processing for acoustic imaging systems'.
Paper K-5-3, 6th I.C.A. Tokyo, Aug. 21-28, 1968.

50. Cutrona, L.J. et.al. 'A high resolution radar combat-surveillance system'.
I.R.E. Trans. MIL-5, pp.127-131, April 1961.

51. Massey, G. 'Acoustic imaging by holography'.
IEEE Trans. SU-15, pp.141-146, July 1968.

52. Greguss, P. 'Techniques and Information Content of Sonoholograms'.
J. Photo. Sci. 14, pp.329-332, 1966.

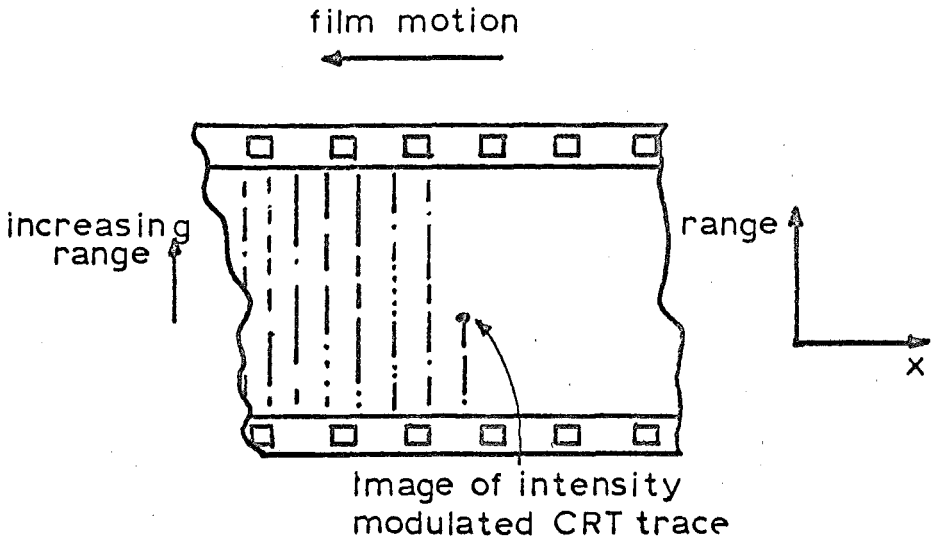

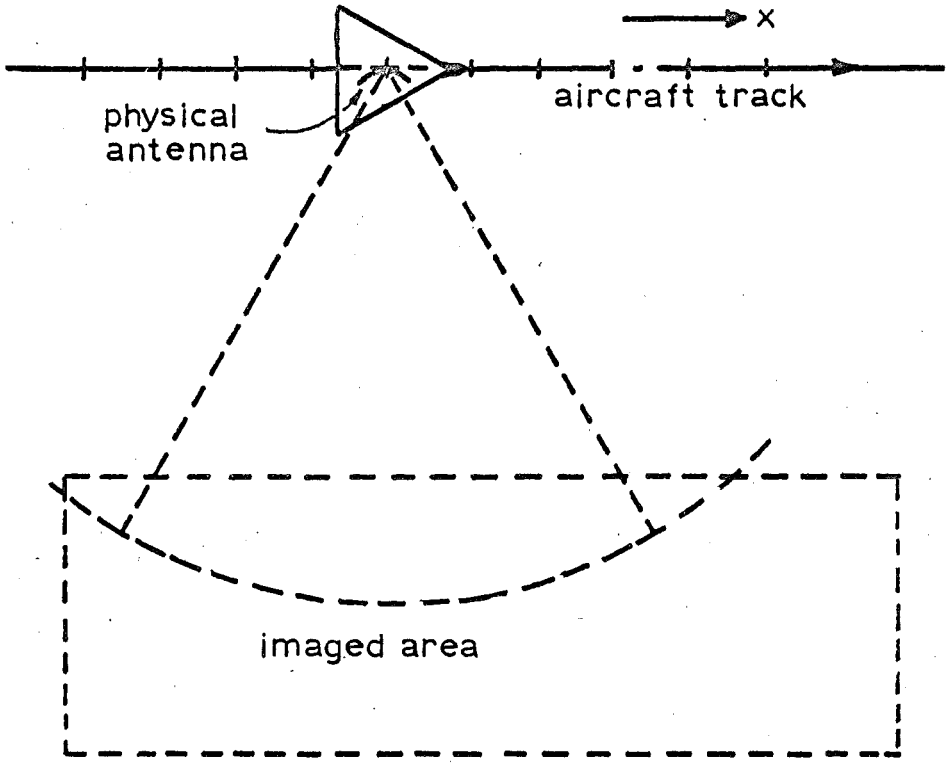

FIG. 2.1: Synthetic aperture radar

CHAPTER 3.

THE SIGNAL PATH IN AN IMAGING SYSTEM

3.1. INTRODUCTION.

This and the succeeding chapters of this section contain an analysis and develop a model of the imaging system. The present chapter considers a typical signal path through the system from the electrical transmitter to the acoustic input of a particular section of the receiving transducer. Chapter 4 discusses the receiving transducer behaviour and Chapters 5 and 6 the combination of these signals to produce an image. In Chapter 7 we consider the effect of errors and noise to complete an overall view of the complete system and arrive at a specification of the potential performance.

This division is somewhat arbitrary as, for example, the spatial imaging characteristics are a function of transducer spatial and temporal responses. However preliminary individual examination of these provides a 'fill' of important blocks in the overall system model although we must make implicit assumptions based on concepts and constraints that will not be developed until later.

3.2. SIGNAL PATH DEFINITION.

In the remainder of this chapter we will be considering the behaviour of part of the arrangement depicted in Figure 3.1.

TX is the electrical transmitter, characterised by an open circuit waveform $w_0(t)$ and internal impedance Z_{TX} as seen from the terminals of the transmitting transducer B. This latter element has an electrical to mechanical impulse response that will be denoted by b(t) and a resultant acoustic field described in the coordinates θ_B, ϕ_B and R_B as depicted in Figure 3.2. The acoustic wavefront produced by B has a form $w_2(t)$ at the transducer surface and the electrical waveform from TX when loaded by the transducer the time variation $w_1(t)$. The acoustic field in V will be scattered by discontinuities such as O and some portion of the incident energy deflected towards the receiving aperture A. In general the scatterer will display a frequency selective response and hence we denote the form of the scattered wavefront distinctly from that incident as $w_4(t)$. This incident wavefront will be a function of the coordinates of O for finitely sized transducers and is shown as $w_3(t)$.

Here we anticipate the next chapter by taking the transducer occupying A as a number of distinct small elements A_1, A_2,--A_i--. For present purposes we consider the response of one of these. (Chapter 4). This element will be subjected to an acoustic field which as will be shown in Chapter 5 may be considered as the superposition of plane wavefronts with some parameter dependence on the angle of arrival denoted by coordinates θ_A, ϕ_A, similar to those defined for the transmitter.

The receiving element will respond with a waveform $w_5(t)$

dependent on the acoustic spatio-temporal signal distribution and the electrical impedance connected to its terminals. This waveform may be further modified by passage through the device (TR) used to scan over the A_i's to that shown as $w_6(t)$. The receiver mechanical to electrical impulse response is taken as a(t) for a normally incident impulsive plane wavefront.

At this point we note the physical assumptions that will be inherent in the analysis;

(1) The transducers will be assumed to be slabs of piezoelectric material firmly bonded to the surface R. One may conceive transducer arrangements (particularly for the receiver) where the transducer material is distributed (say) in a spherical or cylindrical fashion but this would require special contouring of the specimen surface whereas a smooth flat surface is much more practicable.

(2) The signal levels will be assumed small enough that linear superposition of signals can be taken. At the levels adequate for materials inspection this assumption is well justified but high powered transmissions may violate it.[1]

(3) We will concentrate on the direct return from an object considering the dimensions of V to be sufficient that wall echoes and similar artefacts do not interfere with the signal. This is justified by the fact that (as mentioned in Chapter 1) we anticipate the use of quite short pulses from the transmitter and also the time gating of the return signal at A.

Essentially then V is taken as an infinite half space with A and B mounted on its accessible side.

(4) The propagation medium and transducer materials will be assumed lossless over the frequency range of the signals applied. This assumption will be examined more fully when considering the potential resolution and range of application of the system in the next chapters. (See especially Chapter 7).

Further assumptions and constraints of a more specific nature will be applied to various elements of the complete signal path. These will be considered as they arise.

3.3. THE TRANSMITTING TRANSDUCER.

Throughout the development of this project only longitudinal waves have been considered as the sensing radiation for the system. This is to a large extent the result of the growth out of earlier imaging schemes operating in fluid media where this is the only mode of propagation possible. The use of shear wave propagation in solids would have the advantage of shorter wavelengths for a given frequency and hence greater potential resolution. However, against this must be set the necessity (rather than possible advantage) of using solid coupling to the material under examination, variations of object reflectivity with polarization, and the much higher attenuation of shear waves in technical poly-crystalline materials. (The ratio of shear to

longitudinal wave attenuation is typically 20:1 or greater in units of db/unit distance).[2] A further not inconsiderable factor is the ready availability of a wide range of longitudinal wave transducers in the lead-zirconium-titanate (PZT) ceramics whereas shear polarized and electroded units are non-standard.

From these considerations we now proceed to consider the behaviour of the arrangement of Figure 3.3. B is the transducer operating in the thickness expander mode, (i.e., the dimension 'd' varies under the applied electric field). The 'rear' face of B is covered in a perfectly conducting electrode of negligible thickness and the 'front' face is bonded by a uniform material to the bulk of V. This latter is assumed electrically conductive to complete the electrical circuit.* The physical dimensions are such that the lengths of any conducting paths are very small relative to the free space wavelength of electromagnetic radiation at the frequencies involved. The effect of electrical cables is absorbed in $Z_{TX}(\omega)$.

From the earlier assumption of linearity and homogenity for the material of V its acoustic properties may be represented by two constants λ and μ usually referred to as the Lamé constants[3] and the density ρ_o. These lead to the definition of a parameter,

---

* Or is attached by a non-conducting layer sufficiently thin that the capacitance across the bonding layer is much greater than the capacitance of the transducer.

the specific acoustic impedance Z_o, giving the ratio between stress and particle velocity for plane wave propagation ($Z_{o,l} = \rho_o c_l$ where c_l is the propagation velocity = $\left[\frac{\lambda+2\mu}{\rho_o}\right]^{\frac{1}{2}}$ for longitudinal waves).

The equivalent circuit of transducers has been the subject of studies by several authors[4,5,6,7] and no point would be served by repeating the derivation here. We follow the notation and method developed by Mason[8] and defined by the IRE Standards.[9-12] An excellent recent treatment appears in Reference 13. Figure 3.4 shows the equivalent circuit for the transducer.* It is important to examine the validity of the assumptions made in deriving this circuit. These may be summarised as;

(1) The transducer lateral dimensions are very great compared with the thickness (i.e., $\sqrt{A} >> d$) with all points in any plane parallel to the large faces moving in phase. Transducers with small lateral dimensions will commonly exhibit very complex behaviour when excited under mechanically 'free' conditions[14] but these modes are heavily suppressed under loaded conditions. The resultant condition of lateral restraint

---

* This circuit is essentially that of Figure 26, p.239, reference 13 with some symbols changed to suit the present notation. It should be noted that the diagram in the reference is wrongly labelled. The parameter 'l' in the arguments of the sin and tan functions should be 't'. Here we have reserved this symbol for time and use instead 'd'. This should not be confused with the piezoelectric constants 'd_{ij}' which are here used only with the subscripts present.

enables the behaviour to be accurately represented by a one dimensional model.

(2) The material is assumed perfectly insulating with constant electric flux (D_3) in the thickness direction and no transverse field.

The 3,3 indices used relate specifically to piezoelectric ceramics but the model is good for X-cut quartz with these replaced by the 1,1 indices.

Under conditions where the transducer has one face free (i.e., in vacuum or to a good approximation, air) a short circuit is applied to one mechanical terminal pair and the circuit transforms to that of Figure 3.5. One may conceive of a situation where a backing material is applied but this will generally be unnecessary when the transducer is bonded to a mass of metal.

At the remaining terminals an impedance characteristic of the properties of V will appear. In the case where A is large this will simply be $Z_{o,1}$, corresponding to the production of an infinite plane wavefront. Finitely sized transducers will see an impedance which becomes predominantly reactive as the area decreases[15] even under the assumption of pure piston behaviour. For generality then the loading will be represented as (possibly) complex impedance $Z_m(\omega)$.

Letting $d/v_t^D = \alpha$ and proceeding by normal electrical circuit theory* we may reduce the entire transducer plus electrical

---

* Appendix 3.1.

transmitter to a Thevinin equivalent as shown in Figure 3.6. This is per unit area (1 m^2). The actual impedance of TX must be replaced by an equivalent per unit area of transducer. Similarly a normalized expression for the electrical current flowing into the transducer may be derived. (Note that it is <u>not</u> the 'current' in Z_T which is a 'mixed' impedance containing an electromechanical conversion factor).

This system has been programmed for computer solution and the complete results are treated elsewhere.* Here we will note the general behaviour.

(1) The transducer electromechanical transfer function has a basic 'high pass' characteristic. High mechanical output is provoked by rapid (i.e., comparable with the propagation time α of mechanical waves) transitions in the driving waveform $w_o(t)$.

(2) The acoustic response to such a sharp wavefront is concentrated into a pulse of about one cycle of a sinusoid with period equal to twice the mechanical transit time of the transducer plate, (i.e., 2α). Under conditions of strong coupling to typical metals the 'tail' of the pulse decays very fast. See Figure 3.7(a).

(3) The spectrum of the response is concentrated in broad humps around the frequencies corresponding to the

---

* Appendix 3.1.

plate thickness resonances. These occur approximately at the values $\frac{n}{2\alpha}$ Hz (n=1,3,5,----). The PZT ceramics have high coupling factors and the resonances are not in exact harmonic relation.[16]

(4) The obtainable rise times of practical electrical circuits driving these transducers is such that very little excitation will be applied at the 'harmonics' and we may approximate the spectrum of $w_2(t)$ to just the first hump. The general form is shown in Figure 3.7(b). As will be seen in Chapter 6 no radiation should be emitted above a frequency set by the temporal and spatial sampling characteristics of the receiver and a spectrum such as that shown represents reasonable utilization of the available region.

3.4. THE TRANSMITTER SPATIAL FIELD.

3.4.1. Basic response.

This problem has been investigated under conditions relevant to the present case by Miller and Pursey[15] as a theoretical study and by Filipczynski[17,18] and White[19] experimentally. Miller and Pursey derive the field components of a small piston source of radius a applying unit amplitude (sinusoidally varying at angular frequency ω) normal stress to the free surface of the medium as; (see Figure 3.8)

$$u_{R_B} = - \frac{a^2}{2\mu} \frac{e^{-jk_l R_B}}{R_B} \cdot \frac{\cos\theta_B (\nu^2(1-2\nu^2\sin\theta_B))}{(1-2\nu^2\sin^2\theta)^2 + 4\nu^3\sin^2\theta_B\cos\theta_B(1-\nu^2\sin^2\theta_B)} \quad .. \quad 3.1$$

$$u_{\theta_B} = - \frac{a^2}{2\mu} \frac{e^{-jk_s R_B}}{R_B} \cdot \frac{j \sin 2\theta_B (\sin^2\theta_B - \nu^2)^{\frac{1}{2}}}{\cos^2 2\theta_B - 4j\sin^2\theta_B \cdot \cos\theta_B (\sin^2\theta_B - \nu^2)^{\frac{1}{2}}} \quad .. \quad 3.2$$

u_{R_B} and u_{θ_B} being the radial and tangential field components,

$j = \sqrt{-1}$,

k_l and k_s are the propagation constants for longitudinal and shear waves respectively;

$$k_l = \frac{\omega}{c_l} \quad .. \quad 3.3$$

$$k_s = \frac{\omega}{c_s} \quad .. \quad 3.4$$

ω being the angular frequency, $2\pi f$, in rad./sec.

ν is the ratio c_s/c_l which is typically equal to $\frac{1}{2}$,

and we have rewitten the original equations 116 and 117 in the present notation. The $e^{j\omega t}$ factor is suppressed.

Examination of these equations shows two main factors;

(1) a term $\frac{e^{jk_\varepsilon R_B}}{R_B}$ characteristic of a spherically spreading wavefront, propagating at the velocity $\omega/k_\varepsilon = c_\varepsilon$ (ε=l or s);

(2) a term depending on θ_B describing the variation in signal strength as a function of the angle from the

normal to the transducer. In the longitudinal wave case this factor is purely real for all θ_B but that for u_{θ_B} becomes complex for $\theta_B > 30^o$ (and $\nu = \frac{1}{2}$). This term is similar to that arising in electromagnetic antenna theory and is frequently referred to as the 'obliquity factor'.[20] An examination of the factor for u_{R_B} will show that it may be approximated very closely simply by $\frac{1}{4}\cos\theta_B$.

3.4.2. Practical sources.

The above equations give the field at each frequency in the mechanical driving waveform $w_2(t)$ under the conditions of 'a' much smaller than the wavelength at this frequency and $R_B >> a$ or the wavelength. The practical sources used typically have dimensions of the order of 1 to 20 wavelengths at the highest radiated frequency. Hence we must now examine the extent of the spatial region over which 3.1 and 3.2 are an adequate representation of the field and the additional factor required to describe the effect of finitely sized sources.

This latter modification may be accounted for quite simply by invoking the 'directivity product theorem'.[21] We write the total field due to a source which may be visualized as a combination of many elemental radiators as;

$$u(\theta) = K(\theta).D(\theta) \qquad .. \quad 3.5$$

where $D(\theta)$ is the elemental pattern described above and $K(\theta)$ the

pattern of a spatially congruent array of isotropically radiating elements. This factor depends on the overall transducer shape. Two common examples are the rectangular array of sides 2a and 2b giving;

$$K_\varepsilon(\theta_B) = \frac{\sin(k_\varepsilon a \sin\theta_B)}{k_\varepsilon a \sin\theta_B} \cdot \frac{\sin(k_\varepsilon b \sin\theta_B)}{k_\varepsilon b \sin\theta_B} \quad .. \quad 3.6$$

and a circular array of radius a with;

$$K_\varepsilon(\theta_B) = \frac{2J_1(k_\varepsilon a \sin\theta_B)}{k_\varepsilon a \sin\theta_B} \quad .. \quad 3.7$$

(ε = 1 or s as appropriate)

(See e.g., Reference 22, p.166.

It now remains to consider the limit of validity of these expressions. The main concern is with the u_{R_B} component representing the longitudinal wave radiation. The criterion normally applied is derived by a calculation of the point on the normal to the transducer surface where destructive interference between elements of the radiator just ceases. In the present case we observe that for the longitudinal component this will occur at a distance;

$$z_B = k_1 a^2/\pi \quad .. \quad 3.8$$

for a radiator of radius a.

This distance is twice the commonly quoted 'a^2/λ'. The larger value has been taken to give validity to the formulae for off axis conditions.[23]

Thus for the circular piston source;

$$u_{R_B} = -\frac{a^2}{8\mu}\,\frac{e^{j(\omega t - k_1 R_B)}}{R_B}\cdot\cos\theta_B\cdot\frac{2J_1(k_1 a\sin\theta_B)}{k_1 a\sin\theta_B} \qquad .. \quad 3.9$$

$$\text{for}\quad R_B > \frac{k_1 a^2}{\pi}$$

and generalising over the spectrum of $w_2(t)$:

$$u_{R_B}(\omega) = -\frac{a^2}{8\mu}\cdot\frac{e^{j(\omega t - k_1(\omega)R_B)}}{R_B}\cdot\cos\theta_B\cdot$$

$$\cdot\frac{2J_1(k_1(\omega)a\sin\theta_B}{k_1(\omega)a\sin\theta_B}\cdot W_2(\omega) \qquad .. \quad 3.10$$

For $R_B > \dfrac{k_1(\omega_{max})a^2}{\pi} = R_{min}$

where the ω dependence of k_1 has been made explicit.
$W_2(\omega)$ is the Fourier transform of $w_2(t)$.

3.4.3. Numerical calculations.

A typical transducer size of 5mm diameter radiating into aluminium with c_1 = 6300 m/Sec and $\omega_{max} = 2\pi.10^7$ gives R_{min} as 8cm.

This is in fact a typical transmitter to object distance in real situations and hence taking the far field approximation is justified, particularly if the object is near the z_B axis. It will also be recalled that the energy in the pulse is largely concentrated at about half the maximum frequency and partial cancellation of the higher components will have only a minor effect.

For the unit applied stress the peak amplitude of particle displacement on the z_B axis is given by;

$$u_{R_B,\theta=0} = a^2./8\mu R_B \qquad .. \quad 3.11$$

which for the case above gives a value of 0.41×10^{-15}m at 5 MHz and R_B = 8cm. The displacement at transducer excitations of 30 volts (peak) giving a stress of 2.4×10^5 N/m^2 will thus be approximately 1×10^{-10}m or 1Å. This may seem extremely small but is typical for propagation in solids.[24] It may be noted that this value of stress is only about 1/1000th. of the static elastic limit of aluminium.

Experimental measurements made by Filipczynski and White confirm the high accuracy of these equations over the range of interest in the present project. Some measurements taken here when it became obvious that transmitter location and energy distribution were critical in obtaining good imaging provided further confirmation. The first null in the pattern of the 5 MHz component for the 5mm transducer occurs at an angle of $\theta_B = 18.2^\circ$ corresponding to a circle of diameter 5.3cm at 8cm depth. Consideration of the receiving transducer behaviour will show that satisfactory imaging is possible over a much wider cone than this and hence for a transmitter located at (say) the centre of the receiving array or hard up against one edge of it much smaller dimensions are necessary if the image is not to be confused by 'blind spots' or sudden changes in reflected signals due to phase reversals of some spectral components in the minor

* Appendix 3.1.

lobe regions. An advantage of wideband signals becomes apparent in that the overall energy distribution in the transmitter field will be free from sharp nulls if the spectrum occupies at least an octave but this does not prevent anomalies due to selective scattering by the objects. The transmitter should ideally be small enough that the region under inspection is entirely contained within the first null circle at the highest frequency. Allowing imaging out to $\theta_B = \pm 45^\circ$ and $\omega_{max} = 2\pi \times 10^7$ rad/Sec. the transducer radius works out at 0.55mm, a small but quite practicable value. With this radius, R_{min} becomes less than 1mm on the z_B axis.

3.5. REFLECTION OFF SCATTERERS.

3.5.1. Introduction.

In concept the problem of elastic wave scattering presents little difficulty. However to an even greater extent than in the field where the greatest effort is concentrated on the scattering problem-radar[25]-actual solutions of practical cases present extremely laborious tasks. The complication arises from the necessity for a complete solution to take account of the mode conversion phenomena. Longitudinal or shear waves normally incident on a reflecting surface will reradiate in the same mode producing a simple scalar or vector problem respectively. At any angle other than normal incidence partial conversion to the other mode will occur. In the system under examination here the exact form of the scattered shear wave field is not of significance as

it will not be deliberately recorded or used in the imaging process. Shear wave returns coincident with the longitudinal wave return of an object of interest are however quite possible in a multiple object situation. See Figure 3.9. For a perfectly reflecting plane object illuminated by a plane longitudinal wave the amplitude of the shear wave reflection may exceed that of the incident wave and the longitudinal wave reflection be as little as 0.38 the amplitude of that incident at certain angles of incidence.[26]

In this section we shall discuss the general form of solution for scattering, consider simplifications that may be applied in specific cases of interest and derive some measure of the strength of return signals from simple targets. Before proceeding further in the discussion it is necessary to consider what use can be made of detailed knowledge of the scattering characteristics of particular bodies. Without the benefit of apriori information as to scatterer parameters; with the limitations of relative (to the wavelength) aperture sizes which by optical standards are ridiculously small* and the likelihood of many objects being of the order of the wavelength in size, the possibility of being able to unambiguously separate parts of the total return as attributable to particular details is small. Thus the signal processing scheme has proceeded on the assumption

---

* For example, an acoustic aperture of 40mm diameter on aluminium at 5 MHz is about equivalent to an optical aperture of 16 μm.

of 'one to one' matching. That is, the repeated appearance of a return over a number of records from different aperture positions will cause it to be imaged as a distinct scattering zone in some definite small region. In fact of course the signal may have originated from the scattering peculiarities of some body which does not occupy the corresponding object region at all, (e.g., from creeping waves on an extended body). Thus in the sections below, most of the detail is concentrated in determining the echoes from small bodies which offer both simplicity in calculation and more importantly a measure of the lowest signal strengths to be anticipated in the system. Thus an estimate of the ultimate sensitivity possible can be obtained. A short bibliography appears at the end of the chapter giving additional references to elastic media scattering work.

3.5.2. The incident field.

As was shown in 3.4, over the domain of possible imaged sections of V the incident wavefront may be regarded as spherical with time variation in the direction of propagation that of the transducer mechanical output for paraxial components and with progressively greater attenuation of the higher frequencies at increasing values of Θ_B. Particularly for small objects at some distance from the transmitter the incident energy may be approximated to a single plane wavefront but in any case we may represent the wavefront by a suitable superposition of plane waves so that it will suffice to consider the response to this spatial

distribution only. Similarly a general solution is contained within that for a single frequency wave although as we will consider later a rather simplified approach can yield a good approximation to the field under conditions of 'impulsive' incident wavefronts.

With these assumptions then and the previously made ones about material properties we may express the general equation of motion for an elastic solid, viz.; *

$$(\lambda + 2\mu)\nabla\nabla.\tilde{u} - \mu\nabla x\ \nabla x\ \tilde{u} = \rho_o \frac{\partial^2 \tilde{u}}{\partial t} \qquad .. \quad 3.12$$

(where $\tilde{u}$ is the vector displacement and ∇ the 'del operator',[27]) in simpler form by recognising the total displacement to be composed of a scalar (i.e., longitudinal wave) and vector (i.e., shear wave) component and expressing $\tilde{u}$ as a function of scalar and vector potentials as;

$$\tilde{u} = \nabla\Psi + \nabla\ x\ \tilde{\Pi} \qquad .. \quad 3.13$$

Each of these potential functions satisfies a wave equation of the form;

$$\nabla^2\Psi = \frac{1}{c_1^2}\frac{\partial^2\Psi}{\partial t^2} \qquad .. \quad 3.14$$

where c_1 is the longitudinal wave propagation velocity, $\left(\frac{\mu+2\lambda}{\rho_o}\right)^{\frac{1}{2}}$ as before, and similarly for $\tilde{\Pi}$ with c_s $\left(=\left(\frac{\mu}{\rho_o}\right)^{\frac{1}{2}}\right)$, instead of c_1.

Now general plane wave solutions appear as;

---

* In this section we largely follow the development of White.[19]

$$\Psi = f(\hat{a}.\tilde{r}-c_1 t) \qquad .. \ 3.15(a)$$

$$\text{and } \tilde{\tilde{\Pi}} = \tilde{A}g(\hat{a}.\tilde{r}-c_s t) \qquad .. \ 3.15(b)$$

where $\hat{a}$ is the unit vector in the direction of propagation

$\tilde{r}$ defines the direction of interest

$\tilde{A}$ is any constant vector normal to $\hat{a}$, and f,g are arbitrary scalar functions of the indicated variables.

From this point on we will confine the development to longitudinal incident waves only. From the above;

$$\tilde{u}_1 = \nabla\Psi = \nabla f = \hat{a}f(\hat{a}.\tilde{r}-c_1 t) \qquad .. \ 3.16$$

and in particular the particle displacement of a monochromatic unit stress amplitude wave of frequency ω propagating in region 1 (see Figure 3.10) and incident on a scatterer occupying region 2 is given by;

$$\tilde{u}_1 = \hat{a}\, u_o\, e^{+j\omega t} e^{[-jk_{1,1}(x_o \cos\alpha_1 + z_o \sin\alpha_1)]} \qquad .. \ 3.17$$

with u_o the appropriate displacement magnitude and,

$k_{1,1} = \dfrac{\omega}{c_{1,1}}$ similar to equation 3.3 with the additional subscript signifying region 1.

$j = \sqrt{-1}$

3.5.3. <u>The Scattering Body</u>.

Some particular shapes for region 2 will now be considered but first it is appropriate to discuss the occurrence of likely

scattering bodies in practical materials inspection situations.

A field in which there is wide interest in ultrasonic testing is the production of nuclear fuel elements. These are normally bars of the radioactive material coated with a protective sheath of metal. Any sections of poor bonding result in inefficient heat transfer. This form of defect approximates to a very thin gap possibly of considerable area and in terms of Figure 3.10 region 2 becomes a thin sheet occupying the y_o, z_o plane, with very poor acoustic transmission compared with region 1.

Castings are subject to two variations of faults in the form of (possibly multiple) small regions of inhomogenity. The first of these is 'blowholes' which we may approximate by spherical cavities of radius 'b' and the second inclusions of impurities of different composition representable as spheres with Lamé constants λ_2 and μ_2.

In forgings and similarly worked items these cavities are elongated into laminae.

None of these flaws is readily simulated for system assessment but it is easy to produce cylindrical cavities by drilling and in this case region 2 becomes a cylinder lying along the z_o axis and of radius 'b'.

Appropriate coordinates for the spherical scattering problem are the spherical polar set centred on the sphere at the origin of the indicated Cartesian set. These are denoted by the radius

vector $\tilde{r}$ and the angles θ_o and ϕ_o. (θ_o is the angle between $\tilde{r}$ and the z_o axis and ϕ_o the angle in the x_o, y_o plane). For the cylinder problem an $\tilde{r}, \theta_o, z_o$ set is used with $\tilde{r}$ lying in the x_o, y_o plane.

3.5.3.1. Plane reflector.

The case of a lamina reflector is relatively simple and is treated in standard texts.[28] The main conclusion has already been quoted above (3.5.1). The reflected waves are of similar form to Equation 3.17 with $\hat{a}$ now in the direction α_2 as defined by the Snell's law relation;

$$\frac{\sin\alpha_1}{c_{l,1}} = \frac{\sin\alpha_2}{c_{l,1}} = \frac{\sin\chi_2}{c_{s,1}} \qquad .. 3.18$$

for the longitudinal component and χ_2 for the shear wave. (The form of Equation 3.17 for shear waves introduces a unit polarization vector $\hat{p}$ defined from the relation;

$$\tilde{A} = \tilde{p} \times \hat{a} \qquad .. 3.19$$

in place of $\hat{a}$).

From Equation 3.18, $\alpha_2 = \alpha_1$, and thus any incident plane wave (and consequently an arbitrary wavefront) will reflect in the same spatial form.

The relationships are independent of frequency and the time variation of the waveform will be preserved.

The preservation of the wavefront spatial shape constitutes a specular or 'glint' type of reflection identical to that of an

optical mirror. However mode conversion causes a fall off in reflected amplitude with α_1. For a plane longitudinal incident wave the reflected longitudinal component has an amplitude approximately $\cos\alpha_1$ times that incident (within 20% for $\alpha_1 < 60^\circ$).

3.5.3.2. Cylindrical and Spherical Scatterers.

If we simplify the situation to $\alpha_1 = 0$ then for an incident, plane longitudinal wave the scattered field outside the object may be expressed in the form;

$$\Psi = F \sum_{n=0}^{\infty} A_n H_n(kr) G(\eta) \qquad .. \ 3.20$$

with F = -1 (cylinder and sphere)

$G(\eta)$ = $\cos(n\phi)$ (cylinder)

= $P_n(\cos\theta)$ (sphere; $P_n(x)$ is the Legendre polynomial)

$H_n(kr)$ = $H_n^{(1)}(k_{l,1} r)$ (cylinder; Hankel function)

= $h_n^{(2)}(k_{l,1} r)$ (sphere; spherical Hankel function).

If $\alpha_1 \neq 0$ then $k_{l,}$ must be replaced (for the cylinder) by;

$$k'_{l,1} = k_{l,1} \cos\alpha_1 \qquad .. \ 3.21$$

and F becomes $-e^{-jk_{l,1}\sin\alpha_1}$

The incident wave is taken as propagating along the z_o axis towards the sphere to maintain the normal coordinate system usage. Similar expressions for the scattered shear field with coefficients B_n and arguments $(k_{s,1} r)$ may be formed but are not of direct interest. Inside the region 2 the appropriate

expressions are in terms of the corresponding Bessel functions and coefficients C_n and D_n, subscripts of the k's being altered as appropriate.

Solution now preceeds via the application of an appropriate set of boundary conditions producing an infinite set of equations with a typical member of the form;

$$\left[Z_n\right] \begin{bmatrix} A_n \\ B_n \\ C_n \\ D_n \end{bmatrix} = \left[Y_n\right] \qquad .. \quad 3.22$$

where Z_n is a 4 x 4 matrix with elements expressed in terms of the appropriate Bessel or Hankel functions evaluated at the scatterer boundary and the terms of the Y_n vector relate to the boundary stress and displacement terms. Particular examples are displayed in references 29 and 19 for the sphere and cylinder respectively.*

Considerable simplifications appear when the scatterer is a cavity. In this case no internal field exists and all the C_n and D_n coefficients are identically zero. As indicated above this does represent a situation of considerable practical importance. In the case of a sphere Ying and Truell[29] obtain explicit expression for the zeroth order coefficient A_o in the

---

* Equations 20 and 1.33 respectively. Note that in the latter case the formulation has been further generalised to include the case of incident shear waves producing six boundary condition equations instead of four.

general case and for the cases with n $\geqq$ 1 in the limiting case of Rayleigh scattering (i.e., lb << 1,l=$k_{i,j}$;i=l,s;j=1,2.) from an elastic sphere. Explicit expressions for the complete set of coefficients applicable to a spherical cavity of any (lb) value appear in equations 30 and 31 of this paper. These results virtually cover the range of practical interest. For large objects simple approximate methods suffice and for small bodies with k in the Rayleigh region the scattering may be characterized by a scattering cross-section defined as;

$$\gamma = \frac{\text{scattered energy/unit time}}{\text{incident energy/(unit area).(unit time)}} \quad .. \ 3.24(a)$$

which for a small spherical cavity is

$$\gamma = \frac{4\pi}{9} \cdot g_c \cdot \frac{1}{k^2_{1,1}} \cdot (k_{1,1}.b)^6 \quad .. \ 3.24(b)$$

g_c is a function of the parameter $\nu = \frac{c_{s,1}}{c_{l,1}}$ only and in the case of aluminium with $\nu = \frac{1}{2}$ has the value 13. (See Figure 1 of 29). For $\omega_{max} = 2\pi \times 10^7$ rad/Sec. the largest cavity for which the above possesses any validity ($k_{1,1}$ b=1) has a diameter of 0.2mm in aluminium.

Taking half this value gives;

$$\gamma = 3.7 \times 10^{-41} \omega^4 \quad .. \ 3.25$$

which reaches a maximum for $\omega = \omega_{max}$ of 5.7×10^{-10}.

Taking similar conditions to those in section 3.4.3 let us consider the response to an incident wave with particle displacement amplitude of 1Å. For a plane wave in aluminium

this corresponds to an intensity of 167 watts/m^2 or 0.0167w/cm^2 for the 5 MHz component. (For simplicity the phase shift between stress and strain in a spherical wave has been neglected as $k_1R >> 1$). Thus, the scattered power is $167 \times 3.7 \times 10^{-41} \times (\pi \times 10^7)^4$ watts = 5.95×10^{-8} watts. If we make the rather conservative assumption that this power is uniformly distributed in space and since the main concern is with the near backscattering region take all the energy in this direction to be in longitudinal form then $P_b \approx 0.475 \times 10^{-8}$ watts/steradian, for the backscattered signal.

Before leaving this case we note the strong dependence of the scattering on frequency which will result in considerable enhancement of the higher frequency components in $w_4(t)$ compared with $w_3(t)$.

In the case of a cylindrical scattering body the results of White are immediately relevant. He indicates that for the case $k_{1,1}b=2$ scattering in the back direction is nearly uniform over a 120^o arc for normally incidence waves ($\alpha_1 = 0$). Approximately 72% of the incident longitudinal wave energy will be scattered into the same mode (in aluminium). Thus over one centimeter of hole the energy returned will be approximately 7.7×10^{-5} watts/radian. In the case of a cylinder the cross section varies as the cube of frequency (for the Rayleigh region) and the distortion of the reflected wave is consequently lessened.

3.5.3.3. Flat bottomed holes.

A fourth type of discontinuity consisting of a flat bottomed hole is common as a calibrating target in pulse echo testing although the results can be very misleading for real targets which do not exactly resemble the ideal ones.[30] This situation has been studied by Ermolov[31] who points out that the scattered field is of the same form as that from a piston source of the type we have already discussed. The conclusion about the scattered field that he derives is of particular significance. Up to scattering angles of 60° the longitudinal field may be represented to within 20% by that of the corresponding case in a fluid media. Since results for bodies in fluids are much more thoroughly documented this is very helpful as a guide to behaviour.

For this type of scatterer with a normally incident excitation the scattered field is described by an equation of the form of 3.10, with the $K(\theta)$ term suitably altered to fit the shape of the reflecting surface. Assuming this to be reasonably symmetrical, and of radius 'a', then the direct backscattered field is given by Equation 3.11 in the far zone with unit incident stress. The scattered field back in the vicinity of the transmitter will have a displacement amplitude of $.016\mathring{A}$ for conditions as previously and a 1mm radius scatterer. For bistatic conditions (Figure 3.11) and all the radiating and scattering surfaces 'small' the received signal amplitude will exhibit a '$\cos^4$' variation with angle. For all angles in the region of $\approx 30^{\circ}$ the receiver output will be approximately halved.

As the scatterer becomes larger and/or the frequency higher, the region of high backscattering progressively diminishes towards the 'glint' response of the extended lamina (3.5.3.1).

3.5.4. Scattering bodies with characteristic dimensions comparable and larger than the wavelength.

Plots of scattering cross-section against 'kb' characteristically resemble that of Figure 3.12. The 'A' region bounded by kb=1 shows a high power dependence on kb (fourth power in the classical spherical Rayleigh scatterer). There is an intermediate 'B' region frequently referred to as the 'resonance region' because of the rapid large fluctuations in γ. In some scatterers this oscillation continues indefinitely as kb grows[32] but typically will settle to a steady value once dimensions of the order of a wavelength are exceeded. In any case the approximate methods applicable in the 'C' region predict well for large kb even when oscillations continue. This last region is characterised by the increasing accuracy of the Kirchoff[33] or 'physical optics' scattering formulation based on the superposition of radiating fields by Huygens principle. This, together with appropriate allowance for components circumnavigating the reflector one or more times before reradiation - the so-called 'creeping' or 'Franz'[34] waves - can provide satisfactory predictions in most cases. Ultimately a point is reached where the radius of curvature is so great that the concepts of simple geometrical optics become valid. This has already been discussed in the limiting case of a plane reflector.

Some work on the problem of scattering in the resonance region has been performed by the group of Tyutekin.[35,36] Reference 35 discusses the case of a single cylindrical cavity with a formulation similar to that of 15 and 19. While the main interest centres around rubberlike materials (characterised by large (10-500) values of the ratio λ/μ) the results presented indicate that the first resonant peak in metallic media occurs for $kb \approx 1$. Glazanov[36] extends the discussion to a grating of cylindrical cavities. The whole problem of this region is complicated by the failure of any reasonably simple approximations and has received little attention in the present studies. The numerical results of Johnson and Truell[44] do however indicate that for cavities in typical metals the resonant rise is not great and that oscillations in γ do not exist beyond the final peak. The situation is much more complicated for spheres of differing elastic constants. For cavities a value of γ corresponding to twice the physical, cross-sectional area (πb^2) is appropriate for $kb > 2$.

In the high frequency region the method of Freedman[37,38,43] draws immediate attention from its simplicity of concept and natural fit to the case of short duration illuminating waveforms. Basically all one needs is a plot of the variation of illuminated area on the scatterer as the incident pulse sweeps over the surface. The derivatives of this function then give the form of the back-scattered impulse response directly. As pointed out by Freedman this fails to predict the existence of creeping wave components but also may predict components arising from the cut-off at the

geometrical shadow boundary which do not physically exist.[39] In the near monostatic situation however, these may be of small amplitude compared with the main return[40,41] particularly for band limited incident waves.

Overall then in the case of larger bodies we may expect an initial return closely matching the waveform of the incident pulse followed by various delayed returns. As was discussed in the introduction (3.5.1) it is this initial response which holds the most interest. Following Freedman the backscattering cross-section for a sphere becomes;

$$\gamma_B = \pi b^2 \left(1 - \frac{\sin 2kb}{kb} + \left(\frac{\sin kb}{kb}\right)^2\right) \qquad .. 3.26$$

(neglecting shear wave components). Taking for example a sphere of the same radius as the flat disc considered before then over the 1 to 5 MHz range (kb varying from 1-10), γ_B varies about 15% from the classic high frequency value πb^2. This evaluates to $\pi \times 10^{-6}$. Hence in the standard case we have considered before the expected displacement amplitude at the receiver will be 0.017Å a similar value to that for the disc.

We may deduce several likely properties of returns from complex objects applying the concepts of this method. For example the response of a finite length smooth cylinder with non-normal excitation will tend to consist of returns from the ends only and the consequent image to consist of bright spots at these points only.

Similarly, at normal incidence the main response will occur at the leading edge only and the return form (but not amplitude)

become relatively independent of the cylinder diameter. The situation is saved in real cases by the rough boundary to be expected in practical scatterers creating many secondary radiating points and can also be much improved by arranging for the illumination to be incident from as wide an arc as possible. The ultimate aim would in fact be to approximate to the spatially diffuse and uniform illumination that we experience in everyday seeing. Attempts to ascertain the shape of reflective objects with a narrow light beam will 'illustrate' the point. In practice this ideal illumination is difficult to achieve ultrasonically and this failing is a very significant limitation to the ultimate system abilities.

The effect of extended pulses is illustrated by several diagrams in Freedman's work. In the case of a sufficiently extended burst there is a period in the return where the signal consists of contributions from all the reflecting discontinuities on the body. The necessary conditions for this to occur are discussed by Cann.[41] Over this period the returning signal may be characterised by a simple specification of amplitude and phase. In some of the experimental measurements performed this condition was created and the images formed correspond to those formed by the scatterer in strictly monochromatic illumination.

REFERENCES FOR CHAPTER 3.

1. Krasilnikov, V.A. and Zarembo, L.K. 'Non-linear interactions of elastic waves in solids'. IEEE Trans. SU-14, pp.12-17, Jan. 1967.
2. Papadakis, E.M. 'Variation of ultrasonic grain scattering factors with velocity'. J.Acoust.Soc.Am. 43, pp.876-8, April 1968.
3. Kolsky, H. 'Stress waves in solids'. Dover, New York, 1963, pp.8-9.
4. Filipczynski, L. 'Transients and the equivalent electrical circuit of the piezoelectric transducer'. Acustica 10, pp.149-154, 1960.
5. Ghosh, S.K. and Banerji, S.K. 'Responses in a piezo-electrical plate transducer'. Indian J. Phys. 39, pp.486-493, Oct. 1965.
6. Redwood, M. 'Transient performance of a piezoelectric transducer'. J.Acoust.Soc.Am. 33, pp.527-536, April 1961.
7. Redwood, M. 'Experiments with the electrical analog of a piezoelectric transducer'. J.Acoust.Soc.Am. 36, pp.1872-1880, Oct. 1964.
8. Mason, W.P. 'Electromechanical transducers and wave filters'. 2nd Edition Van Nostrand, Princeton, New Jersey, 1948.
9. IRE Standards on Piezoelectric crystals. Proc. IRE. 37, p.1378, 1949.
10. IRE Standards on piezoelectric crystals. Proc. IRE. 45, p.354, 1957.
11. IRE Standards on piezoelectric crystals. Proc. IRE. 46, p.765, 1958.
12. IRE Standards on piezoelectric crystals. Proc. IRE. 49, p.1162, 1961.
13. Mason, W.P. (Ed.) 'Physical acoustics'. Vol.1, Part A, Academic Press, New York, 1964, Chapter 3.
14. Holland, R. 'Contour extensional resonant properties of rectangular piezoelectric plates'. IEEE Trans. SU-15, pp.97-105, April 1968.
15. Miller, G.F. and Pursey, H. 'The field and radiation pattern of mechanical radiators on the free surface of a semi-infinite isotropic solid'. Proc.Roy.Soc. A-223, pp.521-541, 1954.
16. Onoe, M. et.al. 'Shift in the location of resonant frequencies caused by large electromechanical coupling in thickness mode resonators'. J.Acoust.Soc.Am. 35, pp.36-42, Jan. 1963.
17. Filipczynski, L. 'The field of elastic waves radiated into a semi-space by a compressional source'. Proc.Vib.Prob. 4, pp.17-25, 1963.

18. Filipczynski, L. 'Measurements of longitudinal and transverse waves radiated by a compressional source into elastic semispace'.
Proc.Vib.Prob. 5, pp.89-93, 1964.
19. White, R.M. 'Elastic wave scattering at a cylindrical discontinuity in a solid'.
J.Acoust.Soc.Am. 30, pp.771-785, Aug. 1958.
20. Woodward, P.M. and Lawson, J.D. 'The theoretical precision with which an arbitrary radiation pattern may be obtained from a source of finite size'.
J.IEE 95, Part 3, pp.363-370, 1948.
21. Schelkunoff, S.A. 'A Mathematical Theory of Linear Arrays'.
B.S.T.J. 23, pp.80-107, Jan. 1943.
22. Kinsler, L.E. and Frey, A.R. 'Fundamentals of Acoustics'.
2nd Edition, Wiley, New York, 1962.
23. Tucker, D.G. 'Near field effects in electronic scanning sonar'.
J.Sound Vib. 8, pp.355-363, 1968.
24. Alers, G.A. and Fleury, P.A. 'Strain amplitude of Mc/sec ultrasonic waves in solids'.
J.Acoust.Soc.Am. 36, pp.1297-1304, July 1964.
25. Proc. IEEE 53 (8), 'Special issue on radar reflectivity'.
Aug. 1965.
26. Kolsky, H. op.cit. Figure 6, p.29. (Note; In this reference the terms 'dilation' waves and 'distortion' waves are used for the propagation modes referred to as longitudinal and shear waves respectively here).
27. Spiegel, M.R. 'Mathematical handbook'.
McGraw-Hill, New York, 1968, p.119.
28. Kolsky, H. op.cit. p.24-38.
29. Ying, C.F. and Truell, R. 'Scattering of a plane longitudinal wave by a spherical obstacle in an isotropically elastic solid'.
J.App.Phys. 27, pp.1086-1097, Sept. 1956.
30. Gericke, O.R. 'Ultrasonic spectroscopy'.
U.S. Army Materials Research Agency, Watertown, Mass.
Rept. AMRA-TR-66-38. Dec. 1966.
31. Ermolov, I.N. 'Diffraction of sound in the acoustic path of a pulse type flaw detector'.
Sov.Phys.-Acoustics 6, pp.195-201, Oct-Dec. 1960.
32. Garbarcz, R.J. 'Modal expansions for resonance scattering phenomena'.
Proc. IEEE, 53, pp.856-864, Aug. 1965.
33. Born, M. and Wolf, E. 'Principles of Optics'.
Pergamon, London, 1959, p.377.
34. Neubauer, W.G. 'Pulsed circumferential waves on aluminium cylinders in water'.
J.Acoust.Soc.Am. 45, p.1134-1144, May, 1969.
35. Tyutekin, V.V. 'Scattering of plane waves by a cylindrical cavity in an isotropic elastic medium'.
Sov.Phys.-Acoustics 5, pp.105-108, Jan-March 1959.

36. Glazanov, V.E. 'Diffraction of a plane longitudinal wave by a grating of cylindrical cavities in an elastic medium'.
Sov.Phys.-Acoustics 13, pp.303-308, Jan.-March, 1968.
37. Freedman, A. 'A mechanism of acoustic echo formation'.
Acustica 12, pp.10-21, 1962.
38. Freedman, A. 'The high frequency echo structure of some simple body shapes'.
Acustica 12, pp.61-70, 1962.
39. Kennaugh, E.M. and Moffatt, D.L. 'Transient and impulse response approximations'.
Proc. IEEE 53, pp.893-901, Aug. 1965.
40. Rudgers, A.J. 'Acoustic pulses scattered by a rigid sphere in a fluid'.
J.Acoust.Soc.Am. 45, pp.900-910, April 1969.
41. Proc. IEEE 53 (8), 'Special Issue on Radar Reflectivity'. Cover Illustration.
42. Cann, A.J. 'CW-equivalent radar cross-section measurements with a pulse'.
Proc. IEEE (Letters) 53, p.1644, Oct. 1965.
43. Freedman, A. 'Portrayal of body shape by a sonar or radar system'.
J.Brit.I.R.E. 25, p.51, Jan. 1963.
44. Johnson, G. and Truell, R. 'Numerical computations of elastic scattering cross-sections'.
J.App.Phys. 36, pp.3466-3475, Nov. 1965.

Additional Bibliography on Scattering of Elastic Waves.

45. Akubakar, I.I. 'Scattering of plane elastic waves at rough surfaces'.
Proc.Cam.Phil.Soc. 58, 136-157, Jan. 1962.
46. Banaugh, R.P. and Goldsmith, W. 'Diffraction of steady elastic waves by surfaces of arbitrary shape'.
J.App.Mech. 30 series E, p.589, Dec. 1963.
47. Einspruch, N.G. and Truell, R. 'Scattering of a plane longitudinal wave by a spherical fluid obstacle in an elastic medium'.
J.Acoust.Soc.Am. 32, pp.214-220, Feb. 1964.
48. Gilbert, F. 'Scattering of impulsive elastic waves by a smooth convex cylinder'.
J.Acoust.Soc.Am. 32, pp.841-857, July, 1960.
49. Kanevskii, I.M. 'Analysis of the diffraction of a converging cylindrical wave by a cylinder.
Sov.Phys.-Acoustics 5, p.152, April-June, 1959.
50. Knopoff, L. 'Diffraction of elastic waves'.
J.Acoust.Soc.Am. 28, pp.217-229, March 1956.
51. Knopoff, L. and Hudson, J.A. 'Scattering of elastic waves by small inhomogenities'.
J.Acoust.Soc.Am. 36, pp.338-343, Feb. 1964.
52. Miles, J.W. 'Scattering of elastic waves by small inhomogenities'. Geophysics, 25, pp.642-648, June 1960.

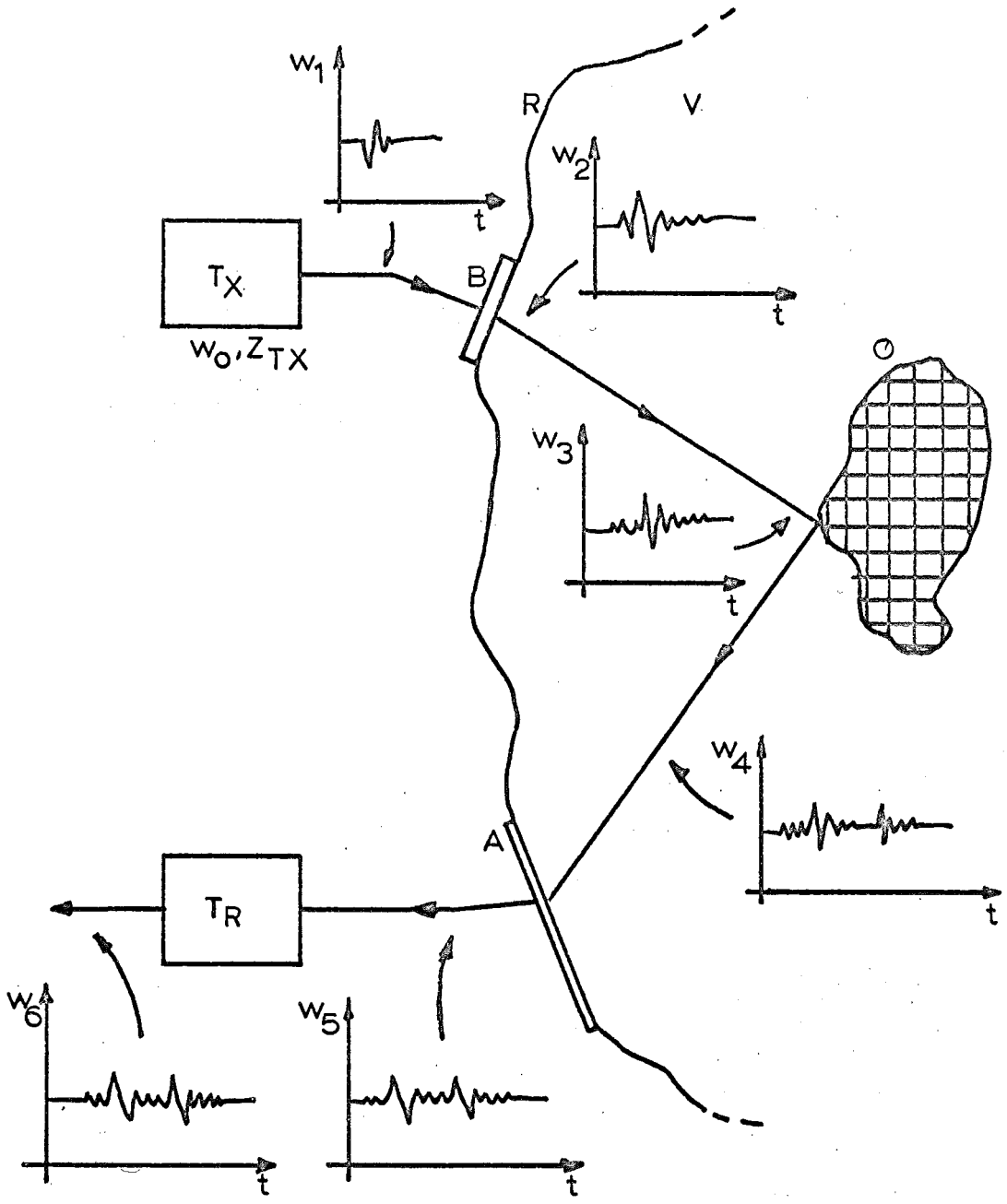

FIG. 3.1: Signal path in the imaging system

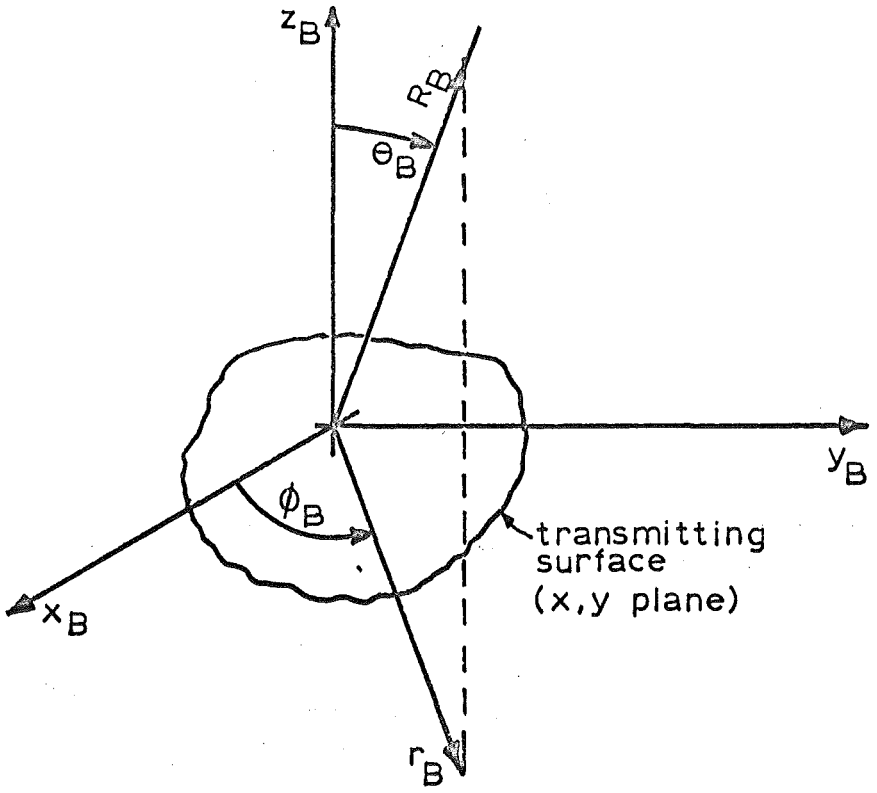

FIG. 3.2: Spatial coordinates

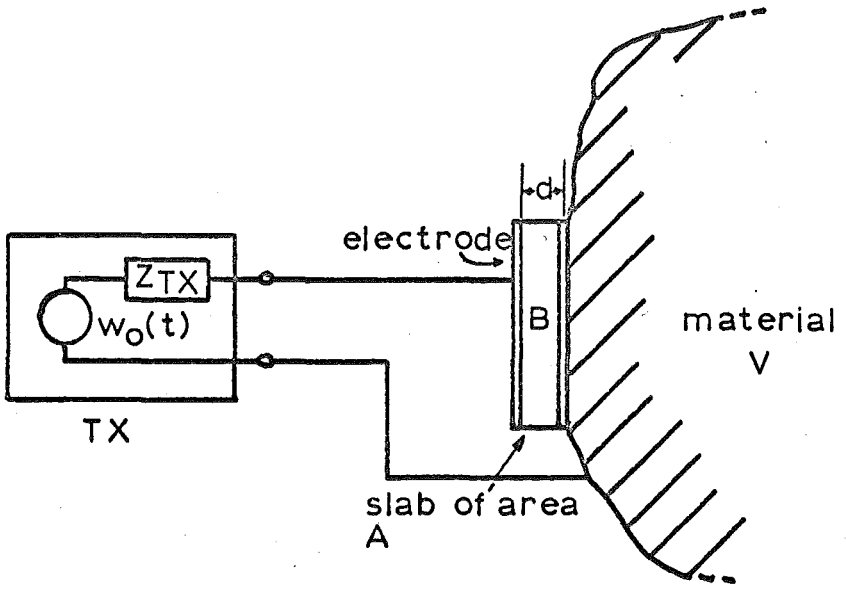

FIG. 3.3: Transmission of acoustic waves

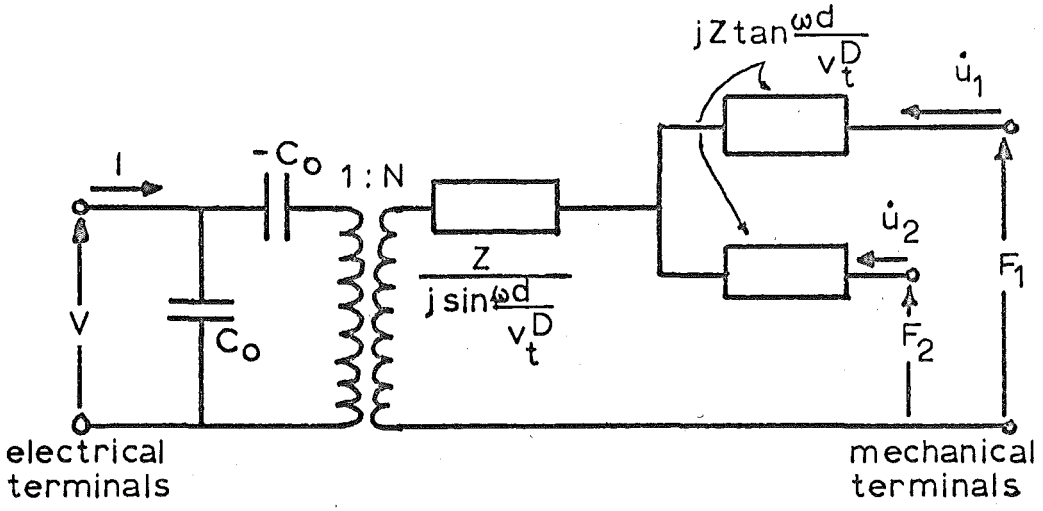

FIG. 3.4: Thickness expander mode transducer equivalent circuit

$C_o = \frac{A\epsilon_{33}^S}{d}$ = clamped capacitance

$v_t^D = \left(\frac{c_{33}^D}{\rho}\right)^{\frac{1}{2}}$ = propagation velocity at constant electric field

$Z = Z_o A = \rho v_t^D . A$, acoustic impedance

$N = C_o h_{33}$, where h_{33} is the piezoelectric stress constant

$\dot{u}$ = particle velocity, F = Force.

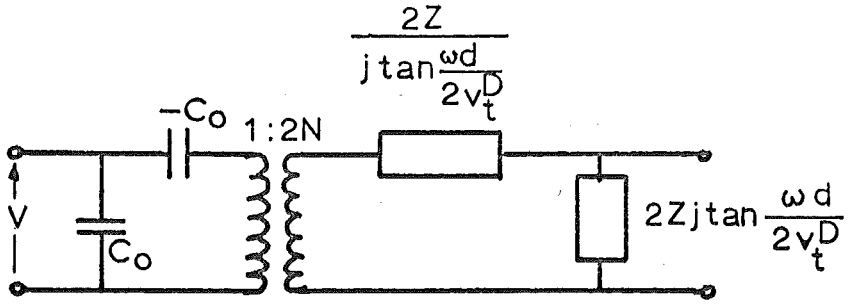

FIG. 3.5: Equivalent circuit with $F_2 = 0$ (i.e. one mechanical terminal pair free)

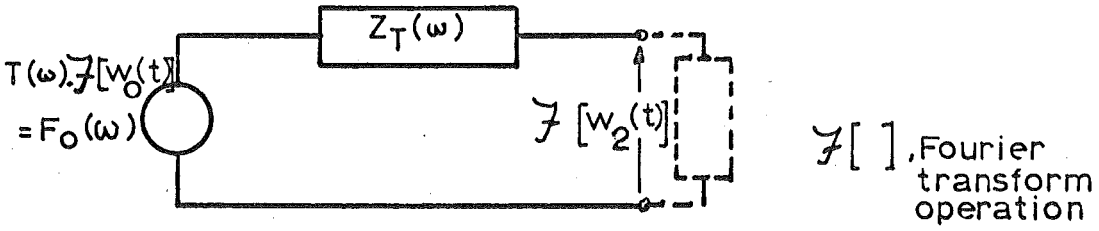

FIG. 3.6: Thevenin equivalent from mechanical terminals

$$Z_T(\omega) = j Z \tan \omega\alpha \left[1 - \frac{2 N^2 \tan \frac{\omega\alpha}{2}}{\omega C_o Z (1 + j\omega C_o Z_{TX}(\omega))} \right] \cdot \left[\frac{N^2 \tan \omega\alpha}{\omega C_o Z (1 + j\omega C_o Z_{TX}(\omega))} \right]^{-1}$$

$$T(\omega) = \frac{1}{N} \cdot \frac{\omega C_o Z \tan \frac{\omega\alpha}{2}}{\left[1 - \frac{\omega C_o Z (1 + j\omega C_o Z_{TX}(\omega))}{N^2 \tan \omega\alpha} \right]}$$

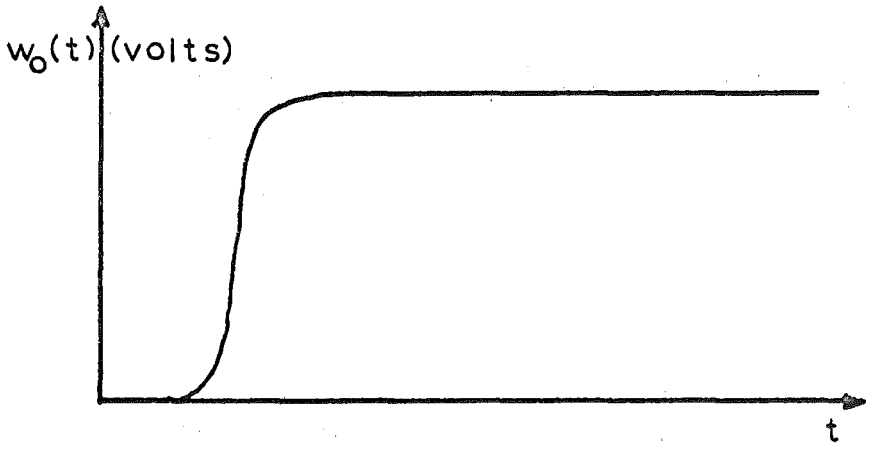

FIG. 3.7(a): Electrical drive and acoustic output

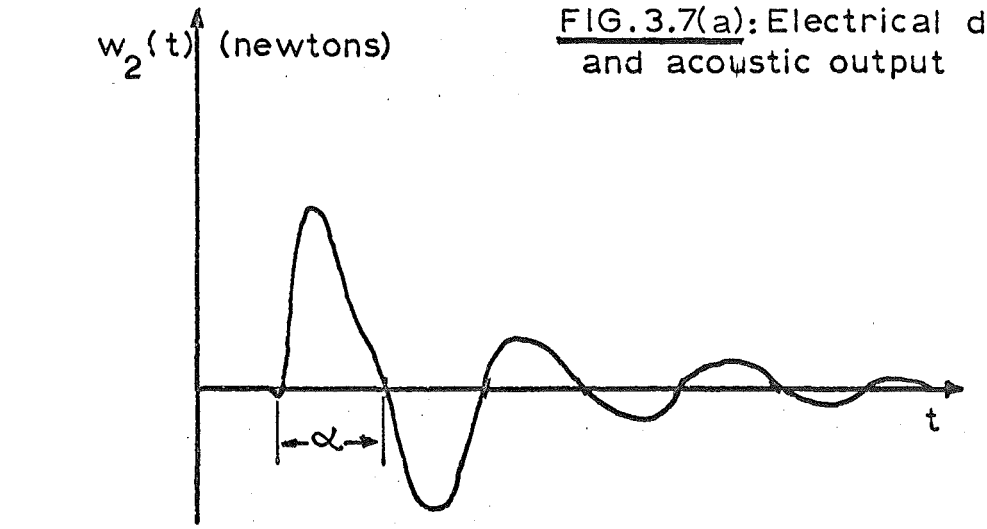

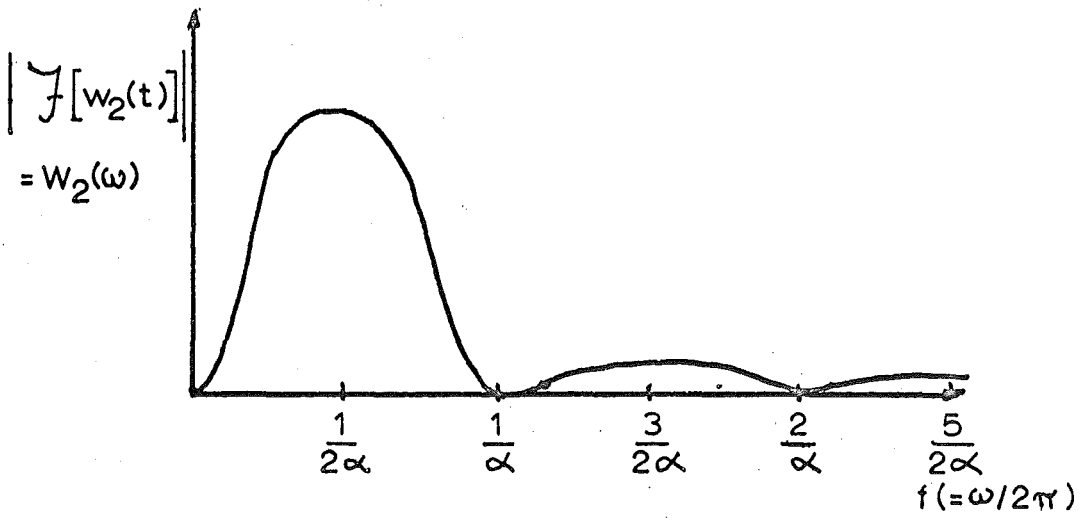

FIG. 3.7(b): Spectrum of $w_2(t)$

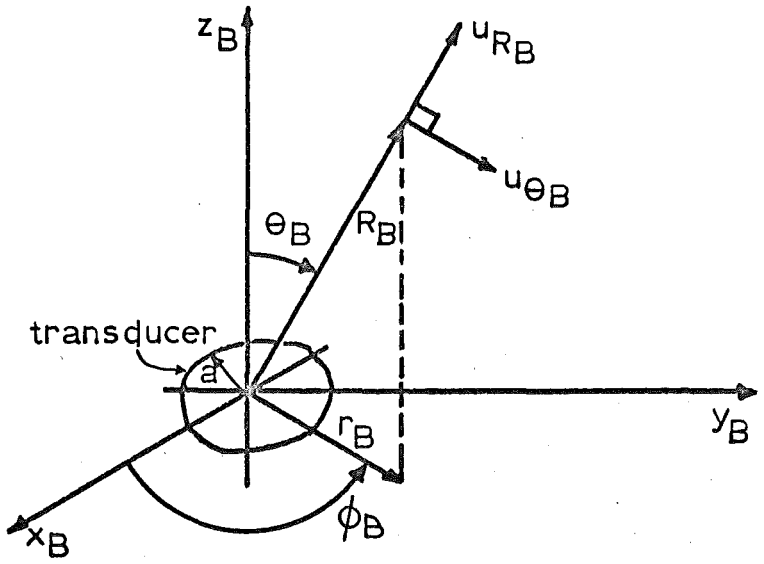

FIG. 3.8: Field components of piston source

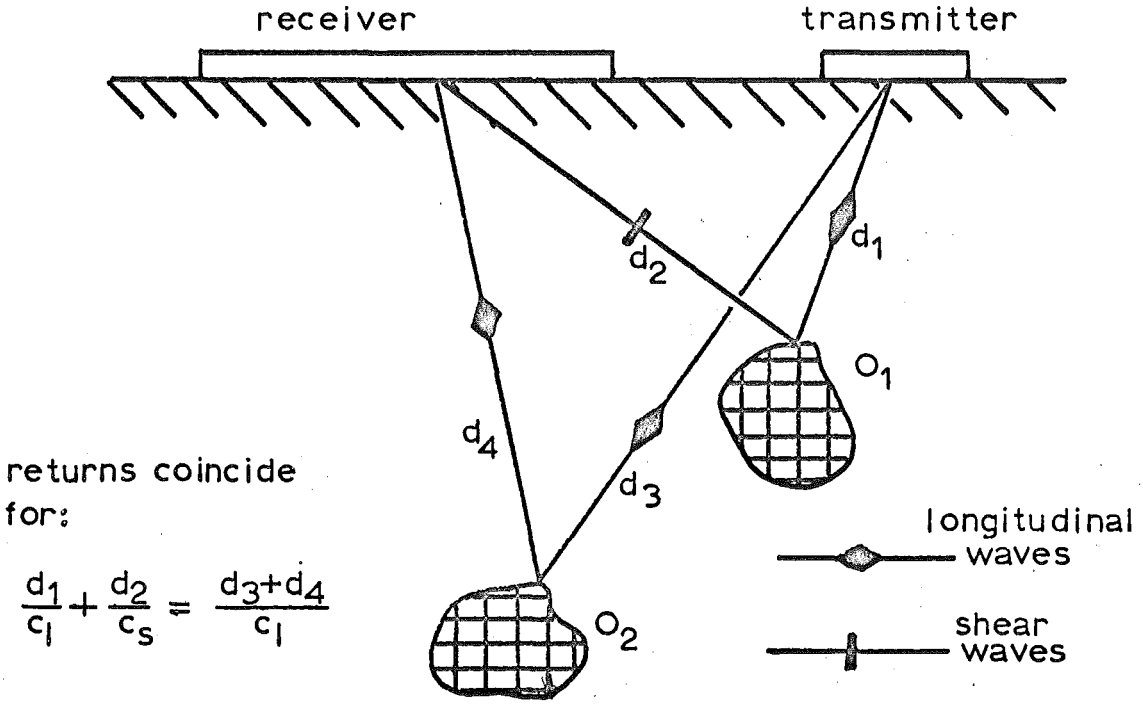

FIG. 3.9: Interference in multiple target situation

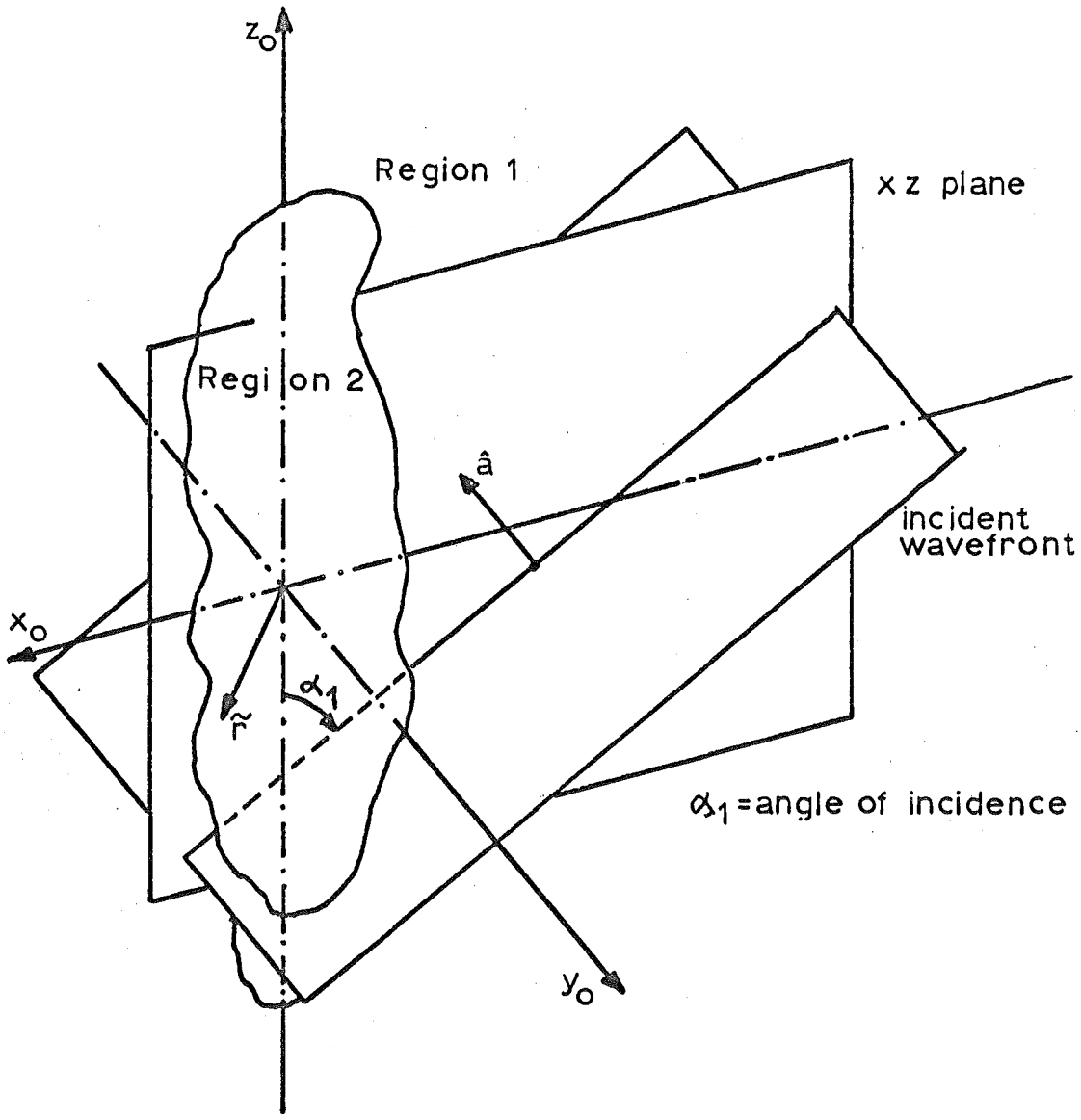

FIG. 3.10: Geometry of scattering problem

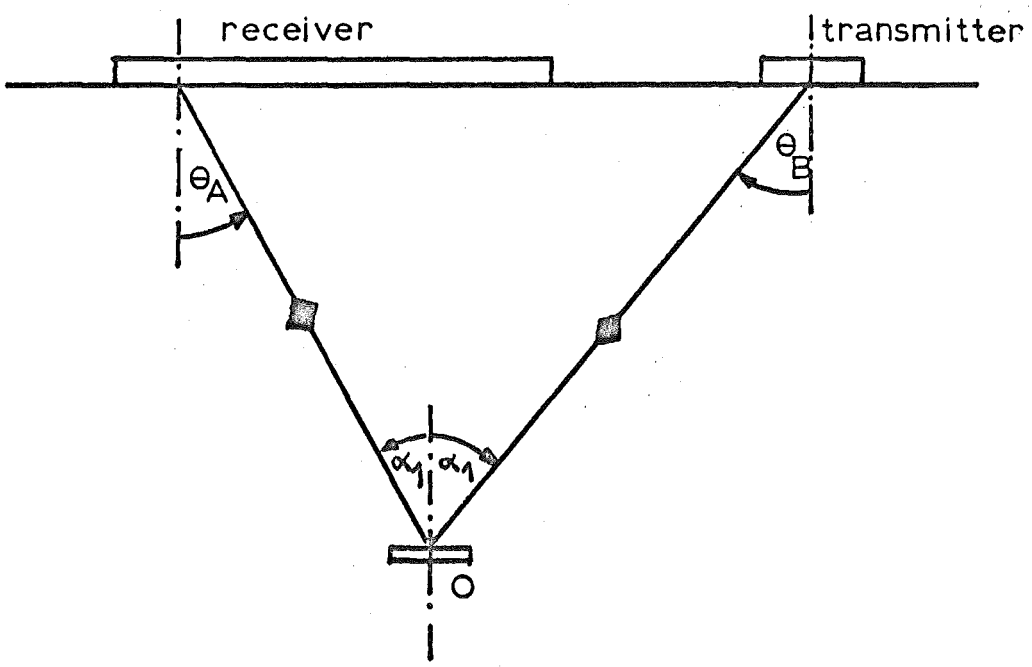

FIG. 3.11: Bistatic scattering

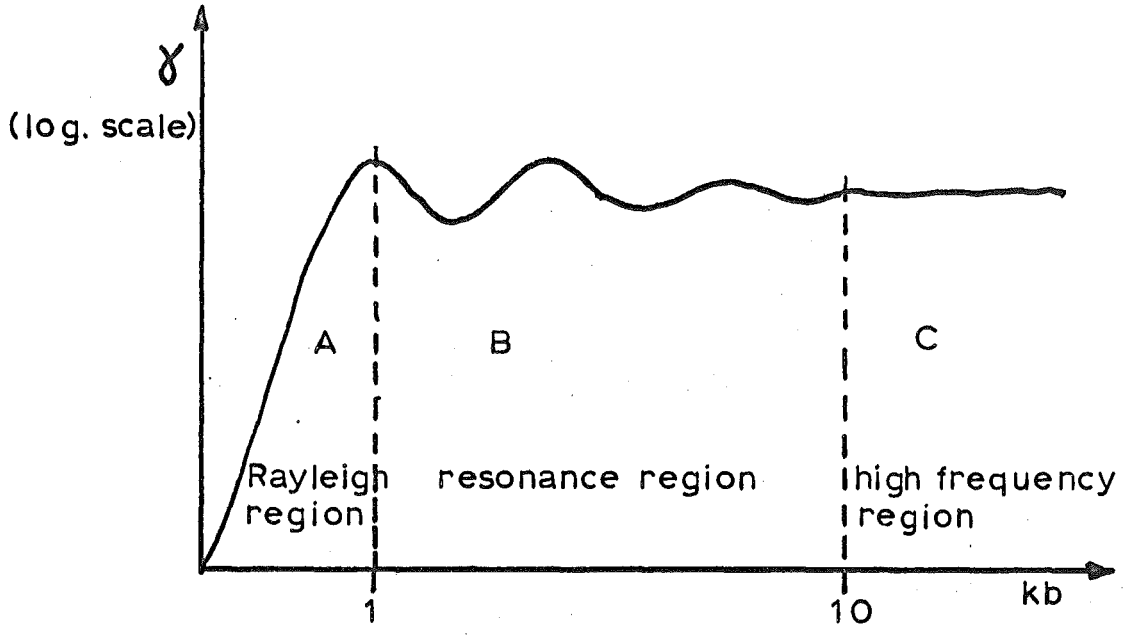

FIG. 3.12: Variation of scattering cross-section with kb

CHAPTER 4.

THE RECEIVING TRANSDUCER

4.1. INTRODUCTION.

This chapter continues the system analysis of Chapter 3. Firstly the response of the receiving transducer to a plane, impulsive, incident wavefront is considered. This is then extended to take account of non-normal incidence. Having thus derived a general description of the basic transducer behaviour the model of the system through from transmitter to receiver output is completed.

The analysis falls into two sections;

(1) Consideration of the mechanical response for a section of transducer imbedded within a large slab.

(2) Development of an acoustic-electrical conversion relation for the transducer element and an examination of the signal response.

4.2. MECHANICAL RESPONSE.

4.2.1. Physical arrangement.

The physical layout of the transducer is shown in Figure 4.1. The lateral dimensions of the transducer are assumed to be very much greater than the thickness while those of any elemental area are small compared with the overall size. These elements may have solid physical definition by virtue of the presence of individual

electrode areas on the back of the transducer slab or merely a transitory appearance when the slab is interrogated by a scanning electron beam. The particular characteristics of different transducer configurations are discussed in a later chapter. (Chapter 8).

4.2.2. Response of an extended plate.

Throughout the project it has been taken that a large transducer slab responds point by point to the incident field with (at least over elements comparable in dimensions with the plate thickness) sufficient decoupling from element to element that the electrical signals are a true representation of the local acoustic conditions. It has frequently been stated in connection with work on imaging tubes that the necessary condition for this is that the plates be fundamentally resonant at the frequency used.[1,2] Work by Hartwig[3] is quoted in support of this contention. The curves produced by Smyth[1] do indicate a very definite degredation in resolution capabilities when thicker plates are used. However all this work has been concerned with very lightly damped plates working between water and vacuum. Under these conditions or even with relatively thin oil couplant films between the transducer and a metal specimen[4] strong resonance occurs greatly increasing the available output signal. However, if the transducer is tightly bonded to a large object of comparable acoustic properties then the resonance is greatly suppressed. (Measurements taken indicate that the combined 'Q' of transmitter and receiver together is about

2 for PZT5A on aluminium). (Figures 12.28-12.31). Additionally we are concerned here with wideband signals (albeit with a maximum at the resonance frequency).

Holland[5,6] has exhaustively considered the behaviour of a multiply electroded piezoelectric transducer but only for driving frequencies well below the first thickness resonance. While in metals inspection there would be no real objection to overcoming the lower sensitivity by increased transmitter power and operating with transducers resonant at very high frequencies, if any potential biological use is considered the transmitter power should be kept as low as possible.

Of more direct relevance to the actual situation is the work by Lyon[7] and Fay and Fourtier.[17] These authors consider the vibration of an infinite elastic plate under localized driving forces. By the assumption of linear superposition we may regard the general problem of arbitrary spatial distribution solved once the solution for a concentrated driving force is established. In the present case we are however more concerned with gathering an appreciation of the degree of 'spreading' to be expected. The main additional assumption needed is that of a very large plate area. Since lateral movement is restrained by bonding of the plate to the material inspected the 'infinite' plate assumption would seem reasonable for the central elements at least.

Lyon's theory is concerned with plates which are completely undamped. Under these conditions the plate surface displacement

(normal component) may be expressed as a sum of terms such as $A_n \cos(k_n s).e^{jk_n s}$ for the region under the exciting force (which is taken to be uniformly applied over an infinite strip 2s wide), and $A_n \sin(k_n s).e^{jk_n x}$ for the region not under the forced area. (k_n is the wavelength constant for the nth mode, and x the distance from the centre of the forced area).

In particular Lyon presents results for the plate excited at 2.5 times the half-wavelength thickness resonance frequency. Several modes are excited, a Rayleigh surface wave, three more waves propagating with distinct phase velocities along the plate and a fifth which decays exponentially away from the source (i.e., k_n is imaginary). In the particular case taken, (2 MHz plate excited at 5 MHz) the vibration decays to 1/e of the initial value within 0.5mm of the edge of the excited region.*

As the plate thickness increases more modes appear further complicating the response. Of more direct interest is the behaviour with thinner plates. At the thickness corresponding to half-wavelength resonance a $k_n=0$ condition occurs (more exactly a closely spaced pair near this frequency - similar behaviour is apparent at the odd multiples of this thickness but becomes progressively less distinct). For this mode the associated A_n goes to infinity and thus also the plate surface displacement in

---

* The results in Lyon's paper have been appropriately scaled for PZT5A material and the different frequency-thickness products used here.

the region under the exciting force. (Remember that no damping has been allowed). For x>s this mode remains infinite despite the sine factor. Two of the other three modes are reduced to zero over the whole plate. The remaining mode is unattenuated and represents a condition intermediate between Rayleigh waves and thin plate propagation. Ideally then the free plate forced at its resonant frequency will exhibit a spread of the displacement over the whole surface. In practical situations motion of the plate surfaces is damped and the k_n's will exhibit a complex value. The imaginary part then contributes damping through the exponential term. (This is distinct from the pure imaginary values of k_n which appear for some modes of thick plates).

This conclusion that considerable spreading must occur appears to be at conflict with the commonly used resonant plates. Nevertheless the effect has been observed experimentally even under heavily damped conditions.[8] Despite this the loss of sensitivity is so great when very thin plates are used that a well damped resonant transducer is practically always necessary. For example a transducer 1/12th. wavelength thick produces only 1/59th. the steady state output of the corresponding resonant device (Appendix 3.2).

As the plate thickness is reduced below resonance the response becomes confined to two modes only. One of these represents thin plate longitudinal waves[9] propagating with the velocity -

$$c = \left[\frac{E}{\rho(1-\sigma^2)}\right]^{\frac{1}{2}} \qquad .. 4.1$$

E = Young's Modulus

ρ = density

σ = Poisson's Ratio

and the other tends toward zero propagation velocity as the plate becomes vanishingly thin. This represents a direct transfer of the applied stress through the plate. The thin plate waves are readily damped and in any case contribute to the surface displacement only indirectly. Ideally then, subject to sufficient output being obtainable, the transducer plate should be as thin as possible. This conclusion is validated in a reciprocal fashion by the work of Feit[10] and others[11,12] on the radiation field from a point excited elastic plate radiating into a fluid medium. In particular for a thin plate radiating into a fluid of high acoustic impedance the pressure field is given by an expression of the form (far field);

$$p(R,\theta) = K.\frac{e^{j(\omega t-kR)}}{R}.\cos\theta \qquad .. 4.2$$

K is a constant

R = the distance from the medium point to the point of force application

θ = the angle from the normal to the plate surface.

This will be recognised immediately as identical in form to Equation 3.9 when the source radius is vanishingly small. (The

cosθ term alone is exact for a liquid medium). Thus under these conditions the plate is simply reproducing the force distribution applied to it and it follows that coupling along the plate is negligible.

4.2.3. Actual arrangements used.

Despite the desirability of a very thin transducer for best spatial resolution (and as will be seen below for best temporal reproduction of the applied acoustic waveform) resonant plates have in fact been used. This is due not only to the increased output obtainable but just as importantly to the ready availability of large slabs in the 1-10 MHz range and their reasonable mechanical robustness. The problem of output voltage is acute when quartz transducers are used because of the high internal impedance and consequent high noise voltage. The low impedance ceramic materials are much superior in this parameter and offer possibilities of using thinner sections.

A major influence towards the use of thick plates in the imaging tube transducer was the necessity of adequate mechanical strength to form part of the vacuum envelope (8.3.2).

Since the plates are heavily damped when mounted on solid materials it has been considered sufficient to analyse the acoustic-electrical response with the same assumptions as were applied in the case of the transmitter (3.3).

4.2.4. Electrical leakage.

Apart from the neglect of mechanical coupling the other source of signal 'spreading', capacitive coupling between elements has also been ignored. Referring to Figure 4.2 the significance of this coupling can be assessed by an estimation of the capacitance between a perfectly conducting electrode (E) of sides a and b and the surrounding electrode (F). This is all the other electrodes tied together. E and F are in intimate contact with a slab of dielectric D representing the transducer material and bounded on the lower surface by a perfectly conducting plate 'G'. The medium above the top electrode will be assumed to have a relative permittivity of 1 (air) and that of the dielectric is ε_r. This will be of the order of 1000 for the ceramic transducer materials and by comparison with that in D the field in the space above the transducer will be negligible. ε_r for quartz however is only 4.6 and some part of the leakage will occur through the air path. Three capacitances appear in this system. C_{EF} between E and F, C_{EG} between E and G and C_{FG} between F and G. The latter one is of no direct significance. Cross coupling appears as the ratio between C_{EF} and C_{EG}.

Assuming a potential to be applied between F and G the problem resolves into determining the potential of E. A two dimensional version (i.e., $b=\infty$) of the problem is readily modelled using a resistive paper analogue. The field plot is shown in

Figure 4.3 for the case a=0.8mm, d=0.42mm and δ=0.1mm.

Measurement on an actual 1mm square element on a 5 MHz PZT5A transducer gave values of;

$$C_{EF} = 15 \text{ pF.}$$

$$C_{EG} = 27 \text{ pF.}$$

(The measurements were done at 16 kHz to avoid electromechanical coupling).

The potential of E is $C_{EF}/(C_{EF} + C_{EG})$ times that of F which in this case gives a figure of 0.36. In the field plot shown the potential of E' relative to G' is 0.25 the potential of F'. (Dashes are used to indicate reference to the two dimensional model). As would be expected this is lower than the value in the true 3D situation but the simplicity of the modelling technique made the exploration of the relative performance of different geometries a rapid process. The results of these experiments are shown in Figure 4.4. It will be seen that reducing 'δ' has only a small effect on the capacitance while reducing 'a' greatly increases the value. The reduced spacing between the sections of F' has caused much less upset of the F'-G' field and consequently elevates the potential of E' nearer to that of F'.

The last two results (Figures 4.4(c) and (d)) are of the greatest interest as not only do they minimise the electrical leakage but are also highly favourable mechanical configurations. In particular the arrangement of (c) offers a method of maintaining high electrical and mechanical element to element isolation while

retaining the advantage of the higher electrical output of a resonant transducer. The mechanical weakness of the notch is not serious when the transducer is mounted on a solid material but Haslett[13] reports use of this arrangement even with an image tube operating in water. However his transducers were five times the thickness of those used in the present project. Lack of suitable equipment to notch the hard and rather brittle ceramic materials prevented an arrangement such as that of Figure 4.4(c) being used here. The electrical circuitry loading the transducers in operation does however greatly reduce the E to G impedance Z_{EG} and results in much less leakage than the open circuit value indicated from this section.

4.3. ACOUSTIC-ELECTRICAL RESPONSE.

4.3.1. Introduction.

In this section we consider the response of an individual transducer element to an arbitrary incident acoustic waveform. The element will be assumed sufficiently decoupled from the remainder of the transducer that the equivalent circuit model developed for the transmitter is an adequate representation of the response. As noted above this assumption of decoupling is valid for very thin transducers but the results must be treated with some caution when the thickness becomes comparable with the wavelengths of the acoustic radiation.

In Section 3.3 the response was analysed (see Appendix 3.1)

via a Fourier transform representation. In analysing the receiving transducer however a slightly different method using Laplace transform methods was adopted.

At the same time the analysis was done, attention was concentrated on the use of the image tube as the system receiving transducer and the electrical side of the receiving device modelled accordingly. In the high voltage tube (8.3.1) the electron beam impedance is high and consequently the analysis was in terms of the open circuit response. With an electrical open circuit the response is particularly easy to calculate by Laplace transform methods. Subsequent work using probe contact to the transducer has involved the use of relatively low impedance electrical loads. Taking the impedance of C_o (Figure 3.4) as representative of the output impedance magnitude then for a 1mm square element of a 5 MHz plate the value is 1200 ohms (for PZT5A at 5 MHz). Short (i.e., length $\ll$ electrical wavelength) cables may be regarded as simple capacitors when terminated in a high impedance. Typical capacitances are 30 pF per foot and hence just the use of a short connection will halve the value of Z_{EG}. Termination of the cable in say 50 ohms results in loading conditions approximating a short circuit over the signal bandwidth of interest and the effect of electrical leakage may be ignored.*

* Use of such a low value of termination may seem at first sight extravagant of the signal developed by the transducer. However we have not yet considered the effect of electrical noise in the system or the distortion of the input caused by the transducer (4.3.2). Over the wide bandwidths used noise can become very great in high impedance circuitry.

4.3.2. Open circuit response.

As for the transmitting case the detailed mathematics are relegated to an appendix (Appendix 3.2) and the discussion here is confined to the pertinent results. Figure 4.5 shows the open circuit impulse response a(t) of the transducer. The form is a function of the relative acoustic impedances of the transducer material and the medium from which the incident stress waveform is coming. This is characterised by a reflection coefficient ρ_2 defined as;

$$\rho_2 = \frac{Z_m - Z}{Z_m + Z} \qquad .. \ 4.3$$

where Z_m = characteristic impedance of medium.
(As given the equation is for unit area of transducer. With Z defined as in Figure 3.4, Z_m must also be multiplied by the area for non unit conditions).

The complete Laplace transform domain expression for the response is;

$$A(s)_\infty = \frac{2h_{33}}{(Z_m+Z)} \cdot \frac{\tanh \frac{s\alpha}{2}}{s} \left[1 - (1+\rho_2)e^{-2\alpha s} + \rho_2(1+\rho_2)e^{-4\alpha s} + ... \right] \qquad .. \ 4.4$$

$$\alpha = d/v_t^D$$

s = Laplace transform variable.

From which

$$a(t)_\infty = \frac{2h_{33}}{Z_m+Z} \cdot F(\alpha,t) \cdot \left[1 - (1+\rho_2)h(t-2\alpha) + ... \right] \qquad .. \ 4.5$$

where: $F(\alpha,t)$ is the squarewave function of period 2α and amplitude $\pm$ 1,

and $h(t-\beta)$ is the unit step function delayed by a time β.

The open circuit impulse response then consists of a series of squarewave functions commencing at successive multiples of 2α, that is after each transit of the mechanical pulse through the transducer and back.

The two responses shown correspond to the cases of aluminium and PZT5A ($\rho_2 = -\frac{1}{3}$) and steel and PZT5A ($\rho_2 = 1/6$). For perfect matching ($\rho_2 = 0$) the response is zero after $t = 2\alpha$.

With open circuit electrical terminals the response is easily deduced on a physical basis. Output voltage is due to current in the short-circuited secondary of the transformer in the equivalent circuit. (The positive and negative capacitances in series have zero impedance for all frequencies). This current develops a voltage proportional to its integral in the capacitance C_o. Up to the transit time through the transducer slab there is no difference between the finite thickness transducer and one of infinite depth. At $t=\alpha$ perfect reflection occurs at the rear face, doubling the particle velocity value and starting an inverted wavefront propagating back through the transducer. At the front face, reached after a further time α, a reflection occurs and a further wave propagates forward through the slab. The magnitude of this depends on the matching between the two materials. The process similarly repeats at the rear face and

so on, the output decaying after each arrival at the front face. The amplitudes of successive components are readily calculated and the results are tabulated in the appendix (Appendix 3.2) for a variety of material combinations.

Having derived the impulse response the behaviour for arbitrary inputs may now be obtained by the relation;

$$w_5(t) = a(t) \not\otimes w_4(t) \qquad .. 4.6$$

($\not\otimes$ denotes convolution)

$w_5(t)$ and $w_4(t)$ are the waveforms of the electrical output and mechanical input respectively. (See Figure 3.1).

The case of $w_4(t)$ in the form of a few cycles of a sinusoid is of special interest as this approximates the waveform of the transmitter. The output $w_5(t)$ in response to a pulse consisting of two complete cycles of such a function is shown in Figure 4.6 under the conditions $\rho_2=0$ and the wavelength of the incident signal twice the transducer thickness. Under prolonged excitation the electrical output eventually settles to a steady amplitude with a $\pi/2$ phase lag on the incident signal. When $\rho_2 \neq o$ new transients continue to appear indefinitely but in practice with typical solid materials the amplitudes decay quite rapidly. Even with $\rho_2 = -\frac{1}{3}$ (which is extreme for metals) the 11th component is only 0.007 of the initial one, and this is neglecting the losses in the transducer material. With the transducer facing into a water medium the results are quite different, typical reflection coefficients being in the range 0.8 to 0.9. These high values drastically prolong

the response. For example with PZT5A and water the value on the 21st reflection is still 83% of the initial response. For this reason it seems very unlikely that the image tube will ever be useful as a transducer in a wideband system if operation in a liquid bath is required. Completely 'solid state' transducer arrangements may allow a backing on the transducer and this overcomes the problem.

4.3.3. Electrically loaded response.

The analytical calculation of this case is considerably more involved than for the open circuit device. Redwood[14] has performed the analysis for the case where the transducer has an infinitely rigid backing, a condition that results in some simplification. Following the same method as for the open circuit situation one may readily derive the form of the response up to the time $t=\alpha$, after this the expression assumes great complexity, but reasoning based on physical grounds can give some indication of the probable behaviour. The details are worked out in Appendix 3.2 from where we derive the expression for $(0<t<\alpha)$ as exactly that for the previous case multiplied by a term,

$$k(t) = \mathcal{L}^{-1}\left[\frac{s}{(s-\xi)(s-\eta)}\right] \qquad .. 4.7$$

($\mathcal{L}^{-1}$ = inverse Laplace transform operation)

$$\text{i.e.,} \quad k(t) = \frac{\eta e^{\eta t} - \xi e^{\xi t}}{\eta - \xi} \qquad .. 4.8$$

Where ξ and η are the roots of the expression,

$$s + \frac{s}{RC_o} - \frac{h_{33}^2(Z_m+2Z)}{Z\,R(Z+Z_m)} \qquad .. 4.9$$

R = loading resistance.

Under conditions where R is small ξ and η are approximately;

$$\xi = \frac{h^2(Z_m+2Z)C_o}{Z(Z_m+Z)} \qquad .. 4.10(a)$$

$$\eta = -\frac{1}{RC_o} \qquad .. 4.10(b)$$

The limit of applicability of these approximations is reached near $R \geqq 500$ ohms for a 1mm square element of (5 MHz) PZT5A. This is considerably higher than the resistance values actually used in practice.

For the PZT5A-Aluminium combination and $1m^2$ area of transducer the parameters have the values;

$h_{33}^2 = 4.3 \times 10^{18}\ V^2/m^2$

$C_o = 30.4 \times 10^{-6} F$

$R = \frac{1}{2000}\ \Omega$ (i.e., 500Ω on $1mm^2$)

$Z_m = 17 \times 10^6$

$Z_o = 34 \times 10^6$

giving

$\xi = 6.4 \times 10^6$

$\eta = -6.6 \times 10^7$

For $t=0, k(t)=1$ and with these values of ξ and η the response for $t>0$ is dominated by the $e^{\eta t}$ term with a time constant of 15 nS. Thus the initial output follows a path such as that in Figure 4.7 when $\alpha=100$ nS. The form of response for $t \geqq \alpha$ has been sketched from physical considerations. Obviously as $R \to \infty$ the voltage must be that of the open circuit device, and this determines the limiting form of the output wave.

For quartz the capacitance will be only about 1/200th. that of PZT5A and the corresponding resistance for the same general response must be higher by the same factor.

Very approximately the effect of low values of resistance is differentiation of the open circuit waveform. For a nearly complete short circuit the output impedance of the transducer becomes approximately that of C_o at frequencies above about one fifth of the resonant value for the transducer and the output current is the derivative of the mechanical-electrical transformer input.

Operating the transducer into a low impedance reduces the impulse response to a series of short pulses spaced α apart in time and diminishing in height at a rate depending on the value of ρ_2. Thus the response to an arbitrary input waveform will consist of the superposition of a number of successively delayed versions of the input. However in this situation the steady state phase shift characteristic of open circuit transducers excited by a sinusoid does not exist. (More generally the

integration of the input waveform apparent with an open circuit transducer is removed). During the build up and decay of the output waveform no displacement from the zero crossing instants of the input waveform occurs. This fact is of considerable advantage in the present system which relies very heavily on accurate timing of the received pulses.*

As mentioned before (4.3.1) terminating resistances of 50 ohms have been used in practice with the 1mm square transducer elements. This well satisfies the conditions both for preservation of signal timing and for low electrical leakage.

4.3.4. Numerical results.

In Chapter 3 (3.5) the amplitude of signal returns was estimated for a variety of targets. From the results of the immediately preceding sections we may now calculate the electrical outputs for these signals.

Typical amplitudes of acoustic signals at 5 MHz in aluminium were found to be 0.017Å. This corresponds to a stress amplitude of 905 N/m^2. Thus the force on a $1mm^2$ element is 9.05×10^{-4} N. From Appendix 3.2 the steady state output voltage for a transducer driven at resonance is given by;

---

* Note that this condition holds only for the input waveform's period matching the transition time of the transducer, that is, the signal must be generated by an identical unit to the receiver.

$$\bar{w}_5 = \frac{4h_{33}\,\bar{F}}{j\omega Z_m . A} \qquad .. 4.11$$

(A = transducer element area).

Thus for $\bar{F} = 9.05 \times 10^{-4}$N (R.M.S.) the output is,

$$\left|\bar{w}_5\right| = 14.5 \times 10^{-3} \text{ volts.}$$

(This is for PZT5A but a similar result holds for X cut quartz as h is comparable).

The peak amplitude for a fast transient comes from Equation 4.5. Let the particle displacement in the medium follow a step function of height 0.017Å. Then $F(t) = \delta(t).0.017 \times 10^{-10}.Z_m.A$

and $$w_{5_{max}} = \frac{2h_{33}F}{(Z+Z_m).A} \qquad .. 4.12$$

giving for PZT5A - aluminium

$$w_{5_{max}} = 2.44 \times 10^{-3} \text{ volts.}$$

These magnitudes correspond very well with observed values in the apparatus.

4.4. NON-NORMAL INCIDENCE OF INPUT WAVE.

There are two factors involved in the necessary modifications to the impulse responses already presented.

(1) A factor to account for the behaviour of flat transducers of any element size. This is simply a representation of the transducer property of responding to the

normal component of incident stress only.[15] The problem is similar to determining the angular directivity function for the transmitter.

In dealing with the field reconstruction problem (Chapters 5-6) it is convenient to deal with the particle displacement rather than with stress. Now in the analysis above there is an implicit assumption of a direct relationship between stress and particle velocity at the transducer terminals. This requires careful examination for non-normal incidence. Ideally the normal force on the transducer should fall off with incident angle along exactly the same function as does the normal particle velocity. As is seen in the next chapter this occurs simply as $\cos\theta_A$. Now the normal component of stress in the medium is given by,[18]

$$\sigma_{zz} = (\lambda+2\mu)\frac{\partial U_z}{\partial_z} + \lambda\left(\frac{\partial U_x}{\partial x} + \frac{\partial U_y}{\partial y}\right) \qquad .. 4.13$$

by noting that $\frac{\partial U_z}{\partial_z} = -jk\cos\theta_A . U_z$, for a plane wave propagating towards the transducer (5.2.2) we may put,

$$-\sigma_{zz} = \frac{\lambda+2\mu}{c}\dot{U}_z\cos\theta_A + \frac{\lambda}{c}(\dot{U}_r\sin\theta_A) \qquad .. 4.14$$

$\dot{U}_r$ is the component of particle velocity in the plane, the dot signifying differentiation with respect to time (i.e., multiplication by $j\omega$).

Typically $\lambda + 2\mu \approx 2\lambda$ and hence,

$$\sigma_{zz} \propto \dot{U}_z\cos\theta_A + 0.5\dot{U}_r\sin\theta_A \qquad .. 4.15$$

For the equivalent circuit to hold we must have $\sigma_{zz} \propto \dot{U}\cos\theta_A = \dot{U}_z$ so that both force and velocity fall off together. With the actual relationship,

$$\sigma_{zz} \propto \dot{U}(\cos^2\theta_A + 0.5\sin^2\theta_A) \qquad .. 4.16$$
$$= \dot{U}\,0.5\,(1 + \cos^2\theta_A).$$

Comparison of $\cos\theta_A$ with $0.5\,(1 + \cos^2\theta_A)$ shows that for $\theta_A \leqq 60^o$ the difference is less than 20%. Thus up to at least this angle of incidence we may retain the equivalent circuit to a good approximation and represent the basic transducer factor simply by;

$$D(\theta_A) = \cos\theta_A. \qquad .. 4.17$$

(2) A factor depending on the size and shape of the transducer element. To investigate this we shall consider a unit impulsive wavefront incident from the direction (θ_A, ϕ_A) as defined in Figure 4.8.

The transducer element is in the z_A=0 plane and has a maximum extent of Δ along the r_A direction. Distance from the 'leading' edge (i.e., that which the incoming waveform meets first) is measured by ε and a function $f(\varepsilon)$ represents the width of the transducer element at any ε. The instant when the incoming wavefront reaches the leading edge is denoted by t_o, relative to an arbitrary time origin.

The phase velocity v of the wavefront over the transducer surface is a function of θ_A viz.;

$$v = c/\sin\theta_A \qquad .. 4.18$$

where c is the velocity normal to the wavefront.

At any time $t(t>t_o)$ the wavefront has travelled a distance ε given by;

$$\varepsilon = v(t-t_o). \qquad .. 4.19$$

Now the transducer responds to the instantaneous spatial average of the incident (normal) force. This mechanical input is given by;

$$m(t,\theta_A) = f[v(t-t_o)] . D(\theta_A); t_o<t<\Delta/v \qquad .. 4.20(a)$$
$$= 0 \text{ otherwise}$$

or, replacing $D(\theta_A)$ from Equation 4.17,

$$m(t,\theta_A) = f[v(t-t_o)] . \cos\theta_A; t_o<t<\Delta/v \qquad .. 4.20(b)$$
$$= 0 \text{ otherwise.}$$

Some particular shapes of E are of interest;

(1) Let E be a rectangular element aligned with the incoming wave and of width a. Then $f(\varepsilon) = a$ and the mechanical input $m_1(t,\theta_A)$ is a square pulse of duration $\frac{\Delta}{v}$ and amplitude $a.\cos\theta_A$ (Figure 4.9(a)).

(2) Circular element of diameter Δ. For this shape $f(\varepsilon)$ has the form;

$$f(\varepsilon) = 2\{\varepsilon(\Delta-\varepsilon)\}^{\frac{1}{2}} \qquad .. 4.21$$

and the input $m_2(t,\theta_A)$ as in Figure 4.9(b).

(3) Square element aligned with the x_A, y_A axes and $\phi_A = \pi/4$. If the element is of side a then $\Delta = \sqrt{2}\,a$

and,

$$f(\varepsilon) = 2\varepsilon \quad (0 \leqq \varepsilon \leqq a/\sqrt{2}$$
$$= 2(\sqrt{2}\,a - \varepsilon) \quad (\frac{a}{\sqrt{2}} < \varepsilon \leqq 2\,a) \qquad .. 4.22$$

giving $m_3(t,\theta_A)$ as in Figure 4.9(c).

This case represents the extreme deviation from the square pulse of the aligned element.

For an arbitrary form of the incoming wave temporal variation the resultant mechanical input to the transducer may be calculated by taking instant by instant the weighted spatial average of the normal components of the signal over the element. The appropriate weighting function is the impulse input as derived above, expressed as a function of ε instead of t. Take the case of a continuous sinusoidal wave, i.e.,

$$w_4(t) = \sin(\Omega t) \qquad .. 4.23$$

incident as in Figure 4.9(a). The signal over the transducer plane at any instant is,

$$s(t,\varepsilon,\theta_A) = \sin\Omega\{t - t_o - \varepsilon/v\} \qquad .. 4.24$$

and the weighted average is;

$$\bar{s}(t,\theta_A) = \frac{1}{\Delta}\int_0^{\Delta} m_1(\frac{\varepsilon}{v},\theta_A)\sin\Omega(t - t_o - \varepsilon/v).d\varepsilon \qquad .. 4.25$$
$$= \frac{a\,v\cos\theta_A}{\Delta\Omega}\left[\cos\Omega(t - [\Delta/v + t_o]) - \cos\Omega(t - t_o)\right]$$

This is the value of the total force on the transducer at any instant t. The R.M.S. value of this force is given by;

$$\bar{s}_{RMS}(\theta_A) = \frac{a v \cos\theta_A}{\Delta\Omega}\left\{\frac{\Omega}{2\pi}\int_0^{\frac{2\pi}{\Omega}}\left[-2\sin\left(\frac{\Omega\Delta}{2v}\right).\sin\Omega\left(t-\left[t_o+\frac{\Delta}{2v}\right]\right)\right]^2 dt\right\}^{\frac{1}{2}} \quad .. 4.26$$

$$= \frac{a}{\sqrt{2}}\left\{\frac{\sin\left(\frac{\Omega\Delta}{2v}\right)}{\frac{\Omega\Delta}{2v}}\right\}\cos\theta_A . \quad .. 4.27$$

When $\Omega\Delta/2v = \pi/2$, i.e., when the dimension of the transducer element in the direction of the wave travel is one half wavelength of the signal on the transducer surface, $(\bar{s}_{RMS}(\theta_A))$ has the value $\frac{a}{\sqrt{2}} . \frac{2}{\pi} . \cos\theta_A$. The RMS value of the signal at normal incidence is just $a/\sqrt{2}$ and hence a signal of this surface wavelength is attenuated by a factor $(2/\pi).\cos\theta_A$.

This effect is analogous to the 'aperture effect'[16] encountered in the temporal sampling of a signal by a function other than the ideal impulse 'comb'. The particular $m(t,\theta_A)$'s may be compared with the shapes of practical finite width sampling pulses. The circular element weights the spectrum by a factor $\frac{2J_1\left(\frac{\Omega\Delta}{2v}\right)}{\frac{\Omega\Delta}{2v}}$, and the square element on a diagonal gives a $\left[\frac{\sin\frac{\Omega\Delta}{2v}}{\frac{\Omega\Delta}{2v}}\right]^2$ weighting. The particular case calculated above corresponds to taking samples consisting of the average of the input function over a period equal to the sampling period, and the factor $2/\pi$ appears similarly* for the signal component of period equal to

---

* The $\cos\theta_A$ is a peculiarity of the particular transducer type and has no direct temporal analogue.

two sampling intervals. In correct sampling practice this would also be the highest frequency applied to the sampler.

In the succeeding chapters it is shown how the maximum permissible size and spacing of elements is related to the bandwidth of the signals and the range of θ_A from which they may appear. The case $\Omega\Delta/2v = \pi/2$ represents the maximum value permitting unambiguous imaging. If for example the highest frequency of interest is 10 MHz and the elements are spaced so as to just clear each other then for $\theta_{A\ max} = \pm 30^{o}$ the maximum value of Δ is the free space wavelength λ ($= 2\pi c/\Omega$). For aluminium this is 0.64mm. If the complete half space were to be viewed (an impractical limiting case because of the $\cos\theta_A$ factor) then the element spacing should not exceed $\lambda/2$.

REFERENCES FOR CHAPTER 4.

1. Smyth, C.N. et.al. 'The ultrasound image camera'. Proc. IEE 110, pp.16-28, Jan. 1963.
2. Jacobs, J.E. 'Applications and limitations of the ultrasound image converter in acoustic imaging'. in; 'Ultrasonic imaging'. (Ed. R.S. Mackay) Mine Advisory Committee, Natl.Acd.Sc., Natl. Res. Coun. NRC:MAC:2016, April 1965.
3. Hartwig, K. 'Uber das Raeumliche Aufloesungsvermogen von Barium Titanat-Und Quarzplatten bei der Ultraschallabbilding'. Acustica 9, pp.109-117, 1959.
4. Filipczynski, L. 'Transients and the equivalent electrical circuit of the piezoelectric transducer'. Acustica 10, pp.149-154, 1960.
5. Holland, R. 'The equivalent circuit of an N-electrode piezoelectric bar'. Proc. IEEE 54, pp.968-975, July 1966.
6. Holland, R. 'Analysis of multiterminal piezoelectric plates'. J.Acoust.Soc.Am. 41, pp.940-952, April 1967.
7. Lyon, R.H. 'Response of an elastic plate to localized driving forces'. J.Acoust.Soc.Am. 27, pp.259-265, March 1955.
8. White, R.M. 'Elastic wave scattering at a cylindrical discontinuity in a solid'. J.Acoust.Soc.Am. 30, pp.771-785, Aug. 1958.
9. Kolsky, H. 'Stress waves in solids'. Dover, New York, 1963, p.86.
10. Feit, D. 'Pressure radiated by a point excited elastic plate'. J.Acoust.Soc.Am. 40, pp.1489-1494, Dec. 1966.
11. Pal'tov, V.A. and Pupyvev, V.A. 'Vibration and sound radiation of a plate under random loading'. Sov.Phys.-Acoustics 13, pp.210-214, Oct.-Dec., 1967.
12. Plakov, D.D. 'Near sound field of an infinite plate driven by a point force'. Sov.Phys.-Acoustics 13, pp.264-265, Oct.-Dec., 1967.
13. Haslett, R.W.G. 'An ultrasonic to electronic image converter tube for operation at 1.2 Mc/s.'. Radio Elect. Eng. 31, p.161-170, March, 1966.
14. Redwood, M. 'Transient performance of a piezoelectric transducer'. J.Acoust.Soc.Am. 33, pp.527-536, April, 1961.
15. Ermolov, I.N. 'Diffraction of sound in the acoustic path of a pulse type flaw detector'. Sov.Phys.-Acoustics 6, pp.195-201, Oct.-Dec., 1960.
16. Bennett, W.R. 'Spectra of quantized signals'. Bell Sys. Tech. J. 27, pp.446-474, July 1948.
17. Fay, R.D. and Fortier, O.V. 'Transmission of sound through steel plates immersed in water'. J.Acoust.Soc.Am. 23, pp.339-346, May 1951.
18. Kolsky, H. op.cit. 'p.27.

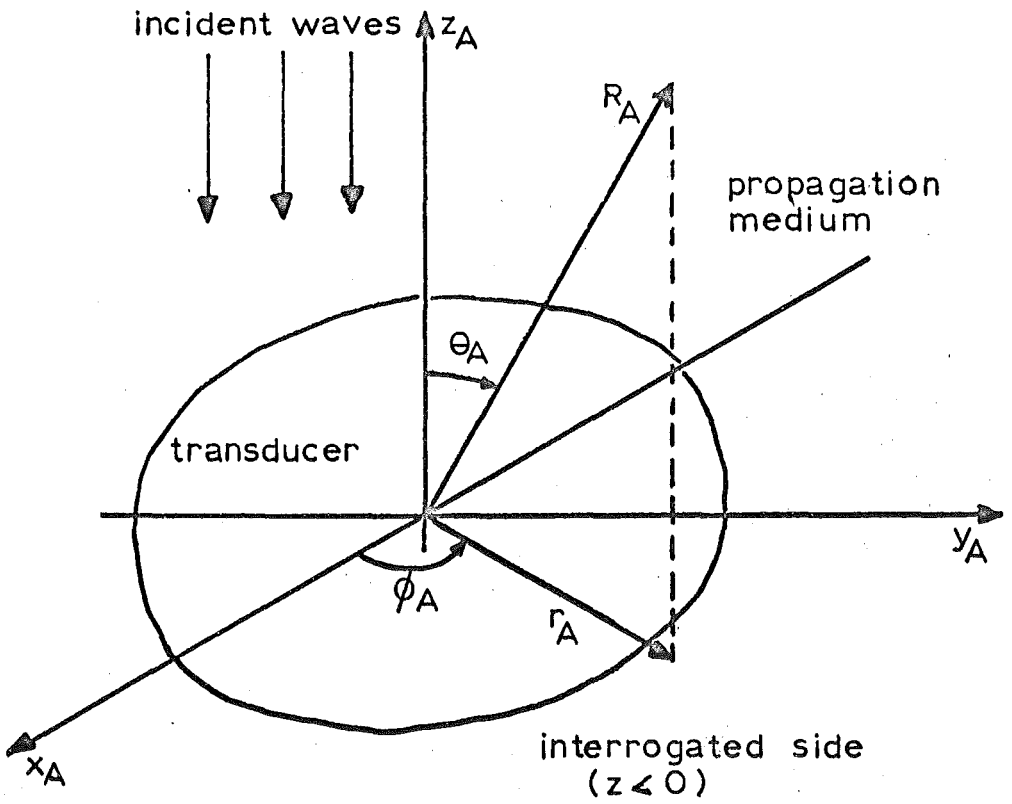

(a) View from incident wave side ('mechanical side')

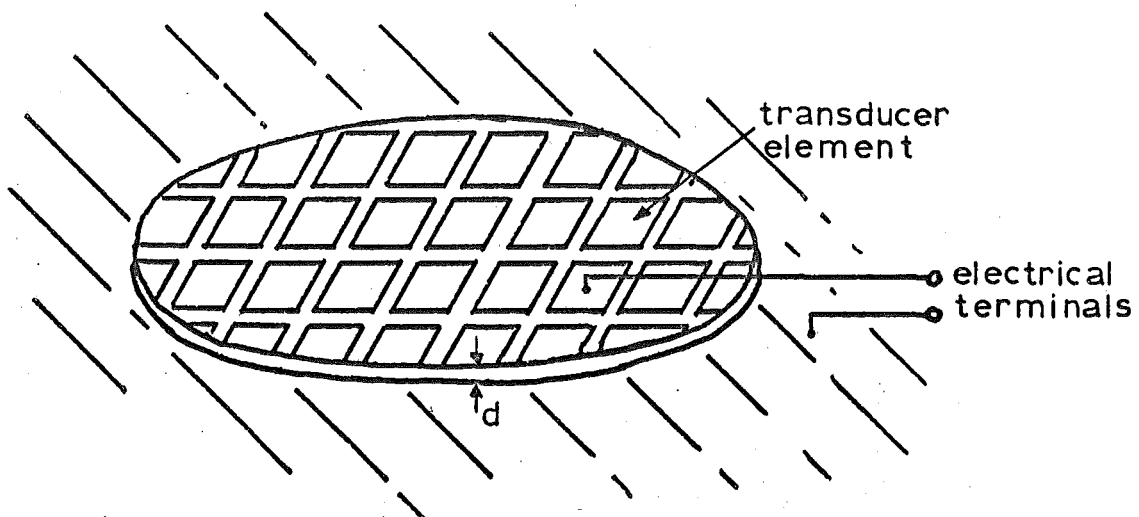

(b) 'electrical side'

FIG. 4.1: Receiving transducer

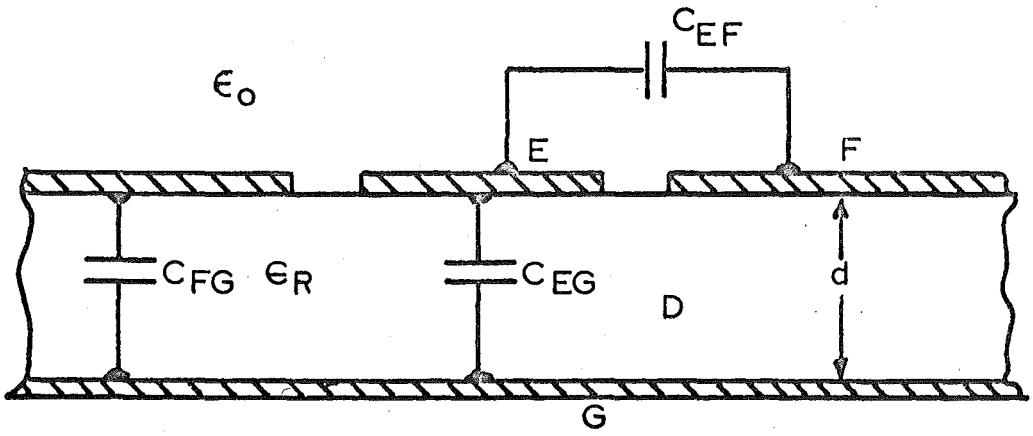

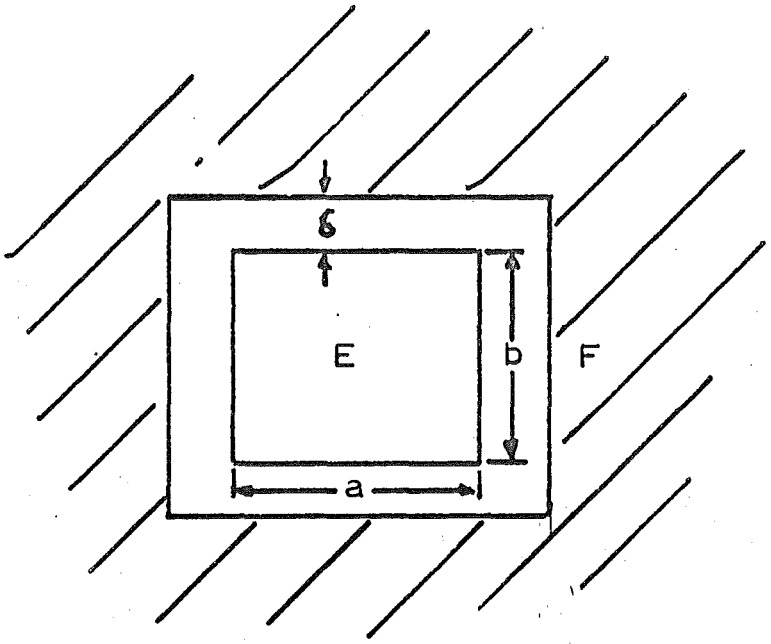

FIG.4.2: Capacitances in transducer array

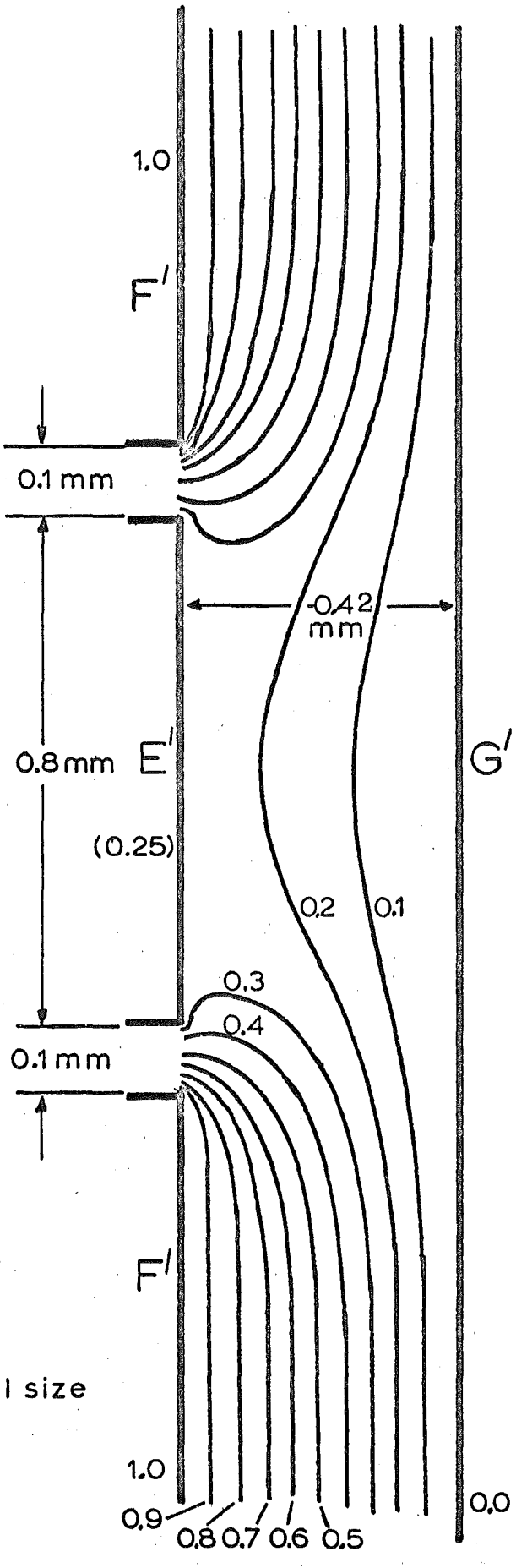

FIG.4.3: Field plot for $\epsilon_R \gg 1$

Scale: 100 times full size

FIG. 4.4(a): (reduced δ)

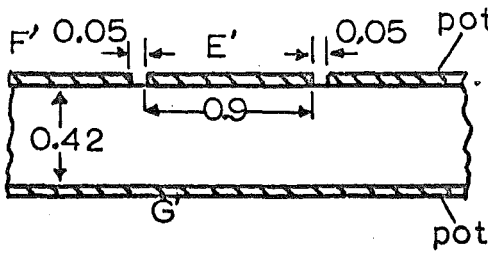

potential of E' = 0.295

FIG. 4.4 (b): (reduced a)

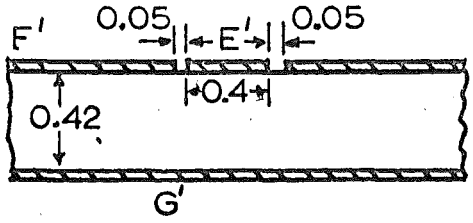

potential of E' = 0.45

FIG. 4.4(c): (notched ceramic)

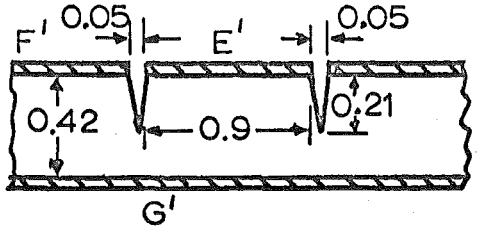

potential of E' = 0.065

FIG. 4.4(d): (thin transducer)

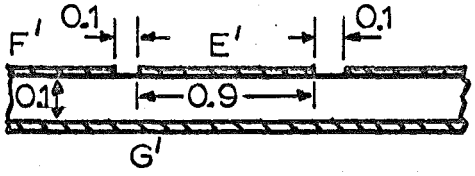

potential of E' = 0.032

FIG. 4.4: Effect of transducer electrode arrangements (all dimensions in millimetres)

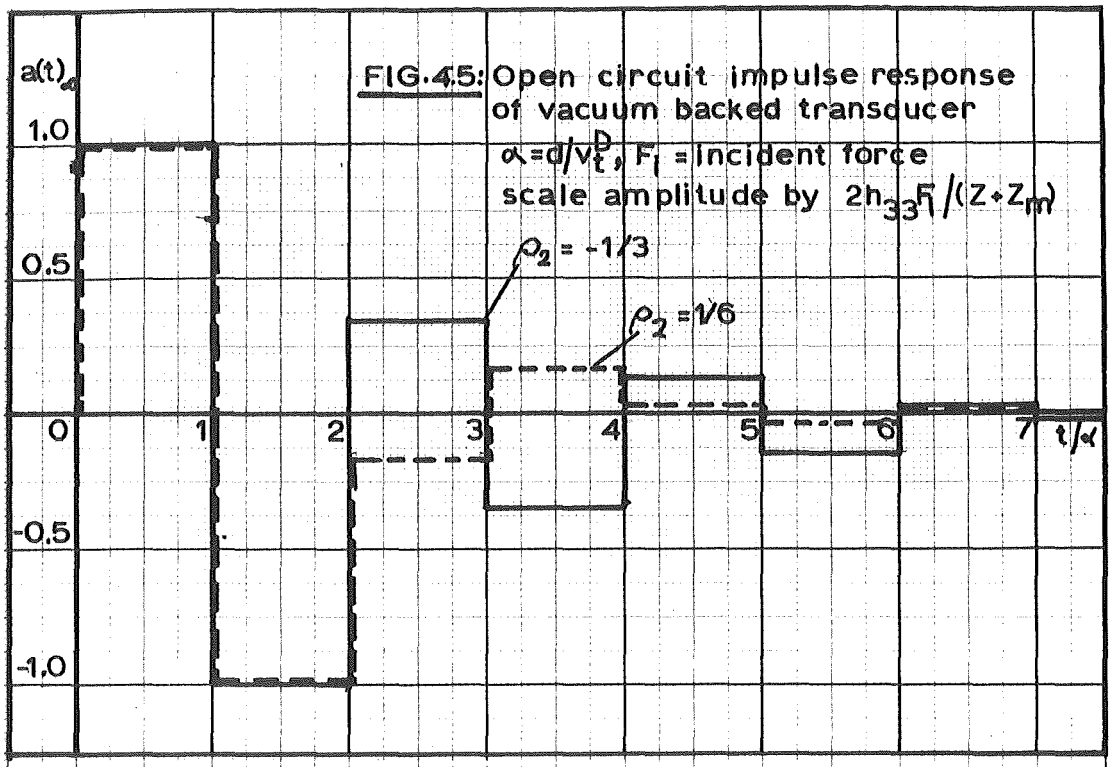

FIG.4.5: Open circuit impulse response of vacuum backed transducer
$\alpha = d/v_t^p$, F_i = incident force
scale amplitude by $2h_{33}F_i/(Z+Z_m)$

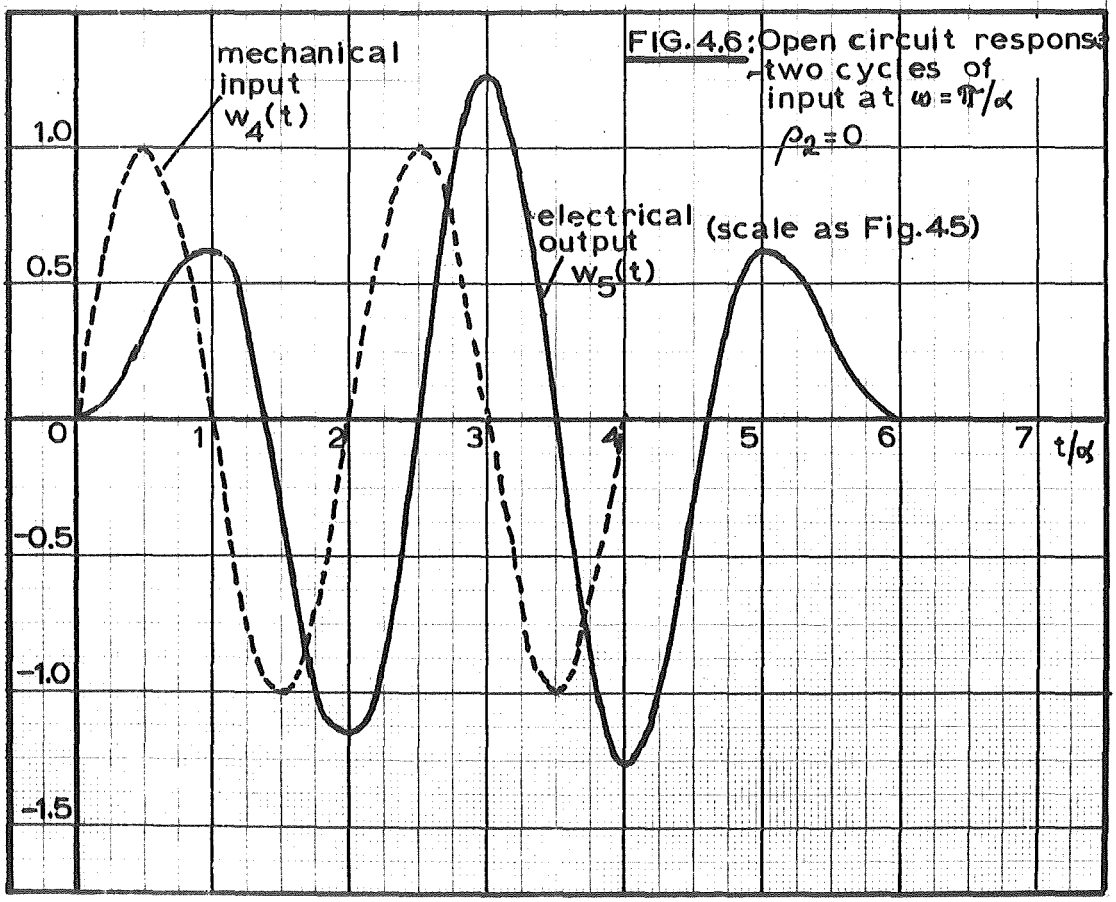

FIG.4.6: Open circuit response two cycles of input at $\omega = \pi/\alpha$
$\rho_2 = 0$

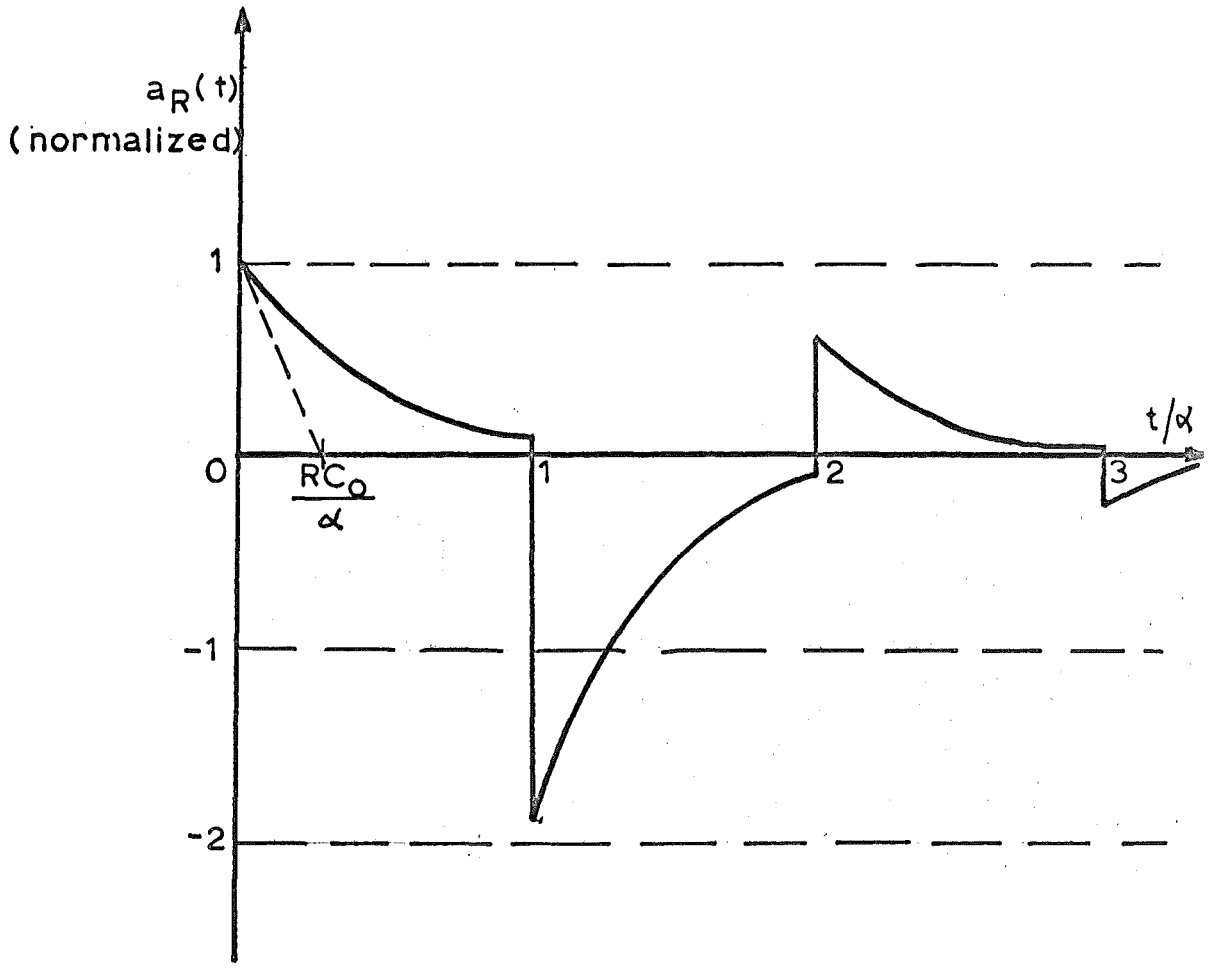

FIG. 4.7: Impulse response of loaded transducer

$\rho_2 \approx 1/3$

$RC_0 = 1/3\alpha$

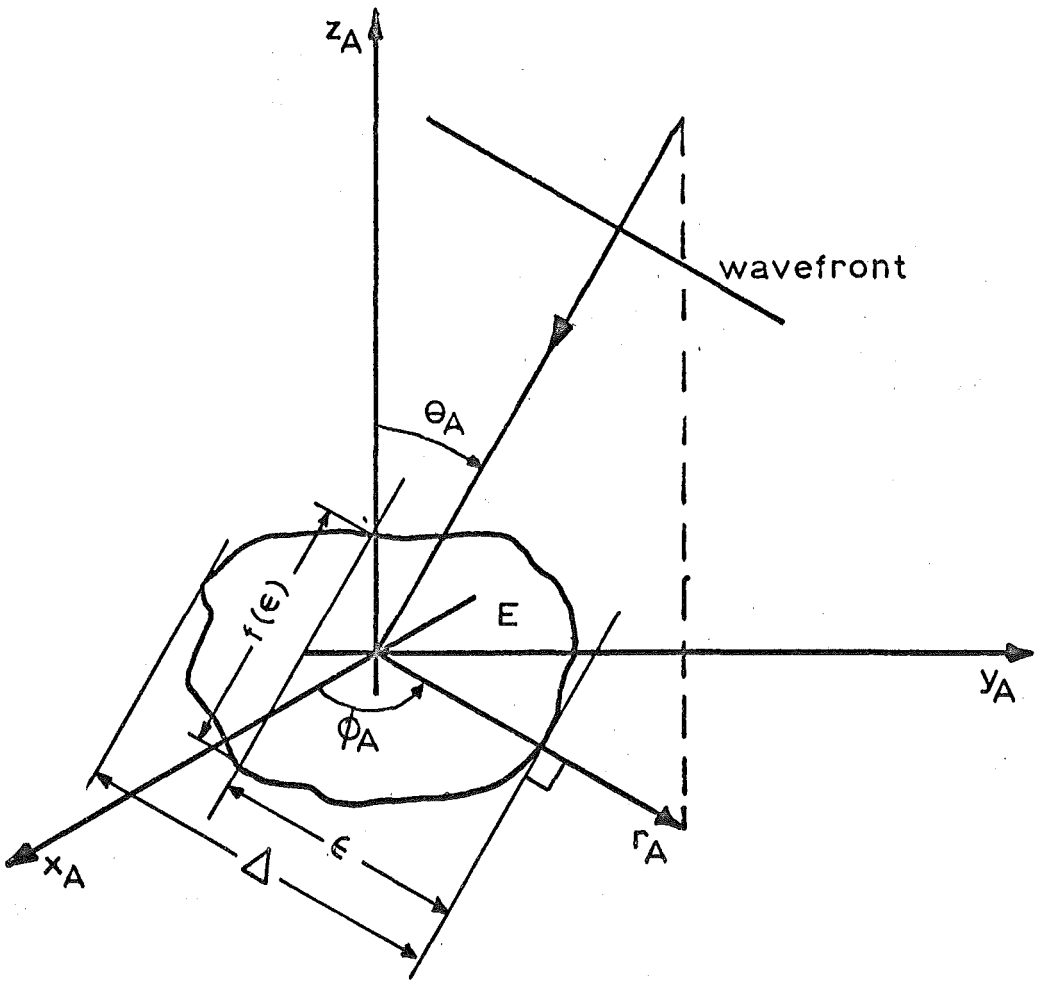

FIG.4.8: Geometry for transducer element

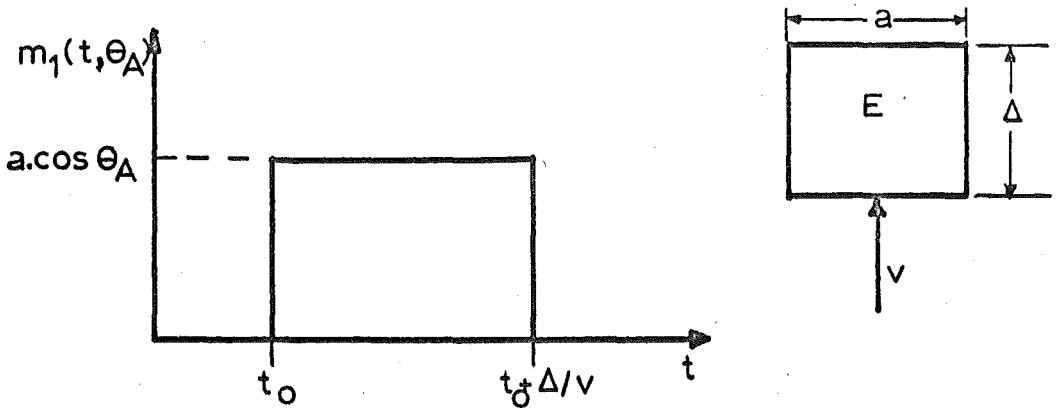

FIG.4.9(a). Rectangular element.

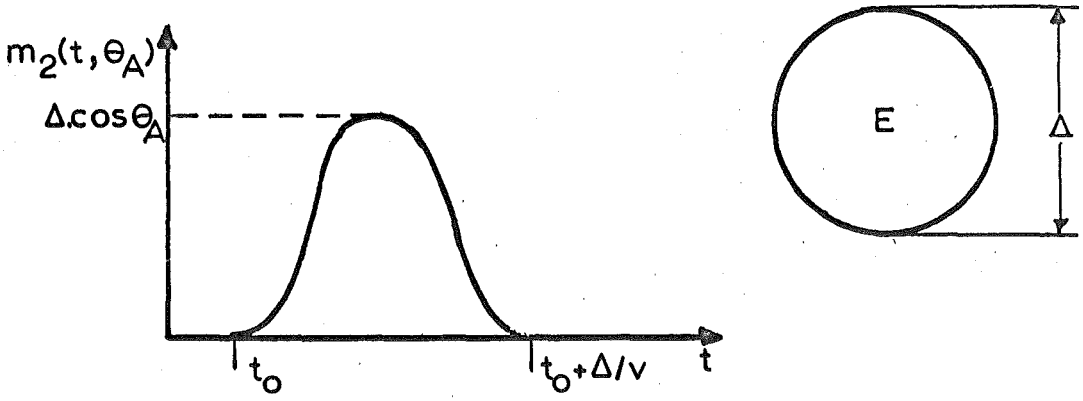

FIG.4.9(b). Circular element.

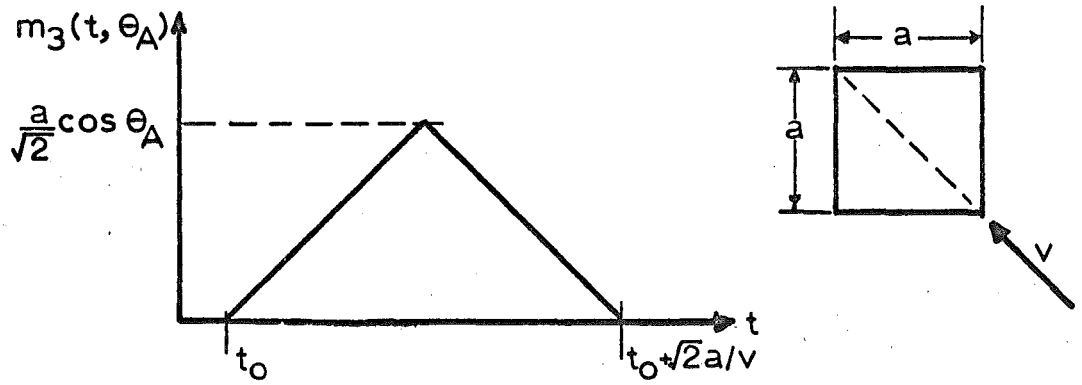

FIG.4.9(c). Square element on diagonal

FIG.4.9: Mechanical input to transducer elements with inclined incident wave.

CHAPTER 5.

INFORMATION PROCESSING IN THE IMAGING SYSTEM

PART I: GENERAL RELATIONSHIPS

5.1. INTRODUCTION.

This and the succeeding chapter establish a representation of an arbitrary acoustic field over an aperture on the surface of a volume and consider how this representation may be manipulated to determine the acoustic field within the volume. To a greater or lesser extent this field represents the back-scattering from objects within the volume, that is, it is an image of the objects in so far as the illuminating radiation is capable of revealing them.

In the present chapter we consider the general relations between the signal distribution over a plane in (or on the boundary of) the field and the volume field regarded as the superposition of an appropriate set of plane waves. In order to determine the actual field at any point within the material it is necessary to summate the contributions from each member of the plane wave set. The technique for this is examined and then we consider an alternative, equivalent method of analysis of the measured field and synthesis of the volume field in terms of spherical waves. The alternative operations are analogous to the calculation of a filter response by transformation of the input function into the frequency domain followed by multiplication with the filter transfer function then inverse transformation back

to the time domain; and convolution of the input function with the filter impulse response respectively. The relative limitations and convenience of these two approaches are discussed.

As the previous chapter has shown, practical transducers are frequency selective devices. Consequently it is necessary to consider the degradation caused by sensing the field through such a transducer. Also, a real transducer can interrogate only a finite area of the field and does this in a sampled rather than continuous manner. Even then practical restrictions may force rejections of a large number of the spatial samples (1.3).

One further operation on the signals remains - sampling and recording of the time waveform from each transducer element. This introduces further errors into the record. Consideration of the effects of these approximations and of random noise and reverberation is postponed to the second and third sections of this analysis (Chapters 6 and 7). The present chapter concludes with a brief discussion of the adequacy of the analytical approach used here and considers the approximation involved in considering only longitudinal waves in a solid.

5.2. THE PLANE WAVE REPRESENTATION OF AN APERTURE FIELD.

The development in this section is largely based on the work by Clemmow[1] dealing with the electromagnetic case. His equations consider the complete vector form of the electromagnetic wave equation, in the present acoustic case they are analogous to the

shear wave components. Here however we will be solely concerned with the longitudinal wave propagation and considerations of polarization do not arise.* In the analysis below the form of equations taken is appropriate to a receiving situation and consequently the plane waves are progressing towards the measurement plane and spherical waves converging onto 'sinks' in the plane. This is mentioned to avoid any confusion with other treatments[2,3,4] where the reciprocal problem of synthesising a suitable transmitter distribution to produce a specified spatial field is usually taken.

5.2.1. The general plane wave.

It will be recalled from Chapter 3 that the total particle displacement may, within a source free region, in a general case be expressed as a function of scalar and vector potentials, viz.;

$$\tilde{u} = \nabla\Psi + \nabla \times \tilde{\Pi} \qquad .. 5.1$$

with each of these potential functions individually satisfying the equation of wave motion. Here we confine attention to the scalar component only. This produces a plane wave solution which was previously expressed (Equation 3.17) in a form equivalent to (in part);

$$\tilde{u} = \hat{a}\, u_o\, e^{-j\omega_o t} e^{-jk_o \hat{a} \cdot \tilde{r}} \qquad .. 5.2$$

where $\tilde{r} = (x,y,z)$

$k_o = \omega_o/c$ ($c \equiv c_{1,1}$ of Equation 3.17).

---

* Note however that simple fluid media acoustic relationships cannot be used, in particular the concept of 'pressure' has no simple meaning in a rigid body.

The zero subscript in k_o and ω_o implies the values in a monochromatic wave case, all other unnecessary subscripts have been dropped, and from here on the temporal variation will be implicit. From Clemmow[5] the wave equation is satisfied only for;

$$\hat{a}^2 = 1 \qquad .. 5.3$$

If $\hat{a}$ is real then its components are simply direction cosines as explicitly displayed in Equation 3.17. However 5.3 may still be satisfied for complex $\hat{a}$ so in general we will take $\hat{a}$ to be;

$$\hat{a} = \hat{a}_r + j\hat{a}_i \qquad .. 5.4$$

where $\hat{a}_r$ and $\hat{a}_i$ are real and satisfy,

$$\hat{a}_r^2 - \hat{a}_i^2 = 1 \qquad .. 5.5(a)$$

$$\hat{a}_r \cdot \hat{a}_i = 0 \qquad .. 5.5(b)$$

that is, the components are orthogonal. Let a set of Cartesian axes, x and y, lie in the directions of $\hat{a}_r$ and $\hat{a}_i$ respectively. Then $\hat{a}$ may be expressed as;

$$\hat{a} = (\cosh\beta, -j\sinh\beta, 0) \qquad .. 5.6$$

where β is real and arbitrary.*

Hence;

$$\tilde{u} = (\cosh\beta, -j\sinh\beta, 0)u_o e^{-k_o y \sinh\beta} \cdot e^{-jk_o x\cosh\beta} \qquad .. 5.7$$

For $\beta = 0$ this is simply;

$$\tilde{u} = (1,0,0)u_o e^{-jk_o x} \qquad .. 5.8$$

the equation of a simple plane wave propagating in the positive x direction.

---

* The introduction of the parameter β is largely a mathematical convenience in allowing separation of the phase and amplitude conditions of the waves.

With $\beta>0$ the lines of equal phase (x = constant) are at right angles to the lines of equal amplitude (y = constant) and the speed of phase propagation for these inhomogenous waves is $c/\cosh\beta$ in the positive x direction. $\beta<0$ corresponds to phase propagation in the negative direction.

For $y>0$ the amplitude of the wave decays with increasing y ($\beta>0$) but if the x,y plane taken is regarded as being within an unbounded medium then this amplitude grows continuously with distance in the -y direction. (In order to maintain consistent solutions only the decaying side must be taken in each half space - see the next section). Normally however we shall be concerned with a situation in which the measurement surface is the boundary of the space and in this case the solutions for $\beta\neq0$ correspond to surface waves on the material. Whether or not it is necessary to consider the contribution of these waves to the total field depends on how far into the medium one wishes to image the object distribution. If the imaged region is far enough away from the surface then they may be largely neglected.

If the medium is lossy the situation becomes more complex and the equi-phase and equi-amplitude lines are in general no longer at right angles for $\beta\neq0$. For the particular case $\beta=0$ the form is simply that of Equation 5.8 multiplied by an additional exponential factor representing the decay of the wave in the direction of propagation. However in this chapter the effect of losses will not be considered.

5.2.2. Relation of plane waves to field in a plane.

Returning to the general plane wave expression (Equation 5.2) we consider the situation where $\hat{a}$ is arbitrarily inclined to the z=0 plane. Then over z=0 $\tilde{u}$ is given by;

$$\tilde{u} = (l,m,n)u_o e^{-jk_o(lx + my)} \qquad .. 5.9$$

where l,m,n are the direction cosines of $\hat{a}$ with the restraint $l^2 + m^2 + n^2 = 1$. Specification of any two of these cosines is sufficient to define the direction of the wave. The amplitude and any initial phase factor is contained in the scalar u_o which we will describe as the 'spectrum function'.

At any point x,y we will suppose that the total displacement may be formed from a superposition of such terms. It will be recognised that if we consider variation in the z=0 plane distribution along a particular line due to any one of the $\tilde{u}$ terms then this is sinusoidal with a wavelength depending on l and m. Thus the condition that a superposition of plane waves represents the total field across a plane is that the distribution be representable as a Fourier integral. With the exponential form of wave equation solution each (l,m) pair refers to a pair of waves incident from opposite half spaces onto the plane and each contributing one half of the total displacement. (The situation is similar to the double sided spectrum representation of temporal waveforms).

If we now write the total displacement at any x,y as $\tilde{U}(x,y)$ then;

$$\tilde{U}(x,y) = \int_{-\infty}^{\infty}\int \tilde{u}\, dl\, dm \qquad .. 5.10(a)$$

$$= \int_{-\infty}\int u_o(l,m).(l,m,n)e^{-jk_o(lx+my)}\, dl\, dm \qquad .. 5.10(b)$$

(The infinite limits imply the inclusion of inhomogenous waves in the solution).

Of particular concern is the normal component of $\tilde{U}(x,y)$ as this is the displacement to which a transducer placed in the plane will respond. Hence;

$$U_n(x,y) = \int_{-\infty}^{\infty}\int u_o(l,m).n.e^{-jk_o(lx+my)}\, dl\, dm \qquad .. 5.11$$

Before considering the behaviour of the integral between the infinite limits it may be helpful to write l,m and n explicitly in terms of angles. With the normal spherical polar set l, m and n appear as;

$$l = \sin\theta\cos\phi \qquad .. 5.12(a)$$

$$m = \sin\theta\sin\phi \qquad .. 5.12(b)$$

$$n = \cos\theta \qquad .. 5.12(c)$$

The region of 'physical' angles is bounded by $l^2 + m^2 \leqq 1$. Waves satisfying this condition (corresponding to $\sin\theta \leqq 1$) are the normal 'homogenous' waves while those with $l^2 + m^2 > 1$ are the inhomogenous waves decaying away from z=0.

Correct physical behaviour at large distances from the plane demands that only the decaying set of waves obtain in each half space. (The requirement that $U_n(x,y)$ be Fourier transformable

prevents any infinite discontinuities and hence any infinite contributions to the field).

Waves in positive half space are represented by n less than zero (remember that we are considering propagation towards the aperture) and those in negative half space by n>0. l=m=0 or n=±1 corresponds to normal incidence - the 'D.C.' component in the temporal analogy.

If the distribution $U_n(x,y)$ is known and $u_o(l,m)$ is required then applying the inverse transform operation;

$$u_o(l,m)\sqrt{1-l^2-m^2} = \frac{k_o^2}{4\pi^2}\iint_{-\infty}^{\infty} U_n(x,y)e^{jk_o(lx+my)}\,dx\,dy \qquad .. 5.13$$

($\sqrt{1-l^2-m^2}$ is of course cosθ or n).

One may note in passing that the complete specification of an electromagnetic field requires two 'spectrum functions' corresponding to the polarizations associated with the x and y components of the aperture distribution (current density). A complete description of the elastic wave case would similarly require additional functions to account for the shear waves and measurement of the displacements parallel to the surface.

Returning to Equation 5.9, due to one plane wave at any value of z, we have for the field, (with correct account being taken for inhomogenous waves of the particular half-space);

$$\tilde{u} = {}_{\#}(l,m,\sqrt{1-l^2-m^2})u_o(l,m)e^{-jk_o(lx+my\,\mp\,\sqrt{1-l^2-m^2}\,.z)} \qquad .. 5.14$$

The upper/lower signs applying for z>0 / z<0, and for the

superposition of these waves at any point (x,y,z),

$$\tilde{U}(x,y,z) = \int_{-\infty}^{\infty}\int (l,m,\sqrt{1-l^2-m^2})\,u_o(l,m)\,e^{-jk_o(lx+my)} \cdot e^{\pm jk_o\sqrt{1-l^2-m^2}\cdot z}\,dl\,dm \qquad .. 5.15(a)$$

or taking the normal (z directed) component;

$$U_z(x,y,z) = \int_{-\infty}^{\infty}\int \left\{\sqrt{1-l^2-m^2}\cdot u_o(l,m)\right\} e^{-jk_o(lx+my)} \cdot e^{\pm jk_o\sqrt{1-l^2-m^2}\cdot z}\,dl\,dm \qquad .. 5.15(b)$$

But this is just the Fourier transform of the measured function, $U_n(x,y)$, multiplied by a phase factor $e^{\pm jk_o\sqrt{1-l^2-m^2}\cdot z}$ and transformed back to the original variable domain. The exponential factor then may be regarded as the spatial 'transfer function'* for the section of material between the measurement plane and a parallel plane situated a distance z away.

Substituting for $u_o(l,m)$ from Equation 5.13 gives,

$$\tilde{U}(x,y,z) = \int_{-\infty}^{\infty}\int (l,m,\sqrt{1-l^2-m^2}) \left\{\frac{k_o^2}{4\pi^2}\int_{-\infty}^{\infty}\int U_n(x_A,y_A)\,e^{jk_o(lx_A+my_A)} \cdot dx_A\,dy_A\right\} \frac{e^{-jk_o(lx+my\ \mp\sqrt{1-l^2-m^2})\cdot z}}{\sqrt{1-l^2-m^2}}\,dl\,dm \qquad .. 5.16$$

Where x_A and y_A are the corrdinates in the measurement plane. With some rearrangement this gives;

---

* The term usually applied is 'propagation function'.[17]

$$\tilde{U}(x,y,z) = \frac{k_o^2}{4\pi^2}\iint_{-\infty}^{\infty} U_n(x_A,y_A)\left\{\iint_{-\infty}^{\infty}(l,m,\sqrt{1-l^2-m^2})\cdot \frac{e^{-jk_o(l(x-x_A)+m(y-y_A)\mp\sqrt{1-l^2-m^2}\cdot z)}}{\sqrt{1-l^2-m^2}}\cdot dl\,dm\right\} dx_A dy_A \quad \text{.. 5.17}$$

This may now be reduced to a scalar form by re-introducing a potential function describing $\tilde{U}(x,y,z)$ to give;

$$\Psi(x,y,z) = \frac{k_o^2}{4\pi^2}\iint_{-\infty}^{\infty} U_n(x_A,y_A)\cdot\left\{\iint_{-\infty}^{\infty}\frac{e^{-jk_o(lX+mY\mp\sqrt{1-l^2-m^2}\cdot z)}}{\sqrt{1-l^2-m^2}}\cdot dl\,dm\right\} dx_A dy_A \quad \text{.. 5.18}$$

with $X = x - x_A$

$Y = y - y_A$

so that,

$$\frac{\partial}{\partial x}\Psi(x,y,z) = -jk_o U_x(x,y,z) \text{ etc.} \quad \text{.. 5.19}$$

The inner integral has a standard solution[6] which is;

$$\iint_{-\infty}^{\infty}\frac{e^{-jk_o(lX+mY\mp\sqrt{1-l^2-m^2}\cdot z)}}{\sqrt{1-l^2-m^2}}\,dl\cdot dm = 2\pi j\frac{e^{jk_oR}}{k_oR} \quad \text{.. 5.20}$$

where $R = X^2+Y^2+z^2$ or $(x-x_A)^2+(y-y_A)^2+z^2$ - i.e., R is the distance between the measurement plane point and the field point.

Thus we have;

$$\Psi(x,y,z) = \frac{k_o^2}{4\pi^2}\iint_{-\infty}^{\infty} U_n(x_A,y_A)\cdot\frac{2\pi j\,e^{jk_oR}}{k_oR}\cdot dx_A dy_A \quad \text{.. 5.21}$$

If in particular we now consider the z directed component of displacement;

$$U_z(x,y,z) = \frac{k_o^2}{4\pi^2} \iint_{-\infty}^{\infty} U_n(x_A,y_A) \cdot \frac{2\pi j}{k_o(-jk_o)} \cdot \frac{\partial}{\partial z}\left(\frac{e^{jk_oR}}{R}\right) dx_A dy_A \qquad .. 5.22$$

$$\text{Now } \frac{\partial}{\partial z}\left(\frac{e^{jk_oR}}{R}\right) = jk_o \frac{z}{R} \cdot \left(\frac{e^{jk_oR}}{R}\right)\left(1 - \frac{1}{jk_oR}\right) \qquad .. 5.23$$

$\frac{z}{R}$ is the cosine of the angle between the normal at the point (x_A,y_A) and the line joining (x_A,y_A,o) to $x,y,z)$. Denoting this as $\cos\gamma$ we have;

$$U_z(x,y,z) = \frac{k_o^2}{4\pi^2} \iint_{-\infty}^{\infty} U_n(x_A,y_A)\cos\gamma \cdot \left(-2\pi j \frac{e^{jk_oR}}{k_oR}\right)\left(1 - \frac{1}{jk_oR}\right) \cdot$$

$$\cdot \; dx_A dy_A \qquad .. 5.24(a)$$

collecting terms;

$$U_z(x,y,z) = \frac{-1}{2\pi} \iint_{-\infty}^{\infty} U_n(x_A,y_A)\cos\gamma \frac{e^{jk_oR}}{R} \cdot \left(jk_o - \frac{1}{R}\right) \cdot$$

$$\cdot \; dx_A dy_A \qquad .. 5.24(b)$$

This form (which closely resembles the Kirchoff diffraction formulation[4]) may be interpreted by writing;

$$F_z(x-x_A,y-y_A) = \frac{-1}{2\pi} \cos\gamma \frac{e^{jk_oR}}{R}\left(jk_o - \frac{1}{R}\right) \qquad .. 5.25$$

giving;

$$U_z(x,y,z) = \iint_{-\infty}^{\infty} U_n(x_A,y_A) \cdot F_z(x-x_A,y-y_A) \cdot dx_A dy_A \qquad .. 5.26$$

The equation is now displayed as a two dimensional convolution between U_n and F_z, and F_z may be defined as the spatial 'impulse response' of the section of material between the plane z=0 and a point in the field. The field is now described as a superposition of spherical waves converging on the measurement plane. This concept has been discussed by Sherman[7] who develops the idea as a complete integral transform technique for diffraction problems. A further application is described in Reference 8 and Devaney and Baron[9] consider convolutive manipulation of a hologram (i.e., a record of the field in one plane) to obtain corresponding holograms for the field examined at other planes.

In general one is not concerned with imaging of objects very close to the surface of the material nor is it practical to do so with ultrasonic apparatus because of the electrical leakage and surface wave interference from the transmitter. For example, if the transmitter is located centrally in a 50mm diameter receiving transducer then with a Rayleigh wave velocity of say 2800 m/S, a dead period of 9 μS must be allowed before reception can commence. Thus the least distance into the material from which a clean signal is possible is about 25-30mm. For $k_oR>6$ the $jk_o\left(1 - \frac{1}{jk_oR}\right)$ term differs from jk_o in magnitude by less than 2% and in argument by less than 10^o. Thus under these conditions the bracketed term may reasonably be neglected. If the minimum value of R is 25mm and $k_oR>6$ then the wavelength must not exceed

approximately 25mm, corresponding in aluminium to a frequency of 240 kHz.

Thus, with the above constraints;

$$U_z(x,y,z) = \frac{-1}{2\pi}\int_{-\infty}^{\infty}\int jk_o U_n(x_A,y_A).\cos\gamma.\frac{e^{jk_o R}}{R}\,.\,dx_A dy_A \qquad .. 5.27$$

In early work on the development of an image construction scheme an attempt was made to maintain the greatest possible generality in permissible geometry and consequently the computer program was constructed to use the relation 5.27 in discrete form. It is very little extra complication to allow the measurement and image surfaces to be of an arbitrary shape when an operation such as that to form R is involved. On the other hand, the operation of Equation 5.15 loses its Fourier transform character if z is allowed to vary with x and y. The two approaches require an equivalent number of computing operations in the general case of arbitrary geometry but if restriction to imaging planes parallel to a flat measurement surface is tolerable then the Fourier transform approach is much to be preferred. A version of the 'fast' algorithm[10] is now readily available in the standard FORTRAN language to handle a complete three dimensional complex array.

The numerical details are discussed later (10.5) but one may note here that the Fourier transform technique requires sufficient core store in the computer to hold simultaneously all the elements of a complex array of dimensionality comparable to

that of the physical array of receiving elements. On the other hand, the direct convolution technique may be programmed to employ a very small fast storage provided back-up storage is available. This factor forced the continued employment of the very slow convolution method throughout the period of this project.

5.3. WIDEBAND SIGNALS.

Returning to Equation 5.2, a complete solution to the scalar wave equation may be expressed in the form;

$$\Psi = Ae^{-jk(\hat{a}.\tilde{r})+j\omega t} \quad .. 5.28$$

or, $$\Psi = Ae^{-j(klx + kmy + knz - \omega t)} \quad .. 5.29$$

If we now define a modified set of 'direction cosines' as;

$$\begin{aligned} \xi &= kl \\ \eta &= km \\ \zeta &= kn \end{aligned} \quad .. 5.30$$

and, remembering that $k=\omega/c$, express the time variable in a scaled form as (ct) then;

$$\Psi = Ae^{-j(\xi x + \eta y + \zeta z - kct)} \quad .. 5.31$$

(A = constant)

with the constraint;

$$\xi^2 + \eta^2 + \zeta^2 = k^2 \quad .. 5.32$$

Similarly to before inhomogenous waves are characterised by,

$$\xi^2 + \eta^2 > k^2$$

Solving for the components of $\tilde{u}$,

$$\tilde{u} = \nabla\Psi = (-j\xi,-j\eta,-j\zeta)Ae^{-j(\xi x + \eta y + \zeta z - kct)} \quad .. 5.33(a)$$

$$= (\xi,\eta,\zeta).(-jA).e^{-j(\xi x + \eta y + \zeta z)} \quad .. 5.33(b)$$

and identifying $-jA$ with u_o the normal component of displacement over the z=0 plane varies as;

$$U_n(x,y,ct) = \iiint_{-\infty}^{\infty} \zeta . u_o(\xi,\eta,k) e^{-j(\xi x + \eta y - kct)} . \, d\xi \, d\eta \, dk$$

$$= \iiint_{-\infty}^{\infty} \sqrt{k^2 - \xi^2 - \eta^2} . u_o(\xi,\eta,k) e^{-j(\xi x + \eta y - kct)} . \, d\xi \, d\eta \, dk$$

(cf. Equation 5.11). .. 5.34

Conversely, (cf. Equation 5.13)

$$u_o(\xi,\eta,k)\sqrt{k^2 - \xi^2 - \eta^2} = \frac{1}{8\pi^3} \iiint_{-\infty}^{\infty} U_n(x,y,ct) . e^{j(\xi x + \eta y - kct)} .$$

$$. \, dx \, dy \, d(ct) \quad .. 5.35$$

and for the 'normal' or z directed component at any point in space;

$$U_z(x,y,z,ct) = \iiint_{-\infty}^{\infty} \sqrt{k^2 - \xi^2 - \eta^2} . u_o(\xi,\eta,k) e^{-j(\xi x + \eta y - kct)} .$$

$$. \, e^{\pm j\sqrt{k^2 - \xi^2 - \eta^2} . z} . d\xi \, d\eta \, dk \quad .. 5.36$$

Once again we have the field expressed as the Fourier transform of the aperture function multiplied by a spatial transfer function and transformed back to the 'real space' domain. Corresponding to Equation 5.24 we get;

$$\Psi(x,y,z,ct) = \frac{1}{8\pi^3}\iiint_{-\infty}^{\infty} U_n(x_A,y_A,ct_A).\frac{4\pi^2 j}{R}.\delta(R+c[t-t_A]) \cdot$$

$$\cdot\ dx_A dy_A d(ct_A) \qquad .. 5.37$$

which expresses the field in an appropriate 'advanced potential' form[11] for the converging waves with time contained in a distance like term rather than the more usual case where distances are divided by the propagation velocity, and,

$$U_z(x,y,z,ct) = \frac{1}{8\pi^3}\iiint_{-\infty}^{\infty} U_n(x_A,y_A,ct_A).-4\pi^2.\frac{\partial}{\partial z}\left(\frac{\delta(R+c[t-t_A])}{R}\right).$$

$$\cdot\ dx_A dy_A d(ct_A) \qquad .. 5.38$$

Now,

$$\frac{\partial}{\partial z}\left(\frac{\delta(R+c[t-t_A])}{R}\right) = \cos\gamma.\frac{1}{R}\left[\delta'(R') - \frac{\delta(R')}{R}\right] \qquad .. 5.39$$

where $\cos\gamma = z/R$ as before

$R = R+c[t-t_A]$

$\delta'(\ )$ is the unit doublet function.[12]

Thus;

$$U_z(x,y,z,ct) = \iiint_{-\infty}^{\infty} U_n(x_A,y_A,ct_A)\left\{-\frac{1}{2\pi}\frac{\cos\gamma}{R}\left[\delta'(R') - \frac{\delta(R')}{R}\right]\right\}.$$

$$\cdot\ dx_A dy_A d(ct_A) \qquad .. 5.40$$

The expression in brackets could analogously be described as the spatio-temporal impulse response of the section of material between the aperture plane and the field point.

By invoking the 'sifting' properties[13] of the impulse and doublet functions, viz;

$$\int_{-\infty}^{\infty} F(\alpha)\delta(\alpha-\beta)\,d\alpha = F(\beta) \qquad .. 5.41(a)$$

$$\int_{-\infty}^{\infty} F(\alpha)\delta'(\alpha-\beta)\,d\alpha = -F'(\beta) \qquad .. 5.41(b)$$

and noting that $\delta'(-\alpha) = -\delta'(\alpha)$ .. 5.41(c)

Equation 5.40 may be reduced to;

$$U_z(x,y,z,ct) = \frac{-1}{2\pi}\iint_{-\infty}^{\infty} \frac{\cos\gamma}{R}\left\{ \dot{U}_n(x_A,y_A,ct+R) - \frac{U_n(x_A,y_A,ct+R)}{R}\right\} \cdot dx_Z dy_A \qquad .. 5.42$$

where $\dot{U}_n(x_A,y_A,ct+R) = \frac{\partial}{\partial(ct_A)}\left(U_n(x_A,y_A,ct_A)\right)\Big|_{R+ct}$ .. 5.43,

$(F(\beta))\big|_{\alpha}$ means that the function is to be evaluated at $\beta=\alpha$) that is $\dot{U}_n$ is essentially the normal component of measurement plane particle velocity. This was inherent in Equation 5.24(b) as for a steady sinusoid the time derivative is given simply by multiplying by $j\omega$, ω there being contained in k_o.

Again if R is large and/or the particle velocity magnitude sufficiently high compared with displacement amplitude (i.e., the frequency high) the second term in the braces may be neglected to give;

$$U_z(x,y,z,ct) = \frac{-1}{2\pi}\iint_{-\infty}^{\infty} \dot{U}_n(x_A,y_A,ct+R).\frac{\cos\gamma}{R}.dx_A dy_A \qquad .. 5.44$$

(cf. Equation 5.27)

and the z directed displacement component is seen to be expressible as a summation of the aperture measurements weighted in amplitude according to their distances and inclinations to the field point, and taken at a time advanced by the travel time from the field point to the aperture point. The field may be visualized as a superposition of convergent, spherical, impulsive wavefronts propagating towards the measurement plane.

Where computer limitations inhibit simultaneous storage of the complete three dimensional set of measurements $U_n(x_A,y_A,ct)$ it is convenient to evaluate the field in terms of a superposition of solutions for each value of k taken separately. This requires a preliminary Fourier analysis of the time record at each (x_A,y_A) but this is a one dimensional operation. The field may be obtained in terms of time variation by final inverse transformation of the k spectrum at each (x,y,z) but since the final image can only be displayed as a single value for each point it will normally be of no consequence whether the field is in frequency or time terms, only a measure of the total energy being required.

Formalizing this we define a function $U_{n,k}(x,y)$ by;

$$U_{n,k}(x,y) = \frac{1}{2\pi}\int_{-\infty}^{\infty} U_n(x,y,ct)e^{-jkct}d(ct) \qquad .. 5.45$$

and inserting the relation (Equation 5.34) for U_n;

$$U_{n,k}(x,y) = \iint_{-\infty}^{\infty} \left\{ \sqrt{k^2-\xi^2-\eta^2} \cdot u_o(\xi,\eta,k) \right\} e^{-j(\xi x + \eta y)} \cdot$$

$$\cdot \; d\xi \cdot d\eta \qquad .. \; 5.46$$

and similarly,

$$U_{z,k}(x,y,z) = \iint_{-\infty}^{\infty} \left\{ \sqrt{k^2-\xi^2-\eta^2} \cdot u_o(\xi,\eta,k) \right\} e^{-j(\xi x + \eta y)} \cdot$$

$$\cdot \; e^{\pm j\sqrt{k^2-\xi^2-\eta^2} \cdot z} \cdot d\xi \cdot d\eta \qquad .. \; 5.47$$

5.4. DISCUSSION OF THE SOLUTION.

It will be noted that solutions for the field in terms of the measurements over a plane in it are expressed as the z directed component only. However as shown, for example, by Equation 5.15(a) (similar expressions may be constructed for the other forms of field synthesis) measurement of just the normal field component is sufficient to permit complete solution for the field vector. The difficulty is of course that the x and y components do not fit exactly into the Fourier transform formulation. For example to obtain $U_x(x,y,z)$ the transform of the measured function must be modified by a factor $1/\sqrt{1-l^2-m^2}$ before multiplication with the spatial transfer function and inverse transformation*. In principle there is no reason why

---

* Except at angles of incidence where $l^2+m^2 \approx 1$ and $1/\sqrt{1-l^2-m^2}$ is a very large factor, allowing extreme magnification of small errors in the measured function.

this could not be done but it would involve approximately triplication of this part of the computing effort.

Since unperturbed echoes cannot be obtained from very shallow objects and transmitter restrictions limit the range of incident radiation directions it follows that in nearly all practical situations the field reconstruction will be possible only for a restricted cone around the normal to the receiving transducer (i.e., for a range of $l^2+m^2<1$). Consequently the z component will dominate the total displacement and measuring the field strength in terms of it alone is an adequate representation. No information is destroyed though and a complete field description is available within this cone at the expense of extra computing.

Although the discussion has been in terms of a set of measurements taken over a plane which may be arbitrarily located in the propagating medium, in a practical situation the measurements will actually be obtained from a boundary of the medium considered as an infinite half space. However the results are nevertheless valid to a good approximation. Consider a fluid medium. At a free boundary the condition of zero normal stress imposes equality of amplitudes on the incident and reflected waves. For normal incidence the boundary displacement must therefore be exactly double the particle displacement in the incident wave. At non-normal incidence the amplitude becomes $2.\cos\theta$ the incident amplitude, where θ is the angle to the normal (more generally $2.\sqrt{1-l^2-m^2}$. to allow for inhomogenous waves).

This doubling effect corresponds exactly to the effect of a second, conjugate set of waves propagating in the space behind the measuring surface and is analogous to the taking of a double or single sided frequency spectrum of a time waveform.* Thus with the restriction to longitudinal wave propagation only the solutions are exact. Either side of the boundary may be taken in the reconstruction. The calculated 'field' for the non-existent space behind the surface will exhibit identical behaviour to that in the actual space but in a spatially and temporally conjugate manner. That is the same field strengths will occur at the points $(-x,-y,-z)$ and (x,y,z) while the field is diverging from one side of the boundary and convergent on the other. The field patterns correspond to the rather unfortunately named 'real' and 'virtual' images of an optical system, respectively.

In a solid material, consideration of the longitudinal waves only represents an approximation that becomes less exact as the angle of incidence increases. Up to an incident angle of 60° (i.e., $l^2+m^2 \leqq 0.75$) the amplitudes of the normal components of the reflected waves sum to a value differing from that of the incident

---

* This must be distinguished from a similar statement made earlier in 5.2.2. In that case the fields on either side of the plane were, in general, independent and the double sided spectrum description applied to the representation of the waves from either side, each as the superposition of two conjugate sets. The conjugate set, while having a coordinate range indicating existence in the opposite half-space, is <u>not</u> part of the field representation in that region. Here the physical field exists only on one side of the measurement surface and similarly the conjugate field is a physical fiction, the true field in the space described by the conjugate field coordinates being zero.

wave normal component by less than 20%. (This result has already been mentioned in 3.5.3.3 from a slightly different view and may be readily demonstrated by construction on, for example, the curves given by Kolsky[5]). Thus for waves incident at angles up to 60^{o} the measured value is an accurate indication of the field to within 10%. For similar reasons the stress-velocity relationship at the transducer terminals fails beyond this angle (4.4).

As was seen in the previous chapter, real transducers do not generally correspond to the idealized device for measuring normal displacements implied above even at normal incidence. A vanishingly thin piezoelectric plate provides a very good approximation but for thicker transducers perfect reflection does not hold and something less than doubling of the incident amplitude will occur. This was accounted for in the derivation of the equivalent circuit model by the introduction of a reflection coefficient. (An interesting discussion of the behaviour of 'ideal' transducer devices in a sound field may be found in Reference 16). Also, the device is sensitive to particle velocity rather than displacement. This is easily accounted for. Consider Equation 5.34. The particle velocity is found by taking the differential with respect to time to give;

$$\frac{\partial}{\partial t} U_n(c,y,ct) = \iiint_{-\infty}^{\infty} \sqrt{k^2-\xi^2-\eta^2}\, u_o(\xi,\eta,k) \cdot jck \cdot e^{-j(\xi x + \eta y - kct)} \cdot d\xi\, d\eta\, dk \qquad .. 5.48$$

and carrying this through the successive transformations gives;

$$\frac{\partial}{\partial t} U_z(x,y,z,t) = \iiint_{-\infty}^{\infty} \left\{ \sqrt{k^2 - \xi^2 - \eta^2} \cdot u_o(\xi,\eta,k) \cdot jck \right\} \cdot$$

$$\cdot \; e^{-j(\xi x + \eta y - kct)} e^{\pm j\sqrt{k^2 - \xi^2 - \eta^2} \cdot z} \cdot$$

$$\cdot \; d\xi \, d\eta \, dk \qquad \cdot\cdot \; 5.49$$

Once again the field component is derived from the Fourier transform of the measured set. Estimation of the energy associated with a given field point requires evaluation of the particle velocity in any case so this is actually the most convenient form.

Having established the general field relationships it now remains to consider the effects of having only a portion of U_n available for measurement and the requirements for sampling this portion. This is treated in the next chapter.

REFERENCES FOR CHAPTER 5.

1. Clemmow, P.C. 'The plane wave spectrum representation of electromagnetic fields'. Pergamon, Oxford, 1966.
2. Woodward, P.M. 'A method of calculating the field over a plane aperture required to produce a given polar diagram'. J.IEE 93, Part IIIA, pp.1554-1558, 1946.
3. Woodward, P.M. and Lawson, J.D. 'The theoretical precision with which an arbitrary radiation pattern may be obtained from a source of finite size'. J.IEE 95, Part III, pp.363-370, 1948.
4. Booker, H.G. and Clemmow, P.C. 'The concept of an angular spectrum of plane waves and its relation to that of a polar diagram and aperture distribution'. Proc.IEE 97, Part III, pp.11-17, Jan. 1950.
5. Clemmow, P.C. op.cit. pp.12-13.
6. Ibid. p.36.
7. Sherman, G.C. 'Integral transform formulation of diffraction theory'. J.Opt.Soc.Am 57, pp.1490-1498, Dec. 1967.
8. Winthrop, J.T. and Worthington, C.R. 'Convolution formulation of Fresnel diffraction'. J.Opt.Soc.Am. 56, pp.588-591, May 1966.
9. Devaney, A.J. and Baron, S. 'An integral transform for the analytical manipulation of holograms'. NASA Electronics Research Centre, Control and Information Systems Lab. 1967.
10. IBM scientific subroutines package (SSP) program 'HARM'. IBM Manual H20-0205-3, p.276, Fourth Edition, 1968.
11. Coulson, C.A. 'Waves'. Oliver and Boyd, Edinburgh, 7th Edition, p.142, 1955.
12. Guillemin, E.A. 'The mathematics of circuit analysis'. Technology Press M.I.T., Wiley, New York, p.542, 1949.
13. Kuo, F. 'Network analysis and synthesis'. Wiley, New York;Toppan, Tokyo, 2nd Edition, pages 41 and 480. 1966.
14. Born, M. and Wolf, E. 'Principles of Optics'. Pergamon, London, pp.337 et.seq., 1959.
15. Kolsky H. 'Stress waves in solids'. Dover, New York, p.29, 1963.
16. Welsby, V.G. 'The signal/noise gain of ideal receiving arrays'. Proc.IEE 109, Part C, pp.108-116, March 1962.
17. Lesem, L.B. et.al. 'Holographic display of digital images'. Proc.AFIPS Conference 31, pp.41-47, Oct. 1967.

CHAPTER 6.

SPATIAL INFORMATION PROCESSING IN THE IMAGING SYSTEM.

PART II: THE BANDLIMITED SYSTEM.

6.1. INTRODUCTION.

The general topics of this chapter have already been outlined (5.1). Essentially the relationships developed in the previous chapter may be regarded as describing a completely unconstrained system in which no limits were placed on the complexity of the field or the spatio-temporal extent over which it could be measured. Here we are concerned with applying the constraints on the field determined by the behaviour of the transmitting source(s) and the response of reflecting objects, then within these constraints determining the requirements on the receiving system and the potential performance of the imaging device. The term 'bandlimited' in the chapter title is intended in the widest sense as applying to both the frequency range of the temporal variation of the signals and the extent of the spatial spectrum function.

Two categories of limits appear:

(1) Limitation of the complexity of the spatial field by determining a restraint on the rate of phase-shift along the measurement plane. This is equivalent to restricting the angle of arrival of the plane waves of which the field may be considered composed. Similarly, a maximum frequency limit may be enforced on the insonifying signal transmitted into the material. This category

of restraint enables the spatio-temporal variation at the measurement plane to be exactly represented by an infinite set of samples taken at sufficiently fine intervals.

(2) Restriction of the sample set to finite membership.

This represents the effects of measuring the field over only a finite region or aperture in the measurement plane and of recording from each aperture sampling element only a finite length of signal.

Once these latter restrictions are made information about the field is irretrievably lost (See 6.4.2.) and the resolution of the system determined. Further resolution may be deliberately sacrificed to facilitate data handling.

6.2. BANDWIDTH OF INCIDENT SIGNALS.

6.2.1. Temporal Signals.

Specification of the bandwidth restraint on temporal signals in the system follows immediately from the bandwidth of the electrical signal applied to the transmitting transducer. In the absence of non-linearities and with the assumption of a fixed object-transducer geometry no components can appear in the frequency spectrum that were not present in the transmitter signal. The relative strengths of different portions of the spectrum may alter drastically in passage through the transmission-reflection-reception path, as for example if the reflection is from a small Rayleigh scatterer.

The spectrum of the radiated acoustic signal $w_2(t)$ will be taken as zero above the frequency corresponding to twice the fundamental thickness resonance frequency of the transmitter (i.e., above $\frac{2}{\alpha}$ in Figure 3.7(b)) and this frequency will be denoted as ω_h for a corresponding maximum value of the wave number $K = \omega_{h/c}$. The 'D.C.' term is zero for transducers with free backing.

The temporal sampling rate follows immediately from the signal bandwidth, the requirement being simply that samples must be taken at at least every $\frac{\omega_h}{\pi}$ seconds. The arrangement actually constructed samples at a 24 MHz rate allowing some margin above the 10 MHz frequency limit.

6.2.2. Spatial bandwidth.

The problem of determining the spatial limitations is more complex. A plane reflector, even if quite close to the small transmitters necessary, sees and reflects unchanged (in bandwidth, not direction) only the range of homogeneous plane wave components necessary to represent the curved wavefront impinging on it. Small objects or ones with curved surfaces scatter energy over a wider arc, broadening the spectrum function of the reflected waves relative to the incident ones. The most extreme situation occurs in the limiting case of a very small spherical target reradiating a virtually uniform field all around itself containing a complete spectrum of plane waves. (This may be seen by regarding the object as a radiator occupying a point in an otherwise source free plane.

This delta function of excitation transforms to a uniform spectrum over all l,m). Under these circumstances no discrete sampling of the field will suffice to represent the complete distribution. However the very small object dimensions also imply that the scattered field must be very weak, and so, with the further limitation that if the object is near in to the measuring plane then no signals can be taken from it in any case, this situation does not pose a major difficulty.

In the rather more realistic case of a small plane reflector subject to a uniform plane field the reflected wave spatial distribution will follow, say, a '$2J_1(s)/s$' curve (circular object, $s = ka(\sin\alpha_1 - \sin\beta)$ as in Figure 6.1). The first null occurs for $s = 3.83$ and the function does not exceed 13% of the maximum value beyond this point. No restriction is implied on the range of s but it is easy to see that for larger values of ka the spectrum function will assume very small values for the range of ($\sin\alpha_1$ - $\sin\beta$) corresponding to inhomogeneous waves. As low frequencies (i.e., small k) are of small amplitude in the transmitted waveform and the inhomogeneous waves at the lower frequencies have correspondingly longer wavelengths (even though these are shorter than the 'free space' value) the broadening of the spectrum function for small k, while increasing their amplitudes, does not necessarily allow significant components with wavelengths shorter than the free space ones of higher k value waves. Perhaps this is best illustrated by a numerical calculation. Let the highest frequency

be 10 MHz and assume that the spectrum of the incident wave falls off linearly to zero in either direction from 5 MHz (i.e., is zero at 0 Hz and 10 MHz). For simplicity, take the incident wavefront, target surface and measurement plane as all parallel. Then $\alpha_1 = 0$ and the waves are described as a function of $\sin\beta$ only ($= \sqrt{l^2 + m^2}$ of the earlier discussion). If a = 2mm then at a frequency of 0.25 MHz the boundary of the inhomogeneous wave region commences at s = 0.5 (for aluminium). However, inhomogeneous components at 0.25 MHz having the same or lesser wavelengths along the measurement plane as the highest frequency free space wavelength correspond to $s \geqq 10$, where $2J_1(s)/s$ is less than .04 in magnitude. Since with the spectrum assumed the 0.25 MHz component is only 0.05 of the peak spectrum value to start with, these inhomogeneous waves have a value of only 0.002 the maximum in the system. The high $\sin\beta$ value also implies that attenuation away from the plane of the target is very rapid, falling off as e^{-20kz} or greater. Thus for z = 25mm say a further reduction by a factor of e^{-120} will occur, reducing the signal to completely negligible proportions.

If we arbitrarily disregard all components less than the first secondary maxima in amplitude then it will be found that none of the stronger components occur at angles greater than 65°. A smaller disc will scatter over a correspondingly wider arc but as the amplitude of the reflection at any frequency will also decline at a rate proportional to at least the linear extent of the target (and up to the square of this) the wide angle components are much reduced.

For the want of any definite means of establishing an absolute limit a rather arbitrary limit of 60° has been taken for system design, in the full realization that this may allow distortions in the spectrum constructed from the aperture spatial samples.* This limit corresponds to the extreme of accurate transducer response.

6.3. SAMPLING OF THE SIGNAL DISTRIBUTION.

6.3.1. Impulse sampling.

Consider that component of the measurement surface field with a particular wave number, k. Along any direction on the surface a wave characterised by (ξ,η) has an effective wavelength (i.e., distance for 2π phase progression) differing from the free space value $\lambda = \frac{2\pi}{k}$. The minimum value occurs along the direction of the projected normal to the wavefront and is given by;

$$\lambda_A = \frac{2\pi}{(\xi^2+\eta^2)^{\frac{1}{2}}} \qquad .. 6.1$$

With the constraint to angles of incidence $<60^{\circ}$, the minimum λ_A is 1.15 the free space value. Thus the fastest rate of spatial variation for the measured signal cannot exceed $1/(1.15\lambda_h)$ cycles/

---

* Note that this is a limit on l^2+m^2. In a situation where the individual sampling elements were omnidirectional, one could alternatively impose the limit on $\xi^2+\eta^2$; that is a restriction on the minimum effective wavelength along any direction on the measurement plane. This would then allow waves of the highest frequency to impinge at up to say the 60° limit and waves of lower frequencies to arrive over progressively wider angles (including inhomogeneous waves) while still remaining within a maximum rate of phase variation across the aperture.

unit distance ($\lambda_h = \frac{2\pi c}{\omega_h}$) in any direction and consequently we may at once apply the sampling theorem[1] to state that the signal must be sampled at not less than $2/(1.15\lambda_h)$ uniformly spaced points per unit distance. For $\omega_{h/2\pi}$ = 10 MHz and c = 6300 m/S (aluminium) this implies sampling every 0.37mm.

There are a number of possibilities in arranging the sampling grid and some of these based on a triangular[2,3] or hexagonal unit[4] allow a reduction in the total number of elements per unit area compared with say a rectangular arrangement.* If a convolutive processing scheme is followed then these arrangements have some advantage. However use of the transform method in discrete form implies measurements over a rectangular array and this is simpler to produce on a transducer slab. Consider Figure 6.2 where the

---

* Figure 6.3 illustrates a possible hexagonal grid. The maximum spacing in any direction is the hexagon side d while the minimum is $\frac{\sqrt{3}}{2}$ d = 0.866d compared with 0.707d for the square grid. Consider the number of points to sample a unit area. The area of the hexagon is $2\sqrt{3}d^2$ and that of the square d^2. For each new hexagon a total of three new points must be used while one is sufficient to extend the square array. Thus the ratio of sampling points p per unit area is;

$$\frac{p_{Hex}}{p_{sq}} = \frac{\frac{3}{2\sqrt{3}d^2}}{\frac{1}{d^2}} \qquad .. 6.2$$

$$= 0.866.$$

In a large array a 13% saving may represent several thousand elements.

sampling points are aligned with the x and y axes. Along either of these directions samples are taken at points d apart and this spacing corresponds to the correct sampling interval. However, along the directions $|x| = |y|$ sampling occurs at intervals of $\frac{d}{\sqrt{2}}$ which is unnecessarily fine and similarly to a lesser extent on any other off axis direction. This means that the field direction constraint may be altered to constraints on l and m separately and the maximum permissible values become $l_{max} = L = m_{max} = M$. This separation of the constraint is convenient in defining the limits over which the Fourier transform of the measured signal needs to be taken. The combined constraint on $l^2 + m^2$ represents a tighter condition and thus the Fourier components calculated within the separate constraints will always be sufficient to describe the spatial field. The geometrical forms of the constraints are shown in Figure 6.4. For cone half angles $> \frac{\pi}{4}$, the ranges of l and m taken separately extend into regions permitting inhomogeneous wave components (i.e., $\sin\theta > 1$) but this is of no moment as the physical limit on the incoming waves implies that these components will be zero.

In this section we have merely assessed the degrees of freedom available to the measurement surface signal over unitary intervals of space and time and derived therefrom the necessary sampling rates. The spatial spectrum and frequency spectrum are taken as identically zero outside defined limits. That is, we may regard the actual spectra as multiplied by functions of unit value over the region of non zero spectral values and zero outside. That is, multiplied by

a function;[5]

$$\text{rect}(\alpha) = 1 \quad |\alpha| < \tfrac{1}{2}$$
$$= 0 \quad |\alpha| > \tfrac{1}{2} \qquad \text{.. 6.3}$$

where α is $\frac{k}{2K}$, $\frac{l}{2L}$ or $\frac{m}{2M}$ as appropriate.*

Define a bandlimited spectrum function by

$$u_1(\xi,\eta,k) = u(\xi,\eta,k)\ (k^2-\xi^2-\eta^2)^{\frac{1}{2}} \cdot \text{rect}(\tfrac{\xi}{2KL}) \cdot \text{rect}(\tfrac{\eta}{2KM}) \cdot \text{rect}(\tfrac{k}{2K}) \qquad \text{.. 6.4}$$

The continuous measurement plane spatial and time distributions can be recovered by convolution of the discrete samples with the transform of the rect function, that is, with the 'sinc(β)'[5] (Figure 6.5), or $\frac{\sin\pi\beta}{\pi\beta}$ function. For the spatial samples denoted by (q,r) taken at spacings d, β is $(\frac{x}{d} - q)$ or $(\frac{y}{d} - r)$ as appropriate and for the 'time' samples indexed by s taken at intervals of $c\tau$, β is $(\frac{t}{\tau} - s)$. Thus the measurement plane signal at any (x,y,t) becomes;**[6]

$$U_n(x,y,ct) = \frac{8\pi^3}{d^2 c\tau} \sum_{q=-\infty}^{\infty} \sum_{r=-\infty}^{\infty} \sum_{s=-\infty}^{\infty} U_n^s(qd,rd,sc\tau) \cdot \text{sinc}(\tfrac{x}{d} - q) \cdot$$
$$\cdot \text{sinc}(\tfrac{y}{d} - r) \cdot \text{sinc}(\tfrac{t}{\tau} - s) \qquad \text{.. 6.5(a)}$$

q,r, and s are integers and;

---

* From here on we will use the limits on l and m separately as fitting a square sampling grid most readily.

** (This assumes that the x and y axes and the origin are occupied by sampling points but the generalization to a displaced grid is trivial).

$$U_n^s = U_n \cdot \delta(x-qd) \cdot \delta(y-rd) \cdot \delta(t-s\tau) \qquad .. 6.5(b)$$

Inserting this relation in Equation 5.35 and denoting the triple product of δ functions in Equation 6.5(b) as $\delta_A(q,r,s)$:-

$$u_1(\xi,\eta,k) = \frac{8\pi^3}{d^2 c\tau} \frac{1}{8\pi^3} \iiint_{-\infty}^{+\infty} \left\{ \sum_{q=-\infty}^{\infty} \sum_{r=-\infty}^{\infty} \sum_{s=-\infty}^{\infty} U_n(x,y,ct) \cdot \delta_A(q,r,s) \cdot \right.$$

$$\left. \cdot \operatorname{sinc}\left(\frac{x}{d} - q\right) \cdot \operatorname{sinc}\left(\frac{y}{d} - r\right) \cdot \operatorname{sinc}\left(\frac{t}{\tau} - s\right) \right\} \cdot$$

$$\cdot e^{j(\xi x + \eta y - kct)} d\,x\,d\,y\,d(ct) \qquad .. 6.6$$

since q,r,s are not involved in the integration we may reverse the order of integration and summation and by invoking the sifting property of the δ function, obtain;

$$u_1(\xi,\eta,k) = \frac{1}{d^2 c\tau} \sum_{q=-\infty}^{\infty} \sum_{r=-\infty}^{\infty} \sum_{s=-\infty}^{\infty} U_n^s(qd,rd,sc\tau) \cdot e^{j(\xi qd + \eta rd - ksc\tau)} \qquad .. 6.7$$

as the sinc terms have zero argument for all q,r,s.

Thus the band limited spectrum function is now expressed as a Fourier series with components determined by the sampled measurements. It should be noted that the function u_1 is a periodically repeating version of $u(\xi,\eta,k)\sqrt{k^2-\xi^2-\eta^2}$ ** with a period of 2KL in the ξ variable* and similarly in the others.

---

* The function repeats for $\xi d = 2\pi n$ (n is any integer)

i.e., for $\xi = \frac{2\pi n}{d} = 2KL\,n$.

** The 'o' subscript has been dropped from $u_o(\xi,\eta,k)$.

6.3.2. Finite sampling elements.

So far the sampling has not destroyed any information about the field in the material. We now introduce the effect of sampling the signal through elements of finite dimensions. Details have already been discussed in Section 4.4. The actual transducers employed in the experiments have square elements with side denoted as Δ ($\Delta < d$).

Generalizing Equation 4.21 to arbitrary incidence and dropping the $\cos\theta_A$ term since we are now working in terms of the normal component;

$$\bar{s}(\xi,\eta) = \text{sinc}\left(\frac{\xi\Delta}{2\pi}\right) \cdot \text{sinc}\left(\frac{\eta\Delta}{2\pi}\right) \qquad .. 6.8^*$$

this now represents the reduction in RMS value of the normal component of the incident signal compared with the value recoverable from spatial 'impulse' sampling.

Thus the spectrum calculable from the measured values is now;

$$\bar{u}(\xi,\eta,k) = u_1(\xi,\eta,k)\ \bar{s}(\xi,\eta) \qquad .. 6.9$$

With $\Delta \doteq d$ and d as calculated above, the value of $\bar{s}(\xi,\eta)$ drops to

---

* Note that $\frac{\Omega\Delta}{2v} = \frac{kc.\Delta}{2c/\sin\theta\cos\phi} = \frac{k\Delta\sin\theta.\cos\phi}{2}$ or $\frac{kl\Delta}{2} = \frac{\xi\Delta}{2}$ and similarly for the y direction. Square elements allow separation of the expression for $\bar{s}$ with respect to l and m. Similarly dircular elements may be expressed as a product of expressions in r and θ.

0.65 along the line $\xi = \eta$ (i.e., $\phi = \frac{\pi}{4}$) at the maximum angle of incidence and to 0.636 ($= \frac{2}{\pi}$) along either of the 'principle planes' (i.e., along the directions $\phi = 0$ or $\frac{\pi}{2}$) for the highest frequency of 10 MHz. Calculation of $\bar{s}(\xi,\eta)$ for intermediate values of ϕ shows similar values. No correction has been included for this factor in the calculating procedure as the attenuation is only significant for the highest frequencies in the signals.

Sampling of the temporal waveform from each transducer element is done with a very narrow pulse and no account need be taken of the analogous effect on the spectrum.

6.4. THE FINITE APERTURE SYSTEM.

The problem examined in this section is that arising in the very practical situation where only a limited portion of the function $U_n(x,y,ct)$ is available; that is, under conditions of finitely sized recording areas in the the spatial domain and a limited number of temporal samples from each sampling element.

6.4.1. Perturbation of the plane wave spectrum.

For convenience we will initially take the aperture to be rectangular in shape and to extend over the range $-\frac{d}{2} \leqq x \leqq (Q-\frac{1}{2})d$, $-\frac{d}{2} \leqq y \leqq (R-\frac{1}{2})d$, that is the aperture is Q by R elements. Time sampling will be taken to commence at $t = H\tau$ relative to some arbitrary time origin (most conveniently the instant of transmission) and continue for S samples until $t = (H+S-1)\tau$. Thus the record

available is;

$$V_n(qd,rd,sc\tau) = U_n^s(qd,rd,sc\tau) \cdot \{[h(x+\tfrac{d}{2}) - h(x-(Q-\tfrac{1}{2})d)] \cdot [h(y+\tfrac{d}{2}) - h(y-(R-\tfrac{1}{2})d)] \cdot [h(c(t-H\tau+\tfrac{\tau}{2})) \cdot - h(t-(H+S-\tfrac{1}{2})\tau)]\} \quad .. 6.10$$

where $h(\alpha)$ is the unit step function, i.e.,

$$h(\alpha) = 0 \quad \alpha<0 \qquad = 1 \quad \alpha>0 \quad .. 6.11$$

Equation 6.10 may be interpreted as confining the data to samples on a rectangular lattice in the x,y,ct 'space' (Figure 6.6) and the three dimensional function in braces may be referred to as a rectangular 'box' function, denoted by B_A. Defining v as the Fourier transform of V_n then, similarly to Equation 6.7,

$$v(\xi,\eta,k) = \frac{1}{d^2c\tau} \sum_{q=-\infty}^{\infty} \sum_{r=-\infty}^{\infty} \sum_{s=-\infty}^{\infty} U_n^s(qd,rd,sc\tau) \cdot B_A \cdot e^{+j(\xi qd+\eta rd-ksc\tau)} \quad .. 6.12$$

(where B_A is expressed in terms of q,r,s).

Multiplication of the spectral components of $\bar{u}$ by the box function corresponds to convolution of $\bar{u}$ with the transform of B_A.

Define the transform of B_A as b_A, then;

$$b_A(\xi,\eta,k) = \frac{1}{8\pi^3} \iiint_{-\infty}^{\infty} B_A \cdot e^{j(\xi x+\eta y-kct)} dx\, dy\, d(ct) \quad .. 6.13$$

$$= \frac{QRSd^2 c\tau}{8\pi^3} \cdot \text{sinc}\left[\frac{Qd\xi}{2\pi}\right] \cdot \text{sinc}\left[\frac{Rd\eta}{2\pi}\right] \cdot \text{sinc}\left[\frac{Sc\tau k}{2\pi}\right] \cdot$$

$$\cdot \; e^{j\left[\frac{Q-1}{2}\xi d + \frac{R-1}{2}\eta d - \left(\frac{H+S-1}{2}\right)c\tau k\right]} \qquad \text{..} \; 6.14$$

The exponential portion of the b_A spectrum will be represented by $P(\xi,\eta,k)$ i.e.,

$$P(\xi,\eta,k) = e^{j\left[\frac{Q-1}{2}d\xi + \frac{R-1}{2}d\eta \; \left(\frac{H+S-1}{2}\right)c\tau k\right]} \qquad \text{..} \; 6.15$$

This term represents the shifting of the sample box from a position symmetrical about the origin. Recalling that $\bar{u}$ is bandlimited we may write;

$$v(\xi,\eta,k) = \int_{-\infty}^{\infty}\int\int \bar{u}(\xi_1,\eta_1,k_1) \cdot b_A(\xi-\xi_1,\eta-\eta_1,k-k_1)\, d\xi_1\, d\eta_1\, dk_1 \qquad \text{..} \; 6.16$$

and noting that $d = \frac{\pi}{KL}$ etc.

$$= \frac{QRS}{8K^3 LM} \int_{-KL}^{+KL}\int_{-KM}^{KM}\int_{-K}^{K} \bar{u}(\xi_1,\eta_1,k_1) \cdot \text{sinc}\left[\frac{Qd}{2\pi}(\xi-\xi_1)\right] \cdot$$

$$\cdot \; \text{sinc}\left[\frac{Rd}{2\pi}(\eta-\eta_1)\right] \cdot \text{sinc}\left[\frac{Sc\tau}{2\pi}(k-k_1)\right] \cdot$$

$$\cdot \; P(\xi-\xi_1,\eta-\eta_1,k-k_1) \cdot d\xi_1\, d\eta_1\, dk_1 \qquad \text{..} \; 6.17$$

Equation 6.17 states that the spectrum derived from the finite sampling aperture is that of the true distribution in space viewed through a 'scanning function' which 'smears' the value of $\bar{u}$ at any point over the whole function. (See Figure 6.7). In the extreme case where $\bar{u}$ has unity amplitude over the complete range of ξ,η and

k and is phase shifted so that U_n aligns with the sampling window, the spectrum is perturbed similarly to that in Figure 6.8 which shows the effect for one dimension.* From the properties of the sine integral[7] the maximum overshoot ε is 9% and occurs at a value of $= \frac{2\pi}{Qd}$ in from the edges of the spectrum. Recalling that $d = \frac{\pi}{KL}$ the main ripple peaks are thus $\frac{2KL}{Q}$ from the edges of the 2KL wide true spectrum. If Q = 64 say, then the spectrum is not perturbed by more than 2% over the central 80%.

In a more realistic case where $\bar{u}$ tapers off to zero near the edges of the band, the effect is correspondingly reduced. For example, if $\bar{u}$ tapers linearly down from unity at the centre to zero at the band limits then the error is about 1% over the whole spectrum.* However it is important to consider the worst case of an abrupt discontinuity.

Since V_n is a bandlimited function it follows that v may be completely described by its values at a set of sampling points. Again following Woodward[1] we may immediately derive an expression for v in the form;

$$v(\xi,\eta,k) = \frac{QRS}{8K^3LM} \sum_{f=-\infty}^{\infty} \sum_{g=-\infty}^{\infty} \sum_{h=-\infty}^{\infty} v\left(\frac{f2\pi}{Qd}, \frac{g2\pi}{Rd}, \frac{h2\pi}{Sc\tau}\right) \cdot$$

$$\cdot \operatorname{sinc}\left[\frac{Qd\xi}{2\pi} - f\right] \cdot \operatorname{sinc}\left[\frac{Rd\eta}{2\pi} - g\right] \cdot \operatorname{sinc}\left[\frac{Sc\tau k}{2} - h\right] \cdot$$

$$\cdot P(\xi,\eta,k) \cdot P^*\left(\frac{f}{Qd}, \frac{g}{Rd}, \frac{h}{Sc\tau}\right) \qquad .. 6.18$$

---

* Refer to Appendix 3.3.

i.e.,

$$v(\xi,\eta,k)\,P^*(\xi,\eta,k) = \frac{QRS}{8K^3LM}\sum_f\sum_g\sum_h v\left(\frac{f2\pi}{Qd},\ \frac{g2\pi}{Rd},\ \frac{h2\pi}{Sc}\right) \cdot$$

$$\cdot\ P^*\left(\frac{f}{Qd},\ \frac{g}{Rd},\ \frac{h}{Sc\tau}\right)\ \mathrm{sinc}\left[\frac{Qd\xi}{2\pi}-f\right] \cdot$$

$$\cdot\ \mathrm{sinc}\left[\frac{Rd\eta}{2\pi}-g\right]\ \ \mathrm{sinc}\left[\frac{Sc\tau k}{2\pi}-h\right] \qquad .. 6.19$$

f, g and h are integers.

Thus the set of spectrum values derivable from the limited aperture measurements may be regarded as a set of independent components describing a smeared version of the true spatial field in the material under examination. This may considered in a slightly different way be comparing Equations 6.17 and 6.19. We have at the independent samples of $v.P^*$ -

$$v\left(\frac{2fKL}{Q},\ g\frac{2KM}{R},\ h\frac{2K}{S}\right) \cdot P^*\left(\frac{2fKL}{Q},\ \frac{2gKM}{R},\ \frac{2hK}{S}\right)$$

$$= \frac{QRS}{8K^3LM}\int_{-KL}^{KL}\int_{-KM}^{KM}\int_{-K}^{K} \bar{u}(\xi_1,\eta_1,k_1)P^*(\xi_1,\eta_1,k_1)\ \mathrm{sinc}\left[\frac{Qd}{2\pi}\xi_1-f\right]$$

$$\mathrm{sinc}\left[\frac{Rd}{2\pi}\eta_1-g\right]\ \ \mathrm{sinc}\left[\frac{Sc\tau}{2\pi}k_1-h\right]\ d\xi_1\,d\eta_1\,dk_1 \qquad .. 6.20$$

Thus the height of each of each line of the phase shifted v spectrum is a weighted sum over the entire shifted $\bar{u}$ spectrum about the line, (scaled by a factor $\frac{QRS}{8K^3LM}$). As Q,R,S increase, the weighting 'sinc' functions become sharper and sharper, bringing less and less of the spectrum into the integral. In the limit the value of vP^* exactly equals that of $\bar{u}P^*$ except right at the spectrum

edges.

If the original field consisted of just one 'line' (i.e., a monochromatic transmission and a distant point reflector or significantly an extended flat reflector at any distance)* then the finite aperture 'sees' this spread out into the sinc function. In more conventional terms this is the 'field pattern' of the 'antenna'. If the field comes from just one direction but is wideband in the k domain then each value of k produces distinct values of ξ and η so if we describe the field in l and m the wideband pattern is 'filled in'; that is, the sidelobes add up to produce a nearly monotonic decay. Consider, for example, the case where the function is uniform over all frequencies between -K and +K. Then, taking the 'boresight' case for simplicity, (i.e., the field source on the z axis) the variation along say, the l axis is given by;

$$s(l) = \int_{-K}^{K} \operatorname{sinc}\frac{Qdkl}{2\pi}\, dk \qquad .. 6.21$$

that is,

$$s(l) = \frac{2}{Qdl} \int_{\frac{-QdKl}{2}}^{\frac{QdKl}{2}} \cdot \frac{\sin\alpha}{\alpha}\, d\alpha \qquad .. 6.22$$

and substituting $\beta = \frac{Qdk}{2}$; the normalised pattern is,

$$s_n(l) = \left\{\frac{Si(l\beta)}{l\beta}\right\} \qquad .. 6.23$$

---

* That is, there is no method of distinguishing between these objects in a monochromatic system.

[Si(x) is the sine integral $Si(x) = \int_0^x \frac{\sin\alpha}{\alpha} d\alpha$]

The function in braces is tabulated for small $l\beta$[7] and readily calculable for the range outside the direct tables. For $l = 0$ the value is 1. At increasing l, s(l) decays monotonically, dropping to a value of $\frac{2}{\pi}$* for $\beta l = 2.9$, that is, for $l = \frac{5.8}{QdK}$. A monochromatic system operating at $\frac{K}{2}$ has a pattern reaching this value at $l = \frac{2\pi}{Qdk}$, i.e., the 'main beam' width is some 10% greater. Note however, that a monochromatic arrangement operating at any wave number greater than 0.54K, will actually have a narrower beam-width and hence greater potential resolution than the wideband system.[8] Whether or not this is any real advantage depends heavily on the shape and other properties of the material examined. Figure 6.9 shows the wideband and $k = \frac{K}{2}$ case along a principle plane (6.3.2).

The practical waveforms do not of course have uniform spectra even on transmission into the material and are further selectively filtered by the responses of the receiving transducer. In this case, the $\text{sinc}\frac{Qdkl}{2\pi}$ factor must be multiplied by the spectrum of the actual waveform after reception. The details of the effect of a waveform having a triangular spectrum, are worked out in Appendix 3.5. For the cases taken in Appendix 3.5, the -4 dB point occurs for $l/L \approx 0.04$. Now if $L = l_{max} = \sin 60^\circ = 0.866$, then $l_{-4dB} =$

---

* This value (corresponding approximately to the '-4 dB' point) has been taken because it is the level at which the patterns resulting from two lines, at the closest spacing consistent with independence, cross.

0.0346 and the corresponding angle is 2.0°. The aperture size taken corresponds to 18 wavelengths at the centre frequency of 5 MHz (for aluminium). Comparison with the usual optical formula for angular resolution;[9]

$$\alpha = \frac{1.22\lambda}{A} \qquad .. 6.24$$

(when α is in radians and A is the aperture size) with these figures gives $\frac{\alpha}{2} = 2^{\circ}$, showing a good agreement.

6.4.2. Object reconstruction.

In this section we will consider the spectrum of the field to be adequately represented* by the independent samples of $v(\xi,\eta,k)$ derived by the discrete Fourier transform operation on the available aperture measurements. That is;

$$v\left(\frac{2KL}{Q}f, \frac{2KM}{R}g, \frac{2K}{S}h\right) = \frac{1}{d^2 c\tau} \sum_{q=0}^{Q-1} \sum_{r=0}^{R-1} \sum_{s=H}^{H+S-1} V_n(qd, rd, sc\tau) \cdot$$

$$\cdot\ e^{j2\pi\left(\frac{fq}{Q} + \frac{gr}{R} - \frac{hs}{S}\right)} \qquad .. 6.25$$

(cf. with Equation 6.12).

Similarly to u_1, v is a periodic function. Every increase in f of Q (and similarly for g and h) returns the expression to the same value. Thus v is completely specified by its (complex) values at QxRxS sampling points, spaced at intervals of $\frac{2KL}{Q}$, $\frac{2KM}{R}$ and $\frac{2K}{S}$ in ξ, η, and k respectively.

Equation 6.25 may be modified to;

---

*Methods of improving the representation are discussed later.

$$v\left(\frac{2KL}{Q}f,\ \frac{2KM}{R}g,\ \frac{2K}{S}h\right) = e^{-j2\pi\frac{Hh}{S}}\ \frac{1}{d^2 c\tau}\left\{\sum_{q=0}^{Q-1}\sum_{r=0}^{R-1}\sum_{s=0}^{S-1} V_n(qd,rd,sc\tau)\ .\right.$$

$$\left.\ .\ e^{2\pi j\left(\frac{fq}{Q} + \frac{gr}{R} - \frac{hs}{S}\right)}\right\} \qquad .. 6.26$$

The term in braces now (apart from the trivial reversal of the time or frequency scale)* exactly conforms to the format of the discrete Fourier transform.[10] Thus the function obtained by this operation on V_n is $v\left(\frac{2KL}{Q}f,\ \frac{2KM}{R}g,\ \frac{2K}{S}h\right).e^{2\pi j\frac{H}{S}h}$.

$$= v_H\left(\frac{2KL}{Q}f,\ \frac{2KM}{R}g,\ \frac{2K}{S}h\right) \qquad .. 6.27$$

To construct the field at a distance z from the measurement plane, Equation 5.36 specifies an operation of the form;

$$V_z(qd,rd,sc\tau) = \sum_{f=0}^{Q-1}\sum_{g=0}^{R-1}\sum_{h=0}^{S-1} v_H\left(\frac{2KL}{Q}f,\ \frac{2KM}{R}g,\ \frac{2K}{S}h\right)\ .$$

$$.\ e^{-j2K\sqrt{\left(\frac{h}{S}\right)^2 - \left(\frac{Lf}{Q}\right)^2 - \left(\frac{Mg}{R}\right)^2}.z}\ .$$

$$.\ e^{-j2\pi\left(\frac{fq}{Q} + \frac{gr}{R} - \frac{hs}{S}\right)} \qquad .. 6.28$$

V_z being the discrete approximation to U_z. Use has been made of the periodic nature of v_H to run the summation over (for ξ) 0 to Q-1, i.e., from $\xi = 0$ to $\xi = \left(2KL - \frac{2KL}{Q}\right)$ rather than from -KL to +KL. The value at +KL and that at -KL must be identical from the periodicity and hence no information is lost).

---

* This time-frequency transform will need to be done separately in any case (10.3).

Once again V_z is periodic in q,r and s in exactly the same fashion as V_n. This reveals the interesting result that the area imaged in the material can be no greater in size than the aperture and is essentially a spatial projection* of it to the required depth (note that the sign for $z<0$ has been taken, this conforms to the geometry of the actual transducer situations used). If this area should be insufficient then it may be enlarged by embedding the aperture measurement set in a larger matrix filled up with zeros. To extend this idea one might consider an extrapolation of the measured values into the region beyond the physical aperture.[11,12] This operation is mathematically feasible but of little practical significance unless the measurements are virtually noise and interference free.

The function actually obtained by the discrete Fourier transform operation, v_H, is a phase advanced version of the representation of the signal and thus V_z is related to v by;

$$V_z(qd,rd,sc\tau) = \sum_{f=0}^{Q-1}\sum_{g=0}^{R-1}\sum_{h=0}^{S-1} v\left(\frac{2KL}{Q}f, \frac{2KM}{R}g, \frac{2K}{S}h\right) \cdot e^{-j2K\sqrt{\left(\frac{h}{S}\right)^2 - \left(\frac{Lf}{Q}\right)^2 - \left(\frac{Mg}{R}\right)^2}\cdot z} \cdot e^{-2\pi j\left[\frac{fq}{Q} + \frac{gr}{R} - \frac{h}{S}(s+H)\right]} \quad .. 6.29$$

---

* One can apply additional phase shifts to v_H to obtain the field over an area displaced from the aperture projection.

Thus, with the time origin displaced to s=H, i.e., to the instant sampling commences from the receiving elements, the fundamental period of V_z commences at s=-H and extends over a range of $s\tau$ in t. Physically, the constraint imposed by a finite time record is a limitation in range coverage in the material. Consider Figure 6.18. Transmission from T commences at t=0. If the signal scattered from an object in the material is to be received within the time $H\tau$ to $(H+S-1)\tau$ at the array point P and the transmitter is taken to be in the centre of the receiving array R_{xy} (here assumed circular and of diameter D,) then the minimum value of R_1+R_2 is $cH\tau$ and the corresponding locus of O,(L_{min}) is a sphere of radius $\frac{cH\tau}{2}$ centred at T. This is for P (nearly) coincident with T. At the other extreme with P at the edge of the array, the signal must not occur later than $(H+S-1)\tau$ and the outer locus L_{max} is formed by sweeping an allipsoidal shell with a fixed focus at T and a moving one at the array edge, around the normal through T. Figure 6.18 shows this in section. Thus the total region that may be satisfactorily imaged resembles the shaded area in section. Any object lying wholly within this volume will have the reflections from itself received and recorded over the whole aperture. Objects only partially within the volume will suffer loss in resolution and possibly distortion in imaging from the complete or partial loss of the returns.

As shown above, a further requirement* is that the imageable

---

* In the simplest form.

volume must contain the projected area of the aperture; that is, $AE \geq \frac{D}{2}$. This restraint imposes a condition on d', the length representing the propagation distance during the recording time $(S-1)\tau$.

An appreciation of the magnitudes involved may be gained by a numerical example. Let D=50mm, $H\tau$ = 20μS and c = 6000m/sec. or 6mm/μS. From Appendix 3.4 we derive A as the point x=0, z=60mm and $(S-1)c\tau$ = 24mm whence $(S-1)\tau$ = 4μS. In the apparatus a value of 10.5 μS is used (mainly to allow for the transmitter being displaced from the array centre to a position at the edge). From the appendix this value allows imaging over a depth of 21mm. With a rectangular array the moving locus of the ellipse varies in distance from T and if a corresponding area is to be imaged, d' must be increased to accommodate the larger ellipse obtained from a section on the array diagonal. If the array is 50mm square then in the above example the useful depth range for the given value of H reduces to about 14mm.

The considerable distortion occurring if the received signal partially 'misses' the sampling window implies that a 'guard band' should be allowed around the imaged slice and if this is 1 μS at each end of the record then the region further reduces to about 8mm in depth.

6.4.3. Summary.

Before proceeding to the next section it may be helpful to summarize the chapter up to the present point.

(i) A limit was placed on the range of the incoming signals in terms of a limit to the maximum angle of arrival at the recording surface and the maximum frequency. This limitation is based mainly on physical grounds.

(ii) This limit enables the incident signal to be fully specified by an (infinite) set of samples in space and time. The particular characteristics of the sampling elements may impose some spatial filtering on the signals but this will in general be slight. This discrete representation (Equation 6.7) is found to be periodic in the direction-wavenumber variables (ξ, η, k) but exactly represents the incident function over the fundamental region defined by the limits earlier imposed.

(iii) The region of the recording surface and the time duration over which samples are taken was deliberately restricted to a finite volume in the x,y,ct space. For reasons associated with the format of the computer operations used to perform the necessary manipulations on these measurements the spatial aperture was defined to be in the +x,+y quadrant only and to be of rectangular shape. (Note that this does not necessarily mean that the physical area from which the recordings are taken need be of this shape; only that it must be contained within the rectangle taken). The time recording was taken as running over a direction commencing some time after an arbitrary origin to represent the delay occurring from the transit of the acoustic signals through the material examined.

(iv) Insertion of the finite sample set in the transform relations showed that the direction-wavenumber function so defined differs from the original continuous function obtainable from the infinite set in;

(a) A phase shift changing linearly with the variables representing the displacement of the finite sample box from a position symmetric about the origin of the x,y,ct space. The spatial shift is of no consequence but merely indicates that the fundamental period of the spatial distribution being imaged has shifted across to a position centred on the normal to the centre of the finite aperture. The time shift serves to define one boundary of the spatial region imaged in depth and the duration of record the other limit.

(b) The function defined from the finite set has a definite restriction on the degrees of freedom available and is fully representable by its values at a set of regularly spaced points in the ξ,η,k space. The spacing of these points is inversely proportional to the sizes of the sample taken in from the x,y,ct space.

(c) Each 'line' in the function is derived from a weighted integration over the whole continuous function and consequently the continuous function constructed by a defined interpolation procedure on the independent values differs from the original distribution by an extent depending on the shape of the original distribution and the position within it being considered.

Additional distortion is introduced if the received signal does not align perfectly with the sampling box. This distortion for any given value of ξ,η, or k, varies with position of the received signal in the sampling window in a similar manner to the variation depending on the value of ξ,η or k when the signal does align.

(v) The finite aperture places a definite resolution limit on the spatial reconstruction. This is really only a different way of stating (iv(b)) but relates the terminology employed here to the conventional theory relating to antennas, the 'field pattern' being essentially the interpolation function applied to expand the line spectrum into a continuous function. This is derived in spatial direction terms by integration over the wave-number spectrum for a variety of spectral forms.

(vi) The field reconstruction derived from the discrete direction-wavenumber spectrum is an approximation to the original field over a limited region in the same sense that the discrete spectrum approximates the original continuous one. (This was not explicitly stated before but note that V_z and v are derivable from each other with no information loss). Again the reconstruction is a periodic function in space and time; the fundamental period in space corresponds to an area which is a projection of the aperture and in time to a definite span in depth located by the time delay allowed before time sampling commenced. The operations are diagrammatically summarized in Figure 6.10.

Since, as we have seen in the previous chapter, the Fourier

transform or plane wave relationships may be manipulated into a form using spherical waves instead, the results regarding resolution, depth of space imageable and distortions apply equally to this latter form.

6.5. SPATIAL TAPERING AND THE OMMISSION OF APERTURE SAMPLE POINTS.

In this section we consider two modifications to the method of spatial sampling. These are directed towards;

(i) Reduction in 'overshoot' in the reproduction by v of sharp discontinuities in the function $\bar{u}$.

(ii) A reduction in the number of aperture elements from which signals are recorded while still maintaining coverage of as large an aperture as possible. (The reason - reduction in data storage - for this modification was discussed in Section 1.3).

These two operations are treated together as the means for implementing both are the same.

6.5.1. Spatial Tapering.

In 6.4.1. we saw that the approximate function derived from the finite aperture measurements is the convolution of the true function with the transform of the sample 'box'. This raises the concept of improving the approximation by modification of the box to a more favourable shape so that b more nearly resembles a sharp spike. This is the familiar 'sidelobe suppression' technique commonly employed in radar systems, in the sense that b represents

the response to the case of $\bar{u}(\xi,\eta,k) = \delta(\xi-\xi_1).\delta(\eta-\eta_1).\delta(k-k_1)$.

A large number of techniques[17] have been proposed for achieving this end but all share one feature in common; as the magnitude of secondary peaks in b are decreased the width of the main lobe increases. Some methods of modifying B, in particular the Dolph[18] and Taylor[19] weightings, minimise this effect but require rather complicated functions. As it was desired to generate the necessary weighting 'on line' something simpler was considered adequate. We will treat this in two parts, firstly B will be modified to a cylindrical shape and secondly further weighting applied depending on the distance of the element from the centre of the array.

6.5.1.1. Circular aperture.

When the project commenced, shapes other than circular were not readily available in the transducer materials and units of this shape have been employed in all the experimental work. However, the requirements of the Fourier transform method in practical computing terms mean the allocation of a rectangular storage array in the computer and the introduction of square transducer plates as standard items, indicates that further development should proceed using these in preference.

The cylindrical form now holding for B simply means that samples are taken only from elements lying within a circle enclosed by the total possible area, Qd by Rd, and the time samples are not altered. The effect of the 'ragged' edge of the circle caused by the square

elements will be neglected and we define;

$$B_c = h(Q_c d - \{[x - \tfrac{Q-1}{2}d]^2 + [y - \tfrac{R-1}{2}d]^2\}^{\frac{1}{2}}) \cdot$$

$$\cdot\ h(ct - [H - \tfrac{1}{2}]c\tau) - h(ct - [H+S - \tfrac{1}{2}]c\tau) \qquad .. 6.30$$

where $Q_c d$ is the radius of the circular area. Q_c must be less than $\frac{Q}{2}$ or $\frac{R}{2}$, whichever is the smaller. The transform b_c, of B_c, will be the same as b_a in the k dimension and hence it is sufficient to consider the (ξ,η) variation only. Thus;

$$b_c(\xi,\eta) = \frac{1}{4\pi^2}\int_{-\infty}^{\infty}\!\!\int B_c\ e^{j(\xi x + \eta y)}\,dx\,dy \qquad .. 6.31$$

$$= \frac{1}{4\pi^2}\int_{-\infty}^{\infty}\!\!\int h(Q_c d - \{[x - (\tfrac{Q-1}{2})]^2 + y - (\tfrac{R-1}{2})d]^2\}^{\frac{1}{2}})\, e^{j(\xi x + \eta y)} \cdot$$

$$\cdot\ dx\,dy$$

which, after some manipulation, gives;

$$b_c(\xi,\eta) = \frac{(Q_c d)^2}{4\pi}\left[\frac{2J_1(Q_c d(\xi^2+\eta^2)^{\frac{1}{2}})}{Q_c d(\xi^2+\eta^2)^{\frac{1}{2}}}\right] P_1 \qquad .. 6.32$$

where $P_1 = e^{j[\frac{Q-1}{2}d\xi + \frac{R-1}{2}d\eta]}$

In more usual terms this may be expressed as;

$$b_c(\theta) = \frac{(Q_c d)^2}{4\pi}\left[\frac{2J_1(Q_c d\ k\ \sin\theta)}{Q_c d\ k\ \sin\theta}\right] P_1 \qquad .. 6.33$$

the portion in square brackets being the well known directivity function for a piston source.[21] In the form this is generally

derived, the expression appears in an equation describing the far-field distribution as the result of approximations introduced by assuming large distances from the aperture. Here the function describes the relative strengths of plane wave components of the field and is valid at all distances. Thus;

$$v(\xi,\eta,k) = \frac{(Q_c d)^2}{8\pi K} S \int_{-KL}^{KL} \int_{-KM}^{KM} \int_{-K}^{K} \bar{u}(\xi_1,\eta_1,k_1) \cdot$$

$$\cdot \frac{2J_1\{Q_c d([\xi-\xi_1]^2 + [\eta-\eta_1]^2)^{\frac{1}{2}}\}}{Q_c d[(\xi-\xi_1)^2 + (\eta-\eta_1)^2]^{\frac{1}{2}}} \cdot$$

$$\cdot \operatorname{sinc}\frac{Sc\tau}{2\pi}(k-k_1) \cdot P(\xi-\xi_1,\eta-\eta_1,k-k_1) \cdot d\xi_1\, d\eta_1\, dk_1 \quad .. \ 6.34$$

If the function $\bar{u}$ consists of just a single line then the system's reproduction of this is the $2J_1(\alpha)/\alpha$ function. (Figure 6.1(b)). If we allow $Q_c = \frac{Q}{2}$ and take a cut along

$$\eta = 0 \text{ for } \bar{u} = \delta(\xi)\delta(\eta)\delta(k) \quad .. \ 6.35$$

then

$$s_k(l) = \frac{2J_1(\frac{Q}{2\pi}dkl)}{\frac{Qd}{2\pi}kl} \quad .. \ 6.36$$

by comparison with $\operatorname{sinc}(\frac{Qdkl}{2\pi})$ having a first zero at $l = \frac{2\pi}{Qdk}$, the above form of $s_k(l)$ goes to the first zero at $l = \frac{7.66}{Qdk}$, and the main lobe is thus some 22% wider. However the maximum height of secondary maxima is now only 13.3% of the main lobe compared with 23% for the sinc function.

Similarly to before, we may derive the spatial pattern for a

wideband system by integration over the k spectrum. The case of a rectangular spectrum gives;

$$s(l) = \int_{-K}^{K} \frac{2J_1\left(\frac{Qd}{2\pi}kl\right)}{\frac{Qd}{2\pi}kl}\, dk \qquad .. 6.37(a)$$

$$= \frac{8}{Qdl}\left\{-J_1\left(\frac{KQdl}{2}\right) + \int_0^{\frac{KdQl}{2}} J_o(u)du\right\} \qquad .. 6.37(b)$$

The integral part of the solution is available in tabulated form[23] and we will denote it by $Ji_o(x)$, i.e.,

$$Ji_o(x) = \int_0^x J_o(\alpha)d\alpha \qquad .. 6.38$$

Similarly to the calculations for the rectangular aperture (Appendix 3.5) the normalized version of this function may be plotted and is shown in Figure 6.19 along with the $2J_1(x)/x$ function characteristic of a monochromatic k spectrum.* Similarly to before, the broadband case has no definite sidelobe structure, decaying steadily as the value of 1/L increases and we see that the monochromatic function at a value of k=K/2 is only slightly broader than the wideband case.

By comparison with the square aperture where the pattern varies

---

* The numerical values chosen are the same as for the previous calculations, viz.; Q=64, K=10^4 and note that:

$$\lim_{x\to 0} \frac{Ji_o(x)}{x} = 1.$$

with the location of the cut taken (always passing through l=m=0) the circular aperture has a constant pattern in all directions.

6.5.1.2. Amplitude tapering of the circular aperture.

As indicated earlier, a great variety of tapers is possible but for simplicity that chosen was the 'cone on a pedestal' form illustrated in Figure 6.11.

Thus B is defined by (dealing only with the spatial variation);

$$B = h(Q_c d - r_1) \cdot T(r_1) \qquad .. 6.39$$

$(r_1 = (x^2 + y^2)^{\frac{1}{2}})$

where $T(r_1)$ is the taper function, in this case having the form;

$$T(r_1) = 1 - r_1/R_P \qquad .. 6.40$$

where $1 - \frac{Q_c d}{R_P} = p$, the pedestal height.

Solution of this for b gives;

$$b_c = \frac{(Q_c d)^2}{2\pi}\left[(1+\frac{Q_c d}{R_P})\frac{J_1(\beta)}{\beta} + \frac{Q_c d}{R_P}(\frac{J_o(\beta)}{\beta^2} - \frac{Ji_o(\beta)}{\beta^3})\right] \qquad .. 6.41$$

with $\beta = Q_c d(\xi^2+\eta^2)^{\frac{1}{2}}$ or $Q_c d\ k \sin\theta$.

For $R_P \to \infty$ this reduces to Equation 6.32 as expected.

For $\bar{u}$ as in Equation 6.35, a slice along $\eta = 0$ gives;

$$s(l) = \frac{(Q_c d)^2}{2\pi}\left[(1+\frac{Q_c d}{R_P})\ \frac{J_1(\frac{\alpha l}{L})}{(\frac{\alpha l}{L})} + \frac{Q_c d}{R_P}\ \{\frac{J_o(\frac{\alpha l}{L})}{(\frac{\alpha l}{L})^2} - \frac{Ji_o(\frac{\alpha l}{L})}{(\frac{\alpha l}{L})^3}\ \}\right] \qquad .. 6.42$$

$$(\alpha = \frac{Q_c \pi k}{K})$$

$$\text{and } s(0) = \frac{(Q_c d)^2}{2}\left[\tfrac{1}{2} + \tfrac{1}{3}\ \frac{Q_c d}{R_P}\right] \qquad .. 6.43$$

In the apparatus developed the pedestal height is adjustable but is typically set in the range p=0.0 to 0.3. The resultant normalized curve for s(l) is shown in Figure 6.12 for p=0.2. Comparison with the unweighted case will show that the present function has a slightly narrower main beam with a small increase in sidelobe level. A number of other cases are shown in Reference 24.

6.5.2. Practical realization of amplitude tapering.

The results just derived assume that the amplitude tapering is applied by the introduction of a suitable attenuator in the signal lead from each receiving transducer element. This has a number of practical disadvantages, firstly in that it requires setting up of the attenuators (or the control of a variable one if the elements are accessed sequentially rather than in parallel, and secondly all the array elements must still be interrogated and recordings made from them. Thirdly, if amplitude quantization is done on the signals then pre-quantization tapering requires a large dynamic range in the quantizer while a post-quantization operation is limited

by the size of the steps taken. For these reasons the technique of density tapering[25] was applied. In this method the suitably normalized desired or model taper is regarded as the probability density function (pdf) of a random binary variable assuming the value 1 with the probability given by the pdf evaluated at any radius from the centre of the array. This variable multiplied with the signal U_n^s from the element(s) corresponding to the radius selects a portion of the signals from any group of elements corresponding in the average to the mean value of the taper function over this area. Thus with p=0.2, near the array centre, recordings will be made from nearly all the elements while at the edges only about 1/5th. of the elements will be chosen.

Schemes that achieve a similar result on a deterministic basis have been reported in the literature[26,27,28] but the calculations involved are not trivial for large arrays and such procedures require non-uniform element spacing.

Obviously any scheme that omits elements effectively increases the average sample point spacing, a move that would seem prone to introducing aliasing and greater ambiguity into the field reconstruction. The random selection 'breaks up' these new large lobes within the fundamental period of the reconstruction and effectively 'smears' their area over the whole pattern. Suitable deterministic selection avoids the problem by precise choices of element location to cause destructive interference of the ambiguous lobes.

6.5.3. Element ommission.

Having once settled on the density tapering method for amplitude control a simple extension provides immediately for the required reduction in data acquisition. Suppose that the data storage can handle only 30% of the total possible signal records. Then for a uniform aperture we simply define the pdf to be 0.3 over the entire sampled area. If weighting is also applied then this already reduces the number of elements as much as 50% (p=0) and in this case the overall pdf would be chosen as 0.6 at $r_1 = 0$ tapering to zero at $r_1 = Q_c d$; similarly for other tapers. The reduction in elements caused by the density tapering alone will be referred to as 'natural' thinning.

The whole of the theory, practical implementation and results of this thinning technique have been extensively treated by Cook[29] and Cook and Johnson[30] in a separate project on the ultrasonic imaging system and it is not proposed to repeat this here in other than general terms. The basic requirement is to determine the effect of the random sampling on the attainable accuracy of v, the approximation to $\bar{u}$.

Cook's evaluations involve firstly the determination of the sample points on the aperture for a particular case and then the calculation of the field pattern that such an array would produce if each element is regarded as a small radiator.* This is of

* In Cook's work an element directivity of $\cos^2\theta_A$ was assumed instead of the correct $\cos\theta_A$ term and hence, although intended to represent the component of field strength along the line radial from the array centre, the calculated values are in fact, (for the far field case) the z directed components with which the present theory is concerned.

course precisely the system response to an incoming plane wave that we have been determining for the deterministic forms of B considered previously. The reference treats a large number of particular cases with both natural thinning and further reductions down to a remainder of only 6% of the elements on a 128 x 128 array. In all cases the pattern is virtually unchanged from that of the completely filled array in terms of main lobe width and size of near-in sidelobes but shows a progressive increase in average sidelobe level over the whole space as the degree of thinning increases,with the sidelobe level remaining constant or even rising slightly rather than falling away from the centre of the pattern.

6.5.3.1. Control of response with thinning applied.

In the actual apparatus constructed the random sequence used to determine the sampling of the array was generated by a feedback shift register and thus was in fact completely predictable although displaying random properties to the usual statistical tests. However, formation of the binary sequence from this psuedo-random series involved the use of relatively low accuracy analogue circuitry introducing some 'jitter' into the ideal sequence. Thus although one could, in principle, construct a complete Fourier transform of the actual random pattern established over the finite aperture it is far more convenient to work in terms of the autocorrelation of this pattern and the power density spectrum derived therefrom by transforming. Thus the expression defining the finite aperture becomes (in spatial coordinates only);

$$B = H(x,y) \circ S(s,y) \qquad .. 6.44$$

Where H(x,y) is a function such as that in Equation 6.10 or Equation 6.30 and serves to define the physical extent of the aperture while S(x,y) adopts the value 1 or 0 in accordance with whether or not readings are taken from (x,y). A slice through B(x,y) along the lines of x=constant or y=constant will resemble the function shown in Figure 6.13. The probability of S having the value b in any interval $(q-\frac{1}{2})d$ to $(q+\frac{1}{2})d$ will be denoted as $P_S(b;q)$ and for the full two-dimensional aperture as $P_S(b;q,r)$. If no amplitude taper is applied then P_S is independent of q and r. Specifying a taper function is to specify P_S in terms of aperture position defined by (q,r). As well as chosing P_S control can also be exercised over the conditional probability density describing the probability of $S(x+\bar{x},y+\bar{y})$ having one of the allowable values given the value at (x,y). This essentially is a specification of the autocorrelation function of B and hence when transformed, of the finite aperture response to impulsive input.

In the apparatus S is generated by producing a random sequence of voltage levels uniformly distributed in amplitude by the summation of the levels from a number of stages of the feedback shift register after binary weighting. That is, the random voltage is formed by a summation such as;

$$V = b_i + 2b_j + 4b_k + 8b_l + 16b_m + \ldots \qquad .. 6.45$$

The b_i are the outputs from stages i etc. of the register and are not necessarily from adjacent stages. All states between 2^m-1

and 0 units of voltage will occur with nearly equal probability, m being the number of stages used in forming the random voltage.* Any system that weights the outputs in this binary fashion will produce the uniform probability of states but the conditional probability of successive states can be made to vary widely by altering the 'tapping points' on the register. Generation of the required binary (0,1) sequence is achieved by a comparison of V with a further voltage generated from the coordinates of the element under consideration in the form for the required $P_S(1;q,r)$. If V is less than this voltage, recording is made from the defined (q,r). For example, if a uniformly taken 35% sample is desired, the voltage representing P_S is simply held constant at $0.35V_{max}$; V_{max} being the largest magnitude of V. Thus the probability of again having b=1 at the displaced point reduces to determining the probability of V being again in the appropriate range.

Since the probability of sampling can be made to vary in a complicated fashion over the aperture, any meaningful theoretical calculation of the likely form of the 'power' response becomes extremely intractable. In Cook's work no attempt was made to do this analysis; instead a large number of cases was examined in a computer model of the entire set-up for a variety of possible connection schemes to the shift register and the one finally chosen

---

* (The exception is 0 which occurs one less time than the other possibilities but in the actual unit used having 20 stages with 6 of them included in the weighting, i.e., m=6, the difference is only one in 16384).

for physical implementation decided on the basis of greatest randomness of aperture sampling.

To summarise: Tapering of the aperture amplitude response provides a smoother match of the reconstructed field to the original. If this tapering is achieved by density control of samples from the aperture and further thinning achieved by additional random ommission then, apart from a scaling factor depending on the number of elements removed, the spatial response to an incident plane wave is unperturbed from that of the unthinned aperture in the immediate vicinity of the true position of the wave direction, but degenerates into a low level random sidelobe background.

Before leaving this section, one further result needed later, is quoted. The average sidelobe level relative to the main peak is given by;

$$\overline{SL} = \frac{1}{\overline{N}_R} - \frac{1}{\overline{N}_T} \qquad .. 6.46$$

where $\overline{N}_R$ is the mean number of elements remaining after thinning and $\overline{N}_T$ is the total number in the unthinned aperture. $\overline{SL}$ is in power units.

6.6. OVERALL IMAGING RESPONSE.

So far, in this portion of the thesis, attention has been devoted to consideration of the elements of the complete imaging system as isolated problems. It now remains to bring these

sections together in an overall assessment of the performance. Obviously any really practical situation poses a problem of immense complexity. For this reason it has seemed best to treat the response in terms of a calculation of the image obtainable from a defined 'test pattern' similarly to the method used in related optical practice.[31] This introduces the problem of selection of a suitable pattern. Among the possibilities a point object is perhaps the most obvious choice as it will produce a scattered field having little dependence on the spatial characteristics of the illuminating field. However, as the scattered field contains waves at all angles in equal strengths, this form of object will violate the assumptions made in the earlier part of the present chapter. Control of the range of angles may be achieved by enlarging the 'point' to a small flat surface say, but then the precise selection of the surface's parameters becomes a difficulty in its own right and the field will still contain non-zero components beyond the allowable range for the receiving array spacing. A further problem arises in that calculation of the point or near point object response does not immediately give any measure of the resolution of the system in terms of its ability to reproduce fine object detail. For these reasons it has seemed most suitable to take an object having a co-sinusoidal variation in reflectivity as in Figure 6.14. For an incident plane wave this produces a scattered field consisting of two plane waves only in the directions as indicated on the Figure. Along the object plane the reflectivity is given by;

$$R(x) = \cos\Omega x \qquad .. 6.47$$

no loss of generality being implied by the restriction of the reflectivity variation to the direction of a coordinate axis as a more generally inclined variation can always be separated into two components along the axes.*

Multiplication of the incident field over the object plane with the reflectivity gives the reflected waves. If the incoming wave is represented by;

$$u_o(\xi,\eta,k) = j W_4(k)\delta(\xi-\xi_i)\delta(\eta) \qquad .. 6.48$$

$W_4(k)$ being the spectrum of the incoming wavefront temporal variation, then at the surface the normal component is given by;

$$U_z(x,y,z_o,k) = j W_4(k)\sqrt{k^2-\xi_i^2}\; e^{-j\xi_i x}.e^{-j\sqrt{k^2-\xi_i^2}\cdot z_o} \qquad .. 6.49$$

for a plane located at $z = z_o$.

The reflected wave is given by;

$$u_r(\xi,\eta,k)\sqrt{k^2-\xi^2-\eta^2} = j W_4(k)\sqrt{k^2-\xi_i^2}\cdot\tfrac{1}{2}[\delta(\xi-\xi_i+\Omega) + \delta(\xi-\xi_i-\Omega)] \cdot$$
$$\cdot e^{-j\sqrt{k^2-\xi_i^2}\cdot z_o}.\delta(\eta) \qquad .. 6.50$$

That is, the reflected wave spatial spectrum consists of two delta functions representing waves reflecting at angles symmetrically spaced about the angle at which the incident plane wave would reflect from a smooth surface.

Thus at the measurement plane the surface distribution is

---

* See Reference 31, Figure A4.

given by;

$$U_n(x,y,k) = \iint_{-\infty}^{\infty} u_r(\xi,\eta,k)\sqrt{k^2-\xi^2-\eta^2}.e^{+j\sqrt{k^2-\xi^2-\eta^2}.z_o}.e^{-j(\xi x+\eta y)} \cdot$$

$$\cdot\ d\xi\ d\eta \qquad .. 6.51$$

$$= j\,W_4(k)\sqrt{k^2-\xi_i^2}\,e^{-j\sqrt{k^2-\xi_i^2}\cdot z_o}.\iint_{-\infty}^{\infty}\tfrac{1}{2}[\delta(\xi-\xi_i+\Omega)+\delta(\xi-\xi_i-\Omega)].\delta(\eta) \cdot$$

$$\cdot\ e^{+j\sqrt{k^2-\xi^2-\eta^2}\cdot z_o}.e^{-j(\xi x+\eta y)}\,d\xi\,d\eta \qquad .. 6.52$$

$$= \left\{j\,W_4(k)\sqrt{k^2-\xi_i^2}\,e^{-j\sqrt{k^2-\xi_i^2}\cdot z_o}.e^{j\left[\left(\frac{\sqrt{k^2-(\xi_i-\Omega)^2}+\sqrt{k^2-(\xi_i+\Omega)^2}}{2}\right)z_o\right]}\right\}.$$

$$\cdot\ \cos\left[\Omega x-\left(\frac{\sqrt{k^2-(\xi_i+\Omega)^2}-\sqrt{k^2-(\xi_i-\Omega)^2}}{2}\right).z_o\right].e^{-j\xi_i x}$$

$$.. 6.53$$

The portion in braces will be denoted as $G(k,\xi_i,\Omega,z_o)$ and the non x-dependent portion of the cosine function as $\gamma(k,\xi_i\Omega,z_o)$. So;

$$U_n(x,y,k) = G(k,\xi_i,\Omega,z_o).\cos(\Omega x-\gamma(k,\xi_i,\Omega,z_o)).e^{-j\xi_i x}$$

$$.. 6.54$$

and we may note that for $\xi_i = 0$ this reduces to;

$$U_n(x,y,k) = W_4(k).jk\,e^{j(\sqrt{k^2-\Omega^2}-k)z_o}.\cos\Omega x \qquad .. 6.55$$

in which form the measurement plane displacement follows that at the reflector, with only a phase shift associated with the distance between the surfaces. The jk term is indicative of the fact that

$U_n(x,y,k)$ is a measure of the particle velocity.

We represent the transducer element transfer function* by E(k) so that for an aperture Qd by Rd in side the signal available to the processing system is;

$$T(x,y,k) = E(k)\{G(k,\xi_i,\Omega,z_o) \cdot \cos[\Omega x - \gamma(k,\xi_i,\Omega,z_o)] \cdot B_A(x,y)\} \not\propto b_A(k)\, e^{-j\xi_i x} \quad .. 6.56$$

where $B_A(x,y)$ is as in Equation 6.10 for the x and y variations only.

The finite record length appears as $b_A(k)$ $(= \frac{Sc\tau}{2\pi} \text{sinc}[\frac{Sc\tau k}{2\pi}] \cdot e^{-j([\frac{H+S-1}{2}]c\tau k)})$. For the purposes of analytical solution the effect of sampling will be neglected so that the manipulation may be continued in integral form. The only really significant difference this makes to the calculated image parameters is the absence of periodic repititions.

In the reconstruction, an operation of the form -

$$v(\xi,\eta,k)\sqrt{k^2-\xi^2-\eta^2} = \frac{1}{4\pi^2}\int_{-\infty}^{\infty}\int T(x,y,k)e^{j(\xi x+\eta y)}dx\,dy \quad .. 6.57$$

is first performed to obtain an approximation to the spectrum function at the aperture and then finally we obtain the system's view of the reflecting surface as;

---

* Together with any further operation such as matched filtering that may be performed on the signals from individual elements.

$$V_z(x,y,z,k) = \iint_{-\infty}^{\infty} \mathbf{v}(\xi,\eta,k)\sqrt{k^2-\xi^2-\eta^2}\,.e^{-j\sqrt{k^2-\xi^2-\eta^2}.z} \;.$$

$$. \; e^{-j(\xi x+\eta y)}\,d\xi\,d\eta \qquad .. 6.58$$

with $z = \mathbf{z}_o$.

Firstly,

$$v(\xi,\eta,k)\sqrt{k^2-\xi^2-\eta^2} = E(k).G.\not b_A(k)\,\frac{QRd}{4\pi^2}\,\mathrm{sinc}\left[\frac{Rd\eta}{2\pi}\right] \;.$$

$$. \; \tfrac{1}{2}\Big[\mathrm{sinc}\left[\frac{Q}{2\pi}(\xi-\xi_i+\Omega)d\right].e^{j\left[\frac{Q-1}{2}\Omega d-\gamma\right]}$$

$$. \; + \mathrm{sinc}\left[\frac{Q}{2\pi}(\Omega-(\xi-\xi_i))\right].e^{-j\left[\frac{Q-1}{2}\Omega d-\gamma\right]}\Big] \;.$$

$$. \; e^{j\left\{\frac{Q-1}{2}d(\xi-\xi_i)\,+\,\frac{R-1}{2}d\eta\right\}} \qquad .. 6.59$$

in which equation we see that the two lines of the spectrum of the incoming waves have been spread into the expected sinc function about the position of each line. The phase shift factor $P(\xi,\eta)$ has appeared to denote the shift of the aperture from a symmetrical position and similarly associated with the sinc function for each line is a phase shift representing firstly the aperture position and secondly the inclination of the original insonifying wave.

Insertion of this relation into Equation 6.58 yields, under assumption that Q and R are fairly large so that the sinc functions decay rapidly, and allowing irrational parts of the exponential arguments to be approximated by a second order expansion, an expression in the form;*

---

* Mathematical details are in Appendix 3.6.

$$V_z(x,y,z_o,k)$$

$$= E(k).U_z \left\{ e^{j\Omega x} \left[F_o\left\{\sqrt{\frac{1}{2\pi\beta_2}}\, X_2'\right\} - F_o\left\{\sqrt{\frac{1}{2\pi\beta_2}}\, X_2''\right\} \right] . \right.$$

$$\cdot \left[F_o\left\{\sqrt{\frac{1}{2\pi\gamma_2}}\, Y'\right\} - F_o\left\{\sqrt{\frac{1}{2\pi\gamma_2}}\, Y''\right\} \right] + e^{-j\Omega x} \left[F_o\left\{\sqrt{\frac{1}{2\pi\beta_1}}\, X_1'\right\} \right.$$

$$\left. \left. - F_o\left\{\sqrt{\frac{1}{2\pi\beta_1}}\, X_1''\right\} \right] . \left[F_o\left\{\sqrt{\frac{1}{2\pi\gamma_1}}\, Y'\right\} - F_o\left\{\sqrt{\frac{1}{2\pi\gamma_1}}\, Y''\right\} \right] \right\} \not\in b_A(k)$$

.. 6.60

Where,

$$\left.\begin{matrix}\beta_1 \\ \beta_2\end{matrix}\right\} = \frac{z_o}{2k\left(1-\left(\frac{\xi \pm \Omega}{k}\right)^2\right)^{\frac{3}{2}}}$$

$$\left.\begin{matrix}\gamma_1 \\ \gamma_2\end{matrix}\right\} = \frac{z_o}{2k\left(1-\left(\frac{\xi_i \pm \Omega}{k}\right)^2\right)^{\frac{1}{2}}}$$

$$\left.\begin{matrix}X_1' \\ X_2'\end{matrix}\right\} = x-(Q-\tfrac{1}{2})d - \frac{z_o\left(\frac{\xi_i \pm \Omega}{k}\right)}{\left(1-\left(\frac{\xi_i \pm \Omega}{k}\right)^2\right)^{\frac{1}{2}}}$$

$$\left.\begin{matrix}X_1'' \\ X_2''\end{matrix}\right\} = x + \frac{d}{2} - \frac{z_o\left(\frac{\xi_i \pm \Omega}{k}\right)}{\left(1-\left(\frac{\xi_i \pm \Omega}{k}\right)^2\right)^{\frac{1}{2}}}$$

$$Y' = y - (R-\tfrac{1}{2})d$$

$$Y'' = y + \frac{d}{2}$$

$F_o(z)$ is the complex Fresnel integral defined as;

$$F_o(z) = \sqrt{2}\, e^{j\frac{\pi}{4}} \int_o^z e^{-j\frac{\pi\alpha^2}{2}}\, d\alpha \qquad .. 6.61$$

and U_z is as in Equation 6.49.

From Equation 6.60 we see that the image obtained contains firstly a reproduction of the illuminating waveform incident on the surface with the spectral components modified by the transducer and data capture operations, and secondly a function of the form $e^{j\Omega x}(F_1(x,y)) + e^{-j\Omega x}(F_2(x,y))$. The significant feature of this expression is that the quality of reproduction of the $\cos(\Omega x)$ function is dependent on the region of the original surface which is being imaged and in particular is seriously perturbed near the image region edges where some of the X and Y terms are small.

For simplicity, in assessing the image distortion we may now take $\xi_i = 0$ rendering $\beta_1 = \beta_2 = \beta$ and $\gamma_1 = \gamma_2 = \gamma$ and consider the x variation along the line $y = \frac{R-1}{2}d$ so that $Y' = -\frac{Rd}{2}$, $Y'' = +\frac{Rd}{2}$ and then as $F_o(-z) = -F(z)$, the y dependent term may be extracted to give;

$$V_z(x, \tfrac{R-1}{2}d, z_o, k) = \frac{H}{4} \cdot F_o\left\{\sqrt{\frac{1}{2\pi\gamma}}\ \frac{Rd}{2}\right\} \cdot \Bigg\{ e^{j\Omega x} \cdot \left[F_o\left\{\sqrt{\frac{1}{2\pi\beta}}\ X_2'\right\} - F_o\left\{\sqrt{\frac{1}{2\pi\beta}}\ X_2''\right\}\right] + e^{-j\Omega x}\left[F_o\left\{\sqrt{\frac{1}{2\pi\beta}}\ X_1'\right\} - F_o\left\{\sqrt{\frac{1}{2\pi\beta}}\ X_1''\right\}\right] \Bigg\} \qquad .. 6.62$$

where H represents the remainder of the expression 6.60.

If further attention is restricted to the region in the immediate vicinity of $x = (\frac{Q-1}{2})d$, (i.e., to the point in the image on the normal to the aperture centre), then the expression further simplifies to;

$$V_z(\tfrac{Q-1}{2}d, \tfrac{R-1}{2}d, z_o, k) = \frac{H}{4}.F_o\left\{\sqrt{\frac{1}{2\pi\gamma}} \cdot \frac{Rd}{2}\right\} 2\cos[\Omega(\tfrac{Q-1}{2})d] \cdot$$

$$\cdot\left\{ F_o\left\{\sqrt{\frac{1}{2\pi\beta}}\left(\frac{Qd}{2} - \frac{z_o\frac{\Omega}{k}}{\sqrt{1-(\frac{\Omega}{k})^2}}\right)\right\}\right.$$

$$\left. + F_o\left\{\sqrt{\frac{1}{2\pi\beta}}\left(\frac{Qd}{2} + \frac{z_o\frac{\Omega}{k}}{\sqrt{1-(\frac{\Omega}{k})^2}}\right)\right\}\right\} \quad .. 6.63$$

in which form the image appears as the correct $\cos[\Omega(\frac{Q-1}{2})d]$ term for this position modified by a complex expression depending on $\frac{\Omega}{k}$. Under the conditions, λ = 1.25mm, k = 5000, Rd = Qd = 40mm and z_o = 40mm also, the factor has the form as shown in Figure 6.15 going to zero for $\frac{\Omega}{k} = 1$. The plot could be continued for $\frac{\Omega}{k} > 1$ but this would violate the hypothesis that inhomogeneous waves are to be excluded.

Despite the great number of assumptions and the neglect in particular of the effects of sampling the received waves, the equation and plot shown reveal considerable data about the limitations of the system. The plot reveals the fidelity with which details in an arbitrary object will be shown at the best resolution position of the image and we see this to vary with the fineness of reflecting surface detail in a manner which is analogous

to the action of a low pass filter. At some values of $\frac{\Omega}{k}$ the phaseshift tends to $-\pi$ and the imaged grating is shown in reversed (albeit very much reduced) contrast. Smaller values of $\frac{\Omega}{k}$ give lesser degrees of shift in the image and more accurate amplitude reproduction. The imaging system may be regarded as a linear filter of spatial frequencies; even at very low frequencies a loss of amplitude occurs together with a small displacement.

Similar plots may be drawn for any number of frequency and imaging geometry situations but the general behaviour is much the same as Figure 6.15.

Apart from the variation in image quality with position in the image shown by the expressions derived, Equation 6.60 also shows that the response to a purely x directed test pattern is dependent on the y dimension (Rd) of the aperture as γ_1, γ_2 are functions (although not very sensitive ones) of $\frac{\Omega}{k}$. The dependence reduces as R becomes very large; for the values taken in the plot the dependence is most significant for $\frac{\Omega}{k} \approx 0.5$.

6.7. DEPTH RESOLUTION.

This may be plotted in a simple case by taking the variation in the calculated field along the line $x = \frac{Q-1}{2}d$, $y = \frac{R-1}{2}d$, (i.e., the receiver axis) for a simple plane reflector so that $\Omega = \xi_i = 0$. The plot is shown in Appendix 3.6 as Figure A3.6/1 but needs to be done for each frequency component in the waves to produce a correct impression. A simpler evaluation may be made by letting $z_o >> Qd$

or Rd so that the depth resolution is not strongly influenced by the aperture details and becomes almost purely a function of the spectrum of the signal waveforms in the system.

With a rectangular spectrum for the transmitted signal corresponding to a 'sinc' time waveform a reflector of negligible thickness at a distance sufficient that the depth resolution is effectively decoupled from variations in l and m will resolve as the sinc function in Figure 6.5 with $\beta = \frac{zK}{2\pi}$. If we consider two objects closely spaced so that the returns overlap then the problem resolves into a consideration of the signal output resulting from the overlap of two of these functions at different displacements, that is;

$$f_r(t) = f(t) + f(f-\tau_1) \qquad .. 6.64$$

Rather than attempt a detailed study of this function it is more useful to consider the resolution in terms of an ambiguity function[13] which, for a real signal suffering no Doppler shift, is simply the autocorrelation function[14] defined as;

$$\phi_{11}(\tau_1) = \int_{-\infty}^{\infty} f(t)f(t+\tau_1)dt \qquad .. 6.65$$

for $f(t) = \text{sinc}(\frac{Kct}{\pi})$ corresponding to the rectangular spectrum of width 2K, this gives;

$$\phi_{11}(\tau_1) = \int_{-\infty}^{\infty} \text{sinc}\frac{Kct}{\pi}\ \text{sinc}\frac{Kc(t+\tau_1)}{\pi}dt \qquad .. 6.66$$

$$= c\ \text{sinc}\frac{Kc\tau_1}{\pi}$$

c is a constant.

If we take the square of this function (normalised) as the ambiguity and somewhat arbitrarily state that resolution is possible for target separations with $\left|\phi_{11}(\tau_1)\right|^2 < (\frac{2}{\pi})^2$ then the necessary time separation for resolution with the given parameter values is 25nS corresponding to a shift of 0.1mm in depth (remembering that the distance between the objects is traversed twice by the signal).

A rather more practical waveform closely resembling those in the actual system has the form and spectrum[15] as in Figure 6.16. If $f(t) = e^{-at}\sin\omega_o t$ then the autocorrelation function has the form;

$$\phi_{11}(\tau_1) = \frac{e^{-a\tau_1}\omega_o^2}{4a} \frac{(\cos\omega_o\tau_1 + \frac{a}{\omega_o}\sin\omega_o\tau_1)}{a^2 + \omega_o^2} \qquad .. 6.67$$

This is plotted in Figure 6.17 for $\omega_o = \pi \times 10^7$ (i.e., 5 MHz) and $a = 10^9/300\text{sec}^{-1}$; normalised to one. Again for $\left|\phi_{11}(\tau_1)\right|^2 \leqq (\frac{2}{\pi})^2$, $\tau_1 \geqq 120$nS and $c\tau_1 \geqq 0.72$mm so the necessary separation is 0.36mm.

This considerably increased value compared with the rectangular spectrum case is a reflection of the less than optimum use of the bandwidth available. Even at this value the use of the auto-correlation function as a measure of resolution implies that the received waveform is compressed into the sharpest pulse consistent with the spectral form by matched filtering[16] or actual correlation with a stored replica. Although an attempt was made to construct a filter matched to the impulse response of the receiving transducer the practical realization suffered from high losses in the delay elements used and was not persisted with. Consequently, the

resolution suffers not only from the prolongation of the transmitted acoustic waveform from the transmitter and the corresponding highly oscillatory autocorrelation, but also from further ringing in the receiver. These imperfections increase the necessary separation for objects to be resolved and a more practical value is about 1-2mm. Thus in the example above (6.4.2) it would not be sensible to take more than about 5 slices from the 8mm useful depth.

REFERENCES FOR CHAPTER 6.

1. Woodward, P.M. 'Probability and information theory, with application to radar'. Pergamon, Oxford, 2nd Edition, 1964, Section 2.4, p.31, et.seq.
2. Cheng, D.H.S. 'Characteristics of triangular lattice arrays.' Proc. IEEE 56, pp.1811-1817, November 1968.
3. Sharp, E.D. 'A triangular arrangement of planar array elements that reduces the number needed'. IEEE Trans. AP-9, pp.126-129, March 1961.
4. Allen, J.L. et.al. 'Phased array radar studies'. Lincoln Lab., M.I.T. Technical Report 228, 12 Aug. 1960, p.150.
5. Woodward, P.M. op.cit. p.29.
6. Ibid. Equation 30, p.34.
7. Abramowitz, M. and Stegun, I.A. 'Handbook of mathematical functions'. Dover, New York, 1965, p.227.
8. Gericke, O.R. and Grubinskas, R.C. 'Utilization of the liquid surface levitation effect as a means of ultrasonic image conversion for materials inspection'. Journ. Acoust. Soc. Am. 45, pp.872-880, April 1969. (See esp. Figure 7).
9. Born M. and Wolf, E. 'Principles of optics'. Pergamon, Oxford, 1965, 3rd Edition, p.419.
10. Cooley, J.W. and Tukey, J.W. 'An algorithm for the machine calculation of complex Fourier series'. Math. of Computation 19, pp.297-301, April 1965.
11. Ksienski, A. 'Spatial frequency characteristics of finite aperture antennas'. in - 'Electromagnetic waves and antennas'. Ed. E.C. Jordan, Pergamon, 1963.
12. Welsby, V.G. 'The angular resolution of a receiving aperture in the absence of noise'. Journ. Brit. IRE 26, pp.115-124, Aug. 1963.
13. Woodward, P.M. op.cit. p.120.
14. Lee, Y.W. 'Statistical theory of communication'. Wiley, New York, 1960, p.37.
15. Lathi, B.P. 'Signals, systems and communication'. Wiley, New York, 1965, p.132. (Note that the analytical expression of the spectrum of this function given on p.136, Table 4.18, No.11, is incorrect. The ω_o^2 term should be in the denominator).
16. Turin, G.L. 'An introduction to matched filters'. IRE Trans IT-6, pp.311-329, June 1960.
17. Skolnik, M.I. 'Introduction to radar systems'. McGraw-Hill, New York, 1962, Section 7.8.

18. Dolph, C.L. 'A current distribution for broadside arrays which optimizes the relationship between beamwidth and sidelobe level'.
Proc.IRE 34, pp.335-348, June 1946.
19. Taylor, T.T. 'Design of line source antennas for narrow beamwidth and low sidelobes.'
IRE Trans. AP-3, pp.16-28, Jan. 1955.
20. Abramowitz, M. and Stegun, I.A. op.cit. p.360, Equation 9.1.21.
21. Tucker, D.G. and Gazey, B.K. 'Applied underwater acoustics'.
Pergamon, Oxford, 1966, p.181.
22. Kinsler, L.E. and Frey, A.R. 'Fundamentals of acoustics'.
Wiley, New York, 2nd Edition, 1962, pp.167-169.
23. Abramowitz, M. and Stegun, I.A. op.cit. pp.492-493.
24. Cook, G.B. 'The ultrasonic camera: a study of the transducer-computer interface'.
M.E. Thesis, University of Canterbury, 1969, Appendix 5.
25. Skolnik, M.J. et.al. 'Statistically designed density tapered arrays'.
IEEE Trans. AP-12, pp.408-417, July 1964.
26. Maffett, A.L. 'Array factors with non-uniform spacing parameter.'
IRE Trans. AP-10, pp.131-136, March 1962.
27. Skolnik, M.I. and Sherman, J.W. 'Planar arrays with unequally spaced elements'.
Radio and Electronic Eng. 28, pp.173-184, Sept. 1964.
28. King, D.D. et.al. 'Unequally spaced, broadband antenna arrays'.
IRE Trans. AP-8, pp.380-384, July 1960.
29. Cook, G.B. op.cit. Appendices 2, 3, 4.
30. Cook, G.B. and Johnson, D.A.H. 'Pseudo-random selection of elements in a multielement array'.
Radio and Electronic Eng. 38, pp.82-88, Aug. 1969.
31. Linfoot, E.H. 'Fourier methods in optical image evaluation'.
Focal Press, London, 1964.

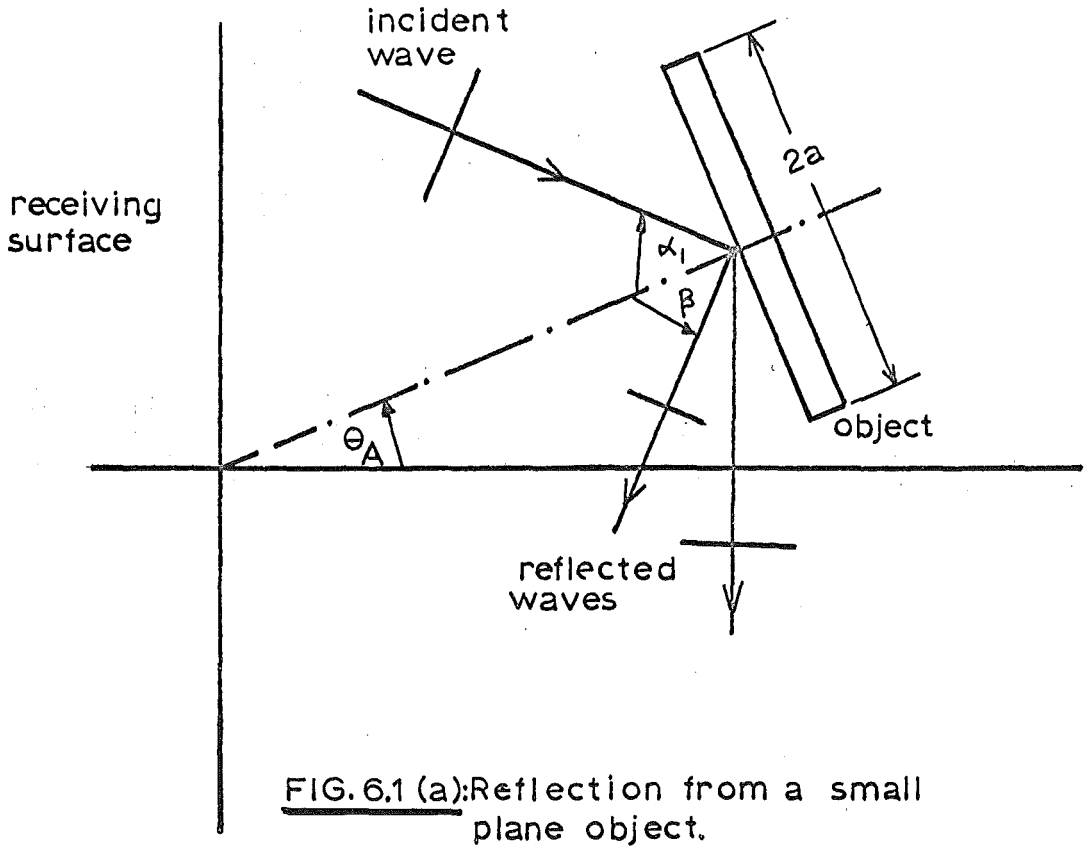

FIG. 6.1 (a): Reflection from a small plane object.

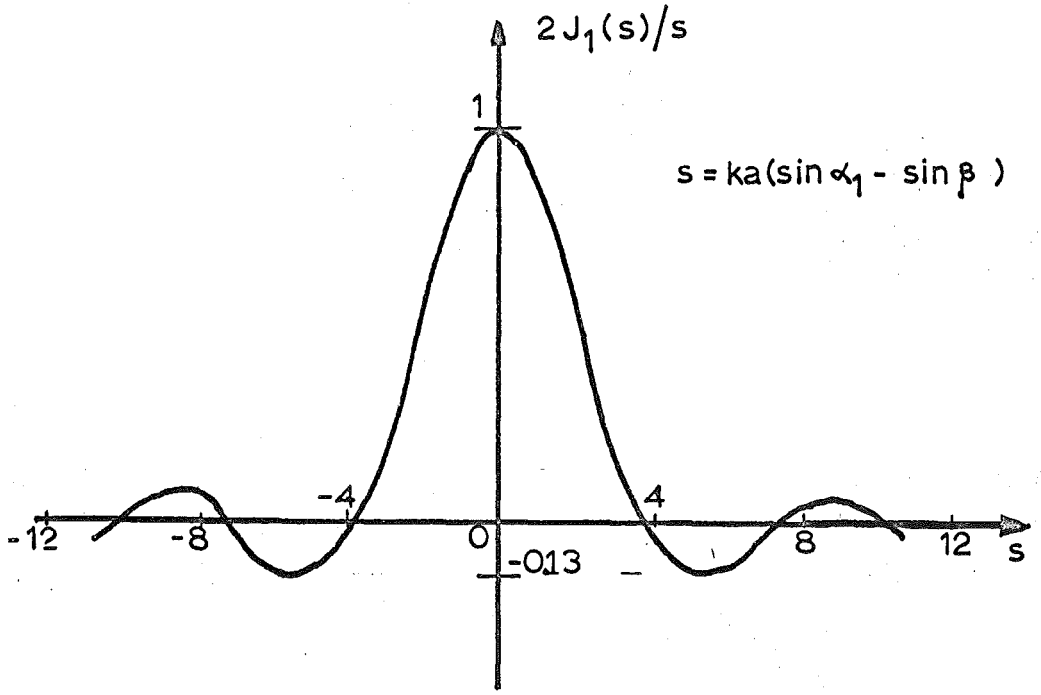

FIG. 6.1(b): Spectrum function

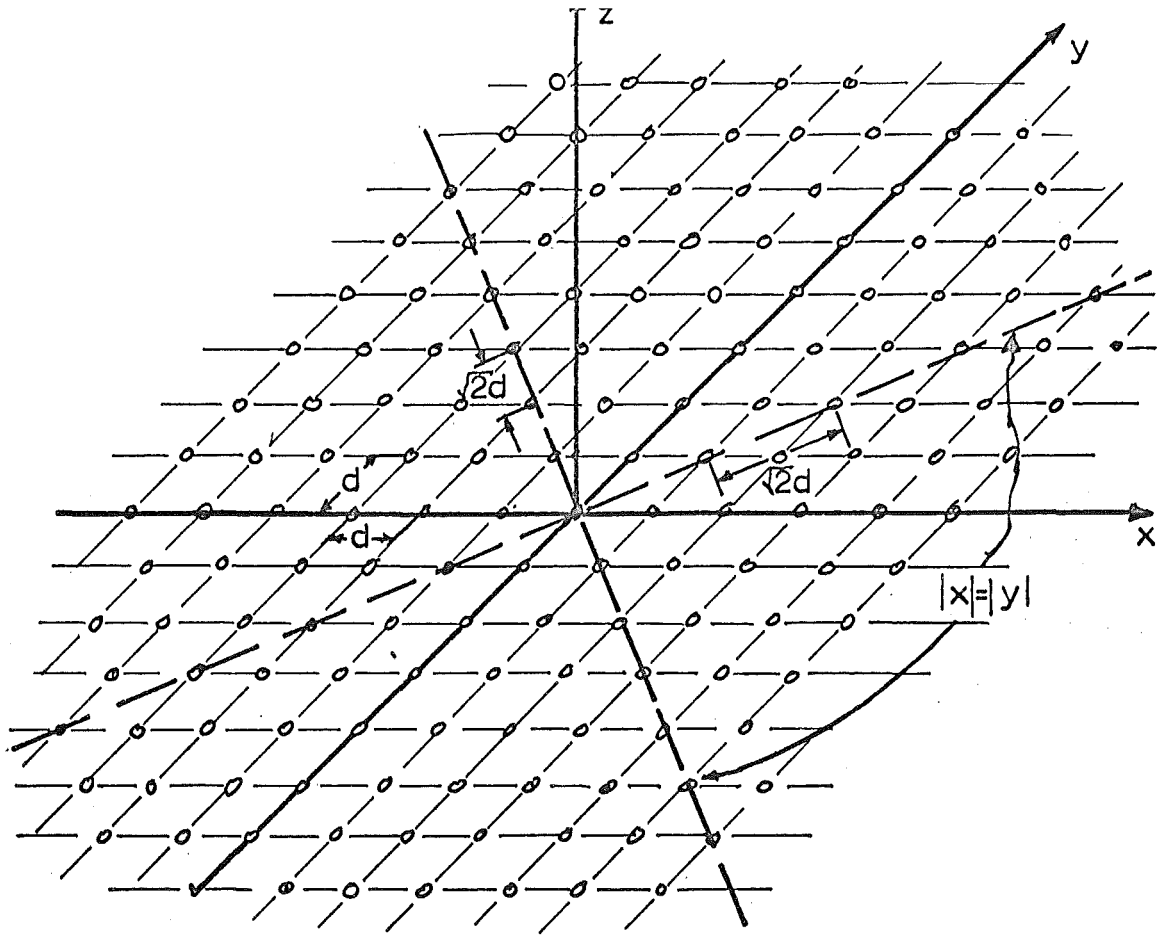

FIG. 6.2: Rectangular sampling grid

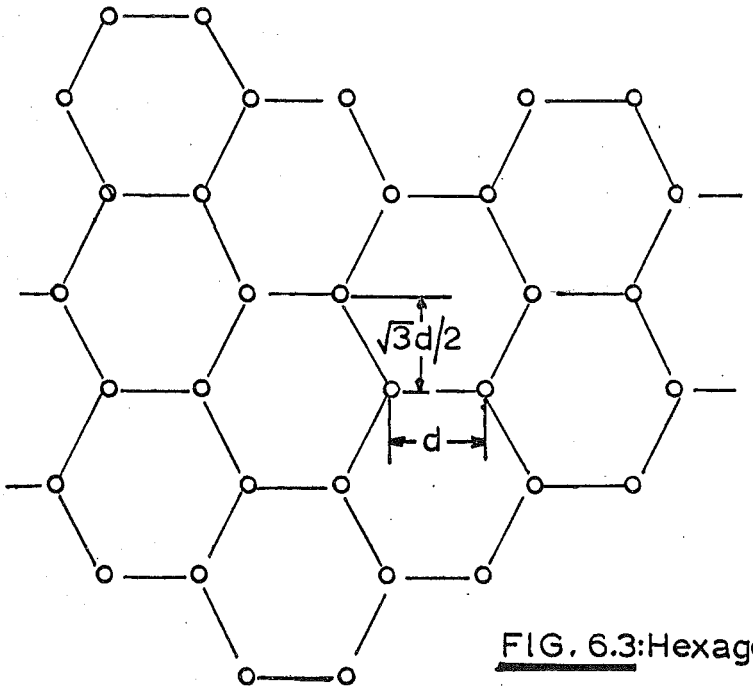

FIG. 6.3: Hexagonal sampling grid

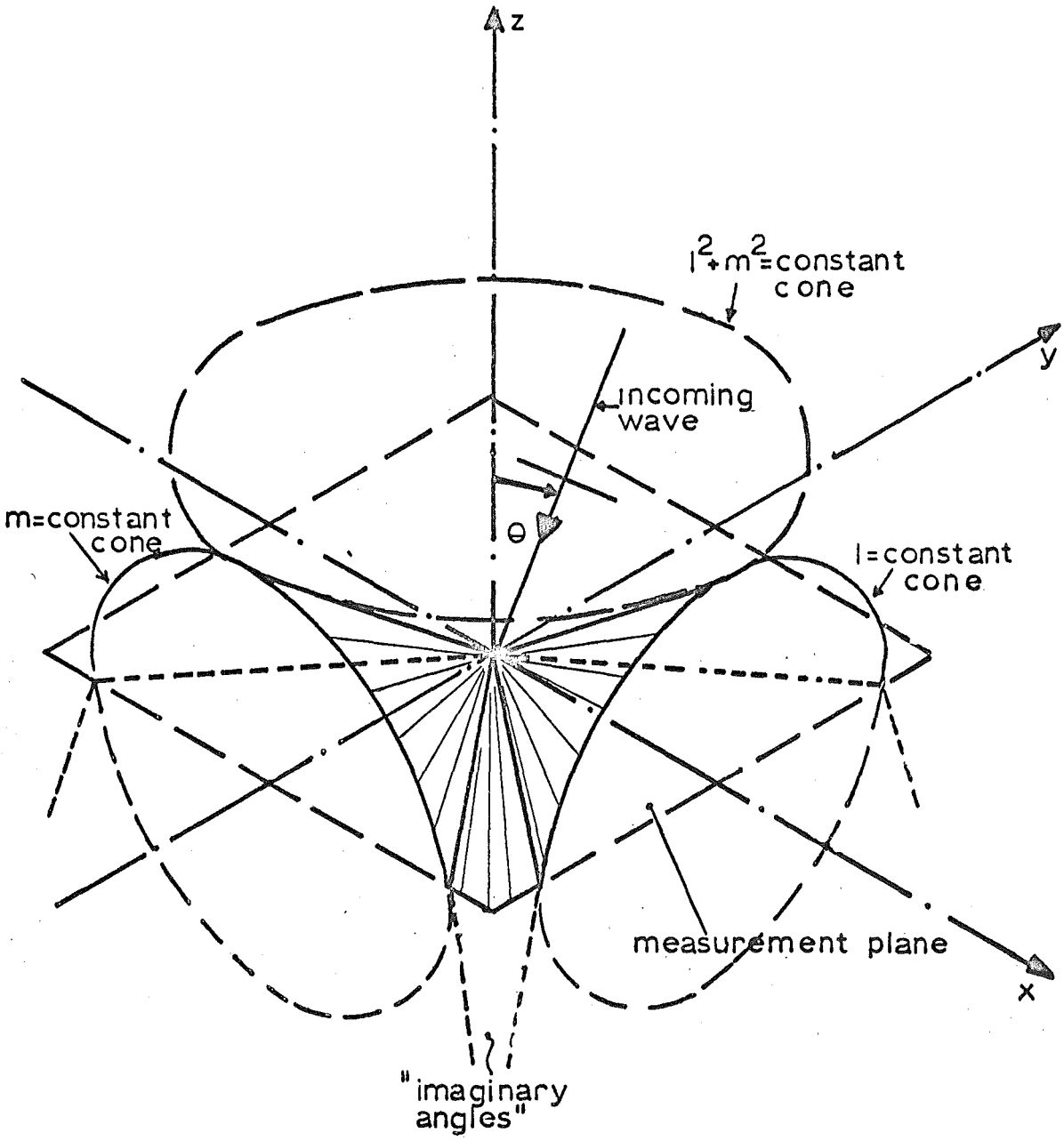

FIG. 6.4: Geometric constraints on angle of arrival

Only those waves having angles of arrival within the regions above the conical (for l^2+m^2=constant) or, for l=constant, m=constant, the indicated surface (shown in part), may be correctly recorded.

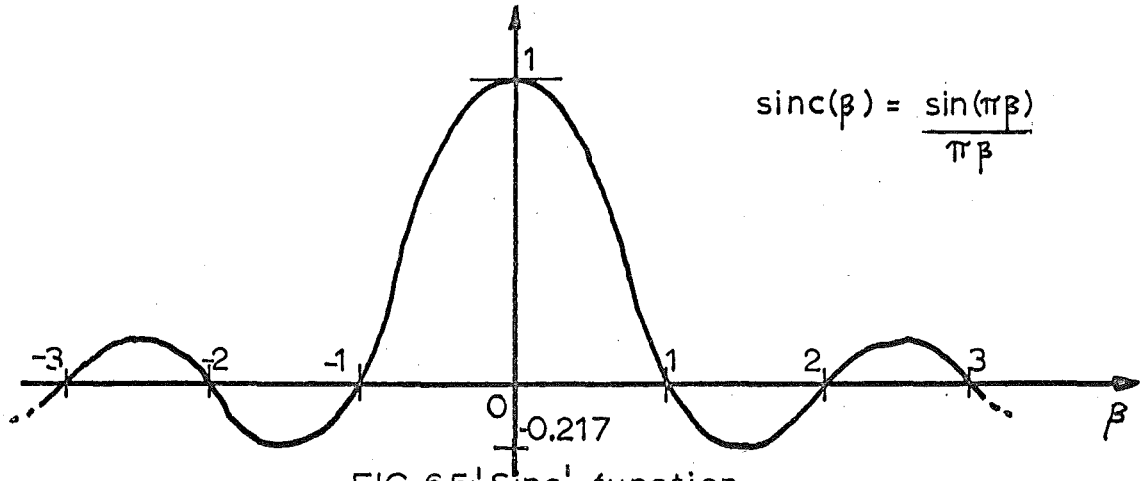

FIG. 6.5: 'Sinc' function

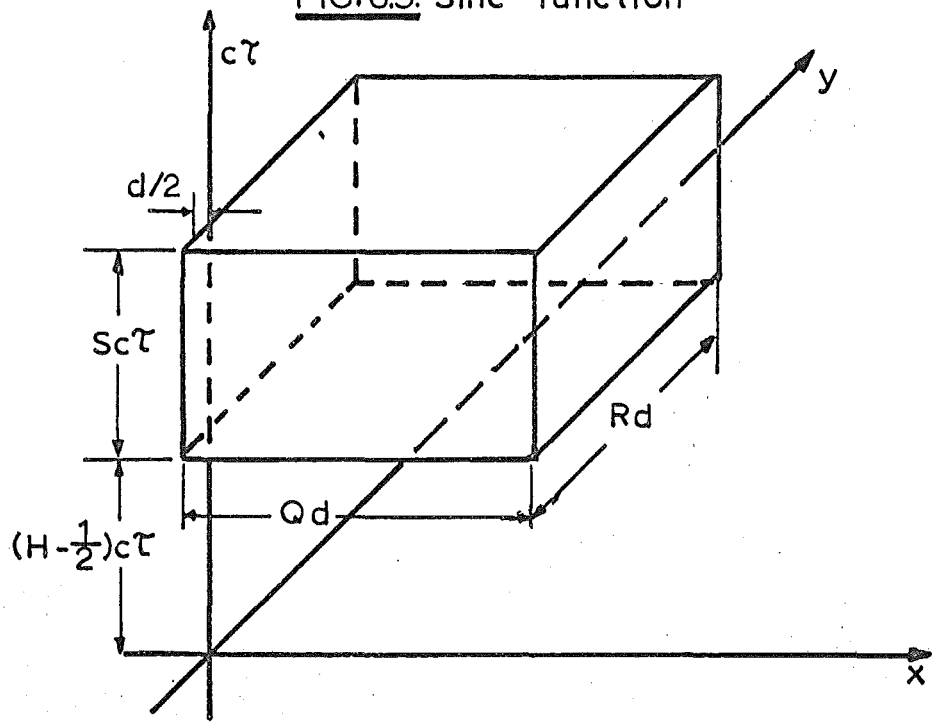

FIG. 6.6: Sample box

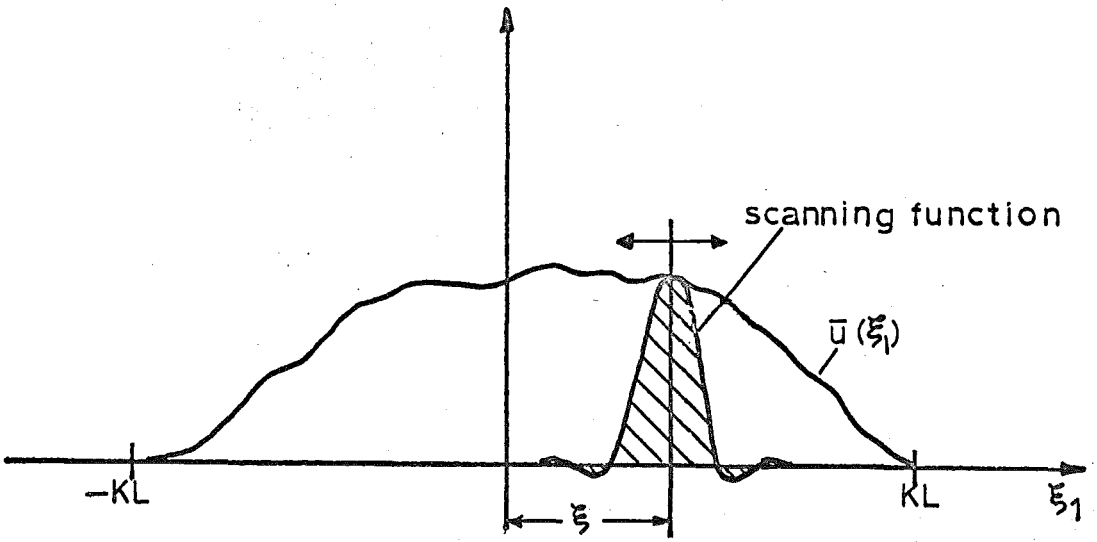

FIG. 6.7: Scanning of distribution by finite aperture

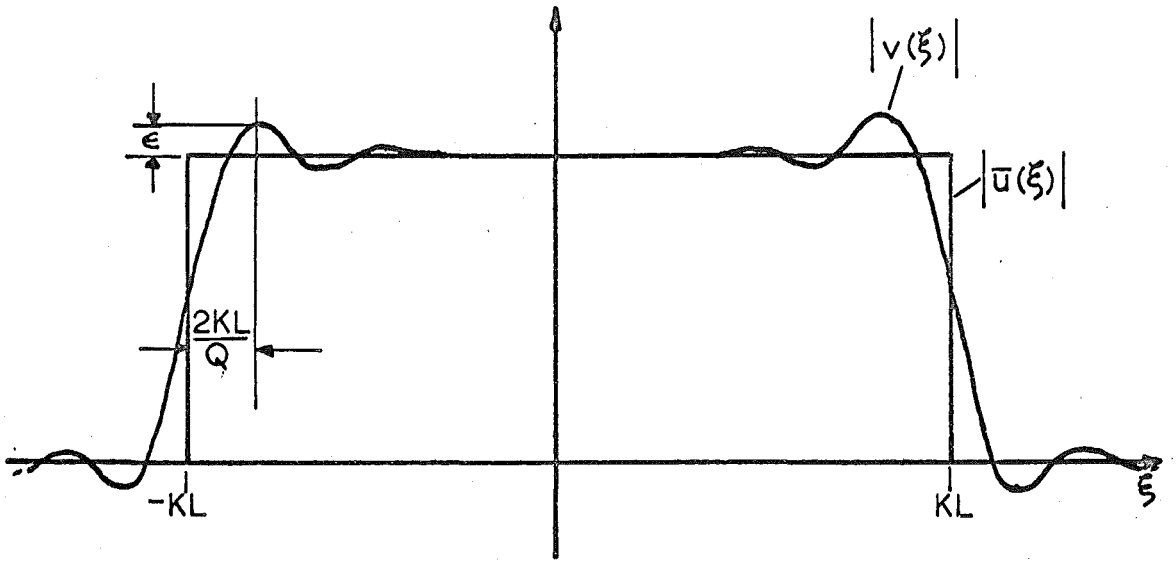

FIG.6.8: Spectrum distorsion with finite aperture

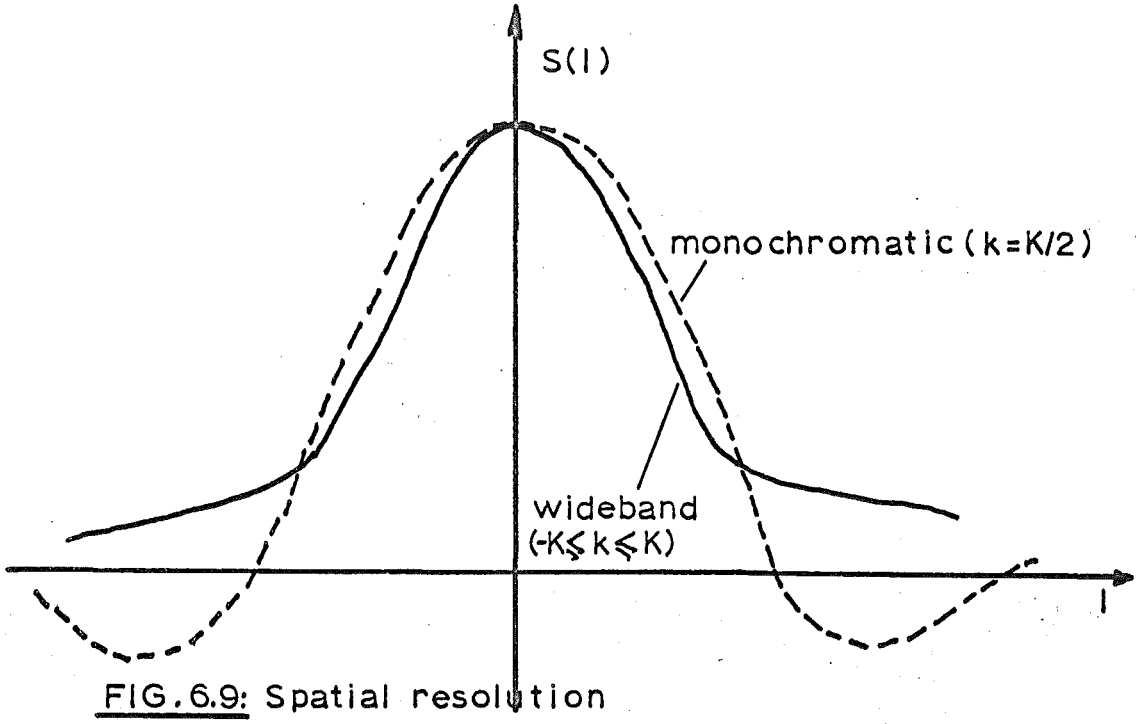

FIG.6.9: Spatial resolution
(see Fig.A 3.5/2 for detailed plot)

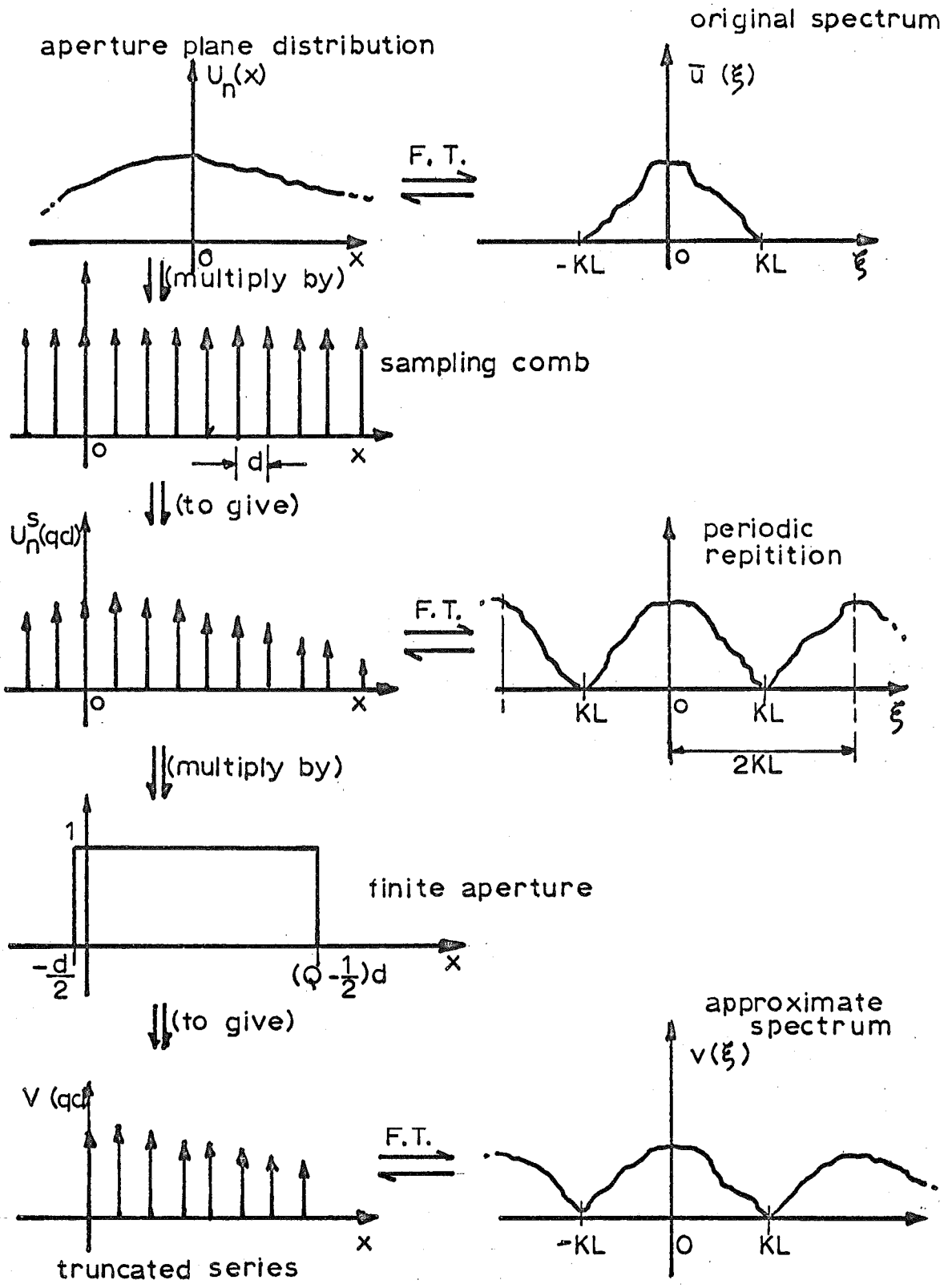

FIG. 6.10: One dimensional representation of signal processing operations.

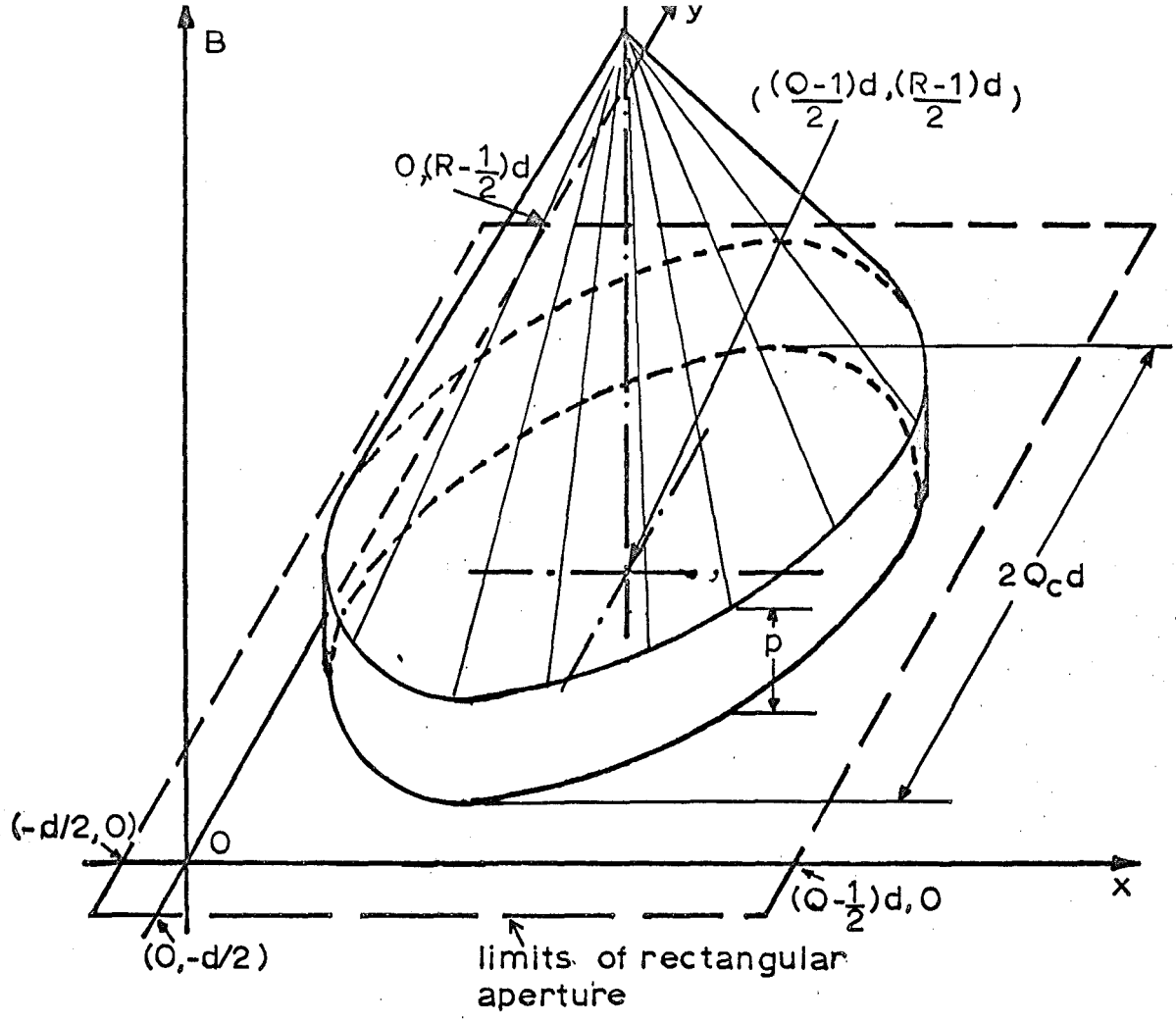

FIG. 6.11: Cone on a pedestal taper

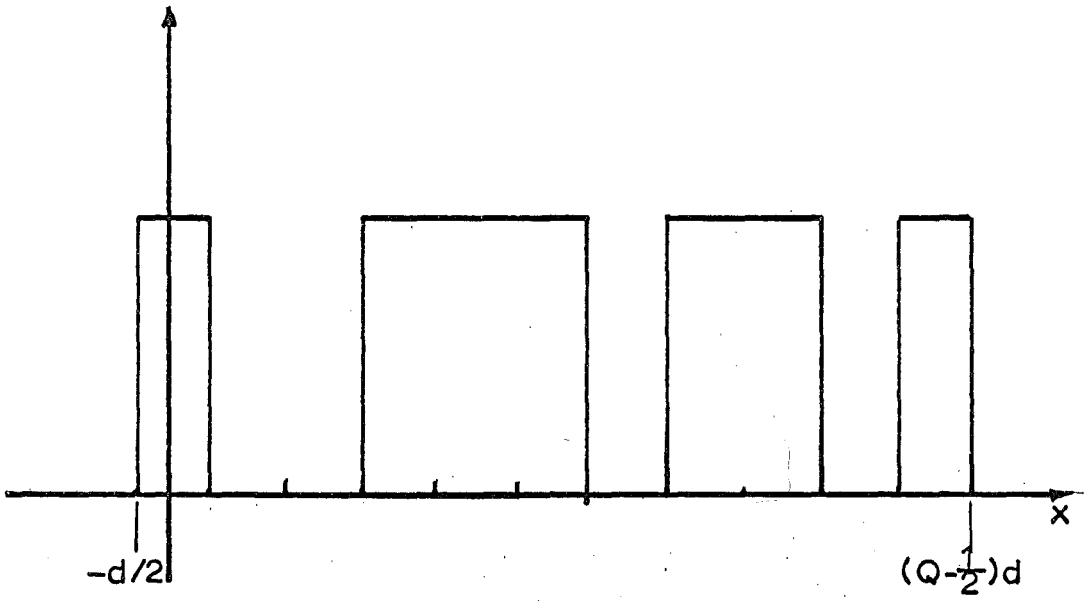

FIG. 6.13: Pertaining to random sampling

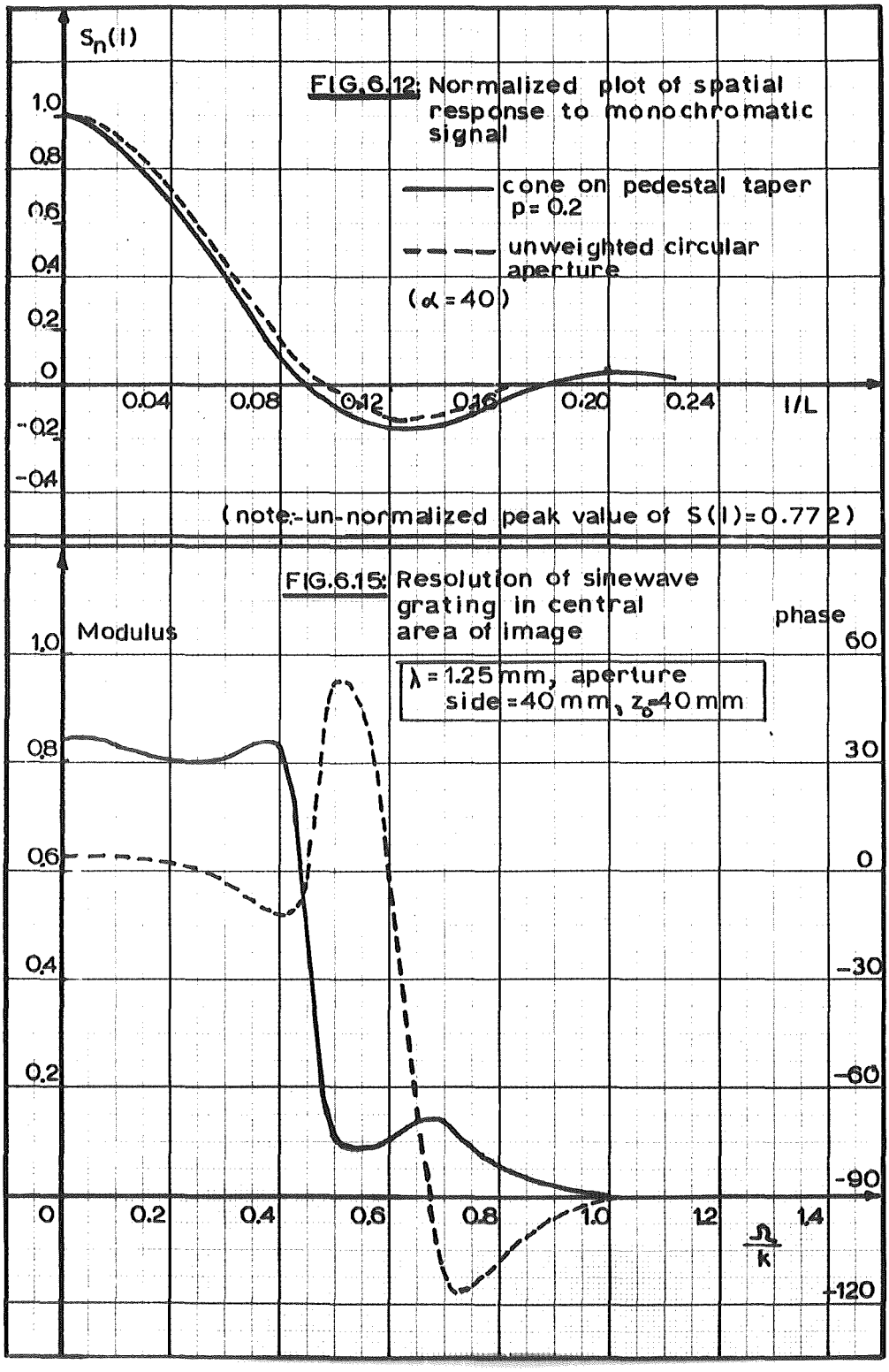

FIG. 6.12: Normalized plot of spatial response to monochromatic signal

FIG. 6.15: Resolution of sinewave grating in central area of image

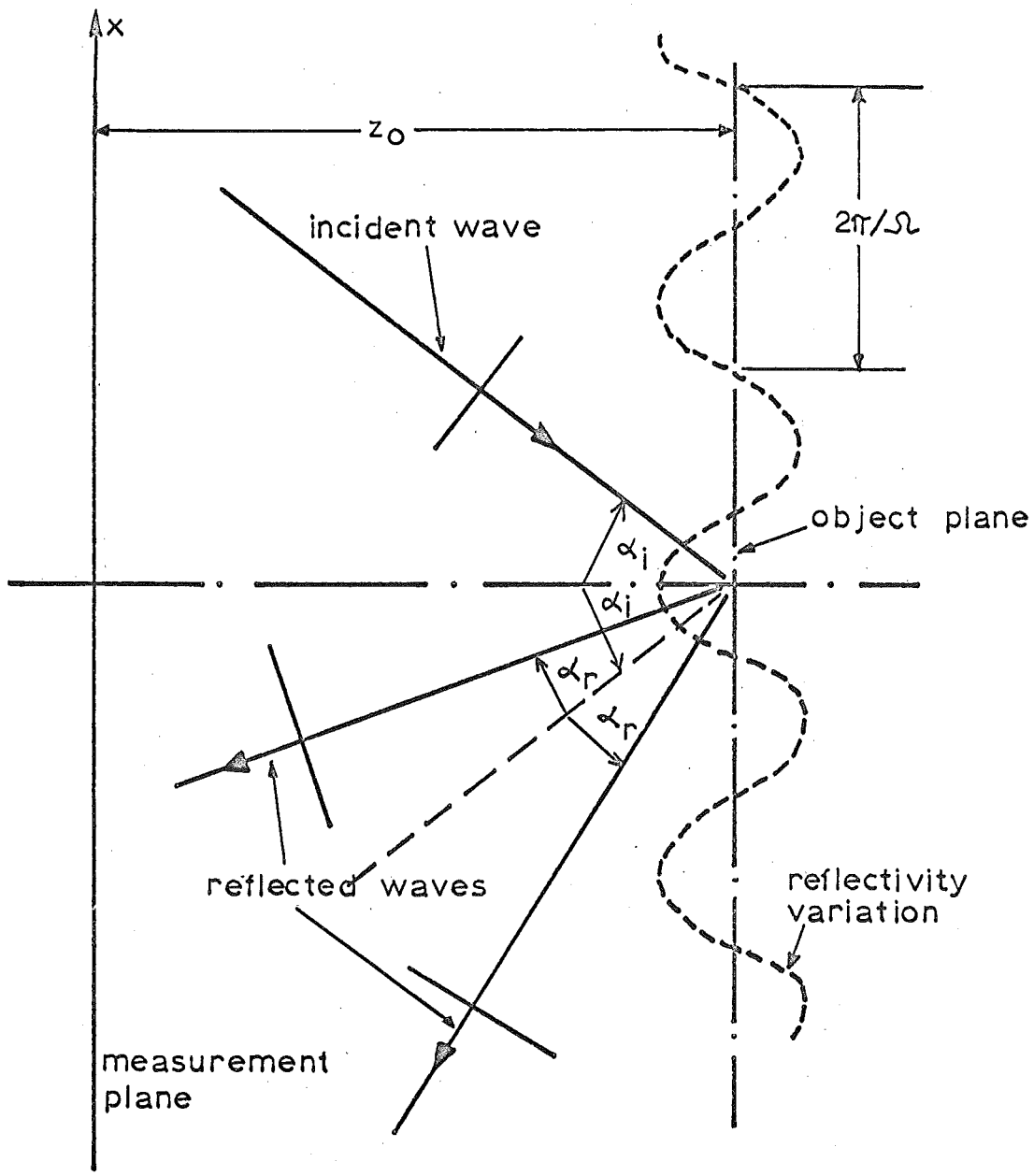

FIG. 6.14: Reflection at "test pattern" object

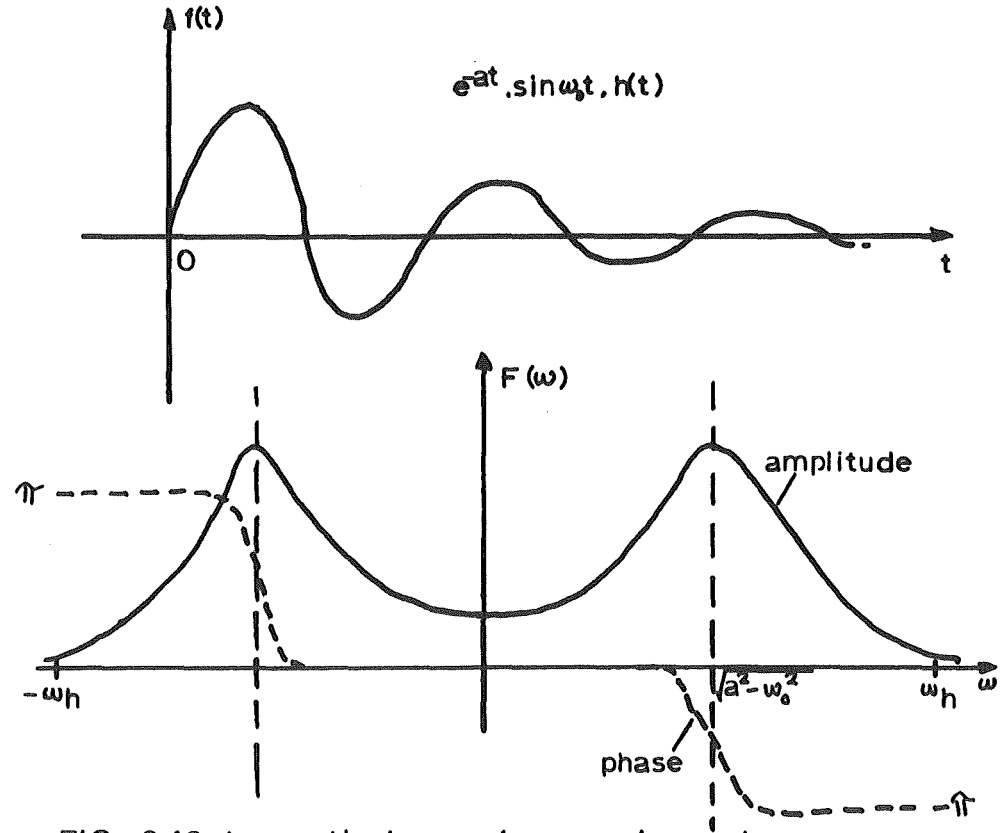

FIG. 6.16: A practical waveform and spectrum.

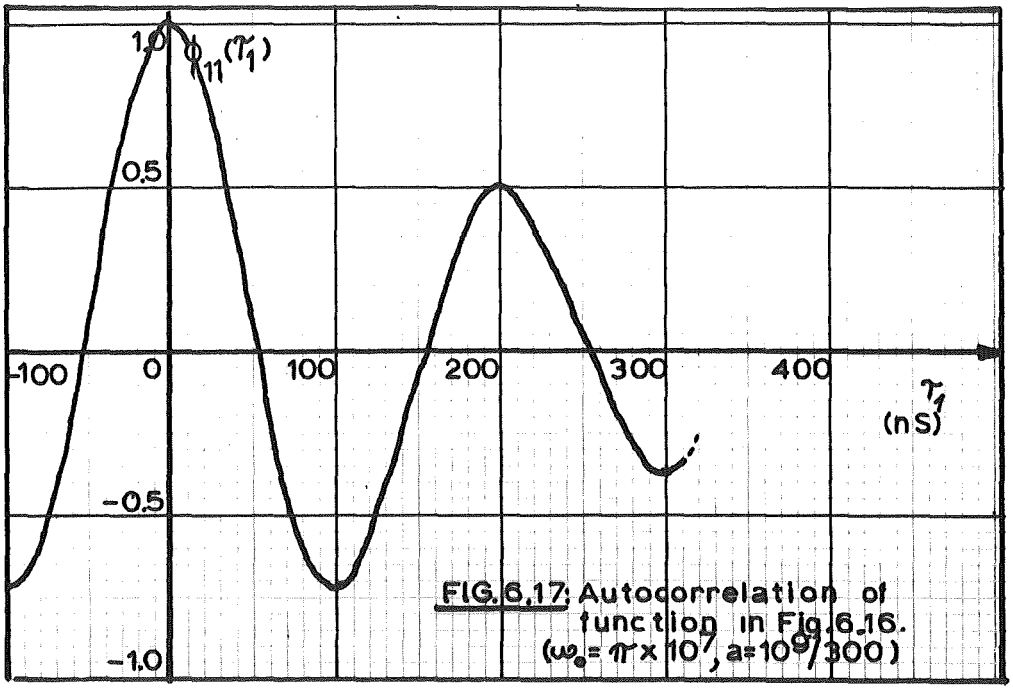

FIG. 6.17: Autocorrelation of function in Fig. 6.16. ($\omega_0 = \pi \times 10^7$, $a = 10^9/300$)

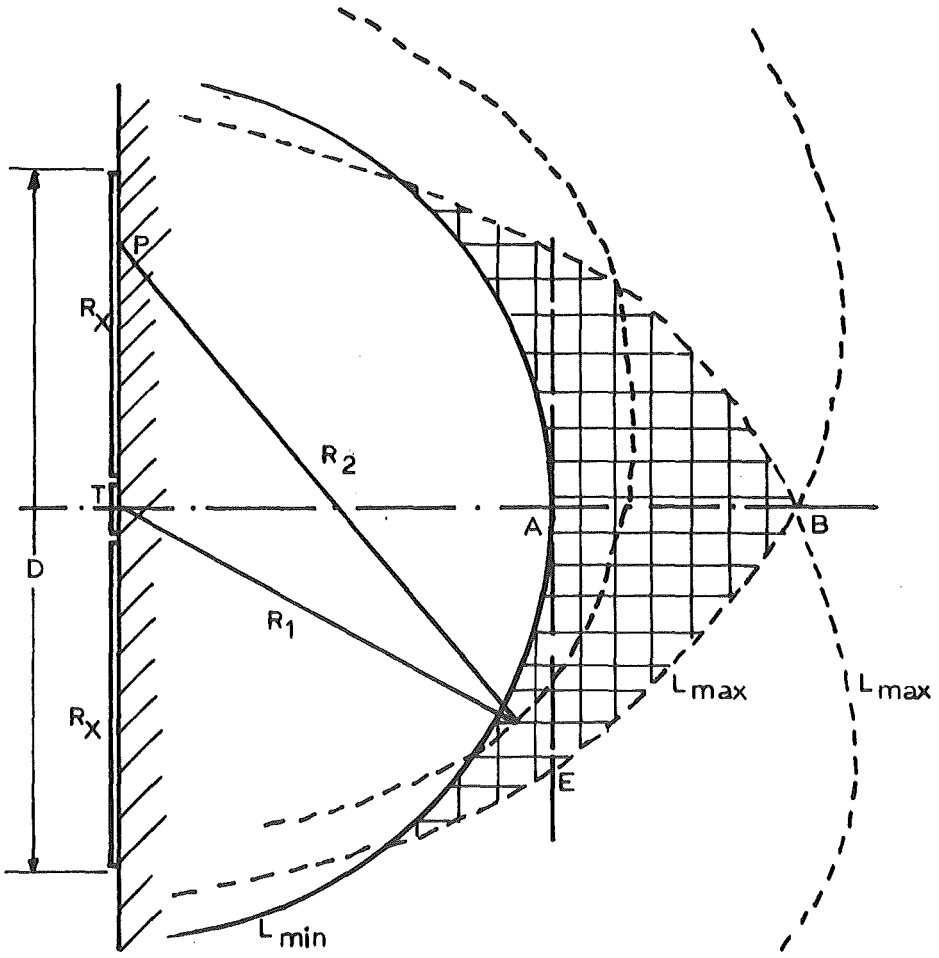

FIG.6.18: Cross-section of receiver transmitter and material geometry.

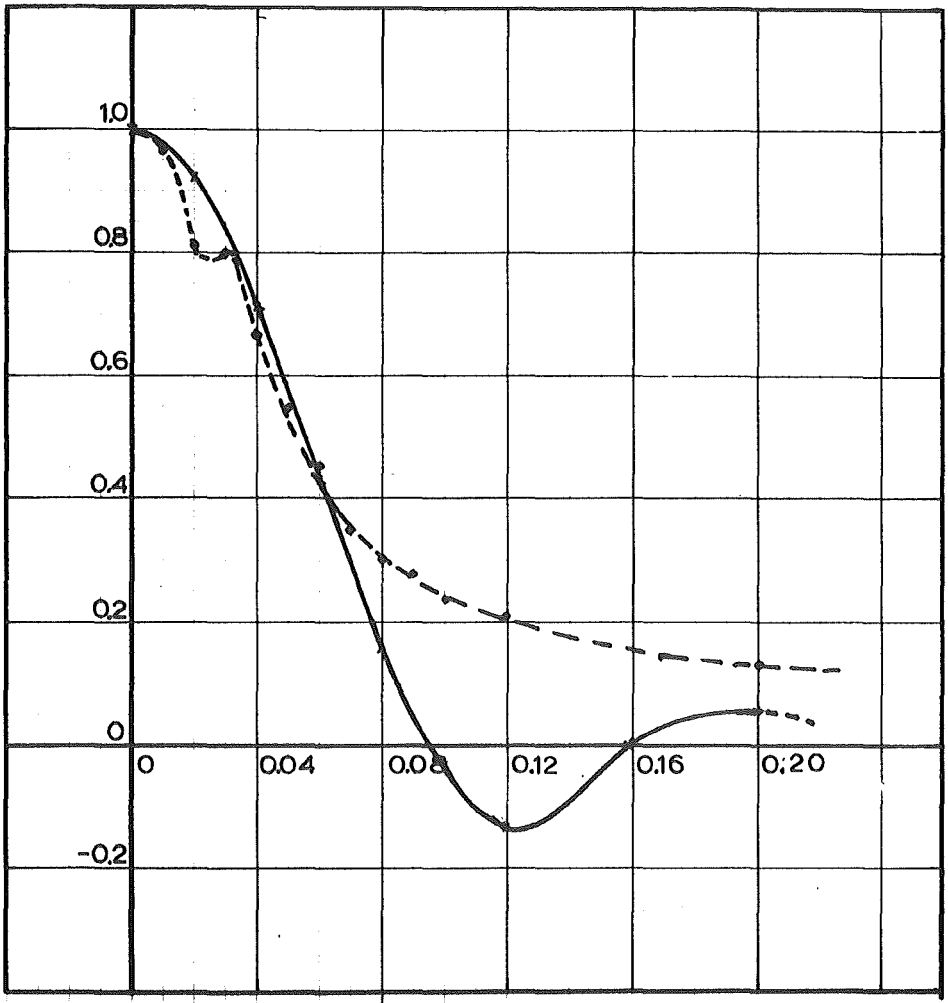

FIG. 6.19: Spatial pattern of unweighted circular aperture

——— monochromatic spectrum

– – – – – rectangular spectrum

CHAPTER 7.

INFORMATION PROCESSING IN THE IMAGING SYSTEM.

PART III. ERRORS AND NOISE: RELATIONSHIP TO RADAR/SONAR SYSTEMS.

7.1. INTRODUCTION.

In this chapter the sources and effects of noise and errors in the imaging system are considered. These resolve into two classes; perturbations which are peculiar to the particular application of imaging principles such as dispersion effects in the propagation medium and grain scatter, and problems common to any image forming arrangement such as timimg errors and thermal noise. The treatment concentrates principally on examining each of the contributions and categorizing them as additive amplitude errors which, in the absence of timing or phasing errors, result primarily in the establishment of a 'background' of random variations in the images, or as timing errors causing primarily a loss in the strength of the correct image relative to the background. Obviously this division is rather arbitrary but provides a convenient classification.

Finally some brief mention is made of the signal processing techniques used in array radars and sonars and these methods are related to those discussed in the three chapters of this portion of the thesis.

7.2. ERRORS AND NOISE.

These two sources of image uncertainty have been taken

together because except for a systematic 'error' such as accidental or deliberate assumption of an incorrect frequency scale in computation it has been found that they may be treated as statistically similar under the conditions prevailing in the apparatus and computing.

7.2.1. Noise and error sources.

(a) 'Amplitude' noise.

(i) Amplitude quantization in the recording process.

(ii) Production of a random spatial background from the sidelobes of the randomly thinned aperture pattern.

(iii) Backscatter from grain boundaries in the medium.

(iv) Thermal noise in the recording apparatus.

(v) Computer errors.

(vi) Display errors.

The first five of these are listed in approximate order of importance but the last, while large in the present arrangement using a line printer with a restricted number of distinct symbols, does not have the same basic significance as much more accurate data is available to produce the final plot and is not lost in the plotting operation.

(b) Timing errors.

(i) Variations from exact geometry in the physical layout of the receiving transducer.

(ii) Phase errors in the spectra of the signals from each

element.

(iii) Drift in the timing reference oscillator.

(iv) Deliberately introduced coarse quantization of phase in the computing operation to save computation time.

(v) Changes in propagation path lengths with changing temperature and the connected effect of velocity variations.

(vi) Systematic error in the choice of frequency values in computation. The relative importance of these errors is to some extent a matter of design in that without affecting such over-riding factors such as available data transfer methods and storage (which largely determine the relative significance of amplitude errors*) or computation time, (b) - (i), (iii), (v) and (vi) can, if necessary, be controlled to a precision several orders of magnitude better than the present system proves to require.

7.3. 'AMPLITUDE' ERRORS.

7.3.1. Amplitude quantization of the temporal record.

Earlier (Chapter 5) it was shown that two possibilities exist in performing the field reconstruction from a wideband signal record. One of these as in Equations 5.35 or 5.47 involves determination of the spectrum of the recorded time variation and the other uses the time samples directly. (Equation 5.44).

---

* For example, a more efficient recording medium than paper tape would permit compact recording of finer amplitude information.

In the previous chapter the effects of time sampling or quantization of the waveform were considered but with the inherent assumption that each time sample was an exact measure of the instantaneous value of the signal at the sample instant (or a weighted average of the value over a small interval around the sample instant). Feeding the signal into a digital computer demands quantization in amplitude as well as time so we now proceed to consider the effects of this operation.

7.3.1.1. Effect on time waveform.

It has been customary to describe the effect of a quantizing device on the signal passing through it as that of acting as a source of noise in the system, the noise introduced having a mean square value of $E_o^2/12$ where E_o is the step size in the quantizer.[1] This requires careful examination when one wishes to use a minimal number of levels to reduce the data storage requirements as there must necessarily be some causal relation between the input signal and the error introduced by the quantization. This problem of dependence of the noise on input signal behaviour has been studied by Widrow[2] through a consideration of the quantizer as a device which takes weighted samples of the probability density function (pdf) of the input signal. With an input signal having a Gaussian spread of amplitudes he shows that even for the level differences in the quantizer as large as twice the standard deviation (or RMS value) of the input the output noise is practically uncorrelated until the input correlation coefficient exceeds about 0.8. Since

any input to the quantizer is already time sampled at a little above the minimum rate for a signal of the bandwidth used, it follows that the input sample to sample correlation cannot be high and hence quite coarse quantization will still allow the quantization error to be treated as first order and uncorrelated, with a uniform probability over the range $-E_o/2$ to $+E_o/2$.

Since the input signals are in general the superposition of reflected signals off independent scatterers it is not unreasonable to invoke the central limits theorem and assume Gaussian statistics for their amplitudes. If we regard the signal as practically confined to the range -3σ to $+3\sigma$ (σ being the RMS value) then from Widrow's results the quantization may be as coarse as three levels without seriously violating the independent noise assumption. Thus for the purposes of evaluating the effect on an operation such as that specified in Equation 5.44 we may treat the quantizer simply as a source of noise in the system. However, before considering this we will examine quantization from the view of recovery of the signal spectrum.

7.3.1.2. Effect on the signal spectrum.

This problem has been treated extensively by Heaps and Willcock[3] and in a related form by Watts.[4] Heaps and Willcock establish a measure of the difference at every frequency between the function calculated via a discrete transform operation and that resulting from a similar operation on the quantized signals. Denoting this error function as $Q(\omega)$ it may be expressed in the form;

$$\tau^{\frac{1}{2}} Q(\omega) \rightarrow q'(T)^{\frac{1}{2}} \qquad .. 7.1$$

τ is the sampling interval and T the total duration of the record (i.e., S_τ). q' is a constant depending on the particular waveform being transformed and the arrow indicates 'tends to' (as $\tau \ll T$).

Initially some consideration was given to quantizing the signal to two levels only by infinite clipping. Heaps and Willcock indicate that the maximum value of q' in this case may also be reached by systems with any degree of quantizing but there is a far more serious objection than the large uncertainty in spectral estimation. This is concerned with the response when the input consists of the summation of a number of separate signals. This problem has been studied by a number of authors both as a general signal operation[5,6,7] and specifically for the cases of clippers included in the signal path of array antenna elements.[8,9,10,11] The main effects are the 'capture' of the limiter by strong signals to the exclusion of other weak ones present and the generation of spurious components in the spectrum of the output signal. For a single signal the additional harmonics generated reflect as new sidelobes in the plane wave response and this is not necessarily serious. However the presence of (say) two monochromatic plane waves at the array, presenting the limiters with the superposition of two similar signals with varying phase relative to each other, and the subsequent time sampling* and addition of the limiter outputs produces a whole spectrum of sum and difference frequencies,

---

* Time sampling would most conveniently be performed after clipping.

(regarding the progressive phase shift of one signal relative to the other as equivalent to a slight frequency difference) tending to appear as spurious large responses in the computed spatial distribution. This sort of behaviour is obviously unacceptable in a system which must deal with an unknown object distribution and which cannot have the array manipulated in the fashion suggested by Gore[8] to suppress the ambiguities.

Since recording of the signals can be most economically achieved by a pure binary coding the choice of a number of quantizing levels resolves down to 2^1, 2^2, 2^3... etc. Having rejected one bit or two levels as likely to lead to serious artefacts in the images and rejected the choice of a large number from storage limitations* practical considerations indicate 4 or 8 levels. Initial design of the apparatus assumed the use of the camera tube as the input transducer and this device results in a relatively low signal to noise ratio. (8.3.1).

An application of Shannon's formula[29] for rate of information transmission;

$$C = W \log_2 \left[\frac{P+N}{N} \right] \qquad .. 7.2$$

P and N being the signal and noise power respectively and W the bandwidth reveals for W = 12 MHz and P/N = 10 which is quite high,

---

* This is more a limitation of the actual recording media than of computer storage as the latter is commonly accessible in units ('Bytes') of not less than 8 binary digits and direct input would enable up to the corresponding number of levels (256) to be used.

that C is approximately 2 bits per sample interval. Experience with direct contact to PZT transducers has shown that much higher P/N ratios can be achieved and to utilise the more precise information, more levels should be used. A ratio of 35/1 for example corresponds to 3 bits per sample interval.

The compromise eventually taken was quantization to four levels enabling the data from 3 successive samples to be recorded on one punching of the paper tape while still leaving two spare channels for a distinct encoding of position identification.

From Heaps and Willcock we find that the maximum value of q' is 0.761 for 2 bit quantization, (although typical signals will generally have values very much less than this) the extreme error occurring for signals which are zero over 94% of the total range T.

The procedure involved in four level quantization is the choice of threshold level h (Figure 7.1). If the signal exceeds h then it is recorded as having the value 'a' and if less than h the value 'ca'. Negative signal values are treated similarly. The value of h that minimises error is a function of the signal amplitude distribution but should be at a level that the signal exceeds about 60% of the time and c set at 0.35. With these values $q' \approx 0.02$ so that with S = 200 say, the maximum error may be up to 40 % at a few values in the spectrum but in general is slight for the dominant components.

The actual signals in the apparatus do peak around the resonant frequency of the transducers and we may expect the region around

this to be well reproduced. Unfortunately some object distributions result in the received signal consisting of a short burst at high levels surrounded by a long period of near zero returns; precisely the condition that results in the largest errors. Ideally the time sampling window should be open for just sufficient time to encompass the returns at any one aperture element. If for example the signal occupies only 1 μS of the 10 μS window then a 3 times (Equation 7.1) reduction in maximum error due to quantizing could be achieved by accurate positioning. This would however be at the expense of increasing the errors caused by finite sample periods as discussed earlier(and in Appendix 3.3). Since the position of the signal from any given object varies within the full sampling window depending on receiving element position in the array, closing up onto it could be satisfactorily achieved only be elaborate 'on line' computation as the aperture interrogation proceeded. No such facilities were available at the design stage of this project and hence the possibility was discarded. Despite the extra information required to establish the time origin of each recording more accurate positioning would allow a considerable reduction in data storage.

An example of the computed spectra from quantized records is shown later (12.4.1.) but no apparatus was available to measure the spectrum of the analogue signals so it has not been possible to assess the errors with the actual arrangement used.

The value of h was arbitrarily set at one half the peak signal

value for all the experimental measurements made but can be easily changed. The value of c is set simply by the values assigned to the four output conditions and may be varied arbitrarily after the recording is made. For all the reported results a value of 1/3 was used.

For the purposes of assessing the effect of quantization on the overall performance it has been regarded as a source of additive independent noise of uniform power spectrum over the range of the signal spectrum.[1] This spectral model accounts for large errors in the computed spectrum at frequencies where the input signal is weak.

In the apparatus h is set at 0.5 volts and the step size an identical value. Thus the RMS noise introduced is approximately $0.5/(12)^{\frac{1}{2}} = 0.145$ volts. The peak input signal level allowable to the quantizer is 2 volts P-P ($= 2E_m$). If this is a single frequency tone then the S/N ratio over the full sampling arrangement bandwidth is $(0.707/0.145)^2 = 24$ or 19 dB. If at the other extreme the signal is essentially uniform over this bandwidth and has the characteristics of Gaussian amplitude noise then to avoid quantizer overload the RMS value cannot be set at more than about 1/3 (Bennett[1] suggests 1/4) E_m and the ratio degenerates to 7.2 dB for the time sampling rate employed.

7.3.2. Backscatter or 'structural reverberation'[12] in the medium.

This interference source is similar in nature to the 'clutter' encountered in radar. Some typical examples of the signals

involved are shown in Figure 12.29(a)-(d) from which it will be observed that these components change considerably from element to element of the receiving array.

A condition of negligible element to element correlation has been assumed and the problem resolves into determining the expected level in relation to the strength of the transmitted signal.

From Merkulov,[12] for the ratio of RMS received stress from grain scatter to transmitted stress, we have the expression;

$$\frac{\sigma_\rho}{\sigma_t} = \sqrt{\alpha_\rho}\ \frac{\exp(-2\alpha r)}{r}\ \sqrt{\frac{c\,T\,m}{4\pi}} \cdot \sqrt{A_r} \qquad .. 7.3$$

where α_ρ is the attenuation coefficient for scattering only,

α the total attenuation coefficient,

(both at the frequency involved)

r, is the distance of penetration into the medium,

c, the velocity of propagation,

T, the duration of the transmitted pulse,

m, a directivity factor depending on the transducers,

and A_r the area of the receiver.

It is further assumed that the transducers are physically adjacent, (or that r is large compared with the spacing).

Merkulov gives results for steel of two different grain sizes and attenuation figures[13,14] for aluminium are readily available. Attention will be concentrated on these two materials as having fairly high and very low attenuation respectively.

m will be taken as one, an approximation that results in a pessimistic estimate, and A_r as $1mm^2$. (This receiver area enters into the equation from the assumption of incoherent returns, the total scatter returns adding in power rather than amplitude).

We will take r as 8cm corresponding to the situations calculated in Chapter 3 (3.4.3.), and the insonification in the form of a pulse 10 μS long of a 5 MHz sinewave. Considering first the case of aluminium with an average grain diameter of 0.18mm then at 5 MHz α and α_ρ are not significantly different and give an attenuation value of 6.6 dB/metre;[14] whence $\alpha = 0.76m^{-1}$.

With these figures Equation 7.3 gives a value of 8.5×10^{-4} for the stress ratio. Now from Chapter 3 with $\sigma_t = 2.4 \times 10^5 N/m^2$ (peak) the stress back at the receiver for a 1mm radius reflecting disc at 8cm was found to be approximately $900N/m^2$, or $640N/m^2$ RMS under conditions of zero attenuation. Corrected for attenuation this reduces to approximately $565N/m^2$. Thus the signal to reverberation ratio for this target at this frequency is about 16 (power ratio) or 18 dB.

Merkulov's paper indicates that for the 8cm depth, 5 MHz is in fact very near to the frequency of maximum reverberation, the greater attenuation at higher frequencies reducing the return.*

---

* Note however that the amplitude of signal returns from small targets will also increase relative to a given transmitted stress at higher frequencies and thus despite the greater attenuation the signal/reverberation ratio can be expected to remain relatively constant. Actual returns with comparable targets to that taken above but over a wide bandwidth do in fact exhibit signal/reverberation ratios of the order calculated (Figure 12.29).

In the case of steel with the 1.2mm grain size considered by Merkulov, at 5 MHz the scatter only losses are approximately 520 dB/metre[13] giving $\alpha_\rho = 60m^{-1}$ and the corresponding stress ratio works out at 6.8×10^{-7}. However the attenuation of the signal components is now a factor of 7.9×10^{-5} and the resultant signal to reverberation ratio at the receiver assuming the same relation between transmitted and received target scattered stress ($\doteq$ 250/1) is now 0.21 (power) or -6.7 dB. Again this value is in good agreement with those actually observed. Figure 7.2(a) shows the return for a situation similar to that calculated here in aluminium and Figure 7.2(b) the return from an identical situation set up in steel of $\approx$ 0.3mm average grain diameter.

7.3.3. Thermal noise.

This interference component arises primarily in the source resistance of the transducer and in the associated amplifiers. As was seen earlier the expected signal amplitudes at the transducer element terminals (4.3.4.) are of the order of a few millivolts. In the actual arrangement used the receiver elements are loaded into a 50Ω resistance and since the actual source impedance of the transducer element alone is several times this value over the whole of the useful bandwidth the effective impedance has been taken as 50Ω.

For this source the MS noise voltage developed is given by the usual formula;[15]

$$\overline{V}^2 = 4kTRB \qquad .. 7.4$$

which with T = 300°K, R = 50Ω and B = 10 MHz, gives a numerical value of 8.3×10^{-12} or an RMS noise voltage of 3 μV. Of greater significance is the additional noise developed in the amplifier necessary to bring the transducer signals up to the 2 volt level needed by the analogue to digital conversion circuitry, (although if an image conversion tube is used the S/N ratio at its output terminals is much lower than the value indicated here). Use of a quartz transducer, even with direct connection, raises the circuit impedance by a factor of 100 or more compared with ceramics and a correspondingly higher noise level is to be expected. Reducing the loading impedance does not improve the situation as the signal voltage will tend to diminish in proportion whereas the noise falls off only as the square root.

For the type of amplifier* used to provide most of the required amplification, the internally generated noise is equivalent to 12μV at the input terminals for the bandwidth and source impedance used here. Thus if we assume a minimum signal voltage of 300 μV (RMS) the S/N ratio from thermal noise is 630 or 28 dB.

The three interference sources just considered apply to the individual element signals and from them we may derive the S/N ratio in the recorded signals supplied to the computer. Figure 7.3 shows the power spectra taken for the signal and various noise sources in the calculation. It is necessary to consider the ratio over each

---

* Fairchild μA733.

small frequency interval separately as the reconstruction process proceeds via calculations at discrete frequencies. The calculated components at each of these frequencies correspond to the weighting over the whole spectrum by a 'sinc' function but it is sufficient to regard the component as derived from a filtering operation using the rectangular filter indicated in Figure 7.3(a). With a total of 256 time samples spaced 41⅔ nS apart the spectral 'lines' calculated are at a spacing of 3/32 MHz and this will be taken as the bandwidth of the rectangular filter (δf).

Thus with the understanding that $\Phi(f)$ refers to the power in unit frequency interval we may write, for the ratio in the recorded signal;

$$SNR_1(f) = \frac{\Phi_s(f)}{\Phi_q(f) + \Phi_r(f) + \Phi_t(f)} \qquad .. 7.5$$

Now for the quadratic Φ_s indicated in Figure 7.3(a) the signal has been assumed a $sinc^2$ function modulating a cosine wave of 5 MHz. If the peak signal voltage allowed is 1 volt then the peak spectral value (A_s) is 0.02 $volts^2$/MHz. (Note that these are single sided spectra).

For the quantization noise the energy density is 0.0021 $volts^2$/MHz and the thermal noise (assuming that an amplification of 2000 is provided to bring a 1mV peak-peak signal up to 2 volts P-P) has a RMS value of 24mV for a further contribution of 5.7×10^{-5} $volts^2$/MHz. The contribution of reverberation depends on the material but taking the case of aluminium the peak spectrum value is 0.125×10^{-3} $volts^2$/MHz. In the case of steel the signal voltage cannot be so great if

overload is to be avoided and if we allow the reverberation to set the overall signal level then (approximately) it will have the value of 0.02 volts^2/MHz and the signal a level of 0.0045 volts^2/MHz.

Thus in the calculated component near 5 MHz (neglecting the small change in signal and reverberation levels over the 3/32 MHz interval involved) we have;

(1) Aluminium

$$SNR_1(5) = \frac{2\times10^{-2}}{2.1\times10^{-3} + 5.7\times10^{-5} + .125\times10^{-3}}$$

$$= 9.1 \text{ (or } 9.6 \text{ dB)}$$

(2) Steel

$$SNR_1(5) = \frac{4.5\times10^{-3}}{2\times10^{-2} + 5.7\times10^{-5} + 0.125\times10^{-3}}$$

$$= 0.22 \text{ (or } -6.6 \text{ dB)}$$

and we see that in the latter case the operations following the transducer element have had little effect on the SNR.

Proceeding similarly, for 3 MHz and 7 MHz in aluminium a figure of 3.2(5.0 dB) is obtained and by 1.5 or 8.5 MHz SNR_1 = 0.82 (-0.85 dB). For steel the ratio will remain similar to the -6.6dB figure over the whole frequency range of practical interest.

7.3.4. Computer amplitude errors.

These are the result of round off errors and similar computing artefacts and may be deliberately permitted to rise in low accuracy computations to speed computation. This action has not been taken

and consequently amplitude errors from computing actions may be considered negligible.

Before proceeding to the errors appearing in the displayed image we must consider the form of the (ideal) operation performed on the signals. Essentially this consists of applying phase shifts so as to bring the signals from each element into phase with each other at the image points. Considering for the moment just a single small object we may immediately state the usual result under the hypothesis of independent noise,* that the 'on target' SNR will be improved by a factor proportional to the number of active elements.

Thus for example with 148 elements (representing the case of most of the results shown in Chapter 12) the gain is 23.4 dB. Even for the worst case in steel the image SNR becomes about 17 dB and may be nearly twice this for the 5 MHz contribution in aluminium. For the full number of elements the recording apparatus is capable of dealing with (1000) the improvement is 30 dB. For image regions well removed from the target position the input noise to the processing operation will contribute a background level (again) proportional in power to the number of elements. If we define the signal power level in the element record at 0 dB then for the 5 MHz case in aluminium the 'on target' power (for 148 elements) is 46.8 dB while in the distant surroundings the level becomes 13.8 dB. For the steel example the figures are similarly 46.8 dB on target with a background at 30 dB.

---

* This may lose some validity at lower frequencies when significant element to element correlation exists in the reverberation.

7.3.5. Random thinning of aperture.

The necessary relation for this has already been quoted (Equation 6.46). Random thinning does not become necessary (unless by deliberate choice for other reasons than exceeding paper tape capacity) until the number of aperture elements exceeds 1000. With the computing facilities presently available an array of approximately 64 x 64 elements can be accommodated so with these two figures we derive the MS sidelobe level as $\frac{1}{1000} - \frac{1}{4096} = 0.75 \times 10^{-3}$ or -31.2 dB for an overall background level -30.7 dB relative to the on target level in the aluminium example and -22.7 dB for steel. In the former case the level is predominantly fixed by element removal and in the latter, noise in the original records is still the most significant.

In Chapter 12 (12.4.3.3) an extreme case of 148 elements thinned down to 16 is considered. In this situation Equation 6.46 gives 0.054 or - 12.7 dB. The noise contributed background is at a level of -21 dB for an overall -12.1 dB background. Assuming Gaussian amplitude statistics this implies that a few background peaks may reach to 0.75 of the target image amplitude. This is confirmed experimentally by the results obtained (Figure 12.44).

7.3.6. Display errors.

The effect here is essentially one of quantizing the range of output image variation. With the symbols available on the line printer used only 8 or 9 distinct levels were possible if some semblance to a normal 'black and white' picture was to be obtained.

From the usual $E_o^2/12$ formula this means a random component of 10^{-3} MS value. Despite this rather small value the pictures have a very coarse visual appearance and other work[16] indicates that 64 or more levels are desirable. However as mentioned before, precise data is retained in computer storage, the problem is simply lack of a more suitable output device.

7.4. TIMING ERRORS.

The basic effect of errors in the timing or phasing of the signals is to upset the accuracy of alignment of the coherent components in the image forming summation process. Since by hypothesis the noise is incoherent, phasing errors have no effect on the power summation involved and the noise background remains at the same absolute level.

7.4.1. Geometrical distortions.

This term is intended to cover departures from placement of the receiving array elements at the precisely regular points assumed. Since the elements average the signal over an area and occupy mutually exclusive positions, deviations from the correct relative positions are not possible.*

At the dimensions involved in the transducers precise

---

* For an electroded transducer plate. For a plate scanned by an electron beam any distortion in the scanning raster will cause errors. In Chapter 12 random element position variation has been introduced but as an artifice to simulate other forms of error.

duplication from element to element is no problem but systematic placement of the elements at a spacing other than that assumed is quite likely. This has the effect of making the phase progression of the incoming waves along the aperture appear faster or slower than the correct values depending on whether the actual spacing is closer or greater than assumed. The effect of this is similar to that of a deliberate frequency change which is discussed below.

7.4.2. Phase distortion in the element signals.

This problem is caused by the phase characteristic of any amplifiers or filters placed in the path of the element signals, including the phase characteristics of the element mechanical-electrical response. (In a phased array radar the main phase problem is that caused by differences from element amplifier to amplifier but here all the signals use the same path and are all affected equally). Some spectral components, as supplied to the image computing program, will have phases which are considerably in error from those at the transducer element terminals. Consequently reconstructions of the acoustic field will be in error especially at the higher frequencies relative to the low ones. However as the ultimate picture will of necessity represent an incoherent power summation of all frequencies this common perturbation in all element signals does not ultimately matter.

7.4.3. Path length changes and reference oscillator drift.

These temporarily distributed errors take the place of the

spatially distributed errors in a phased array system. A similar problem arises in holography where typically, a figure of 1/10th. wavelength stability in all distances is required over the photographic exposure time.

7.4.3.1. Path changes.

These may be caused by mechanical force applied to the material under test or by thermal expansion. No significance attaches unless changes occur over the recording time but as this may reach 20-30 minutes, thermal drifts in particular, need investigation.

The two effects involved are, (a) change in path length due to linear thermal expansion, (b) changes in velocity caused by changes in density and elastic constants.

In terms of the shear modulus and Young's modulus (for which temperature coefficient data is available[17]) the longitudinal wave velocity is given by;

$$c^2 = \frac{\mu(4\mu-E)}{\rho(3\mu-E)} \qquad .. 7.6$$

and the time for a wave to travel to a depth l and back again by;

$$t = \frac{2l}{c} \qquad .. 7.7$$

Taking the first order expansion for small changes in E, μ, ρ, and l, for the variation in t, gives;

$$\frac{\delta t}{t} = \frac{\delta l}{l} - \frac{E\mu}{2(3\mu-E)(4\mu-E)} \frac{\delta E}{E} + \frac{1}{2}\left[\frac{\mu E}{(3\mu-E)(4\mu-E)} - 1\right]\frac{\delta \mu}{\mu} - \frac{1}{2}\frac{\delta v}{v}$$

(v = volume, has been substituted for density) .. 7.8

Inserting the numerical values for aluminium gives;

$$\frac{\delta t}{t} = \frac{\delta l}{l} - 3.35\,\frac{\delta E}{E} + 2.85\,\frac{\delta \mu}{\mu} - 0.5\,\frac{\delta v}{v} \qquad .. 7.9$$

therefore, with

$\alpha_l = 0.26\times10^{-4}/^{\circ}C$

$\alpha_E = -21.3\times10^{-4}/^{\circ}C$

$\alpha_\mu = -13.5\times10^{-4}/^{\circ}C$

and taking $\frac{\delta v}{v} = \frac{3\delta l}{l}$

for the time delay thermal coefficient we have a figure of $33.8\times10^{-4}/^{\circ}C$. Similarly steel gives $-7.6\times10^{-4}/^{\circ}C$. For path lengths of the order of 160mm producing delays of about 28 μS these figures would imply changes of +95nS/°C for aluminium and -21nS/°C for steel, constituting a severe drift.

Measurements taken on an aluminium block with a total delay of 70 μS showed an increase in delay of 0.23 μS for a 20°C temperature rise; a figure which is only 1/20th of that predicted from the above calculations.* Consequently a figure of 1.7×10^{-4} has been adopted and implies that for the 28 μS delay case, shifts of no more than 5nS/°C which is only 1/20th of a cycle at 10 MHz.

The considerable thermal inertia of the large blocks of material

---

* The only reason that can be advanced for this discrepancy is a difference in properties between the actual sample used and those for pure aluminium to which the quoted coefficients relate. Because of the differing signs of the various components of the total thermal coefficient, quite small changes in material properties can considerably influence the final $\frac{\delta t}{t}$ value.

used inhibit any rapid temperature changes under normal laboratory conditions but this factor could be of considerable significance in an industrial environment.

7.4.3.2. Reference oscillator drift.

Consider Figure 7.4 showing, in outline, the transmitter and received signal sampling. Transmission is initiated through gate G_1 at a particular point on the oscillator (O) waveform indicated as occurring at time t_o. Inevitably a small 'jitter' will exist in the time interval between t_0 and a defined point at t_t in the electrical waveform produced by the transmitter T. Inspection has shown that this does not exceed 1nS.

Simultaneously with transmission a delay is initiated by counting of pulses from O in the dividing circuit D_F. (This provides the delay $H\tau$). Again the output from this may have jitter $\approx$ 1nS. Ignoring D_v for the moment the output from D_F triggers a further pulse generator P at the instant the leading portion of the desired signal reaches the end A of a delay line L. Propagation of the sampling pulse and the signal through each other gives a series of outputs at the tappings T_1-T_4 corresponding to the required samples. This whole transmission process is then repeated with an additional delay D_v introduced, corresponding (in the case illustrated to 4τ) to the increase in time of arrival of the next four samples of the waveform from the particular receiver element under interrogation. Most conveniently this delay increment is one cycle of the

oscillator frequency and so if τ = 50nS say, and four samples are taken per transmission, 0 would be at 5 MHz. (This apparatus is described fully in References 19 and 20). A little consideration will show that the effect of oscillator drift is to cause variations in the interval between the successive groups of samples. (Internal group timing is set by the delay line). Basically then the problem resolves into a determination of the variations that may occur over the complete recording period in the time required to accumulate a given number of oscillator cycles in D_F. This total recording time may reach 20 minutes. The worst case will be caused by a steady drift in one direction so that the oscillator period gradually changes over the recording time. Since with a paper tape record the intervals between transmissions are several orders of magnitude greater than the duration of each 'transmit-record sample group' period, we may assume that the frequency of the oscillator is essentially constant while each count for D_F is accumulated and changes at a rate δf_1 Hz/sec. between transmissions. A further drift at δf_1 Hz/sec. occurs during the period T_2 required to index from element to element. Thus if each element requires a total of N transmissions spaced T_1 sec. apart and there are M elements, the total drift will be;

$$\Delta f = N M \delta f_1 T_1 + (M-1) \delta f_1 T_2 \qquad .. 7.10$$

The relative oscillator drift $\frac{\Delta f}{f}$ (f = nominal frequency) will cause a corresponding opposite change in time measurements made by counting a fixed number of cycles.

With a maximum delay of 130 μS, (as in the apparatus) if the error reaches x nS then the drift is $\frac{x}{130} \times 10^{-3}$. If we allow a maximum misalignment between the first and last set of samples taken of say, 10nS, then $\frac{\Delta f}{f} < 7.6 \times 10^{-5}$ over the recording time $NMT_1 + (M-1)T_2$. This latter may reach 20 minutes so the required stability is 2.3×10^{-4}/hour, a figure readily obtainable with simple crystal oscillators. Temperature stability of AT-cut crystals over the normal termperature range is a few parts in 10^7 and will cause any significant performance degredation.

Overall then it may be seen that with only moderate effort phasing errors due to fluctuations in the material dimensions and timing reference in the apparatus may be contained within quite negligible proportions, (i.e., a few nanoseconds). In particular, timing stability may be further increased by the use of a larger amount of temporary storage in the apparatus to decrease N and higher speed transfer medium such as magnetic tape to reduce T_1 down to the minimum for reverberation to decay. T_2, while large, with manual or mechanical scanning is capable of considerable reduction if electron beam or switching array scanning is used. (Chapter 8).

7.4.4. Phase errors in the computed spectra.

The above discussed errors cover the situation up to the output of the quantization process in the apparatus. In the computed spectra of signals two forms of errors may occur -

(i) A systematic error due to the finite sample length. This is common to all elements and merely indicates

incorrect phases will be obtained for some of the calculated spectral components. Since ultimately the final plot can be of intensity only this will not affect the overall result.*

(ii) Random phase error caused by the finite SNR of the signal applied to the Fourier transform process.

If similarly to before we regard the Fourier transform process as one of passing the signal through a narrow band filter as illustrated in Figure 7.3, then for the pdf of the output phase (denoted as θ) with the correct value zero for convenience, we have the expression;[22]

$$pdf(\theta) = \frac{e^{-s^2}}{2\pi} + \frac{1}{2}\sqrt{\frac{s^2}{\pi}}\cos\theta . e^{-s^2\sin^2\theta}[1 - erf(s\cos\theta)] \quad .. 7.11$$

where s^2 is the power SNR and $erf(x)$ the error function.

With the value of $s^2 = 9.1$ obtained previously for 5 MHz in aluminium this function has approximately the form of a Gaussian distribution with variance $= \frac{1}{2s^2} = 0.055$ or RMS value of 0.24 radians. The other conditions considered produce pdf's with considerably more spread degenerating to a uniform probability over $-\pi$ to $+\pi$, with vanishing SNR.

Fairly obviously the contribution to phase error from noise in the system greatly exceeds any caused by thermal changes or oscillator drift and timing jitter and these latter contributions may be ignored.

---

* This does assume that the spectra of the signals does not vary greatly from element to element.

7.4.5. Quantization of phase.

In the computations it was found convenient to use a precomputed table of sines and cosines at certain fixed intervals rather than go through the full procedure each time. Basically this operation is similar to amplitude quantization except that now phase is being taken instead. If the quantization is done in steps of x radians then the MS error introduced is $x^2/12$. With $x = \pi/18$ (10^o) this gives 0.0025 rad.^{2}; much less than the error due to noise as calculated in the previous section.

7.4.6. Overall loss due to phase errors.

As already noted, the power sum of N cophasal signals of equal amplitude is $N^2 = P_o$. For the signals perturbed in phase by an amount drawn from a Gaussian population of RMS value σ the average power sum becomes;[23]

$$\overline{P} = N^2 e^{-\overline{\sigma}^2} + N(1-e^{-\overline{\sigma}^2}) \qquad .. 7.12$$

corresponding to a value between the completely coherent case and the completely incoherent value (N.)

(i) N = 148, $\sigma^2 = 0.058$ corresponding to the 5 MHz situation treated in the experiments;

$\frac{\overline{P}}{\overline{P}_o} = 0.942$, a gain loss of 0.25 dB.

With this small value of phase error the value of N has no direct significance and the gain loss on the peak remains at 0.25 dB for any N value greater than 3 or 4.

(ii) $N = 148$, $\sigma^2 = 0.155$ (corresponding to the 3 and 7 MHz situations) gives a gain loss of 0.75 dB, again independent of N. These very small losses indicate that phase errors are not of great significance in the system, a conclusion which is supported by the behaviour observed under conditions of deliberately introduced large errors (12.4.3.4).

7.4.7. Deliberate changes in frequency scale.

The behaviour of the image in a system where recording is made at a wavenumber k_o and reconstruction of the field at a wavenumber ak_o can be readily deduced from Equation 5.15(b) or 5.27. Considering the former, if we write ak_o for k_o it will be observed that exactly the same result will be obtained if all the distance variables x,y and z are scaled by 1/a to give;

$$U_z(x,y,z)\Big|_{k_o} = U_z\left(\frac{x}{a},\frac{y}{a},\frac{z}{a}\right)\Big|_{ak_o} \qquad .. 7.13$$

thus if $a>1$ the scale of the image is reduced and similarly expanded for $a<1$.* Obviously this effect in no way influences the relative accuracy of the picture obtained but the absolute dimensions may be in error when referred to the original objects.

In practice the most likely cause of an effective change in frequency scale is uncertainty as to the exact propagation velocity

---

* This effect is well known in holography and in fact was the impetus behind the original work by Gabor where greatly magnified versions of electron microscope images were sought by reconstruction at optical wavelengths, (i.e., $a<<1$). The opposite case occurs in optical reconstructions from holograms made from acoustic fields (2.3.2).

in the material being examined. If published values are relied upon these may differ by several percent from the actual value in any given specimen of nominally the same material.

The result of Equation 7.13 holds equally for the wideband case if all frequencies are scaled by the same factor. (Not by the same absolute amount).

7.5. SUMMARY OF ERROR BEHAVIOUR.

From the discussion above it may be seen that the predominant error source with most materials will be reverberation. Aluminium is somewhat exceptional among common materials for its low attenuation. Steel and brass have attenuations from one to nearly two orders of magnitude greater and the losses are greater still in copper and in nickel alloys of the type used in gas turbine manufacture.

With aluminium some significant performance improvement would be possible by finer quantization (16 levels would cause reverberation to predominate) but this additional complication would be of no benefit in any other likely material.

By comparison with a conventional ultrasonic inspection system, the present arrangement gains by providing the maximum gain possible by coherent addition of the signals over the transducer face for any size of receiver. Larger probes, averaging over the whole face, gain only up to a point as their size increases and may actually produce lower SNR's when the dimensions are so large that some parts of the

received wavefront are in antiphase with others.

Phase errors are seen as of comparatively minor importance.

7.6. RADAR/SONAR SYSTEMS.

As was mentioned in Chapter 1, some initial attention was devoted to a number of radar and sonar systemsusing various methods for electronically scanning the field under observation. In particular the sector scanning sonar of Welsby et.al.[24] in its many versions, and the techniques involved in phased array radars attracted interest.

In terms of the discussion presented here we may classify all these systems as devices which essentially perform some approximation to the operation of Equation 5.13,* i.e., determination of the plane of the plane wave spatial spectrum at a single frequency (or more accurately over a small relative bandwidth). This plane wave spectrum describes the far field of the system in terms of a distribution of point sources, each one responsible for a reflected wave which, over the aperture dimensions, presents a practically plane wavefront. Means for performing the more complicated operation of Equation 5.15(b) necessary to describe the near field are not provided although recently some interest has been shown in

---

* In particular the Butler[28] matrix performs the Fourier transform in hardware exactly paralleling the Fast Fourier transform technique with a large reduction in complexity compared with other beam scanning arrangements.

methods to obtain at least a quadratic approximation[26,27] (similar to that in Equation A3.6/5) to the z dependent term and so permit the increasingly larger arrays to operate at full resolution near to the aperture.

The other restriction of these techniques is the limited bandwidth of operation possible unless pure delay elements are provided instead of the usual phase shifters. Once delay is demanded the quantity of equipment rapidly becomes prohibitive for anything having more than a few receiving elements and all the advantages of the ingenuous techniques such as those of Welsby are lost.

The big advantage of these techniques is in the availability of real time image formation and it was this possibility that prompted the original study.

REFERENCES FOR CHAPTER 7.

1. Bennett, W.R. 'Spectra of quantized signals'.
   Bell Syst. Tech. Journ. 27, pp.446-474, July 1948.
2. Widrow, B. 'A study of rough amplitude quantization by means of Nyquist sampling theory'.
   IRE Trans. CT-3, pp.266-276, December 1956.
3. Heaps, H.S. and Willcock, P.W. 'The use of quantizing techniques in real time Fourier analysis'.
   Radio, Elect. Eng. 27, pp.143-148, March 1965.
4. Watts, D.G. 'A general theory of amplitude quantization with applications to correlation determination'.
   Proc. IEE, 109C, pp.209-218, March 1962.
5. Jones, J.J. 'Hard limiting of two signals in random noise'.
   IEEE Trans. IT-9, pp.34-42, January 1963.
6. Doyle, W. and Reed, I.S. 'Approximate band pass limiter envelope distributions'.
   IEEE Trans. IT-10, pp.180-185, July 1964.
7. Sollfrey, W. 'Hard limiting of three and four sinusoidal signals'.
   IEEE Trans. IT-15, pp.2-7, January 1969.
8. Gore, W.C. 'Non-linear processing in receiving arrays'.
   IRE Trans. AP-10, pp.656-662, November 1962.
9. Kanefsky, M. 'Detection of weak signals with polarity coincident arrays'.
   IEEE Trans. IT-12, pp.260-268, April 1966.
10. Kovaly, J.J. Statistical description of non-linear signal processing in array antenna systems'.
    IEEE Trans. MIL-9, pp.237-246, July-Oct. 1965.
11. Rudnick, P. Small signal detection with the 'DIMUS' array'.
    J.Acoust.Soc.Am. 32, pp.871-877, July 1960.
12. Merkulov, L.G. 'Modern ultrasonic inspection'.
    App.Mat.Res. 1, pp.98-106, July 1962.
13. Papadakis, E.M. 'Variation of ultrasonic grain-scattering factors with velocity'.
    Journ.Acoust.Soc.Am. 43, pp.876-878, April 1968.
14. Gooberman, G.L. 'Ultrasonics-Theory and application'.
    E.U.P. London, 1968, p.171.
15. Pierce, J.R. Physical sources of noise'.
    Proc. IRE 44, pp.601-608, May 1956.
16. Nathan, R. 'Digital video data handling'.
    N.A.S.A. Tech. Rept. 32-877, January 5, 1966.
17. Kaye, G.W.C. and Laby, T.H. 'Tables of physical and chemical constants'.
    Longmans-Green, London, 10th Edition, 1948, p.39.
18. Ibid. p.68.
19. Cook, G.B. 'The ultrasonic camera - a study of the transducer-computer interface'.
    M.E. Thesis, University of Canterbury, 1969, Chapter 7.

20. Cashin, P.M. and Johnson, D.A.H. 'A novel method of analysing singly occurring pulses with nanosecond resolution'. Radio.Elect.Eng. 38, pp.1-4, July 1969.
21. Mason, W.P. 'Physical acoustics. Vol.1. Part A'. Academic Press, New York, 1964, p.374.
22. Schwartz, M. 'Information transmission, modulation and noise'. McGraw-Hill, New York, 1959, p.410-413.
23. Ruze, J. 'Antenna tolerance theory - a review'. Proc. IEEE 54, pp.633-647, April 1966.
24. Welsby, V.G. and Dunn, J.R. 'High resolution sector scanning sonar'. Journ.Brit.IRE 26, p.205, September 1963.
25. Proc. IEEE. 'Special issue on electronic scanning'. 56, November 1968.
26. Hatcher, B.R. Collimation of row-and-column steered phased arrays'. Proc. IEEE 56, pp.1787-1790, November 1968.
27. Shah, C.V. 'Comments on "Electronic scanning of focussed arrays".' Journ.Sound.Vib. 10, p.352-355, September 1969.
28. Butler, J. and Lowe, R. 'Beam forming matrix simplifies design of electronically scanned antennas'. Electronic Design, pp.170-173, April 12, 1961.
29. Shannon, C.E. 'Communication in the presence of noise'. Proc. IRE 37, pp.10-21, January 1949.

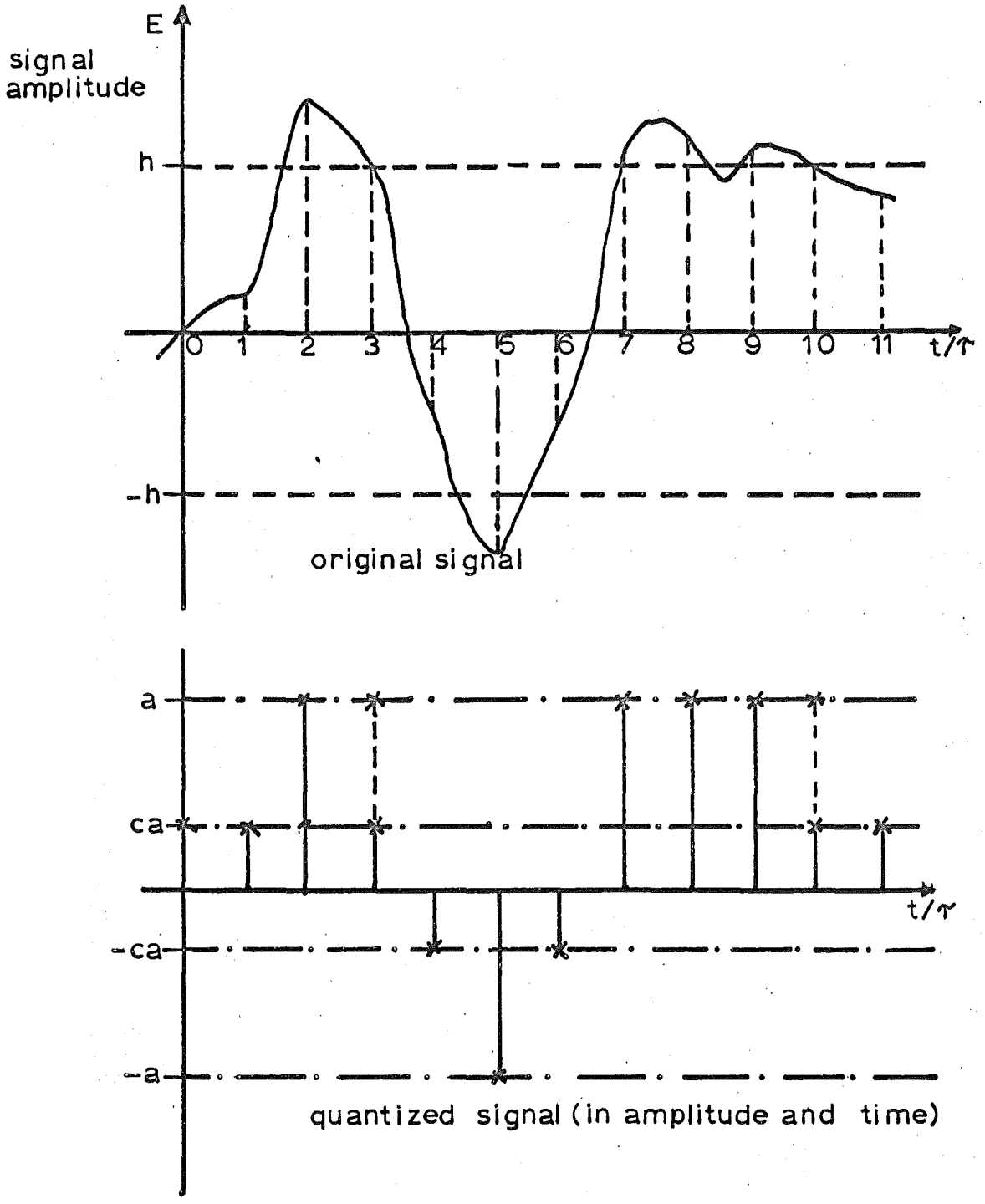

FIG. 7.1: Amplitude quantization.

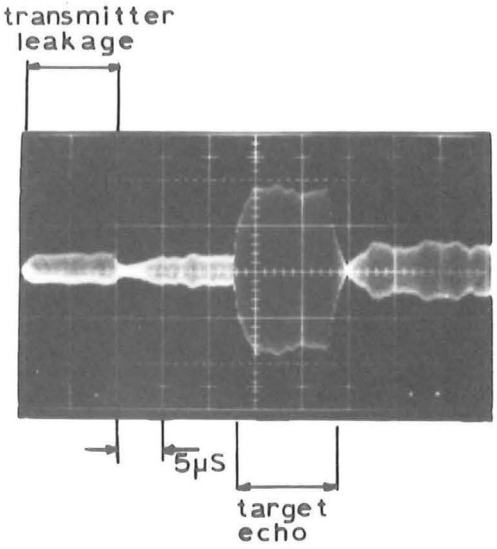

(a) returns in aluminium

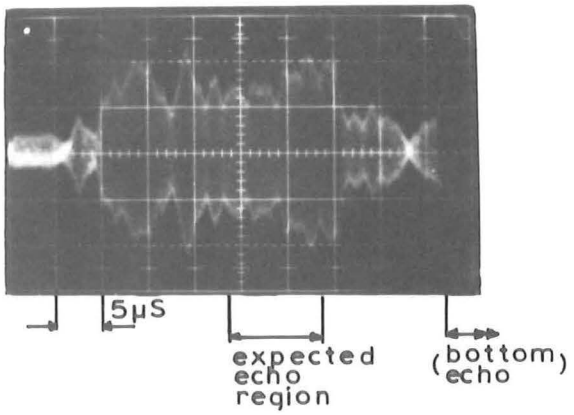

(b) similar situation in steel

FIG.7.2: Signals and reverberation in aluminium and steel.

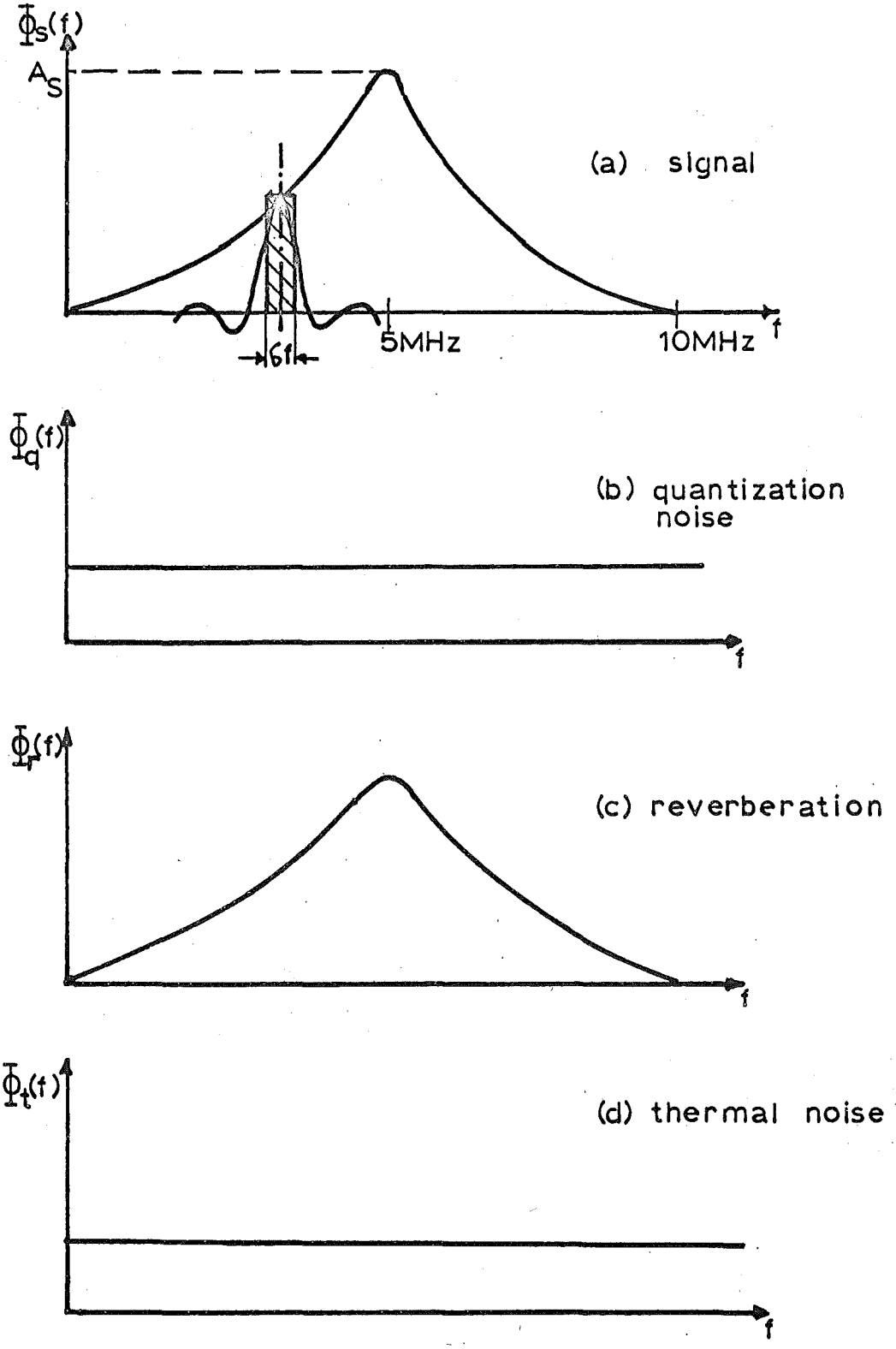

FIG. 7.3: Noise and signal power spectra.

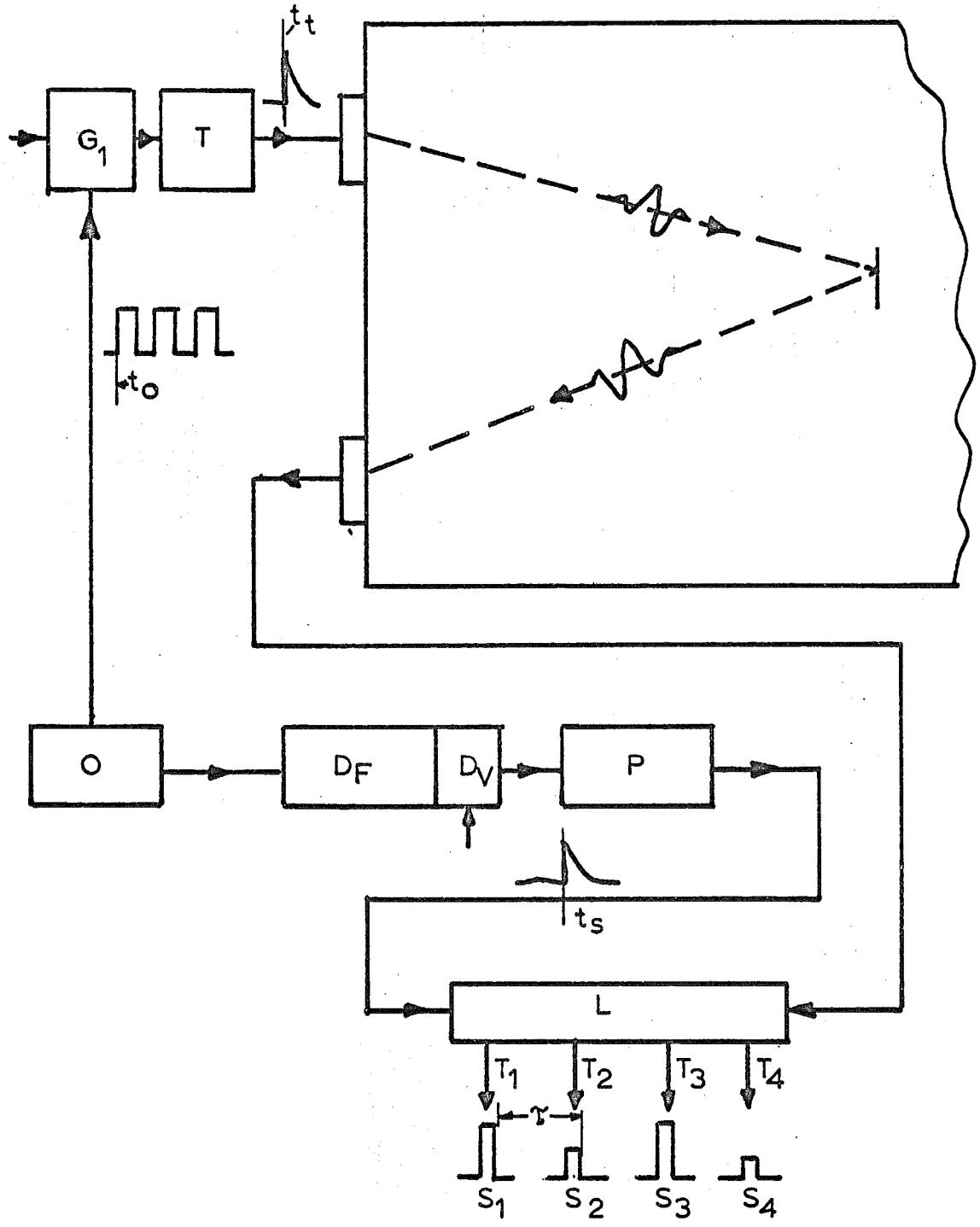

FIG. 7.4: Pertaining to reference oscillator drift.

CHAPTER 8.

INTERROGATION OF THE RECEIVING TRANSDUCER ARRAY.

8.1. INTRODUCTION.

This chapter is concerned with the details of available and proposed methods for accessing the individual elements of the receiving array. The methods discussed are;

(i) The image conversion tube, using electron beam commutation.

(ii) High conductivity contacts using mechanically scanned probe or electronic switching matrix, connecting to the elements formed on a slab of normal transducer material.

(iii) Complete integration of the transducer elements with the switching arrangements using a piezoelectric semiconductor material.

Of these, (i) is well established, (ii) has reached the initial prototype stage and, so far as is known, (iii) has not yet been reduced to practice.

When the transducers are operated under conditions that do not permit damping to be applied to the acoustic-electric response considerable 'ringing' occurs, severely restricting the useful operating bandwidth. Some attention was given to the possibilities of compensation for this effect by means of a matched filter and

this is also discussed.

8.2. BASIC REQUIREMENTS.

These may be stated as;

(1) Sample spacing. For operation in normal metals the finest element spacing needed is approximately 0.3 - 0.4mm. This limit presents some difficulties for electron beam scanning because of the problem of maintaining electron beam focus within a moderately sized tube at the operating currents needed and over the deflection angles required. A mechanically scanned probe moving over the rear face of the transducer can meet this spacing requirement without great difficulty through the use of stepping motors actuating a worm drive and 0.3mm is relatively large by the standards of integrated electronics permitting quite complex switching circuits to be used for each element if necessary.

(2) Aperture size. This must ultimately be set by the free plane area available on the specimen but if we require that the size should extend to the 128 x 128 elements that the present apparatus will scan* then the aperture should be capable of extension to at least 50mm in diameter. Apart from the rapidly increasing number of switching elements required this poses no problem for a switching matrix method; nor is there any difficulty in extending a mechanical scanner over this dimension. In the

---

* This size can be increased considerably with very little complication.

normal use of the image tube however, the situation is much more difficult as the transducer slab must withstand considerable mechanical stress and if chosen for resonance at a particular frequency is immediately limited in diameter. However, if the transducer is applied to a non-porous solid material capable of being cleaned to a sufficient extent to allow a high vacuum to be maintained in contact with it, this difficulty can be overcome. A more pressing objection is the one of maintaining geometric accuracy in the scan over a large area as this demands a precision electron gun, which, with the vacuum obtainable in the tube, needs frequent replacement or reconditioning.

(3) Signal transfer characteristics. Here the image tube fails badly, firstly on account of the transfer of the signal over an electron beam thereby introducing shot noise, and secondly by the high impedance of the 'connection' to the transducer element which effectively isolates the transducer from any external circuitry that might be used to improve the damping. With the direct connection of a probe or a switch both of these problems are avoided.

(4) Artefacts. Again spurious signal pickup can be considerable in the image tube without extensive shielding as a consequence of the high impedances in the signal circuitry, while the low impedances in the 'solid' arrays overcome this problem.

(5) Physical convenience. This is probably the most pressing objection to the image tube as in association with the necessary vacuum gear it becomes virtually a fixed object and specimens must be brought to it rather than vice versa. Mechanical scanning does, of course, require a certain amount of setting up and alignment of the apparatus but the problem is much less, while in the ultimate form of an electronic switching matrix or completely integrated array one would envisage a device of similar appearance to a large probe of the type used in conventional pulse echo testing systems and with the corresponding ease of application.

(6) Scanning time. In this respect the image tube or a switching matrix can provide nearly instantaneous access to any element while a mechanical scanning device must inevitably consume considerable time. This is not so serious so long as paper tape is used for data transfer but would virtually negate any advantage in recording time obtained by the use of, say, magnetic tape recording. A short recording time is not essential for purely laboratory application but becomes a decisive factor if any hopes of application in industrial situations or to medical examination are entertained.

8.3. THE ULTRASONIC IMAGE CONVERSION TUBE.

Since the image conversion tube is a well established device and has already been exhaustively considered by the present author[1]

only a brief survey of the main features will be presented here. This device initially appeared to hold considerable promise as a transducer for the imaging system but as in fact successful operation was never fully achieved and the trend is towards the use of 'solid state' scanning, the current importance does not warrant extensive treatment.

At the time the work reported here commenced, characteristics of the transducer tubes used in developments of Sokoloff's original idea (1.2.3) were;

(1) Use of resonant face plates one half wavelength thick under conditions of very light damping.

(2) Continuous wave operation.

(3) Relatively small active faces (2 - 5cm diameter).

(4) Use of the transducer plate as part of the vacuum envelope.

Two systems of scanning the transducer plate were developed; one by Smyth et.al.[2] employing a low velocity electron beam which results in rectification of the piezoelectrically generated signal and the other, developed by Jacobs[3], using high velocity electrons which allowed preservation of the signal phase. Although both these tubes are available commercially[4,5] only the latter type is of any potential use for the present system.

To a large extent the features listed above are interrelated and a result of operating the device with a fluid medium. If

operation with solid materials only is sufficient then at one stroke all these disadvantages can be eliminated by bonding the transducer plate directly to the solid and sealing the vacuum envelope onto the solid. This gives good damping to the transducer, permitting wideband operation and by removing all static mechanical stress enables extension to any size of aperture.

8.3.1. Tube electrical performance.

Figure 8.1 shows diagrammatically the signal path in the tube. The transducer plate, being an insulator, produces secondary emission at the point bombarded by the electron beam with the mean current leaving equal to that arriving. Some of this electron stream, modulated by the piezoelectrically induced signal V_E, is captured by the electrostatic screen while the remainder appears at the input to an electron multiplier within the tube envelope emerging in amplified form at A. The amplifier indicated is external to the tube but may be significant in determining the SNR.

In practical devices a considerable portion of the current is lost to the electrostatic screen but its insertion is essential to prevent a large interfering signal being transferred by the capacitance between the transducer plate and the multiplier.[6]

The whole arrangement of this tube is similar to the 'image orthicon' tube[7] developed in early television practice.

In Figure 8.2 an equivalent circuit of the tube is shown. R_E and C_E represent the resistance and capacitance of the source

impedance of the transducer element over the frequency interval under consideration. R_B is the resistance of the electron beam regarded as a signal transfer path. Z_L represents the impedance presented by the input stage of the multiplier while I_{n_1} and I_{n_2} are the equivalent noise currents inserted in the signal by the electron beam and the multiplier. C_E is simply the static capacitance of the transducer element, while R_E has the value;[1]

$$R_E = 4h^2/\omega_o^2 \, Z_m A \qquad .. 8.1$$

h being the piezoelectric stress constant (h_{11} for quartz), ω_o the transducer resonant frequency, A the element area and Z_m the specific acoustic impedance of the material from which the acoustic signal is coming.

This equation is valid near resonance only, but in practice this is of no significance as R_B is very high and swamps the transducer impedance.

The voltage V_E modulates the electron beam to an extent that can be described by defining a 'beam modulation factor' as,

$$M = \frac{\text{peak value of alternating current}}{\text{steady component of current.}} \qquad .. 8.2$$

and this typically has a value of 5% per volt RMS of signal.[3]

In the ultrasonic image tube where no charge storage occurs, there is no heavy discharge current from the element being interrogated[7] and the equivalent beam impedance is very high, being of the order of 50 MΩ. By comparison, the impedance of C_E even for quartz is about only 1 MΩ, and the transducer

impedances for ceramic materials only a few thousand ohms. Consequently any loss in the developed voltage may be neglected.

Noise sources - noise enters into the signal path from;

(1) Equivalent resistance of the transducer element, giving a contribution;[8]

$$\overline{V}^2 = 4kT R_E B \quad .. 8.3$$

(2) Shot noise in the scanning beam - this contribution is given by;[8]

$$\overline{I}_{n_1}^2 = 2e_o I'_B B (\Gamma\delta)^2 \quad .. 8.4$$

e_o being the electron charge. Γ is a factor to account for smoothing of the electron distribution by the presence of a space charge. A pessimistic estimate of noise will be obtained by taking this as 1. δ accounts for the increased velocity spread in electrons resulting from secondary emission and a suitable value for image tube operating conditions is $\delta^2 = 2$.

(3) Electron multiplier noise - the MS output noise current from the multiplier is given by;[29]

$$\overline{I}_{n_2}^2 = 2e_o I'_B B \cdot \frac{G^{\frac{n+1}{n}} - 1}{G^n - 1} \quad .. 8.5$$

G being the gain per stage and n the number of stages.

Taking these in order, with a $1mm^2$ element R_E varies from 5200Ω for quartz on aluminium down to 1200Ω for PZT5A on steel giving rise to noise contributions (all over 1 Hz bandwidth) of 86×10^{-18} volts^2 and 20×10^{-18} volts^2 in the region near the 5 MHz

resonant frequency.

In the tube actually used* I_B may typically have the value 2 μA** and the current reaching the electron multiplier about half this value. (These are measured values in an actual tube).

With $I'_B = 1 \times 10^{-6}$A the shot noise contribution comes to $64 \times 10^{-26} A^2$. In this case the noise spectrum is 'white'.

With the value of M quoted above the transducer noise voltage will modulate the electron current to a maximum of about 22×10^{-32} A^2 which is quite negligible in comparison with the shot noise.

The spectrum of shot noise contribution at the input to the electron multiplier depends on the impedance presented by Z_M, the equivalent input impedance of the multiplier. Because of the 'constant current' nature of the source current I'_B any small capacitances will result in some shunting of the higher frequencies in the modulation. However the rise-time figures commonly quoted for multiplier outputs[9] are of the order of a few nanoseconds, so within the bandwidth of the present system any loss is negligible.

The stage gain of the multiplier is a function of the applied voltage differential between dynodes, the dynode surface material

---

* James Electronics, Type C-4906

** This is much less than the cathode current value recommended by the manufacturer. Most of the cathode emission (50-100μA) is returned through the accelerating electrodes in the tube and does not reach the transducer plate.

and the history of the multiplier. This latter factor is of considerable importance in a tube subjected to repeated exposure to the atmosphere and materials that will withstand this treatment (beryllium-copper commonly[10]) have secondary emission factors somewhat less than the values of 8 or 9 that can be achieved in permanently sealed photomultipliers. At the applied voltage in the James Electronics tube, the stage gain is typically 2. Thus with n = 10 the overall gain is given by;[9]

$$G_T = G^n = 1024^* \qquad .. 8.6$$

and for the noise source $\overline{I}^2_{n_2}$ we have a value of $3.5 \times 10^{-28} A^2$. The beam noise $\overline{I}^2_{n_1}$ will emerge at a level of $64 \times 10^{-20} A^2$ which is far in excess of the internal multiplier noise and the latter may be neglected.

The output voltage developed from the multiplier is a function of the load impedance Z_L applied. This is quite a complicated network of resistors and capacitors but basically amounts to approximately 2000Ω in parallel with 22 pF giving a time constant of 44 nS.** If operation up to 10 MHz is needed this time constant is too great and although it was not actually done as work on the tube was suspended, the resistive component should be reduced to

---

** Some modification to the values of the coupling capacitors supplied was needed to produce acceptable low frequency response.

* Note that in any case more gain than this cannot be comfortably used because of the large D.C. component at the multiplier input which will, with the figures quoted, give upwards of 1 mA at the multiplier anode.

less than 800Ω for satisfactory performance. If we take this value then the RMS noise voltage in the operating frequency range would be (in 1 Hz);

$\sqrt{\overline{V^2}} = 64 \times 10^{-8}$ volts.

Now for a signal at the transducer of V_E volts RMS, the resultant beam current (RMS) will be $0.035 \times 10^{-6}\ V_E$ amps and the output signal voltage $V_O = 28 \times 10^{-3} V_E$.

For the single frequency operation conventionally used with image tubes the amplifiers provided* define the system bandwidth at approximately 1.5 MHz giving a noise level of 8.0×10^{-4} volts, RMS. Thus for a SNR of 1 at the multiplier load, V_E must have the value of 29 mV and to achieve a SNR approaching those attainable with direct connection, the element signal must be an appreciable fraction of a volt.

For operation over the full 10 MHz bandwidth the signal must have an RMS value of 70 mV (assuming the signal has a 'white' power spectrum). As we have already seen, signals of a fraction of a millivolt are adequate to completely swamp any noise incurred in the necessary amplification when direct contact is made to the transducer elements. In the present case this can be obtained only by a large increase in the transmitter power, an achievable but inconvenient operation. In passing we may note that a signal of 30 mV (at a 5 MHz resonant frequency of the transducer) can be achieved in a water bath system with a received intensity of $7 \times 10^{-6} W/cm^2$ in line with the magnitude of figures normally

* James Electronics, Type C-4995.

quoted for limiting sensitivity[5] but the higher impedance of metals results in figures 10-30 times greater than this.

The main advantage of the electron multiplier lies in the high level of amplification that may be achieved with negligible degredation of the SNR together with the wide bandwidth possible. This latter parameter is restricted by the inevitable input capacitance of any amplifier applied directly to an electrode picking up the secondary emission from the transducer, combined with the very high source impedance.

Up to a point, SNR can be improved by operating the tube at a higher current I_B as the signal current increases directly with this for a given transducer voltage while the noise grows only as the square root, but this is ultimately limited by saturation in the transfer characteristic between transducer voltage and signal current component,[30] difficulty of maintaining focus of the electron beam and d.c. capacity of the electron multiplier.

8.3.2. Mechanical considerations.

Although the main mechanical problems can be overcome by the direct attachment of the transducer to a solid, it is relevant to consider a situation (as in medical examination) when no such support can be provided.

Two parameters are important; (a) stress produced by atmospheric pressure, and (b) deflection of the transducer plate from a plane surface. The first of these is obviously relevant

in any mode of operation of the tube but the second is significant only if accurate phase information about the acoustic field is needed, a requirement that does not exist in the conventional system. In principle, any known amount of deflection* could be compensated for in determining the field but it is far better if the measurements do come from a surface flat to a small fraction of a wavelength.

(a) Stress: Taking the transducer as circular and simply supported at the edges[15] the maximum allowable diameters for 5 MHz plates of quartz and PZT5A are 27mm and 18.5mm respectively.

(b) Deflection: If we restrict the plates to 16mm diameter the central deflection comes to 0.06 wavelengths for quartz and 0.17λ for PZT5A (5 MHz wavelength in water or oil). The quartz value is tolerable but the transducer size is somewhat inadequate. This may be improved by internal support bars behind the plate, dividing the supported areas up into small rectangles. For the support structure in the James Electronics tube the maximum deflection over the 45mm diameter useful area comes to approximately 0.01λ. The support bars appear in the picture in

---

* It has been suggested that deliberate curvature[11] of the transducer be incorporated as an aid to resisting the atmospheric pressure but this and the other possibility of providing a metal faceplate with the transducer on the inner surface[12] would introduce undesirable effects for the present application. The 'Charlotte plate'[13] method of Grasyuk et.al.[14] overcomes the objection of curvature or insertion of an additional material in the acoustic path but particularly with quartz increases considerably the capacitive coupling between elements.

the conventional use but the effect when focussing is done after the transduction process is much less significant and the support structure could readily be extended to much larger plates, or so as to allow the use of several individual plates.

8.3.3. Summary.

By comparison with the other possibilities the image conversion tube suffers from physical inconvenience, high noise levels and lack of electrical control over the transducer response but has the advantages of fast element access and well established manufacture.

8.4. MECHANICAL ADDRESSING.

This method is mentioned briefly for completeness. Basically the equipment consists of a probe which may make direct electrical contact with the electrode on the back of the transducer elements (as used in the experiments, Chapter 12), or a capacitive pickup[16,17] with a suitable means for moving the probe over the transducer in a systematic manner. This latter part may consist of no more than a jig to guide manual placement (Figure 12.15) to a complete mechanism resembling that of an 'X-Y' plotter. Some applications[18] use a single small transducer element moved over the field to be measured instead of a single large, stationary transducer but this is really practical for a water bath system only, because of the difficulty of maintaining consistent acoustic coupling to the surface of a solid.

When other than completely regular scanning patterns are needed (e.g., when random deletion of elements is required) a simple feedback arrangement may be incorporated to sense the probe position and move it into correspondence with the demanded coordinates. Such a device is under development as part of the continuing effort on this project as a stopgap pending the production of an electronically scanned device, such as that outlined in the next section.

8.5. SWITCHING MATRIX SCANNING.

The concept of this method is shown in Figure 8.3. Each transducer element $E_{i,j}$ is connected to an analogue switch $S_{i,j}$ controlled by voltages applied to the connections X_i, Y_j. When X_i and Y_j are both activated the signal from element $E_{i,j}$ is connected through to the output O. The arrangement is similar to that of a magnetic core storage array.

Development of devices similar to that required here has already reached a high level in optical applications,[19,20] presently reported devices having reached 360 x 360 elements at 25 μm spacing. Since the present ultrasonic application requires no more than 128 x 128 elements at 10-20 times this spacing it will be obvious that the required techniques are well in advance of the need.

A paper by Harrold[21] has appeared recently, describing the first moves towards the production of an ultrasonic device. This uses individual wire contacts to the 2 x 2mm elements of a 10 x 10

array operating at 1 MHz switched through a matrix constructed of discrete components.

The requirements of the switching matrix may be stated as;

(1) Linear input-output characteristic over a range of input voltages from a few tens of microvolts to (say) 100mV.

(2) Bipolar capability.

(3) Ability to incorporate resistive damping of the transducer elements either via the switch element or with separate loading resistors.

(4) Low level of 'cross-talk' into the output from the elements not being addressed.

(5) Frequency response up to ≈ 10 MHz.

(6) Freedom from artefacts in the output signal caused by the operation of the switching circuits.

(7) Simplicity of the switches. (This is purely an economic consideration because of the large number needed for a practical device. The space available at each element is more than adequate for very complex arrangements constructed as integrated circuits).

(8) Low noise insertion.

Of these requirements (1) and (2) may be readily achieved with very simple circuits using conventional[21] or field effect

transistors.[22] * (3) will normally require a distinct resistor for the purpose as the switch 'on' resistance for typical semiconductors will be of the order of 1000Ω and variable from unit to unit whereas values of the order of 50Ω are required. In Harrold's arrangement a resistance is incorporated at the appropriate position and merely needs to be changed to a suitable value.

The cross-talk problem is a function of the 'off' impedance of the switch units. This impedance will be largely capacitive and result from capacitances of the order of 1 pF (with FET's) to 10 pF (with ordinary transistors). The relevant equivalent circuit is shown in Figure 8.4. Taking the worst case when all the element voltages are in phase (and have the value E) with a total of N elements connected to R_L and a frequency of 10 MHz, then if the transducer element source impedance is effectively determined by the 50Ω load and R_L tends to zero (e.g., by running the signals into a 'virtual earth' provided by an amplifier) I_o will have the value $E/1000 + (N-1)jE/16000$ so for a phase error in the output $< 30^o$ N must be 10 or less. The problem of high frequency response is connected with that of cross-talk. If R_L has any appreciable magnitude then shunting of the signals by the switch capacitances will occur as the impedance to ground on the transducer side of the switch is much less than the switch impedance.

---

* These are the most common elements in the optical devices.

This leakage problem may be reduced by a number of means, a reduction in the on impedance of the switch being perhaps the most obvious. However, the simple application of an emitter follower circuit is not entirely suitable as this will also reduce the impedance of the interfering sources as well; it will be necessary to control the supply voltages to this stage with the switching voltages to the gate element. Variations in switch impedance level can be swamped by the inclusion of a stabilising resistor* in series with the output from the emitter follower to ensure that all transducer elements are treated equally.

A variety of possible switch circuits are discussed in Reference 20, but from the considerations above it appears that it will be necessary to connect to the transducer as a number of sub-arrays each say comprising one row of elements.

Item 6 is of importance in a system where the transducer is continuously scanned and the pattern obtained presented as a television image but has no significance here as a 'settling time' can be allowed before reading off the section of signal required from each element.

The noise inserted by such a matrix is essentially that generated in the gate $S_{i,j}$. This is considered in more detail below but if a FET gate is used, the noise introduced in a 10 MHz bandwidth amounts to approximately $10^{-13}A^2$. With a signal of

---

* Which obviously must be much smaller than the switch impedance of $\approx 1000\Omega$ to serve any useful purpose.

1mV on the transducer the MS signal current will be $10^{-12}A^2$ giving a SNR of 10. Internal transducer noise is insignificant.

This ratio is inferior to that obtained by direct connection (7.3.3) but can readily be improved by a modest increase in transmitter power.

8.6. INTEGRATED TRANSDUCER ARRAY.

The basic idea here is similar to that of the previous section except that the separate transducer material is replaced by a semiconductor which also is used to form the switching devices. A number of materials, including cadmium sulphide and gallium arsenide, have both piezoelectric and semiconductor properties. The concept is one of fabricating the transducer with the electrical configuration of a FET so that the piezoelectrically induced charge on the gate electrode acts in exactly the same manner as an externally applied signal in the normal application, to modulate the source-drain current.

A number of papers[22,24] have appeared on single FET transducers and from the latter we derive the performance of a device in the following form;

Firstly the drain current depends on the gate voltage in the manner;

$$I_d = \frac{I_{d_o}(V_g - V_o)^n}{V_o} \qquad .. 8.7$$

V_o is the gate offset voltage

V_g is the gate voltage

I_{d_o} the drain current for $V_g = 0$, and n is 2-3 for most practical devices.

The offset voltage is a function of the surface charge density and the capacitance of the channel region. The effect of stress is to alter V_o by an amount ΔV_o given by the normal piezoelectric relations for the type of transducer (see below) and we get;

$$\frac{\Delta I_d}{I_d} = \left[1 - \frac{\Delta V_o}{V_g - V_o}\right]^n - 1 \qquad .. 8.8$$

I_{d_o} is given by;

$$I_{d_o} = \mu \varepsilon_i w V_o^2 / 2 t_i L \qquad .. 8.9$$

with;

μ = surface mobility

ε_i = permittivity of insulating layer

t_i = channel thickness

w = channel width

L = channel length

refer to Figure 8.5.

If the transducer portion of the FET is very thin* compared with the wavelength of operation then defining the sensitivity as

---

* This condition provides good frequency response and is practically unavoidable if the transducer is formed by the usual vacuum deposition method.

stress induced current/unit stress we have;

$$S_T = \frac{\Delta I_d}{T} = \mu w(V_g - V_o) \frac{d_{33}}{L} \qquad .. 8.10$$

d_{33} being the piezoelectric stress coefficient for thickness distortion of the structure.

With CdS μ may have the value $10^{-2} m^2/S$ and by bending the structure around after the manner illustrated by Becke and White[25] a value of $w/L = 1000$ may be achieved in a compact space so with $V_o = 0.5$ volts and $V_g = 2$ volts, say, a sensitivity of 1.6×10^{-10} $A/(N/m^2)$ may be obtained. With the stresses of the order of the 10^3 N/m^2 derived earlier (Chapter 3) a current of 1.6×10^{-7}A may be expected which, if passed through a 1000Ω load resistor, will give 160 μV - comparable with the voltages developed from a conventional transducer.

8.6.1. Optimization of the transducer.

Three factors enter;

(1) Sensitivity

(2) Noise

(3) Bandwidth.

Over the frequency range of interest the low frequency '1/f' noise is of no concern and the main contribution is from thermal noise. This is given by;[26]

$$\overline{I}_n^2 = 4kT \cdot \frac{\mu \varepsilon_i}{L t_i} (V_g - V_o) H(u) \cdot B \qquad .. 8.11$$

$$u = \frac{V_d}{V_g - V_o}$$

V_d = drain voltage

k = Boltzmann's constant

T = absolute temperature

and over normal ranges of the parameter u, H(u) has the approximate value of 0.9.

Normally the insulating layer is SiO with a $\varepsilon_i = 3.75$ so with $T = 300^oK$, $t_i = 400\mathring{A}$ and $L = 25\ \mu m$, $\overline{I}_n^2 = 8.8 \times 10^{-14} A^2$ over 10 MHz.

The bandwidth of the device as a transistor is a function[23,27] of μ/L^2 so we have, (i) sensitivity varies linearly as the factor $\frac{\mu w d_{33}}{L}$, (ii) noise is a function of μ/L, (iii) bandwidth $\alpha\ \mu/L^2$, and we define a 'Figure of Merit' for the present application as;

$$F = \frac{\text{sensitivity x device bandwidth}}{\text{noise power}}$$

$$= K \cdot \frac{\frac{\mu w d_{33}}{L} \cdot \frac{\mu}{L}}{\mu/L} = \frac{K \cdot \mu w d_{33}}{L^2} \qquad .. 8.12$$

K is a constant depending on the bandwidth required, and the source-drain voltage.

For a given thickness of the insulating layer the significant geometrical parameter is w/L^2 which can be increased within a given transducer area by more elaborate convolutions of the structure.[25]

For the two materials examined, CdS and GaAs, the latter would appear to possess a better potential performance because although d_{33} for GaAs is 1/10th the value in CdS (10^{-11}C/N - comparable with quartz) GaAs is a superior semiconductor having a value of μ some 50 times that for CdS.

With the figures quoted above the SNR is approximately 0.2 and consequently this device will require a substantial boost in transmitter power compared with the use of a ceramic transducer material.

Switching of the elements can be performed by the connection of the source and gate leads to appropriate X,Y switching lines, similarly to the arrangement sketched before (Figure 8.3).

Despite the aesthetic attractiveness of a completely integrated transducer, the idea would in fact appear to have little else to offer. The sensitivity is not high and the overall performance (for a given field strength) markedly inferior to the 'hybrid' arrangement using the most appropriate materials for each section of the complete transducer, i.e., a high performance ceramic transducer material switched by a separate array provided by the methods of the highly developed silicon or thin film technologies and formed on an insulating layer deposited over the top electrodes of the transducer elements.

None of the other interrogation methods approach the sensitivity of direct connection to the elements by a moveable probe but this technique is slow and clumsy.

8.7. COMPENSATION OF TRANSDUCER RESPONSE.

When considering the possibilities of a water bath system employing the image tube, some attention was given to the design of an electrical network with characteristics compensating those of the transducer response. The transducer in the image tube may be regarded as open-circuited on the electrical side and the impulse response is that given in Equation 4.4. (4.3.2).

If this equation is further expanded by writing the 'tanh' function in terms of exponentials and represented as a Fourier transfer function we obtain;

$$A(\omega) = \frac{k}{j\omega}\left[1 - 2e^{-j\omega\alpha} + (1-\rho)\, e^{-2j\omega\alpha} + 2\rho\, e^{-3j\omega\alpha} + \ldots.\right] \qquad .. 8.13$$

where ω is the angular frequency and k a constant depending on the piezoelectric properties and the medium impedance.

The general terms in the expansion are given by;

c_n = coefficient of $e^{-nj\omega\alpha}$

$$c_n = (-\rho)^{(n/2-1)}(1-\rho) \quad \ldots \text{ n even, } \geq 2,\ c_0 = 1 \qquad .. 8.14$$

$$c_n = -2(-\rho)^{\frac{n-1}{2}} \quad \ldots \text{ n odd}$$

(ρ_2 has been replaced by ρ for simplicity).

For all non-zero values of ρ, $A(\omega)$ contains infinitely many terms but for transducers well coupled to typical solids, ρ will not usually exceed $\frac{1}{2}$ and for this, c_n for $n>15$, are less than 1/100.

Under conditions where a large noise component contaminates the signal the best approximation (in a least squares sense) to the signal is given by a matched filter receiver.[28] If the transfer function of the signal generating filter is $A(\omega)$ then the required matched filter must have the transfer function $A^*(\omega)$ (the complex conjugate).

With the form of $A(\omega)$ in Equation 8.13, the signal may be regarded as formed by the application of an impulse to a network comprised of a series of delay elements, weighting filters, a summer and an integrator as indicated in Figure 8.6 (any other waveform will produce its appropriate response). In the present case each of the G_n is independent of frequency and is purely a numerical multiplier. The spacing of the tapping points gives delays of α between taps, so at position n the delay is $n\alpha = \Delta_n$.

For the matched filter we have;

$$A^*(\omega) = \frac{k}{-j\omega}\left(c_0 + c_1 e^{j\omega\Delta_1} + c_2 e^{j\omega\Delta_2} + c_3 e^{j\omega\Delta_3} + \ldots c_n e^{j\omega\Delta_n} + \ldots \right) \qquad \ldots 8.15$$

The $\exp(j\omega\Delta_n)$ terms represent time advances so in order to produce a physically realisable device it is necessary to truncate the series at say c_N and introduce a time delay $\geq \Delta_N$ to give;

$$A^*(\omega) \qquad \frac{k}{-j\omega}\ (c_0 e^{-j\omega\Delta_N} - c_1 e^{-j\omega(\Delta_N-\Delta_1)} + c_2 e^{j\omega(\Delta_N-\Delta_2)} \quad ---$$

$$--- \quad + \quad c_n e^{-j\omega(\Delta_N-\Delta_n)} \quad ---$$

$$--- \quad + \quad c_N .) \qquad\qquad .. 8.16$$

This extra delay means that a signal incident on the transducer at $t = 0$ will not emerge until $t = \Delta_n$ but this fixed delay is of no consequence.

The form of the required filter appears as in Figure 8.7.

Of the major components needed; (1) delay line - approximately 1-2 μS of total delay is needed for very good compensation. A bandwidth of the order of 10 MHz is necessary. (2) N wideband amplifiers to realize the c_n's. This function is easily fulfilled by standard integrated amplifiers of the 'μA 702' type. A similar amplifier could be employed for the summing and integrating operation.

The coefficients c_n have been calculated for a variety of transducer-material combinations, some of which are given in Appendix 3.2. The results indicate that with a PZT5A transducer no more than 10 stages are necessary in the delay line for a representation accurate to 1%, when the transducer is on a metal surface.

REFERENCES FOR CHAPTER 8.

1. Maginness, M.G. Deptl Memo. No.3, April 1967, Electrical Engineering Department, University of Canterbury, Chapter 4.
2. Smyth, C.N. et.al. 'The ultrasound image camera'. Proc. IEE 110, pp.16-28, Jan. 1963.
3. Jacobs, J.E. et.al. 'An investigation of the limitations to the maximum obtainable sensitivity in acoustical image converters'. IEEE Trans UE-10, pp.83-87, Sept. 1963.
4. 20th Century Electronics Ltd, Croydon, England. Type UC9.
5. James Electronics Inc., Chicago, U.S.A. Type C-4906.
6. Semennikov, Iu. B. 'Certain aspects of the operation of an electron-acoustic image converter'. Sov.Phys. Acoustics 7, pp.56-59, July-Sept. 1961.
7. Zworykin, V.K. et.al. 'Theory and performance of the iconoscope'. Proc. IRE 25, p.1071, Aug. 1937.
8. Pierce, J.R. 'Physical sources of noise'. Proc. IRE 44, pp.601-608, May 1956.
9. Data Handbook. Electron tubes, Part 6. pp.1-12. Philips Electrical, July 1969.
10. 'Electron multipliers and particle detectors. DuMont SPM structures'. Publication of Fairchild-DuMont Electron Tubes, Clifton, New Jersey, U.S.A.
11. Schätzer, E. 'An ultrasonic to electronic image converter with an enlarged image field'. Ultrasonics 5, pp.233-4, Oct. 1967.
12. Smyth, C.N. 'Light beam scanning ultrasonic camera'. British patent, 801,294.
13. Charlotte, H.F. 'A direct recording CRT. Electronic Eng. 29, p.373, Aug. 1957.
14. Grasyuk, D.S. et.al. 'An ultrasonic "introscope" with the new U-55 electronic-acoustic image converter'. Sov.Phys.Acoustics 11, pp.376-379, April-June 1966.
15. Timoshenko, S. and Woinowsky-Krieger, S. 'Theory of plates and shells'. McGraw-Hill, New York, 1959.
16. Suckling, E.E. 'Observations on resolution and on field variations in near field sonic optical systems'. Journ.Acoust.Soc.Am. 31, pp.678-680, June 1959.
17. Suckling, E.E. and Ben-Ziv, S. 'Formation of images by ultrasonic rays'. Trans N.Y. Acad. Sci. 28, pp.588-595, 1966.
18. Kreuzer, J.L. 'Ultrasonic holography for non-destructive testing'. Mater. Eval. 26, pp.197-202, Oct. 1968.

19. Horton, J.W. et.al. 'The scanistor - a solid state image scanner'.
Proc. IEEE 52, pp.1513-1528, Dec. 1964.
20. Weimer, P.K. et.al. 'Multielement self-scanned mosaic sensors'.
IEEE Spectrum 6, pp.52-65, March 1969. (This paper contains an extensive list of references).
21. Harrold, S.O. 'Solid state ultrasonic camera'.
Ultrasonics 7, pp.95-101, April 1969.
22. Harrold, S.O. Private communication.
23. Mueller, R.S. and Conragan, J. 'Transducer action in a metal-insulator-piezoelectric-semiconductor triode'.
Appl.Phys.Lett. 6, pp.83-85, March 1965.
24. Mueller, R.S. and Conragan, J. 'A metal-insulator-piezo-electric-semiconductor electromechanical transducer'.
IEEE Trans ED-12, pp.590-594, Nov. 1965.
25. Becke, M.W. and White, J.P. 'Gallium arsenide FET's outperform conventional silicon MOS devices'.
Electronics 40, p.82, June 12, 1967.
26. Jordan, A.G. and Jordan, N.A. 'Theory of noise in metal oxide semiconductor devices'.
IEEE Trans ED-12, pp.148-156, March 1965.
27. Mauser, J.R. 'Small signal properties of field effect devices'.
IEEE Trans ED-12, pp.605-618, Dec. 1965.
28. Turin, G.L. 'An introduction to matched filters'.
IRE Trans IT-6, pp.311-329, June 1960.
29. Zworykin, V.K. et.al. 'The secondary emission multiplier - A new electronic device'.
Proc. IRE 24, p.351, March 1936.
30. Haslett, R.W.G. 'An ultrasonic to electronic image converter' tube for operation at 1.2 Mc/s.
Radio Elect. Eng. 31, p.161, March 1966.

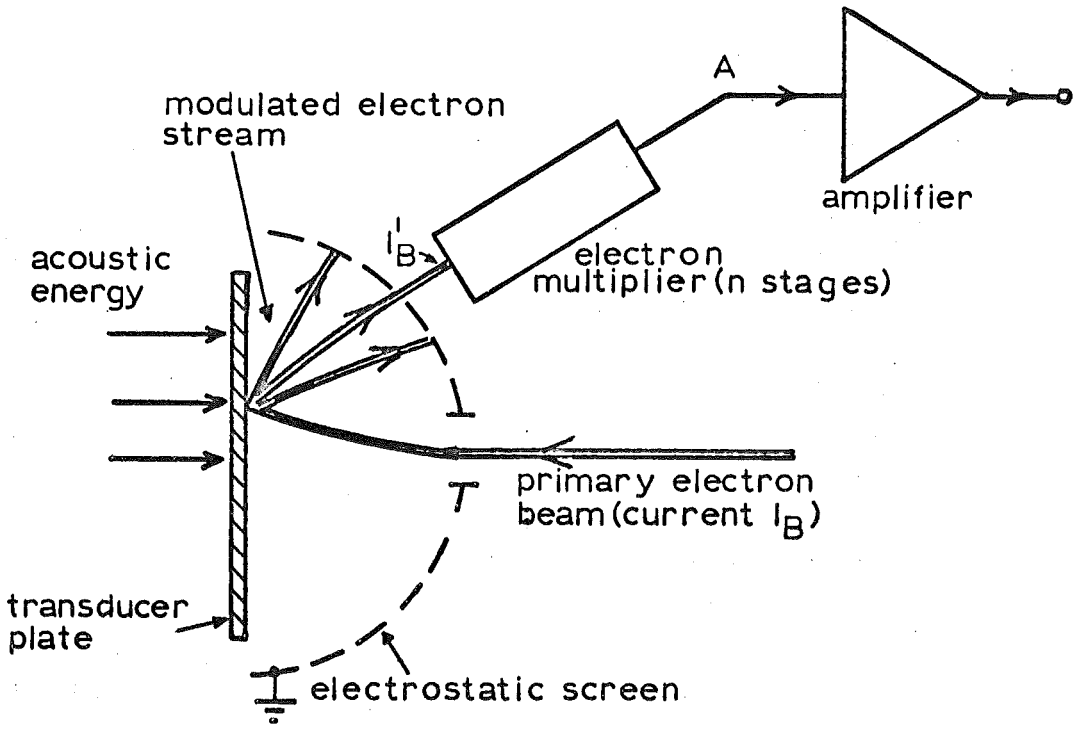

FIG. 8.1 : Diagrammatic layout of tube

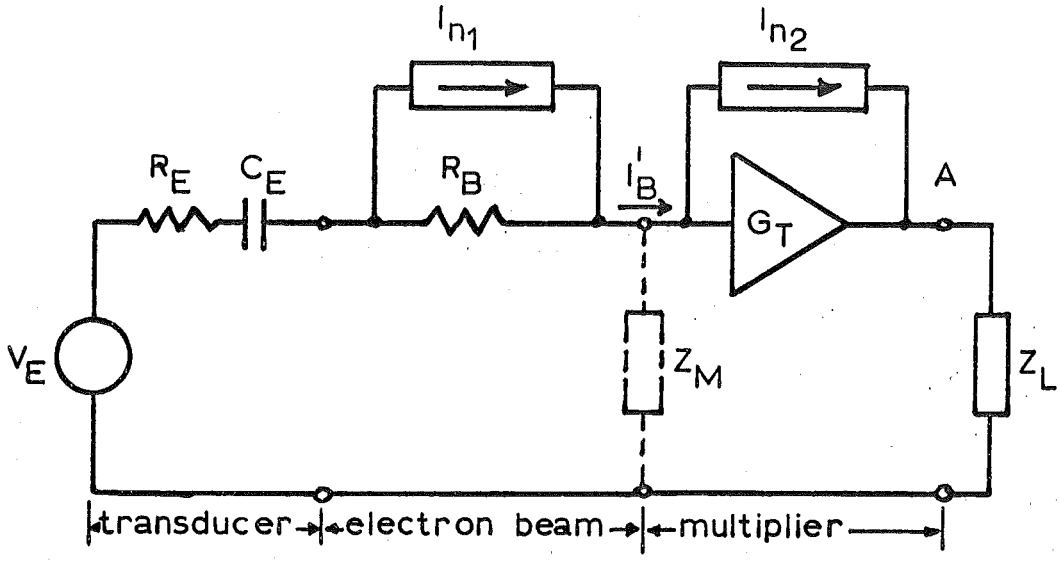

FIG. 8.2 : Equivalent circuit

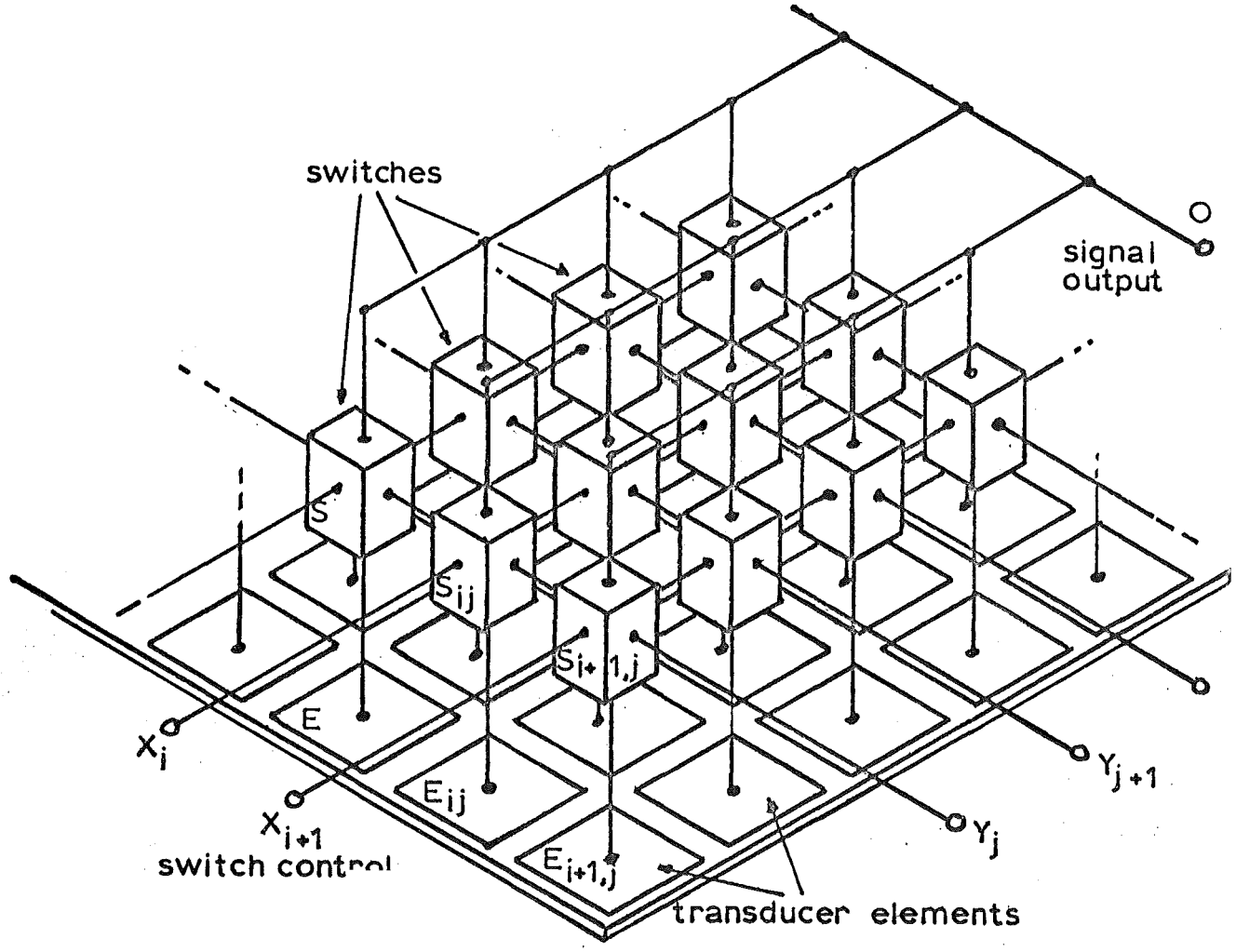

FIG. 8.3: BASIC SWITCHING MATRIX ARRANGEMENT

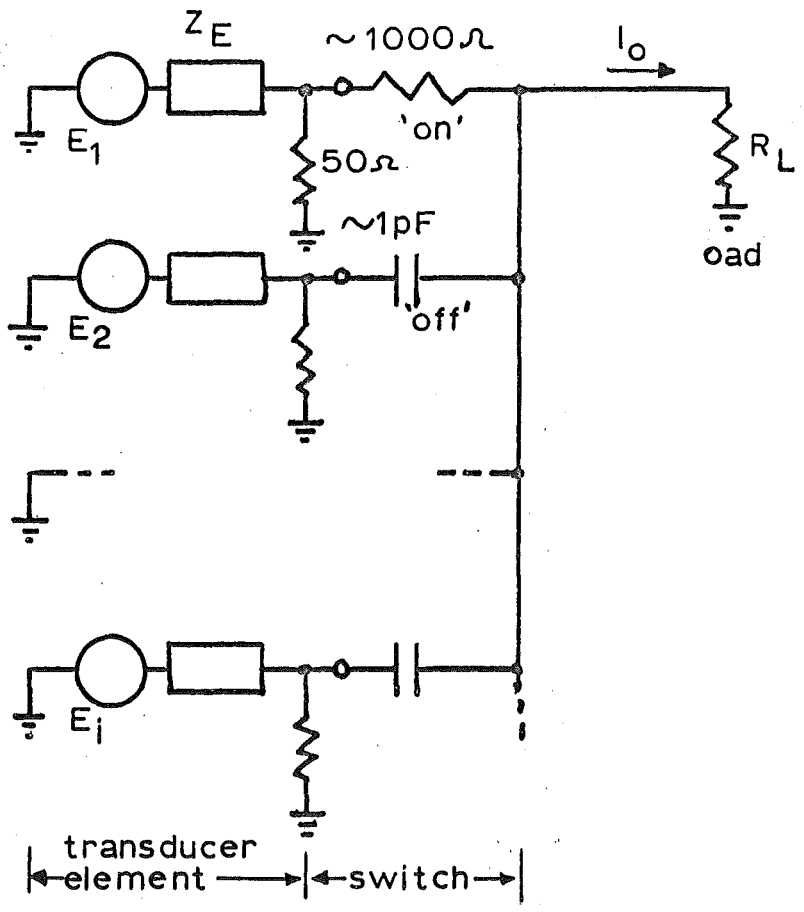

FIG. 8.4: Pertaining to cross-talk in the switching matrix.

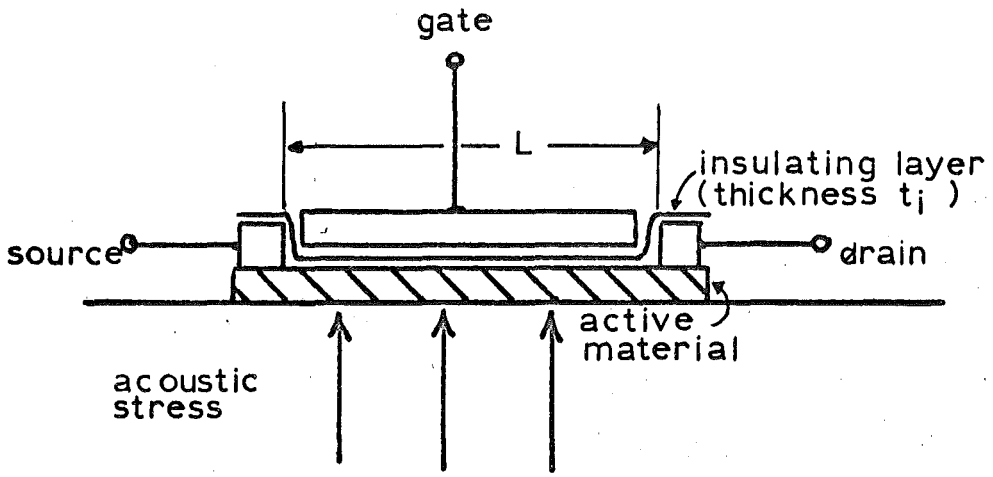

FIG. 8.5: Cross-section through FET transducer.

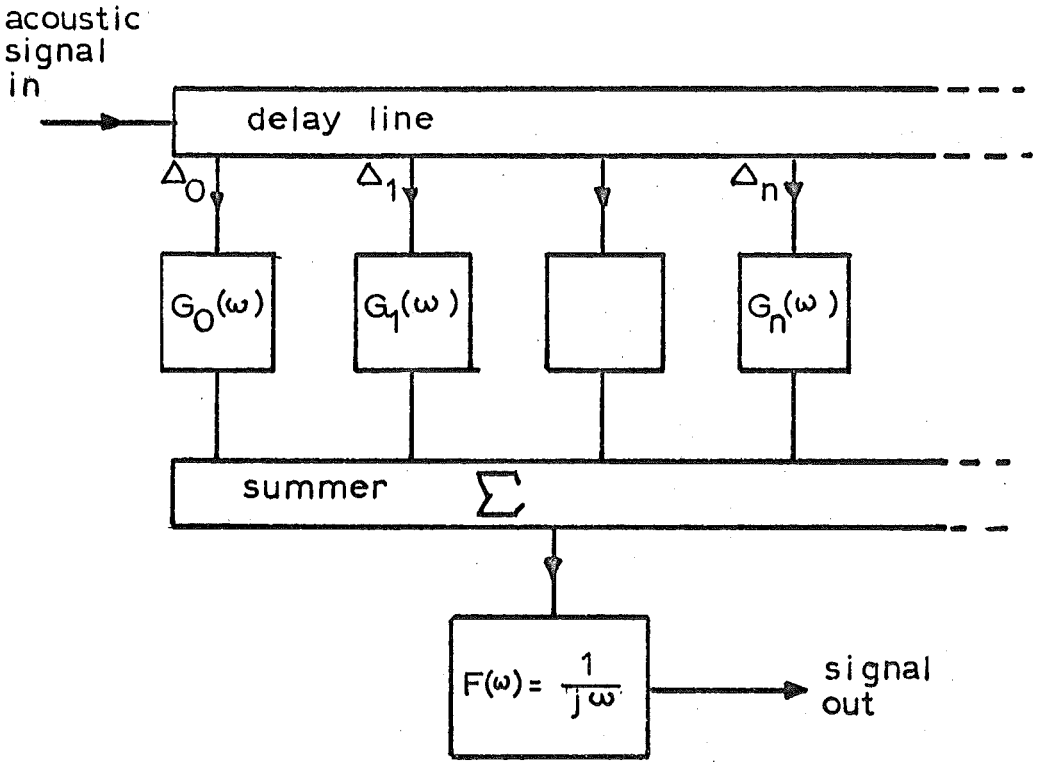

FIG.8.6: Tapped delay line transducer model

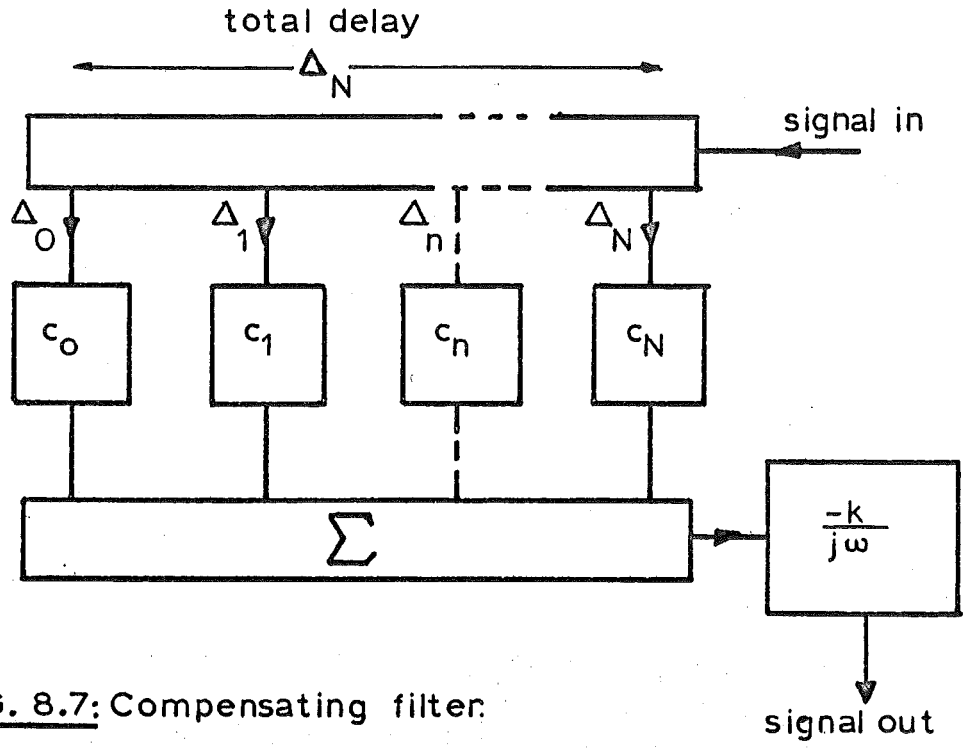

FIG. 8.7: Compensating filter

CHAPTER 9.

SIGNAL CAPTURE AND RECORDING.

9.1. INTRODUCTION.

It has already been necessary to make reference to some of the detailed functions of the apparatus in discussion of the system design (Section II) and this chapter has been introduced to bring together, within a coherent outline, the various functions involved in the capture of data from the transducer and the recording for transfer to the computer. No detail is entered into as this apparatus has formed the topic of a separate project and is exhaustively described in the thesis of Cook.[1]

The basic functions needed are;

(1) Definition of the required aperture positions by the generation of suitably coded signals that can be used to control scanning apparatus as described in the previous chapter and recorded with the data to reference each element signal.

(2) Provision for omission of element signals from the complete set.

(3) Timing of the successive operations of transmission, allowance for propagation delay and reception of the signals.

(4) Time sampling and amplitude quantization of the received signals, together with any necessary buffer storage to match the information rate of the incoming signals with that of the

recording medium.

(5) Provision and control of a suitable recording medium which is compatible with the available computer.

Each of these functions is considered in turn with a discussion of possible modifications to the existing apparatus for the purpose of improving recording accuracy and speed.

9.2. DESIGN CONCEPTS.

As was noted earlier (1.3.), some attention was initially given to the possibilities of a completely self-contained device that would accept the element signals and produce an image therefrom, without reference to external devices. The impracticability of this approach reduced the role of specially built apparatus to essentially that of data acquisition. Despite this limitation the apparatus constructed is of considerable complexity and includes some 600 semiconductors alone, of which half are integrated circuits. It cannot be claimed even now that the device represents a particularly elegant solution to the problems involved but at the stage of system design it appeared a reasonable compromise with the computing facilities available and projected. The only operation performed by the apparatus (beyond basic data recording) is that of aperture thinning (6.5.3) and this is necessitated by the need for data storage on a modest amount of paper tape rather than by any fundamental limitation of the computing process.

9.3. SCANNING OF APERTURE.

The method adopted is shown in Figure 9.1. Two 7 stage binary scaling chains are connected in sequence and the input of that giving the required 'X' position fed from a 'clock' source C. As the 'X' counter S_x fills, the position is indicated in binary form on the lamps L_{x1}-L_{x7} which may be visually inspected to give the position when a manual scanning method used. On the 128th pulse from C the S_x counter resets to zero and the 'Y' position required is incremented by 1 in S_y. This produces a simple 'raster' scan, the end of which is indicated by the overflow from S_y after 128 lines have been scanned. To scan a device requiring analogue deflection signals, digital to analogue converters $D.A.C._x$ and $D.A.C._y$ are incorporated. Use of an image tube requires scanning voltages with a maximum value of 150 volts. These are provided by switching appropriate fractions of a high voltage source in the D.A.C.'s by reed relays and a network of precision resistors. The overall accuracy is better than 0.1%. All the normal focussing and astigmatism adjustments are incorporated in such a manner as to be independent of the deflection and the actual scan area can be altered as required (or compensation made for variable deflection sensitivity).

For scanning a solid state array the usual approach is to have two shift registers with one stage per row and column, with an 'on' voltage level propagating from stage to stage. Suitable signals for this clocking process appear at X' and Y'.

The binary coded position information in the counters provides the levels fed to the tape punch as position information after the signal from each interrogated element has been recorded and may also be used to control the position of a mechanical scanning device.

The normal condition of C is free running at any of four speeds from 100 Hz to 10 kHz until interrupted by the scanning control logic deciding to take a recording from the transducer element just reached. This interrupting signal is indicated at G.

It will be seen that provision for all the possible scanning methods is incorporated in this design and operation is simply a matter of connecting the desired device. One additional refinement is provided, the facility to set the counters at any desired position and hold this indefinitely.

9.4. SCANNING CONTROL LOGIC.

This is outlined in Figure 9.2 and performs three functions:

(1) Setting the overall shape and size (in terms of number of elements) of the area scanned.

(2) Providing for random deletion of specified fraction of the elements.

(3) Controlling the deletion in such a way as to produce the desired taper function (6.5.1.).

Referring to the figure we have on the left, two further digital to analogue converters operating from 6 bits obtained by converting

the 7 bit outputs of S_x and S_y in the digital function generator to give a binary code representing position from the centre of the scanned area (to within $\frac{1}{2}$ an element spacing). The resultant analogue voltages X and Y represent, in orthogonal form, the scan position from the array centre to within approximately 1%. These voltages are taken as inputs to a function generator H using a resistor-diode network to approximate, at the output A, the aperture taper function, and at output B a voltage proportional to position from the centre of the scanned area. Preset adjustments 1 and 2 are provided on the front of the apparatus to set the relative height of the pedestal (6.5.1.2) in the taper function and the average density of sampling, i.e., the total number of elements to be taken.

Output B is compared with a further preset voltage E in comparator 2 to control the overall area. The condition B>E indicates that the positions generated in the scanning counters are outside the aperture radius desired.

A random sequence of voltage levels is generated by the psuedo-random number generator (PRNG) (6.5.3.1) and introduced at C to a second comparator (comparator 1), the other input of which is the taper function. The PRNG is clocked by the scanning clock C and thus advances to a new state for every increment in S_x or S_y. The comparator outputs D and F are further compared in an AND gate to give an output at G only if the point is one accepted by the random selection process and is within the desired aperture size. G forms

the inhibiting input to the scanning clock C, halting the apparatus at the element to be interrogated.

The preset adjustments permit deletion of up to 90% of the elements in the full scannable area and reduction of this area down to a diameter 10% of the full size. The full size can be scanned as a square if desired, with the loss of only a few corner elements (6 at each corner).

This description of the scanning controls omits a vast amount of important detail regarding in particular the synchronisation of the operations but will serve to illustrate the versatility of the design.

9.5. TRANSMISSION-RECEPTION TIMING.

Some attention has already been given to this section of the apparatus in connection with the stability requirements (7.4.2.). The cycle of timing operations is initiated after the scanning logic has caused a pause on an element to be taken. Initiation may be directly controlled by the signal G, by a delayed version of this to allow "settling time" in the scanning, by a signal feedback from the actual scanning mechanism, or by manual operation of a push button. Suitable interlocking brings the control signal into synchronism with the timimg reference oscillator as discussed earlier. The propagation delay is provided by a chain of flip flops counting the reference oscillator cycles. This chain may be preset to initiate the time sampling of the incoming signals at any time up to 127.5 μS after transmission, in 0.5 μS steps, by means of

switches on the front panel. There is a further delay in the signal from switching times and amplifier delays but this is very small (<0.5 μS) and constant.

This maximum delay allows for depths of up to 400mm in aluminium and similar figures in other metals. More delay could easily be provided but this range involves a large attenuation of the acoustic signals even in aluminium (≈20 dB at 10 MHz) and is well beyond any reasonable depth in steel.

After the first 6 samples from a given element have been taken, the transmissions are additionally synchronised to the paper tape punch operating cycle, a new transmission being allowed to commence at the completion of punching the current samples.

9.6. SAMPLING OF THE SIGNALS.

The present arrangement in the apparatus takes only 6 samples from the element signals after each transmission, to an accuracy of 2 bits. Some consideration was given to providing sufficient buffer storage to hold the complete record from each element but this would necessitate a number of shift registers equal to the number of bits, each having a number of stages equal to the number of samples (252), and capable of being clocked at the sampling rate (24 MHz). Little advantage could be had from such an arrangement, apart from some simplification of the timing arrangements, as long as the data was recorded on paper tape and at the design stage such registers were not readily obtainable as integrated components. However, noting

that the record from each element taken in approximately 10 μS of signal and that the 250 odd samples extracted from this interval could be fed into the store of a modern computer in no more than 400 μS*(1.5 μS storage cycle time) compared with the 770mS required for recording with the present tape punch (110 punching/sec), such a buffer store represents a possible future extension to the apparatus.

The present analogue to digital conversion circuitry could be extended to one more bit without troubles from amplitude jitter but is basically a design chosen more for economy than performance.

9.7. RECORDING MEDIA.

The only methods available for transferring data into the computer used** are paper tape and 80 column punched cards. Without resorting to elaborate coding, at least 3 cards would be required per element interrogated for a maximum of about 3500 cards over the 1100 elements that can be comfortably accommodated on a standard reel of paper tape (300m). With a 250 cards per minute cardpunch this would take 14 minutes. The present tape punch can record the same data in 14.4 minutes. From the relative prices (15-20/1 in favour of the tape punch) and physical sizes of the machines, the choice to be made was obvious.

Since the project began, a further computer+ has become available

---

* Note that in practice, at least 1mS and probably more must be allowed between transmissions to allow complete decay of the echoes in the material.

** IBM 360/44.

\+ EAI 640.

offering direct access but the presently installed storage is quite inadequate for the data involved even with the small receiving transducers actually used.

An intermediate solution is seen in the use of magnetic tape recording. At say, a 100 kHz rate, data recording from one element would take 2.5mS, agreeing with the periods needed for echoes to decay. Even at the relatively modest density of say 50 digits/cm, the length of tape required comes to only 55m for 1100 elements and the recording time to less than 3 seconds plus any time needed to shift from element to element with the scanning arrangement used. This latter time becomes of considerable significance with faster methods of data recording and any improvements in recording speed must be matched with a fast scanning arrangement. (Image tube or electronic switching matrix).

9.8. TAPE FORMAT.

The layout of data on the paper tape is illustrated in Figure 9.3. The record from each element takes up 87 punchings on the tape organized as follows:

(1) Signal data; this occupies the first 84 punchings in any record. Channel 7 of the tape is punched continuously to identify this section. Data is in Channels 0 through 5. Channels 0 and 1 of punching 1b contain the two bits representing the first sample from the signal, Channel 0 containing the most and Channel 1 the least significant bit. Channels 2 and 3 have sample 2 with the most significant bit in Channel 2. Similarly Channels

4 and 5 hold the third sample with Channel 4 the most significant. Samples 4, 5 and 6 are in punching 2b from bottom to top, 7, 8 and 9 in 3b and so on up to 84b containing samples 250, 251 and 252. Figure 9.4 shows the relationship between the original analogue signal and the coded numbers.

(2) Position punchings 85b and 86b contain the x,y coordinates of the position from which the preceding data has come. The basic form of the coordinate records omits the Channel 7 punchings and has the positions 1-127 indicated in pure binary code in Channels 0-6 with Channel 0 the most significant bit. Position 0 cannot be represented by a blank 'punching' as this will simply be skipped by the tape reader, so is given the special code of Channels 6 and 7 punched. Since Channel 6 is not used for data, this produces no confusion. In fact, unless the full area the scanning system is capable of is used, the zero condition does not occur.

(3) End of record. On the 87th punching a distinct character consisting of all channels punched is inserted to provide an easy visual check on the tape and facilitate computer examination for correct operation when reading in the tape.

This whole sequence is repeated for each successive element examined.

REFERENCE FOR CHAPTER 9.

1. Cook, G.B. 'The ultrasonic camera - a study of the transducer-computer interface.
M.E. Thesis, University of Canterbury, 1969.

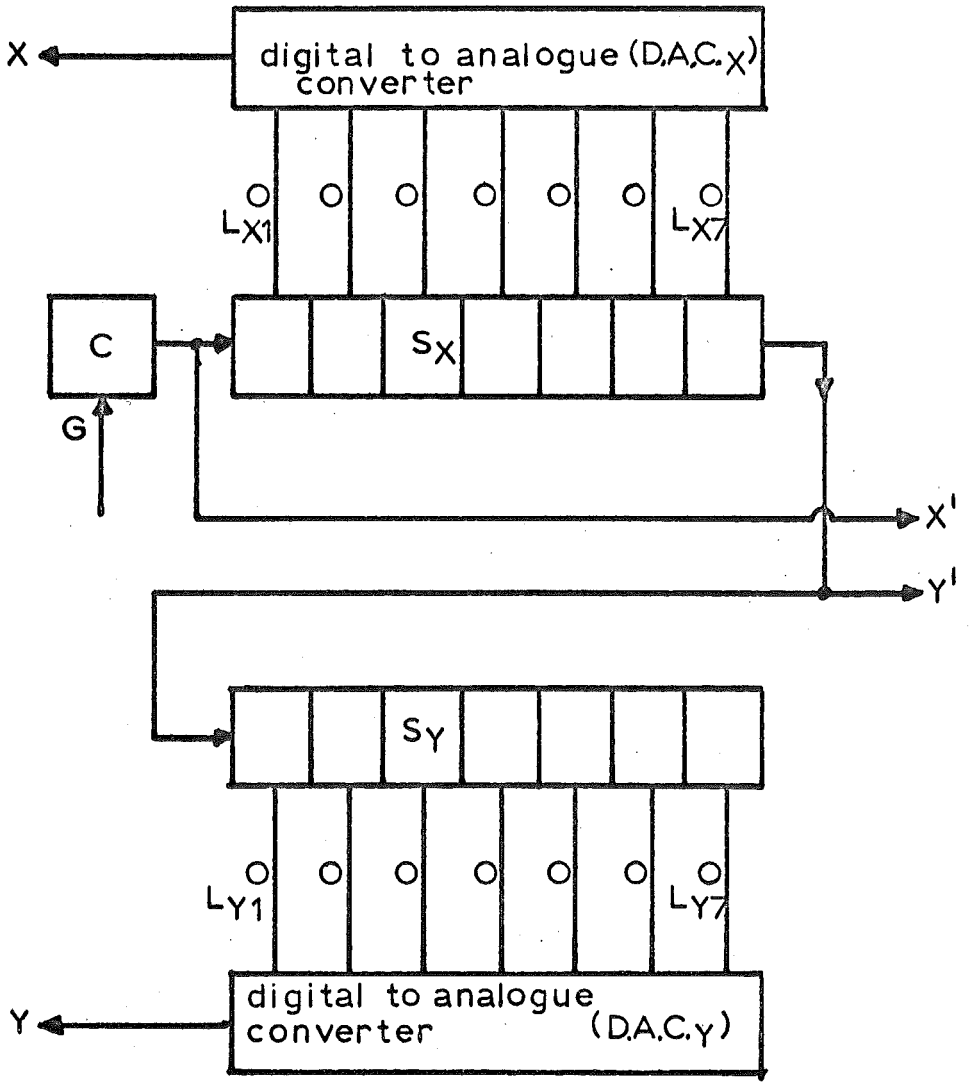

FIG. 9.1: Block diagram of X—Y scan control.

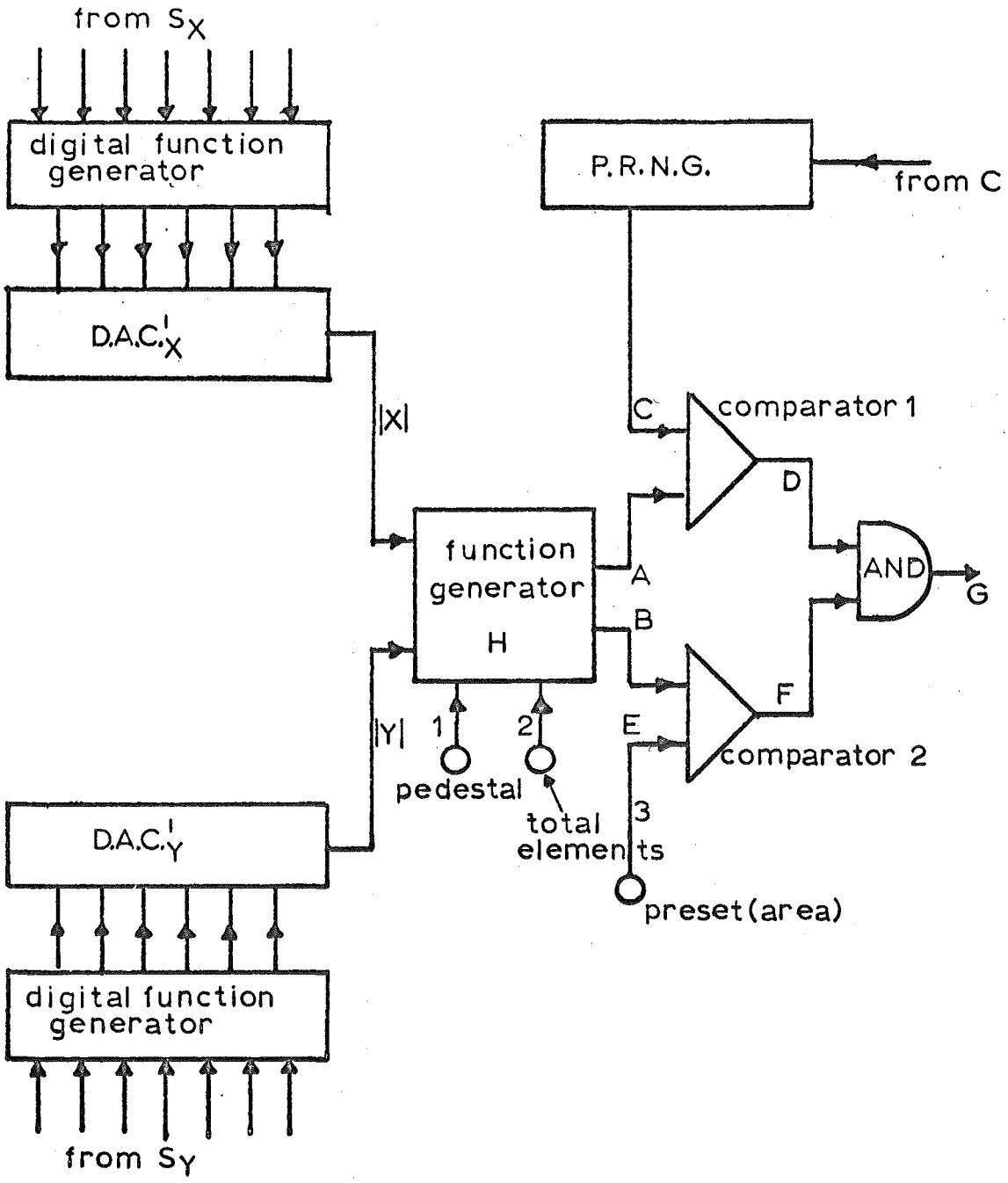

FIG. 9.2: Scanning control logic.

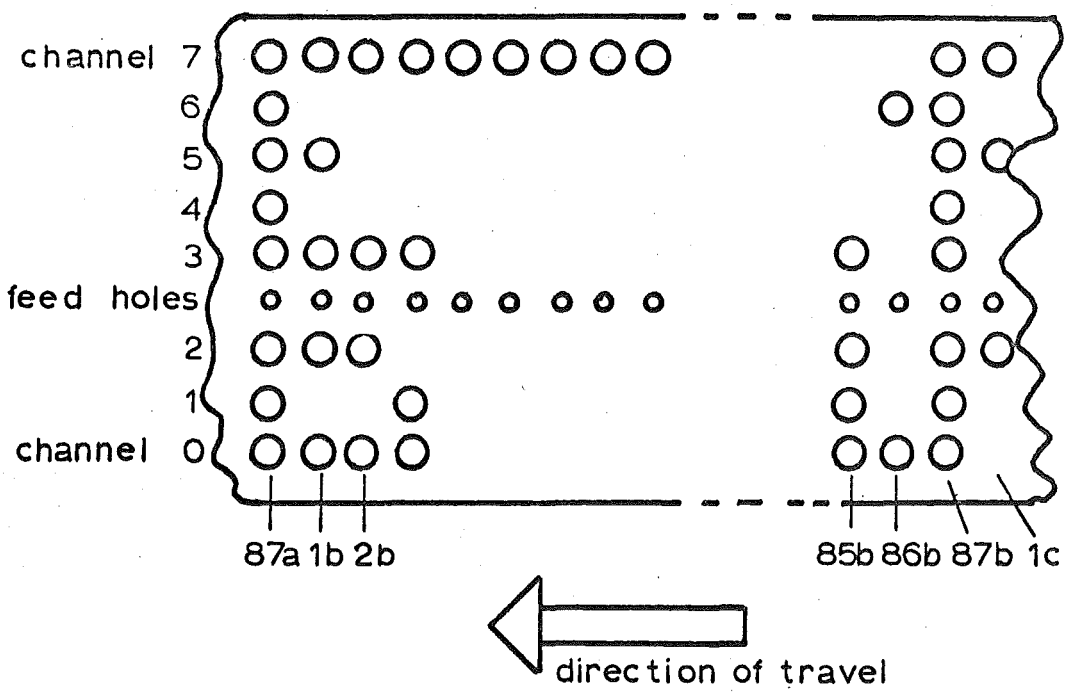

FIG. 9.3: Paper tape format.

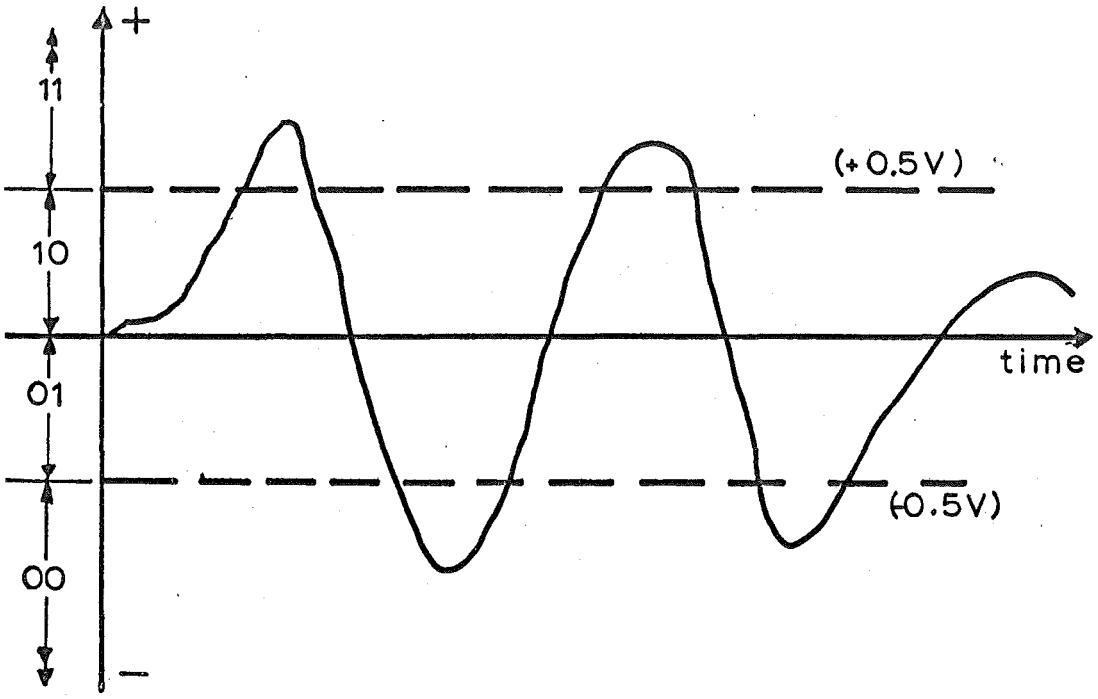

FIG. 9.4: Relation of coding levels to original signal.

CHAPTER 10.

COMPUTER ORGANIZATION.

10.1. INTRODUCTION.

It is considered that little point would be served by a detailed description of the particular computer program used in the image construction experiments described in Chapter 12. Of more concern than the exact specification of what is basically a very simple set of operations (complicated only by the large number of repetitions needed) is a discussion of the requirements that such image forming operations impose on a computing facility and means of efficient organization within the limits set by a given machine.

In line with this idea only a brief outline of the necessary operations in the program will be given. These will serve to illustrate some of the general problems involved in such computer applications. The numerical results derived relate specifically to a particular computer installation but it is convenient to discuss the problem by way of an example.

Although for reasons of storage limitation over the period of the project it has not been practicable to use a 'Fourier transform' (Chapter 6) type of computation, the storage and time requirements of this approach are discussed. For a large receiving array this approach offers possibilities of large reductions in computing time.

10.2. COMPUTER FACILITIES.

For the first 18 months of this project the only machine available was an IBM 1620 with a 40,000 word core store. Although reasonably generous in storage, no work beyond some initial simulations of image forming processes was possible on this machine because of the very slow speed.

All the work reported in Chapter 12 was done on the machine installed later, with the specifications;

Type; IBM System/360, model 44.

Storage; core - 16k words of 32 bits each, in four 8 bit 'bytes' or 64k bytes (k ≡ 1024 i.e., 2^{10}).
disk - 2, type 2315 disk cartridges, each with a nominal capacity of 1,048,576 bytes.

Inputs; 600 cards/minute (80 column cards) reader,
500 characters/second paper tape reader.

Outputs; 600 lines/minute line printer,
125 cards/minute, card punch.

The core storage has very recently been extended to 32k words. Most of one disk ('system residence disk') is occupied by compilers and other standard programs, leaving a space of 1024 blocks (each of 360 bytes) available for program use.

All the programs* on this disk were written in the FORTRAN IV language which, in the IBM System/360 version, contains a large number of features not provided in the basic form. This, together with the peculiarities of disk storage usage in this machine are the

* With the exception of one to interpret the paper tape code.

main reasons why complete program listings are considered of little value.

In normal use approximately 29,000 bytes of core storage are absorbed by input-output routines and similar functions leaving 36,000 bytes for program and data in the 64k byte form. In the expanded version 101,000 bytes are available, an increase of approximately three times.

10.3. OPERATIONS COMMON TO CONVOLUTION AND TRANSFORM COMPUTATIONS.

Regardless of the type of operations performed in proceeding from the raw data set of the transducer array to the image, the following are needed;

(1) Reading and storage of the paper tape data.

(2) Time-frequency Fourier transform operations on each element record. Despite the fact that this operation can be combined with the spatial transformations or convolution in one operation, (5.3, 6.4) simultaneous manipulation of the complete three dimensional data set requires storage space far beyond any reasonable core storage size.

(3) Display of the image formed.

These operations fit into the overall pattern as indicated in Figure 10.1.

10.3.1. Tape reading and storage of data.

For purposes of reading and initial storage it is convenient

to regard the data in each tape punching as a single number between 1 and 255 (inclusive) represented in pure binary code. (Zero has a special representation). With this representation each group of three samples may be stored together and individually extracted later by breaking up the numbers. Using this artifice, each element interrogated contributes 87 numbers, each of which may be stored as a half word (the smallest individually accessible unit) of two bytes. Thus a maximum length tape with 1100 records requires 95,700 half words of storage or 191,400 bytes. This amount is available in the 1024 blocks of 360 byte storage on the system residence disk and the data was placed here, 2 element data sets per block, together with a reference number attached for identification and checking, to give a total of 352 bytes used in each block. ((2 x 87) + 2 reference numbers, each as a half word of 2 bytes). The total capacity extends to 2048 elements with this scheme and provision was made for up to 1280 in the tape reading subprogram.

This record is not perturbed by subsequent operations and provides a semi-permanent file of the data. Reading a complete tape takes 4 minutes (and there is no automatic respooling!) so the internal record is of some importance.

10.3.2. Time-frequency transform.

The transform was achieved by first recovering the record from the disk, element by element, and expanding each stored punching

of data into the three individual samples for a total of 252 numbers. This array of numbers was inserted into the real parts of a 256* element complex number vector with two dummy numbers at each end. At this stage the tape codes of 00, 01 10 and 11 were represented by the numbers -3, -1, +1 and +3 respectively, restoring the original sample polarities. Passing the sample vector through the transform routine produced a set of complex numbers in place of the original time sample values, representing in sampled form the frequency spectrum of the time record. (This transform corresponds to the 'h,s' part of Equation 6.26). The 256 complex numbers obtained are 'spaced' an interval $1/(256\tau)$ Hz apart, which for $\tau = 41\frac{2}{3}$ nS was 3/32 MHz, beginning with a value at d.c. and proceeding to the sample immediately before the sampling frequency of 24 MHz. Since the time record was a purely real function the values for frequencies above half the 24 MHz rate are redundant, being merely the complex conjugates of those in the corresponding positions below 12 MHz.** If these are dropped, 129 complex numbers remain, i.e., the output has the same number of degress of freedom as the input.

---

* The Fourier transform routine works on input sample sets in sizes that are powers of 2 ($256 = 2^8$), 252 is the nearest multiple of 6 (i.e., the number of samples taken in one operation by the apparatus built) below 256.

** That is, the next value above 12 MHz is the conjugate of that immediately below, and the last value at $23\frac{29}{32}$ MHz the conjugate of that at 3/32 MHz.

(Strictly speaking, the 12 MHz value conveys no information as the original signal should have had no energy near this frequency).

The form of operation described was a fairly basic application of the transform to raw data and some improvement could be made in the accuracy of the spectrum estimation by application of techniques such as those suggested by Richards.[1] However, extreme accuracy was scarcely possible considering the SNR of the signals and not ultimately of great importance because of the noise reduction effected by the spatial image forming processes. (Chapter 7).

Adhering to the standard representation in the machine, each complex number occupies 2 words or 8 bytes representing a precision which is ridiculously in excess of the accuracy of the computed spectrum. However no consideration was given to special representation and the waste has been tolerated.* Some saving may be effected by discarding the values from the very low and very high frequencies as being practically meaningless but even then one is left with approximately 100 complex numbers per element interrogated, so with 1100 elements a total of 880,000 bytes are needed for storage In practical terms this means occupying a whole disk since the coordinates of the aperture point must also be accommodated and these require approximately a further 10,000 bytes.

---

* A two to one compression could be achieved by treating the real and imaginary parts separately as integer numbers each taking a half word but this would involve expansion back into the full two words for actual computation, or special arithmetic routines.

Because the actual image formation carried out was restricted to only a few frequencies it has not been necessary to store all the transformed data and at the present stage of development the numbers representing the signal component at any given frequency are extracted from each element record and punched into cards for transfer to the actual image forming program. Since the biggest aperture used was 14 x 14 elements the complete record for any frequency together with coordinate information could comfortably be accommodated on 30 cards. However extension to a greater number of frequencies or a larger aperture requires storage as discussed above.

10.3.3. Image display.

If it is taken that the final image should resemble an optical picture in form then the display must appear as a variation in apparent density following the calculated intensity of the acoustic field. It is also possible to present a picture of the field amplitude at any one frequency and this form of representation has been adopted for all the images shown in Chapter 12. Intensity plots are also available.

There are four main problems associated with the image display.

(1) Range of 'grey' levels.

(2) 'Fill' of the display area to an extent sufficient to permit visual 'running together' of the display points.

(3) Generation of spurious patterns by interaction between the image and a regular display grid.

(4) Geometric distortion.

The first of these has already received some mention in connection with the error introduced (7.3.5). The only available output medium was a line printer fitted with a standard print train which limited the range of possible symbols. Basically the idea was to obtain variations in density by using characters covering variable fractions of the area of the unit character 'cell' of 0.1 by 0.125 inches. After some experimenting, the range finally employed was; ⊛, ⊖, ✱, +, =, -, . and blank. The first two symbols are formed by overprinting the capital 'O' with an asterisk and a dash respectively, the others being standard. These achieved roughly the required variation in area coverage but the apparent density of the symbols viewed directly is not in accordance. This arises from the action of the printer. Each symbol is struck with the same force onto the paper and consequently those occupying a smaller area produce a darker impression. However, this can be remedied to some extent by taking a high contrast photograph and thus bringing all the symbols to the same blackness.

As presented, the images are in 'negative' form; areas of high reflectivity in the field appear darker. This can be reversed if desired but the effect is not considered to be as good.

For any computed image there are only a limited number of independent picture elements, depending on the number of aperture elements. Ideally the information in these independent samples

can be interpolated* to provide a continuous picture but in practice this constitutes a major operation. In computing the Chapter 12 results a large number of redundant points were calculated to allow the image spread over the largest possible area (approximately 1 foot square) so that a reduction to true size appeared reasonably 'smooth' in intensity variation. However, this wasteful procedure cannot be followed with a larger amount of input data and some form of interpolation using the information in immediately surrounding elements[2] is more suitable. This essentially approximates the mathematically correct interpolation procedure.

When an image is plotted on a coarse grid there is always the possibility of spurious apparent patterns appearing through the Moiré effect.[2,3,4,14] Images of small objects are particularly prone to this effect as they tend to consist of a series of concentric rings. Basically the problem is one of under-sampling the higher frequency Fourier components of the image resulting in 'aliasing' of the pattern repititions which should occur outside the fundamental image area (6.4.2) back into the fundamental period. The problem can be avoided by a sufficiently fine display grid; a condition that should be satisfied automatically if at least one display cell is available for each independent image point.

---

* By 'filtering' the complete picture array through a low pass filter so that each point sample spreads into a sinc function after the manner of Equation 6.18.

Carter[4] indicates that in practice it is advisable to be more generous than this. In none of the images shown in Chapter 12 is this effect apparent, but it is suppressed in any case by the disappearance of the finer diffraction structure around the main peaks below the level of the first plotting symbol.

Geometric distortion of the image results from the use of a line printer unless compensation is made for the different cell dimensions across and down the page. With the particular printer used the characters were at 0.1 inch spacing with a displacement of 0.125 inches between lines. Thus, if the points were from a uniformly spaced array, the vertical dimension expands by 25% in the printed image. This was compensated for in the convolution technique by increasing the spacing of the computed points in the 'y' direction but with a Fourier transform method the x and y directions are treated simultaneously and have the same relative scales in the computed image as the original transducer array element spacings. Changing these from equal x and y spacing is possible but implies either redundancy or under-sampling depending on whether the x spacing is compressed or the y spacing expanded. Probably the most suitable method of compensation is to interpolate values for each set of three display points between the positions where the two grids align from the four values that appear in this interval.

Most of the problems mentioned here were basically the result of attempting to use an unsuitable piece of apparatus for the job.

Difficulties of coarse spacing, grey levels and distortion can be solved by the use of a device such as a film plotter[2] or if this is too slow, a CRT display. (The latter suffers from poor range of intensities in direct use but some form of 'half-tone' display[5] can be used to overcome this).

10.4. IMAGE FORMATION BY CONVOLUTION TECHNIQUE.

This method was adopted very early in the project mainly because the amount of direct access storage needed can be very small. Basically, the operations involved were taking the values of phase and amplitude at each aperture point for each frequency, one by one, and using a discrete form of Equation 5.27, computing the contribution made by each of these components to the signal at each of the image points. After progressing over every aperture point for a given image point and successively adding the contributions as each was computed, a single complex number was obtained which described the field at the image point for the particular frequency chosen. This whole process was then repeated for each image point. With a total of M aperture points and N image points, a total of M x N operations was needed with each operation essentially a complex multiplication.* However the only data required at each step was the value of the aperture signal at one point and the accumulated value of the image signal at one point, to which the

---

* In the actual program the real and imaginary parts were treated separately as no complex arithmetic subroutines were available when it was written.

latest computed value was added. In practice, it was more convenient to have as much of the aperture data as possible, and the array in which the image was accumulated, together in core storage.

The actual sizes of aperture used in all the experiments on solid materials did not exceed 16 x 16 elements and provision was made accordingly to hold the complete aperture data pertaining to one frequency in core store. With the program and standard routines also present a space sufficient to hold one quarter of the 120 x 96 image array was available and the remainder was stored on the disks until required. This image array contains many redundant points but was used in anticipation of larger apertures.

Provision was made in the program for computing only a portion of the full number of image points so as to bring the amount of information manipulated into a better relation to the true information content of the data.

Other work on the manipulation of images and holograms in computers has used convolution[6] but once any appreciable size of aperture is used the time savings possible by the transform technique have resulted in all recent work being done by this method.[7,8].

Before proceeding to discuss this we may note that a convolution method can be used for any size of aperture and any geometry given only sufficient backing storage in the computer.

This flexibility is not shared by the transform method unless

a direct form of Fourier transform operation is resorted to and in this case the whole advantage of speed is lost.

10.5. IMAGE FORMATION BY TRANSFORM TECHNIQUE.

The main point in using the transform approach to image formation lies in the possibility of employing the 'fast' algorithm[9] for the transform operations. The implementation of this requires the complete array of numbers representing the aperture readings at a particular frequency to be held in storage at once. If the transducer array was randomly sampled then the samples available must be inserted in an array in core storage having dimensions sufficient to have accommodated the complete number of transducer elements. Also, this storage must have dimensions sized in powers of two.* Since each sample is a complex number, 8 bytes are required. For an array of 64 x 64 elements this implies a storage consumption of 32,768 bytes. Ultimately the image computed appears in the same locations but if intensity values are retained to combine several frequencies, a separate array providing at least one half word per point is needed for a further storage requirement of 8,192 bytes. The Fourier transform algorithm occupies 5988^{10} bytes for a total of just under 47,000 bytes. With a further 29,000 bytes required for standard routines, a total of 76,000 bytes is reached which exceeds the storage of the available computer.

Even with 128k bytes the array cannot be extended to 128 by 128 (the next jump in powers of two) but there is ample room left

---

* (See comments at the end of this Chapter).

for the program with a 64 x 64 array.

From the material in Chapter 6 it will be seen that the operations involved consist of;

(1) A Fourier transform of the aperture data.

(2) A complex multiplication operation between each computed plane wave component and the phase or 'propagation factor' appropriate to the component.

(3) An inverse transform operation to give the image.

If we adopt the usual procedure of regarding the computing time as proportional to the number of complex multiplications[11] required then each transform has approximately $4N^2 \log_2 N$ operations for an N by N array. The second operation involves another N^2 multiplications for a total of $N^2(1+8\log_2 N)$. For an equivalent manipulation the convolution method involves N^4 multiplications. Thus the transform method becomes more economical when N is greater than the solution to -

$$N^4 = N^2(1+8\log_2 N) \qquad .. 10.1$$

which is approximately N = 4. For N = 64 the saving is by a factor of 83 times.

In both methods the operations besides complex multiplication are very similar, the most arithmetically complex being the calculation of R. (Equation 5.27), or the irrational exponent in Equation 6.28.

10.6. DISCUSSION.

From the above considerations it will be apparent that the image formation procedures actually followed are open to considerable improvement. In particular any fully practical scheme involving image formation at many frequencies should definitely employ the transform approach as this will enable a complete image to be formed in little more time than one at a single frequency takes via the convolution method.

At the input end of the processing, opportunities exist for the correction of the transducer response with a software 'filter' simulating the function of the matched filtering discussed in 8.7.

The initial time-frequency transform could possibly be implemented via a device such as those discussed by Bergland and Hale.[12] This initial operation however constitutes only a small part of the total computation required and unless direct transfer of the spectra to the computer were possible, would result in an expansion of the data to be accommodated on the tape. (Requantizating the spectral values to only two bits adds a large noise component).

Improvements at the output end could follow the line of extracting the information content of the image in the most favourable form by enhancement techniques.[13] For this to be a profitable exercise a considerable improvement in the means of image display is necessary.

Some considerable economy in storage and a possible increase in computing speed are possible by a more economical representation of the data. High accuracy is not needed in individual operations because of the small final effect of even quite large errors. To take advantage of these features would have required writing the programs in a lower level language than FORTRAN, probably 360 Assembler Language, and for the purposes of this project the convenience of FORTRAN was an over-riding consideration.

Possibly the worst feature of using standard computer arrangements for implementing the transform method is the very wasteful storage utilisation. Algorithms are now available that permit data set sizes to be other than powers of two.[15] This avoids the large jumps between 'binary' sizes and represents a method of fitting, more exactly, the size of storage used with the size of the transducer array. Similarly some extra programming complications can compensate for a restricted fast storage.[16]

REFERENCES FOR CHAPTER 10.

1. Richards, P.I. 'Computing reliable power spectra'. IEEE Spectrum 4, pp.83-90, Jan. 1967.
2. Schroeder, M.R. 'Images from computers'. IEEE Spectrum 6, pp.66-78, March 1969.
3. Oster, G. and Nishijima, Y. 'Moiré patterns'. Sci.Am. 208, p.54, Jan. 1963.
4. Carter, W.H. 'Aliasing in sampled holograms'. Proc. IEEE (Letters) 56, pp.96-98, Jan. 1968.
5. Kennedy, W.K. Private Communication.
6. Devaney, A.J. and Baron, S. 'An integral transform for the analytical manipulation of holograms'. NASA, Electronics Research Centre, Control and Information Systems Laboratory, 1967.
7. Lesem, L.B. et.al. 'Holographic display of digital images'. Proc. AFIPS Conference 31, pp.41-47, Oct. 1967.
8. Lesem, L.B. et.al. 'Computer synthesis of holograms for 3-D display'. Comm. ACM. 11, pp.661-74, Oct. 1968.
9. Cooley, J.W. and Tukey, J.W. 'An algorithm for the machine calculation of complex Fourier series'. Math. of Comp. 19, pp.297-301, April 1965.
10. IBM Scientific Subroutines Package (SSP), Program 'HARM'. IBM Manual H20-0205-3, Fourth Ed., 1968.
11. Cochran, W.J. et.al. 'What is the fast Fourier transform'. Proc. IEEE 55, pp.1664-1674, Oct. 1967.
12. Bergland, G.D. and Hale, H.W. 'Digital real-time spectral analysis'. IEEE Trans. EC-16, pp.180-185, April 1967.
13. Oppenheim, A.V. et.al. 'Non linear filtering of multiplied and convolved signals'. Proc. IEEE 56, p.1264-1291, Aug. 1968.
14. Rosen, L. 'Moiré effects in computer generated holography'. Proc. IEEE (Letters) 55, p.1736-1737, Oct. 1967.
15. Singleton, R.C. 'An algorithm for computing the mixed radix fast Fourier transform.' IEEE Trans AU-17, pp.93-103, June 1969.
16. Brenner N.M. 'Fast Fourier transform of externally stored data.' IEEE Trans AU-17, pp.128-132, June 1969.

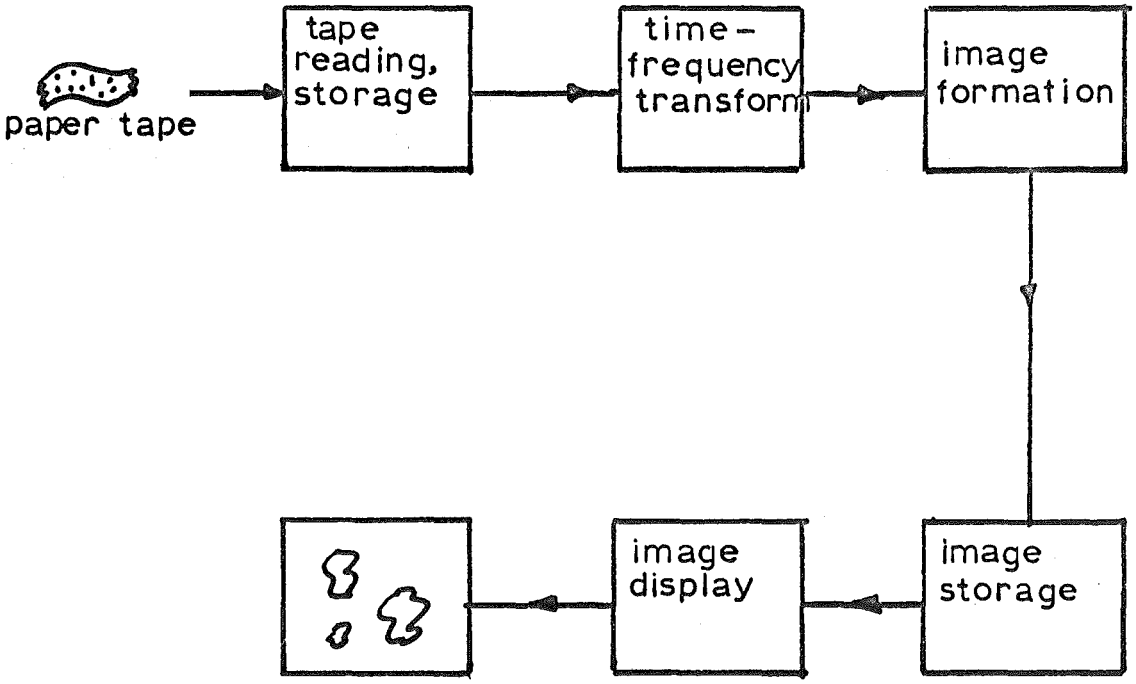

FIG.10.1: Basic operations of image construction program.

CHAPTER 11.

PRACTICAL APPLICATION OF TRANSMITTING TRANSDUCERS.

11.1. INTRODUCTION.

This chapter describes some measurements of the acoustic fields produced by a number of different transmitter arrangements. All the measurements were made on the apparatus shown diagrammatically in Figure 11.1. The excitation applied to the transmitter consisted of a burst of 5 MHz sinusoid, similar to that shown in Figure 12.18(a), approximately 25 μS long.

Except for the case where a scattering spacer was inserted between the transducer and the aluminium block the transmitter was bonded to the block with gallium. (Appendix 1.2). The receiving transducers consisted of a 5mm diameter, 5 MHz disc of PZT5A and similar elements ground to 3mm or 1mm diameter. Acoustic contact was made to the polished top surface of the block via a thin layer of glycerine, with a stiff spring forcing the transducer down, and the received signals were indicated on an oscilloscope. The plots are a cross-section (including the transmitter axis) through the field. Block thickness was chosen at $2a^2/\lambda$ (a = radius, λ = wavelength) for the largest transmitter tested (15mm diameter). This distance corresponded to that quoted earlier (3.4.2) as necessary for 'far field' conditions, at least near the transmitter axis, and was approximately the transmitter-object distance in the imaging experiments (Chapter 12).

The present experiments were not intended as a precise means of measuring the field of any particular arrangement; rather the aim was to investigate the relative fields resulting from different transmitters and in particular to assess the effect of deliberately introducing a diffusing section into the acoustic path. Spatial diffusion of the insonification provides a means of overcoming some of the highlight effects apparent when a smooth object is subject to energy coming from one direction only.

The work reported here has since been extended considerably as part of a further project within the overall acoustic imaging effort, to the case of several transmitters (up to five) distributed over the face of the block. Accurate correction of these latter readings for the measuring system geometry and the directivity of the receiving transducer has led to measured fields in agreement with those predicted and measured by other investigators (3.4.1), but the results shown here served to indicate directly the z directed component of the field at a plane within the material and thus corresponded with the theory presented in Chapters 5 and 6.

11.2. 15mm DIAMETER TRANSMITTER.

The relative field strength measured is shown in Figure 11.2, with maximum value corresponding to a signal of 0.57V. peak to peak on the 3mm diameter receiving transducer for 50V. P-P on the transmitter. Between the half amplitude points the pattern had a width of 18.5mm.

Application of the formula*;

$$U_z = C \frac{2J_1(ka\sin\theta)}{(ka\sin\theta)} \cdot \cos^2\theta \qquad .. 11.1$$

giving the component normal to the surface (C is a constant) indicated an angle of $\theta = 0.06$ rad. for half amplitude, ($k = 5000$, $a = 7.5$mm) corresponding to a circle of radius 5.3mm at a depth of 88.5mm. However a more detailed examination of the path lengths involved (Figure 11.3) showed that the main lobe far field condition of no cancellation of signals from different parts of the transmitting surface was valid only for an area of 4mm radius around the normal to the transducer centre. The geometry is shown in Figure 11.3. The observed broadened pattern is typical of near field behaviour with an unfocussed transducer[1] and it will be noted that it has a width comparable with that of the transmitter diameter.

Accurate measurement of the field with a receiving transducer of appreciable size requires allowance for its directivity. With a 3mm receiver on a plane 88mm from the source some portions of the receiver are in antiphase with others for a displacement along the measuring surface greater than 20mm from the transmitter axis.

This became of significance in the case of a 5mm transmitter where the energy was spread over a wider arc.

11.3. 5mm DIAMETER TRANSMITTER.

Figure 11.4 shows the measured field with a 3mm receiver as

---

* This comes from Equation 3.9 for the radially directed term multiplied by an additional cosθ term for the receiving transducer.

recorded' and the field corrected for the receiver directivity.

With the 5mm transmitter, some cancellation occurs for distances greater than 11.5mm from the axis so once again the pattern was somewhat broader in angle than the far field one. (The far field pattern should have a null at 18°, corresponding to a distance of 29.7mm from the axis at 88.5mm and be at half amplitude for a distance of 15.3mm from the axis).

With correction made for the receiver directivity, the response was one half at 19mm radius from the axis.

Perhaps the most significant observation to be made is that this pattern was only twice as broad as the 15mm transducer at the depth involved. Thus, in order to spread the insonification over a still wider arc, a transducer with a diameter of 1.3mm was formed by etching away the outer portion of the electrode coating on the free face of a 5mm diameter element.

11.4. PARTIALLY ELECTRODED TRANSMITTER.

For measurements with this transmitter the receiving element was 1mm diameter to reduce the correction needed. Some considerable difficulty was experienced in obtaining a consistent reading because of a tendency for the small receiver to seat with only one edge in good contact with the surface of the block. The range of readings obtained are indicated on the plot (Figure 11.5) together with a line drawn through the average reading at each position. (It may be noted that the maximum signal in this

arrangement was approximately 60 mV for 50 volts on the transmitter, a drop of ten times compared with the 3mm receivers at the same transmitter excitations, corresponding to the reduced receiver area). The plot corrected for receiver directivity is also indicated; the maximum correction within the range of the measurements amounting to 15%.

With the broad beam obtained with this smaller transmitter the expression 11.1. lost accuracy as the measurement surface now departed considerably from one at constant radius from the transmitter centre point assumed by neglecting the $\frac{1}{R}$ term in Equation 3.9. However, even with correction for this factor allowed, the field pattern was considerably narrower than that which should have been obtained from a transmitter of 1.3mm diameter. Working back from the indicated half amplitude width gave a 'ka' value of 8, corresponding to an effective transducer radius of 1.6mm.

This result agreed with the spreading effect noted by White[2] using partially electroded plates operating at their thickness resonant frequency and indicates that a very wide spread of energy could be obtained only by a physically small transducer and not by merely reducing the electrode area on a larger one.

11.5. SCATTERING SPACERS.

The physical arrangement is sketched in Figure 11.6. The transducer was bonded to one end of a bar of material and the other end of the bar forced into contact with the under-surface of the

aluminium block through a film of glycerine.

A number of scatterers were investigated, all with a 15mm transmitter.

(1) Cast iron. The distance l was 2.5cm and the diameter of the spacer (d) also 2.5cm. With this material the losses were so great that no signal could be detected at the measuring face of the aluminium block.

(2) A similar section of steel bar was treated at 800°C for twelve hours to induce grain growth. The average grain size achieved was of the order of 0.4mm. This spacer proved unusable as a whole succession of delayed pulses were obtained from reflections at the steel-aluminium interface travelling back and forth through the steel. Measurements on the first received pulse indicated that no appreciable broadening of the field was obtained.

(3) To overcome the interface reflection problem a further spacer of aluminium with l = 5cm was fabricated and turned into a scattering path by drilling some 200 holes in a range of diameters from 1 to 3mm through the block. These holes were orientated randomly in inclination to the spacer axis and in the location of the ends on the spacer surface.

The transducer was fixed with gallium but after the measurements shown below had been taken the metallurgical effect described in Appendix 1.2 was observed, rendering the spacer useless for any further tests.

Figure 11.7 shows the observed field on two 'slices' at right

angles to each other. While these measurements (taken with the 3mm diameter receiver) have a maximum value one tenth that obtained with the transmitter directly attached to the block, (showing considerable loss in the spacer), they are quite narrow and indicate that the main parameter determining the distribution inside the block was the diameter of the radiating end of the scatterer.

A situation relevant to the design of a material which effects as much phase fluctuation* as possible without a great amplitude loss has been described by Knollman.[3,4] He considered the case of both plane and spherical waves in a medium perturbed by random spheroidal inhomogeneities, deriving results for the mean square amplitude and phase fluctuations at different distances from the transmitter. From Reference 3, the greatest phase and least amplitude perturbations result from inhomogeneities having dimensions in the direction of wave propagation which are of the order of 10 wavelengths or more and preferably much greater dimensions in the direction across the propagation, (although particularly with spherical waves, spherical discontinuities will be nearly as effective). Total path lengths containing only a few discontinuities minimise amplitude fluctuations.

These papers suggested the possibility of fabricating a scatterer by embedding spheroids in a bulk of material by casting.

---

* A random phase distribution over the transmitting area prevents the formation of definite beam patterns and tends to spread energy more or less uniformly over a wide core.

However this idea was not pursued, attention being concentrated instead on providing a multiplicity of small transmitters mounted directly on the material under inspection.

REFERENCES FOR CHAPTER 11.

1. Kay, L. and Bishop, M.J. 'The effect of a linear phase taper on the near field of an ultrasonic multi-element array'. Radio Electron. Eng. 29, pp.207-212, April 1965.
2. White, R.M. 'Elastic wave scattering at a cylindrical discontinuity in a solid'. Journ. Acout. Soc. Am. 30, pp.771-785, Aug.1958. (Table IV).
3. Knollman, G.C. 'Wave propagation on a medium with random spheroidal inhomogeneities'. Journ. Acoust. Soc. Am. 36, pp.681-688, April 1964.
4. Knollman, G.C. 'Correlation of amplitude and phase fluctuations for wave propagation in a medium with random spheroidal inhomogeneities'. Journ. Acoust. Soc. Am. 36, pp.2306-2310, Dec. 1964.

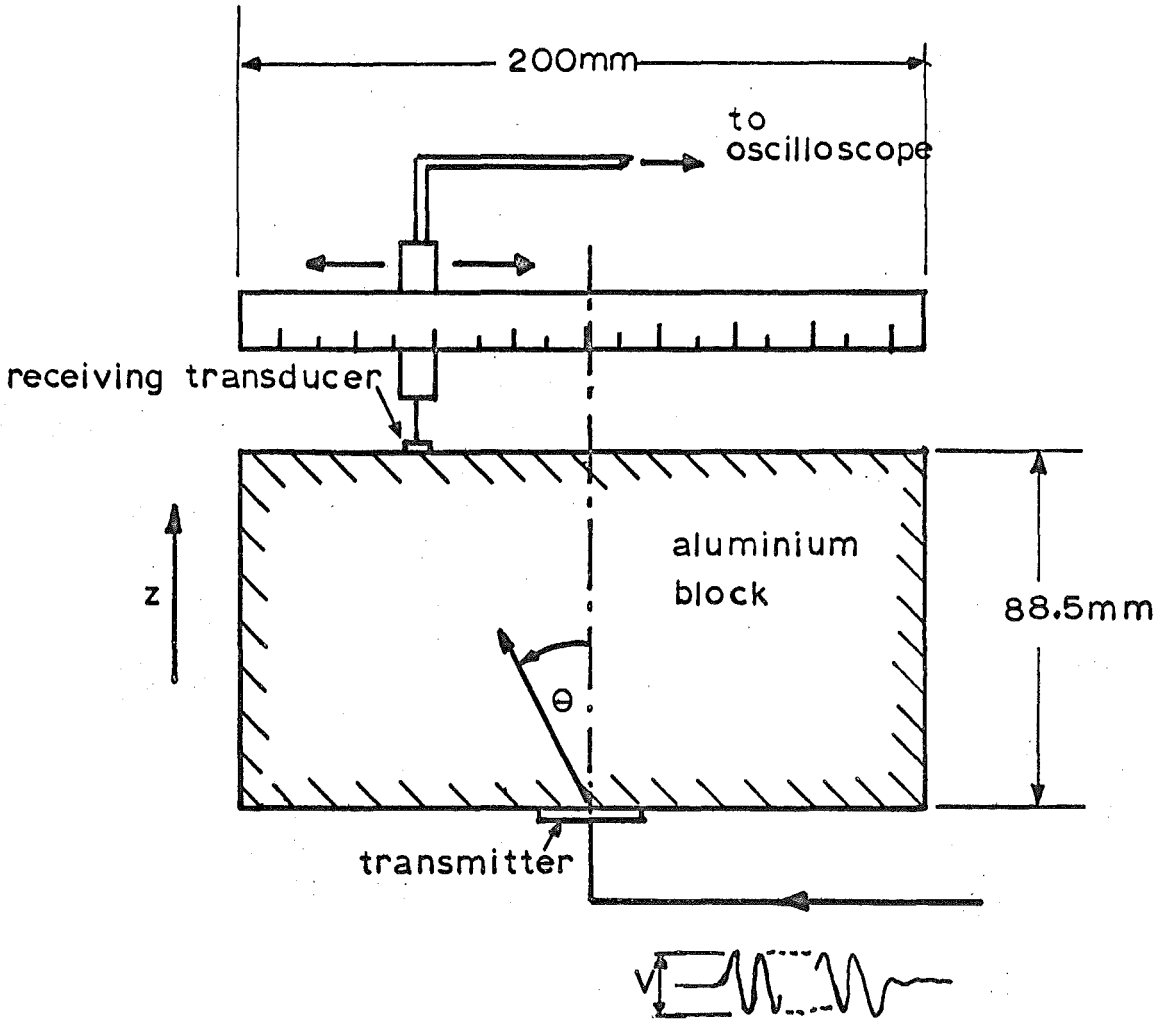

FIG.11.1: Sketch of apparatus for transmitter field pattern measurements.

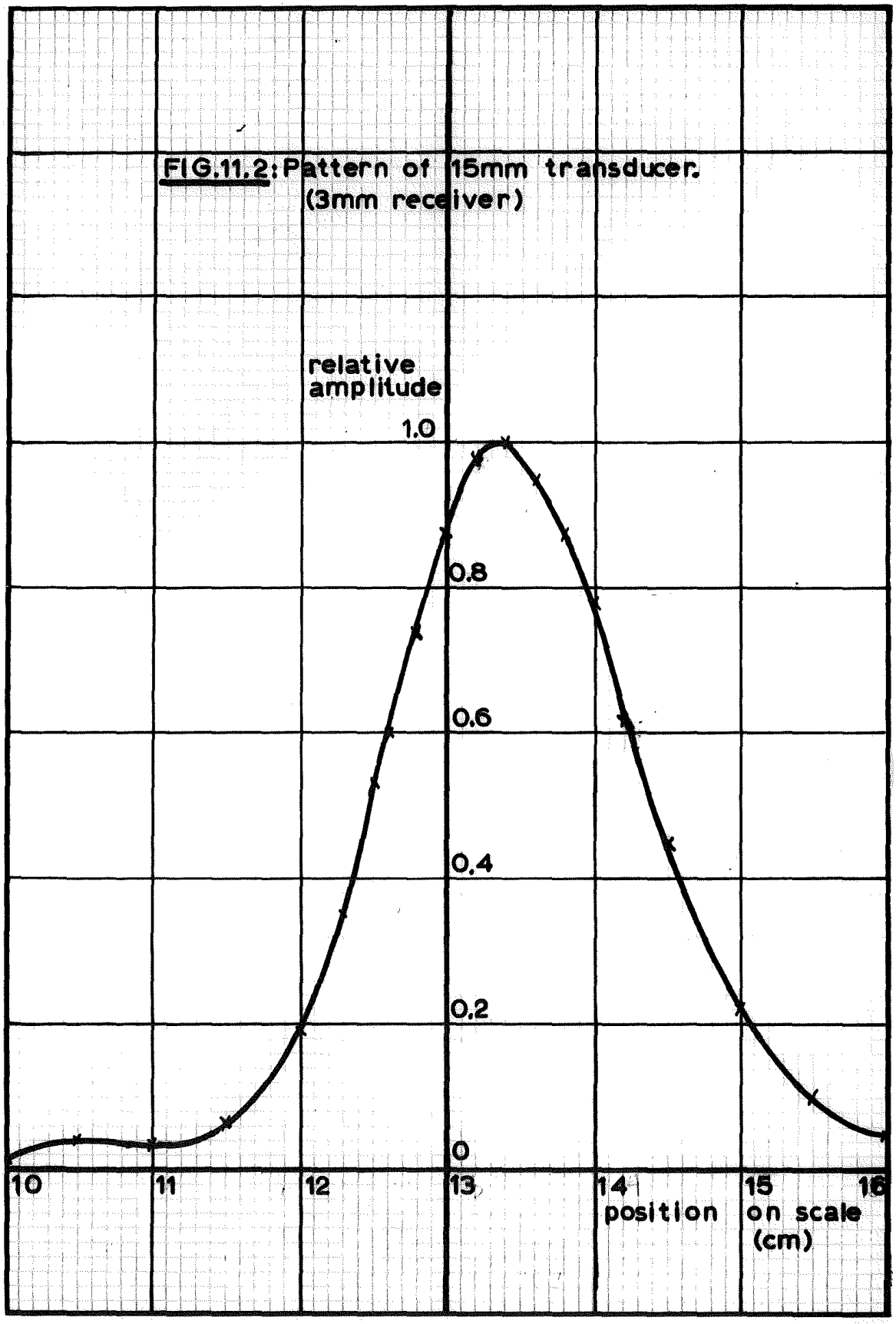

FIG.11.2: Pattern of 15mm transducer. (3mm receiver)

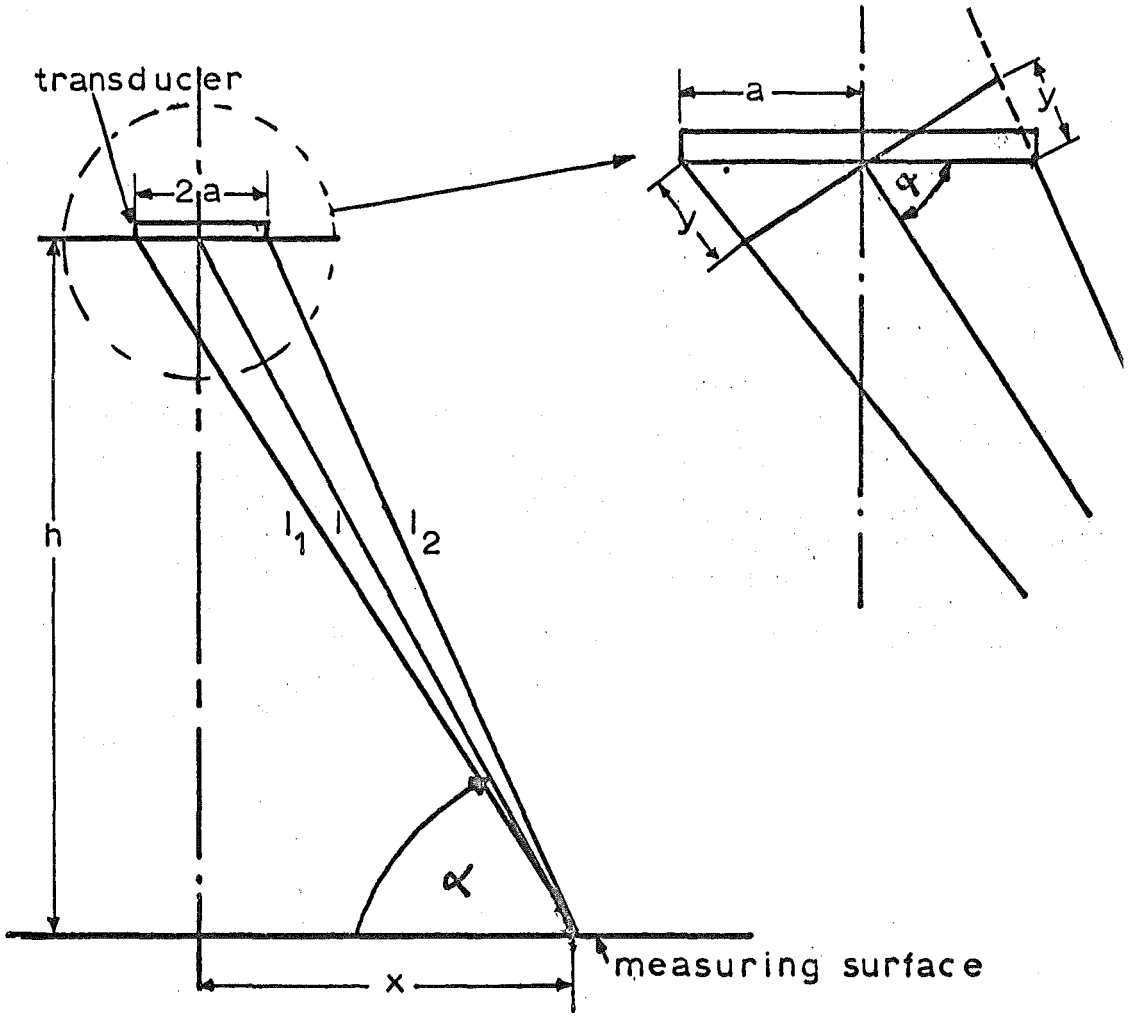

path difference $= |l_1 - l_2| = 2y$

$\approx 2a.\cos\alpha$

$= \frac{2ax}{l}$

for $2y \leq 0.64$ mm $(\lambda/2)$ and $x \ll h$, then for $h = 88.5$mm and $a = 7.5$ mm,

$x \leq 3.9$ mm.

FIG. 11.3: Cancelation effects in main 'lobe' of transducer near field pattern.

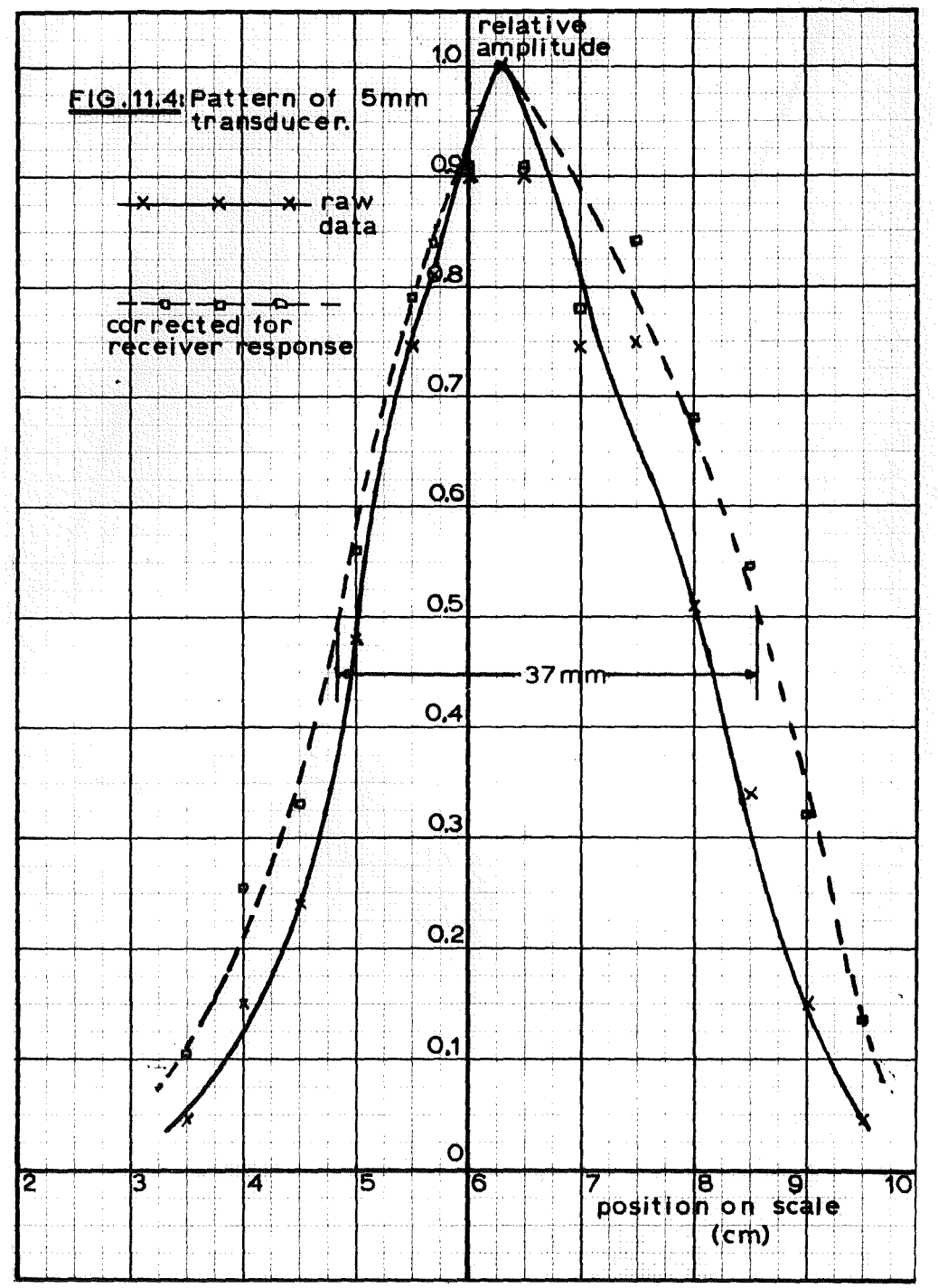

FIG. 11.4: Pattern of 5mm transducer.

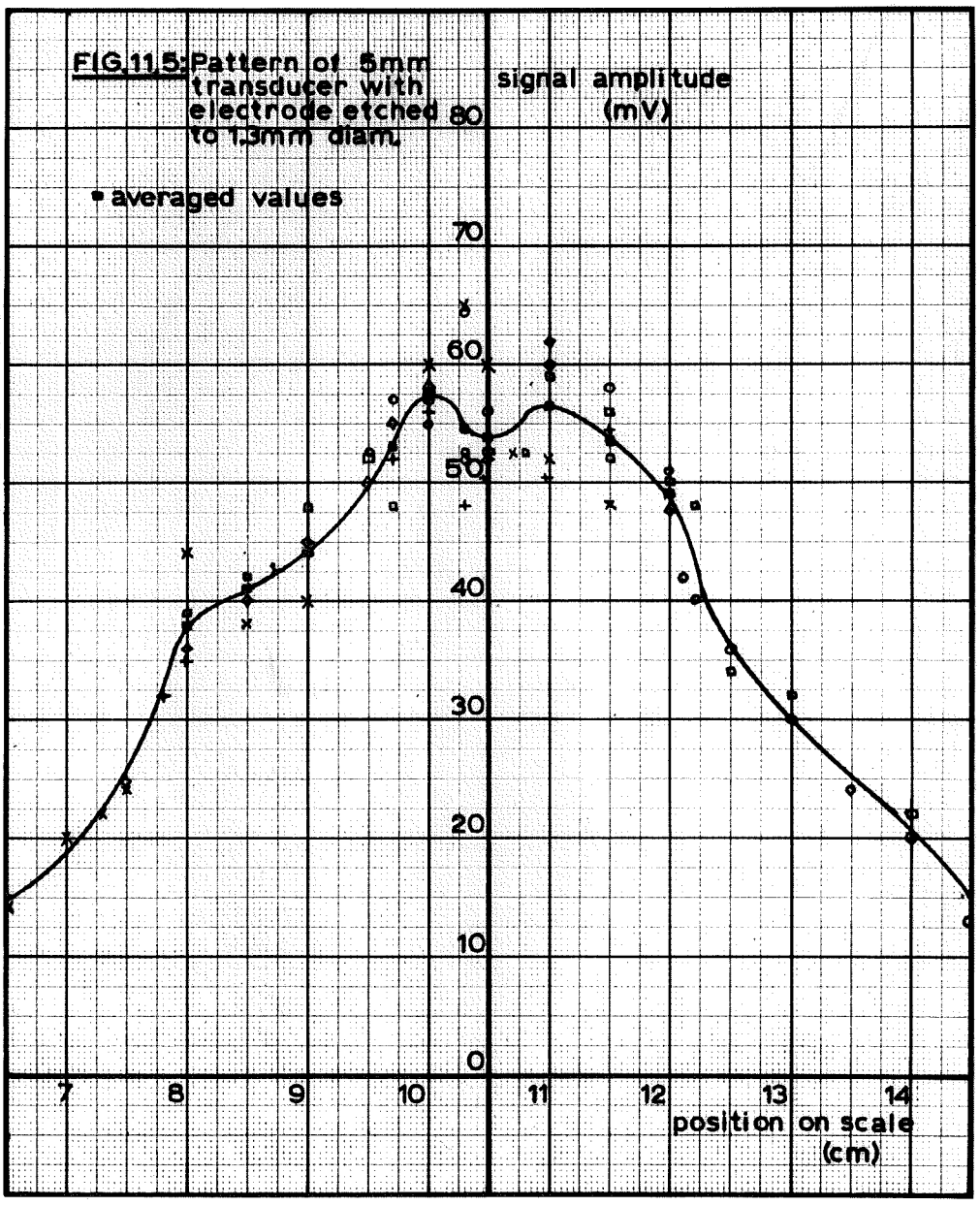
FIG.115: Pattern of 6mm transducer with electrode etched to 1.3mm diam.
• averaged values
signal amplitude (mV)
80
70
60
50
40
30
20
10
0
7
8
9
10
11
12
13
14
position on scale (cm)

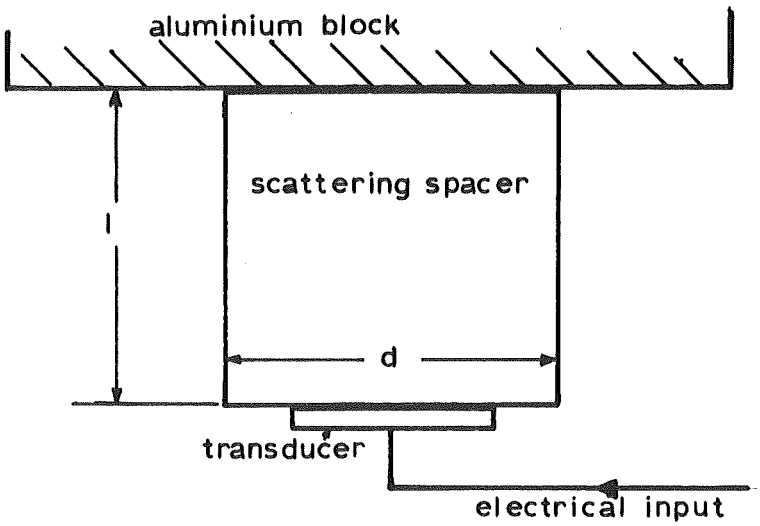

FIG.11.6: Scattering spacer.

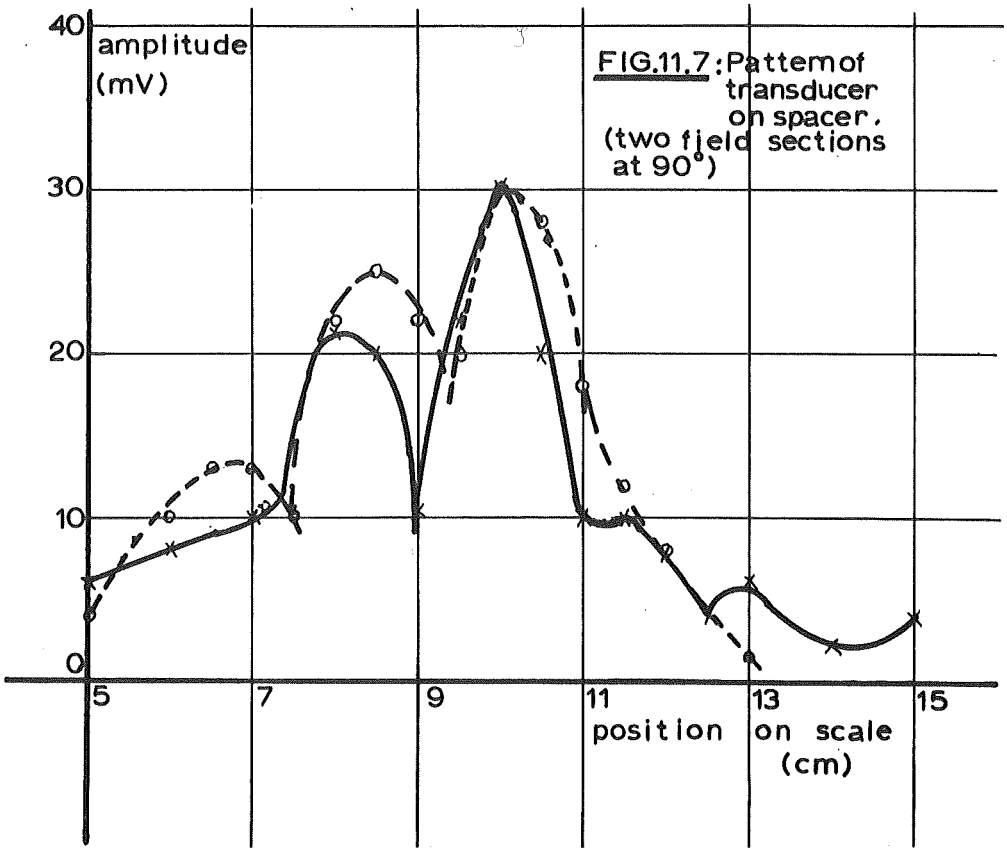

FIG.11.7: Pattern of transducer on spacer, (two field sections at 90°)

CHAPTER 12.

EXPERIMENTAL ARRANGEMENTS AND RESULTS.

12.1. INTRODUCTION.

The experiments on imaging fall into three distinct categories;

(i) Some initial measurements and processing done on transducers and reflecting objects suspended in a water tank. These are 'two dimensional' in the sense that the receiving transducer was scanned along a single line and not over an area of the field.

(ii) Measurements made on the surface of an aluminium block employing a quasi-continuous wave illuminating signal (3.5.4) and manual measurement of the amplitudes and relative phases of the signals on each element of the receiving array which now extends over an area of the surface.

(iii) Measurements made using the apparatus developed by Cook to automatically record the signals from each element under conditions of wideband illumination.

The first of these experiments was conducted largely to assess the practicability of maintaining the required stability over the extended period of the recording process but did indicate the ability of the processing program to satisfactorily operate with 'live' signals containing considerable errors. Results obtained in a fluid medium with a moving transducer do not however provide

any definite indication that a similar set of measurements taken from the surface of a metal block with a large, divided transducer will also be sufficiently representative of the true acoustic conditions to enable an image to be formed. Thus while awaiting completion of the automatic recording apparatus, the second group of experiments was conducted. These were necessarily restricted by the considerable time (several hours) necessary to manually record measurements from the 150 array elements examined. The extremely short period over which C.W. conditions could be maintained without encountering spurious reflections from the walls of the block and the very low 'duty cycle' of the transmission made any possibility of constructing a device for automatically measuring the necessary phases and amplitudes into a major project in its own right. However the results obtained did serve to demonstrate the general practicability of the project which depended critically on the behaviour of the receiving transducer.

Measurements made with the special apparatus have shown the generally correct functioning of the entire system but it has not been possible to fully utilise the wideband information obtained in the recording and computed results are confined to separate images constructed at a number of discrete frequencies. Consequently they exhibit the usual characteristics of monochromatic images - poor depth resolution.

Since the size of receiving array that has been used up to the present was too small to necessitate thinning, the effect of

this has been investigated by simulating the process on the recorded data. This is described in Section 12.4.3.3. To gain an appreciation of the effect of random and systematic errors in recording these have been similarly simulated in the computer and the results so far obtained demonstrate a considerable tolerance especially when it is remembered how much noise and distortion has already been introduced by the actual physical recording. This is described in Section 12.4.3.4.

Some work has been done using similar transducer arrangements on steel blocks rather than the aluminium material which the present author has confined attention to,and despite the much greater level of 'background' signals produced in steel, images have been formed. This work is being extended as a further project covering a variety of common engineering metals and the problems of obtaining more diffuse illumination over the interior of the material.

12.2. IMAGING EXPERIMENTS IN WATER.

12.2.1. Experimental setup.

The experimental apparatus is shown diagrammatically in Figure 12.1, and a photograph of the tank and scanning apparatus in Figure 12.2. The free space in the tank is approximately 45cm by 30cm by 30cm deep and the walls and bottom are completely lined with strips cut from rubber matting* after the fashion

---

* A rather larger size of spiked material than that in the reference was used and the supression of wall echoes is not particularly good.

suggested by Wood.[1] The transducers consisted of PZT5A ceramic cylinders 1,6mm in outside diameter by 1.6mm long with a 0.25mm wall thickness* mounted at the end of $\frac{1}{8}$th. inch brass tubes as shown in Figure 12.3. These tubes were coated with a latex material[1] to reduce spurious reflections. Despite the relative crudity of the mounting (partially enclosing some of the transducer body) no appreciable effects could be observed from pickup on the support tubes.**

The electrical side of the apparatus consisted of a stable 5 MHz source A derived from a crystal oscillator. The output from this was gated synchronously through a gating circuit D (Appendix 2., Section A2.1(a)), the gating pulse being derived by division from the 5 MHz to ensure that the transmitted pulses commenced on exactly the same part of the cycle. The length of transmission T was regulated by the 'pulse width' control on the pulse generator C and could be varied from one cycle up to several hundred. Power amplifier E provided a signal of approximately 50 volts peak to peak (P-P) into the transmitter.

Simultaneously with the commencement of transmission, the delayed sweep facility of the observing oscilloscope was triggered, providing a synchronised time-base against which to view the

---

* Brush-Clevite, Type 1-1010-5A.

** A more sophisticated support arrangement is described in Reference 2.

receiver signals. The signal was examined to determine that period over which the pickup from all positions examined by the receiver exhibited a steady value and the centre of this portion of the trace expanded for phase comparison with the signal directly from the oscillator. The expansion of one cycle over the whole screen enables phase comparison to be made to about 5% with some care and 10% accuracy is easily achievable. Phase shifts occurring in the preamplifier, oscilloscope, cables, etc., are of no consequence as they affect readings from all spatial positions equally and the measurement is concerned with only the relative phases of the received signals.

Some typical signal waveforms are shown in Figure 12.4.

12.2.2. Measurement of wavefront from transmitter.

For this measurement the arrangement was as in Figure 12.5 and the transducers were mounted at a common level with no other bodies in the tank. Readings of received signal were taken at 0.5mm intervals out to 11.5mm on each side of the point O with the results plotted in Figure 12.6. No significant variation in amplitude could be observed. (Note that the sampling interval d is smaller than the transducer size but none the less, changes in phase occur from point to point as the transducer is averaging over a different part of the field. Similar measurements made in connection with some acoustical holography experiments[3] have had a like arrangement).

Figure 12.6 reveals that the receiver axis zero point did not in fact quite coincide with the line at right angles to this axis through the transmitter centre but was displaced about 1mm. With correction made for this displacement the distance ΔL was calculated for each measurement point and converted to an equivalent phase shift. This is essentially one of the operations done by the computer program corresponding to the calculation of the exponential argument k.R in Equation 5.27. Integral numbers of wavelengths are of no consequence. Subtracting this computed phase shift produced a set of phase angles representing those applying after phase shifting in image construction. It was found that the standard deviation of these residual values was 16° with a maximum deviation of $\pm 30^{\circ}$ from the mean. Ideally of course these deviations would be zero but the values obtained indicated that the measurement accuracy was more than adequate for satisfactory imaging.

One further point should be noted. Figure 12.6 shows that the distance along the measurement surface for a 2π phase change is about 15mm, 50 times the 'free space' wavelength, from which it will be obvious that a transducer of 1.6mm width is several times samller than necessary to correctly sample the field.

12.2.3. Image construction from recorded data.

The data recorded as above was used to define the amplitude and phase of a corresponding number of point radiators and the

resultant field in the surrounding space computed along lines parallel to and at the same depth below the water surface as the measurement line as indicated in Figure 12.7. The procedure used is that of Equation 5.27 and this style of calculation has been used for all the results presented here.

It will be seen from Figure 12.8, showing the amplitude of the computed fields, that;

(i) A definite sharp peak is found in the plot taken through the position of the transmitter. This has a width of 4mm at the $2/\pi$ points. Calculation of the resolution for a 23mm aperture operating at a wavelength of 0.294mm (fresh water at 16°C) gives a value of 0.0155 radians which corresponds to 3.9mm at 250mm distance, this is in excellent agreement.

For an array of this size the far field region commences at approximately 1800mm for paraxial regions and the 'object' (in this experiment self luminous) is thus well within the near field zone.

(ii) The main peak is surrounded by sidelobes which vary from side to side of the main peak due to errors in the measurements but the average value of the two closest in lobes is 0.27 of the main lobe, in fair agreement with the 0.23 value to be expected from a linear, uniformly weighted array.

(iii) Plots taken in the region well removed from the object show a diffuse structure tending to a maximum around the angular location of object but lacking any definite main peak. A number of plots taken very close to the true position show plots

almost identical to A of Figure 12.8 but with a slight increase in main beam width as the displacement increases.

12.2.4. Imaging of transmitter and passive reflector.

The apparatus for this experiment was similar to that of the previous one with the addition of a passive reflector as indicated in the sketch of the apparatus in Figure 12.1, in the form of a vertically mounted length of steel tubing 22mm in diameter. The precise geometry is shown in plan view in Figure 12.9, and two photographs of the received signal for different transmission periods T giving, (a) conditions of separation of the direct transmitter-receiver signal and the latter arrival from the reflector and (b) overlap of the two components are shown as Figures 12.10(a) and (b).

The resultant computed fields are shown in Figure 12.11 for distances of 175 and 100mm from the measurement plane. The actual positions of the centre lines of the transmitter and reflector are indicated by the vertical arrows. In this case no definite single peaks have appeared at the respective positions but there are maxima in the pattern in the correct places. It is believed that this rather complicated pattern is largely due to multiple reflections occurring between the reflector and the transmitter and to reflections off the back wall of the tank. This latter signal had no effect on the earlier readings as a much shorter pulse length was needed to establish quasi-monochromatic conditions

and the interfering reflection did not overlap with the direct signal. The results here illustrate well the need to make the illuminating signal as short as possible when the objects are within a restricted volume with reflecting walls.

The significant features of these plots are;

(i) Despite the large size of the reflecting tube the signal from reflection off it is much smaller in amplitude than the direct transmission. Referring back to Figure 12.9, the tube has smooth walls of radius>>wavelength and thus will act as a specular reflector. Only energy incident on the tube over the small arc marked as β will reflect to within the length over which measurement was made. With the dimensions shown β is 2.5° and the strip of the tube actually 'seen' only 0.5mm wide, less than one third of the transmitter width.

(ii) The centres of the two peaks move in towards the centre line of the plot (C-D in Figure 12.9) as the distance from the aperture decreases. The arrangement is plotted to scale in Figure 12.13. The line drawn from the centre of the measurements, D,to the position of the reflector R, will be found to intersect the plot line B at R', 32mm from CD. Similarly the line from the transmitter site to D intercepts at T', 6mm from CD. Inspection of plot B of Figure 12.11 will show that these distances correspond to the apparent positions of the objects. This has shown a further characteristic of monochromatic systems when the object distance is>>aperture size, a very extended focal region

in the depth dimension.** The information to be derived from the measurements is thus purely of angular position of the objects.

A similar effect to the one seen here is apparent in field reconstructions made from measurements on the aluminium blocks.

12.3. MONOCHROMATIC ILLUMINATION IN THE ALUMINIUM BLOCK.

12.3.1. Experimental arrangement.

The arrangement for these experiments was functionally identical to that shown in Figure 12.1 except that the water tank was replaced by the aluminium block as sketched in Figure 12.14. Both transmitter and receiver are 15mm diameter discs of PZT5A nominally resonant at 5 MHz in the thickness mode.* The precise composition of the 'aluminium' material is unknown but is is of the type normally used in the manufacture of extruded sections.

The receiving transducer has the back face electrode divided into 1mm square elements (0.78 wavelengths at 5 MHz) by etching narrow strips away from the silver electrode. Connection to any element was made by means of a spring loaded probe guided by a

---

* Brush-Clevite, Type BMF/15B-5A.

** Cook[4] has calculated the 'depth of focus for a C.W. system when the object depth is comparable or greater than the aperture size as $\delta x = \pm \frac{\lambda}{8\sin^2 \alpha/2}$, δx being the displacement in depth from the true object position at which the phase shift from the true position = $\pi/2$, and α is the half angle subtended by the aperture at the object, with object distance/aperture diameter = 9 as in the present case, δx = 60mm.

perspex jig. These components are illustrated in Figure 12.15. There are a total of 156 complete square elements on the transducer. Bonding of the transducers to the block was accomplished by soldering using gallium metal. Initially an attempt was made to use an oil coupling layer for the sake of greater convenience in positioning the receiving array but an examination of the ringing occurring with oil eliminated this idea in that later extension to short pulses was required. Figure 12.16(a) shows the signals on identical receiving transducers resulting from the reflection at the bottom of the block from a transmission of a few cycles as shown in Figure 12.16(b).* The reduced output from the oil coupled transducer is caused by the voltage division effect of the capacitance introduced in series with the transducer by the oil film. Only sufficient pressure was applied to cause the transducer to 'wring' onto the surface, that is, the conditions were similar to those found in conventional pulse-echo ultrasonic inspection apparatus.

The importance of a suitable bond is shown even more graphically in Figure 12.17(a) when the electrical waveform applied the transmitter was essentially a single half cycle of a 5 MHz wave as in Figure 12.17(b).

In all the above results the transmitter was bonded with

---

* The acoustic waveforms resulting from this and the waveform shown in Figure 12.17(b) are considered in Appendix 3.1.

gallium.*

Typically for the 'C.W.' measurements the electrical drive to the transmitter resembled Figure 12.18(a). The superimposed low frequency ringing is caused by the restricted bandwidth of the power amplifier tuned circuits which had a 'Q' factor of approximately 10 and is essentially the same in form as would be expected from a low pass filter of 500 kHz bandwidth subjected to a rectangular pulse.[5] The ceramic transducers are extremely difficult loads to force rapidly changing high level signals into because of their very high capacitances. For a 15mm 5 MHz disc this shunt capacitance C_o is approximately 7000 pF and has an impedance of only 5 ohms at 5 MHz. Usual matching networks such as the 'pi coupler'[6] cannot achieve the necessary impedance transformations without high 'Q' tuned circuits in the power valve anode circuits resulting in the response as in the figure.

The received signal from the bottom reflections with this transmitter waveform is shown in Figure 12.18(b). For these long pulses allowing steady state conditions to build up there is no real difference in performance between oil or solid coupling and either may be used for the 'C.W.' measurements.

It was found that with the size of metal block used transmissions could not be spaced closer than 2mS without significant

---

* It was later found that under some conditions the gallium forms an alloy with the aluminium which tends to penetrate the bulk material and seriously affect its properties. This is discussed further in Appendix 1.

overlap of echoes from one pulse on those from the next. For manual recording direct from the oscilloscope it is essential to repeat the trace at least every 20mS to avoid flicker. (In the automated recording mode the paper tape punch limits the repetition period to 18mS). A value of approximately 9mS was used for all the recordings.

12.3.2. Measurements with holes in the block.

Three distinct situations were set up and readings of phase and amplitude taken from the 156 array positions on the centre portion of an extended pulse.

These were;

(i) with a single hole in the block approximately midway between the transmitter and receiver at a depth of 77mm, (Data Set 1);

(ii) with two holes, the second being parallel to the first and at the same depth, (Data Set 2);

(iii) with two holes and an additional transmitter excited in parallel with the first one, (Data Set 3).

The geometrical arrangements are shown in Figure 12.19. Note that the holes are parallel to the flat faces of the block and of 3mm diameter. To a large extent the geometry was arbitrarily determined by initial attempts to secure adhesion to the block by the gallium. Once the transducers were actually fixed it was

considered more profitable to leave them in place and proceed with an attempt at field reconstruction rather than rearrange the locations so that, in particular, the region under the receiver was more directly illuminated by the transmitter.*

In the actual measurements it was noted that the signals on adjacent elements differed in phase by up to 180° although changes of the order of 60° were much more typical. This illustrates the high degree of decoupling between adjacent elements attainable, the extreme case representing areas 1mm apart moving in opposite directions.

12.3.2.1. Single hole, single transmitter. Data Set 1.

Four deliberate (and one inadvertent) plots were made with this data. These are shown as Figures 12.20-23. (The inadvertent plot was made over an area widely removed from the correct position of the object and had no values greater than 1/100th. those prevailing in the object region).

---

* A 15mm transducer operating at the 5 MHz wavelength of 1.28mm has a main lobe width of 12° which places the hole at 20mm spacing from the transmitter approximately in the centre of the second sidelobe and the illumination relative to a point directly under the transmitter only 0.06, while that at the second hole is down by a further factor of 5. However, these figures are misleading; for a depth of 77mm, the 'far field' conditions for which the patterns are calculated hold over only a small area directly under the transducer (11.2). Actual measurements (Figure 11.2) indicate a relative strength at the first hole of about 0.07 - in fortuitous agreement.

(i) Figure 12.20.

This was made at the depth corresponding to that of the hole.

(a) The reflection from the hole is highly specular. Only that short portion which is favourably orientated relative to the transmitter and receiver has resulted in a measurable field.

(b) The diameter of the 'bright spot' (i.e., the most densely printed area) at $2/\pi$ relative to the maximum is about 9mm. A 14mm aperture at λ = 1.28mm gives an angular resolution of 0.11 radians for paraxial objects. At 80mm distance (to allow for the slant range) this corresponds to 8.8mm.*

(c) The portion imaged corresponds to that section of the hole facing the receiver and is not exactly located on the true position.

(d) There is a noticeable elongation of the focal area along the line joining the centre of the image to the position of the aperture due to the reduced aperture area 'seen' by the object in this direction.

(ii) Figure 12.21.

This is a plot at 85mm depth. This plot is very similar to Figure 12.20 but careful examination will reveal that the centre of the image has moved about 1mm further down and

---

* Note that a conventional pulse echo test system with a transducer of the same radius cannot have better resolution than the transducer diameter at any depth.

about the same to the left.

(iii) Figure 12.22.

This plot at 70mm depth is again similar to Figure 12.20 with the centre shifted 2mm to the right and 2mm upwards.

(iv) Figure 12.23.

This plot at 40mm depth shows:

(a) A break up of the central spot correlating with that observed in the water tank experiments. (Figure 12.8).

(b) A shift in the most intense area by 4mm upwards and 5mm to the right.

Figure 12.24 shows a vertical cross-section containing a line drawn from the array centre to the centre of the image at 77mm. Comparison with the displacements found in the plots will indicate fair agreement with those in the diagram considering the degree of uncertainty as to the precise location of the maxima caused by the coarse level quantization in the printout.

No definite sidelobes can be observed in the plots. This is a combination of errors in the measurements tending to break up any regular structure and the fact that for a circular array the maximum sidelobe level does not exceed 13% even for perfect phasing and this is below the maximum of the first level in the 7 level plot.

12.3.2.2. Two holes with a single transmitter. Data Set 2.

Only two plots were made from the data in this case.

(i) Figure 12.25 whows a plot in the plane of the holes. The centre of the plot has been shifted to a position directly below the receiving transducer. The spot on the lower left is that corresponding to the original hole. The centrelines of the holes are shown dotted. Note that the plotting symbols have been changed from those previously to give 8 levels.

(a) The reconstruction for the original hole is essentially the same as that obtained from the previous data set, allowing for the change in level representation.

(b) The maximum level in the plot of the second hole is approximately two-thirds that in the first one. This correlates with the reduced level of illumination expected. However the distance of 85mm between the transmitter and object is insufficient to allow accurate 'far field' assumptions about transmitter field patterns, particularly considering the wide angle and thus the figure of 1/5th. estimated previously must be treated with caution.

(c) The apparent position of the second hole is slightly to the left of the true centre line. This is to be expected from the relative positions of the illuminating source and the receiver.

(d) The most significant feature is the correct relative and absolute positioning of the two holes and their clear separation.

(ii) In order to check for spurious images in the region well removed from the actual holes a second plot was done with the scale expanded 3 times. This resulted simply in a smaller version of the previous plot surrounded by a region of negligible returns and is not shown.

12.3.2.3. Two transmitters and two holes. Data Set 3.

This situation was set up in an attempt to secure a more uniform illumination of the holes and so obtain an image having closer resemblance to the original shapes. Unfortunately an injudicious placement of transmitter two resulted in nearly complete cancellation of the reflections from the second hole. Consequently, while hole one has appeared much as before, the region of hole two and the space between it and the first hole has become confused. (Figure 12.26). However one might note that there is little chance of the situation not being recognised as distinctly different from that obtaining with one hole only.

One further plot made with this data at a depth of 30mm revealed a spatially compressed version of the same plot moved in towards the normal to the receiver face.

12.3.3. Summary.

These readings and field reconstructions made in the above experiments revealed;

(i) The receiving array is capable of satisfactorily

reproducing the elastic wave field incident on it to an accuracy that permits resolution at the theoretical limit imposed by the system parameters.

(ii) The image seen is determined to a large extent by the illuminating energy incident on the objects and the reflecting properties of these objects and may (commonly) have little resemblance to even a very low definition optical view of the same scene.

(iii) A considerable 'depth of focus' effect is apparent and similarly to the water tank experiments if the depth of the object is not known beforehand then only its angular position may be determined to any degree of accuracy. In connection with this, note that the field determined for the slices well removed from the actual target area is the 'trace' of the targets as seen through a restricted aperture, not the actual signals (if any) coming from these areas, as these were not included in the piece of return signal from which measurements were taken.

(iv) Imaging is possible out to an angle of at least 20^{o} from the array centre line.

The extremely tedious measurement procedure inhibited any further readings being taken by this method and all further results were obtained via the automatic recording apparatus.

12.4. WIDEBAND ILLUMINATION AND AUTOMATIC RECORDING.

12.4.1. Experimental arrangement.

A block diagram is shown in Figure 12.27. The pulse transmitter and transducer amplifiers are described in Appendix 2. For all these measurements the receiving transducer element being interrogated was fed into a 50Ω load. The electrical waveform driving the transmitting transducer was as shown earlier in Figure 12.17(b) for a 15mm diameter transducer and as in Figure 12.28 when driving a 5mm diameter one. With 3mm diameter holes in the block the voltage at the receiving elements from the backscattering was of the order of 1.5mV, P-P and a total gain of approximately 2000 was necessary to bring the signals up to a level sufficient to fill the dynamic range of the analogue to digital converter.

Recordings were made of the signals over a period of 10.625 μS commencing 20 μS after the instant of transmission. Figure 12.29(a) shows a typical received waveform and Figure 12.29(b) the waveform from an immediately adjacent element. It will be noted that the first trace shows evidence of only one reflector (at 4μS) whereas in the second there is a distinct second return approximately 1 μS later from the second hole. This is shown more distinctly in Figure 12.29(c) taken from a further element. In some cases overlap of the returns occurs; this is illustrated in Figure 12.29(d).

Examination of the areas of the traces not containing echoes

from the artificially introduced objects reveals considerable changes in detail, justifying the assumption made in Chapter 7 that these multiple small echoes are random from element to element. All the signals in Figure 12.29 were generated by the 15mm transmitter, the physical arrangements being exactly as for the C.W. experiments.

Figure 12.30 shows the computed (from the quantized samples) spectrum of the signal in Figure 12.29(b). The high D.C. value is due to imperfect balance in the analogue to digital converter and the tendency to rise around the highest frequency is caused by a combination of finite sample length and aliasing due to the increased bandwidth of the quantized samples presented for analysis. To gain some appreciation of the resolution attainable over considerable path lengths a series of traces were recorded of the echo from the bottom of the block as received at 5 elements spaced at the extremities and centre of the receiver. The total acoustic path for these signals was 630mm. Figures 12.31(a)-(e) show the traces and Figure 12.31(f) the plan view of the element positions. In all five traces it will be noted that the wave-forms and amplitudes are virtually identical. Taking the main positive peak as the reference a total shift in time of arrival of 130nS occurs between elements (a) and (c). Some trigonometrical analysis of the signal path shows that the difference from a to c is 0.86mm which at the measured velocity in the block (6.42mm/μS) gives a time difference of 136nS. Thus even for this considerable

depth the small differences in path length are easily and accurately reproduced by the receiver.

12.4.2. Measurements and results.

Four sets of measurements have been made with the wideband illumination.

(i) Data Set 5; this was obtained using the 15mm transmitter as in 12.3. A large number of plots has been made from this data -

(a) At frequencies from 1 to 10 MHz in the plane of the holes.

(b) At 5 MHz in planes above the holes.

(c) A series of comparative plots made at 5 MHz in the plane of the holes with various proportions of the total element readings deleted at random. This models, in an extreme case, the random thinning action possible in the scanning apparatus. (This could not be applied directly because the array used is too small to allow consistent scanning behaviour).

(d) A second series of plots in which the stated positions of the array elements were perturbed by independently generated normally distributed random numbers in their x and y coordinates. This is, as such, an unlikely error on a solid transducer system with mechanical scanning but serves to introduce random errors into the phasing of the computed components from each element at the image plane

and provides a practical indication of the error tolerance of the system.

(ii) Data Set 6; for these readings hole one was enlarged to 9mm diameter and threaded (5/16" whitworth tap). Results obtained with the 15mm transmitter were somewhat confusing and only one plot was made from this data.

(iii) Data Set 7; conditions for these readings were identical to (ii) except that the 5mm, transmitter 2, was used as the illuminating source.

(iv) Data Set 8; similar to Set 8 except that the 3mm diameter hole was also threaded (1/8" whitworth thread) to give more diffuse scattering.

12.4.3. Image plots. Data Set 5.

12.4.3.1. Data Set 5; plots at various frequencies.

Figures 12.32-38 show the plots obtained from the data at the depth of 77mm. The centre of the plots has again been shifted from the previous situation. Figure 12.36 has the receiver and transmitter positions marked.

(i) Figure 12.34. This appears as basically similar to the earlier plot (Figure 12.25). The resolution indicated by the spot diameters again agrees with the theoretical value. One additional feature has appeared, a maxima of one half the on target spots directly under the transmitting transducer.

With the 10.6 μS sample length taken any scattering from this region is included on the received signal. (See Figure 12.38). Since the transmitter field strength is approximately 20 times greater immediately below the transmitter position than it is in the nearest object region this peak is considered due to scattering in the aluminium at grain boundaries and similar small discontinuities.* The two holes have imaged at the same brightness despite the difference in illumination which prevails at the sites and which is apparent in the received signals (Figure 12.29). This normalisation effect is caused by the coarse steps in the analogue to digital conversion. Any signals from the weaker set which exceed about one half those from the stronger scatterer will have their maximum levels recorded at the same value. This can be readily seen by an inspection of the quantized data in comparison with the original analogue version. This effect is inherent in any quantizing scheme but has been exaggerated by the very few levels employed.

(ii) Figure 12.32. This plot is quite meaningless in terms of the actual objects present, a result which should not be entirely unexpected from the fact that the receiver is only 2 wavelengths in diameter at this frequency of 1 MHz.

---

* Taking the difference in signal levels at the two locations to be 20/1 and the difference in backscattering as 2/1, the relative power levels of the grain scattering and the hole scattering are 1/1600 .

(iii) Figure 12.33, 2 MHz. This plot is just beginning to show some resemblance to the correct situation. The elongation of the focal spot mentioned earlier is very apparent but measurement of the '$2/\pi$' width of the most intense area gives a value of 18mm, in fair agreement with the theoretical value of 22mm.

(iv) Figure 12.34, 3 MHz. This plot shows distinct separation of the two objects. Hole one has imaged much more intensely than hole two because of more favourable illumination at this frequency. The return from the below transmitter region has disappeared from a similar cause; all the plots are normalised at the strongest point and any image components below about one-eighth of this level disappear. The focal spot resolution is now 15mm in near exact agreement with prediction.

(v) Figure 12.35, 4 MHz. This plot shows almost exactly the opposite behaviour from the immediately previous one. Hole two has appeared brightest and the scattering from under the transmitter reappeared. Once again the $2/\pi$ diameter of the spots agrees exactly with the theoretical value.

(vi) Figure 12.37, 7 MHz. This plot still has distinct peaks in the correct areas but is beginning to exhibit a higher level of background than was apparent at the lower frequencies. The focal spots have reduced to 6.5mm diameter still maintaining excellent agreement.

(vii) Figure 12.38, 10 MHz. At this frequency the echoes

from the holes are lost in the background. It should be noted however that the maximum level in this plot is only 0.08 the maximum in the 5 MHz plot and if they were presented on the same scale not even the tips of the three highest spots observed would appear above the first level.

In the seven plots the maximum levels relative to the peak in the 5 MHz plot are:

Frequency	Relative Level
1 MHz	1.75
2 MHz	0.56
3 MHz	0.85
4 MHz	1.12
5 MHz	1.0
7 MHz	0.17
10 MHz	0.08

Table 12.1

12.4.3.2. Data Set 5; plots at 5 MHz in planes above holes.

Two plots were made, one at 12mm above the holes (65mm depth) and another at 47mm above (30mm depth). The first of these is almost identical to Figure 12.36 except for the usual compression and movement of the spots in towards the receiving array normal. Figure 12.40 shows the second plot. Comparison of the positions of the images of the two holes and the transmitter direct scatter with the distances on the scale diagram Figure 12.39 shows agreement to within 0.5mm. Note that this plot is above the region from which actual signals were recorded and similarly to Figure 12.23 the image is a trace of the targets, not actual returns from the region at 30mm depth.

12.4.3.3. Data Set 5; random deletion of elements.

A total of six plots was made from Data Set 5 under identical conditions except that in turn approximately 10, 20, 30, 50, 70 and finally 90% of the signals from the elements were omitted at random. The plots shown should be compared with Figure 12.36 which is the same case with all the elements included.

Figures 12.41-44 show the plots for the 20, 50, 70 and 90% deletions respectively and Table 12.2 lists the actual numbers of elements deleted (from 148) and the relative strengths of the peak values in each plot.

Table 12.2. Parameters of Plots 12.41-12.44

Plot	Nominal omissions (%)	No. of elements deleted	Actual (%) remaining	Peak value	Normalised
12.41	20	29	80.4	6.3	0.81
12.42	50	76	49.6	3.79	0.49
12.43	70	99	33.1	2.76	0.35
12.44	90	132	10.8	1.08	0.14

Normalisation relative to plot 12.36.

(i) Figure 12.41, 20% deletion.

This plot is nearly identical with the prototype except for the small increase in background levels appearing as an increase in the plot area covered by the second level symbol (.).

(ii) Figure 12.41, 50% deletion.

In this plot the general background has increased significantly but the two main spots are still distinct. Some loss is appearing in the spot for hole two however.

(iii) Figure 12.43, 70% deletion.

This shows in more exaggerated form the effects becoming apparent in the previous plot.

(iv) Figure 12.44, 90% deletion.

By this stage, with only 16 elements active, evidence of hole two has virtually gone and the plot is becoming strongly obscured by rising background levels.

From these plots we may note:

(a) The degredation progresses 'gracefully' as the number of active elements is reduced. There is no sudden cut-off at which the whole pattern dissolves completely.

(b) As would be expected from the progressive increase in random sidelobe level characteristic of the patterns of increasingly thinned arrays the plots exhibit increasing amounts and higher levels of signals surrounding the main peaks.

(c) The positions of the hole images do not shift with thinning, correct relative geometry being maintained down to a level of thinning where the whole pattern is being lost.

(d) The relative levels of the image peak values drop in almost exact proportion to the number of elements remaining. In other terms the 'gain' of the array varies linearly with the number of elements.

(e) Overall these plots provide experimental verification of the random thinning concept at a point well beyond that

required from the actual apparatus where thinning becomes necessary only for arrays exceeding approximately 1500 elements, ten times the size here.

12.4.3.4. Data Set 5; random perturbation of element positions.

As mentioned earlier this provides a means of introducing timing or phasing errors into the signals beyond those already suffered in the transduction and recording processes. Five plots were taken with the positions of the elements perturbed according to a bivariate Gaussian distribution of the parameters as in Table 12.3.

Table 12.3.

Plot	$\sigma_x = \sigma_y$	$\text{mean}_x = \text{mean}_y$
1	0.05λ	0
2	0.25λ	0
3	0.56λ	0
4	0.62λ	0.20λ
5	0.25λ	0.20λ

That is, in 5 the element positions varied randomly and uniformly with angle about a position displaced 0.2 wavelengths in x and the same in y according to a Gaussian distribution with standard deviation 0.25 wavelengths. In this particular case a few elements could be 'displaced' up to 1.3 wavelengths from the correct position and in 4, up to 3 wavelengths. In all cases the full number of elements was taken.

Figures 12.45-47 show the conditions 2, 3 and 5 in Table 12.3. These should be compared with Figure 12.36.

(i) Figure 12.45, $\sigma = 0.255$.

By comparison with Figure 12.36 this shows an increased background level and some suppression of the peaks corresponding to hole one and the transmitter scatter. This may be explained by a consideration of the fields these two objects present across the array compared with the scatter from hole two. If we concentrate on just the component plane waves at the angles of the lines joining the array centre and the holes, then hole one and the transmitter scatter region produce waves having a considerably greater rate of phase change across the aperture than the most direct component from hole two which is nearly directly underneath the aperture. For hole one (at 14.5°) the aperture wavelength is approximately four times the free space value λ and thus a perturbation of 0.25λ corresponds to an error with standard deviation 0.065 wavelengths or 0.41 radians. For a uniformly weighted aperture with zero mean phase error this results in a gain loss (see 7.4.5) of 10%, sufficient to depress the peak of the hole one focus by one level as observed in the plot. For the transmitter scatter the gain loss is 43%, for an error twice that of hole one, and as observed from the plot, the spot peak has gone down from 1 to 2 levels in 4, which range contains the 43% depression.

(ii) Figure 12.46, $\sigma = 0.562$.

This shows a similar effect of gain loss to the previous plot, the peak of hole one now being approximately one half that of hole two. Theoretical gain loss is 44%. The transmitter scatter has now been lost in the rising background. The plot taken with $\sigma = 0.62$ shows a still further loss.

(iii) Figure 12.47, $\sigma = 0.25$, mean = 0.2.

This plot very closely resembles Figure 12.45 down to quite fine detail and indicates, as might be expected, that bodily shift of the receiving array has little effect. The spatial resolution in the plots is too coarse to determine whether any corresponding shift has occurred in the apparent positions of the objects.

These plots then serve to illustrate that the system has some considerable tolerance to errors and that degredation from the no error case proceeds smoothly and predictably.

12.4.4. Image plots, Data Set 6.

For these readings the situation was identical to that with Set 5 except for the enlargement and threading of hole one. Two plots were made, one at 5 MHz and one at 7 MHz. The former is shown as Figure 12.48 with the positions of the holes and transducers marked. By comparison with Figure 12.36, this plot reveals, (a) a high background level, (b) elongation of the plot of hole two along the line of the hole, and (c) maxima in the

vicinity of hole one but a lack of definite resolution, together with at least one high peak distinctly removed from the hole position.

These effects can be largely explained by considering the scattering that must now occur at hole one. The depth of the threading is approximately a $\frac{1}{2}$ wavelength at 5 MHz and this hole will thus exhibit a considerable amount of diffuse scatter some of which falls on hole two, increasing the length which is favourably illuminated to reflect back into the receiver. Since hole two is still a specular reflector it might be expected to have a much stronger signal than hole one. The spurious spots may be accounted for by multiple reflections between the holes caused by the much greater range of scatter angles made possible by having one hole (at least partially) a diffuse reflector.

All these statements are supported by an examination of the signals on the receiver elements. Figure 12.49(a) shows a typical example. Four distinct components of signal are discernable. The first (a) is direct reflection from hole one. This is followed by two smaller returns (B) and (C), the second of which is in nearly anti-phase with the return from hole two (D) as evidenced by the sudden dip at the 5.2 μS point. The signal from hole two is considerably stronger and lasts up to twice as long as those shown in Figure 12.29. A further return at 9 μS shows only indistinctly in this particular trace but is of

considerable strength in some of the returns. See Figure 12.49(b). The 7 MHz plot is too confused to show any useful image.

12.4.5. Image plots, Data Set 7.

For this set of readings illumination was provided by the 5mm diameter transducer (transmitter two of Figure 12.19). Plots were taken at 5 and 7 MHz and are shown as Figures 12.50 and 12.51. Figure 12.52 shows typical element signal; one may note immediately how 'clean' this signal is compared with those caused by transmitter one, and that the specularly reflecting hole is now returning a distinctly stronger signal despite the fact that the transmitter is now almost directly over the larger threaded hole. These observations are reflected in the plots. The strong background apparent in Figure 12.48 has disappeared from Figure 12.50. Hole two has produced a distinct spot indicating strong specular reflection whereas the image of hole one is weak (and disappears at 7 MHz). The imaged portions of hole one consist just of the strongly illuminated section immediately under the transmitter and one further region favourably orientated for a direct reflection, marked as 'A' in Figure 12.50). At 7 MHz A is in a much weaker region of the transmitter field and has not shown at all. It should be noted that the relative amplitudes of the two plots are 5/1 in favour of the 5 MHz image.

12.4.6. Image plots, Data Set 8.

This set of data was derived in a situation identical with

that for Data Set 7 except that a 1/8" whitworth tap was passed through hole two in order to roughen the scattering surface. The effects of this are shown in Figure 12.53. By comparison with the situation in 12.4.5, the weaker return from hole two has enabled the main reflection from hole one to stand out at a level twice that observed previously. Relativity between the 'under transmitter' signal and region A reflection has been maintained. The relative strengths of the maximum points in Figure 12.50 and Figure 12.54 are in proportion to the rise in hole one signal.

12.5. OVERALL COMMENTS.

Overall the results obtained over the period reported here show the general correctness and satisfactory performance of the receiving transducers and signal acquisition and processing concepts.

The plots from Data Sets 5, 6, 7 and 8 show very distinctly the effects of the illuminating signal and specular reflections compared with diffused scatter, on the images obtained. It would seem that these two parameters of the imaging situation are of considerably more importance than the capabilities of the receiving transducer and any image forming operations performed. In all cases the resolution spots that have appeared have corresponded to theoretical values with a high precision and the deliberate perturbations of the received data have caused changes in a given image in full accord with those anticipated from analysis but the

actual form of the image varies dramatically with transmitter-scatterer characteristics.

The conclusion one might draw from these results is that the main problems in ultrasonic imaging lie not in the province of what can be done with the signals after they have been received but (as seems to be traditionally the situation in this whole field) in how the illumination of the objects can be brought to the situation prevailing in normal daylight vision where objects are subject to spatially diffuse illumination. (The situation of very strong specular reflections swamping the signals from diffuse scatter is of course not unknown in vision as for example driving on a sunny day against the glare of windscreen reflections illustrates, but is the exception rather than the most common case).

In a further project a continuance of the work reported here has tackled this problem by the provision of multiple transmitters judiciously spaced around the receiver and results so far obtained reveal considerable improvements with extended sections of the holes showing up as rows of spots lying along the hole positions. Some attempt was made to investigate the possibilities of diffusing the illumination by means of a scattering layer between the transmitter and the material but without much success (11.5).

REFERENCES FOR CHAPTER 12.

1. Wood, A.B. 'Model experiments on sound propagation in shallow seas'.
Journ.Acoust.Soc.Am. 31, pp.1213-35, Sept. 1959.

2. Heuter, T.F. and Bolt, R.H. 'Sonics'.
Wiley, New York, p.151, 1955.

3. Kreuzer, J.L. 'Ultrasonic holography for non-destructive testing'.
Mater. Eval. 26, pp.197-202, Oct. 1968.

4. Cook, G.B. (see Reference 19, Chapter 7).
Appendix 1.

5. Everitt, W.E. and Anner, G.E. 'Communication Engineering'.
McGraw-Hill, New York, 1956, 3rd Edition, p.577.

6. Orr, W.J. (Ed.) 'The Radio Handbook'.
Editors and Engineers, Summerland, California,
6th Edition, 1962, p.449.

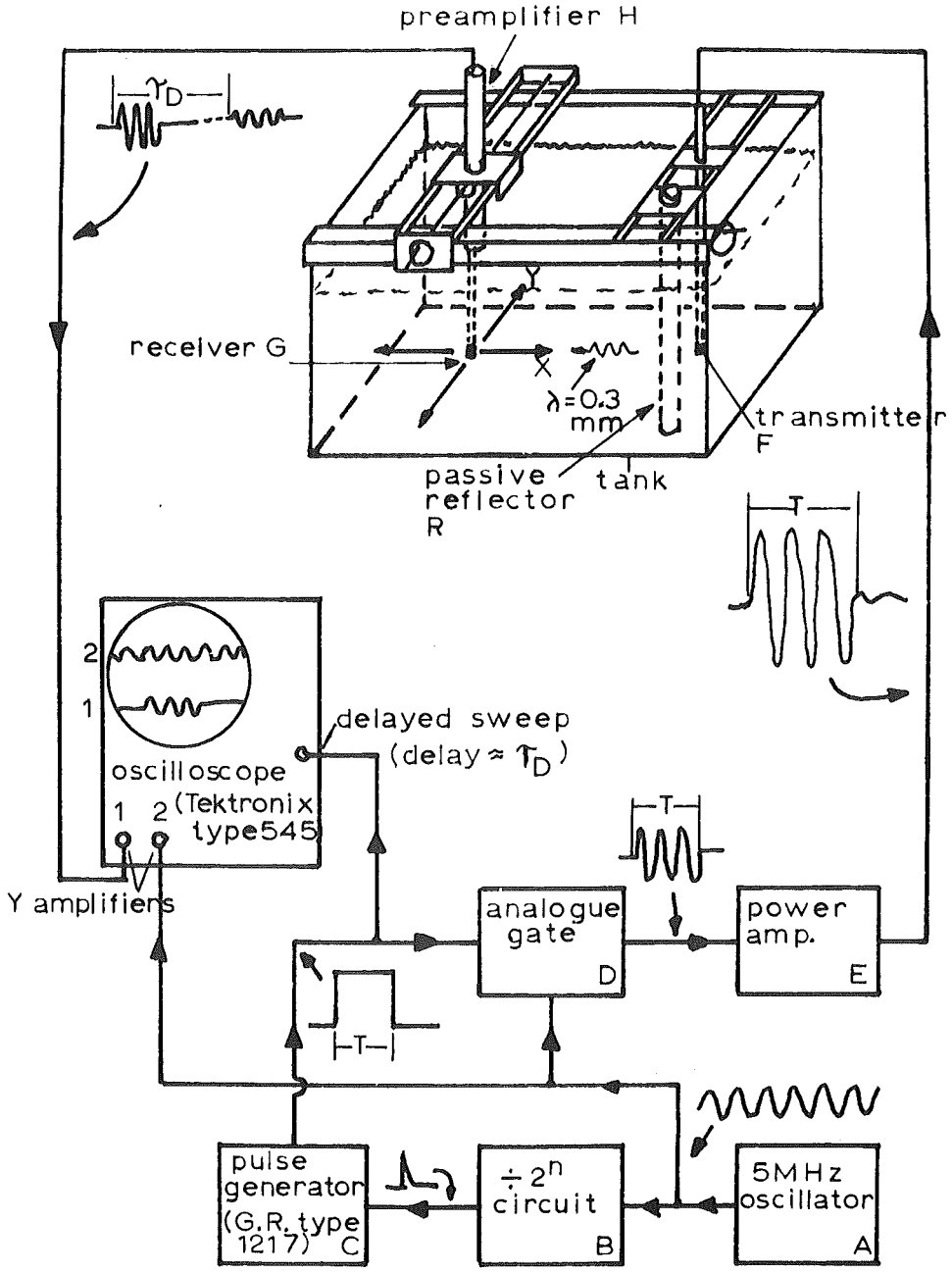

FIG.12.1: Experimental arrangement for measurements in water tank.

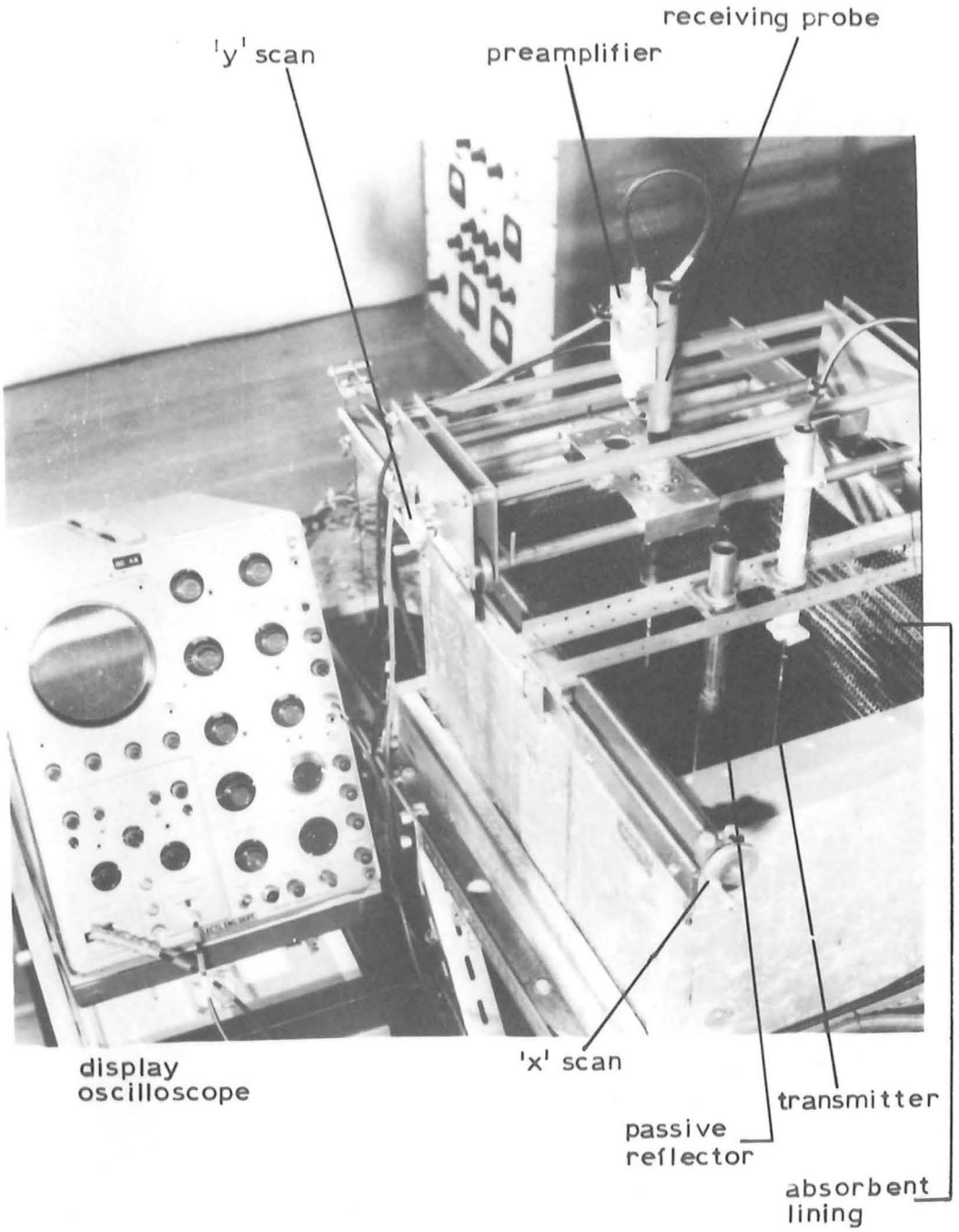

FIG.12.2: Water tank apparatus

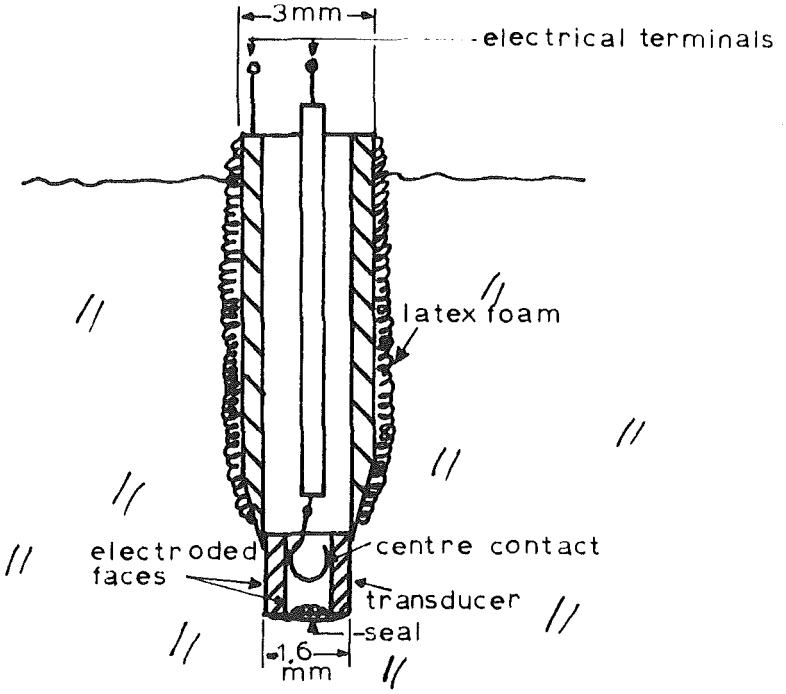

FIG. 12.3: Cross-section through transducer mounting.

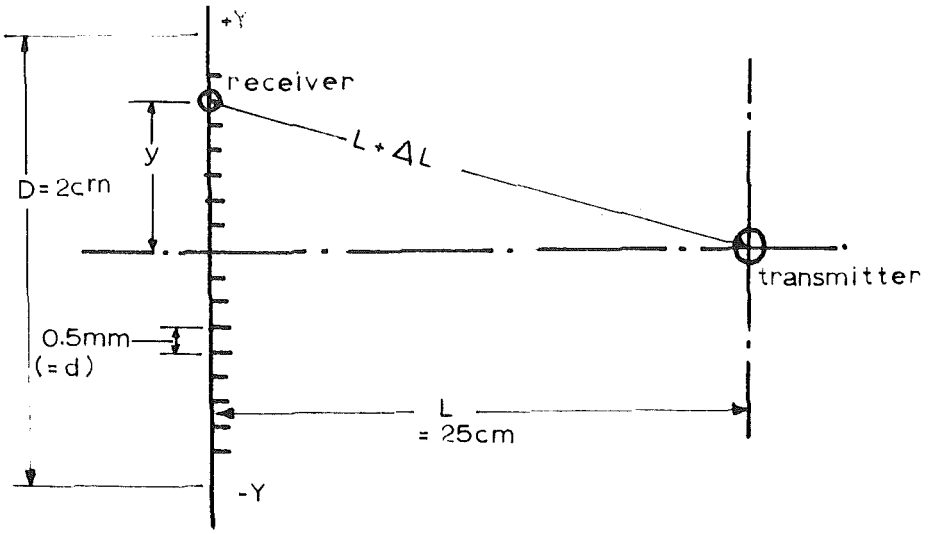

FIG. 12.5: Plan view of arrangement for transmitter field measurements.

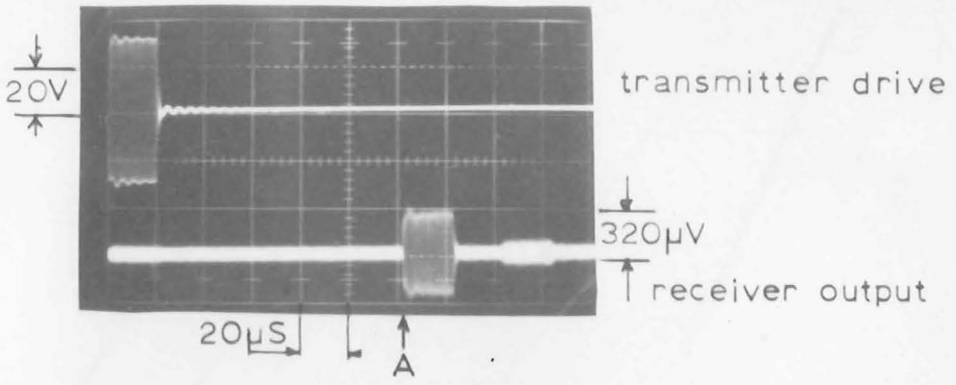

FIG.12.4(a): Signal waveforms in water tank experiments

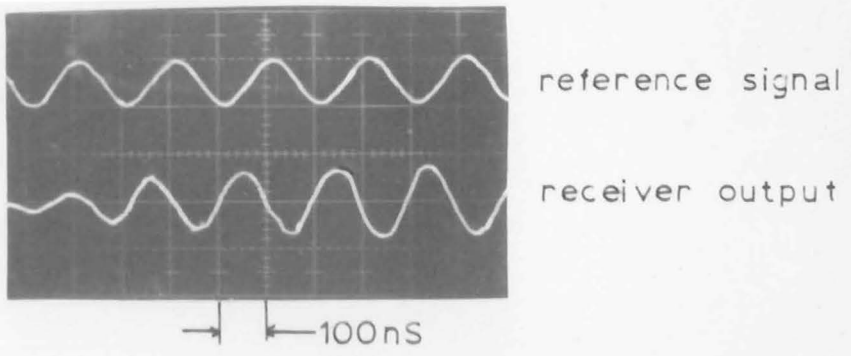

FIG.12.4(b): Expansion near point A in previous figure, with reference wave,

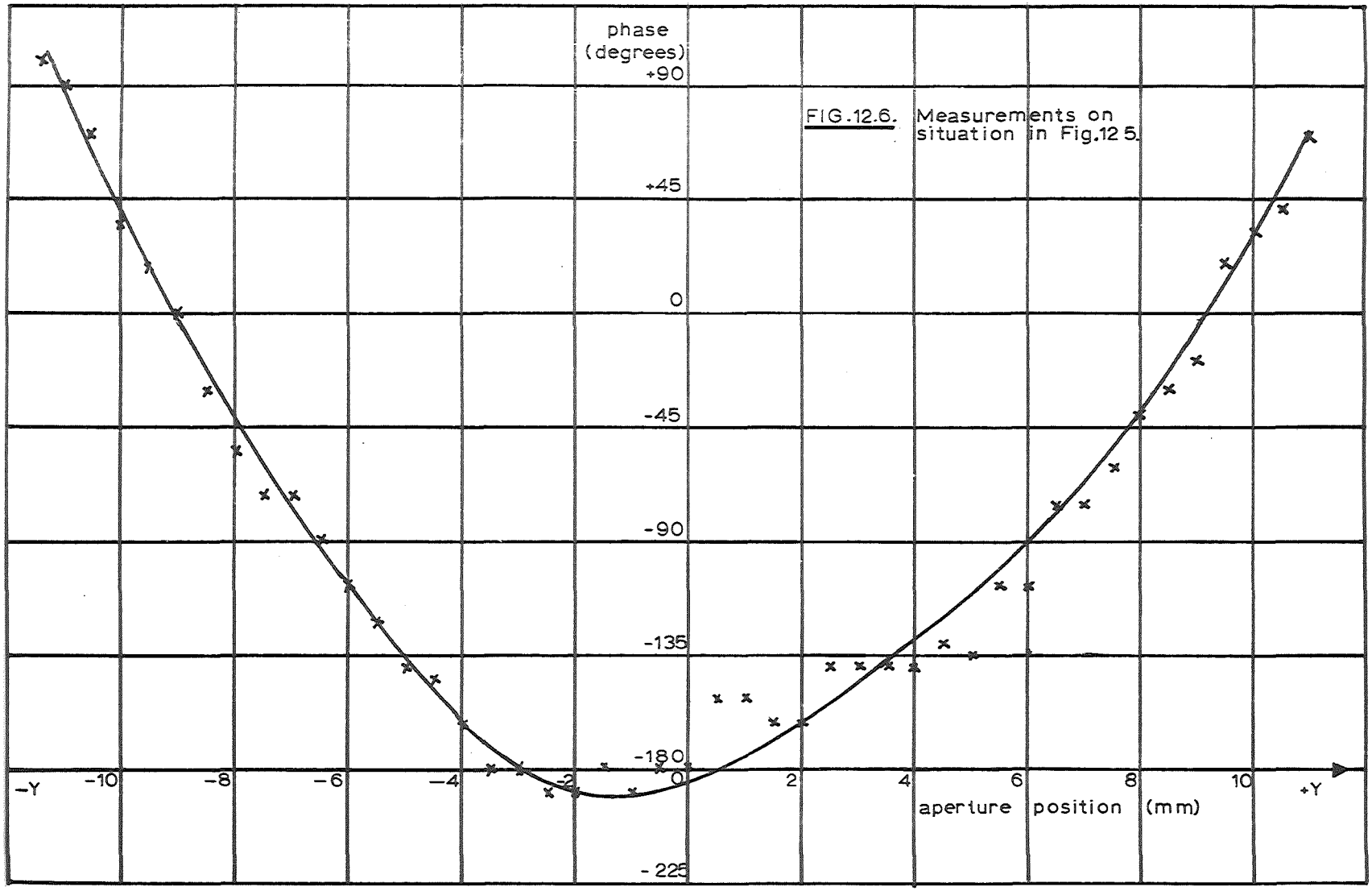

FIG.12.6. Measurements on situation in Fig.12 5.

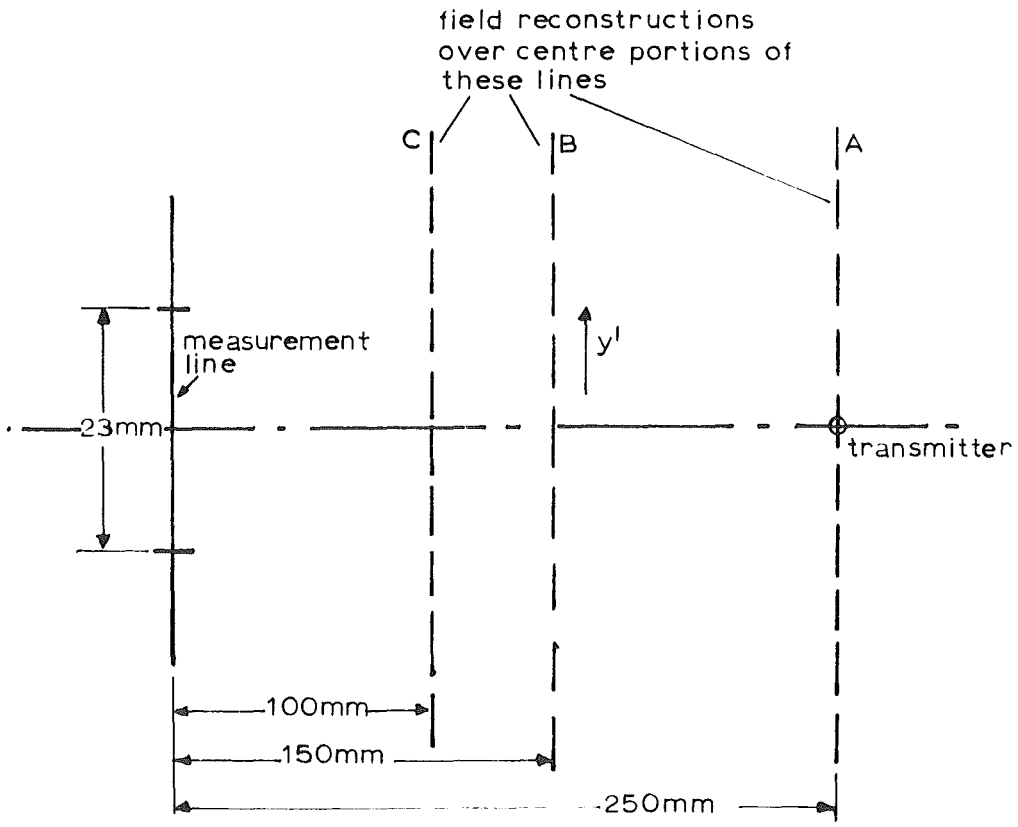

FIG. 12.7: Plan view showing positions of field reconstructions.

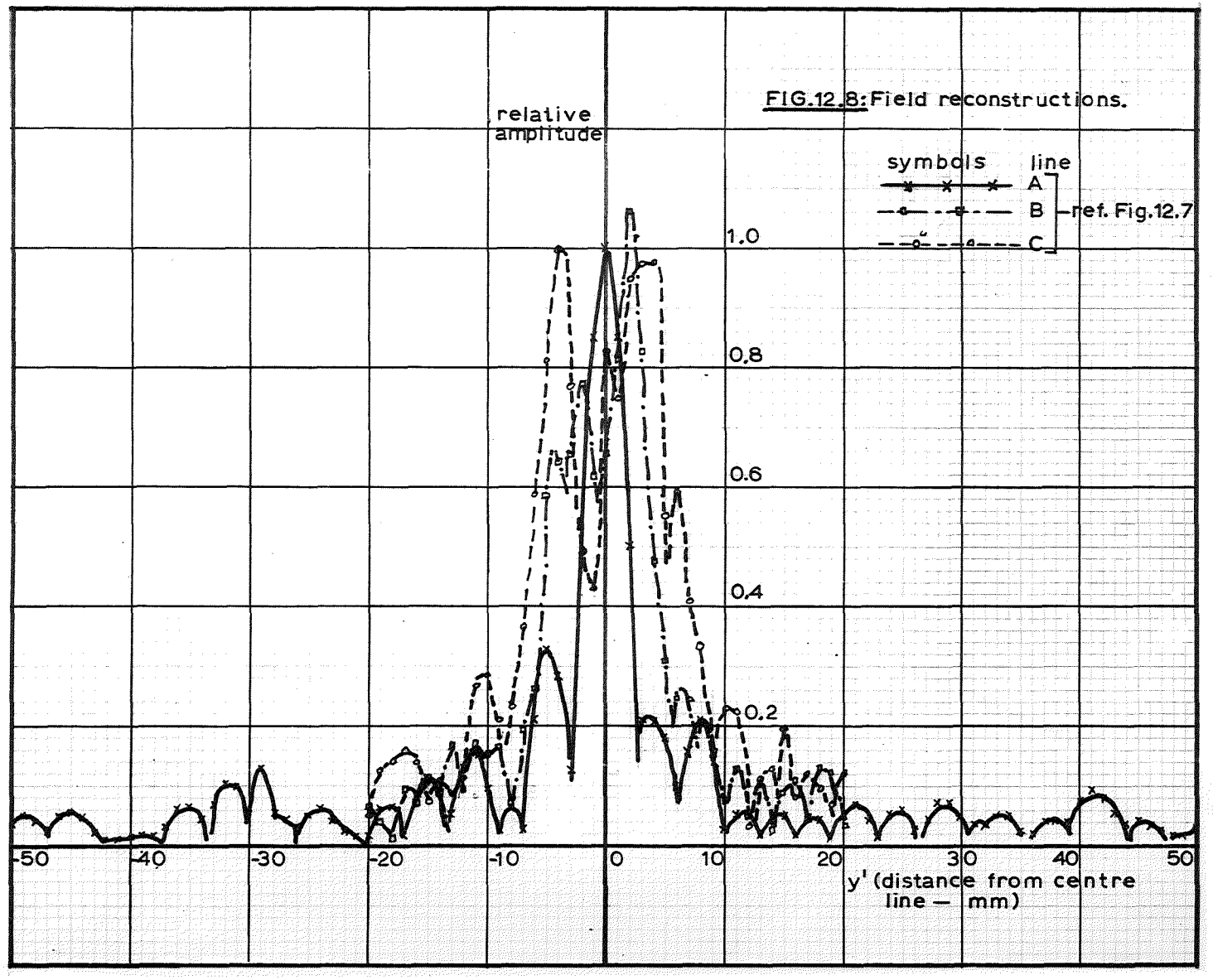

FIG.12.8: Field reconstructions.

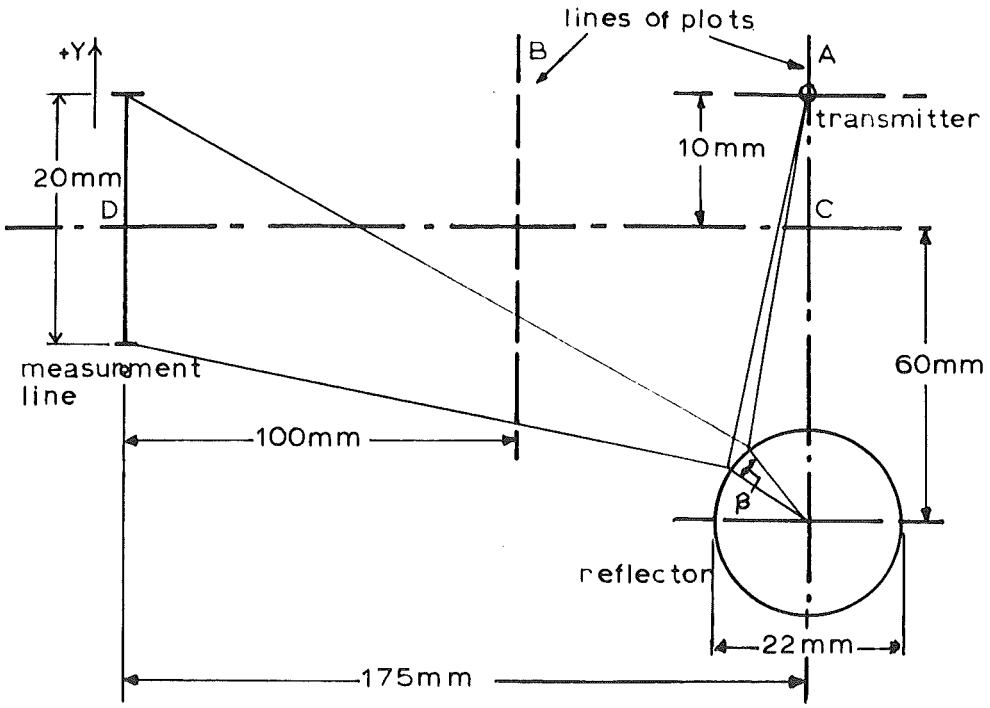

FIG.12.9: Experimental arrangement with passive reflector

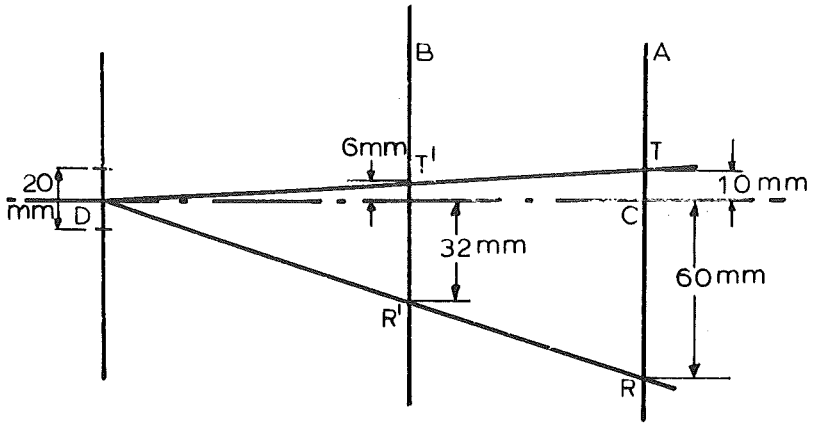

FIG.12.13: Shift in apparent object positions.

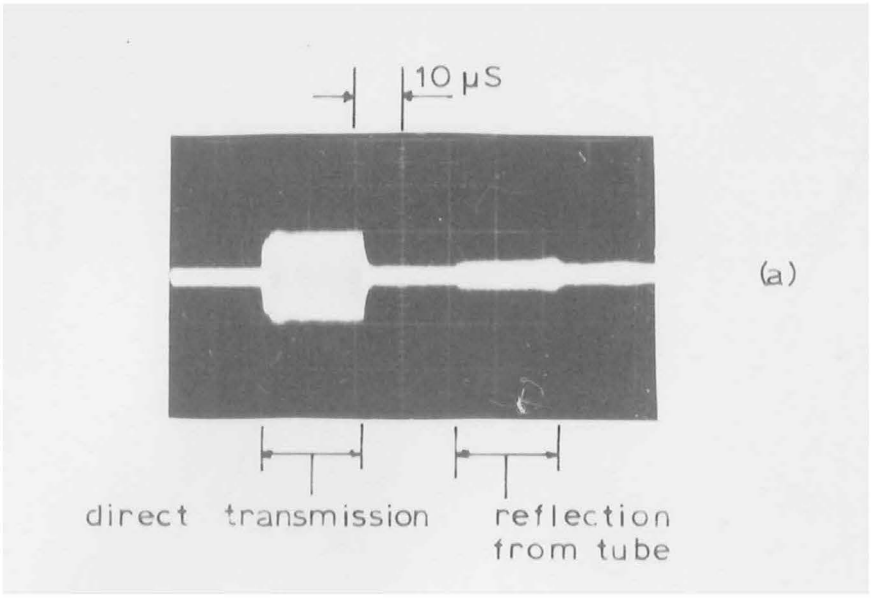

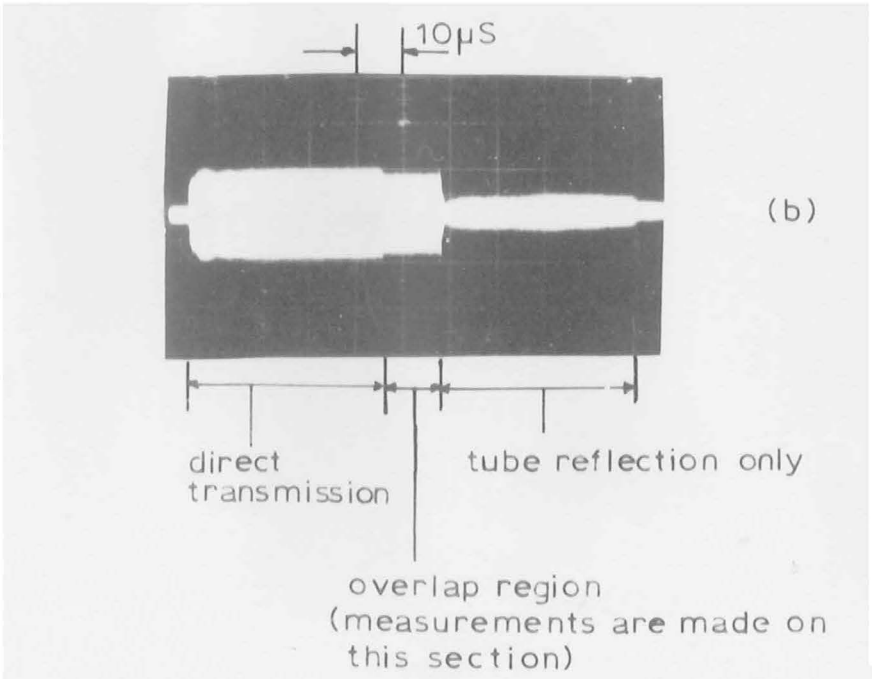

FIG. 12.10: 20 and 40µS transmissions showing (a) separation, and (b) overlap, of the received components.

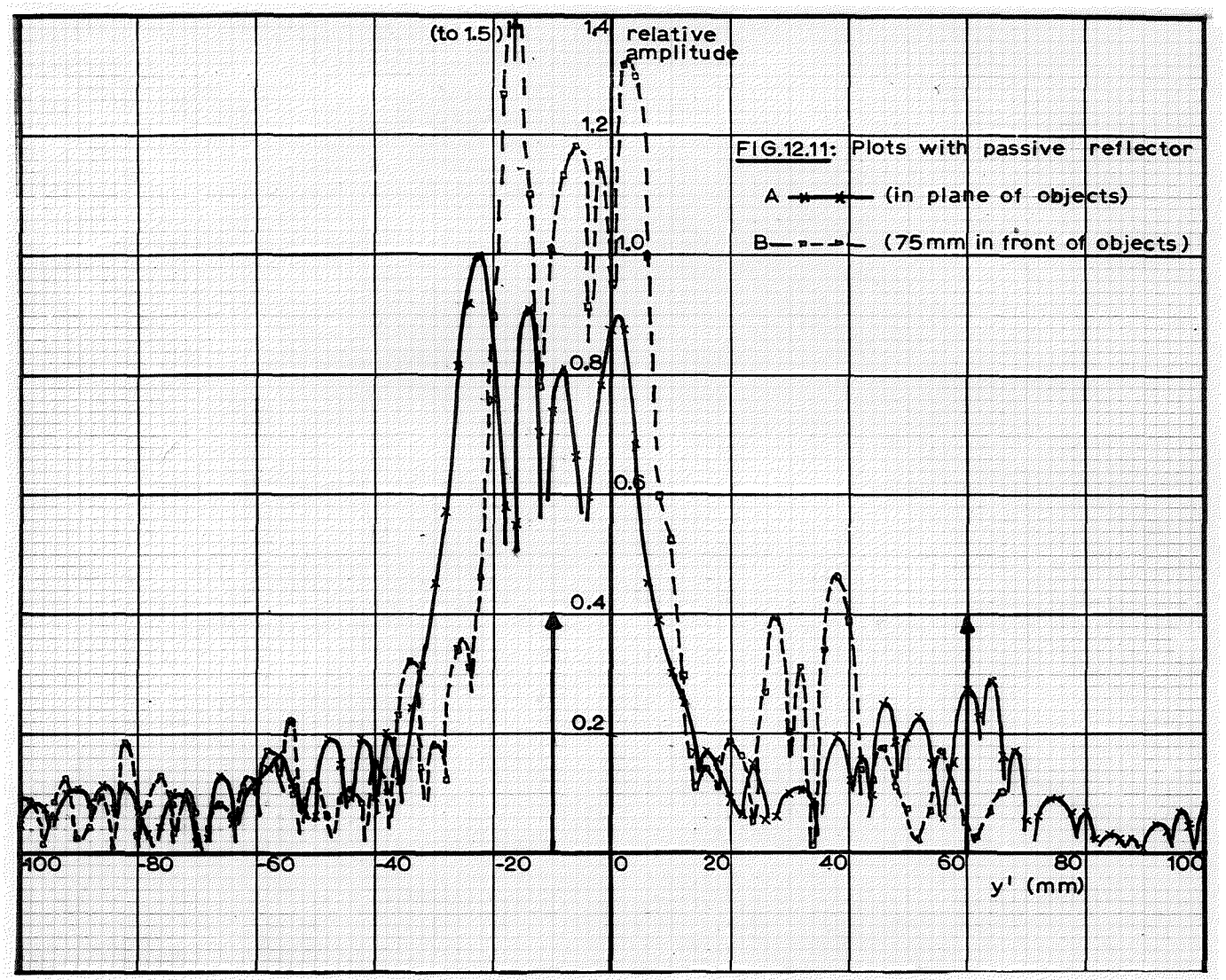
(to 1.5)
1.4
relative amplitude
1.2
1.0
0.8
0.6
0.4
0.2
-100
-80
-60
-40
-20
0
20
40
60
80
100
y' (mm)
FIG.12.11: Plots with passive reflector
A (in plane of objects)
B (75mm in front of objects)

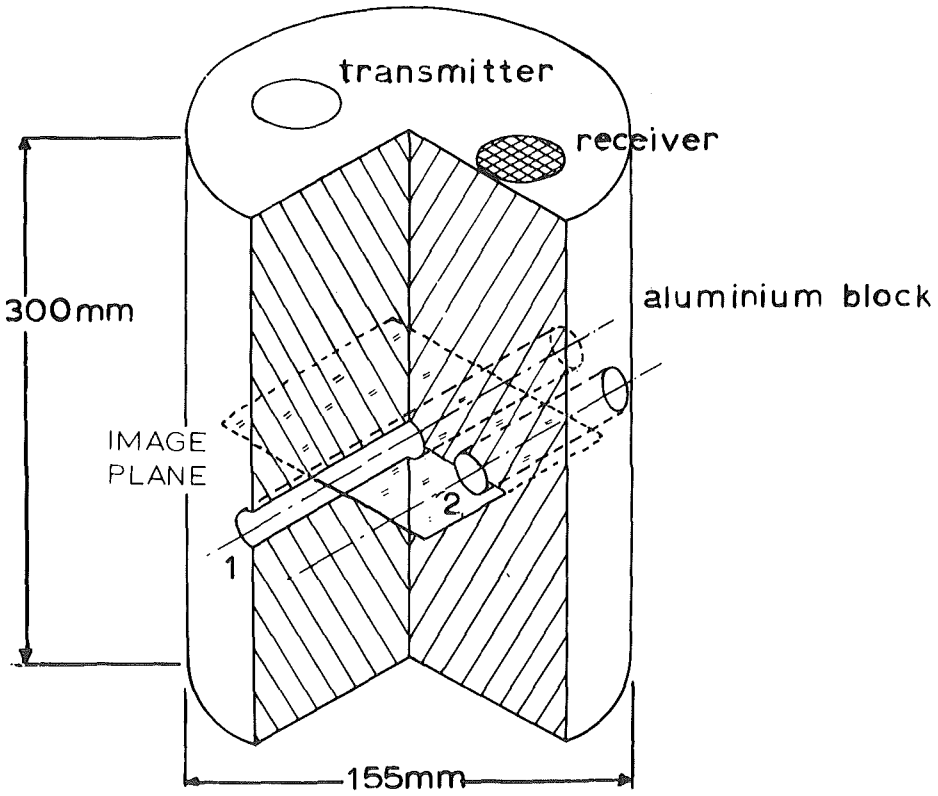

FIG. 12.14: Cutaway view of physical arrangement.

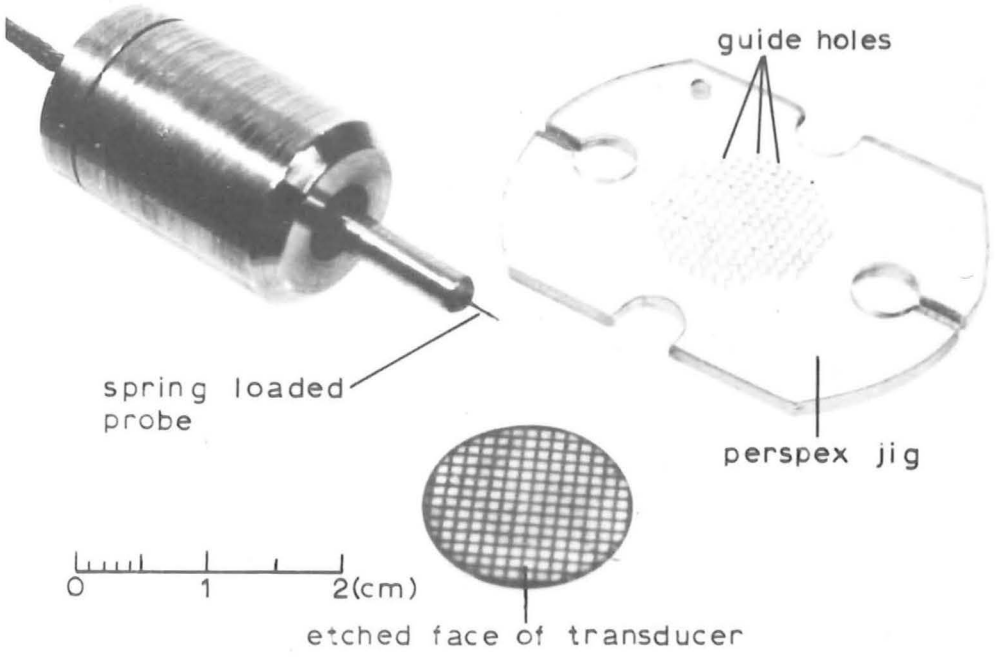

FIG.12.15: Receiving transducer with probe and guide.

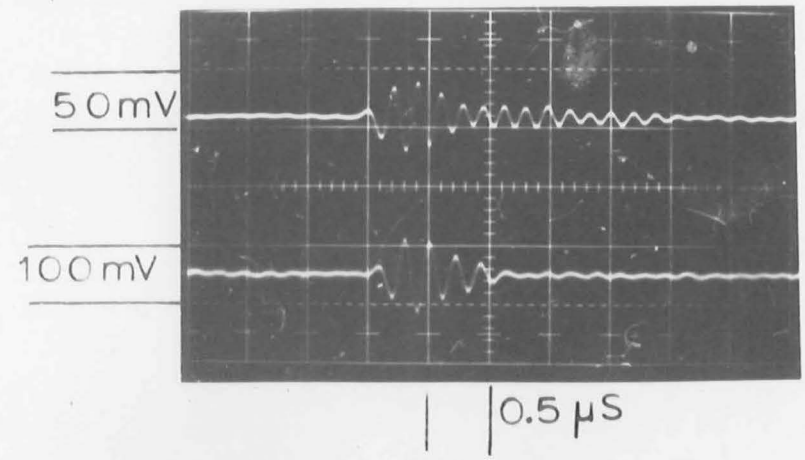

FIG. 12.16(a): Received signals on 5mm diameter transducers

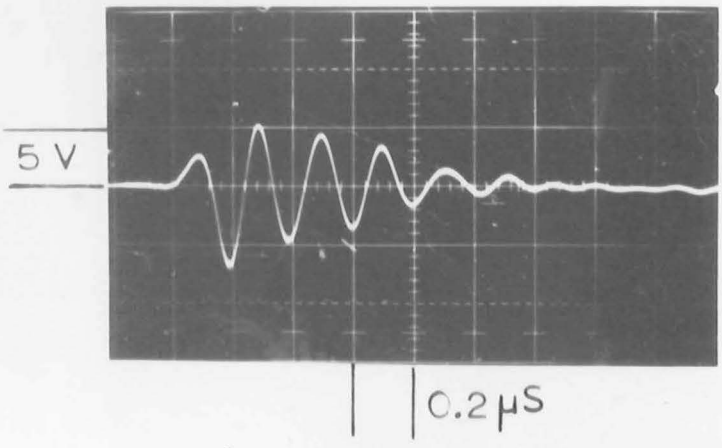

FIG. 12.16(b): Electrical signal on transmitter

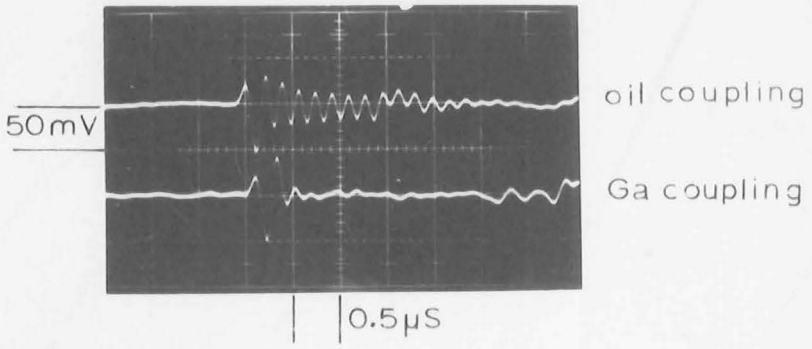

FIG: 12.17(a): Received signals on 5mm. diameter transducers.

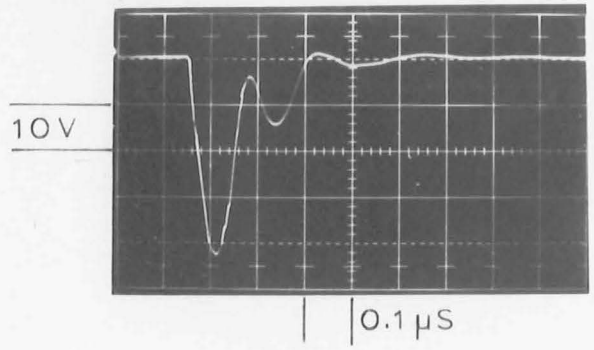

FIG. 12.17 (b): Electrical signal on transmitter.

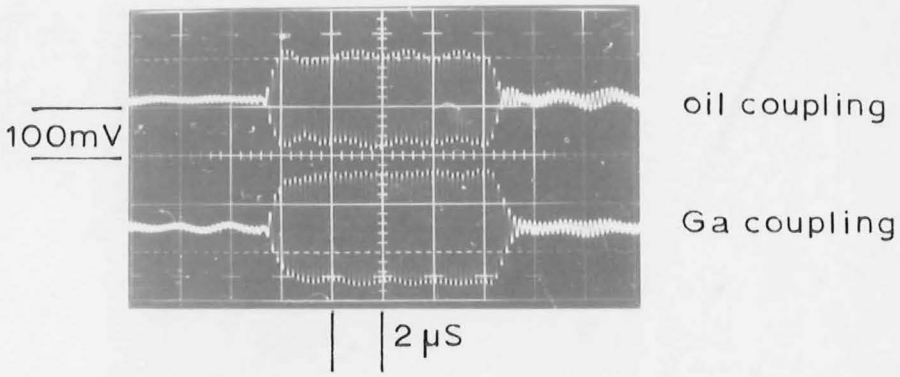

FIG.12.18(a): Received signals on 5mm diameter transducers.

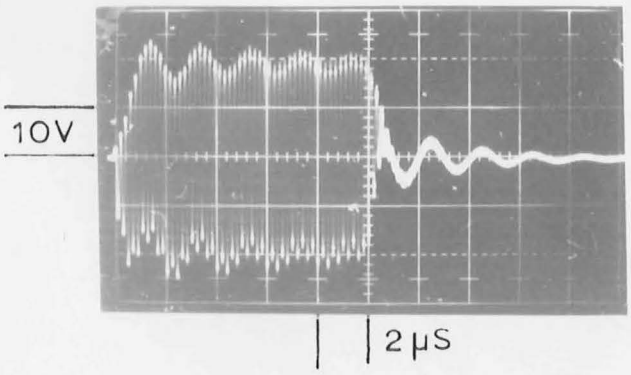

FIG.12.18(b): Electrical signal on transmitter.

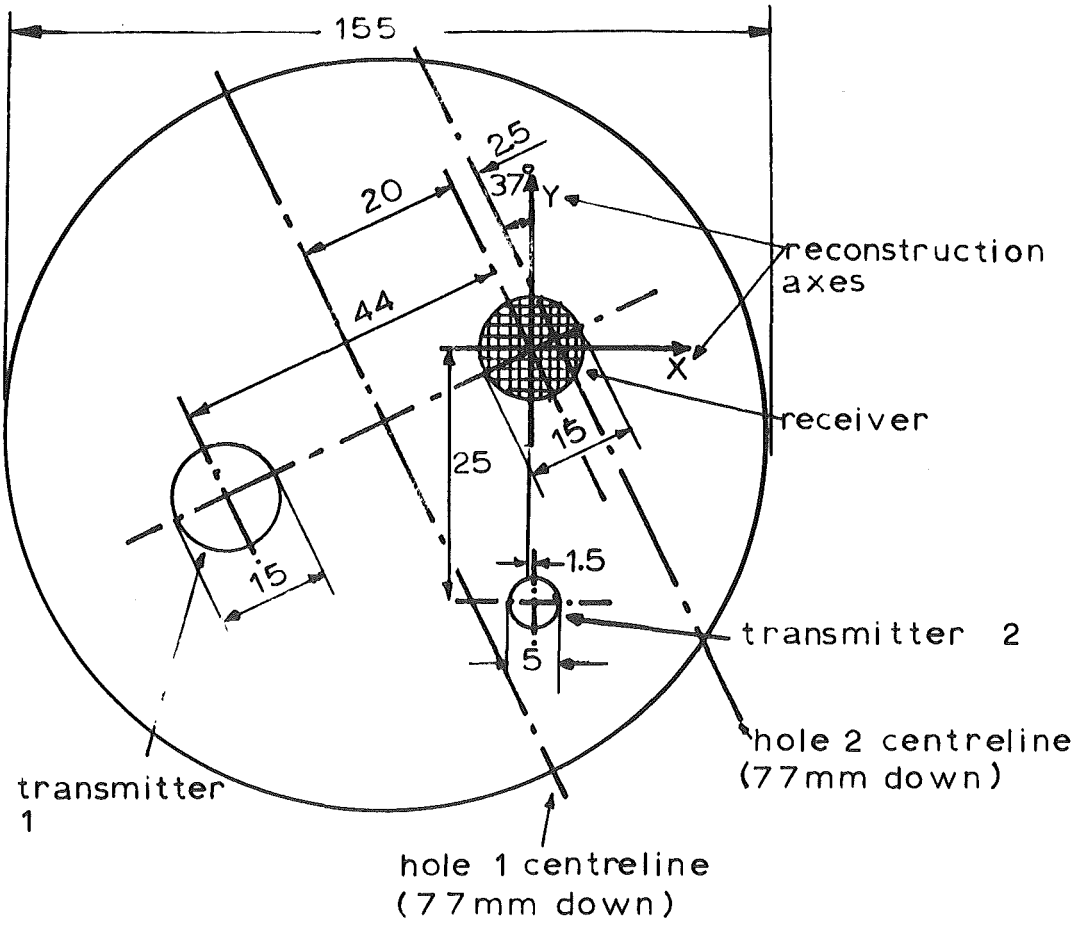

FIG. 12.19: Plan view of arrangementon aluminium block.
(Dimensions in mm)

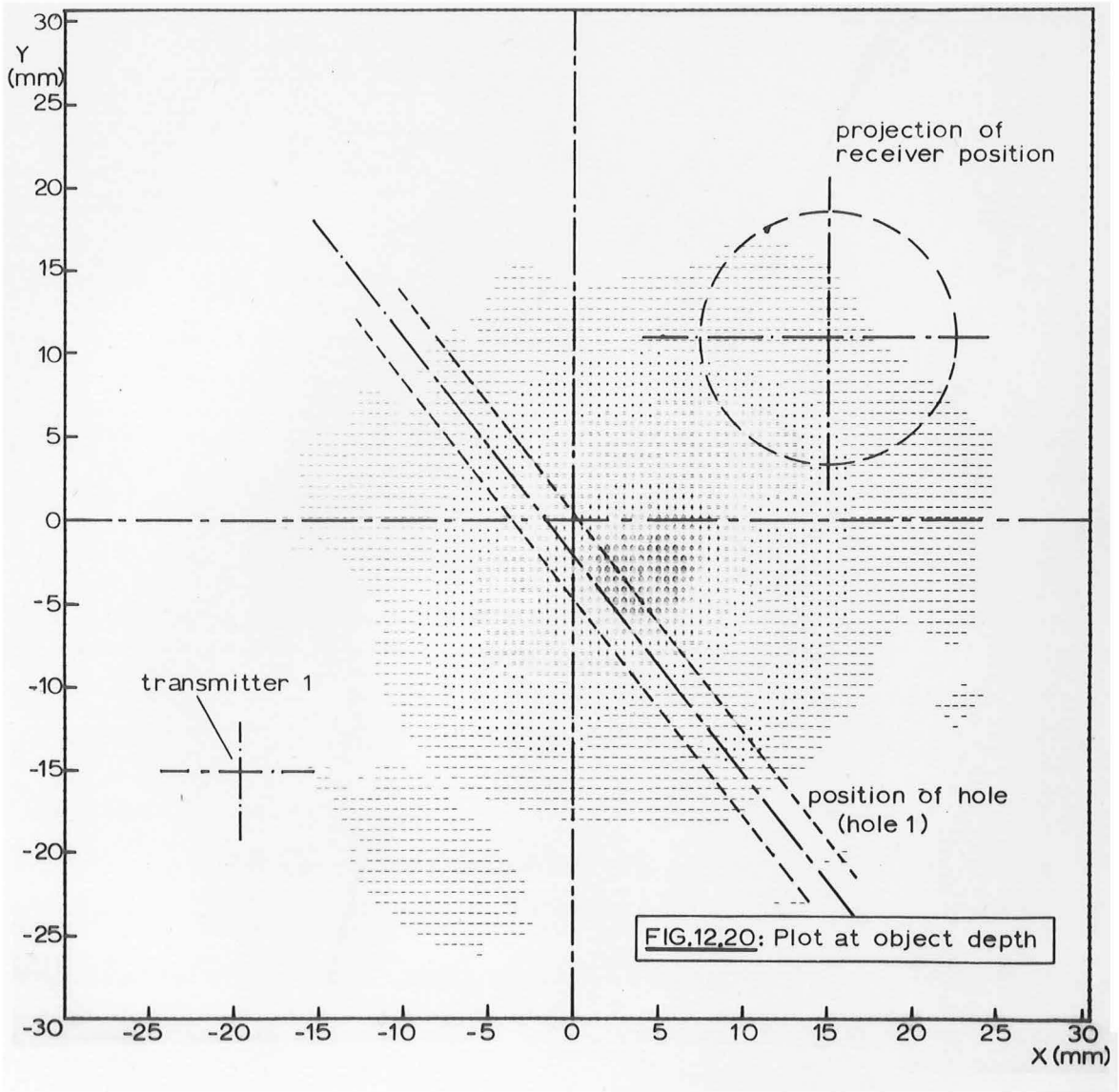

FIG.12.20: Plot at object depth

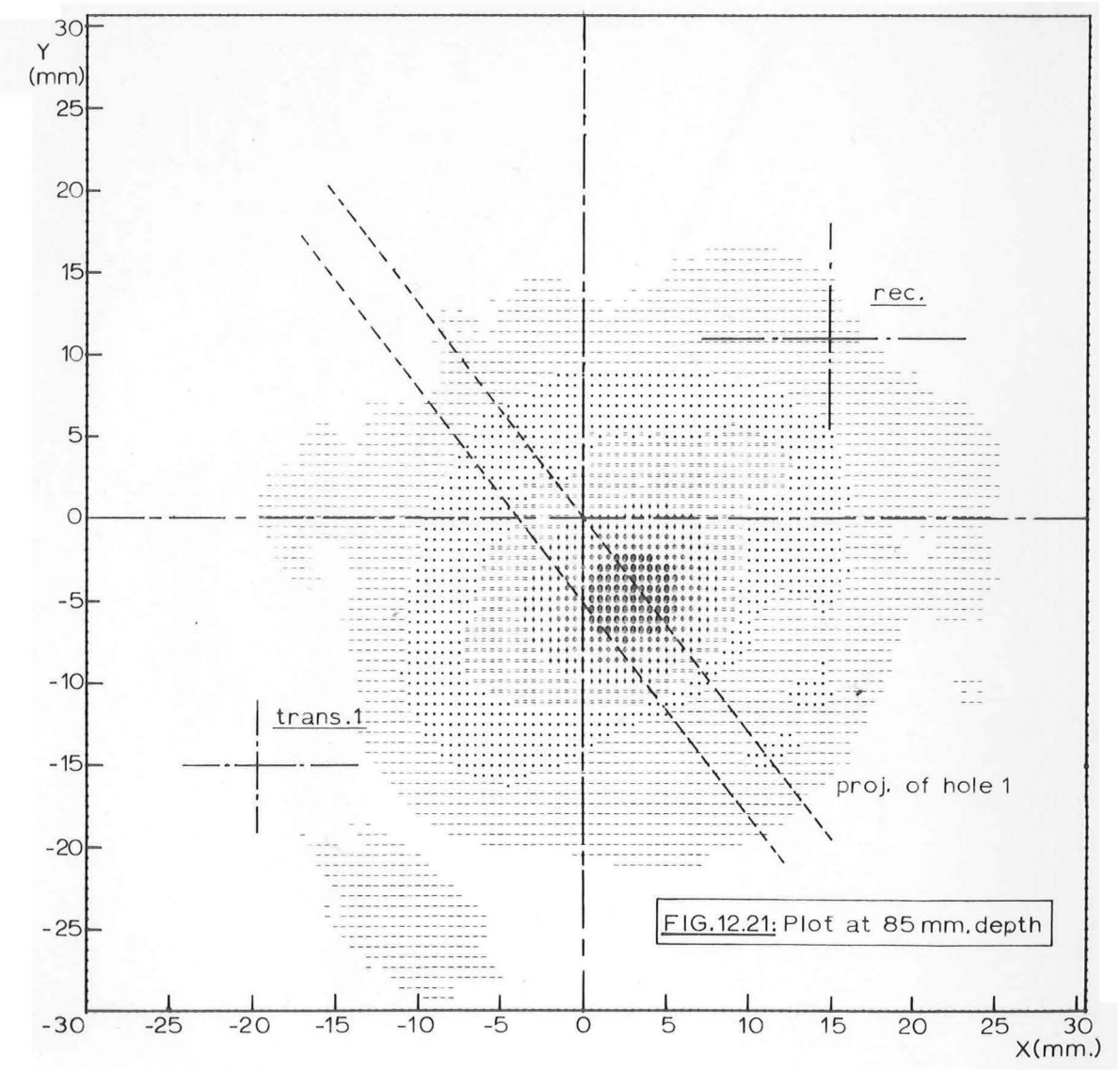

FIG.12.21: Plot at 85 mm. depth

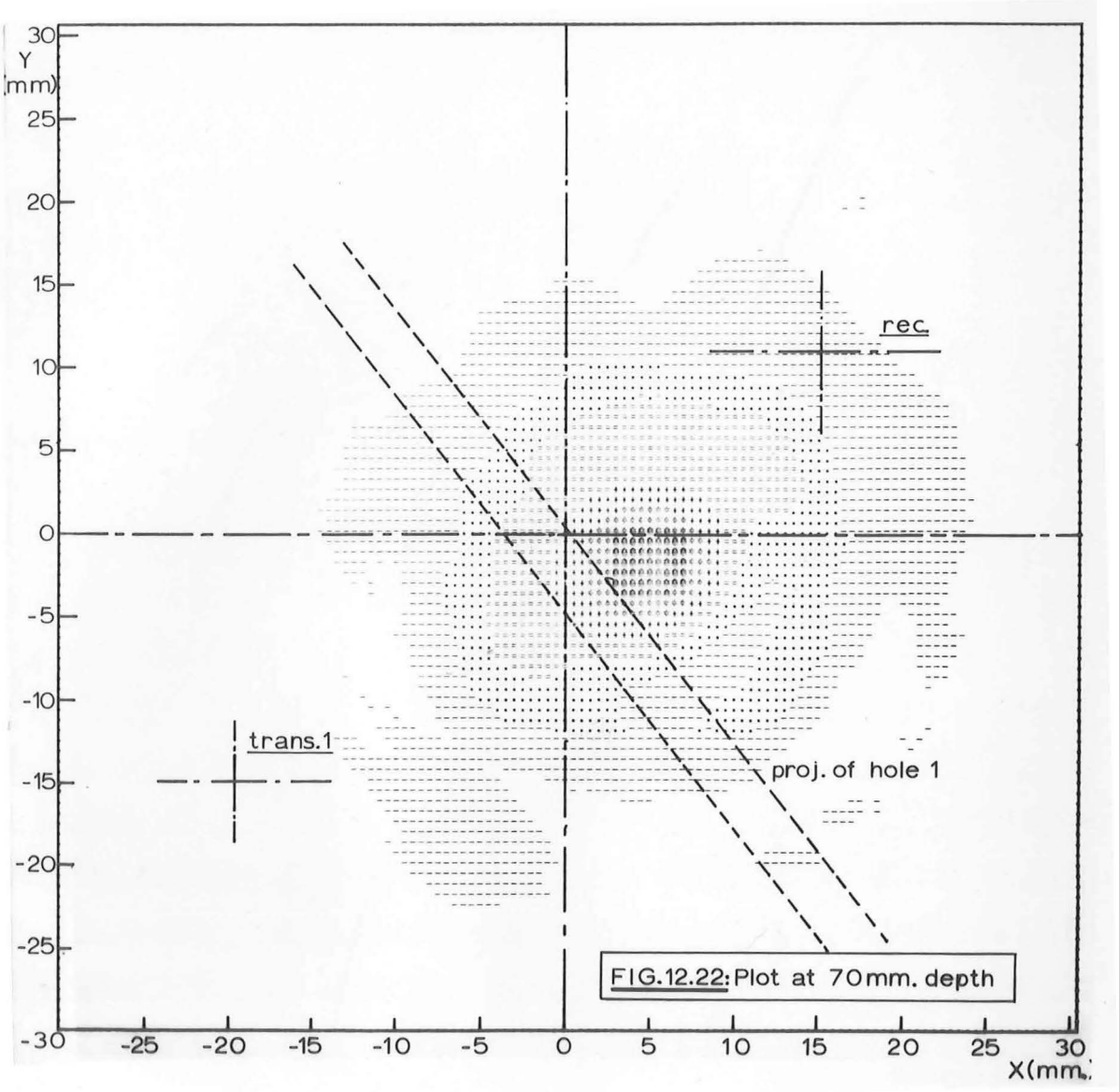

FIG.12.22: Plot at 70mm. depth

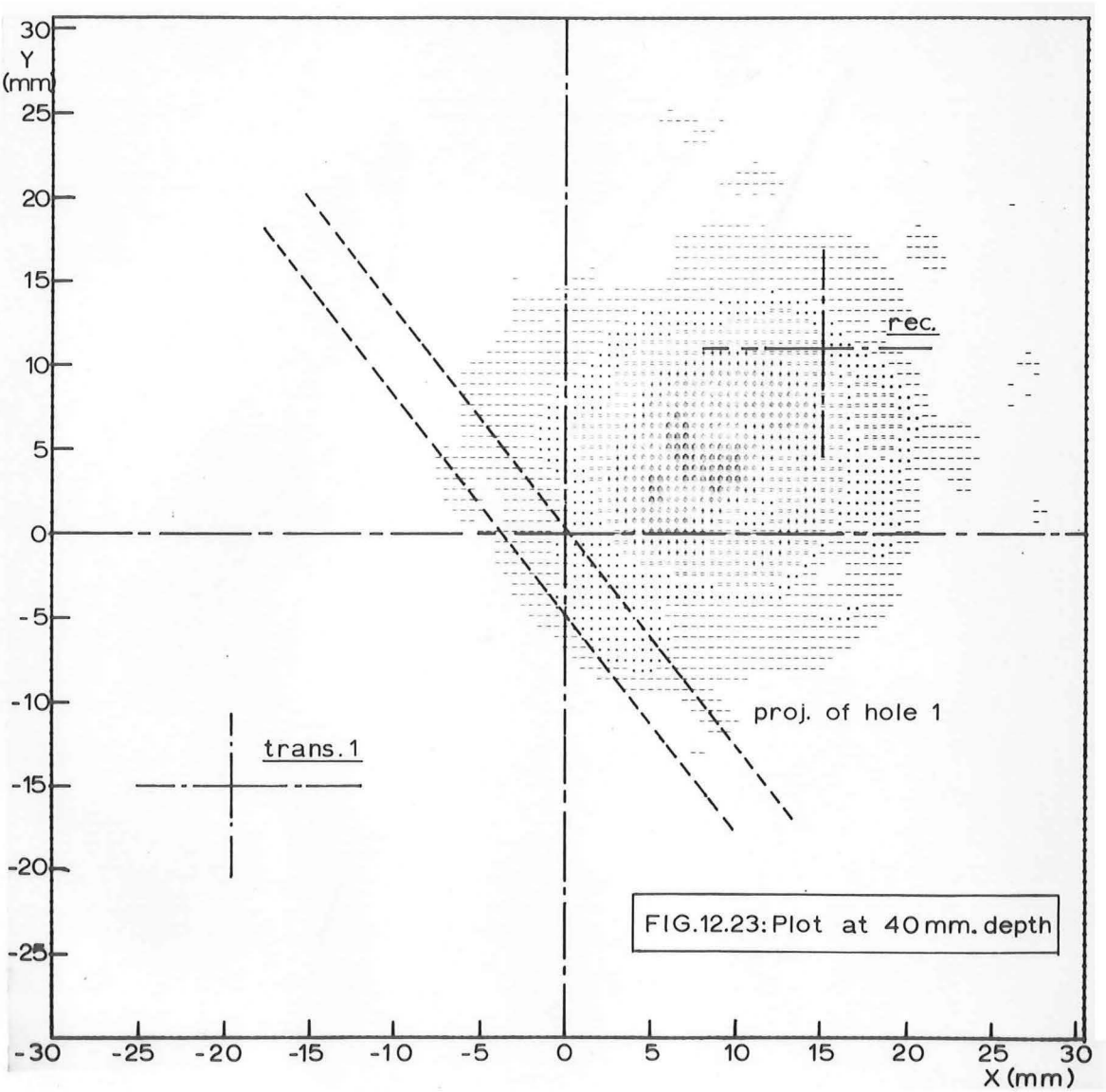

FIG.12.23: Plot at 40 mm. depth

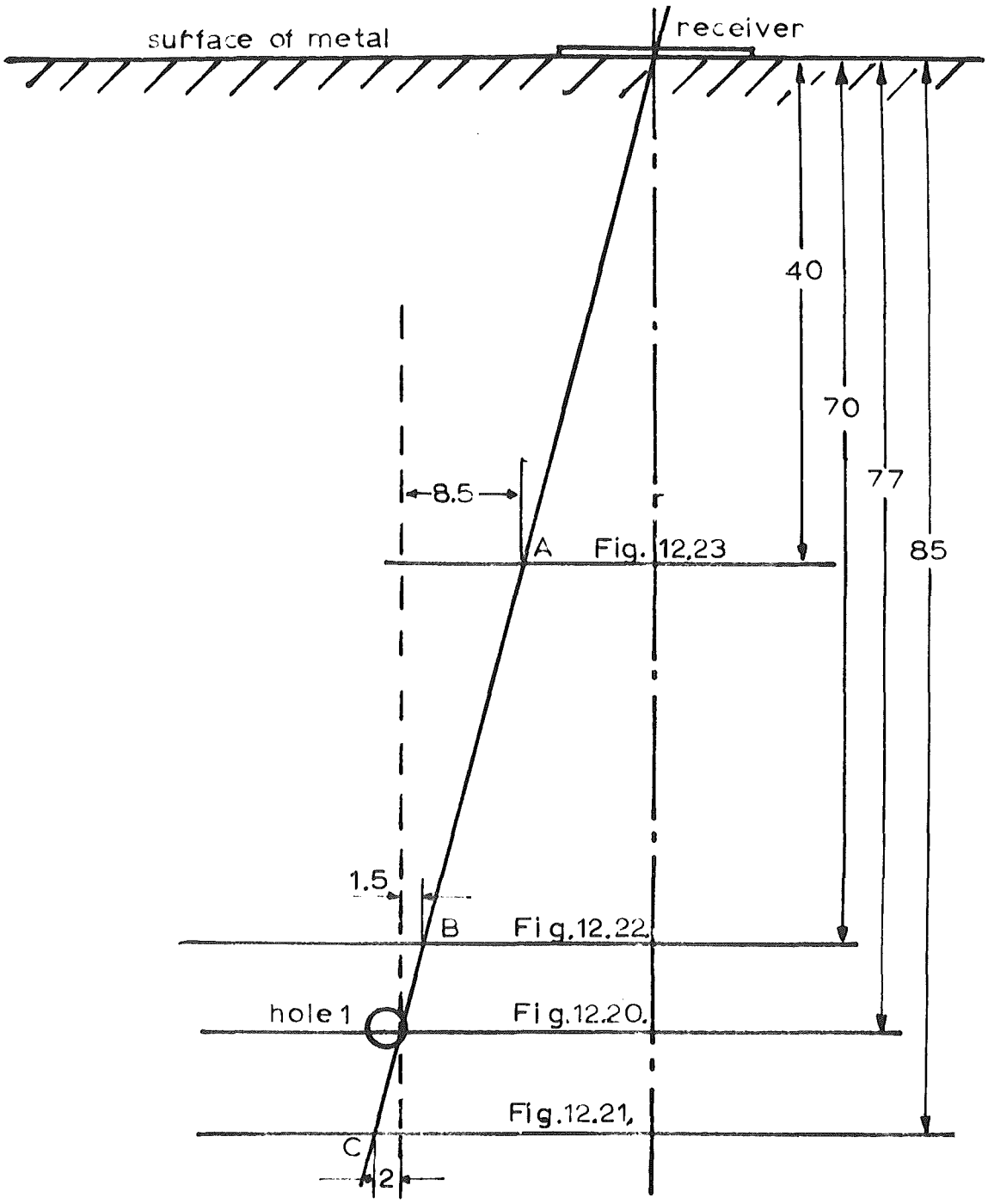

FIG. 12.24: Cross-section showing location of images: single hole. (dimensions in mm.)

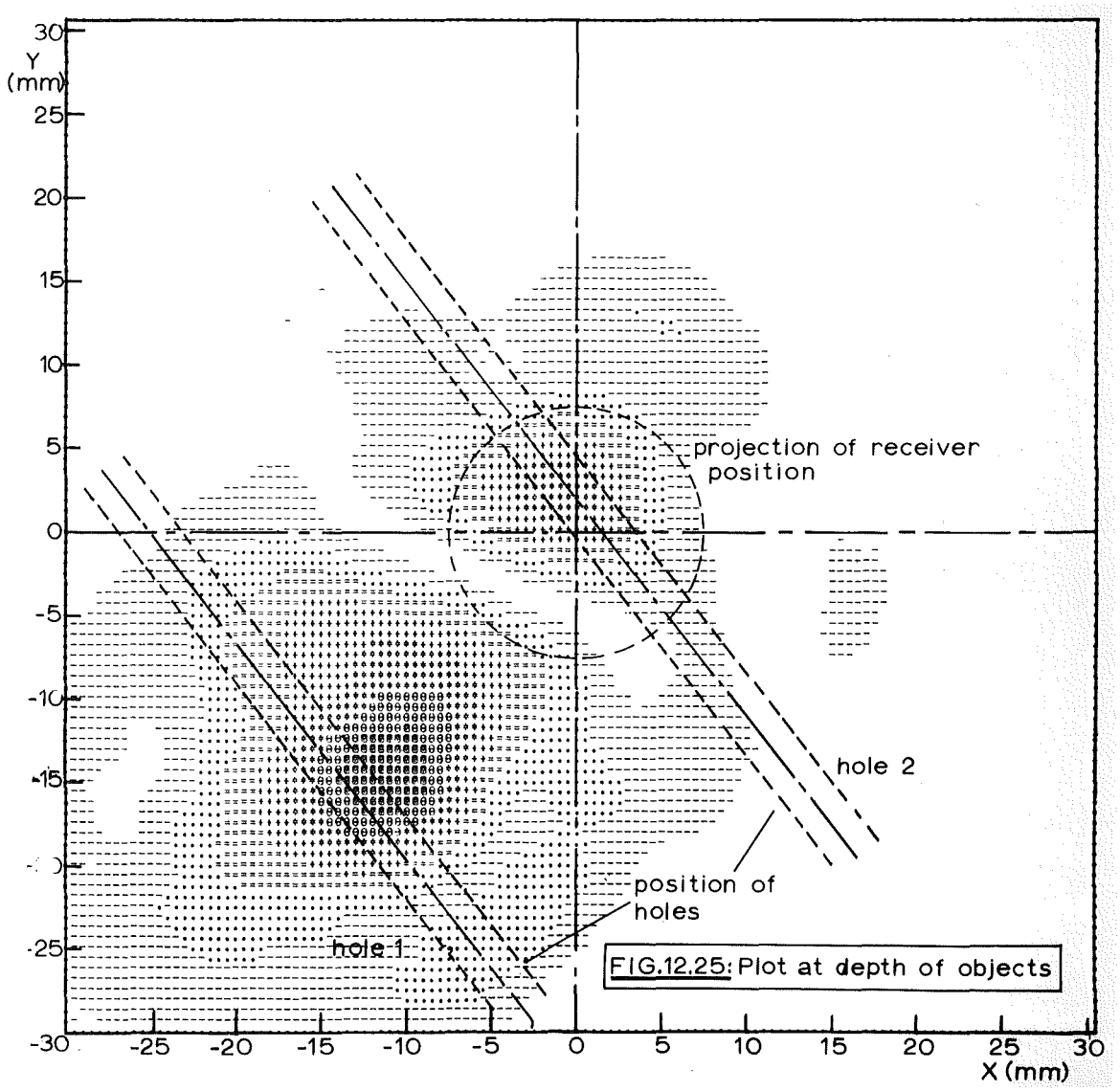

FIG.12.25: Plot at depth of objects

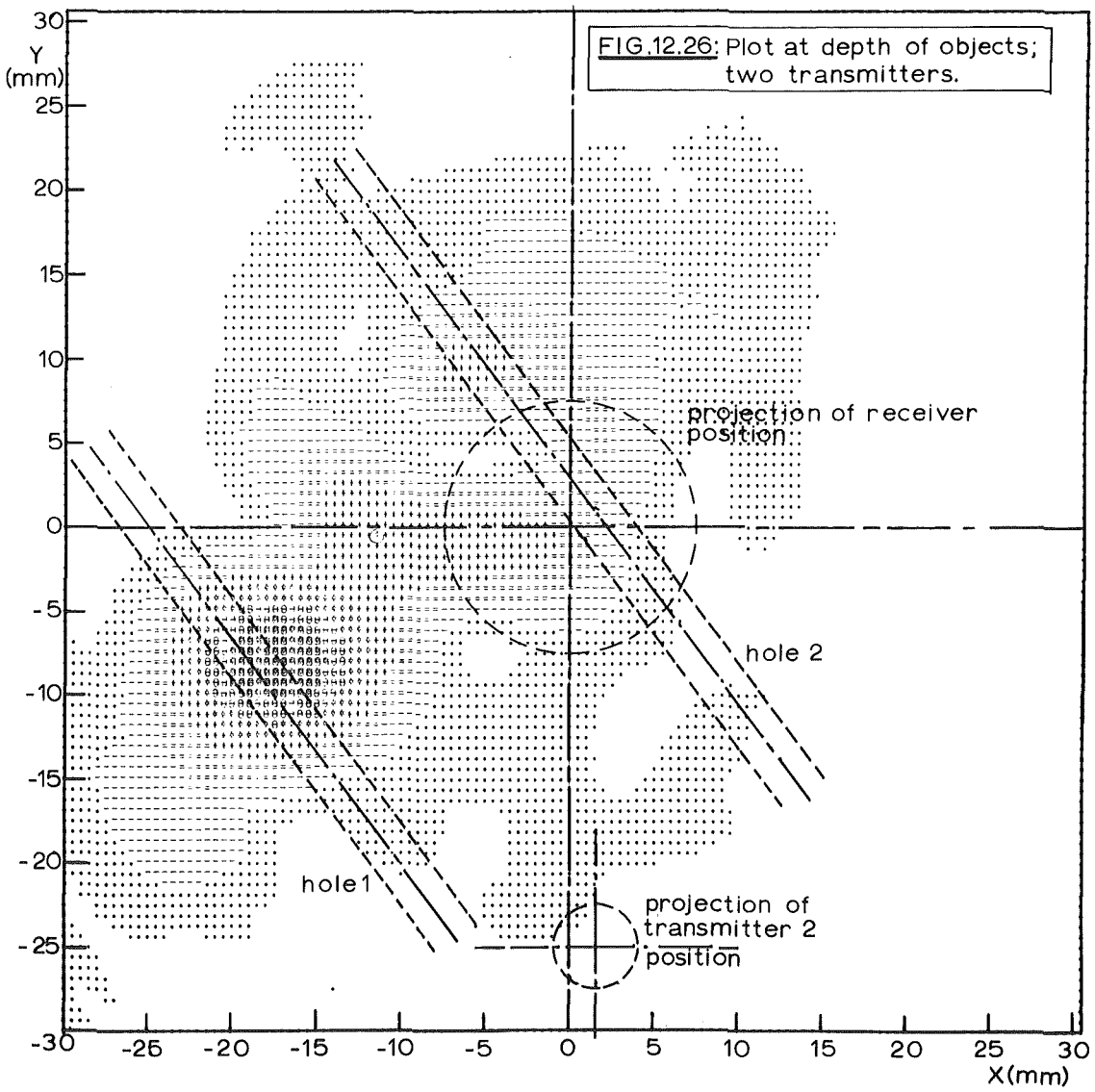
FIG.12.26: Plot at depth of objects; two transmitters.
Y (mm)
30
25
20
15
10
5
0
-5
-10
-15
-20
-25
-30
-25
-20
-15
-10
-5
0
5
10
15
20
25
30
X(mm)
projection of receiver position
hole 2
hole1
projection of transmitter 2 position

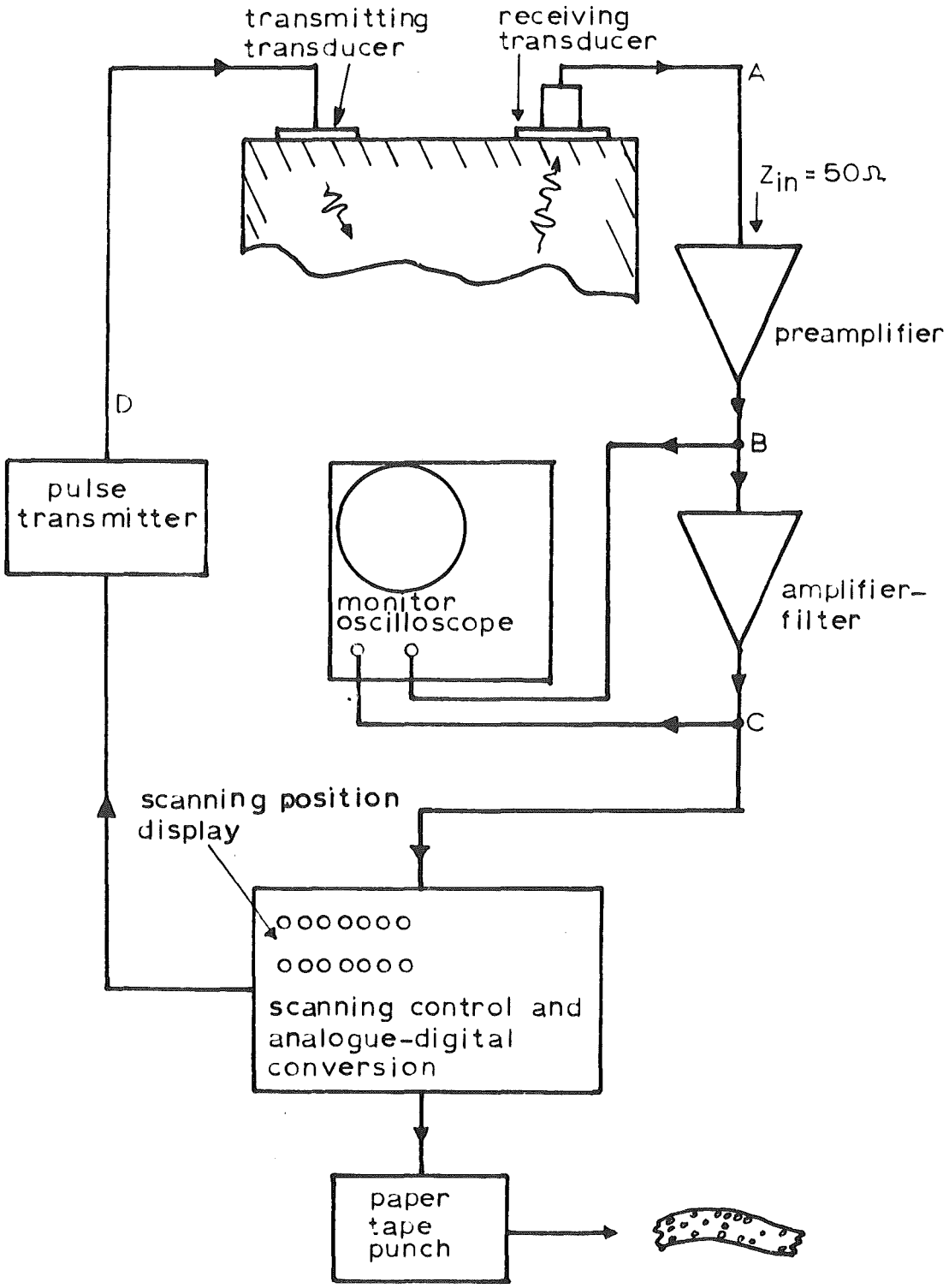

FIG. 12.27: Measurement setup for wideband transmissions.

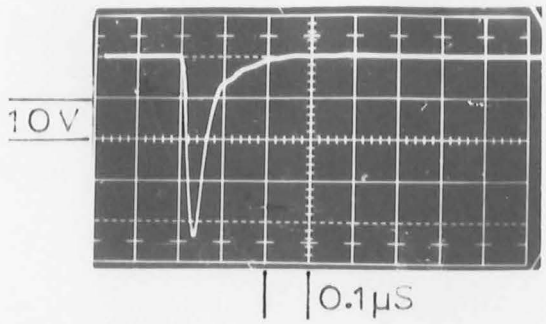

FIG.12.28: Electrical waveform at point D (Fig.12.27) when driving 5mm diameter transducer.

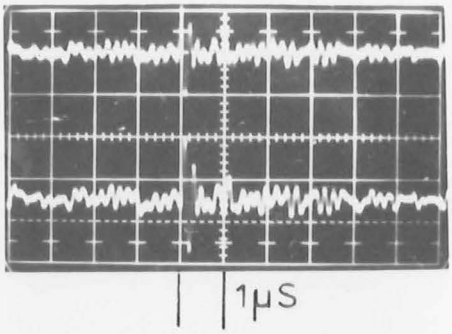

FIG.12.29(a)

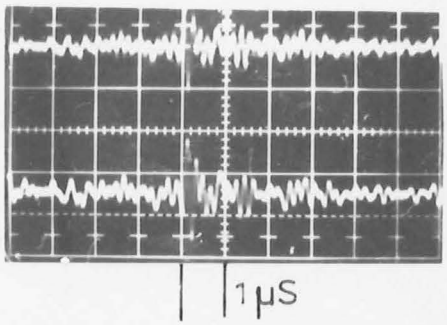

FIG.12.29 (b)

Received signals from adjacent elements: top trace – preamplifier output (point B), lower trace – ADC input (point C).

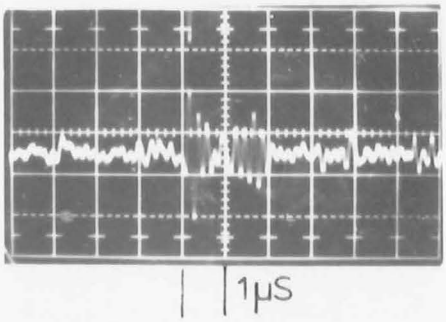

FIG.12.29(c)

Example showing separation of returns.

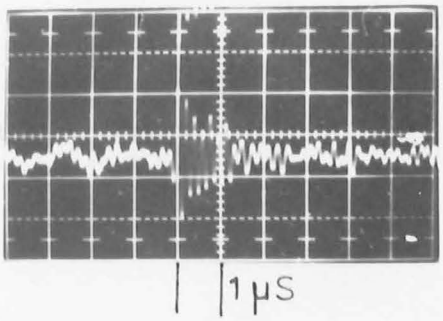

FIG.12.29(d)

Example showing return overlap.

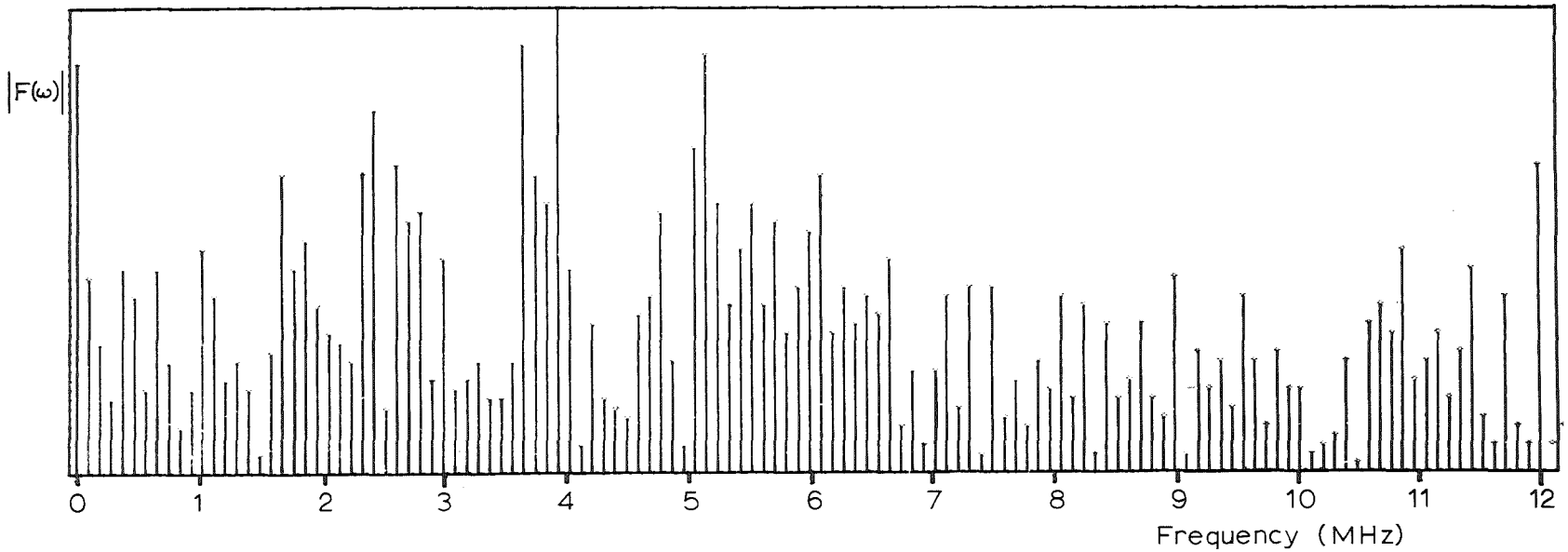

FIG.12.30: Example of computed spectrum of element signal

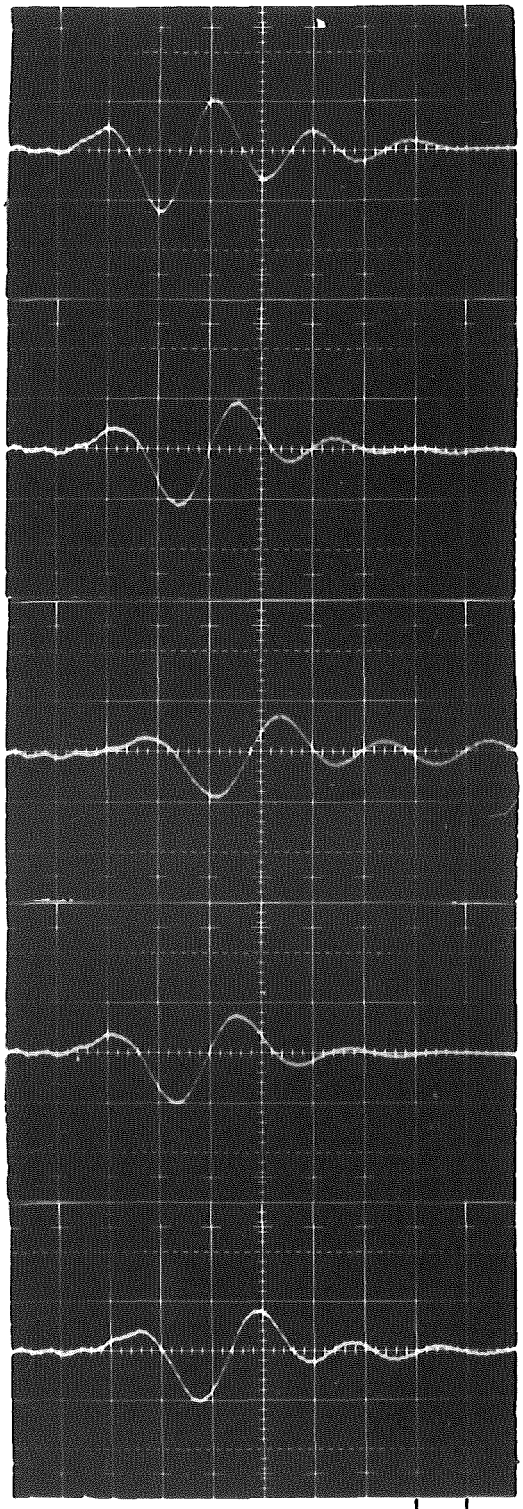

FIG.12.31(a)-(e): Bottom echos showing variations in arrival time

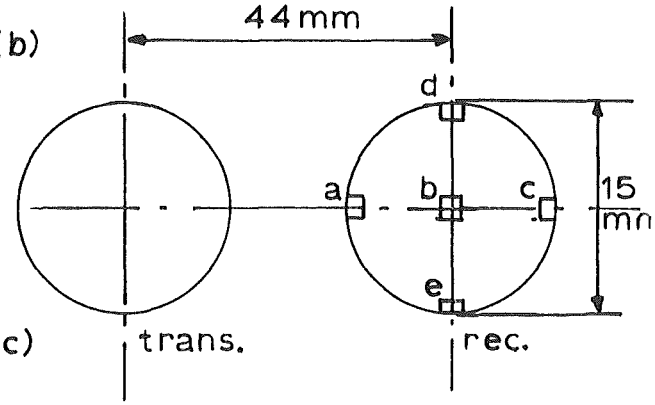

FIG.12.31(f): Element position

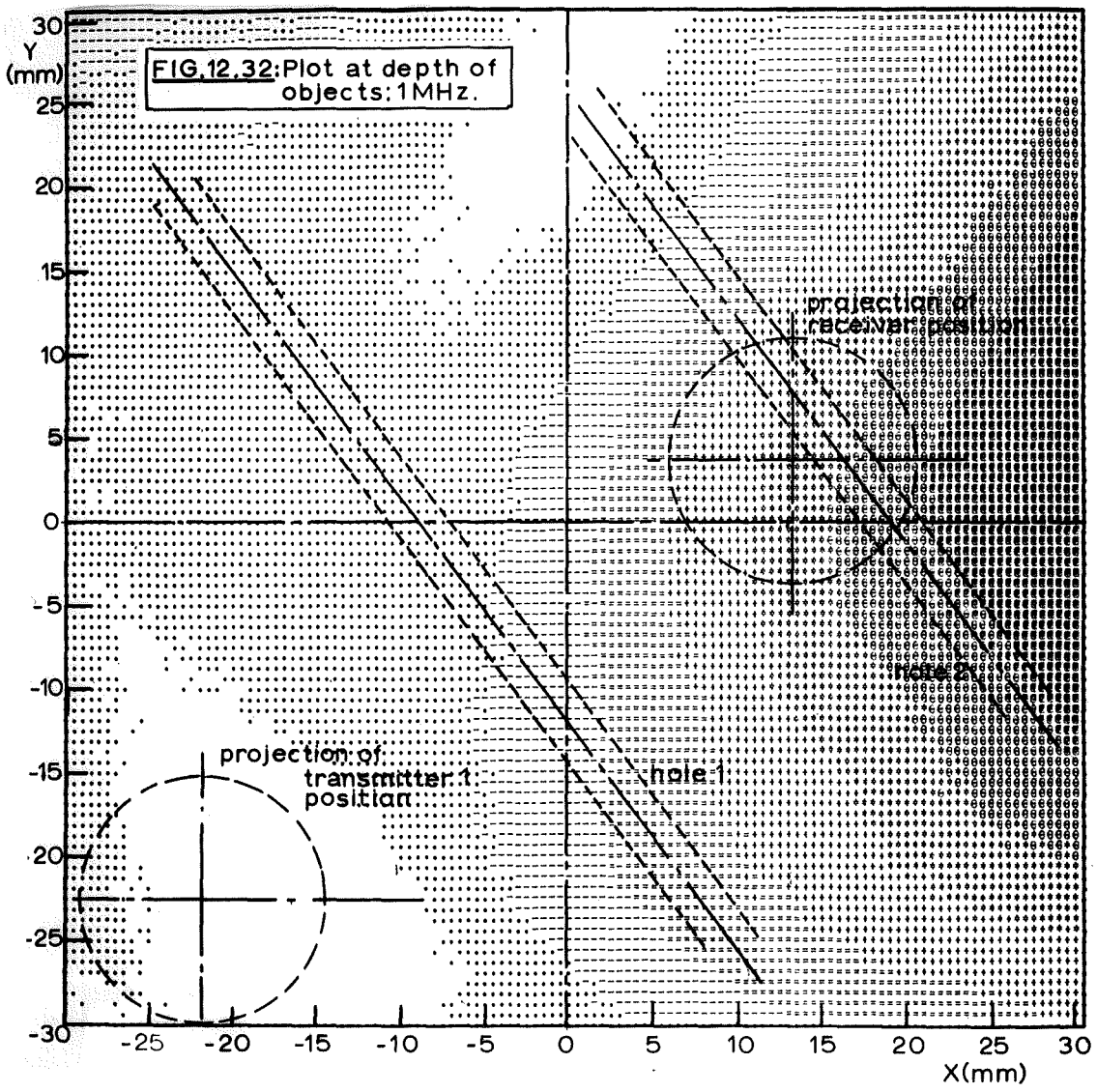
FIG.12.32:Plot at depth of objects:1MHz.
Y (mm)
30
25
20
15
10
5
0
-5
-10
-15
-20
-25
-30
-25
-20
-15
-10
-5
0
5
10
15
20
25
30
X(mm)
projection of transmitter 1 position
hole 1
projection of receiver position
hole 2

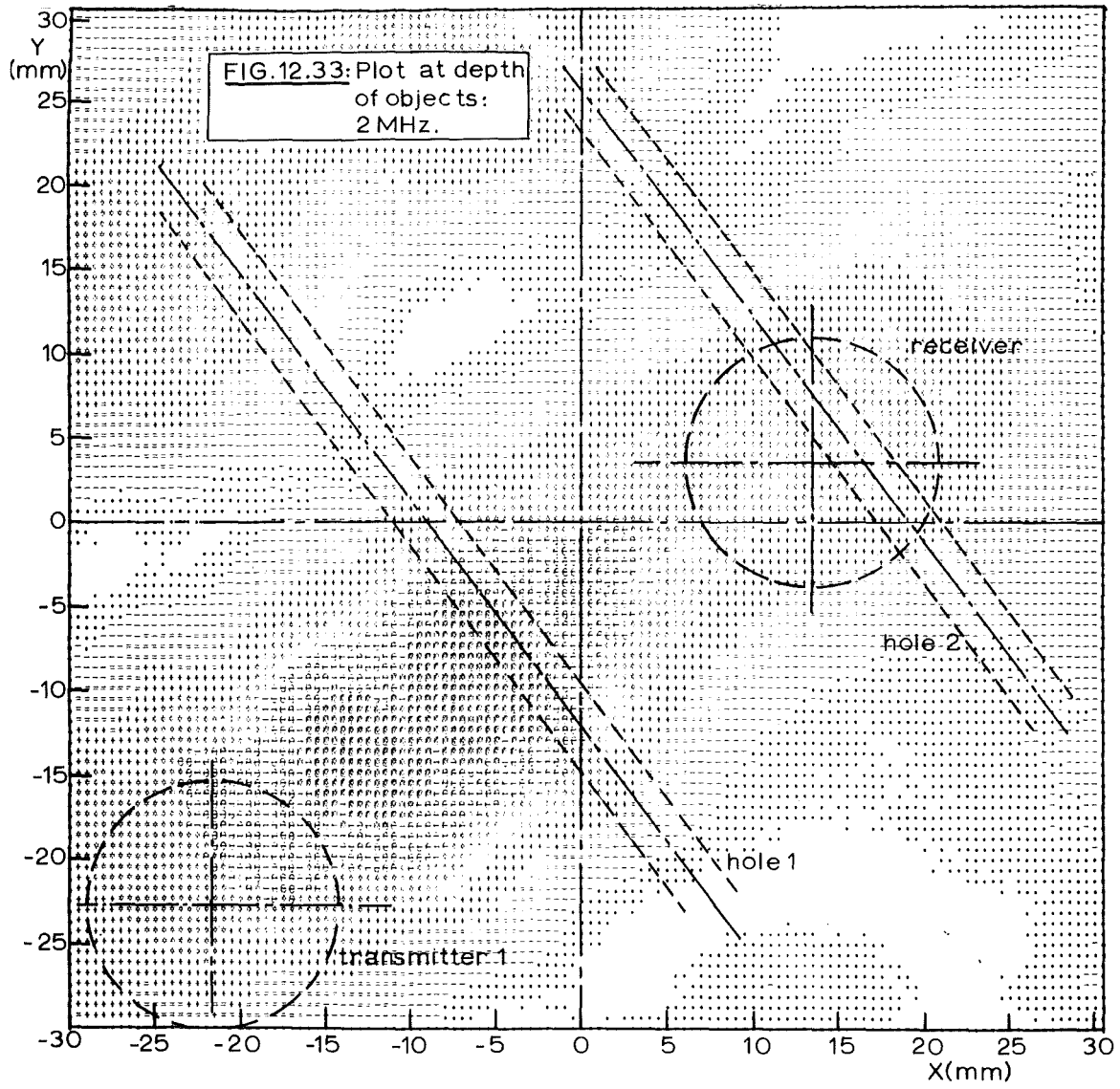
FIG.12.33: Plot at depth of objects: 2 MHz.
Y (mm)
30
25
20
15
10
5
0
-5
-10
-15
-20
-25
-30
-25
-20
-15
-10
-5
0
5
10
15
20
25
30
X(mm)
receiver
hole 2
hole 1
transmitter 1

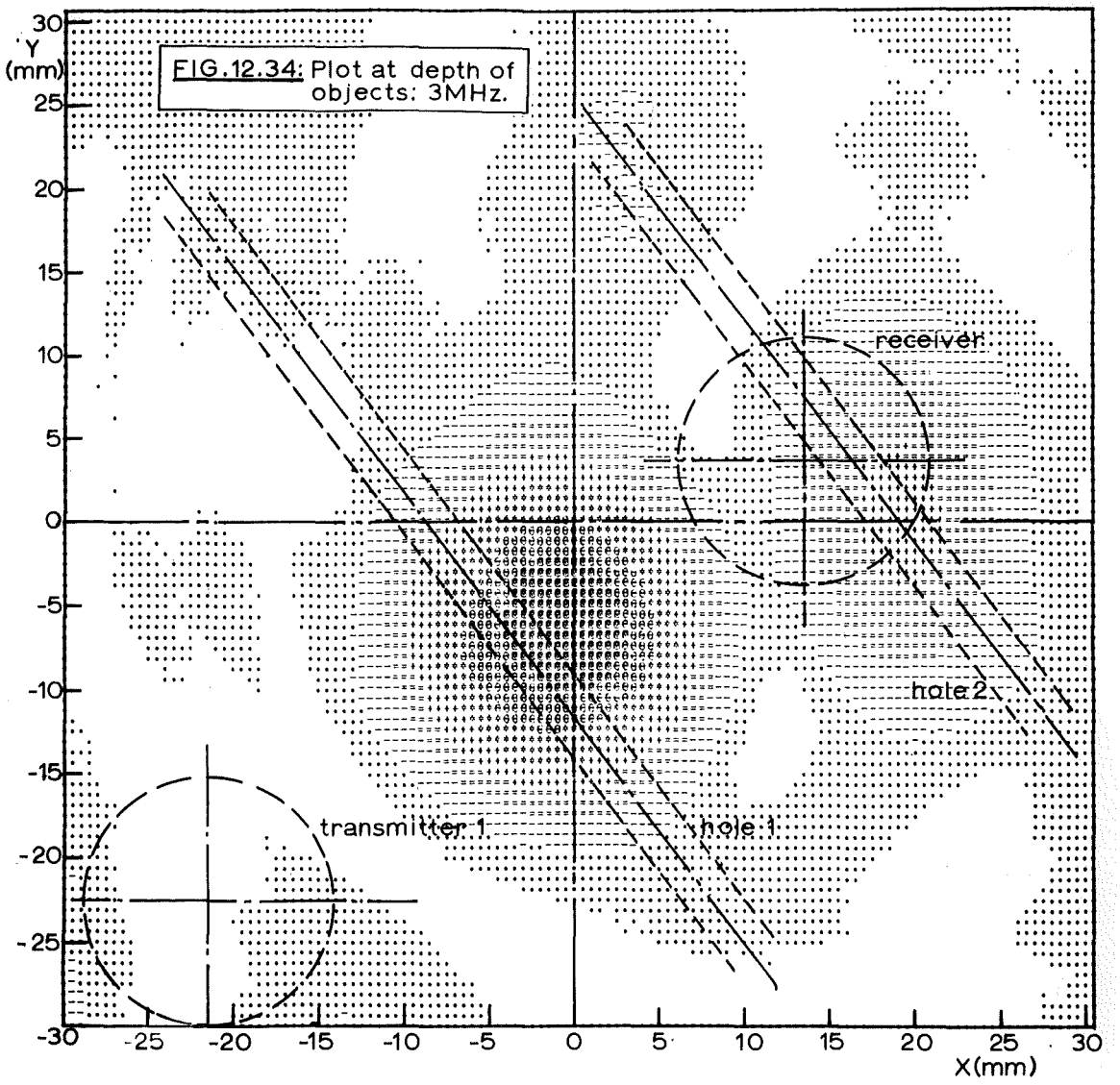
FIG.12.34: Plot at depth of objects: 3MHz.
Y (mm)
30
25
20
15
10
5
0
-5
-10
-15
-20
-25
-30
-25
-20
-15
-10
-5
0
5
10
15
20
25
30
X(mm)
receiver
hole 2
transmitter 1
hole 1

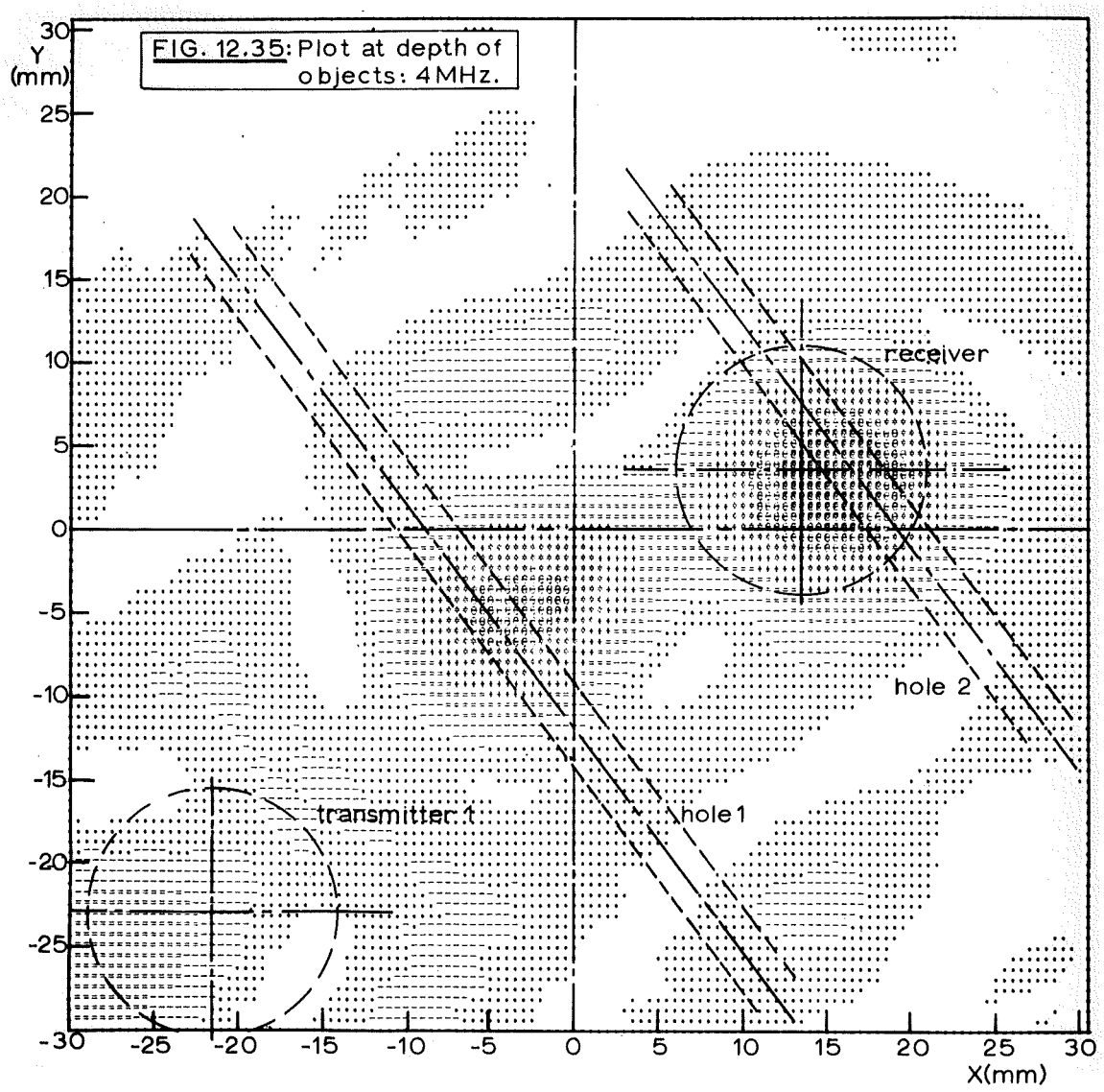
FIG. 12.35: Plot at depth of objects: 4 MHz.
Y (mm)
30
25
20
15
10
5
0
-5
-10
-15
-20
-25
-30
-25
-20
-15
-10
-5
0
5
10
15
20
25
30
X(mm)
receiver
hole 2
hole 1
transmitter 1

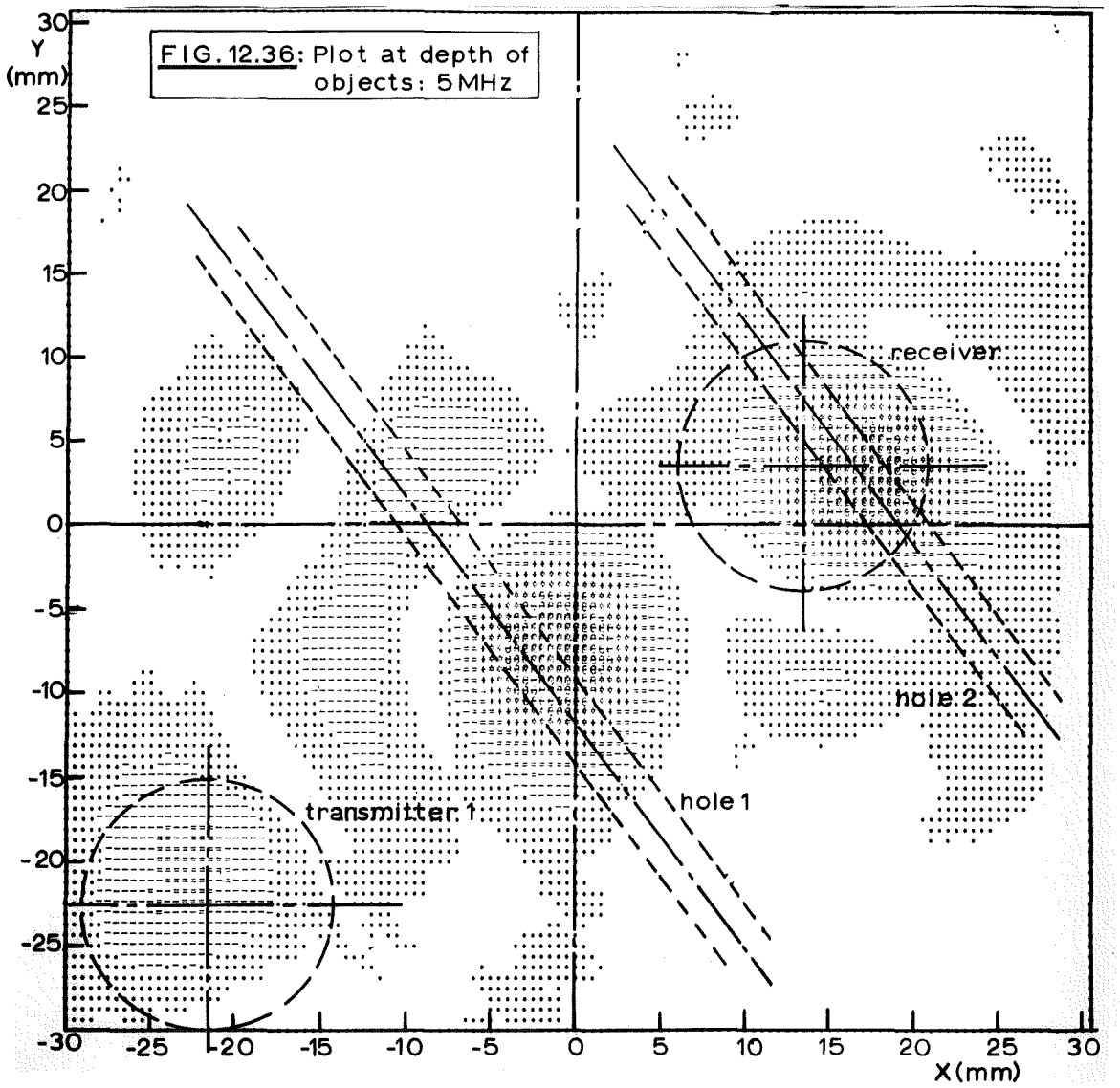
FIG. 12.36: Plot at depth of objects: 5 MHz
Y (mm)
30
25
20
15
10
5
0
-5
-10
-15
-20
-25
-30
-25
-20
-15
-10
-5
0
5
10
15
20
25
30
X (mm)
receiver
hole 2
hole 1
transmitter 1

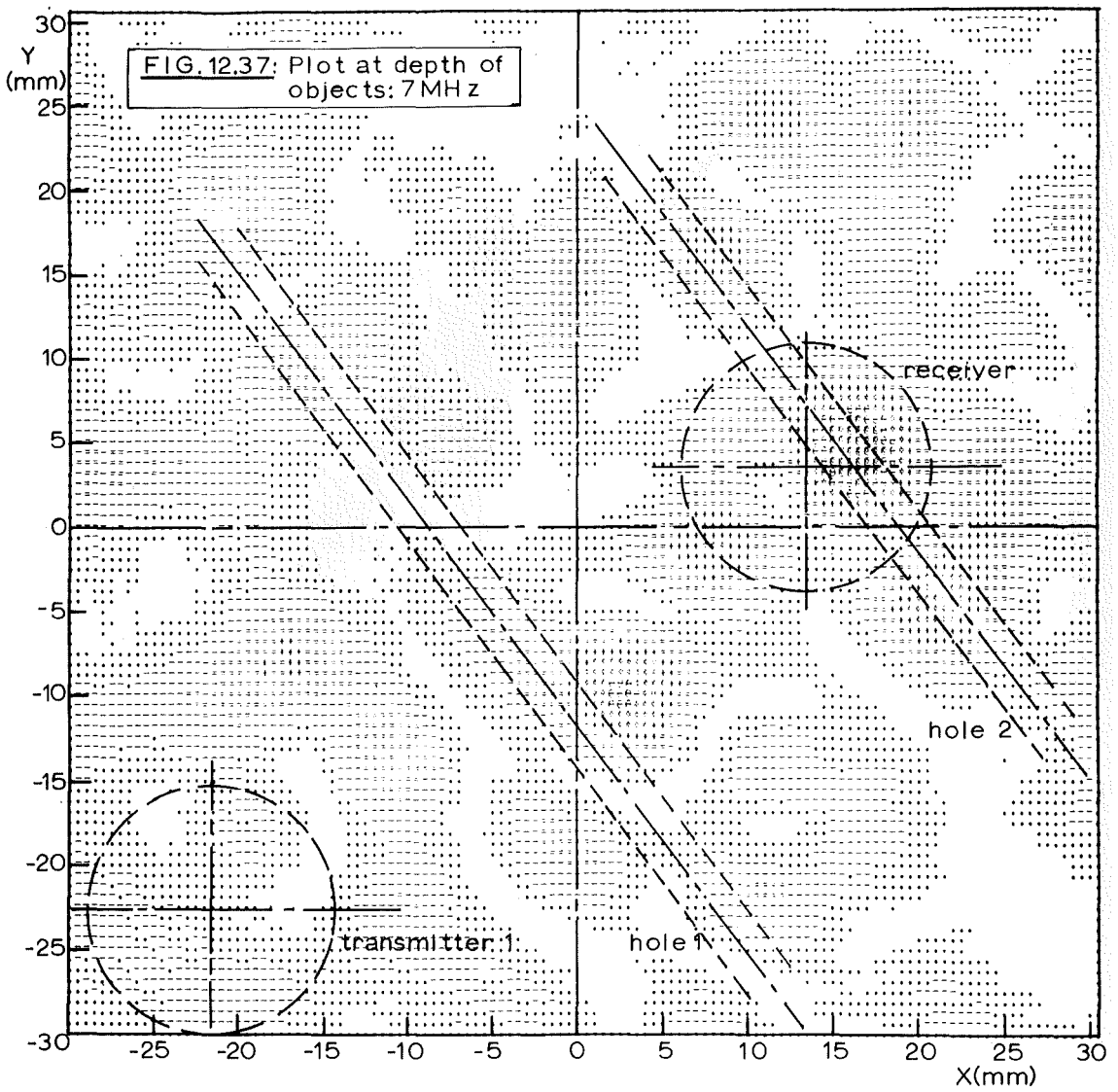
FIG. 12.37: Plot at depth of objects: 7 MHz
Y (mm)
30
25
20
15
10
5
0
-5
-10
-15
-20
-25
-30
-25
-20
-15
-10
-5
0
5
10
15
20
25
30
X(mm)
receiver
hole 2
transmitter 1
hole 1

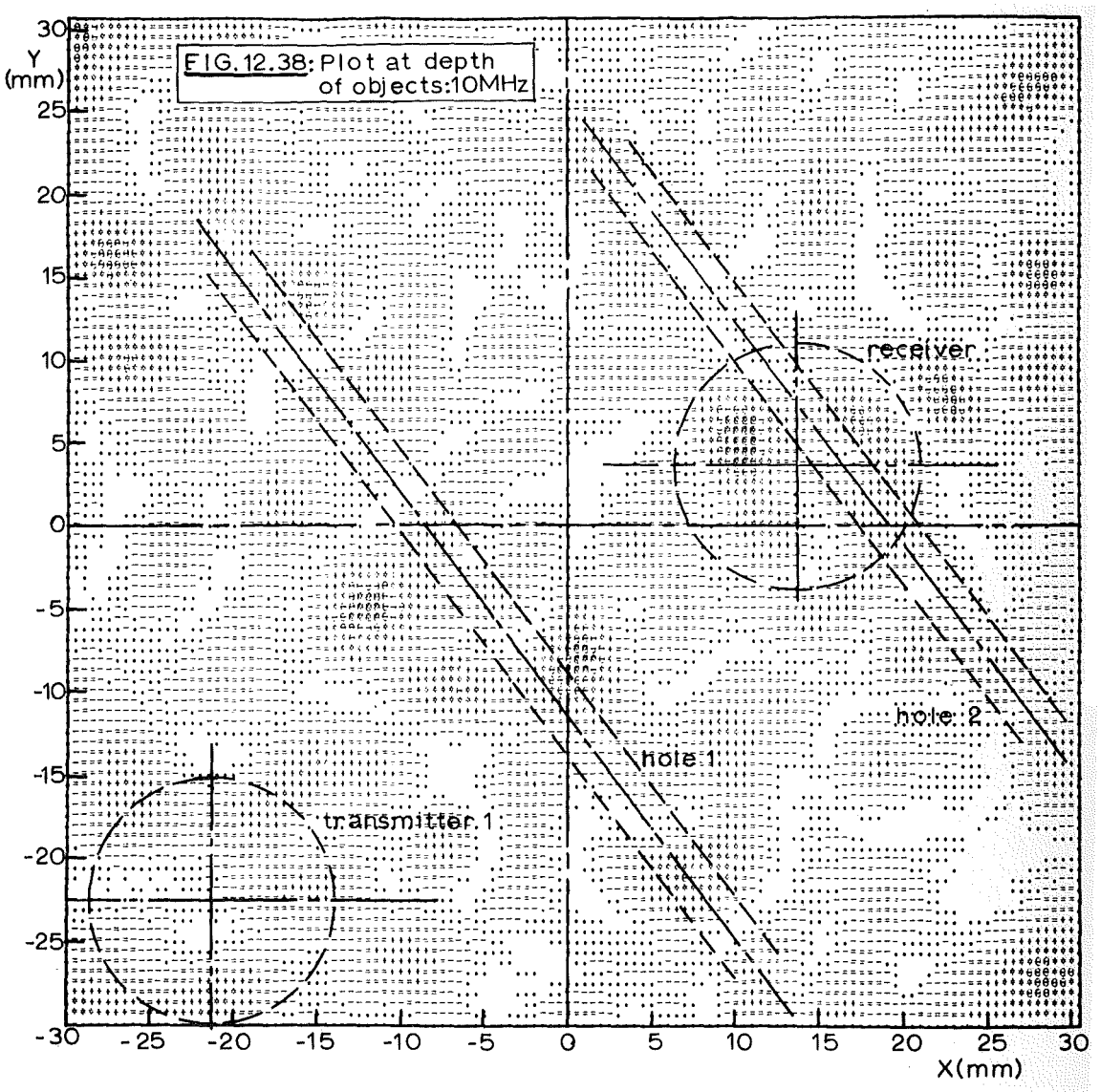
FIG. 12.38: Plot at depth of objects: 10MHz
Y (mm)
30
25
20
15
10
5
0
-5
-10
-15
-20
-25
-30
-25
-20
-15
-10
-5
0
5
10
15
20
25
30
X(mm)
receiver
hole 2
hole 1
transmitter 1

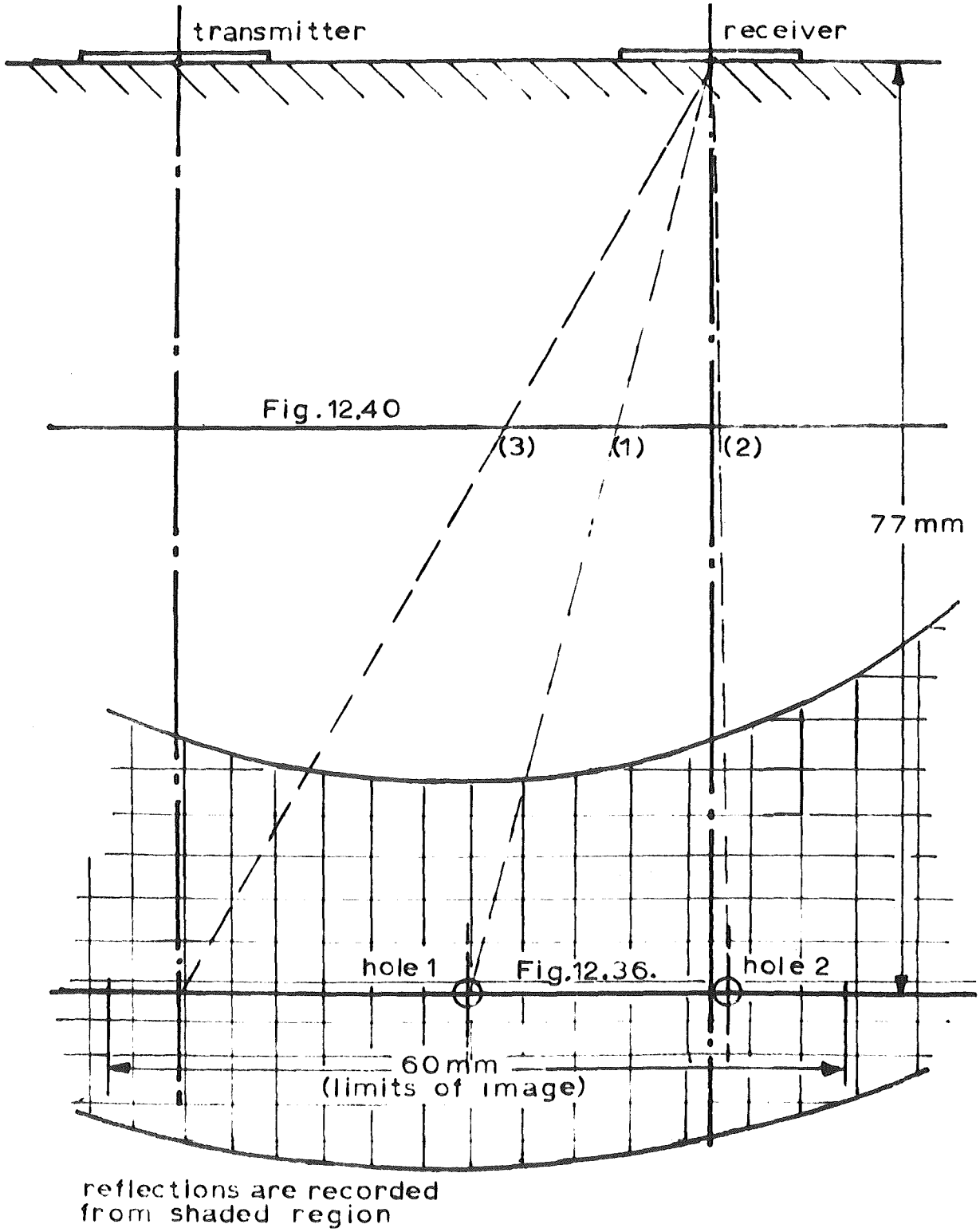

FIG.12.39: Cross-section showing record and image regions for Figs.12.32–38 and Fig.12.40.

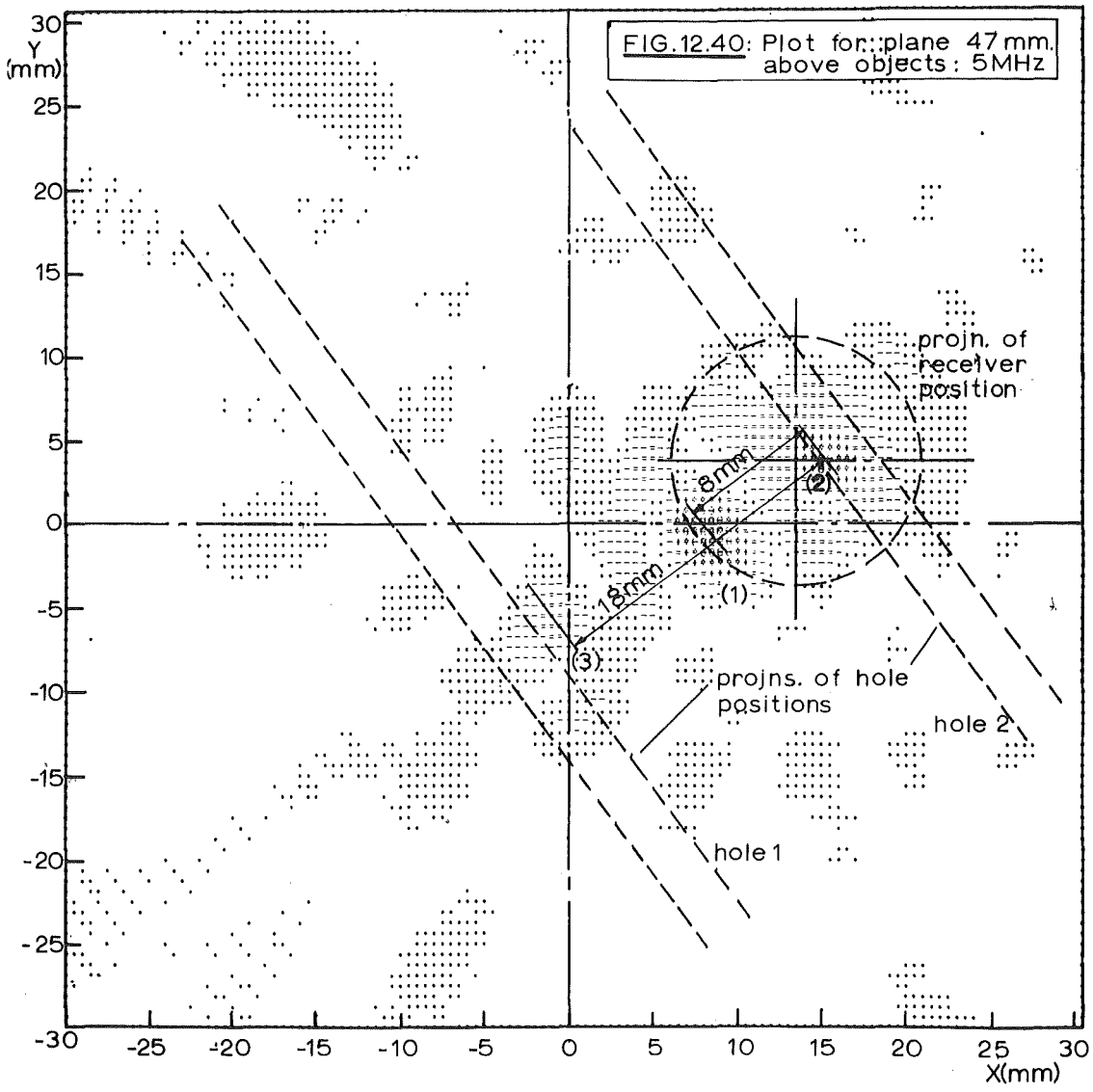
FIG.12.40: Plot for plane 47 mm. above objects: 5MHz
Y (mm)
X(mm)
projn. of receiver position
8mm
18mm
(1)
(2)
(3)
projns. of hole positions
hole 2
hole 1

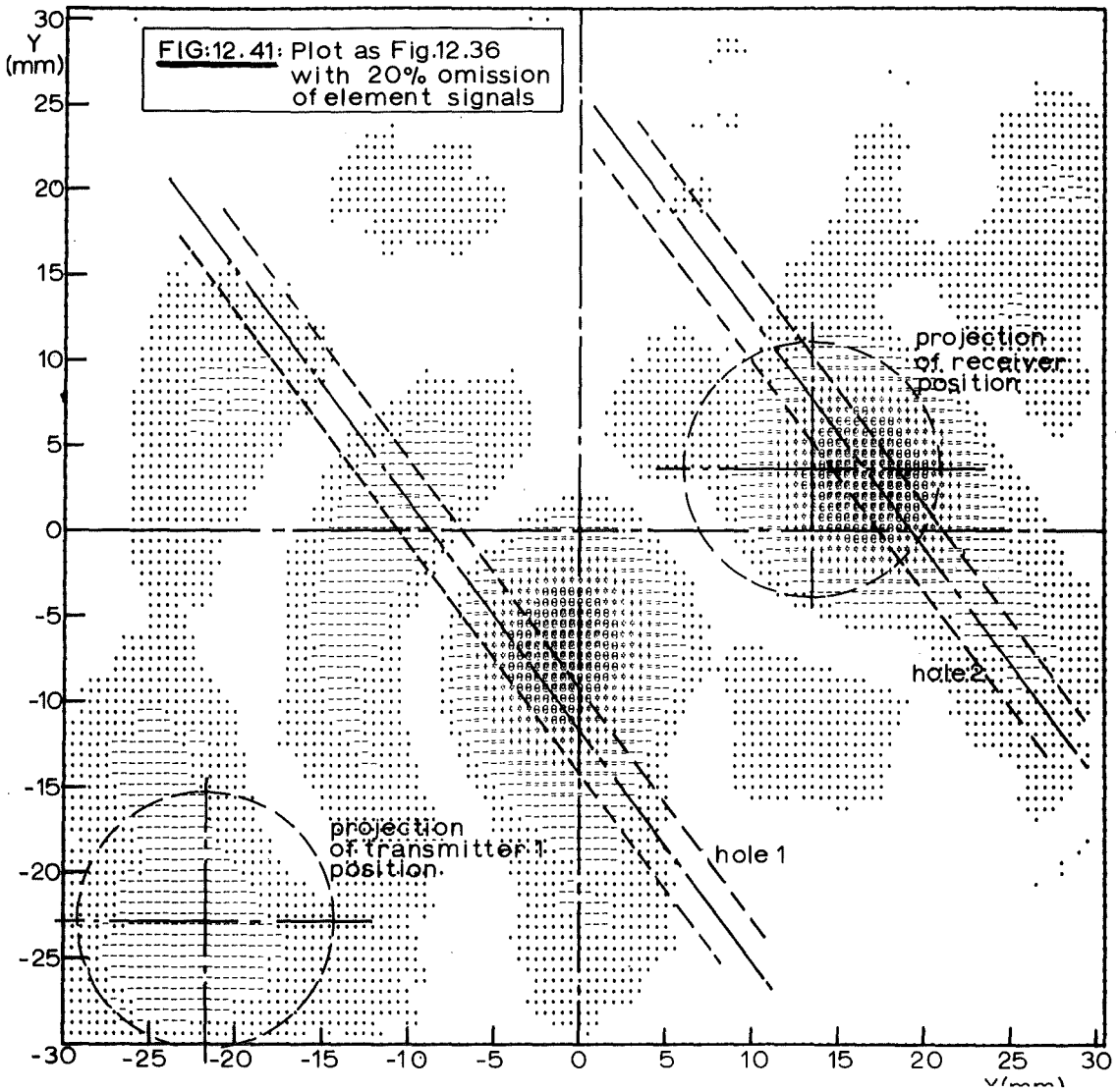
FIG:12.41: Plot as Fig.12.36 with 20% omission of element signals
Y (mm)
30
25
20
15
10
5
0
-5
-10
-15
-20
-25
-30
-25
-20
-15
-10
-5
0
5
10
15
20
25
30
projection of receiver position
hole 2
hole 1
projection of transmitter 1 position

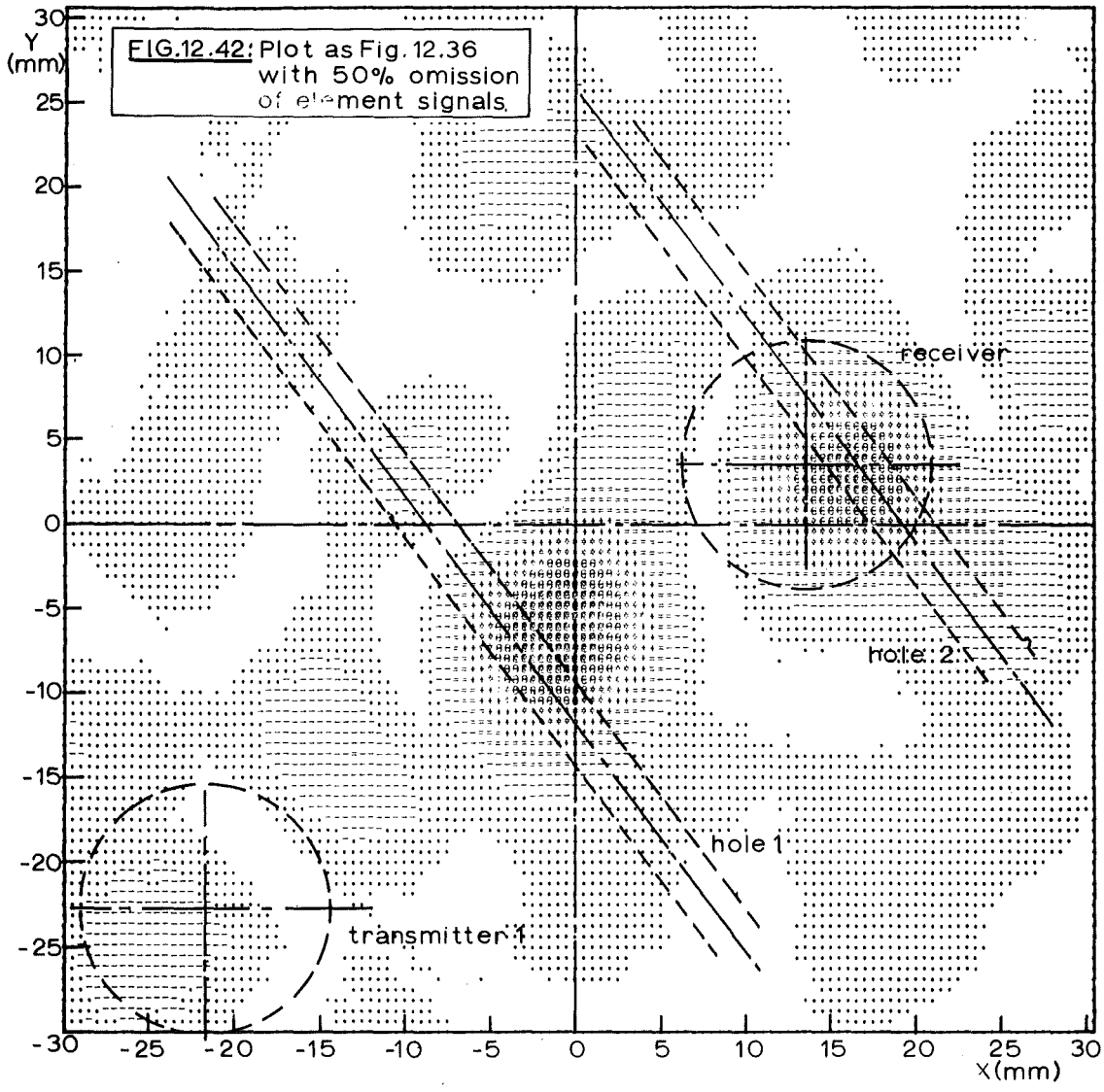
FIG.12.42: Plot as Fig. 12.36 with 50% omission of element signals.
Y (mm)
30
25
20
15
10
5
0
-5
-10
-15
-20
-25
-30
-25
-20
-15
-10
-5
0
5
10
15
20
25
30
X(mm)
receiver
hole 2
hole 1
transmitter 1

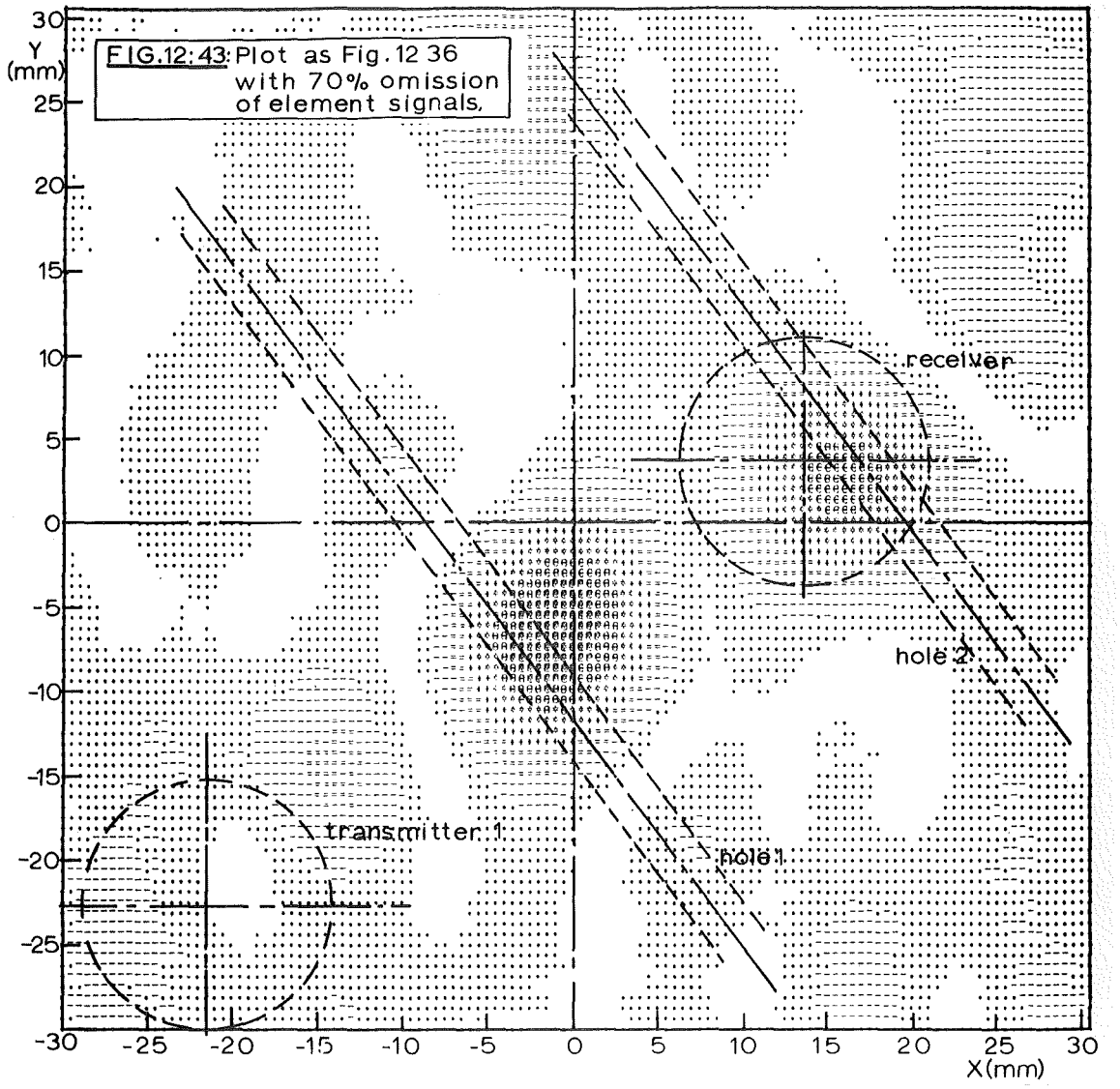
FIG.12:43: Plot as Fig. 12 36 with 70% omission of element signals.
Y (mm)
X(mm)
receiver
hole 2
hole 1
transmitter 1
30
25
20
15
10
5
0
-5
-10
-15
-20
-25
-30
-25
-20
-15
-10
-5
0
5
10
15
20
25
30

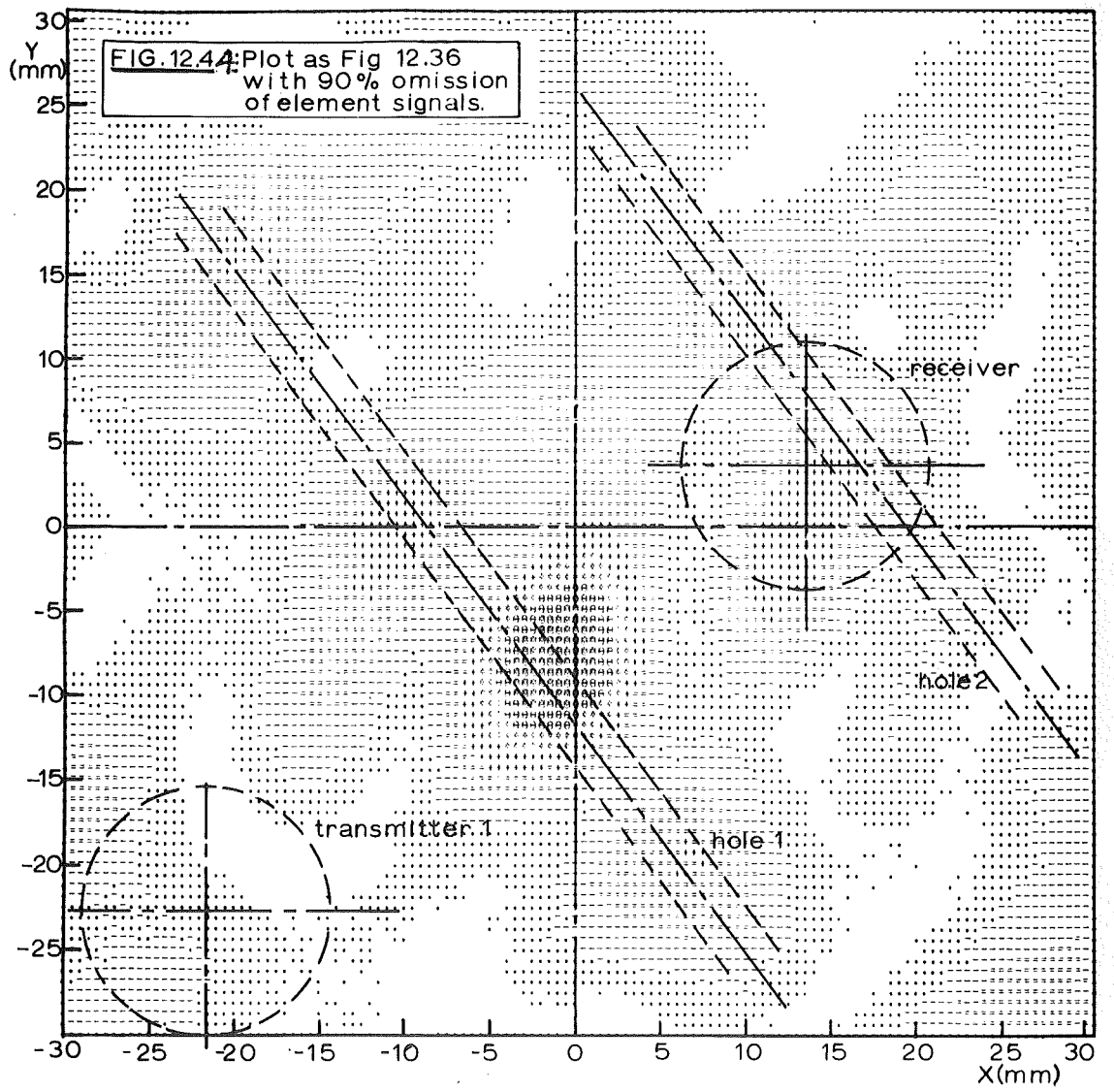
FIG. 12.44: Plot as Fig 12.36 with 90% omission of element signals.
Y (mm)
30
25
20
15
10
5
0
-5
-10
-15
-20
-25
-30 -25 -20 -15 -10 -5 0 5 10 15 20 25 30
X(mm)
receiver
hole 2
hole 1
transmitter 1

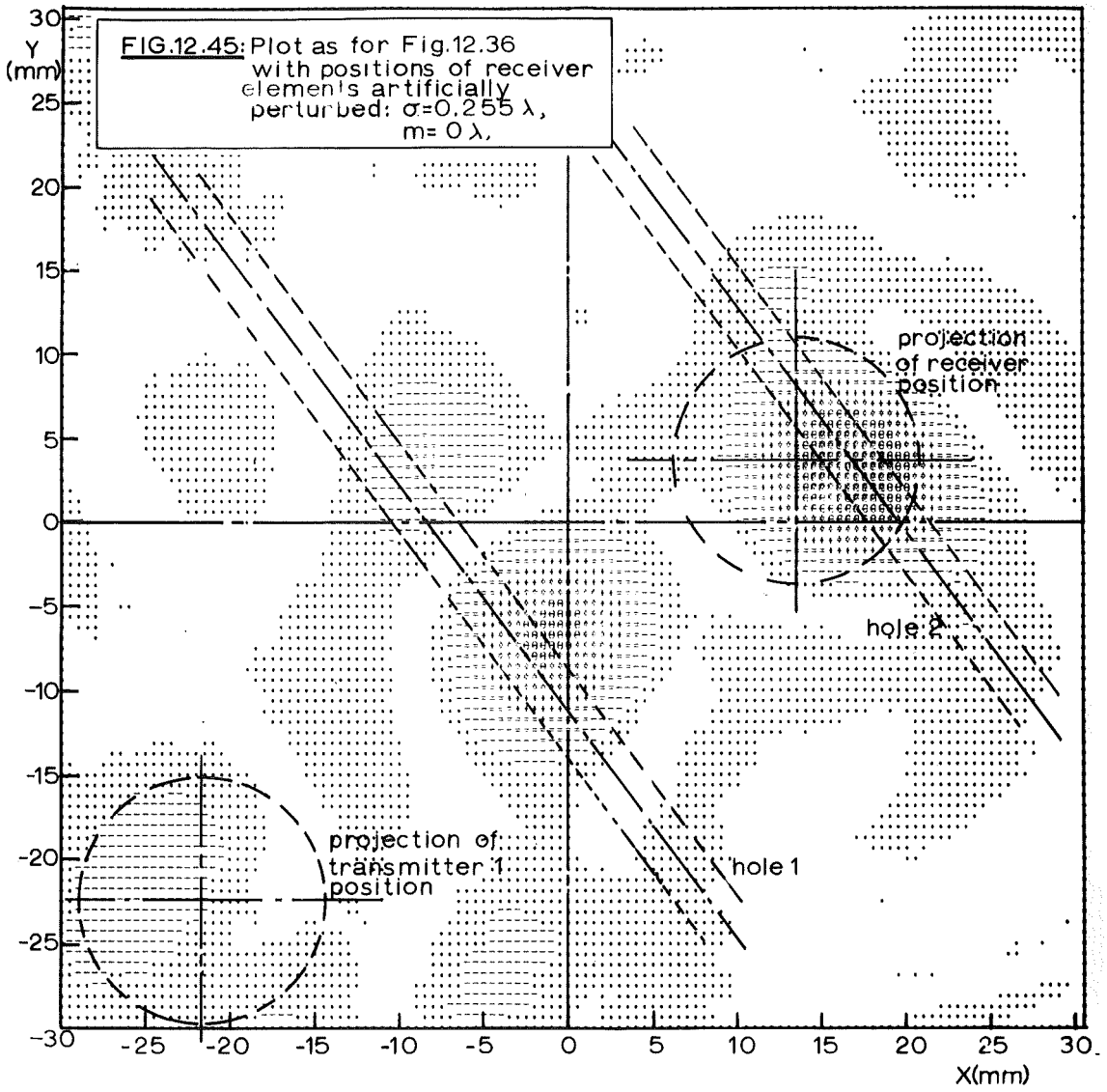
FIG.12.45: Plot as for Fig.12.36 with positions of receiver elements artificially perturbed: σ=0.255 λ, m= 0 λ,
Y (mm)
X(mm)
projection of receiver position
hole 2
hole 1
projection of transmitter 1 position
30
25
20
15
10
5
0
-5
-10
-15
-20
-25
-30
-25
-20
-15
-10
-5
0
5
10
15
20
25
30

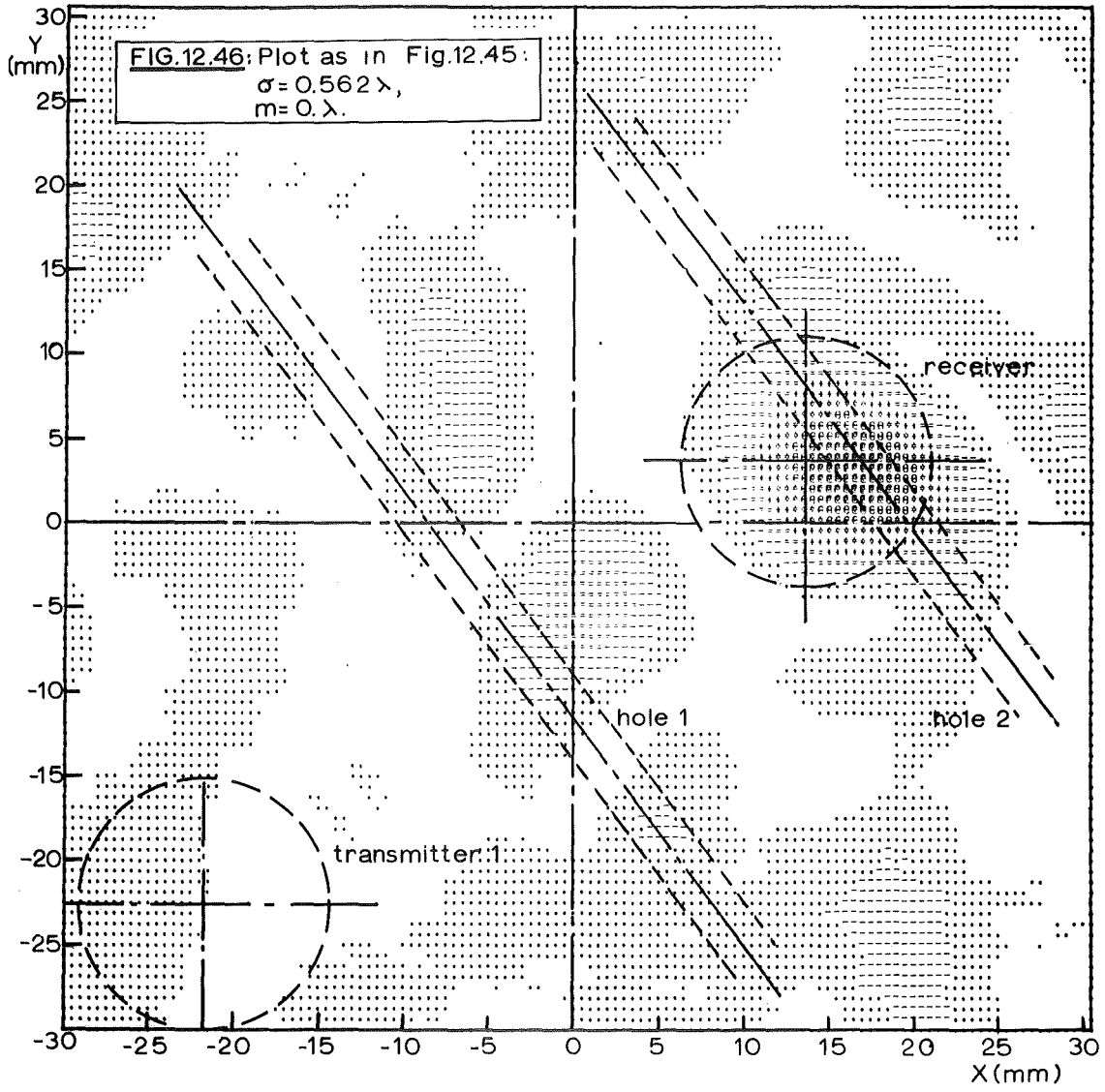
FIG.12.46: Plot as in Fig.12.45:
σ = 0.562 λ,
m = 0. λ.
Y (mm)
X (mm)
receiver
hole 1
hole 2
transmitter 1
30
25
20
15
10
5
0
-5
-10
-15
-20
-25
-30
-25
-20
-15
-10
-5
0
5
10
15
20
25
30

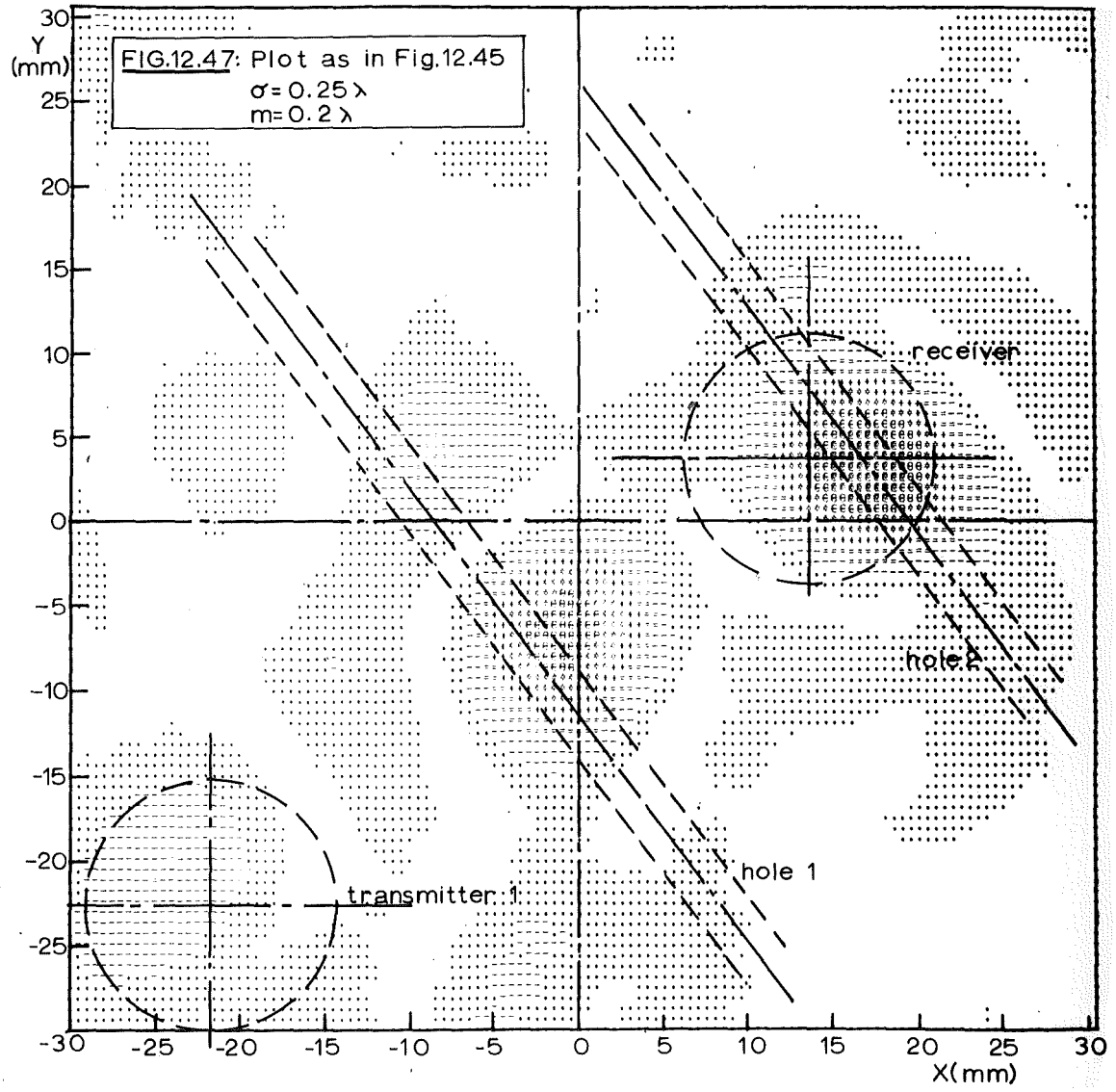
FIG.12.47: Plot as in Fig.12.45
σ= 0.25 λ
m= 0.2 λ
Y (mm)
30
25
20
15
10
5
0
-5
-10
-15
-20
-25
-30
-25
-20
-15
-10
-5
0
5
10
15
20
25
30
X(mm)
receiver
hole 2
hole 1
transmitter 1

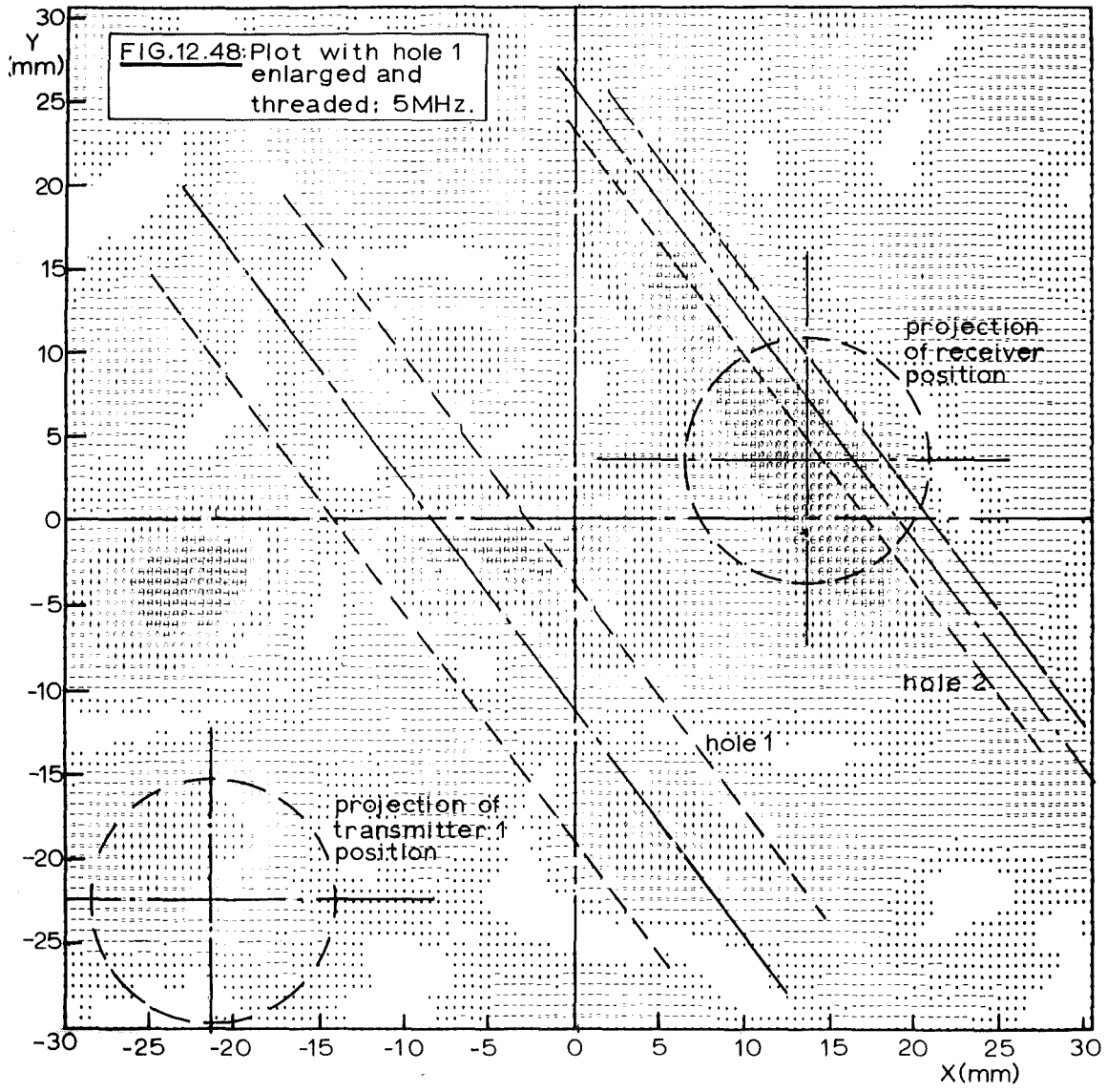
FIG.12.48: Plot with hole 1 enlarged and threaded; 5MHz.
Y (mm)
X(mm)
projection of receiver position
hole 2
hole 1
projection of transmitter 1 position
30
25
20
15
10
5
0
-5
-10
-15
-20
-25
-30
-25
-20
-15
-10
-5
0
5
10
15
20
25
30

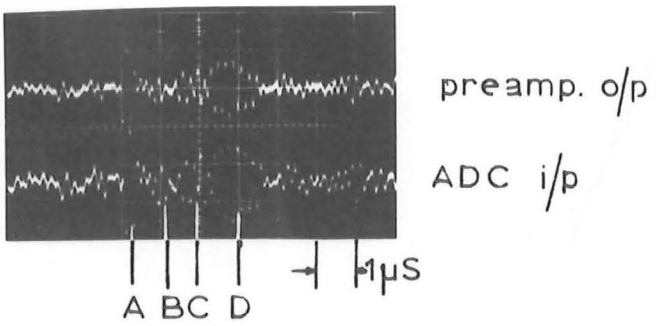

FIG.12.49(a): Typical element signal: data set 6.

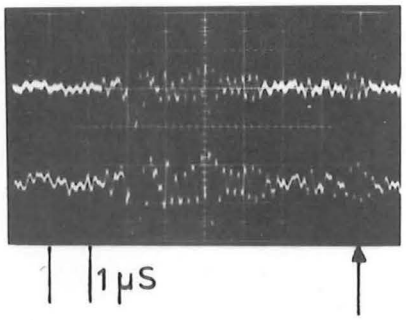

FIG.12.49(b): Similar to above with additional strong return at 9μS.

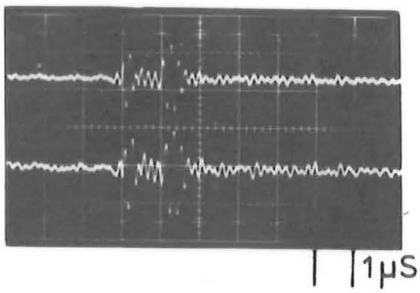

FIG.12.52: Typical element signal: data set 7.

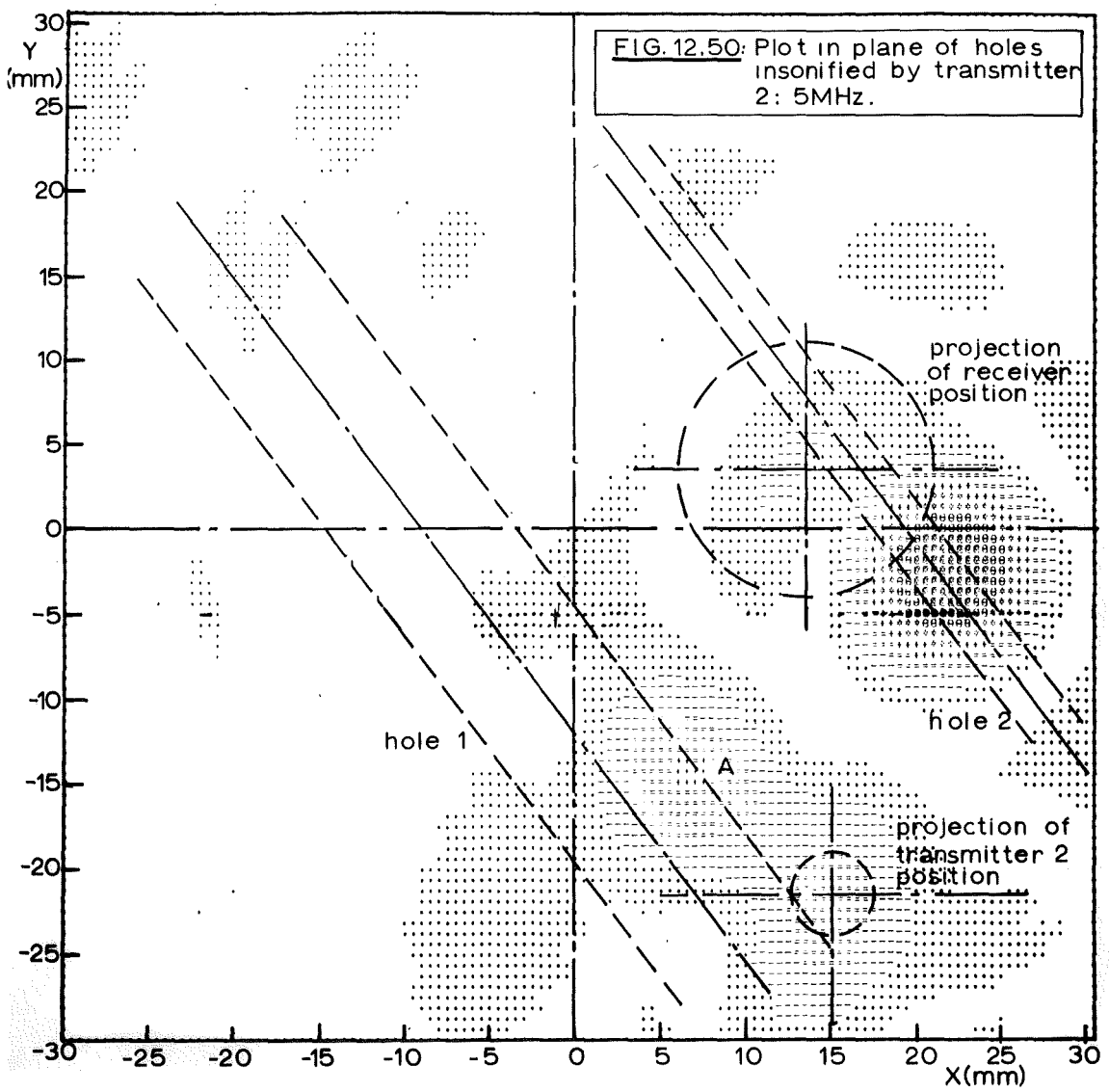
FIG. 12.50: Plot in plane of holes insonified by transmitter 2: 5MHz.
Y (mm)
30
25
20
15
10
5
0
-5
-10
-15
-20
-25
-30
-25
-20
-15
-10
-5
0
5
10
15
20
25
30
X(mm)
projection of receiver position
hole 1
hole 2
A
projection of transmitter 2 position

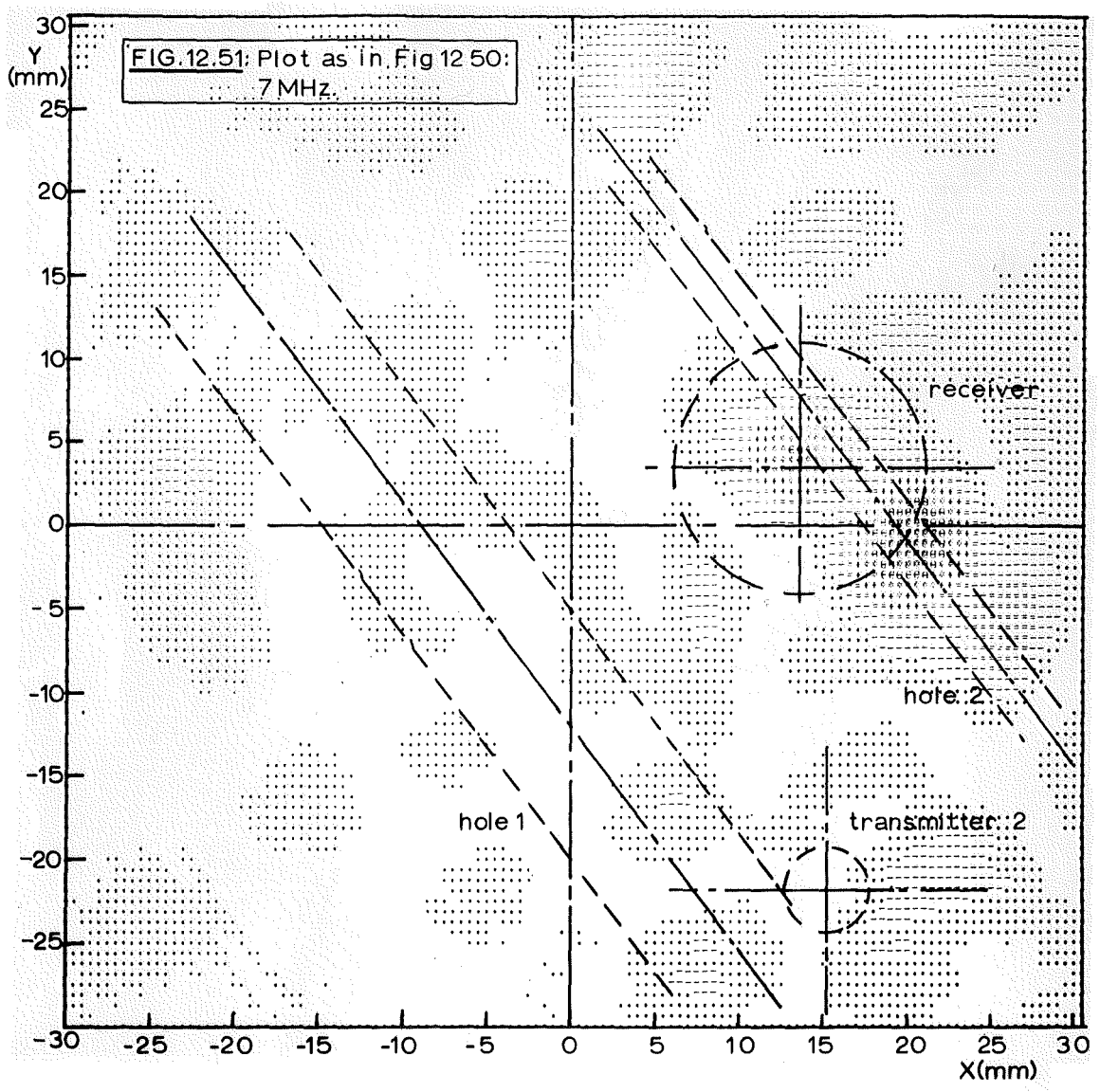
FIG.12.51: Plot as in Fig 12 50: 7 MHz.
Y (mm)
30
25
20
15
10
5
0
-5
-10
-15
-20
-25
-30
-25
-20
-15
-10
-5
0
5
10
15
20
25
30
X(mm)
receiver
hole 2
hole 1
transmitter 2

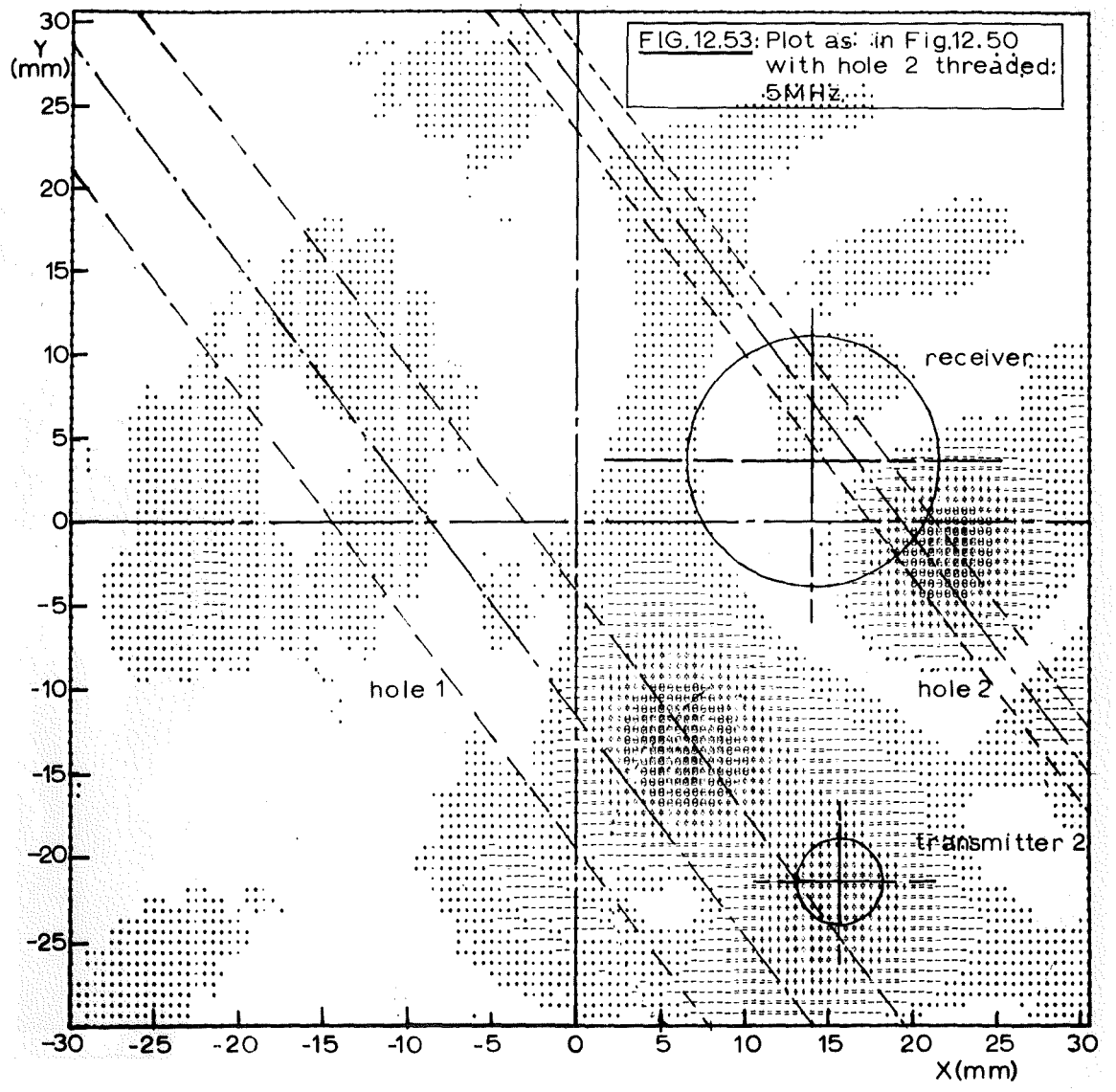
FIG.12.53: Plot as in Fig.12.50 with hole 2 threaded: 5MHz.
Y (mm)
30
25
20
15
10
5
0
-5
-10
-15
-20
-25
-30 -25 -20 -15 -10 -5 0 5 10 15 20 25 30
X(mm)
receiver
hole 1
hole 2
transmitter 2

CHAPTER 13.

GENERAL COMMENTS AND SUGGESTIONS FOR FURTHER DEVELOPMENT.

13.1. INTRODUCTION.

To assess the degree of success achieved by the project we may recall the stated aims in Section 1.1., viz.;

> "Applicability of the method to a range of typical technical materials and possibly bilogical tissue.
>
> Development in a form that encompassed the prototype of a practicable testing apparatus for industrial use."

The stage of development reached over the period reported in this thesis has touched these initial goals in some places, notably in sections of the data collection apparatus built; over a much greater portion the present methods are inadequate but means of achieving the desired ends in a much more efficient fashion have been conceived and in some cases initial work done towards their realization. This category of incomplete development contains the methods of insonifying the materials and interrogating the receiving transducer, transfer of the data to the computer and the actual mathematical techniques used in image formation.

Some aims have not been even partially fulfilled. In particular no work has been done on inspection of biological materials.

The next sections of this chapter follow through the various operations involved in the complete imaging system and discuss for

each, the level of development reached, outstanding problems and the most apparently profitable line for future work.

13.2. INSONIFICATION OF THE MATERIAL.

The most outstanding lack in this portion of the system is the ability to secure adequate spatial diffusion of the acoustic energy and so reduce the dominance of specular reflectors in the images. The technique of introducing a scattering spacer discussed briefly in Chapter 11 corresponds most closely to the usual optical technique of placing a ground glass screen in the path of the illumination and has the practical advantage that the transmitter becomes a single object rather than a number of small items to be attached to the material separately. The main disadvantage is the need to provide an acoustically matching spacer for each material tested so as to avoid reflection effects at the spacer-material interface.

There is no objection to the placement of transmitters at sites, say, on the side of a block of material under examination, provided that echoes from the region of interest in the block reach the receiver within the sampled period. To extend this idea electrical delays can be incorporated to compensate for a wide spread of transmitter positions, allowing objects to be insonified from a wide range of angles simultaneously.*

---

* This technique has been the subject of a patent[1] although with the aim of reducing the spatial spread of insonifying energy rather than increasing it as required here.

Use of a well damped transducer nominally resonant at a frequency below half the maximum frequency permitted by the time sampling on reception, is a convenient and simple way of tailoring the spectrum of the transmitted waveform over the permitted band. Any need for more precise spectrum control demands the use of a thin transducer and passage of the applied excitation through an electrical filter. In any case it is necessary to suppress low frequency components as these add little to the overall resolution and present difficulties when approximations are applied in the processing steps, (as in passing from Equation 5.24(b) to Equation 5.27). Removal of low frequencies also eliminates any effect of normal mechanical vibration acting on the measurement apparatus.

Extra insonifying power is attainable by increasing the exciting voltage applied to the transmitting transducer. The simple avalanche transistor circuit (Appendix 2.1) is limited to an output of 30-40 volts but the arrangement is extendible to provide several hundred volts if needed.[2]

The only difficulty foreseen here, is one of electrical breakdown if a thin transducer element is in use. (The most likely cause being leakage or sparking around the sides of the element).

In the arrangements used the transmitting transducers have been bonded directly to the material under examination. By providing a a backing block for mechanical damping and transmitting into the material through an oil film, the whole arrangement can be rendered far more convenient. Rigid clamping is necessary to maintain a

constant acoustic path during the complete period required to interrogate the receiving array but the more or less permanent bonding was an experimental convenience only.

13.3. RECEIVING TRANSDUCER.

This remains the major difficulty in the whole system. A fully adequate theory of the behaviour of a large, multiply electroded transducer slab more than a small fraction of the acoustic wavelengths thick, still remains to be expounded. One may justify the present usage by the fact that it demonstrably works but a precise quantitative knowledge of the ultimate limitations is lacking. Improved reproduction of the acoustic field demands either reducing the transducer thickness to a very small value and accepting the consequent loss in sensitivity, or increasing the mechanical isolation by notching the plate between elements and compensating for the waveform distortion of the thicker transducer by electrical means such as the matched filter discussed in Section 8.7. Actually there is no reason why the array should not be composed of completely separate piezoelectric elements embedded in a backing material mosaic fashion, particularly if an electronic switching matrix is used for addressing the elements. This would not of course be suited to the image tube because a backing material adequate to stand the static pressure would inevitably be stiff enough to reintroduce close mechanical coupling between the elements. (Quite apart from the problems of electron beam access).

Attachment of the receiver to the material remains a problem

where this is relied on to provide mechanical damping. Provision of a backing block for the receiver is complicated by the need for electrical contact to a large number of points, as preferably the block should be a material of comparable acoustic properties to the transducer material and this cannot be readily achieved with insulating substances. It is considered that a suitable compromise has been reached through the use of a contact adhesive which provides a high bond strength with a very thin layer (of the order of 10μm) between the transducer and examined material but disintegrates when subjected to a modest temperature, (i.e., less than 200°C) or exposed to an appropriate chemical solvent.*

Rather obviously, this is not suitable for fixture of the transducer to organic materials but a very 'flat' arrangement of a switching matrix would permit application of a backing material over the electronics; these, being composed mainly of silicon, silicon oxides and metal, would not represent a great acoustic discontinuity between the transducer material and the backing.

It is felt that the ultimate practicality of acoustic imaging schemes in general, rests with the development of a self-contained, compact receiving array. Permanently sealed tubes go some way towards this aim but where fast, geometrically accurate access to the transducer and minimal disturbance to the signals is required, then some form of switching matrix attached directly to the

---

* A currently available example is Eastman Kodak 910 adhesive.

transducer (and possibly including in the one packet, the necessary scanning shift registers) appears as the best line for development. No other method can approach the ultimate sensitivity of plain mechanical scanning but this is slow; continuously evacuated tubes are electrically noisy and delicate while a completely integrated array, transducers and all, seems an inferior approach to that of separating transducer and switching functions.

13.4. CONTROL OF RECEIVER SCANNING.

This is one area where it is felt that, within the constraints of the overall scheme adopted, the initial requirements of the project have been fully met. The apparatus built provides for all the possible means of scanning that have been discussed and is capable of following a variety of scanning plans. Extension or reduction to any likely size of array is possible merely by adding or removing some standard circuit blocks.

13.5. DATA COLLECTION.

In this section of the system the main shortcomings of the present arrangement are the slow speed of data recording and restricted duration of the samples from each element. Both of these can be overcome by adoption of a more suitable recording media as outlined in Chapter 9. In particular, if it is desired to take an extended record from each transducer element, then magnetic tape storage offers an excellent solution; only the actual section of each recorded return required for the imaging of a particular slice

of the material need be extracted from the tape and placed in the computer central processor at any one time, thus overcoming some limitations of restricted fast storage.

A greater accuracy in the analogue to digital conversion process provided offers some advantage with low reverberation materials but as indicated in Chapter 7, extension to more than twice the present number of 'bits' would be pointless, (except in the unlikely event of a need to image the interior of a tungsten block, this metal has losses only 1/1000th. of those in aluminium).

With the increasing availability of small cheap digital computers comes a further possibility; replacement of the logical control operations presently performed in the special apparatus by a program in the computer. For maximum versatility this program should control all the sequencing of events in the data collection and take over all but the basic scanning operations. Further candidates for implementation in such a computer are the initial one dimensional Fourier transform operation (time to frequency) on the data and transfer of data onto magnetic tape.

The main advantage derivable from this method of control is flexibility beyond anything that could be realistically expected from special hardware. Considering the size of machine necessary to perform the actual imaging operations, a further extension to bypassing any intermediate record of the data on tape and proceeding directly with the image construction in a coupled computer seems remote. This would however bring the whole system back to the very

first concepts of a 'balck box' attached to a transducer at one end and producing pictures at the other.

13.6. IMAGE FORMATION.

From the discussion in Chapter 10 it should be obvious that, despite the geometrical restrictions imposed in the simplest mode of application, any further serious work with usefully sized apertures must use the transform approach. If one wishes to form an image other than 'square on' to the original aperture position, then the extra operations involved do reduce the time advantage compared with a direct convolution, but the reduction of minutes of convolution method time to approximately the same number of seconds for the transform technique cannot be ignored. (This 60/1 factor is derived in 10.5, larger arrays than the 64 x 64 considered there mean even larger relative savings).

In retrospect, it would have been desirable to implement a transform program at the time when the algorithm became available in directly usable form even though only a very small aperture size could have been handled. That this was not done was partially the result of a reluctance to abandon what was by that stage a fully operational and tested convolution program and partially a hope of moving more rapidly to an array size that exceeded the available computing capacity for the transform technique.

13.7. IMAGE DISPLAY.

The present arrangement as described in Chapter 10, and the

pictures produced as in Chapter 12, have rather obvious deficiencies. Noise levels in the signals make an extremely wide variation in presented intensities pointless but an advantage in visual interpretation would be gained by a more 'photographic' type of output.

In the present author's view, the two most pressing lines for further development are the production of a 'solid state' receiving transducer and the performance of image construction by the transform method using the 'fast' Fourier transform algorithm. Once these are achieved the other suggestions for improvement are largely refinements of existing technique.

13.8. OVERALL ASSESSMENT.

Overall, the project has raised many more problems involved in acoustic imaging than it has been possible to resolve. One cannot help admitting a certain frustration at the inadequacies of the work presented here especially when the amount of time spent on fruitless endeavours to achieve satisfactory operation with the image conversion tube is compared with that actually needed to obtain the rather crude results presented in Chapter 12. However, it is felt that the general feasibility of the whole concept of wideband imaging of the interior of solids has been demonstrated. The very poor image quality is a direct function of the basic physics of the situation and while the present approach is capable of providing considerable improvement, one must always be ultimately constrained

by the physical properties of the materials dealt with. Nothing can be done to alter the loss characteristics of given metals and thus extend the frequency band of operation; nor can the undesirable scattering properties of some types of objects be modified, in many practical cases restricted performance must be expected from limitations on the surface area available for insonifying the material and receiving the scattered energy. These limitations set bounds on the potential resolution and the degree to which the images obtained can resemble a normal optical picture, which cannot be overcome by any amount of engineering ingenuity in the apparatus.

REFERENCES FOR CHAPTER 13.

1. Halliday, W. U.S. Patent 3086 195, April 16, 1963.

2. O'Dell, T.H. 'Series operation of avalanche transistors'. Electronics Letters 5, pp.94-95, 6 Nov. 1969.

APPENDIX 1.1.

VACUUM APPARATUS.

The apparatus finally assembled for the image tube has the layout shown in Figure A1.1/1. For satisfactory operation of the tube a vacuum better than 10^{-6} Torr is necessary with 10^{-5} Torr as a limit for any operation. The attainment of this vacuum is critically dependent on a good seal being obtained at the faceplate of the tube which is held in place purely by atmospheric pressure. With the pump presently installed, full capacity is maintained down to 10^{-6} Torr at the pump mouth. The baffles, cold trap and valve, reduce the capacity to approximately one fifth* of the unbaffled value but are essential to prevent pump fluid contamination of the tube cathode. (Hydrocarbon fluids, e.g., 'Apiezon B', decompose to form carbon deposits on the hot cathode but these can be tolerated to some extent as removal is possible by over-running the cathode for brief periods. The modern silicone fluids however decompose to a silica layer, ruining the cathode completely).

With an effective capacity of 30 litres/sec. and a required pressure of 10^{-6} Torr the maximum tolerable leak[1] is;

$$Q_L = P_u S_E \qquad .. \text{A1.1/1}$$

---

* Estimated from the discussion in Reference 1.

P_u = pressure

S_E = effective pumping capacity

from which, $Q_L = 3 \times 10^{-5}$ Torr litre/sec.

If this leak is concentrated in a single hole and is effectively a tube of length 2mm say, then the hole diameter cannot exceed 9 μm. Little can be done to improve this as the image tube itself places a length of about 15cm of 30mm internal diameter tubing between the faceplate and the pump connection limiting the maximum pumping speed to 20 litres/sec.[2] regardless of the actual pump capacity.

With this arrangement it was found to be possible to reach 10^{-6} Torr and the main trouble came from contamination in the tube due to exposure to the atmosphere rather than leaks. For this reason the tube should be kept sealed at a low pressure when not in use.

REFERENCES FOR APPENDIX 1.1.

1. Yarwood, J. 'High vacuum technique'. Chapman and Hall, London, 4th Edition, 1967, p.187.

2. Ibid. Figure 70, p.154.

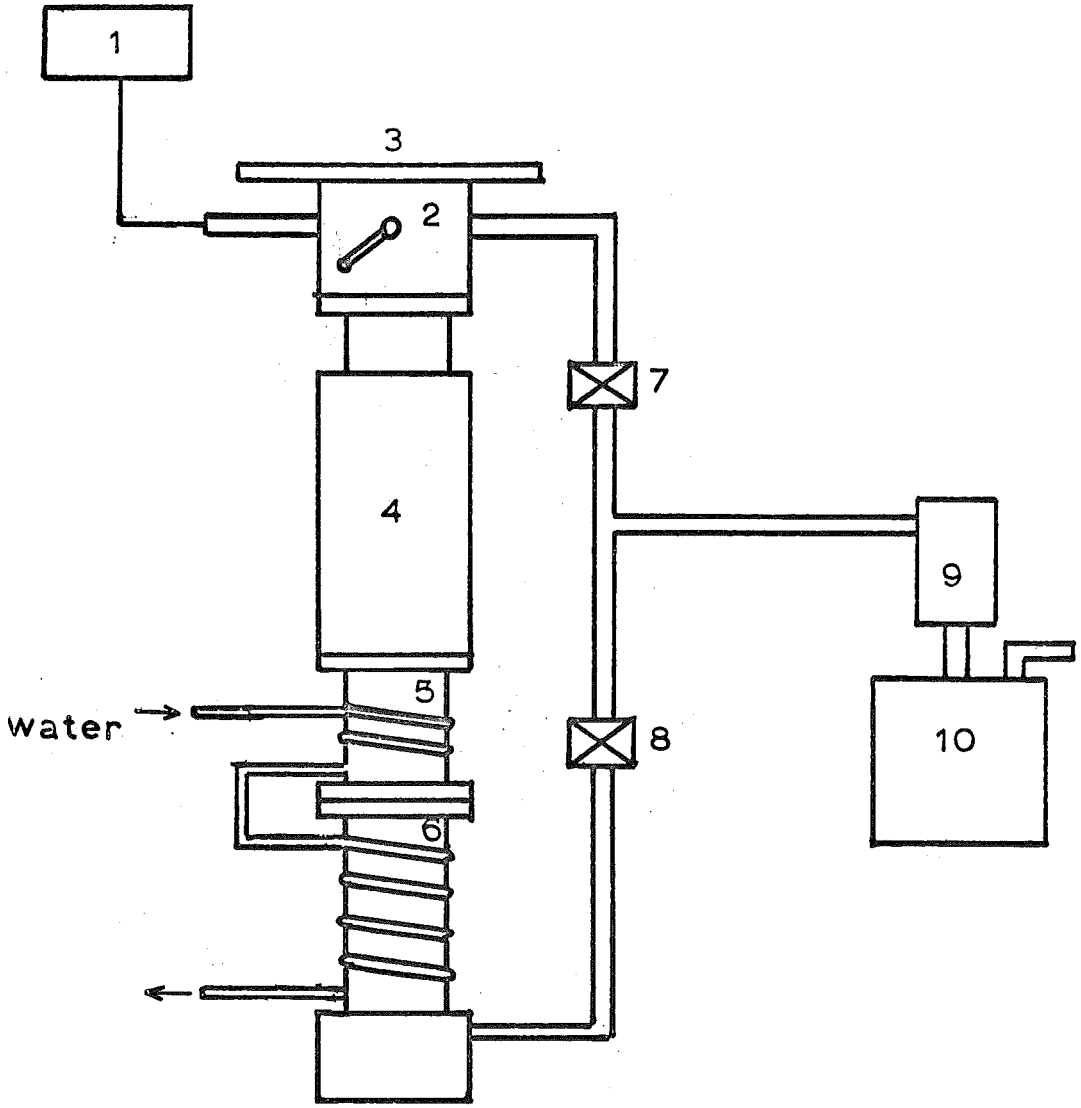

1. vacuum gauge (Dynavac IG 107, 2×10^{-3} – 10^{-7} torr)
2. baffle valve, (2 inch, Dynavac SV 2)
3. work face
4. cold trap
5. oil trap
6. 2 inch water cooled diffusion pump (Dynavac OD 150, 150 litres/sec)
7, 8. valves
9. moisture trap
10. rotary pump (Metrovac DR 1)

FIG. A1.1/1: Vacuum apparatus

APPENDIX 1.2.

MECHANICAL CONSIDERATIONS IN BONDING THE TRANSDUCERS.

Two methods of attaching the transducers have been used;

1. Gallium metal.
2. Contact adhesive.

1. Gallium bonding.

The use of low melting point metals is well established for the bonding of transducers and provides a convenient means of establishing a conducting bond with acoustic properties similar to those of the transducer material. The difficulty of controllably heating the large metal blocks used led to a desire for the lowest melting point metal possible. Bonding to aluminium presents well known difficulties because of the oxide layer and the only metals that seemed promising for bonding without elaborate surface preparation were gallium and indium. (This latter is very common for transducer bonding). The very low melting point of gallium ($29^{\circ}C.$) made heating the material very easy and for a normal laboratory environment it was considered that this temperature would be adequately above any encountered.

Some difficulty was experienced in getting the bond to solidify and refrigeration down to $\approx 5^{\circ}C.$ proved necessary to induce crystallization. However the acoustic results obtained appeared perfectly satisfactory and this method was used for all the transducers employed in the experiments of Chapter 12. When the

method was used on the aluminium spacer described in Chapter 11 the result appeared initially satisfactory but after some hours it was noted that a distinct colour change had occurred in the metal progressively spreading from the surface bonded to the transducer. This was permanently* arrested by cooling the metal but the mechanical properties of the aluminium were drastically altered. In the affected region the metal became soft and 'crumbly' and could easily be penetrated by a fingernail.

No detailed metallurgical data appears to be available on aluminium-gallium alloys but a phase diagram[1] for aluminium-indium (Figure A1.2/1) indicates that for very small percentages of indium a liquid phase (L) can persist down to temperatures well below the solidifying temperature of pure indium (156°C). Presuming that a similar effect occurs with gallium then the observed effects are explained. The grains of aluminium become surrounded by the liquid Al-Ga alloy and the whole metal has the strength of only this alloy.

A similar effect must have occurred in the much larger blocks used for the experiments but the severity has presumably been reduced by the much greater bulk of aluminium as no colour change of the bulk metal has become apparent over a period of a year. However, the possibility of this contamination of the material under examination rules out the use of gallium for applying transducers to valuable specimens of aluminium. No similar effects have been

---

* In six months, no further change has occurred.

observed with steel and there appears to be no reason why gallium (or indium) cannot continue to be used for this metal. In any case, low melting point solders can be used for metals without the tenacious surface layer of aluminium.

2. Contact adhesive.

As an alternative to metal bonds a very thin film of adhesive may be employed. This has the disadvantage of placing a capacitor in series with the transducer unless these are obtained with the 'bottom' electrode continued around the side of the element. The device of inserting a metal mesh between the transducer and the block cannot be employed as the thinnest meshes available are a significant part of a wavelength thick at the MHz frequencies of operation.

Some considerable success has been achieved with a contact adhesive marketed as 'Aron Alpha 201'*. Bond thicknesses obtained with moderate pressure on the setting adhesive have been sufficiently thin to give overall responses through two transducers comparable to those observed with a metal bond.

Measurement of the input impedance of the transducer elements at a low frequency (1 kHz) reveals that the high capacitance value observed with the free element (effectively C_o - Appendix 3.1) diminishes only slightly when a measurement is taken between the free electrode and the metal to which the transducer is attached.

---

* Toagosei Chemical Industry Co. Ltd, Tokyo.

The values obtained indicate apparent bond thickness of the order of 0.1 μm, a figure which is considered unlikely. Most probably some ohmic contact is occurring through 'high spots' on the electrode and material surfaces.

Removal of transducers fixed by these adhesives presents some problems. Various organic solvents are recommended but the action is very slow for a thin film sandwiched between surfaces of any area. The alternative is heating but temperatures as high as 230°C. are needed to cause decomposition. This will not damage the transducer elements (Curie temperature of PZT5A is 350°C.) but is sufficiently high that some metallurgical effects are possible, particularly with aluminium alloys.

REFERENCE FOR APPENDIX 1.2.

1. 'Metals Handbook'.
Am.Soc. Metals. 1948, p.1162.

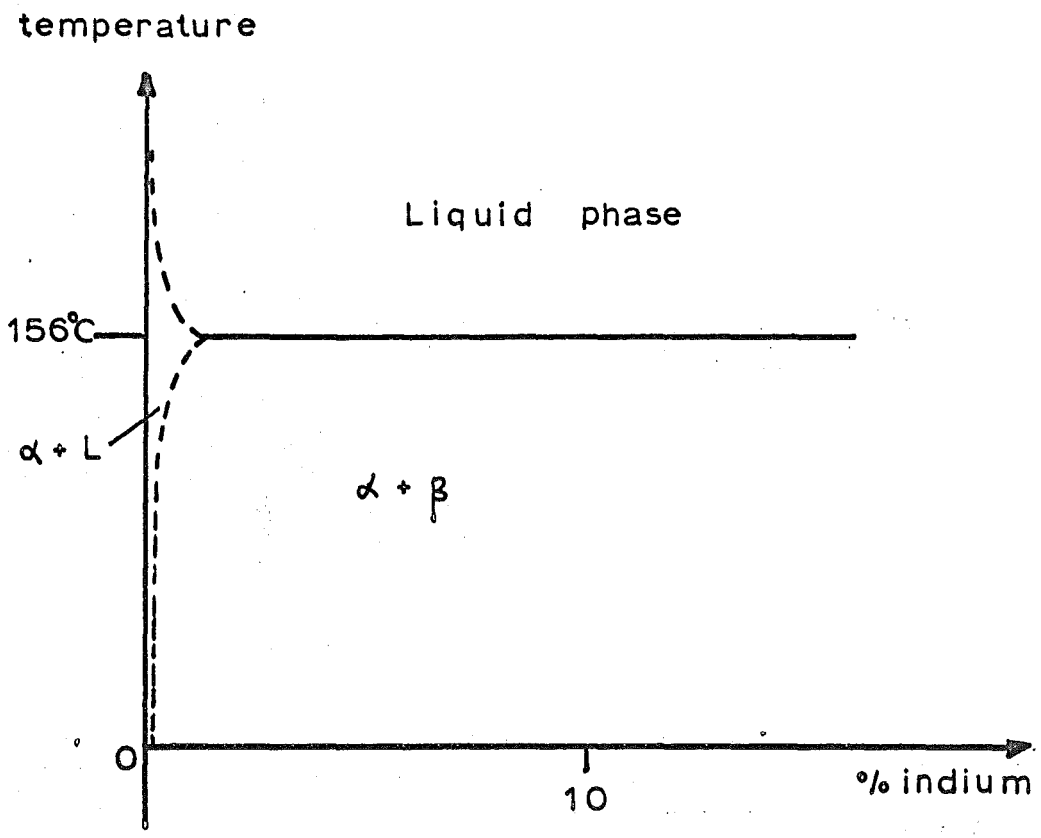

FIG.A 12/1: Al– In phase diagram

α phase is pure indium
β phase is pure aluminium

APPENDIX 2.

DETAILS OF SPECIAL ELECTRICAL APPARATUS.

This appendix is provided purely as a reference to various items that it was found necessary to construct in the course of the experiments. None of items represent any unique examples of electronic circuits. The items detailed here are supplementary to those constructed and described by Cook.

A2.1. ELECTRICAL TRANSMITTERS.

(a) The transmitter used in the 'wideband' measurements is basically a simple avalanche pulse generator with the pulse determining circuit elements (C_1 in particular) rather larger in value than in usual 'sub-nanosecond' pulse applications. Some additional pulse shaping circuitry has been included to ensure highly consistent triggering from the control signals.

Some consideration was given to charging the capacitance C_o of the transducers directly and discharging this abruptly rather than transferring charge from a separate capacitor C_1 but if resistive damping is needed the damping resistor (R_1) prevents operation of the circuit unless C_1 is present.

The circuit is shown in Figure A2/1. Normally the circuit is connected to the transducer element through about 30cm of 50Ω coaxial cable with a further 10Ω damping resistor mounted directly across the transducer.

The output waveform produced depends on the load. Some examples are shown in Figure 12.17(b) and in Appendix 3.1.

(b) To produce the 'tone burst' waveforms shown in Figure 12.18, the gating circuit depicted in Figure A2/2 was used followed by a simple 'Class A' power/amplifier using two type EL500 tubes in parallel, with an anode supply of 350 volts for the final stage. The coupling to the transducer uses a 'Pi coupling' network. Operation is possible over a range of 1 MHz about 5 MHz.

The analogue gating circuit performance is depicted in Figure A2/3 from which it will be seen that the output is completely free from 'offsets' or significant transients. Leakage in the 'off' condition is 46dB down on the 'on' signal at 5 MHz. The basic concept in the circuit is the elimination of transients by cancellation in the balanced output - the phase split signal components passed through the two identical gates are recombined in phase while the transients have the same polarity at both D and E and cancel. Capacitor C compensates for the input capacitance of the next stage driven from the 'upper' transistor.

A2.2. RECEIVING TRANSDUCER AMPLIFIER.

This amplifier had the design criteria of low noise amplification of input signals as low as a few hundred microvolts over at least a 10 MHz bandwidth. The analogue to digital converter in Cook's apparatus requires an input signal of 2V P-P so the total

gain necessary in the signal path may be as high as 10,000. In the experiments with aluminium blocks, transducer signals were more typically 1-2 mV and the required gain 1000-2000.

This was provided in two sections, firstly a gain of up to 150 times in the preamplifier described immediately below and secondly a further gain of up to 20 times in the amplifier discussed later. (In some of the experiments conducted with steel blocks an additional gain of 2-5 times was obtained from a Tektronix type 1A1 amplifier).

The preamplifier is a simple application of an integrated circuit 'video' amplifier (Fairchild μA733). This device is a balanced amplifier with a gain of 10, 100 or 400 controlled by connecting appropriate terminals. In the 'single ended' mode approximately one half these gains are obtainable. (With the particular device used gains of 4,40 and 145 were realized).

A standard impedance of 50Ω was adopted for all wideband analogue signal interconnections and feeding into this value of impedance the linear range of amplification is restricted to outputs below about 0.4 volts peak. This was however quite adequate in the present application. The circuit is shown in Figure A2/4. The noise performance has already been considered in Chapter 7 (7.3.3). The amplifier has an essentially 'flat' frequency response to beyond 15 MHz.

The further gain necessary has been provided by part of a circuit that was originally constructed as part of a conventional

imaging system display and the amplifier is complicated with provision for functions that are not needed in the present arrangement. For this reason only a summary of performance is given. This amplifier has frequency characteristics which serve to shape the overall response of the prequantizing signal path to a form appropriate to the sampling frequency. The response is shown as Figure A2/5. The 12 MHz response is 10 dB down and falls at approximately 24 dB per octave from this frequency on.

The amplifier phase shift affects all elements equally and is of no concern in the overall imaging process (7.4.2.).

A signal of 5 volts P-P can be obtained without distortion at the output of this amplifier when operating into a 50Ω load.

A2.3. PAPER TAPE PUNCH CONTROL CIRCUITRY.

This item receives the encoded signals to be punched in parallel form and provides a power amplification from the input signals at the standard logic levels in the apparatus ('0' 0 to 0.3 volts, '1', > 1.0 volts) to the 28 volt, 1 ampere signal required on the magnets of the tape punch.* Two further inputs provide a 'punch' command and allow the tape advance after each punching to be externally controlled if desired. The synchronising pulse derived from a magnetic pickup on the machine is shaped to the standard logic form and provided as an output.

---

* Teletype, Type BRPE.

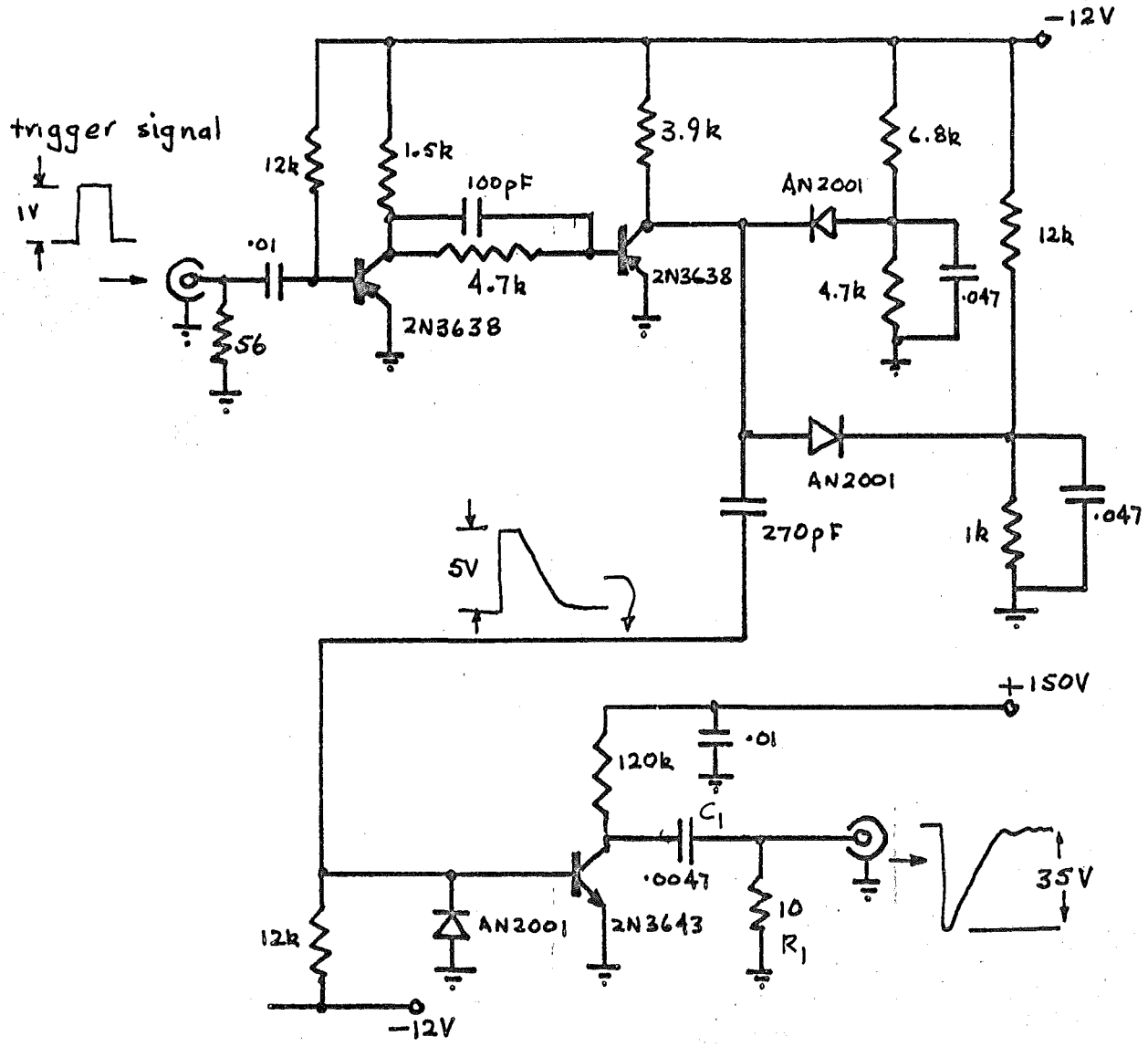

FIG.A2/1: Pulse transmitter

resistances in ohms

capacitances in μF (except as noted)

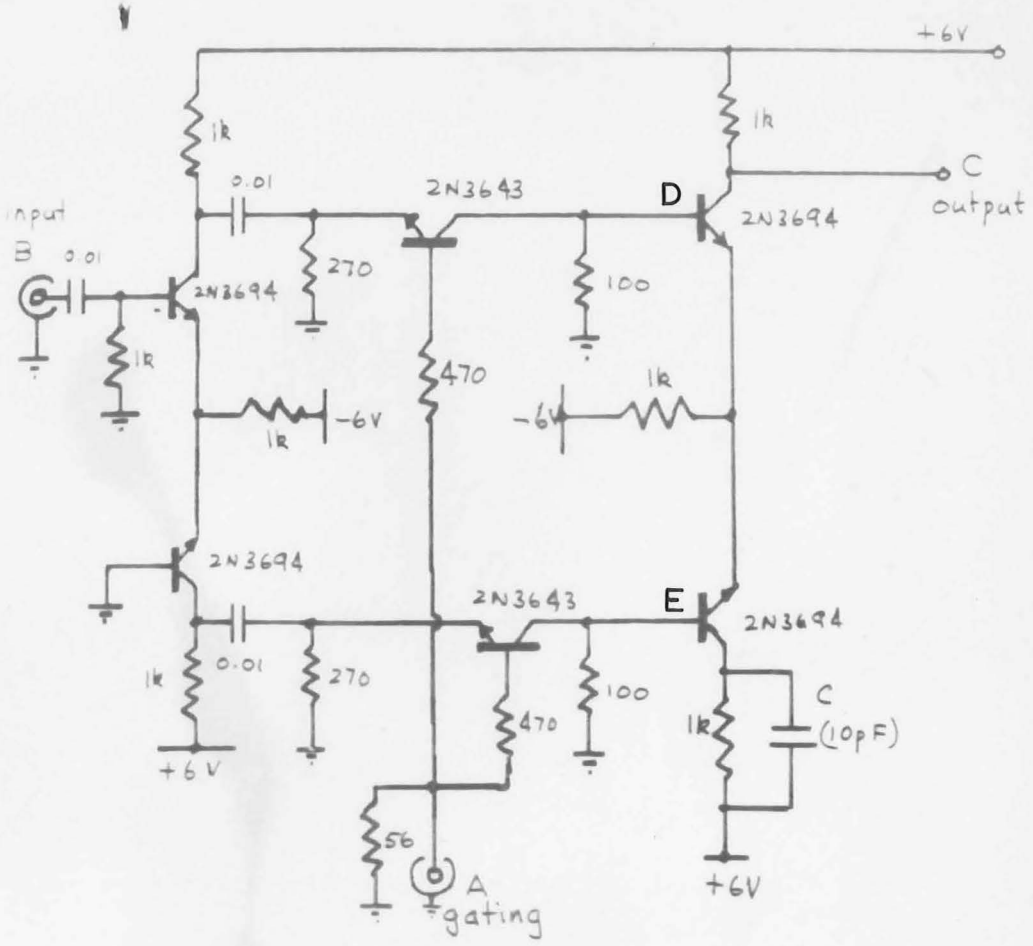

FIG. A 2/2: Analogue gate for 'tone burst' transmission

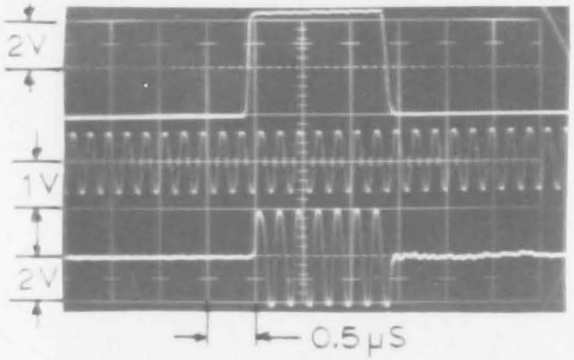

FIG. A 2/3: Gate performance

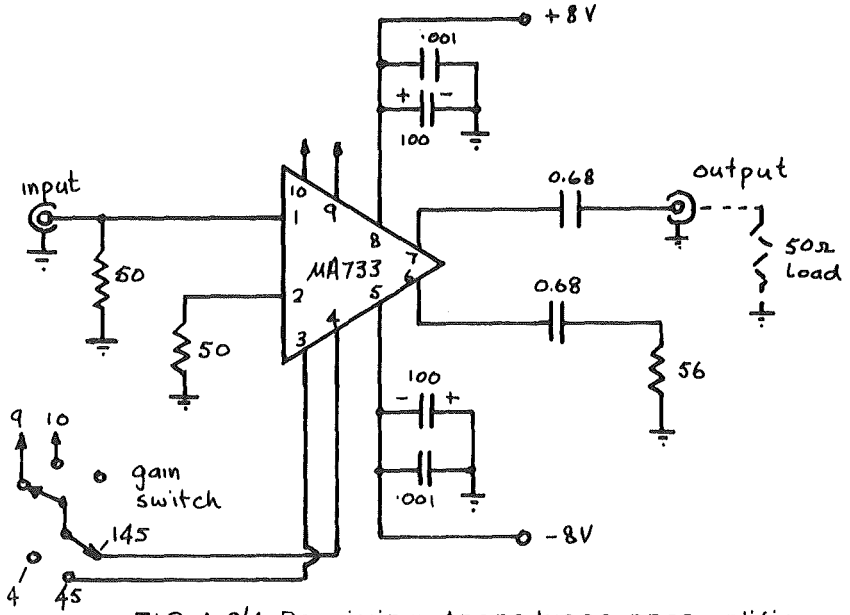

FIG. A·2/4: Receiving transducer preamplifier

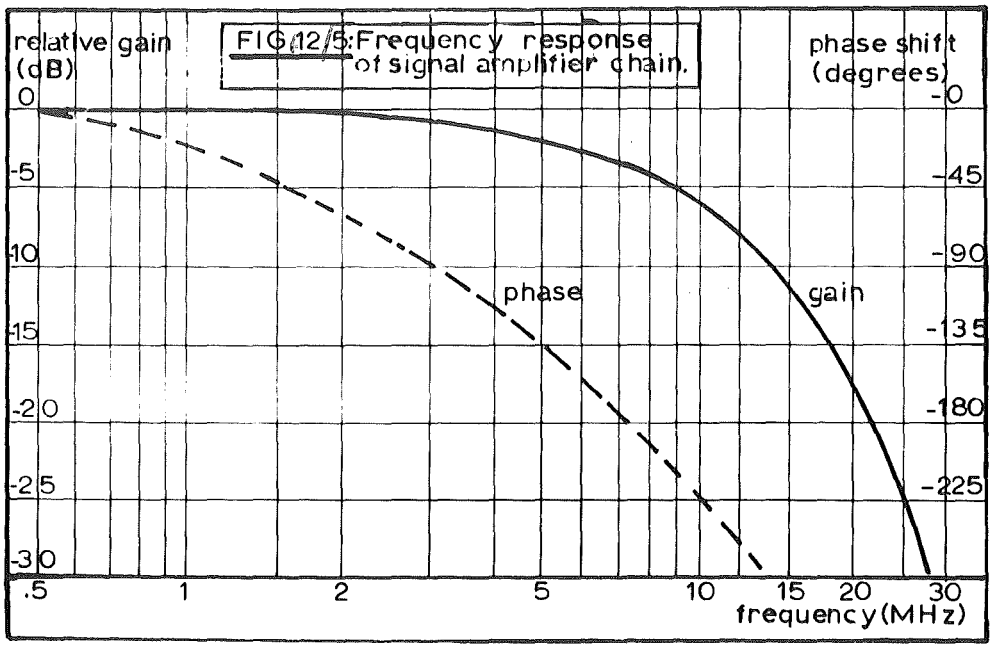

APPENDIX 3.1.

ELECTRO-ACOUSTIC RESPONSE OF THE TRANSMITTING TRANSDUCER.

The basic assumptions made in deriving the equivalent circuit model for a thickness mode transducer bonded to a semi-infinite space on one face and free on the other have been detailed in Section 3.3. The circuit under examination is shown in Figure A3.1/1.

The basic requirement is to determine the force developed at the mechanical terminals given some form of the driving voltage $w_o(t)$.

The calculation proceeds via a Thevenin equivalent circuit approach. The impedance looking back into the mechanical terminals A,B is found for $w_o(t)$ short-circuited and then the driving 'voltage' (really force, as this is on the mechanical side of the transformer in the circuit model) determined as a function of frequency. $w_o(t)$ is a known waveform in the apparatus and thus $w_2(t)$ may be determined as a function of time (or frequency as $W_2(\omega)$).

As a means of providing an experimental check on the calculated waveforms the current I flowing into the transducer electrical terminals is also computed and can be measured in an actual arrangement. Direct measurement of the actual acoustic waveform demands either a receiver of very uniform response up to 15 MHz or

extensive compensation for the response of a thicker transducer. As this compensation would also depend on the same circuit model for the response of the receiver then obviously the check thereby obtained is open to doubt. No very thin receiving transducers were available and the only other readily measurable variable influenced by the transducer response is the input current.

Looking into the transducer from A-B with $w_o(t)$ shorted we have;

$$Z_T(\omega) = (2Zj\tan\tfrac{\omega\alpha}{2}) \,||\, 1 \left[\frac{2Z}{j\tan\frac{\omega\alpha}{2}} + 4N^2 \left(\frac{1}{j\omega(-C_o)} + \frac{1}{j\omega C_o} \,||\, 1 \; Z_{TX}(\omega) \right) \right]$$

.. A3.1/1(a)

with $\alpha = \frac{d}{v_t^D}$ and $||1$ meaning "in parallel with".

$$= \frac{2j\,Z\tan\frac{\omega\alpha}{2}\left\{ \frac{2Z}{j\tan\frac{\omega\alpha}{2}} + \frac{4N^2}{j\omega C_o}\left[\frac{Z_{TX}(\omega)\cdot j\omega C_o}{1+Z_{TX}(\omega).j\omega C_o} - 1 \right] \right\}}{2j\,Z\tan\frac{\omega\alpha}{2} + \frac{2Z}{j\tan\frac{\omega\alpha}{2}} + \frac{4N^2}{j\omega C_o}\left[\frac{Z_{TX}(\omega)\cdot j\omega C_o}{1+Z_{TX}(\omega).j\omega C_o} - 1 \right]}$$

.. A3.1/1(b)

Simplifying this by standard algebraic manipulation gives;

$$Z_{T(\omega)} = \frac{2\,Z\,j\tan\frac{\omega\alpha}{2}\left\{ 1 - \frac{2N^2\tan\frac{\omega\alpha}{2}}{ZC_o(1+Z_{TX}(\omega)\cdot j\omega C_o)} \right\}}{1 - \left[\tan^2\frac{\omega\alpha}{2} + \frac{2N^2\tan\frac{\omega\alpha}{2}}{Z\omega C_o(1+Z_{TX}(\omega)\cdot j\omega C_o)} \right]}$$

.. A3.1/2(a)

and by the substitution, $1-\tan^2(\frac{\omega\alpha}{2}) = \frac{2\tan(\frac{\omega\alpha}{2})}{\tan(\omega\alpha)}$

we derive Z_T in the form;

$$Z_T(\omega) = Z\, j \tan\omega\alpha \left\{ \frac{1 - \frac{2N^2 \tan\frac{\omega\alpha}{2}}{\omega ZC_o(1+Z_{TX}(\omega).j\omega C_o)}}{1 - \frac{N^2 \tan\omega\alpha}{\omega ZC_o(1+Z_{TX}(\omega).j\omega C_o)}} \right\} \quad .. \text{ A3.1/2(b)}$$

The Thevenin equivalent 'voltage' is derived by considering the voltage at A-B when these terminals are open circuited. This may be done by consideration of the circuit in Figure A3.1/2. Z_p represents the reflected impedance on the electrical side of the transformer and since this is a frequency domain analysis we must replace the time varying voltage $w_o(t)$ by its spectrum $W_o(\omega)$.

Using the loop currents method gives;

$$W_o(\omega) = I_1 Z_{TX}(\omega) + (I_1 - I_2)\frac{1}{j\omega C_o} \quad .. \text{ A3.1/3(a)}$$

$$0 = \frac{-I_1}{j\omega C_o} + I_2\left(-\frac{1}{j\omega C_o} + Z_p + \frac{1}{j\omega C_o}\right) \quad .. \text{ A3.1/3(b)}$$

which solves for I_2 in the form;

$$I_2 = \frac{j\omega C_o W_o(\omega)}{j\omega C_o Z_p(1+j\omega C_o Z_{TX}) - 1} \quad .. \text{ A3.1/4}$$

and the resultant secondary 'current'(strictly particle velocity) is $\frac{I_2}{2N}$, for an output 'voltage' across A-B of;

$$V_T(\omega) = \frac{I_2}{2N} \cdot 2j \tan\frac{\omega\alpha}{2}$$

$$= W_o(\omega) \frac{j\omega C_o \cdot 2j Z_o \tan\frac{\omega\alpha}{2}}{2N[j\omega C_o Z_p(1+j\omega C_o Z_{TX}(\omega)) - 1]} \quad .. \text{A3.1/5}$$

further noting that Z_p is $\frac{1}{4N^2}$ times the secondary impedance given by;

$$Z_o = 2Z\left\{\frac{1}{j\tan\frac{\omega\alpha}{2}} + j\tan\frac{\omega\alpha}{2}\right\} \quad .. \text{A3.1/6(a)}$$

$$= -4Zj\cot\omega\alpha$$

$$\text{or} \quad Z_p = \frac{Z}{N^2 j\tan\omega\alpha} \quad .. \text{A3.1/6(b)}$$

we obtain finally,

$$V_T(\omega) = \frac{W_o(\omega)}{N} \frac{\omega C_o Z \tan\frac{\omega\alpha}{2}}{1 - \frac{\omega C_o Z}{N^2 \tan\omega\alpha}(1+j\omega C_o Z_{TX}(\omega))} \quad .. \text{A3.1/7}$$

Hence the mechanical output of the transducer $W_2(\omega)$ may be immediately derived from the reduced circuit in Figure A3.1/3 as;

$$W_2(\omega) = \frac{V_T(\omega)\ Z_m}{Z_T(\omega) + Z_m} \quad .. \text{A3.1/8}$$

and the time waveform obtained by a Fourier transform operation on $W_2(\omega)$.

The current into the transducer cannot be derived directly from the Thevenin circuit but must be obtained by calculating the electrical impedance the transducer element presents to the driving waveform. The relevant circuit is shown in Figure A3.1/4. From this we have;

$$Z_{in}(\omega) = \frac{\frac{1}{j\omega C_o}\left\{-\frac{1}{j\omega C_o} + \frac{1}{4N^2}\left[\frac{2Z}{j\tan\frac{\omega\alpha}{2}} + \frac{2Z\, j\tan\frac{\omega\alpha}{2}.Z_m}{Z_m+2Z\, j\tan\frac{\omega\alpha}{2}}\right]\right\}}{\frac{1}{j\omega C_o} - \frac{1}{j\omega C_o} + \frac{1}{4N^2}\left[\frac{2Z}{j\tan\frac{\omega\alpha}{2}} + \frac{2Z\, j\tan\frac{\omega\alpha}{2}.Z_m}{Z_m+2Z\, j\tan\frac{\omega\alpha}{2}}\right]} \quad .. \text{ A3.1/9}$$

which emerges in the form;

$$Z_{in}(\omega) = \frac{1}{j\omega C_o} + \frac{2N^2\, j\tan\frac{\omega\alpha}{2}}{\omega^2 C_o^2 Z\left[1 - \frac{Z_m\tan^2\frac{\omega\alpha}{2}}{Z_m+2Z\, j\tan\frac{\omega\alpha}{2}}\right]} \quad .. \text{ A3.1/10}$$

This equation reveals that for low frequencies the input impedance is almost purely capacitive and attributable to the static capacitance C_o. At zero frequency the input impedance is infinite and no energy is radiated from the transducer, (taking the limiting case of Equation A3.1/8 as $\omega \to 0$ gives $W_2(0) = 0$). At frequencies where $\frac{\omega\alpha}{2}$ is an odd multiple of $\frac{\pi}{2}$ the impedance reduces to;

$$Z_m = \frac{1}{j\omega C_o} - \frac{4N^2}{\omega^2 C_o^2 Z_m} \quad .. \text{ A3.1/11}$$

The real part of this represents the 'radiation resistance' of the transducer at its resonant frequencies, $\omega = n\frac{\pi}{\alpha}$, $n = 1,3,5--$. The negative sign arises from the current flow convention implicit in the present derivation. Here the 'current' at terminals A,B has been taken as flowing from A to B for the positive direction. The original derivation of the transducer model has the opposite direction for positive 'current' (particle velocity) at these

terminals, so Z_m should be considered here as negative to give a positive radiation resistance.

The actual electrical current into the electrical terminals of the transducer is given by;

$$I(\omega) = \frac{W_o(\omega)}{Z_{TX}(\omega) + Z_{in}(\omega)} \qquad .. A3.1/12$$

The equations for the mechanical force developed and the input current to the transducer have been set up for automatic computation. The program accepts as input samples of the waveform $w_o(t)$ at intervals of 10 nS over a total of 256 samples giving approximately 2.6 μS of signal, sufficient to contain any of the short transient excitations used. The spectrum $W_o(\omega)$ is computed as sample values at 1/2.56 MHz intervals from D.C. and the various frequency dependent impedances calculated at these frequencies, from information giving the values of transducer thickness, propagation velocity, acoustic impedance, piezoelectric constants and relative permittivity. The value of the electrical impedance Z_{TX} must also be given at each frequency together with Z_m.

The program performs the appropriate operations indicated above to derive the spectrum of the mechanical signal and the current then finds the corresponding time waveforms. The time waveforms $w_o(t)$, $w_2(t)$ and of the current, are printed graphically together with the spectra of the input waveform and of the mechanical output. The program assumes that the transducer has unity area (1 metre^2) so the computed force can be regarded as the

stress in N/m^2 produced by the transducer. The magnitude of the current waveform calculated must be multiplied by the actual area of the transducer used and the transmitter impedance Z_{TX} also scaled by the area. For example, if Z_{TX} is 5Ω say, and the transmitter is feeding a transducer $20mm^2$ in area, then for the purposes of the program the value given must be $\frac{5 \times 20}{10^6}$ or $10^{-4}\Omega$. Normally the impedance Z_{TX} will be representable as a resistance and inductance in series. The inductance must also be scaled in the same manner as the resistance. More complex forms of Z_{TX} can be treated by reducing them to a series R-L-C circuit and the capacitance scaled inversely to the area. However, the simple R-L form is most likely. (In fact, one may wish to make L large enough to resonate with C_o if the transducer is to operate with long pulses of a single frequency).

Although only cases of direct interest to the present system have been computed the program is quite general and could easily be extended if necessary to accommodate driving waveforms of much longer duration, or take account of the reactive component in Z_m introduced by very small transducers. Any frequency range for which the original model is valid can be accommodated with small alterations.

Examples:

1. Burst of sinusoid (6 cycles at 5 MHz).

The relevant functions are shown in Figure A3.1/5. Part (a) shows the open circuit driving waveform $w_o(t)$ applied behind a

a 12Ω impedance (Z_{TX}). (b) shows the computed spectral magnitude with the characteristic |sinx/x| form centred on 5 MHz. In (c) the computed spectrum of the mechanical output is displayed. This is seen to be similar to that of the driving waveform but with reduced magnitude at high and low frequencies, illustrating the bandpass filter effect of the transducer. The computed mechanical output $w_2(t)$ is shown in part (d). With the 2 volt peak-peak input voltage assumed in the calculations $w_2(t)$ has a peak value of $7.5 \times 10^4 N/m^2$. With the actual amplitude in (a) (1.5V P-P) a value of $5.6 \times 10^4 N/m^2$ would be anticipated.

Figures A3.1/5 (e) and (f) show the computed and measured (on a 5mm diameter transducer) input current waveforms. For a $1m^2$ transducer and 2 volts P-P excitation the computed maximum current was 687A. Appropriate area scaling gives 13.6mA, and allowing for the lower $w_o(t)$, 10.2mA. The measured value (e) was 11mA.

2. Short pulse.

This driving waveform (shown in Figure 3.1/6(a)), was that produced by the transmitter shown in Figure A2/1. Z_{TX} with this transmitter was 5Ω in series with approximately 25nH. (b) shows the computed spectrum exhibiting a gradual roll off in amplitude with frequency.

The spectrum of the acoustic waveform (c) reflects the greatly broadened spectrum of the excitation compared with the

case of a sinusoidal burst. Significant energy now appears around odd multiples of the fundamental resonant frequency of the transducer. The section between 0 and 10 MHz corresponds to that assumed in calculations of system sensitivity (7.3.3).

Figure 3.1/6(a) shows the computed mechanical waveform. With suitable correction for the actual value of $w_o(t)$ the maximum stress generated was $1.07 \times 10^6 N/m^2$. The waveform approximates to the e^{-at}sinbt from assumed in some calculations. Computed and measured input currents are shown in parts (e) and (f) of the figure. Suitably corrected, the calculated peak value of 47024A for 34 volts excitation on a $1m^2$ transducer, becomes 1.15A (for a 5mm diameter transducer). The measured value is 1.05A.

3. 'Square' pulse.

This waveform did not correspond to any driving waveforms actually used but was convenient to generate. The various time waveforms and spectra are shown as before in Figures 3.1/7(a)-(f). The computed current maximum for a 10 volt pulse behind 12.5Ω was 5075A into a $1m^2$ transducer. With the 2 volt pulse actually used and a 5mm diameter transducer, the expected amplitude becomes 20mA compared with an indicated value of 19mA.

In all these cases good quantitative agreement has been obtained between the measured and calculated peak values of currents. Agreement between the actual and calculated waveshapes

is considered reasonable considering the difficulties of accurately accounting for the small parasitic inductances in Z_{TX}. For example in Figure 3.1/7(f) the actual current dips nearly to zero after the main peak whereas the computed value (assuming Z_{TX} was purely resistive) shows only a small dip. Inductance tends to emphasise 'ringing' behaviour and a few tens of nanohenries in Z_{TX} suffice to account for the observed form. The measuring current probe* contributes some additional inductance (≈2nH). At 10 MHz a 30nH inductance has an impedance of nearly 1Ω which is significant compared with the resistance components. This inductance value is typical of the 30cm lengths of 50Ω coaxial cable (when terminated in low resistances) used to couple the pulse sources to the transducers and was not accounted for in examples 1 and 3.

---

* Tektronix, Type P6021.

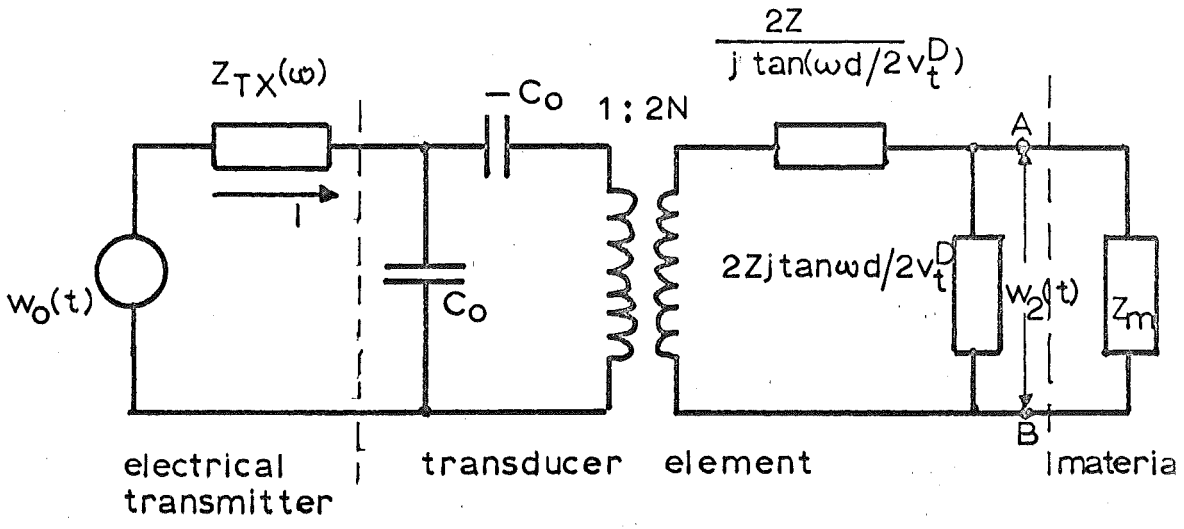

FIG. A3.1/1: Equivalent circuit model for transducer

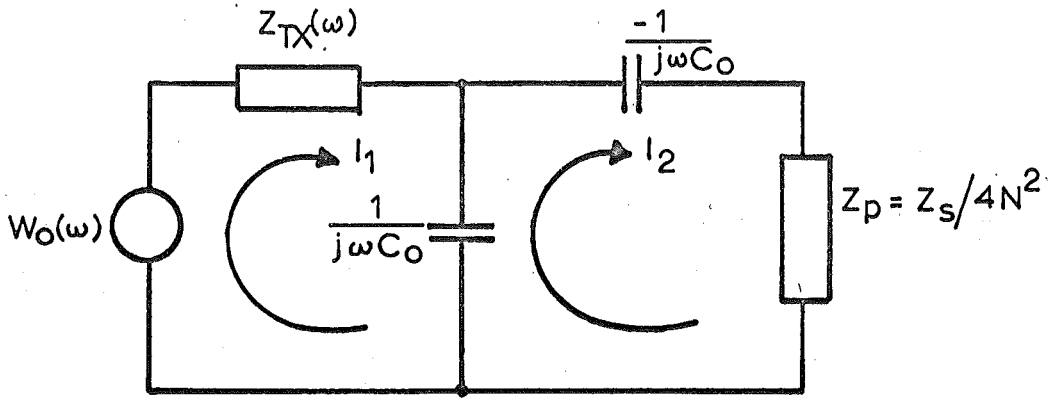

FIG. A3.1/2: Pertaining to Thevenin equivalent voltage

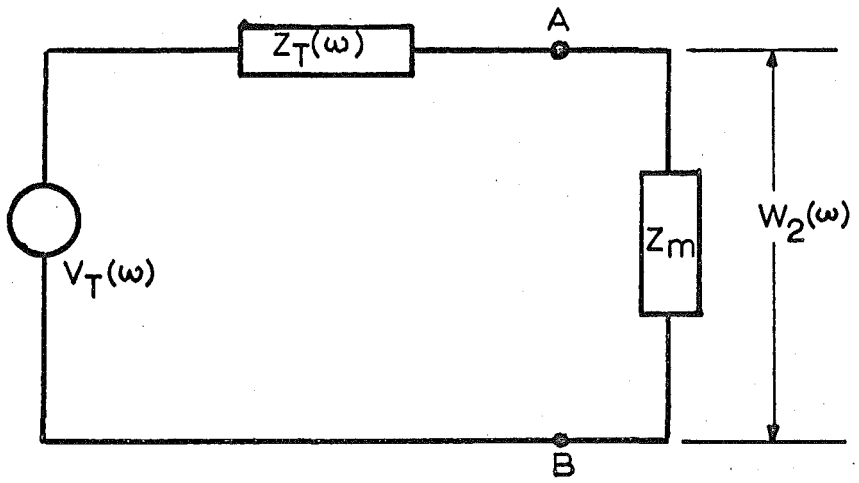

FIG. A3.1/3: Thevenin equivalent circuit.

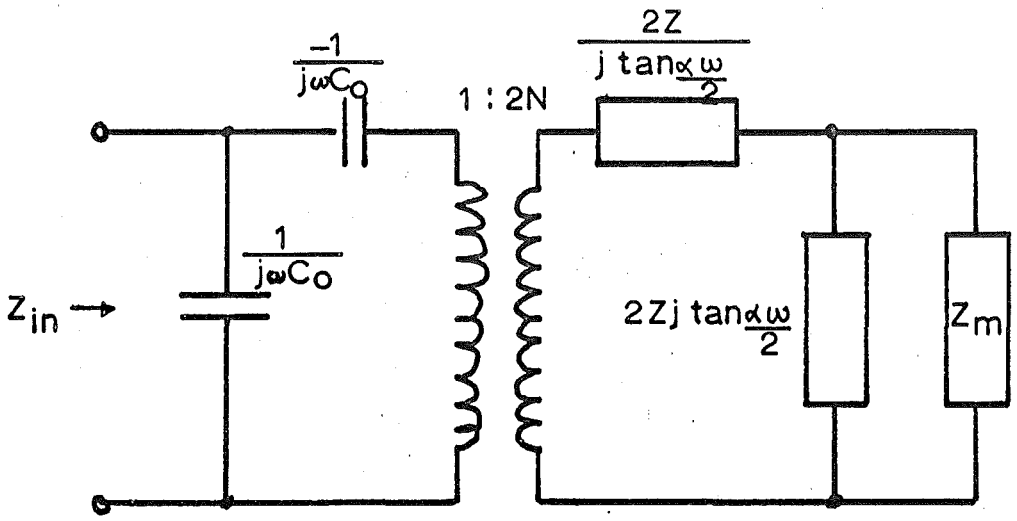

FIG. A3.1/4: Electrical input impedance.

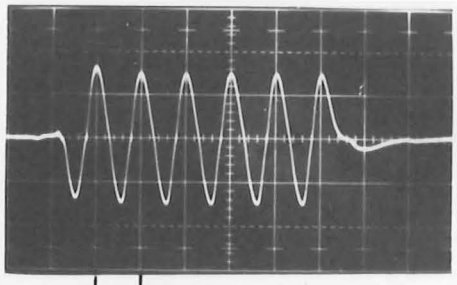

(a) drive voltage

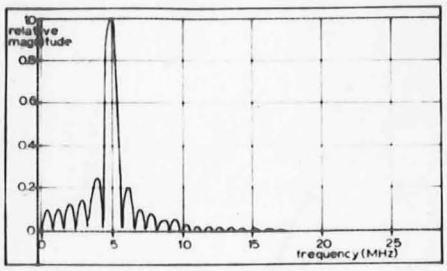

(b) spectrum of (a)

FIG. A 3.1/5: Sinusoidal burst excitation

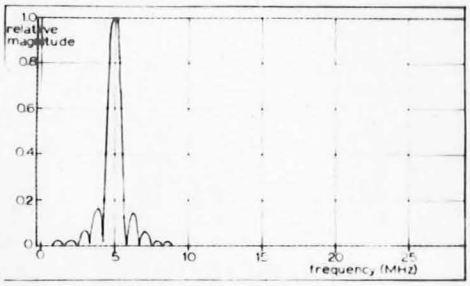

(c) spectrum of acoustic output

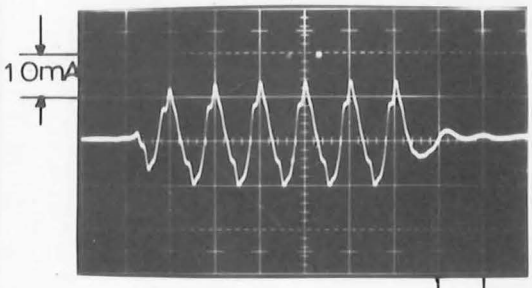

(f) actual current

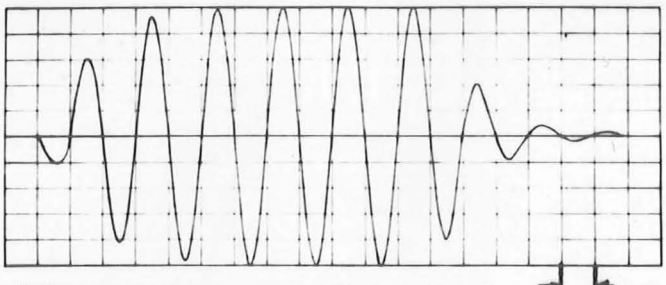

(d) computed acoustic output

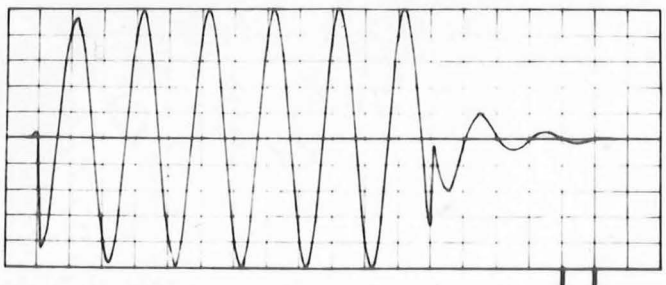

(e) computed current

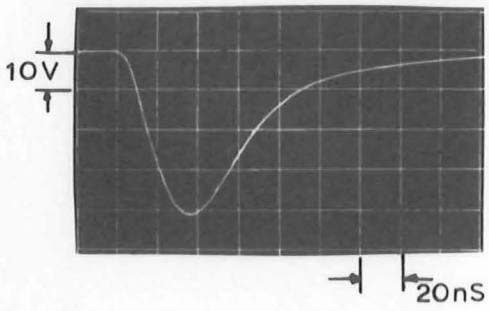

(a) drive voltage

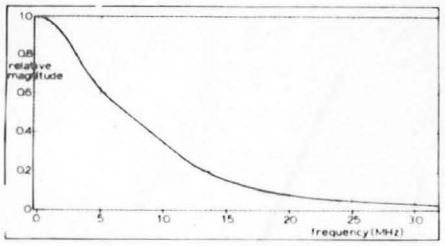

(b) spectrum of (a)

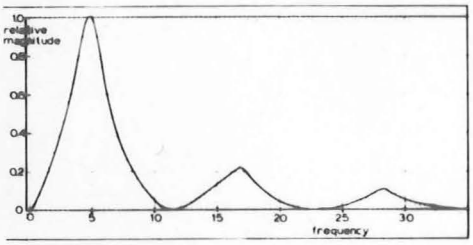

(c) spectrum of acoustic output

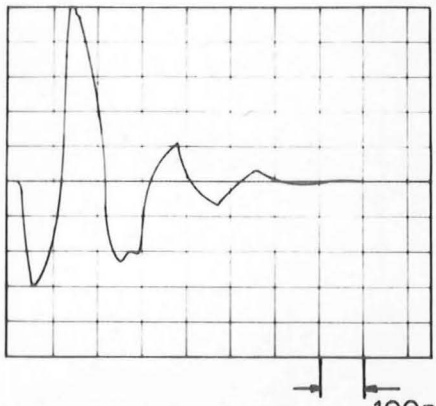

(d) computed acoustic output

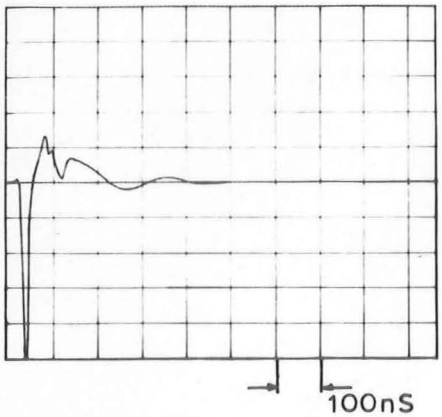

(e) computed current

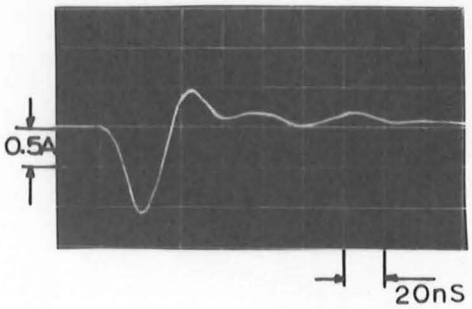

(f) measured current

FIG.A 3.1/6: Pulse excitation.

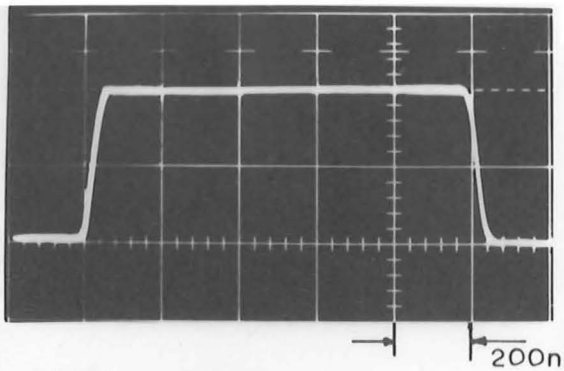

(a) drive voltage

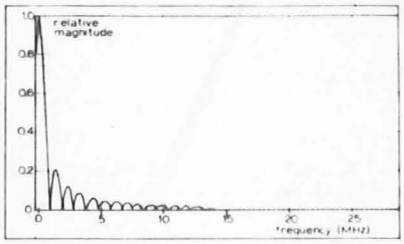

(b) spectrum of (a)

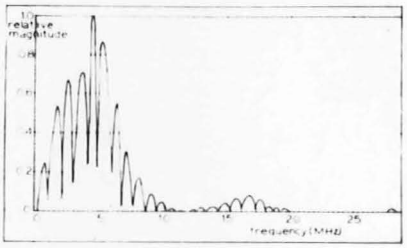

(c) spectrum of acoustic output

(d) computed acoustic output

(plots (d), (e) and (f) show response to leading edge of (a) only)

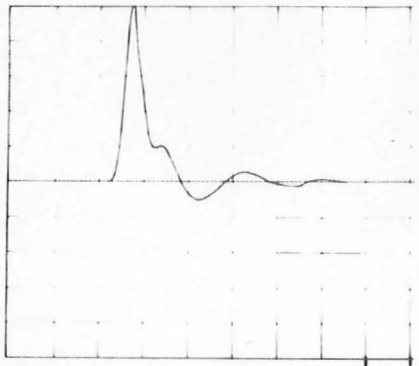

(e) computed current

100 nS

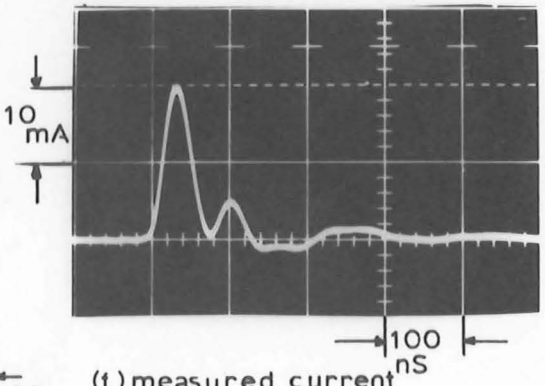

(f) measured current

FIG. A 3.1/7 Square pulse excitation

APPENDIX 3.2.

RECEIVING TRANSDUCER ACOUSTIC-ELECTRICAL RESPONSE

The analysis of the receiving transducer is essentially similar to that of the transmitter treated in the previous appendix. However the use of Laplace transform methods can result in easily interpretable analytic solutions for some conditions and was adopted instead of the Fourier method used in Appendix 3.1.

Under conditions of no initial charges or currents in any of the equivalent circuit capacitors or transmission line sections the circuit elements have transform impedances as indicated on Figure 3.2/1. F(s) is the driving force incident from a medium of specific acoustic impedance Z_m. Unity area of the transducer is again assumed.

(a) Open electrical termination.

This case is extremely simple. The secondary (electrical side) of the transformer appears as a short circuit and the input impedance presented by the transducer at terminals A-B is;

$$Z_{in}(s) = \frac{\frac{2Z}{\tanh\frac{\alpha s}{2}} \cdot 2Z\tanh\frac{\alpha s}{2}}{\frac{2Z}{\tanh\frac{\alpha s}{2}} + 2Z\tanh\frac{\alpha s}{2}} \qquad .. \text{A3.2/1(a)}$$

$$= Z\tanh\alpha s \qquad .. \text{A3.2/1(b)}$$

From this we find the force developed at the transducer terminals by a plane incident wavefront by considering the analogous problem in the termination of electrical transmission lines. (Z_m is a distributed 'characteristic impedance' not a lumped element). Defining a reflection coefficient as;

$$\rho_1 = \frac{Z_{in}(s) - Z_m}{Z_{in}(s) + Z_m} \qquad .. \text{A3.2/2}$$

for waves from the medium into the transducer the total force developed at the interface is given by $1 + \rho_1$, i.e.;

$$F_i(s) = F(s).(1+\rho_1) = \frac{2Z_{in}(s)}{Z_{in}(s) + Z_m} \qquad .. \text{A3.2/3}$$

Similarly for waves travelling from the transducer into the material a similar coefficient ρ_2 is defined as;

$$\rho_2 = \frac{Z_m - Z}{Z_m + Z} \qquad .. \text{A3.2/4}$$

Consider the incoming force f(t) to be an impulse of strength F. Then F(s) = F and the force at the terminals A-B is;

$$F_i(s) = \frac{2Z_{in}(s)}{Z_{in}(s) + Z_m} . F \qquad .. \text{A3.2/5}$$

Consequently a 'current' (particle velocity) is generated in the transformer primary of;

$$I_p(s) = F_i(s) . \frac{\tanh \frac{s\alpha}{2}}{2Z} \qquad .. \text{A3.2/6}$$

and the infinite load output voltage or impulse response is;

$$A_\infty(s) = I_p(s) . 2N . \frac{1}{sC_o} \qquad .. \text{A3.2/6(a)}$$

$$= \frac{2NF}{sC_o} \frac{\tanh \frac{s\alpha}{2}}{2Z} \cdot \left\{ \frac{2Z \tanh s\alpha}{Z \tanh s\alpha + Z_m} \right\} \qquad .. \text{A3.2/6(b)}$$

After expansion of the bracketed tanh terms as exponentials and recalling the definition of ρ_2 we obtain;

$$A_\infty(s) = \frac{2NF}{C_o} \frac{\tanh \frac{s\alpha}{2}}{s} \cdot \frac{1}{Z+Z_m} \left\{ \frac{1-e^{-2s\alpha}}{1+\rho_2 e^{-2s\alpha}} \right\} \qquad .. \text{A3.2/6(c)}$$

Now $e^{-2s\alpha}$ is always less than one from the definition of the Laplace transform variable[1] and from the definition of ρ_2 this is also less than one in magnitude. Thus expanding the denominator of the bracketed term we obtain;

$$A_\infty(s) = \frac{2NF}{C_o} \frac{\tanh \frac{s\alpha}{2}}{s} \frac{(1-e^{-2s\alpha})}{Z_m+Z} (1-\rho_2 e^{-2s\alpha} + \rho_2^2 e^{-4s\alpha} \ldots .) \qquad .. \text{A3.2/6(d)}$$

and thus finally;

$$A_\infty(s) = \frac{2NF}{C_o(Z_m+Z)} \cdot \frac{\tanh \frac{s\alpha}{2}}{s} [\, 1-(1+\rho_2) e^{-2\alpha s} + \rho_2 (1+\rho_2) e^{-4\alpha s}$$

$$- \rho_2^2 (1+\rho_2^2) e^{-6\alpha s} + \ldots . \,] \qquad .. \text{A3.2/7}$$

The $\frac{\tanh \frac{s\alpha}{2}}{s}$ portion is a standard form having a square wave inverse transform shown in Figure A3.2/2 as S(t). The exponential terms each give rise to a delayed version of S(t)

with amplitudes defined by the ρ_2 dependent coefficients. For $\rho_2 = + 1/3$ the form of $a_\infty(t)$ is as in Figure A3.2/3. The forms for $\rho_2 = - 1/3$ and $+ 1/6$ are shown as Figure 4.5.
($a_\infty(t) = \mathcal{L}^{-1}\ (A_\infty(s))$.

We may note some limiting cases;

(1) Z_m very small, $\rho_2 \approx -1$. All the terms of a_∞ except the first are nearly zero and the full amplitude square wave continues indefinitely. (Neglecting losses in the transducer material).

(2) If Z_m is very large $\rho_2 \approx + 1$ and the coefficients after the first are all equal to 2 in magnitude. Again the wave continues indefinitely.

(3) $Z_m = Z$ gives $\rho_2 = 0$ and the response consists of a single cycle of the S(t) function.

From the transfer function $A_\infty(s)$ with F = 1 we may readily determine the response to any of the likely waveforms in the acoustic part of the system.

(i) Sinusoidal wave commencing at t=0. For this $F(s) = a/(s^2+a^2)$ where the wave has the form sin at for t>0.

For these waveforms it is convenient to expand the remaining tanh function in $A_\infty(s)$ in terms of exponentials to give;

$$A_\infty(s) = \frac{h_{33}(1+\rho_2)}{Z_m} \cdot \frac{1}{s} \cdot [1-2e^{-s\alpha}+(1-\rho_2)e^{-2s\alpha} \ldots]$$

.. A3.2/8

where we have further replaced N/C_o by h_{33} ($N = h_{33}C_o$) and replaced $Z + Z_m$ in terms of ρ_2.

Thus dropping unnecessary subscripts, for the sine wave;

$$F_o(s) = \frac{h(1+\rho)}{Z_m} \cdot \frac{1}{s} \cdot \frac{a}{s^2 + a^2} [1 - 2e^{-s\alpha} + (1-\rho_2)e^{-2\,s\alpha} \ldots] \quad .. \text{A3.2/9}$$

This is the transform of a train of sinusoidal waves commencing at successive multiples of α, each with relative amplitudes given by the corresponding coefficients of the exponential term, and the whole superposition of these waves integrated once.

For $\rho_2 = 0$ only three components appear and so for all times greater than $t=2\alpha$ the differential of the output is given by;

$$f'_o(t) = \frac{h}{Z_m} \cdot [\sin at - 2\sin a(t-\alpha) + \sin a(t-2\alpha)] \quad .. \text{A3.2/10}$$

or

$$f_o(t) = \frac{h}{aZ_m} [-\cos at + 2\cos a(t-\alpha) - \cos a(f-2\alpha)] \quad .. \text{A3.2/11}$$

and the steady state response reduces to the combination of three phasors of relative magnitudes and phases such as those indicated in Figure A3.2/4 for the case where the period of the wave is 1.5α i.e., $2\pi/a = 1.5\alpha$.

These give a steady state response as;

$$f_o(t) = \frac{3h}{aZ_m} \sin(at + 4\pi/3) \quad .. \text{A3.2/12}$$

Thus the steady state response is essentially the original waveform after a phase shift and integration. In the particular case where the transducer is resonant at the frequency of the incoming tone (i.e., $2\pi/a = 2\alpha$) $f_o(t)$ reduces to;

$$f_o(t) = \frac{-4h}{aZ_m} \cos at \qquad \text{.. A3.2/13}$$

indicating that a pure integration has occurred.

In the time $0<t<2\alpha$ the output builds up similarly to the fashion shown in Figure A3.2/5 for $2\pi/a=1.5\alpha$. Removal of the excitation after steady state conditions are established results in a similar form of decay.

For this form of input we note that in general the time required for the output to approach to within some given small deviation from the behaviour at $t=\infty$ depends on ρ_2. High magnitudes of this reflection coefficient (e.g., such as would occur with the transducer facing water, PZT5A - water gives $|\rho_2| = 0.86$) allow many delayed contributions of significant amplitude.

Even with perfect matching the steady value cannot be reached in less than 2α.

(ii) Decaying sinusoid input.

This form closely approximates that transmitted (Appendix 3.1). For $f(t) = \sin(at).e^{-bt}$, $F(s) = a/[(s+b)^2+a^2]$ and the response again consists of the integral of superimposed, successively delayed versions of the original waveform. The

output is indicated in Figure A3.2/6. Inspection of Figure 12.31 (which was obtained with a high impedance load) will verify the correctness of these predicted waveforms. The case of $a = \pi/\alpha$ is the most relevant as the waveforms have been generated by transducers of identical thickness to those used in receiving. The case actually shown in the photographs corresponds to $\rho_2 = -1/3$. For this the component commencing at $t = 3\alpha$ has a relative strength of 0.64 and all those after 6α are less than 0.07. However, the waveform indicated in Figure A3.2/6 is correct up to the time $t = 2\alpha$ for any value of ρ_2.

(iii) A few cycles of sinusoid.

This case produces the response shown in Figure 4.6. The values of the coefficients determining the amplitudes of the delayed terms have been calculated for a variety of material-transducer combinations and those for PZT5A on aluminium, steel, copper and water are listed in Tables A3.2/1-4. These materials cover a range of $|\rho_2|$ from 0.1 to 0.9.

The general form of the coefficients is given in Equation 8.14.

(iv) Steady state response of thin transducers.

Reverting back to the form in Equation A3.2/6(b) and rewriting the response as a Fourier transfer function (since we are now dealing with continuous sinusoids this is the most suitable form) we have;

$$G_{\infty}(\omega) = 2h \frac{\tan \frac{\omega\alpha}{2}}{\omega} \cdot \frac{j \tan \omega\alpha}{Z\, j \tan \omega\alpha + Z_m} \qquad \therefore \text{A3.2/14}$$

as the open circuit response to a sinusoid of angular frequency ω. The two cases of especial interest are;

(i) Half wave plate, $\alpha = \frac{\pi}{\omega}$, or $d = \frac{\pi v_t^D}{\omega}$ $(\alpha = \frac{d}{v_t^D})$

(ii) Thin plate, $\alpha << \frac{\pi}{\omega}$, or $d << \frac{\pi v_t^D}{\omega}$

Case (i) leads to the form;

$$G_\infty(\omega_o) = \frac{2h}{\omega_o}\left\{\lim_{\beta\to\frac{\pi}{2}} \tan\beta.\tan 2\beta\right\}\frac{j}{Z\, j \tan\pi + Z_m} \qquad .. \text{A3.2/15}$$

(ω_o is the resonant frequency)

The limiting process gives a value of -2, for;

$$G_\infty(\omega_o) = \frac{-4jh}{Z_m\omega_o} \qquad .. \text{A3.2/16}$$

corresponding to the expression obtained above for the response after transients have decayed (Equation A3.2/13). The expression A3.2/16 agrees with that usually quoted for the resonant response but is often expressed in terms of the intensity of the incoming wave. If the RMS value of the input force is B then the intensity J is given by $J = \frac{B^2}{Z_m}$ so that the RMS value of output voltage becomes;

$$G_\infty(\omega)_{RMS} = \frac{4h}{\omega_o}\sqrt{\frac{J}{Z_m}} \qquad .. \text{A3.2/17}$$

Case (ii). If we denote the resonant thickness of the transducer as d_o $(= \frac{\pi v_t^D}{\omega_o})$ then Equation A3.2/14 may be put in the form;

$$G_\infty(\omega) = \frac{-2h}{j\omega} \tan\left(\frac{\pi d}{2d_o}\right) \cdot \frac{\tan\left(\frac{\pi d}{d_o}\right)}{Z\, j \tan\left(\frac{\pi d}{d_o}\right) + Z_m} \qquad \text{.. A3.2/18}$$

and for $\frac{d}{d_o} << 1$;

$$G_\infty(\omega) \approx \frac{-h}{j\omega} \cdot \frac{\pi d}{d_o} \cdot \frac{\frac{\pi d}{d_o}}{Z\, j \left(\frac{\pi d}{d_o}\right) + Z_m} \qquad \text{.. A3.2/19}$$

Typically Z and Z_m are comparable and hence the imaginary term in the denominator may be deglected. (For $d = \frac{d_o}{10}$ the amplitude error is less than 5% and the phase error less than 20^o when $Z = Z_m$). Thus;

$$G_\infty(\omega) \approx \frac{4h}{j\omega Z_m} \cdot \frac{\pi^2}{4} \left(\frac{d}{d_o}\right)^2 \qquad \text{.. A3.2/20}$$

this differs from the resonant response by a factor;

$$\frac{\pi^2}{4} \left(\frac{d}{d_o}\right)^2 = S(d) \text{ say} \qquad \text{.. A3.2/21}$$

For $\frac{d}{d_o} = 1/12$ say $S(d) = 0.0171 = 1/59$ approximately.

(b) Electrically loaded response.

We shall confine the electrical load to a pure resistor connected across C_o as indicated in Figure A3.2/1. In this case an impedance appears in the electrical side of the transformer of the value;

$$Z_E(s) = \frac{1}{-sC_o} + \frac{\frac{1}{sC_o} \circ R}{R + \frac{1}{sC_o}} = \frac{-1}{sC_o(1+sC_oR)} \quad \text{.. A3.2/22}$$

and reflects into the mechanical side as $-4N^2/(sC_o(1+sC_oR))$.

Thus $Z_{in}(s)$ is modified to the value;

$$Z_{in}(s) = Z \tanh s\alpha \quad \frac{1 - \frac{2N^2 \tanh \frac{s\alpha}{2}}{sC_oZ(1+sC_oR)}}{1 - \frac{N^2 \tanh s\alpha}{sC_oZ(1+sC_oR)}} \quad \text{.. A3.2/23}$$

The particle velocity in the mechanical side of the transformer is thus given by;

$$I_p(s) = F_i(s) \circ \frac{\tanh \frac{s\alpha}{2}}{2Z} \left\{ \frac{1}{1 - \frac{2N^2 \tanh \frac{s\alpha}{2}}{sC_oZ(1+sC_oR)}} \right\} \quad \text{.. A3.2/24}$$

and the electrical side current by 2N times this value.

Thus the loaded output response is given by;

$$F_o(s) = I_p(s) \circ 2N \circ \frac{R}{(1+sC_oR)} \quad \text{.. A3.2/25}$$

inserting the various relationships above,

$$F_o(s) = \frac{2NR}{1+sC_oR} \circ \frac{\tanh \frac{s\alpha}{2}}{2Z} \left\{ \frac{1}{1 - \frac{2N^2 \tanh \frac{s\alpha}{2}}{sC_oZ(1+sC_oR)}} \right\} \circ$$

$$\circ \frac{2Z_{in}(s)}{Z_m(s) + Z_m} \quad \text{.. A3.2/26}$$

Substituting the exponential form $(1-e^{-2a})/(1+e^{-2a})$ for tanh a, replacing N with $h_3 C_o$ and defining a further factor ρ_3 as $(Z_m-2Z)/(Z_m+2Z)$ gives; (after a tedious but straightforward algebraic manipulation)

$$F_o(s) = \frac{2h}{Z_m+Z} \tanh\frac{s\alpha}{2} \cdot (1-e^{-2\alpha s}) \cdot \frac{s}{s^2+\frac{s}{RC_o} - \frac{h^2(Z_m+2Z)}{RZ(Z_m+Z)}} \cdot$$

$$\cdot \left[1 + \left\{\frac{4h^2 e^{-\alpha s}}{R(Z+Z_m)} + \left[\rho_2 s^2 + \frac{\rho_2 s}{RC_o} + \frac{\rho_3 h^2(Z_m+2Z)}{ZR(Z_m+Z)}\right]e^{-2\alpha s}\right\} \cdot \right.$$

$$\left. \cdot \left\{s^2 + \frac{s}{RC_o} - \frac{h^2(z_m+2Z)}{RZ(Z_m+Z)}\right\}^{-1}\right]^{-1} \qquad \text{.. A3.2/27}$$

The term in large square brackets may be brought into the numerator as a $(1+a)^{-1} = (1-a+...)$ type of expansion and the remaining $\tanh(\frac{s\alpha}{2})$ numerator term expanded as exponentials to give a final form for $F_o(s)$ as;

$$F_o(s) = \frac{2h}{Z_m+Z} \cdot \frac{s}{s^2 + \frac{s}{RC_o} - \frac{h^2(Z_m+2Z)}{RZ(Z_m+Z)}} \cdot \left\{1 + c_1 e^{-\alpha s} + c_2 e^{-2\alpha s} \ldots\right\}$$

.. A3.2/28

the successive coefficients c_1, c_2 etc., become progressively more complicated. c_1 has the form;

$$c_1 = -\left(2 + \frac{4h^2}{R(Z_m+Z)}\right)\left(s^2 + \frac{s}{RC_o} - \frac{h^2(Z_m+2Z)}{RZ(Z_m+Z)}\right)^{-1} \qquad \text{.. A3.2/29}$$

which reduces to -2 for $R = \infty$ in agreement with the previously derived result.

A similar form of solution to that given here has been derived by Redwood[2] for the case of infinitely rigid backing of the transducer, a situation that results in some amount of simplification.

Regarded as an output voltage the equation for $F_o(s)$ should have a further minus sign to account for the convention in the equivalent circuit model.

Up to the time $t = \alpha$ the time waveform produced by a unit impulse of mechanical force is given by;

$$f_o(t) = \frac{-2h}{Z_m+Z} \cdot \mathcal{L}^{-1} \frac{s}{(s-\xi)(s-\eta)} \quad , \; 0 \leqq t < \alpha \qquad .. \text{A3.2/30}$$

where ξ and η are given by;

$$\xi, \eta = -\left(\frac{1}{2RC_o}\right) \pm \left[\left(\frac{1}{2RC_o}\right)^2 + \frac{h^2(Z_m+2Z)}{RZ(Z_m+Z)}\right]^{\frac{1}{2}} \qquad .. \text{A3.2/31}$$

thus;

$$f_o(t) = \frac{-2h}{Z_m+Z} \cdot \frac{\eta e^{\eta t} - \xi e^{\xi t}}{\eta - \xi} \quad , \; 0 \leqq t < \alpha \qquad .. \text{A3.2/32}$$

For R small the parameters ξ, η reduce to;

$$\xi = \frac{h^2(Z_m+2Z)C_o}{Z(Z_m+Z)}$$

$$\eta = -\frac{1}{RC_o} \qquad .. \text{A3.2/33}$$

A numerical example in the text (4.3.3.) produces values of $\xi = 6.4\times10^{6}$ sec^{-1}, $\eta = -6.6\times10^{7}$ sec^{-1} for a 1mm^2 PZT5A element on aluminium with α = 100nS, and loaded by 500Ω. Now at t = 0 the bracketed term in Equation A3.2/32 has the value 1 and hence the initial peak in the response is of the same amplitude as that obtained at the same instant with an electrical open circuit.

In many of the experimental measurements the transducer elements were loaded into a 50Ω resistance. With this value η becomes -6.6×10^{8} sec^{-1} and the dominant time constant in the response has a value of 1.5nS. Thus with this value of termination the initial transient will have decayed almost completely within 10nS compared with the 100nS needed before the next term appears at $t = \alpha$.

With c_1 as in Equation A3.2/29 the component commencing at $t = \alpha$ has the form;

$$f_o(t) = \frac{-2h}{Z_m+Z} \cdot \left[\frac{-2s}{(s-\xi)(s-\eta)} - \frac{4h^2}{R(Z_m+Z)} \cdot \frac{s}{(s-\xi)^2(s-\eta)^2} \right]$$

$t \geqq \alpha$ .. A3.2/34

Overlap from the component commencing at t = 0 will be completely negligible with $RC_o << \alpha$ and we see that the response consists now of a similar term to that obtained at t = 0 only inverted and of twice the amplitude with an additional term given by;

$$f_\alpha(u) = \mathcal{L}^{-1} \frac{4h^2}{R(Z_m+Z)} \frac{s}{(s-\xi)^2(s-\eta)^2} \quad .. \text{ A3.2/35}$$

$u = t-\alpha$

$$f_\alpha(u) = \frac{4h^2}{R(Z_m+Z)(\eta-\xi)^2}\left[\frac{\eta e^{\eta u} - \xi e^{\xi u}}{\eta - \xi}(u(\eta-\xi) - 1) + \frac{\eta e^{\xi u} - \xi e^{\eta u}}{\eta - \xi}\right] \quad .. \text{ A3.2/36}$$

at $t=\alpha$ or $u=0$, this gives the initial value of this component as zero. The factor $\frac{4h^2}{R(Z_m+Z)(\eta-\xi)^2}$ has the value of approximately 10^{-6} for R as large as 500Ω and is an order of magnitude less for R = 50Ω. In practical terms then this contribution can be neglected and we find the response starting at $t = \alpha$ as an inverted replica of the initial response. The form is shown in Figure A3.2/7. Essentially the response is a differentiated form of the open circuit waveform. At $t = 2\alpha$ a further pulse of a height depending on the reflection coefficient ρ_2 will occur and so on at successive multiples of α. With input waveforms that do not alter significantly in times comparable with RC_o the transducer response is just a superposition of delayed versions of the original waveforms, the successive components having amplitudes given very closely by the coefficient values computed for the open circuit case (e.g., as in Tables A3.2/1-4). With the case computed before for a steady sinusoid the steady state response becomes ($\rho_2 = 0$) approximately;

$$f_o(t) = \frac{-h}{Z_m}\left[\sin at - 2\sin a(t-\alpha) + \sin a(t-2\alpha)\right] \quad .. \text{ A3.2/37}$$

$(t > 2\alpha)$

or with $2\pi/a = 1.5\alpha$;

$$f_o(t) = \frac{-3h}{Z_m} \sin(at - \frac{\pi}{3}) \qquad .. \text{A3.2/38}$$

and in this case there is no 1/a term.

REFERENCES FOR APPENDIX 3.2.

1. Churchill, R.V. 'Operational Mathematics'. McGraw-Hill, New York, 1958, (2nd Edition), p.4.

2. Redwood, M. 'Transient performance of a piezoelectric transducer'. Journ.Acoust.Soc.Am. 33, pp.527-536, April, 1961.

TABLE A3.2/1

PZT5A $Z = .3370 \times 10^8$ $h_{33} = .2150 \times 10^{10}$

ALUMINIUM $Z_m = .1730 \times 10^8$ REFLECTION COEFF. = -.32156

COEFF. No.	VALUE	COEFF. No.	VALUE
0	1.00000	11	-.00687
1	-2.00000	12	.00454
2	1.32156	13	-.00221
3	-.64313	14	.00146
4	.42497	15	-.00071
5	-.20681	16	.00046
6	.13665	17	-.00022
7	-.06650	18	.00015
8	.04394	19	-.00007
9	-.02138	20	.00004
10	.01413	21	-.00002

TABLE A3.2/2

PZT5A $Z = .3370 \times 10^8$ $h_{33} = .2150 \times 10^{10}$

STEEL $Z_m = .4670 \times 10^8$ REFLECTION COEFF. = .16169

COEFF. No.	VALUE	COEFF. No.	VALUE
0	1.00000	11	.00022
1	-2.00000	12	-.00009
2	.83830	13	-.00003
3	.32338	14	.00001
4	-.13554	15	.00000
5	-.05228	16	-.00000
6	.02191	17	-.00000
7	.00845	18	.00000
8	-.00354	19	.00000
9	-.00136	20	-.00000
10	.00057	21	-.00000

TABLE A3.2/3

PZT5A	$Z = .3370 \times 10^{8}$	h_{33}	$= .2150 \times 10^{10}$
COPPER	$Z_m = .4250 \times 10^{8}$	REFLECTION COEFF.	= .11548

COEFF. No.	VALUE	COEFF. No.	VALUE
0	1.00000	7	.00308
1	-2.00000	8	-.00136
2	.88451	9	-.00035
3	.23097	10	.00015
4	-.10214	11	.00004
5	-.02667	12	-.00001
6	.01179		

TABLE A4.3/4

PZT5A	$Z = .3370 \times 10^{8}$	h_{33}	$= .2150 \times 10^{10}$
WATER	$Z_m = .1480 \times 10^{7}$	REFLECTION COEFF.	= -.91586

CEOFF. No.	VALUE	COEFF. No.	VALUE
0	1.00000	11	-1.28877
1	-2.00000	12	1.23456
2	1.91586	13	-1.18034
3	-1.83172	14	1.13068
4	1.75466	15	-1.08103
5	-1.67760	16	1.03555
6	1.60702	17	-.99007
7	-1.53645	18	.94842
8	1.47181	19	-.90677
9	-1.40717	20	.86862
10	1.34797	21	-.83047

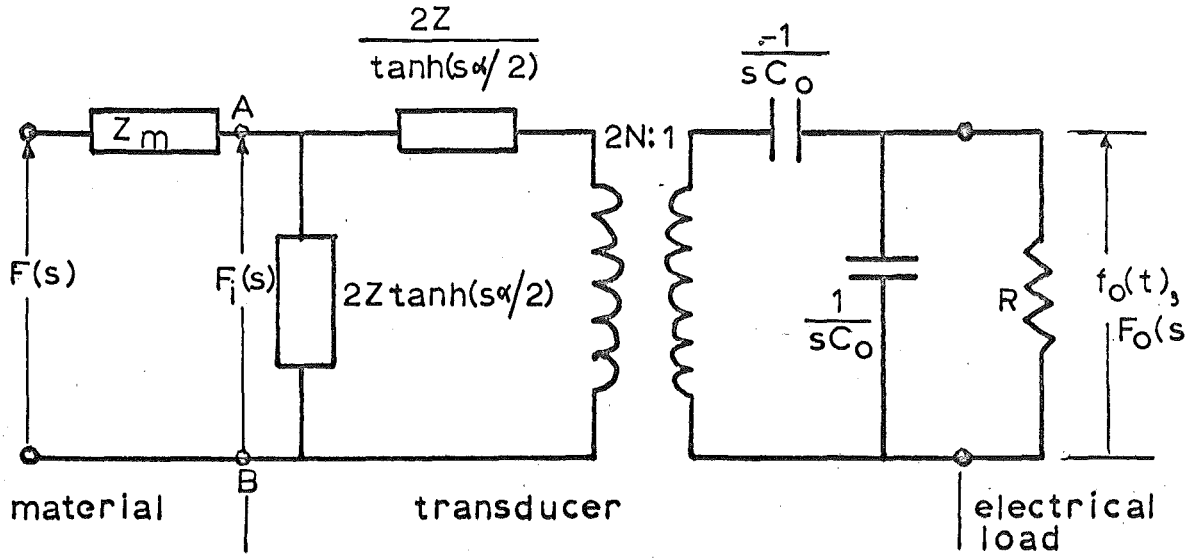

FIG.A3.2/1: Equivalent circuit in Laplace transformed parameters.

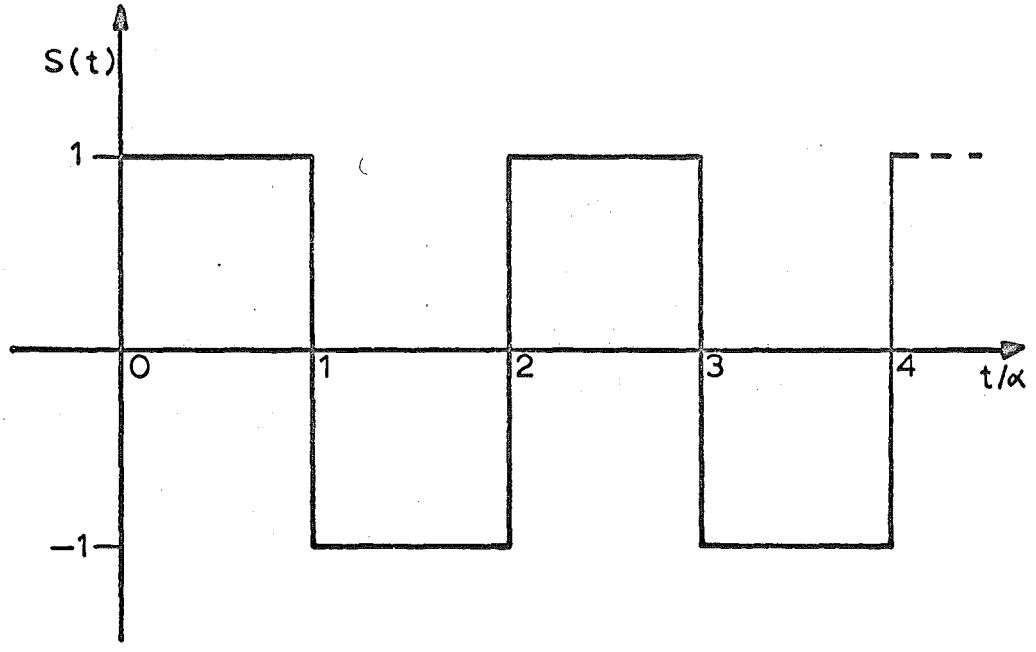

FIG.A3.2/2: Normalized impulse response of free transducer plate.

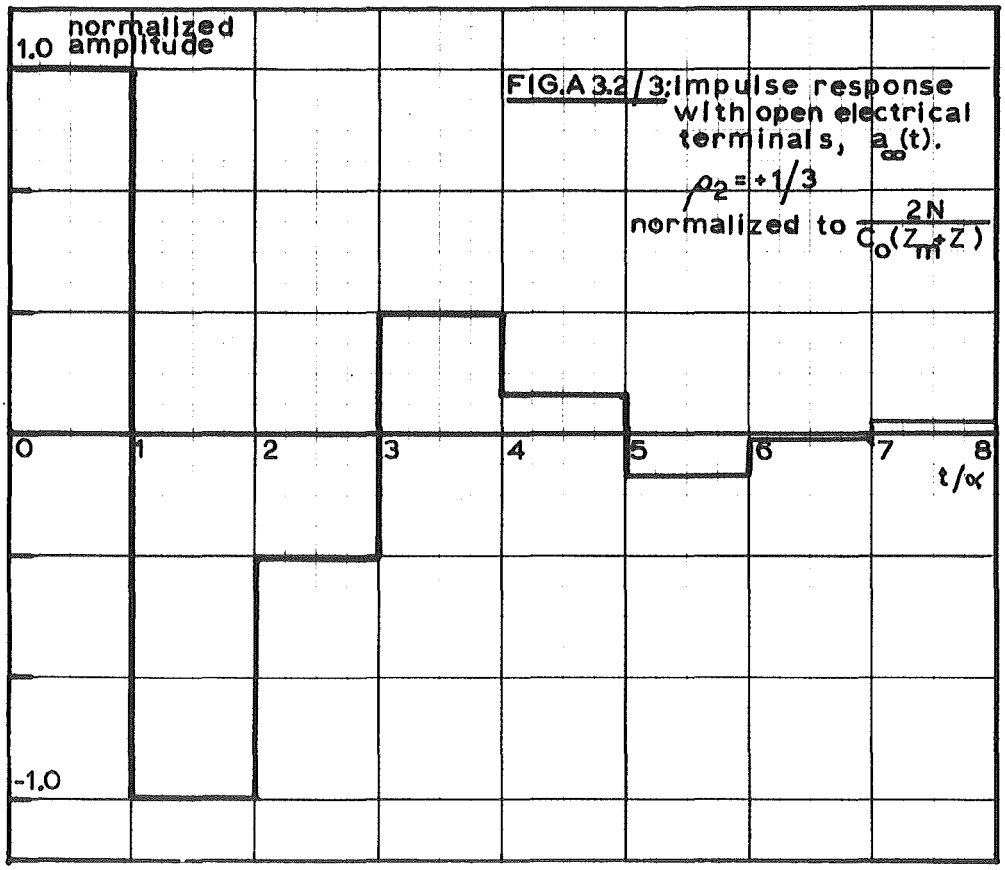

FIG.A 3.2/3: Impulse response with open electrical terminals, $a_\infty(t)$.
$\rho_2 = +1/3$
normalized to $\frac{2N}{C_0(Z_m + Z)}$

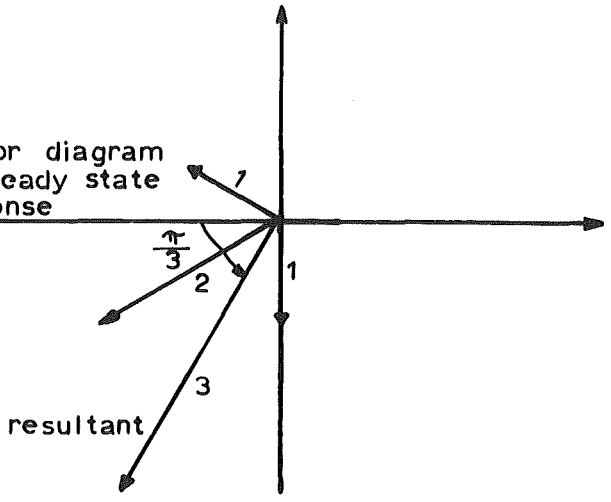

FIG.A 3.2/4: Phasor diagram for steady state response
$\rho_2 = 0$

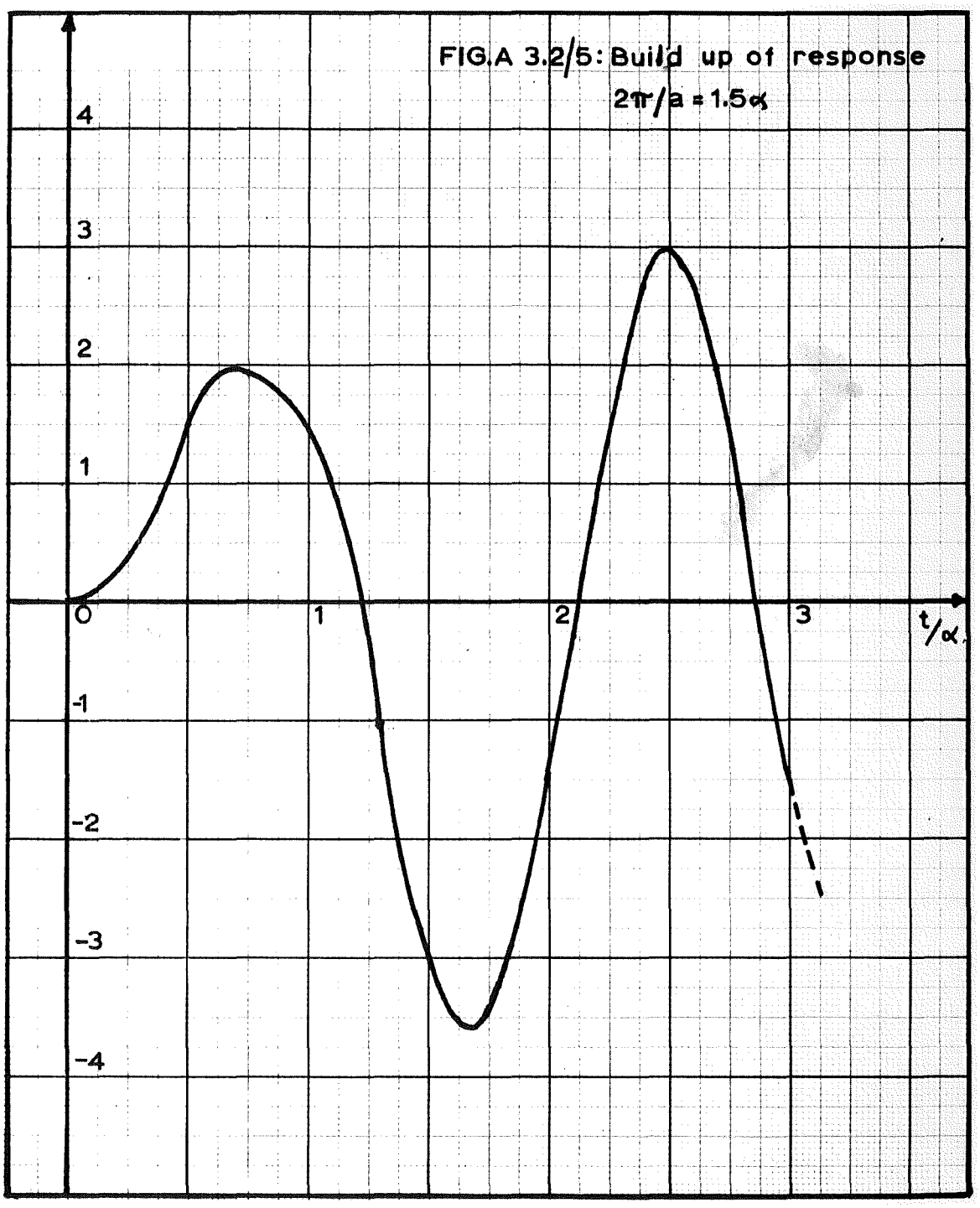

FIG.A 3.2/5: Build up of response
$2\pi/a = 1.5\alpha$

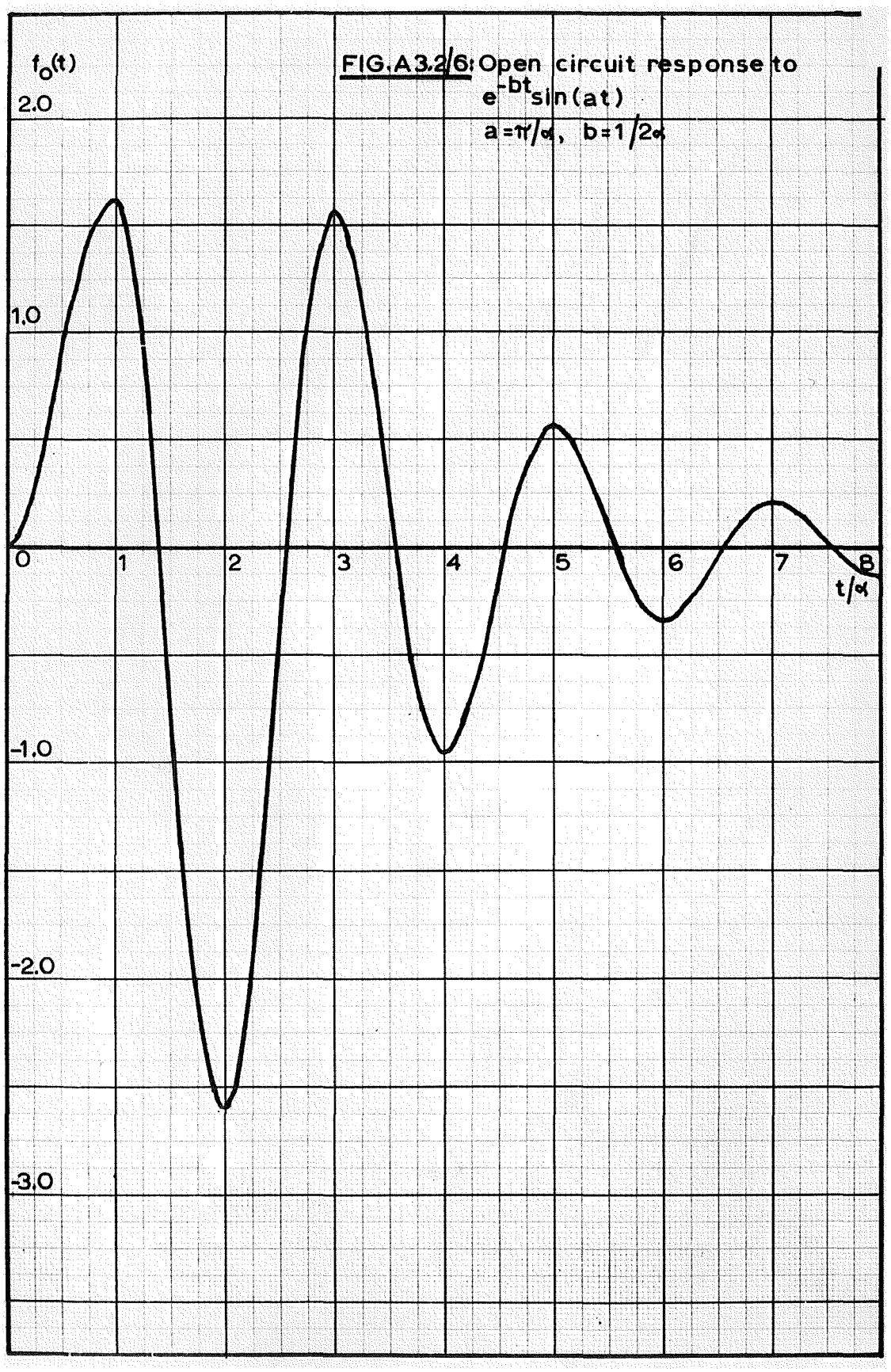

FIG. A3.2/6: Open circuit response to $e^{-bt}\sin(at)$
$a = \pi/\alpha$, $b = 1/2\alpha$

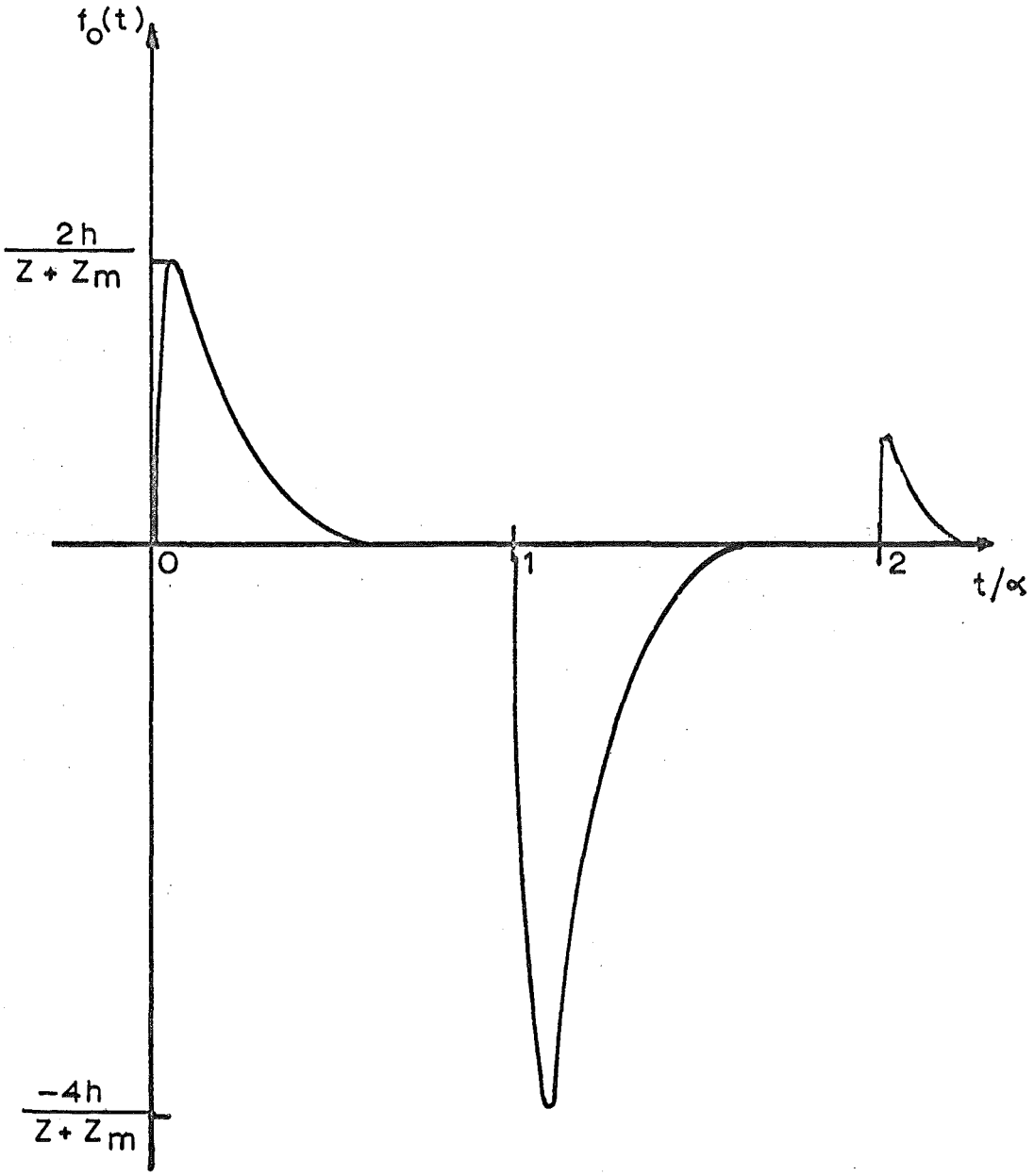

FIG. A 3.2/7: Form of response with $RC_o \ll \alpha$ to acoustic impulse.

APPENDIX 3.3.

CONVOLUTION OF THE SIGNAL SPECTRUM WITH THE TRANSFORM OF THE RECTANGULAR LATTICE FUNCTION.

The problem to be solved is defined in Equation 6.17. We will here consider a one-dimensional reduction taking the time-frequency part only as it is the most general form.

Thus we have;

$$v(k) = \frac{S}{SK}\int_{-K}^{K} \bar{u}(k_1).P(k-k_1)\,\mathrm{sinc}\left[\frac{S\tau'}{2\pi}(k-k_1)\right]dk_1 \qquad .. \text{ A3.3/1}$$

$(\tau' = c\tau)$

An extreme situation is represented by assuming $\bar{u}(k)$ to be uniform over the range $-K' \leqq k \leqq K'$ within the fundamental period $-K \leqq k \leqq K$ and zero outside, as this puts a sharp discontinuity into the function. $c\tau$ domain delay of the signal corresponding to this spectrum is allowed for by a factor $e^{-jk\gamma}$, that is a linear plane shift in the k domain. (See Figure A3.3/1).

The integral then becomes;

$$v(k) = \frac{S}{2K}\int_{-K'}^{K'} e^{-j(H+\frac{S-1}{2})\tau'(k-k_1)}\,\mathrm{sinc}\left(\frac{S\tau'(k-k_1)}{2\pi}\right)e^{-jk_1\gamma}dk_1 \qquad .. \text{ A3.3/2}$$

$$= \frac{S}{2K}\left\{\int_{k}^{K'} \mathrm{sinc}\frac{S\tau'(k-k_1)}{2\pi}\left[\cos\left\{\left[H+\frac{S-1}{2}\right]\tau'(k-k_1) + k_1\gamma\right\}\right.\right.$$

$$\left. -j\sin\left\{\left[H+\frac{S-1}{2}\right]\tau'(k-k_1) + k_1\gamma\right\}\right]dk_1$$

$$\left. - \int_{k}^{-K'} (\qquad\qquad)dk_1\right\} \qquad .. \text{ A3.3/3}$$

$$= \frac{S}{2K}(I_1 - I_2)$$

$$\alpha = (k-k_1)\frac{S\tau'}{2}$$

Then,

$$e^{j\gamma k} I_1 = \frac{-2}{S\tau'}\left\{\int_0^{\frac{S\pi K'}{2K}(\frac{k}{K'}-1)} \frac{\sin\alpha}{\alpha}.\cos\left[\left[\frac{2H}{S}+\frac{S-1}{S}\right]\alpha + \frac{2\gamma\alpha}{S\tau'}\right]d\alpha\right.$$

$$\left. -j\int_0^{\frac{S\pi K'}{2K}(\frac{k}{K'}-1)} \frac{\sin\alpha}{\alpha}.\sin\left[\left[\frac{2H}{S}+\frac{S-1}{S}\right]\alpha + \frac{2\gamma\alpha}{S\tau'}\right]d\alpha\right\}$$

.. A3.3/4

$$= \frac{-2}{S\tau'}(I_3 - I_4)$$

using the relation $\tau' = \frac{\pi}{K}$.

The relation is similar for I_2 with an upper limit of $\frac{S\tau'}{2}(\frac{k}{K'}+1)\frac{K'}{K}$ instead.

We see then that it suffices to consider integrals of the form;

$$I_{c,s} = \int_0^a \frac{\sin\alpha}{\alpha}\begin{matrix}\cos\\ \sin\end{matrix}\{S'+\gamma'\}\alpha\, d\alpha \qquad \text{.. A3.3/5}$$

with $S' = \frac{2H}{S} + \frac{S-1}{S}$, $\gamma' = \frac{2\gamma}{S\tau'}$.

Taking I_c first this has a standard solution[1] in the form;

$$\int_0^a \frac{\sin\alpha}{\alpha}\cos(S'+\gamma')\alpha\, d\alpha = \tfrac{1}{2}\left\{Si[a(S'+\gamma'+1)] - Si[a(S'+\gamma'-1)]\right\}$$

Si(x) is the sine integral function[2] $Si(x) = \int_0^x \frac{\sin u}{u}\, du$

.. A3.3/6

This function represents the real part of the solution.

For I_s the solution may be split into two parts to give;

$$I_s = \int_0^\infty \frac{\sin\alpha}{\alpha}\sin\{S'+\gamma'\}\alpha \, d\alpha - \int_a^\infty \frac{\sin\alpha}{\alpha}\sin\{S'+\gamma'\}\alpha . d\alpha \qquad .. \text{A3.3/7}$$

Denoting these parts by I_{s_1} and I_{s_2} respectively and using the relation;

$$\sin A . \sin B = \tfrac{1}{2}\{\cos(A-B) - \cos(A+B)\} \qquad .. \text{A3.3/8}$$

gives;

$$I_{s_1} = \tfrac{1}{2}\int_0^\infty \frac{\cos\alpha\{S'+\gamma'-1\} - \cos\alpha\{S'+\gamma'+1\}}{\alpha} d\alpha \qquad .. \text{A3.3/9(a)}$$

$$= \tfrac{1}{2} \ln\left[\frac{S'+\gamma'+1}{S'+\gamma'-1}\right] \qquad .. \text{A3.3/9(b)}$$

Similarly expanding I_{s_2} gives;

$$I_{s_2} = \tfrac{1}{2}\int_0^\infty \frac{\cos\{S'+\gamma'-1\}\alpha}{\alpha} d\alpha - \tfrac{1}{2}\int_a^\infty \frac{\cos\{S'+\gamma'+1\}\alpha}{\alpha} d\alpha \qquad .. \text{A3.3/10(a)}$$

$$= \tfrac{1}{2}\int_{S'+\gamma'-1}^\infty \frac{\cos\beta}{\beta} d\beta - \tfrac{1}{2}\int_{S'+\gamma'+1}^\infty \frac{\cos\beta}{\beta} d\beta \qquad .. \text{A3.3/10(b)}$$

$$= \tfrac{1}{2}\left\{ci[(S'+\gamma'-1)a] - ci[(S'+\gamma'+1)a]\right\} \qquad .. \text{A3.3/10(c)}$$

Where ci(x) is the cosine integral function defined as,

$$ci(x) = \int_x^\infty \frac{\cos\alpha}{\alpha} d\alpha \qquad .. \text{A3.3/11}$$

Thus;

$$I_s = I_{s_1} - I_{s_2} = \frac{1}{2}\left\{ \ln\left[\frac{S'+\gamma'+1}{S'+\gamma'-1}\right] + ci[(S'+\gamma'+1)a] - ci[(S'+\gamma'-1)a]\right\}$$

.. A3.3/12

giving;

$$e^{j\gamma k}I_1 = \frac{-2}{S\tau'}\cdot\frac{1}{2}\left\{ Si\left[\frac{S\pi K'}{2K}\left(\frac{k}{K'}-1\right)(S'+\gamma'+1)\right]\right.$$

$$- Si\left[\frac{S\pi K'}{2K}\left(\frac{k}{K'}-1\right)(S'\gamma'-1)\right]$$

$$-j\left[\ln\left[\frac{S'\gamma'+1}{S'\gamma'-1}\right] + ci\left[\frac{S\pi K'}{2K}\left(\frac{k}{K'}-1\right)(S'+\gamma'+1)\right]\right.$$

$$\left.\left.-ci\left[\frac{S\pi K'}{2K}\left(\frac{k}{K'}-1\right)(S'+\gamma'-1)\right]\right]\right\}$$

.. A3.3/13

I_2 is of identical form with $\left(\frac{k}{K'}\right)+1$ instead of $\left(\frac{k}{K'}\right)-1$.

Thus;

$$e^{jk\gamma}v(k) = \frac{1}{2K\tau'}\left\{ Si\left[\frac{S\pi K'}{2K}\left(\frac{k}{K'}+1\right)(S'+\gamma'+1)\right] - Si\left[\frac{S\pi K'}{2K}\left(\frac{k}{K'}-1\right)(S'+\gamma'+1)\right]\right.$$

$$- Si\left[\frac{S\pi K'}{2K}\left(\frac{k}{K'}+1\right)(S'+\gamma'-1)\right] + Si\left[\frac{S\pi K'}{2K}\left(\frac{k}{K'}-1\right)(S'+\gamma'-1)\right]$$

$$-j\left[ci\left[\frac{S\pi K'}{2K}\left(\frac{k}{K'}+1\right)(S'+\gamma'+1)\right] - ci\left[\frac{S\pi K'}{2K}\left(\frac{k}{K'}-1\right)(S'+\gamma'+1)\right]\right.$$

$$\left.\left.- ci\left[\frac{S\pi K'}{2K}\left(\frac{k}{K'}+1\right)(S'+\gamma'-1)\right] - ci\left[\frac{S\pi K'}{2K}\left(\frac{k}{K'}-1\right)(S'+\gamma'-1)\right]\right]\right\}$$

.. A3.3/14

This relationship could be expressed more compactly in terms of the exponential integral with imaginary argument but it is more convenient to examine the real and imaginary parts separately.

(1) H=0, γ=0, i.e., sampling commences at zero and there is no delay in the signal. The condition H=0 pertains for the spatial sampling in x and y. Recalling $S' = 2\frac{H}{S} + \frac{S-1}{S}$ then for these conditions v(k) becomes;

$$\mathrm{Re}\{v(k)\} = \frac{1}{2K\tau}\left\{\mathrm{Si}\left[\frac{\pi}{2K}(k+K')(2S-1)\right] - \mathrm{Si}\left[\frac{\pi}{2K}(k-K')(2S-1)\right] - \mathrm{Si}\left[\frac{\pi}{2K}(k+K')(-1)\right] + \left[\mathrm{Si}\,\frac{\pi}{2K}(k-K')(-1)\right]\right\} \quad .. \text{ A3.3/15}$$

and similarly for the imaginary part.

Consider the region near k = -K' and for definiteness take $K' = \frac{K}{2}$. With S>>1, $-\mathrm{Si}\left[\frac{\pi}{2K}(k-\frac{K}{2})(2S-1)\right] \approx \frac{\pi}{2}$ for $K \approx -\frac{K}{2}$, $\mathrm{Si}\left[\frac{\pi}{2K}(k-\frac{K}{2})(-1)\right] \approx \mathrm{Si}(\frac{\pi}{2})$ for $k \approx \frac{K}{2} \approx \frac{\pi}{2.2}$ and $\mathrm{Si}\left[\frac{\pi}{2K}(k+\frac{K}{2})(-1)\right] \approx 0$.

Thus,

$$\mathrm{Re}\{v(k)\} = \frac{1}{2K\tau}\left[\frac{\pi}{2} + \mathrm{Si}\left[\frac{\pi}{2K}(k+\frac{K}{2})(2S-1)\right] + \frac{\pi}{2.2}\right] \quad .. \text{ A3.3/16}$$

which behaves as in Figure A3.3/2.

By symmetry the behaviour is an inverted replica of this about k=K'. At k=0 both the first and second terms have magnitudes closely approaching $\frac{\pi}{2}$ and the last two terms add to $2\mathrm{Si}(\frac{\pi}{4}) \approx \frac{\pi}{2.1}$.

Figure A3.3/2(b) illustrates the behaviour of the imaginary component, viz.;

$$\mathrm{Im}\{v(k)\} = \frac{-1}{2K\tau}\left\{ ci\left[\frac{\pi}{2K}(k+\frac{K}{2})(2S-1)\right] - ci\left[\frac{\pi}{2K}(k-\frac{K}{2})(2S-1)\right] \right.$$
$$\left. - ci\left[\frac{\pi}{2K}(k+\frac{K}{2})(+1)\right] + ci\left[\frac{\pi}{2K}(k-\frac{K}{2})(+1)\right]\right\}$$

A3.3/17

Using the relation $ci(-x) = ci(x) + j\pi$ to alter the last two terms.

Again for $k \approx -\frac{K}{2}$ the second term has a large negative argument and gives $(-0 - j\pi)$. The fourth term has an argument of $\frac{-\pi}{2}$ and gives $j\pi - 0.47$ for a total contribution of -0.47.

The first and third components at $k = -\frac{K}{2}$ have values of $\pm\infty$ respectively and cancel. The first component oscillates much more rapidly than the second for an overall behaviour as in the Figure. At k=0 $\mathrm{Im}\{v(k)e^{jk\gamma}\} = 0$. From these diagrams it will be obvious that the distortion is very great especially near the discontinuities and furthermore, even for S very great, a large error remains due to the 'single sided' sampling. This is perhaps more obvious by considering that with the spectrum discussed the waveform seen by the sampling window is as in Figure A3.3/4.

(2) Exact alignment: Consider the signal delayed such that the peak of the waveform falls exactly in the middle of the sampling window.

In temporal terms the system inherently deals with delayed signals and hence the converse of the above statement would be more justified, (i.e., delay sampling until the signal arrives).

Spatially, the shift corresponds to considering the signals to have come from a plane which is centered on the axis of the measuring aperture, i.e., at $x = \frac{Q-1}{2}d$, $y = \frac{R-1}{2}d$,. Thus γ becomes $-(H + \frac{S-1}{2})\tau'$ and the expression for v(k) reduces to;

$$v(k) = \frac{1}{K\tau}\left\{Si\left[\frac{S\pi}{2K}(k+K')\right] - Si\left[\frac{S\pi}{2K}(k-K')\right]\right\} .e^{-j\gamma k} \quad .. A3.3/18$$

This function is shown in Figure A3.3/3 and we find v(k) to be an exact reproduction of $\bar{u}(k)e^{-jk\gamma}$ in phase over the relevant interval, in good agreement in amplitude over the central portion of the spectrum and having maximum 'overshoots' of 9% at distances $2\frac{K}{S}$ from the discontinuities. This situation corresponds to exact alignment of the sampling window with the delay or displacement of the signals.

(3) More commonly the signal will be largely within the window but displaced from the centre. This corresponds to cases intermediate between those considered above with the distortion progressively increasing as the shift increases.

A further case that may be treated fairly simply is provided by taking the spectrum as triangular.

i.e., $\bar{u}(k) = (1 - \frac{|k|}{K'}), - K' \leq k \leq K'$

$= 0$ otherwise.

For simplicity the phase factor will be assumed to place the waveform centrally in the sampling window.

Then;

$$v(k) \alpha \int_{-K'}^{K'} \left(1 - \frac{|k_1|}{K'}\right) \text{sinc}\left[\frac{S\tau'}{2\pi}(k-k_1)\right] dk_1 \quad .. A3.3/19$$

Proceeding similarly to above we derive (with $K' = \frac{K}{2}$) ;

$$v(k) = C\left\{(1 + \frac{2k}{K})\left[\mathrm{Si}\left[\frac{S\pi}{4}(\frac{2k}{K} + 1)\right] - \mathrm{Si}\left[\frac{S\pi k}{2K}\right]\right]\right.$$

$$+ (1 - \frac{2k}{K})\left[\mathrm{Si}\left[\frac{S\pi}{4}(\frac{2k}{K} - 1)\right] - \mathrm{Si}\left[\frac{S\pi k}{2K}\right]\right]$$

$$\left. - \frac{4}{\pi S}\sin\frac{S\pi k}{2K}\sin\frac{S\pi}{4}\right\} \qquad .. \text{A3.3/20}$$

(C is a constant)

If we further allow S to be a multiple of 4, writing $S = 4n$, then;

$$v(k) = C\left\{(1+\frac{2k}{K})\left[\mathrm{Si}\left[n\pi(\frac{2k}{K} + 1)\right] - \mathrm{Si}\left[\frac{2n\pi k}{K}\right]\right]\right.$$

$$\left. + (1 - \frac{2k}{K})\left[\mathrm{Si}\left[n\pi(\frac{2k}{K} - 1)\right] - \mathrm{Si}\left[\frac{2n\pi k}{K}\right]\right]\right\} \qquad .. \text{A3.3/21}$$

at $k = 0$

$v(0) = C.2\mathrm{Si}[n\pi]$

For n = 16 say, v(0) differs from unity be less than 0.014.

Near $k = -K_1$ the second term is nearly zero for n large and,

$$v(k) \approx (1 + \frac{2k}{K})\left(\mathrm{Si}\left[n\pi(\frac{2k}{K} + 1)\right] - \mathrm{Si}\left[\frac{2n\pi k}{K}\right]\right)$$

$$\approx (1 + \frac{2k}{K})\left(\mathrm{Si}\left[n\pi(\frac{2k}{K} + 1)\right] + \frac{\pi}{2}\right) \qquad .. \text{A3.3/22}$$

for n = 16 this behaves as in Figure A3.3/5 from which it may be seen that the maximum error is about 1% of the spectrum peak compared with 9% for the rectangular spectrum.

REFERENCES FOR APPENDIX 3.3.

1. Kreyszig, E. 'Advanced Engineering Mathematics'. Wiley, New York, 1962, p.506.

2. Abramowitz, M. and Stegun, I.A. 'Handbook of Mathematical Functions'. Dover, New York, 1965. pp.227-251 deal with this and the related cosine and exponential integrals. Note that the cosine integral Ci(x) as defined in this reference is the negative of the function ci(x) used here.

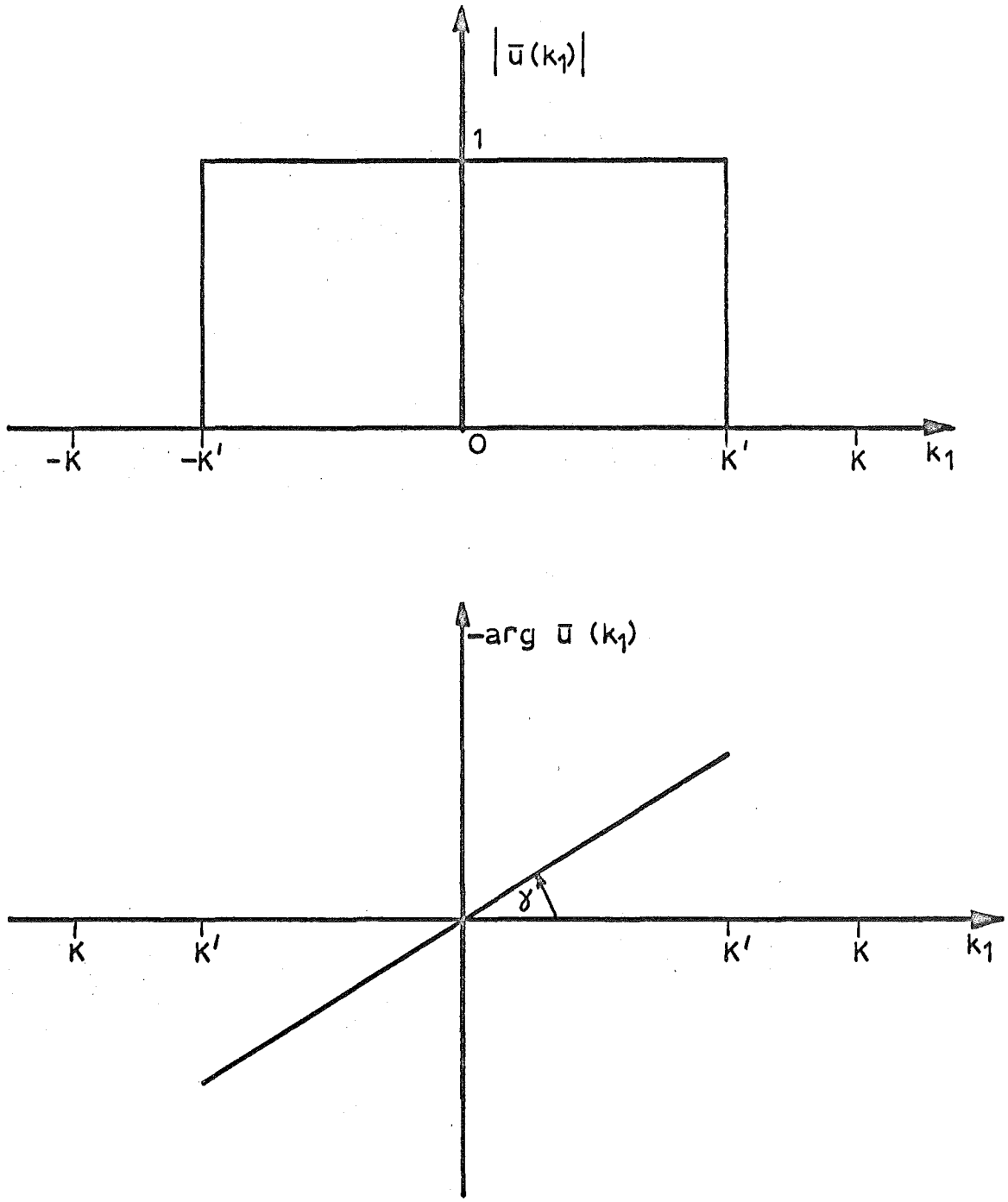

FIG. A 3.3/1: Signal spectrum $\bar{u}(k_1)$

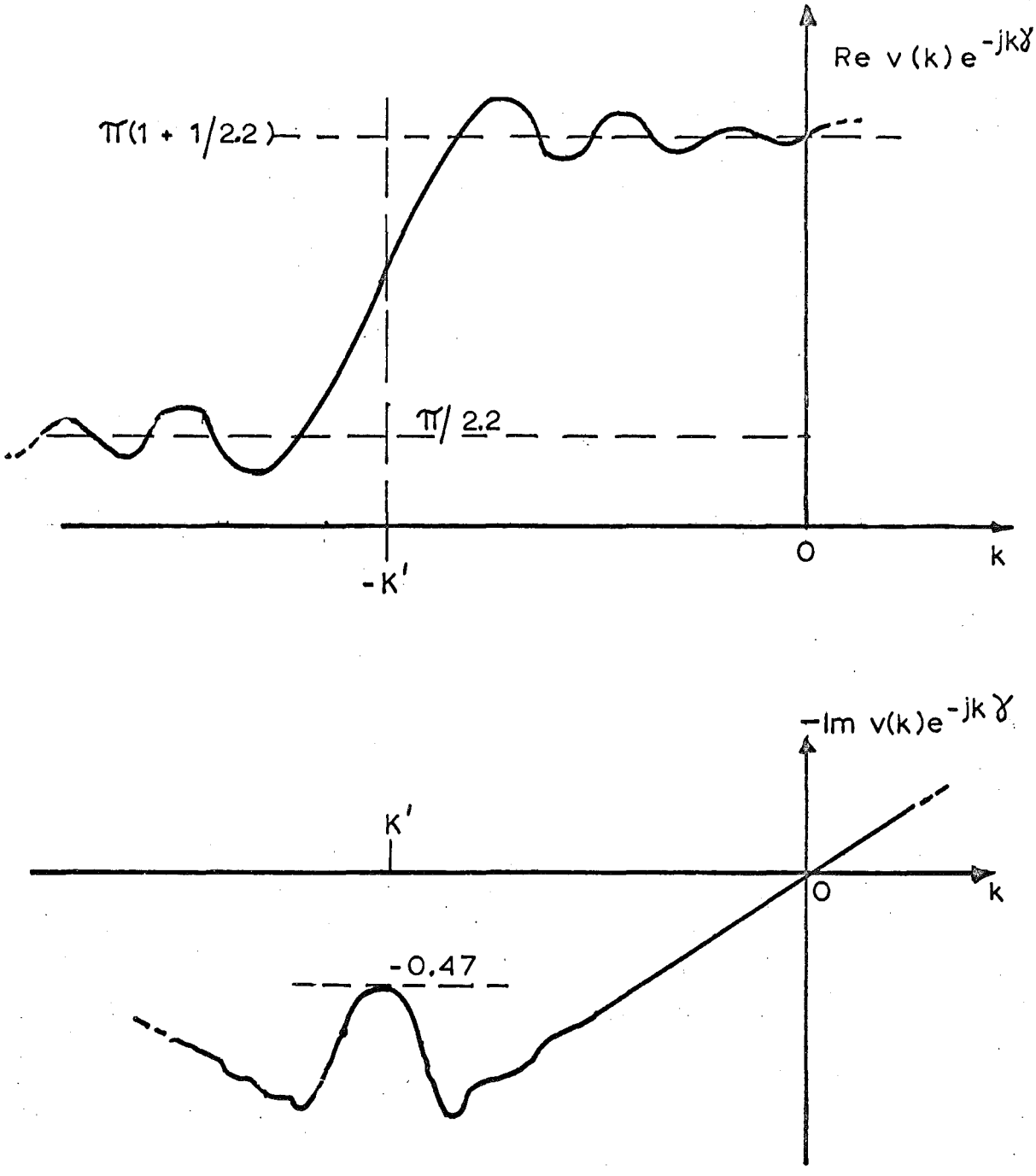

FIG. A 3.3/2: Real and imaginary parts of output spectrum for $\bar{u}(k)$ as Fig.A 3.3/1 and sampling commencing at ct=0. (Scale by $1/2K\tau'$)

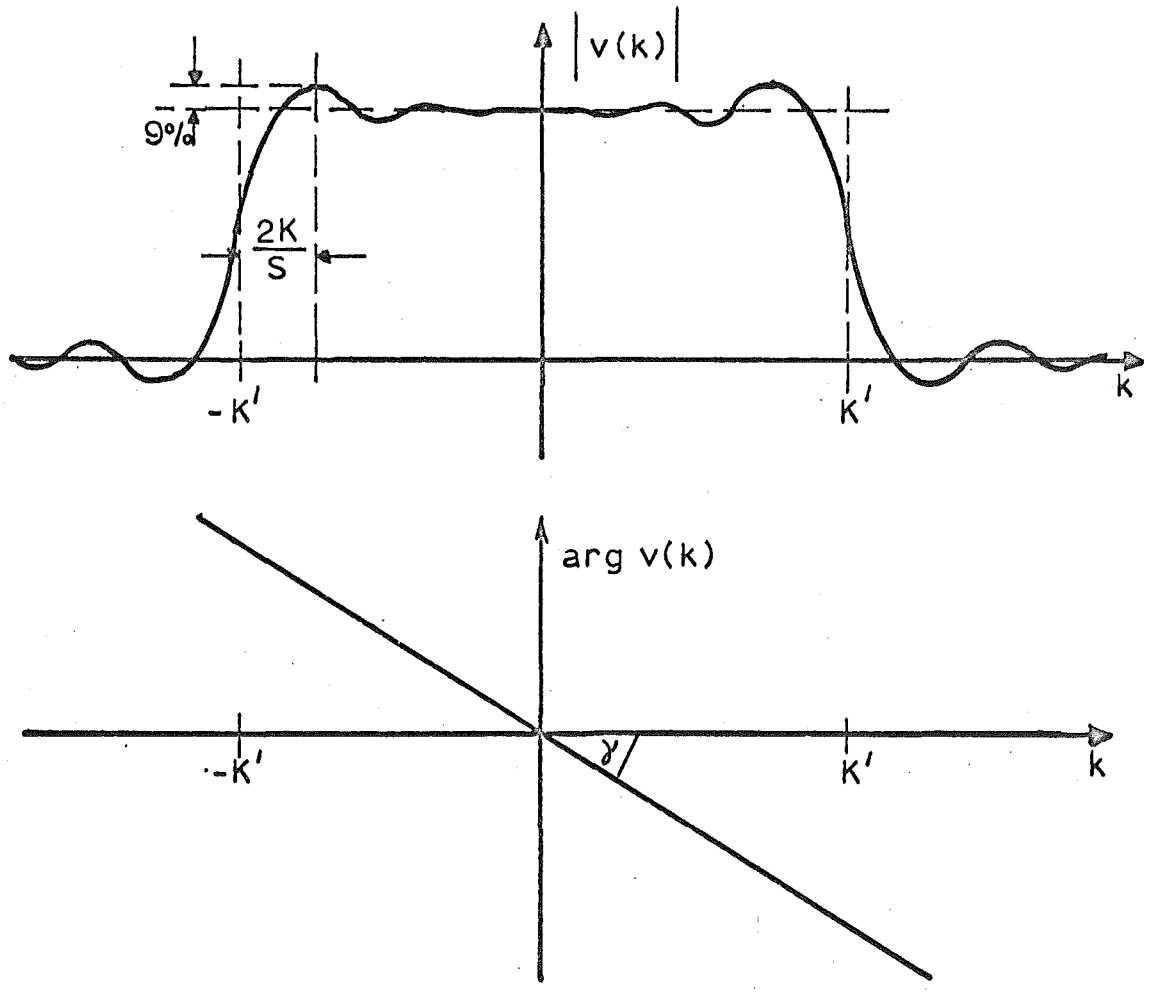

FIG. A 3.3/3: Response with sampling symmetrical about time origin.

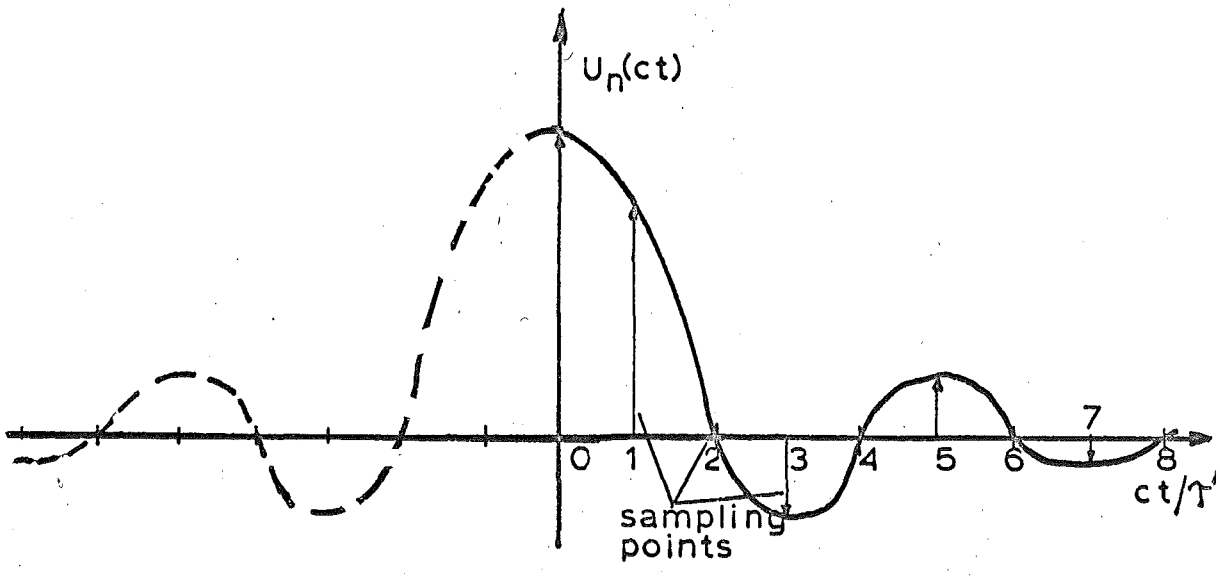

FIG. A 3.3/4: Waveform seen by sampling window ($K' = K/2$)

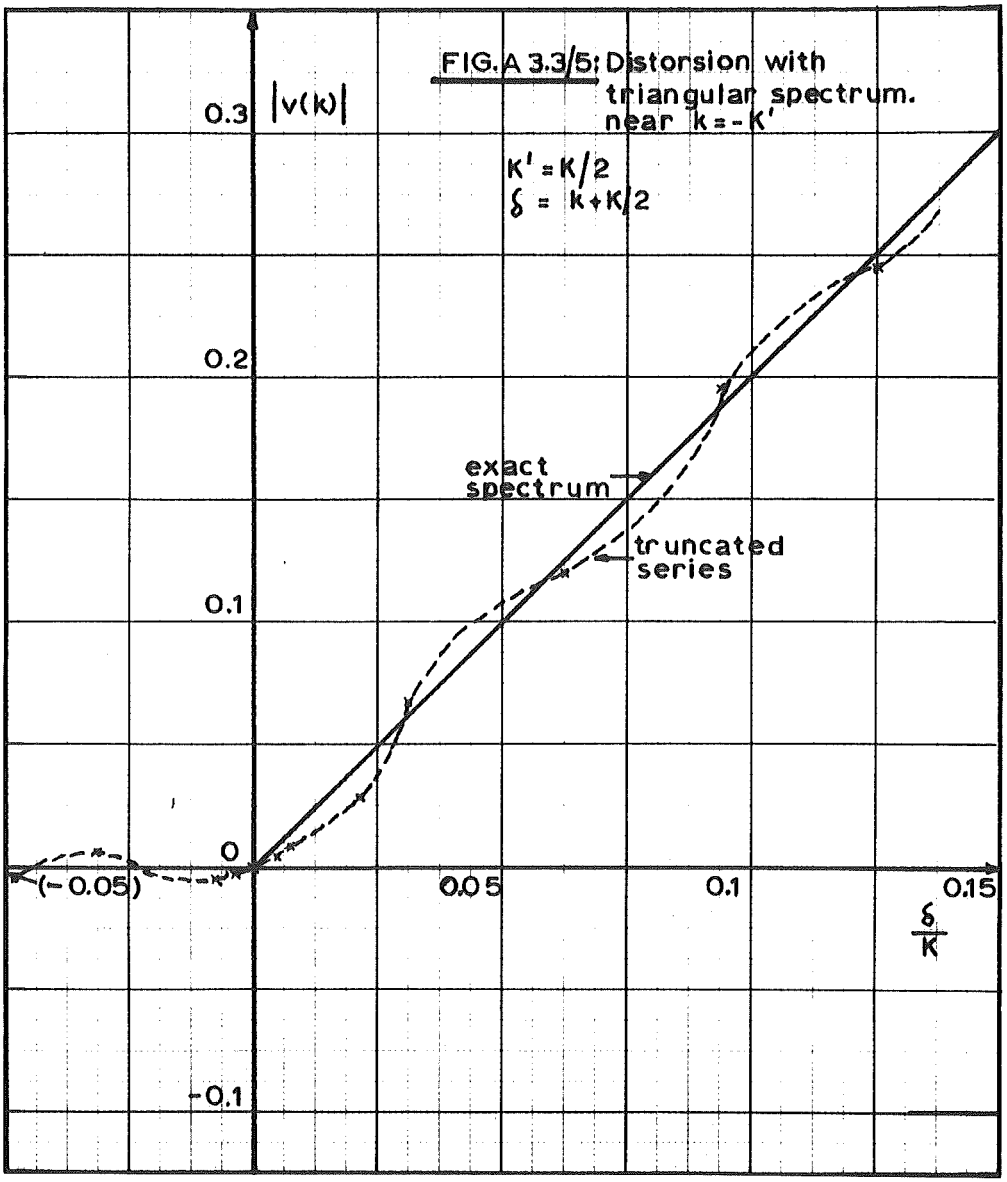
FIG. A 3.3/5: Distorsion with triangular spectrum. near k = -K'
K' = K/2
δ = k + K/2
|v(k)|
0.3
0.2
0.1
0
-0.1
(-0.05)
0.05
0.1
0.15
δ/K
exact spectrum
truncated series

APPENDIX 3.4.

VARIATION IN IMAGEABLE REGION WITH RECORDING DELAY AND RECORDING TIME.

The problem resolves to a study of the figure shown in Figure A3.4/1 and is essentially solved by locating A,B,C, and E.

For the circle the polar equation is simply r = R and for the ellipse with one focus at the origin;

$$r = \frac{a(1-e^2)}{1-e\cos\theta} \qquad .. \text{ A3.4/1}$$

where a is half the major axis and e the eccentricity of the ellipse.

Letting $R_1 + R_2 = 2a = 2R + d'$ then $e = (\frac{D}{4})/a$ and at B;

$$r_B = \frac{\frac{(2R+d)}{2}\left(1 - \left[\frac{D}{2(2R+d')}\right]^2\right)}{1 - \frac{D}{2(2R+d')}} \qquad .. \text{ A3.4/2}$$

$$= \frac{2R+d'}{2}\left(1 + \frac{D}{2(2R+d')}\right)$$

and the variation of r_B with 2R+d' is therefore a linear one, viz.;

$$r_B = \frac{2R+d'}{2} + \frac{D}{4} \qquad .. \text{ A3.4/3}$$

At the point C;

$$R = \frac{\frac{2R+d'}{2}\left(1 - \left[\frac{D}{2(2R+d')}\right]^2\right)}{1 - \frac{D}{2(2R+d')}\cos\theta_C} \qquad \text{.. A3.4/4}$$

$$\text{whence } \cos\theta_C = \frac{2(2R+d')}{D}\left\{1 - \frac{2R+d'}{2R}\left[1 - \left[\frac{D}{2(2R+d')}\right]^2\right]\right\} \text{. A3.4/5}$$

As all of R,d' and D may vary independently this represents a complex interrelationship. However we may impose the requirement that the region to be interrogated must include the projection of the aperture. Then as point C will always be closer to the aperture than A the problem may be shifted to a determination of point E, i.e., to determining the intersection of L_{max} and the line z = R, with the requirement that this point should have an x coordinate of at least $\frac{D}{2}$.

Expressing the condition in Cartesian coordinates and solving for $a^2 = \left[\frac{2R+d'}{2}\right]^2$ gives;

$$a^2 = \frac{5D^2+8R^2}{16}\left[1 \pm \left(1 - \left\{\frac{3D}{5D^2+8R^2}\right\}^2\right)^{\frac{1}{2}}\right] \qquad \text{.. A3.4/6}$$

If D = 5cm then the solution for d' is as in Figure A3.4/2. (The positive value of the radical must be taken and the positive root of a). Lesser values of D produce a lower value of d' for a given R. A related problem with the transmitter located at one side of the array (corresponding to the situation in the actual experiments) is discussed similarly elsewhere.[1]

In the apparatus d' is chosen at a value satisfactory for the closest objects of interest and is about 60mm. (The recording time is fixed and hence d' varies with propagation velocity). At larger R values then the condition $x = \frac{D}{2}$ on the ellipse is not reached until a depth greater than R and hence the useful region extends over some depth in the material. If we now take d' constant and consider the variation in z for the $x = \frac{D}{2}$ condition we obtain;

$$z = (a^2 - \frac{D^2}{16}) \left(1 - \frac{9D^2}{16a^2}\right) \qquad .. A3.4/7$$

and the useful depth (z - R) varies as in Figure A3.4/3 for D = 50mm and d' = 60mm. As would be expected for very large R, z - R tends to $\frac{d'}{2}$.

REFERENCE FOR APPENDIX 3.4.

1. Cook, G.B. 'The Ultrasonic Camera: A Study of the Transducer Computer Interface'. M.E. Thesis, University of Canterbury 1969. p.3.5.

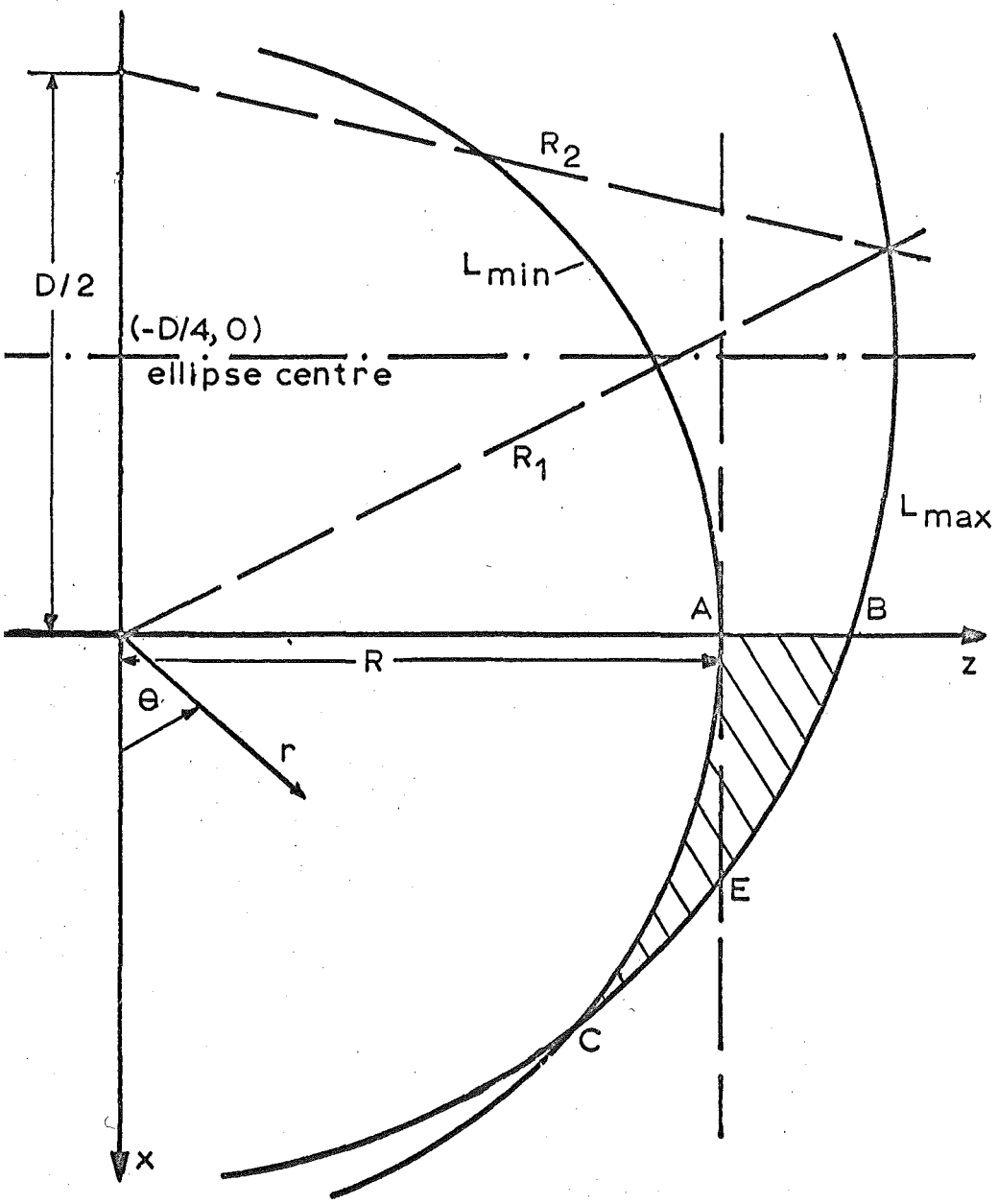

FIG.A 3.4/1: Geometry relavent to the determination of imageable depth.

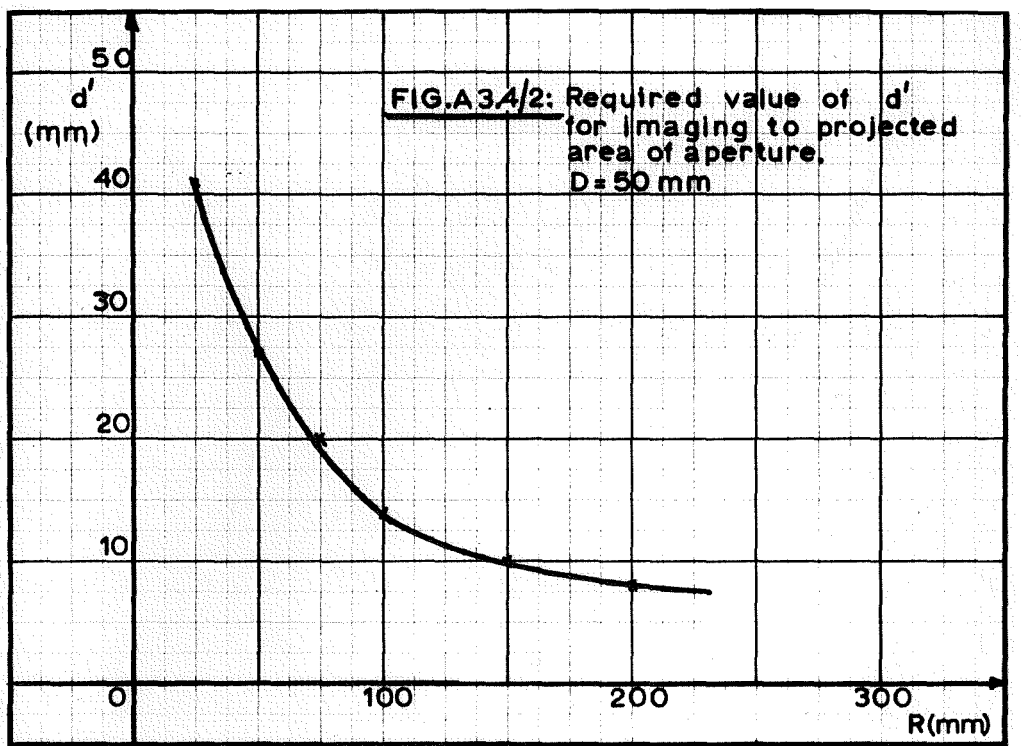

FIG.A3.4/2: Required value of d' for imaging to projected area of aperture. D = 50 mm

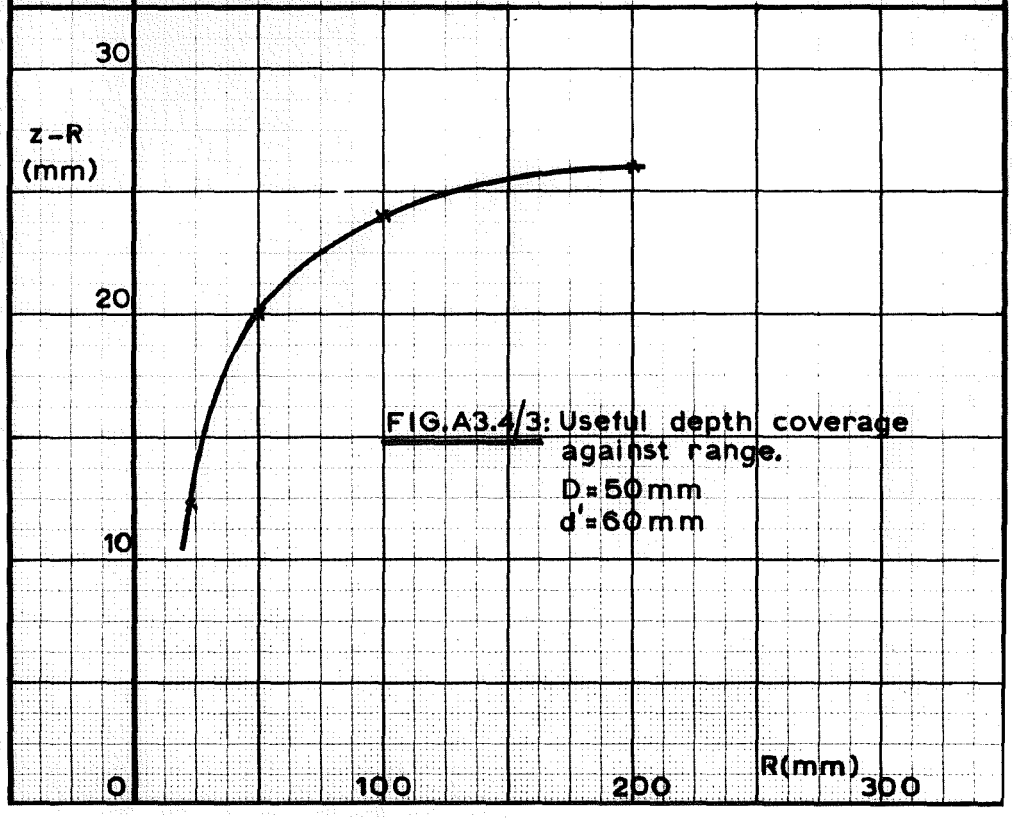

FIG.A3.4/3: Useful depth coverage against range.
D = 50 mm
d' = 60 mm

APPENDIX 3.5.

SPATIAL PATTERN OF WIDEBAND SYSTEMS

The case assumed is that of a single reflector producing a single spatial line in the function $\bar{u}(\xi,\eta,k)$ but broadband in k. The case when the spectrum is uniform over the range -K to +K has already been treated in the text. At any wave-number k the spatial response of the finite aperture system to a single incident plane wavefront which for simplicity will be assumed as on 'boresight' (i.e., wave propagation along the normal to the aperture) may be expressed in the form;

$$s_k(l,m) = \text{sinc}\frac{Qdlk}{2\pi}\ \text{sinc}\frac{Rdmk}{2\pi} \qquad .. \text{A3.5/1}$$

Again for simplicity we will take a cut of this function through a principle plane, choosing m = 0. Then;

$$s_k(l) = \text{sinc}\left(\frac{Qdlk}{2\pi}\right) \qquad .. \text{A3.5/2}$$

The pattern of variation against l is given by a summation of the response at each frequency weighted by the spectrum of the particular signals used. This spectrum is by hypothesis confined to the interval -K to +K and hence;

$$s(l) = \int_{-K}^{K} \text{sinc}\frac{Qdlk}{2\pi} F(k)\,dk \qquad .. \text{A3.5/3}$$

F(k) is the spectrum of the signal after reception and includes the frequency selectivity of the receiving transducer. Figure A3.5/1 shows the waveform and spectrum of the particular example selected. This function has a strong resemblance to the actual form of the received waveforms in the actual apparatus. Thus, writing $\beta = \frac{Qdl}{2}$, Equation A3.5/3 becomes;

$$s(l) = \int_{-2k_o}^{-k_o} (2k_o+k)\frac{\sin(\beta k)}{\beta k}dk + \int_{-k_o}^{o} -k\frac{\sin(\beta k)}{\beta k}dk + \int_{o}^{k_o} k\sin\frac{(\beta k)}{\beta k} + \int_{k_o}^{2k_o} (2k_o-k)\sin\frac{(\beta k)}{\beta k}\,dk \quad .. \text{A3.5/4}$$

and this has the solution;

$$s(l) = \frac{4k_o}{\beta}(Si(2\beta k_o) - Si(\beta k_o)) + \frac{\cos(\beta k_o)}{\beta^2}(\cos\beta k_o - 1) \quad .. \text{A3.5/5}$$

Now $s(0) = 2k_o^2$

and we may thus normalize the function by this factor to give;

$$s_n(l) = \frac{2}{\beta k_o}\{Si(2\beta k_o) - Si(\beta k_o)\} + \frac{2}{(\beta^2 k_o^2)}(\cos\beta k_o)[\cos\beta k_o - 1] \quad .. \text{A3.5/6}$$

For an example we take;

$Q = 64$

$k_o = 0.4K = 0.5 \times 10^4$ (i.e., k_o corresponds to 5 MHz).

Then recalling that $d = \frac{\pi}{KL}$;

$k_o\beta = 401/L$.

This function (Appendix 3.5/6) is plotted in Figure A3.5/2 where the patterns for a signal with a uniform spectrum over the range $-2k_o$ to $+2k_o$ and a monochromatic signal at $k = k_o$ are also shown for comparison.

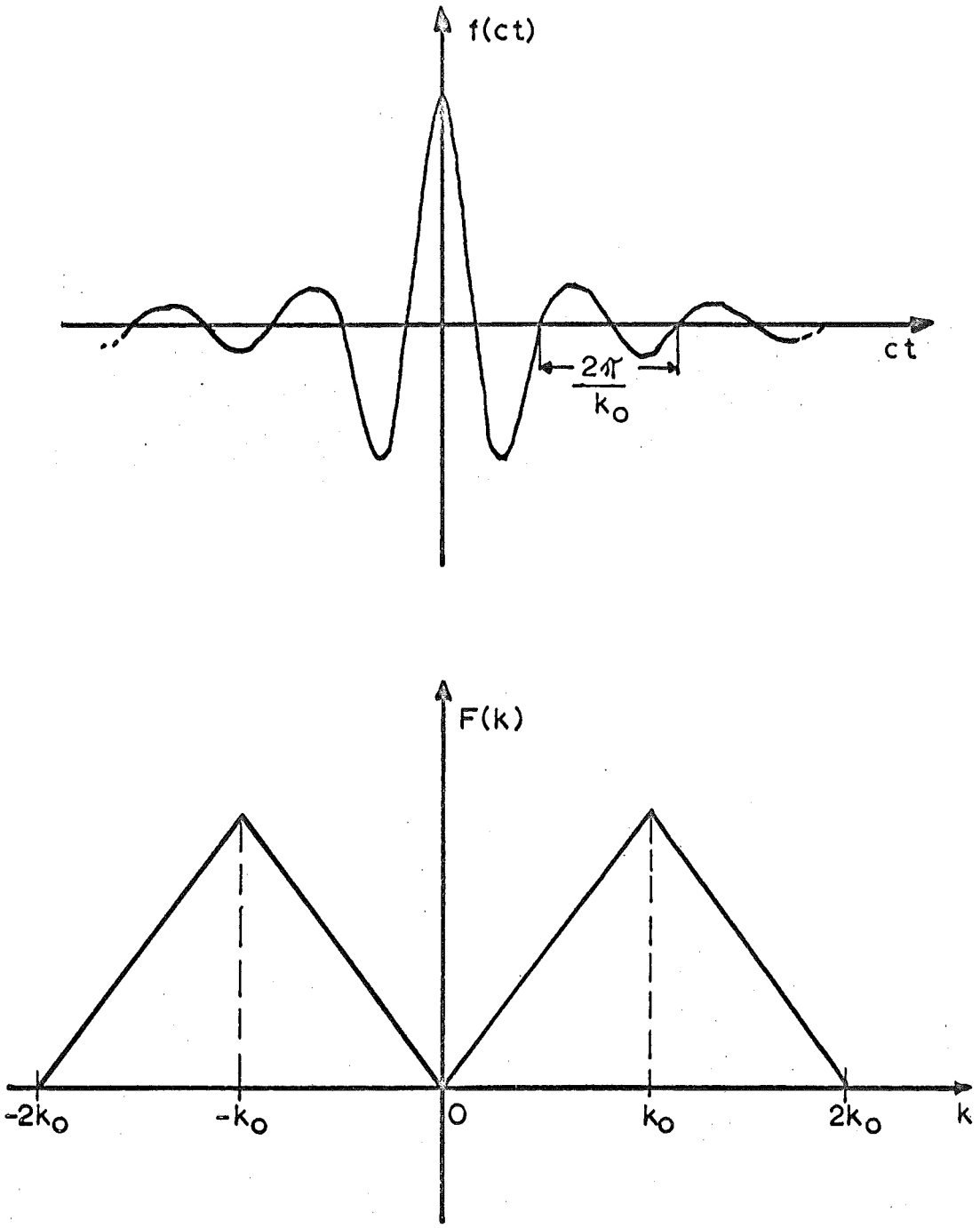

FIG.A 3.5/1: Waveform and spectrum of signal

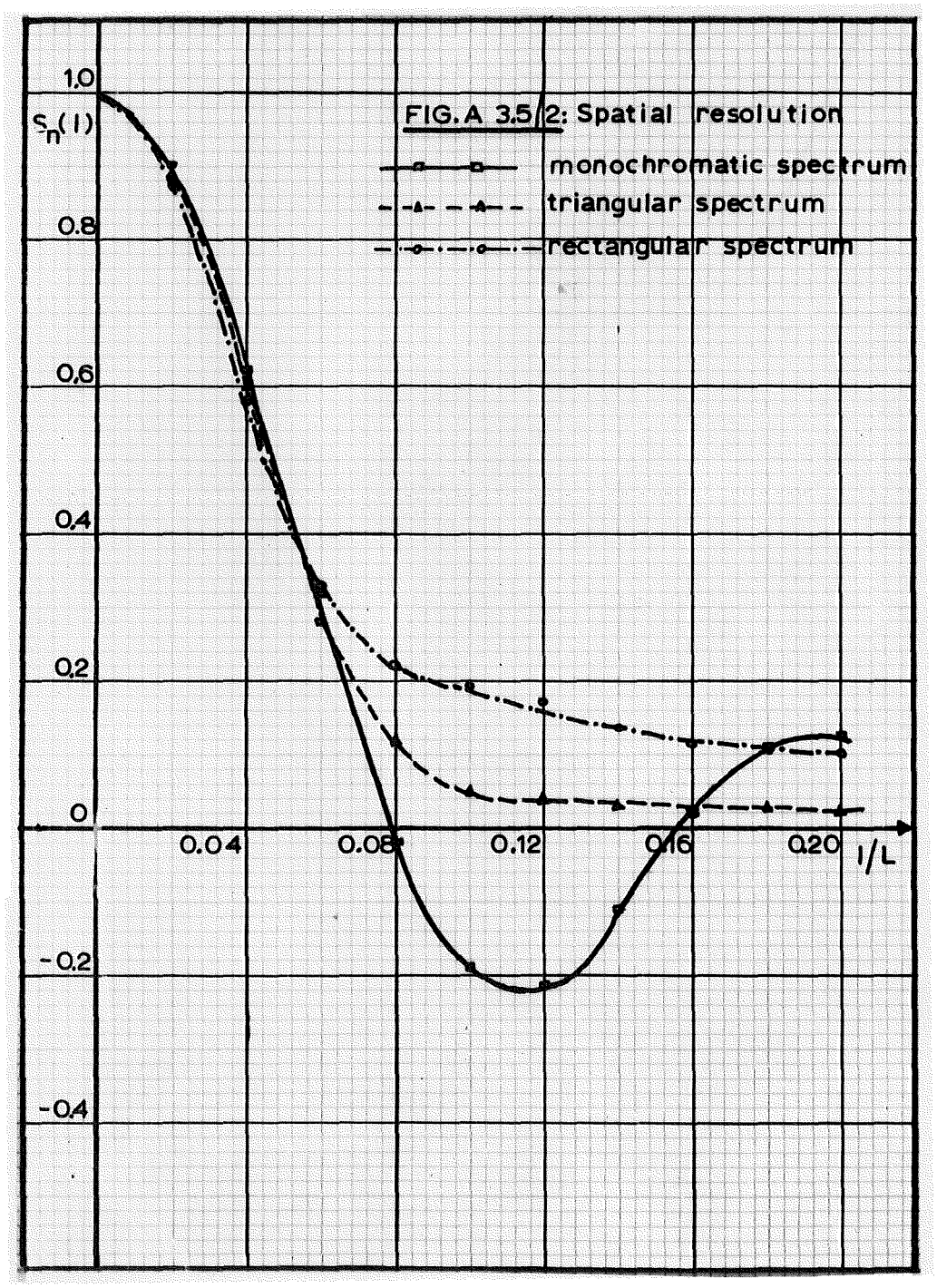
FIG. A 3.5/2: Spatial resolution
monochromatic spectrum
triangular spectrum
rectangular spectrum
$S_n(l)$
1.0
0.8
0.6
0.4
0.2
0
-0.2
-0.4
0.04
0.08
0.12
0.16
0.20
l/L

APPENDIX 3.6.

IMAGE RESOLUTION OF A FINITE APERTURE.

This appendix contains the mathematical details of the results in section 6 of Chapter 6.

From Equation 6.58 the z directed component of particle displacement at the point (x,y,z) is given by;

$$V_z(x,y,z,k) = \left(E(k)G.\not{\sigma}\, b_a(k)\right) . \frac{QRd^2}{4\pi^2}\exp(-j x \xi_i) \iint_{-\infty}^{\infty} \operatorname{sinc}\frac{Rd\eta}{2\pi} .$$

$$. \exp(-j\eta(y - \frac{R-1}{2}d) . \tfrac{1}{2}\Big[\operatorname{sinc}\{\frac{Qd}{2\pi}(\xi-\xi_i+\Omega)\} .$$

$$. \exp(j[\frac{Q-1}{2}\Omega d-\gamma]) + \operatorname{sinc}\{\frac{Qd}{2\pi}(\Omega-(\xi-\xi_i)\} .$$

$$. \exp(-j[\frac{Q-1}{2}\Omega\, d-\gamma])\Big] \exp(-j x \xi) .$$

$$. \exp(j z\sqrt{k^2-\xi^2-\eta^2}) . \exp(j\frac{Q-1}{2}d(\xi-\xi_i)) . d\xi\, d\eta$$

.. A3.6/1

making the substitutions;

$$u = (\xi-\xi_i+\Omega)$$

$$v = (\xi-\xi_i-\Omega)$$

.. A3.6/2

we may rewrite the integral portions in the form;

$$I = \tfrac{1}{2}\left\{ \iint_{-\infty}^{\infty} \operatorname{sinc}\frac{R d\eta}{2\pi} \cdot \exp\left(-j\eta\left(y - \frac{R-1}{2}d\right)\right) \cdot \operatorname{sinc}\frac{Q du}{2\pi} \cdot \exp\left(-ju\left[x - \frac{Q-1}{2}d\right]\right) \cdot \right.$$

$$\cdot \exp(j\Omega x - \gamma) \cdot \exp\left(-j z \sqrt{k^2 - (u+\xi_i - \Omega)^2 - \eta^2}\right) du\, d\eta$$

$$+ \iint_{-\infty}^{\infty} (\text{as first part with } \exp(-j(\Omega x - \gamma)), \text{ and } v$$

$$\left. \text{replacing } u, \text{ with } \xi_i + \Omega \text{ in irrational portion}) \right\}$$

$$= \tfrac{1}{2}\{I_1 + I_2\} \qquad .. \text{ A3.6/3}$$

Taking the first integral I_1 as representative and introducing that portion of G which does not appear in the expression for the reflected wave at the object surface* (i.e., $\exp\left(\frac{jz_o}{2}\left[\sqrt{k^2-(\xi_i-\Omega)^2} + \sqrt{k^2-(\xi_i+\Omega)^2}\right]\right)$, in combination with the $\exp(-j\gamma)$ term in I_1 gives a term $\exp(jz_o\sqrt{k^2-(\xi_i-\Omega)^2})$ (and similarly in I_2 $\exp(jz_o\sqrt{k^2-(\xi_i+\Omega)^2})$.

The z dependent irrational exponential argument;

$$F\left(\frac{u}{k},\frac{\eta}{k}\right) = -j z k \sqrt{1 - \left(\frac{u+\xi_i-\Omega}{k}\right)^2 + \left(\frac{\eta}{k}\right)^2} \qquad .. \text{ A3.6/4}$$

may, under the condition of Q and R both large so that the sinc functions decay rapidly with small values of u and η, be approximated by a Taylor expansion as;

---

* Some liberties have been taken with the convolution operation as this applies to this part of G and also strictly to the $\exp(j\gamma)$ terms already inside the integral. However we will assume that these phase terms are not appreciably upset by the convolution over the range of k where significant contributions to the image are made.

$$F\left(\frac{u}{k},\frac{\eta}{k}\right) \approx F(0,0) + \left(\frac{u}{k}\right) F_{\left(\frac{u}{k}\right)}(0,0) + \left(\frac{\eta}{k}\right) F_{\left(\frac{\eta}{k}\right)}(0,0)$$

$$+ \frac{1}{2}\left(\frac{u^2}{k^2} F_{\left(\frac{u}{k}\right)\left(\frac{u}{k}\right)}(0,0) + 2\frac{u\eta}{k^2} F_{\left(\frac{u}{k}\right)\left(\frac{\eta}{k}\right)}(0,0) \right.$$

$$\left. + \frac{\eta^2}{k^2} F_{\left(\frac{\eta}{k}\right)\left(\frac{\eta}{k}\right)}(0,0) \right) \qquad \text{.. A3.6/5}$$

It should be noted that this does not imply any limitation on the values of $\left(\frac{\xi_i \pm \Omega}{k}\right)$ and is rather a statement about the system's ability to reproduce the original 'lines' at these angles. The 'sharper' the reproduction the better the Taylor approximation will be.

Calculation of the various derivatives and evaluation at (0,0) gives the expression;

$$F\left(\frac{u}{k},\frac{\eta}{k}\right) = -jkz\left\{\left(1 - \left(\frac{\xi_i - \Omega}{k}\right)^2\right)^{\frac{1}{2}} + \frac{u}{k} \cdot \frac{-\left(\frac{\xi_i - \Omega}{k}\right)}{\left(1 - \left(\frac{\xi_i - \Omega}{k}\right)^2\right)^{\frac{1}{2}}}\right.$$

$$\left. + \frac{1}{2}\left[\left(\frac{u}{k}\right)^2 \cdot \frac{-1}{\left(1 - \left(\frac{\xi_i - \Omega}{k}\right)^2\right)^{\frac{3}{2}}} + \left(\frac{\eta}{k}\right)^2 \cdot \frac{-1}{\left(1 - \left(\frac{\xi_i - \Omega}{k}\right)^2\right)^{\frac{1}{2}}}\right]\right\}$$

.. A3.6/6

Which, reinserted in I_1 gives;

$$I_1 = \iint_{-\infty}^{\infty} \text{sinc}\frac{Rd\eta}{2\pi} . \exp(-j\eta[y - \frac{R-1}{2}d]) . \exp\left[\frac{\frac{jkz}{2}(\frac{\eta}{k})^2}{\left(1 - \left(\frac{\xi_i - \Omega}{k}\right)^2\right)^{\frac{1}{2}}}\right] .$$

$$. \quad \text{sinc}\frac{Qdu}{2\pi} . \exp\left[-ju(x - \frac{Q-1}{2}d - \frac{z\left(\frac{\xi_i - \Omega}{k}\right)}{\left(1 - \left(\frac{\xi_i - \Omega}{k}\right)^2\right)^{\frac{1}{2}}})\right] .$$

$$. \quad \exp\left[\frac{\frac{jkz}{2}(\frac{u}{k})^2}{\left(1 - \left(\frac{\xi_i - \Omega}{k}\right)^2\right)^{\frac{1}{2}}}\right] \, du \, d\eta \, . \exp\left[jk(z_o - z) \right. .$$

$$. \quad \left. \left(1 - \left(\frac{\xi_i - \Omega}{k}\right)^2\right)^{\frac{1}{2}} \right] . \qquad .. \text{A3.6/7}$$

and similarly for I_2 with $\xi_i + \Omega$ instead.

Observing that the integral is now separable in u and η and taking the η integral as typical the basic form is seen to be;

$$I_3 = \int_{-\infty}^{\infty} \text{sinc}\frac{Rd\eta}{2\pi} . \exp(-j\eta Y) . \exp(j\gamma_2 \eta^2) d\eta .$$

$$I_3 = Rd \int_{-\infty}^{\infty} \frac{\exp(j\frac{Rd\eta}{2}) - \exp(-j\frac{Rd\eta}{2})}{j\eta} \exp(j(\gamma_2\eta^2 - Y\eta)) \, d\eta \quad .. \text{A3.6/8}$$

which may be further expanded as two integrals;

$$I_3 = \frac{2\pi}{Rd}\left\{\frac{1}{2\pi}\int_{-\infty}^{\infty}\frac{\exp(j\gamma_2\eta^2 + j(\frac{Rd}{2} - Y)\eta)}{j\eta}\,d\eta + \right.$$

$$\left.\frac{1}{2\pi}\int_{-\infty}^{\infty}\frac{\exp(j\gamma_2\eta^2 + j(-\frac{Rd}{2} - Y)\eta)}{j\eta}\,d\eta\right\} \qquad \text{.. A3.6/9}$$

$$= \frac{2\pi}{Rd}(I_4 + I_5).$$

In which form we interprete the integrals as Fourier transform operations between the variable η and the variables $\frac{Rd}{2} - Y$ and $(-\frac{Rd}{2} - Y)$ respectively and from the properties of Fourier transforms the $\frac{1}{j\eta}$ term may be accounted for by indefinite integration of the transform of $\exp(j\gamma_2\eta^2)$. Thus the first solution required is that to;

$$I_6 = \frac{1}{2\pi}\int_{-\infty}^{\infty}\exp(j[\gamma_2\eta^2 + \alpha\eta)\,d\eta$$

$$= \frac{1}{2\pi}(1 + j)\sqrt{\frac{\pi}{2\gamma_2}}\,e^{\frac{-j\alpha^2}{4\gamma_2}} \qquad \text{.. A3.6/10}$$

and the full solution is given by;

$$I_4 = \frac{1}{2\pi}(1 + j)\sqrt{\frac{\pi}{2\gamma_2}}\int\exp(-\frac{j\alpha^2}{4\gamma_2})\,d\alpha$$

$$= \frac{1}{2\pi}(1 + j)\cdot\sqrt{\frac{\pi}{2\gamma_2}}\cdot\sqrt{\frac{\pi}{2(\frac{1}{4\gamma_2})}}\left\{C\left[\sqrt{\frac{2\cdot(\frac{1}{4\gamma_2})}{\pi}}\,\alpha\right] - \right.$$

$$\left. jS\left[\sqrt{\frac{2\cdot(\frac{1}{4\gamma_2})}{\pi}}\,\alpha\right]\right\} \qquad \text{.. A3.6/11}$$

where C and S are the Fresnel integrals,

$$C[z] = \int_0^z \cos(\tfrac{\pi}{2} t^2)dt \ , \ S[z] = \int_0^z \sin(\tfrac{\pi}{2} t^2)dt \quad .. \text{ A3.6/12}$$

collection of terms gives,

$$I_4 = \tfrac{1}{2}(1+j)\left\{ C\left[\sqrt{\frac{1}{2\pi\gamma_2}}\ \alpha \right] - jS\left[\sqrt{\frac{1}{2\pi\gamma_2}}\ \alpha \right] \right\} \quad .. \text{ A3.6/13}$$

and introducing the complex Fresnel integral defined as,

$$F_o[z] = \sqrt{2}\, e^{j\frac{\pi}{4}} \int_0^z e^{-j\frac{\pi}{2}t^2} dt \quad .. \text{ A3.6/14}$$

I_3 may be expressed in the form;

$$I_3 = \frac{2\pi}{Rd} \cdot \tfrac{1}{2}\left[F_o\left[\sqrt{\frac{1}{2\pi\gamma_2}}\ (\frac{Rd}{2} - Y) \right] - F_o\left[\sqrt{\frac{1}{2\pi\gamma_2}}\ (-\frac{Rd}{2} - Y) \right] \right]$$

.. A3.6/15

By remembering $Y = y - \frac{R-1}{2}d$ and noting;

$$F_o[-z] = -F_o[z] \quad .. \text{ A3.6/16}$$

we get,

$$I_3 = \frac{-\pi}{Rd}\left\{ F_o\left[\sqrt{\frac{1}{2\pi\gamma_2}}\ (y - (R-\tfrac{1}{2})d) \right] - F_o\left[\sqrt{\frac{1}{2\pi\gamma_2}}\ (y + \frac{d}{2}) \right] \right\}$$

.. A3.6/17

Proceeding similarly for the u integration and for the other portion of the complete solution, I_2, then for $z = z_o$ the expression given in Equation 6.60 is obtained. For $z \neq z_o$ all the z_o's

should be replaced by z and a term $\exp(jk(z_o-z)\sqrt{1-\left(\frac{\xi_i-\Omega}{k}\right)^2}$ associated with $\exp(j\Omega x)$ and the corresponding term with $(\xi_i+\Omega)$ associated with $\exp(-j\Omega x)$.

Numerical calculations.

Taking the centre of the image the expression for V_z reduces to a more manageable form as; (cf. Equation 6.63)

$$V_z\left(\frac{Q-1}{2}d,\ \frac{R-1}{2}d,\ z_o,\ k\right) = \frac{H}{2}.\cos\left[\Omega\left(\frac{Q-1}{2}\right)d\right].F_o\left[\left(\frac{2}{z_o\lambda}\right)^{\frac{1}{2}}\left(1-\left(\frac{\Omega}{k}\right)^2\right)^{\frac{1}{4}}.\frac{Rd}{2}\right].$$

$$.\left\{F_o\left[\left(\frac{2}{z_o\lambda}\right)^{\frac{1}{2}}\left(1-\left(\frac{\Omega}{k}\right)^2\right)^{\frac{3}{4}}.\left(\frac{Qd}{2}-\frac{z_o\left(\frac{\Omega}{k}\right)}{\left(1-\left(\frac{\Omega}{k}\right)^2\right)^{\frac{1}{2}}}\right)\right]+\right.$$

$$\left.F_o\left[\left(\frac{2}{z_o\lambda}\right)^{\frac{1}{2}}\left(1-\left(\frac{\Omega}{k}\right)^2\right)^{\frac{3}{4}}.\left(\frac{Qd}{2}+\frac{z_o\left(\frac{\Omega}{k}\right)}{\left(1-\left(\frac{\Omega}{k}\right)^2\right)^{\frac{1}{2}}}\right)\right]\right\}$$

.. A3.6/18

(where ξ_i has been taken as 0).

Which with Qd = Rd = z_o = 40mm and λ = 1.25mm (5 MHz in Al.) gives the values plotted in Table A3.6/1.

TABLE A3.6/1

$\bar{k}$	'y'	'x'	'x' . 'y'	$+90^{\circ}$
0	$0.625\angle -40^{\circ}$	$1.31\angle -40^{\circ}$	$0.85\angle -80^{\circ}$	$0.85\angle +10^{\circ}$
0.25	$0.625\angle -45^{\circ}$	$1.28\angle -45^{\circ}$	$0.8\angle -90^{\circ}$	$0.8\angle 0^{\circ}$
0.40	$0.69\angle -52^{\circ}$	$1.21\angle -51^{\circ}$	$0.83\angle -103^{\circ}$	$0.83\angle -13^{\circ}$
0.477	$0.74\angle -51^{\circ}$	$0.676\angle -48^{\circ}$	$0.5\angle -99^{\circ}$	$0.5\angle -9^{\circ}$
0.50	$0.782\angle -48^{\circ}$	$0.132\angle +14^{\circ}$	$0.103\angle -34^{\circ}$	$0.103\angle +56^{\circ}$
0.707	$0.615\angle -47^{\circ}$	$0.236\angle -161^{\circ}$	$0.145\angle -208^{\circ}$	$0.145\angle -118^{\circ}$
0.866	$0.641\angle -37^{\circ}$	$0.048\angle -148^{\circ}$	$0.03\angle -185^{\circ}$	$0.03\angle -95^{\circ}$
1.00	0			

In the table, 'x' represents the sum of the Qd dependent functions and 'y' the value of the Rd dependent component. The $(2)^{\frac{1}{2}}\exp(j\frac{\pi}{4})$ terms are not included in 'x' and 'y'; the amplitude portion cancels with $\frac{1}{2}$ in Equation A3.6/18 and the product of the two phase terms is represented by the 90° added to produce the final column in the table. The abbreviated notation $A\angle\alpha = A.\exp(j\alpha)$ has been employed.

Depth resolution.

To gain an appreciation of the variation in field with depth the simple case where $\Omega = 0$ has been taken and then along $x = \frac{(Q-1)}{2}d$ $y = \frac{(R-1)}{2}d$, V_z reduces to the particularly simple form;

$$V_z\left(\frac{Q-1}{2}d, \frac{R-1}{2}d, z, k\right) \doteq H\left(F_o\left[\left(\frac{2}{\lambda z}\right)^{\frac{1}{2}} . \frac{Qd}{2}\right]\right)^2 e^{jk(z_o - z)} \qquad .. \text{ A3.6/19}$$

taking R = Q.

With values of z ranging from 10 to 80mm this has the modulus as listed in Table A3.6/2.

TABLE A3.6/2

z	Modulus
10	0.922
20	0.895
30	1.19
40	0.85
50	1.10
60	0.97
70	1.23
80	0.82

The phase of the F_o term remains practically stationary within 15^o of 0^o at all values of z and hence the phase is nearly purely a function of the distance from the true image position. As may be seen from the plot (Figure A3.6/1) the axial field varies in an oscillatory manner about 1 not reducing significantly until $(z\lambda)^{\frac{1}{2}}$ becomes appreciably larger than Qd. This corresponds to 'far field' conditions (Equation 3.8) being reached and in the present case does not occur until z > 160mm. The correct limiting behaviour of the expression derived is indicated from the limiting value as the argument goes to zero, i.e.,

$F_o(a) \doteq a$ for $a \to 0$ and here $a = \frac{\text{constant}}{\sqrt{z}}$ so that the expression in Equation A3.6/19 decays as $\frac{1}{z}$ for z very large, with the phase term acting as if there was an effective radiating aperture located $(\frac{1}{4})\lambda$ from the correct image plane.

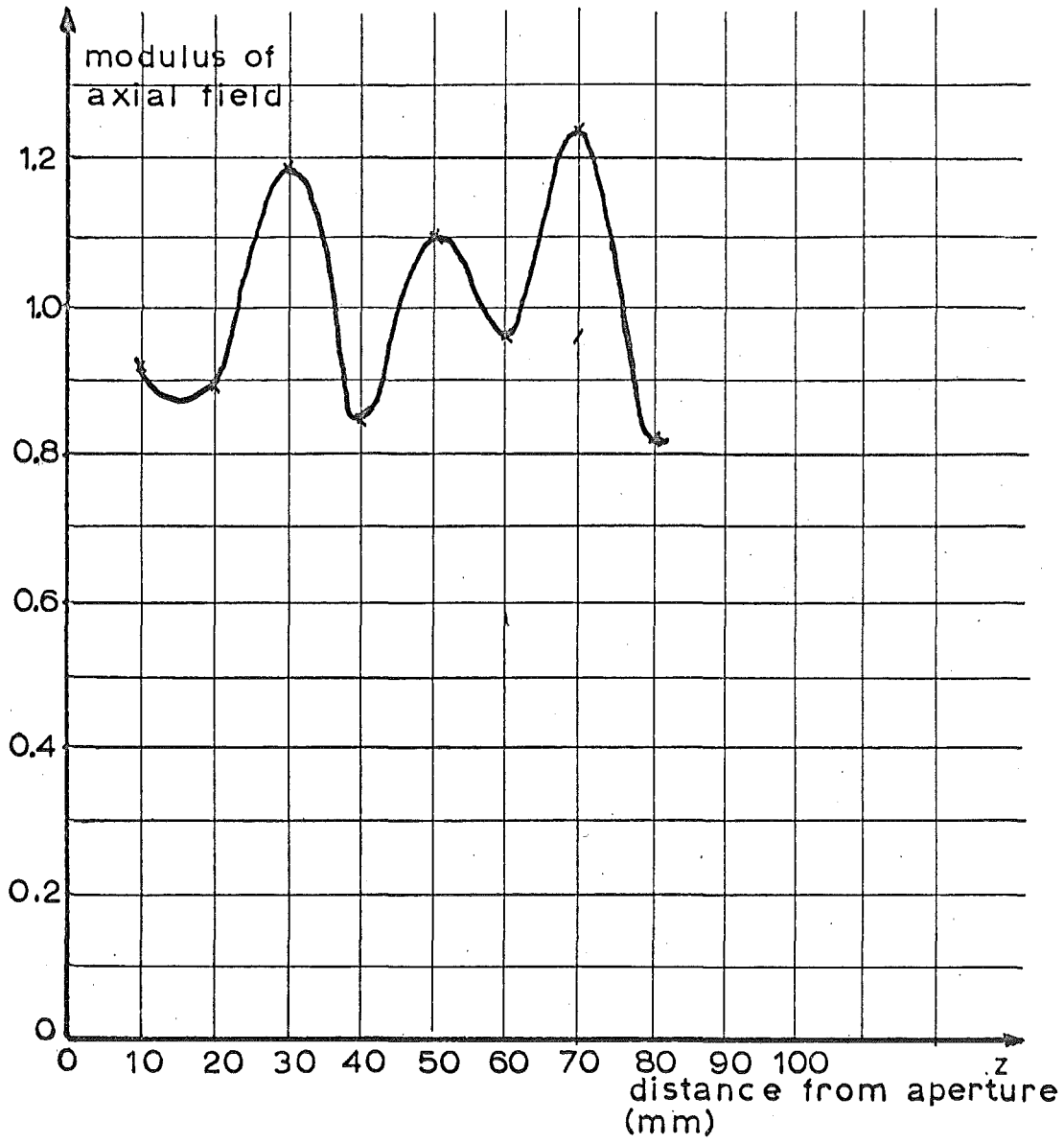

FIG. A3.6/1: Axial field of 40 mm square aperture
λ = 1.25 mm
z_o = 40 mm